MARINE MICROBIAL-DERIVED MOLECULES AND THEIR POTENTIAL MEDICAL AND COSMETIC APPLICATIONS

EDITED BY: Jinwei Zhang, Antje Labes and Runying Zeng
PUBLISHED IN: Frontiers in Microbiology

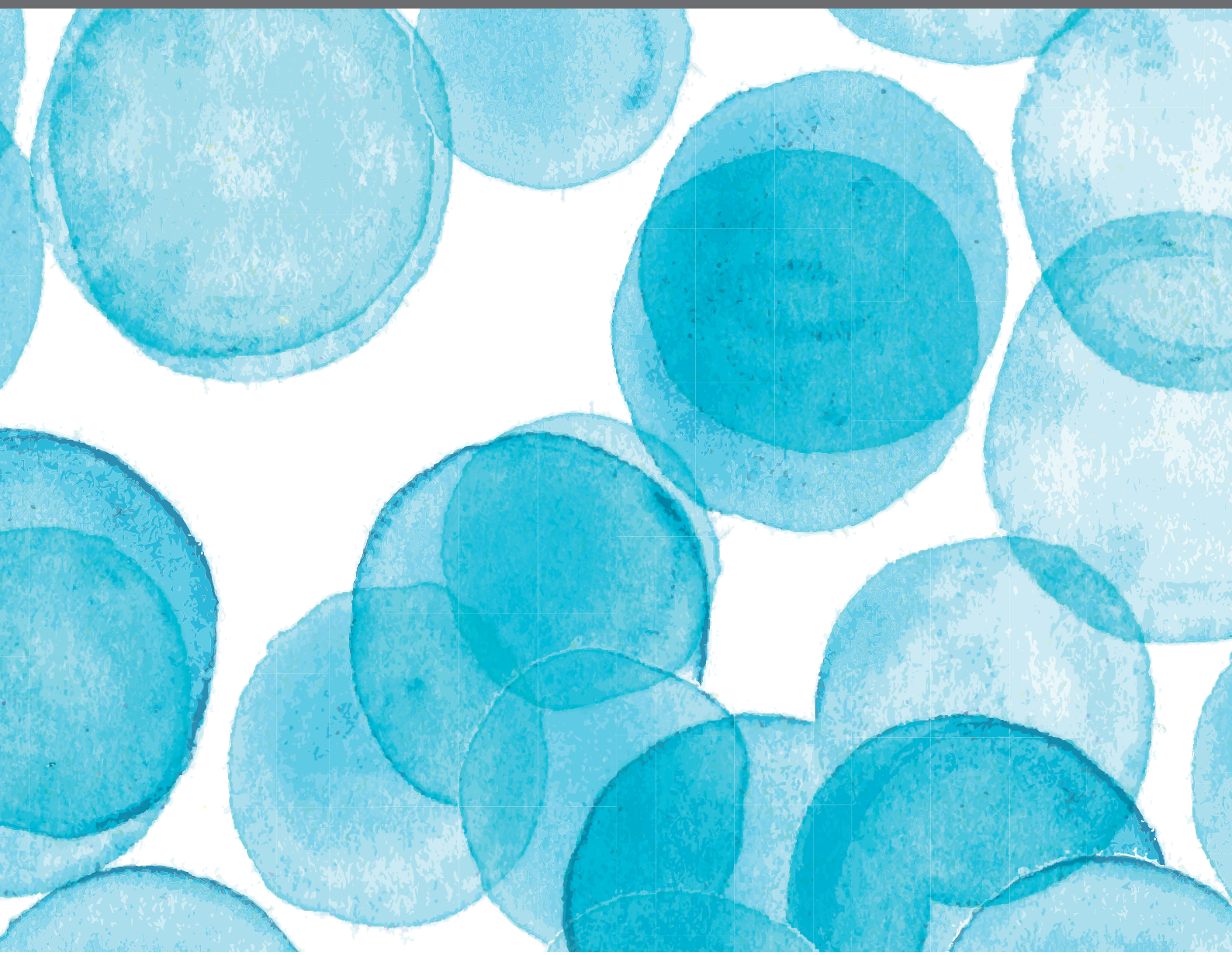

frontiers Research Topics

ISSN 1664-8714
ISBN 978-2-88971-331-8
DOI 10.3389/978-2-88971-331-8

About Frontiers

Frontiers is more than just an open-access publisher of scholarly articles: it is a pioneering approach to the world of academia, radically improving the way scholarly research is managed. The grand vision of Frontiers is a world where all people have an equal opportunity to seek, share and generate knowledge. Frontiers provides immediate and permanent online open access to all its publications, but this alone is not enough to realize our grand goals.

Frontiers Journal Series

The Frontiers Journal Series is a multi-tier and interdisciplinary set of open-access, online journals, promising a paradigm shift from the current review, selection and dissemination processes in academic publishing. All Frontiers journals are driven by researchers for researchers; therefore, they constitute a service to the scholarly community. At the same time, the Frontiers Journal Series operates on a revolutionary invention, the tiered publishing system, initially addressing specific communities of scholars, and gradually climbing up to broader public understanding, thus serving the interests of the lay society, too.

Dedication to Quality

Each Frontiers article is a landmark of the highest quality, thanks to genuinely collaborative interactions between authors and review editors, who include some of the world's best academicians. Research must be certified by peers before entering a stream of knowledge that may eventually reach the public - and shape society; therefore, Frontiers only applies the most rigorous and unbiased reviews.
Frontiers revolutionizes research publishing by freely delivering the most outstanding research, evaluated with no bias from both the academic and social point of view. By applying the most advanced information technologies, Frontiers is catapulting scholarly publishing into a new generation.

What are Frontiers Research Topics?

Frontiers Research Topics are very popular trademarks of the Frontiers Journals Series: they are collections of at least ten articles, all centered on a particular subject. With their unique mix of varied contributions from Original Research to Review Articles, Frontiers Research Topics unify the most influential researchers, the latest key findings and historical advances in a hot research area! Find out more on how to host your own Frontiers Research Topic or contribute to one as an author by contacting the Frontiers Editorial Office: frontiersin.org/about/contact

MARINE MICROBIAL-DERIVED MOLECULES AND THEIR POTENTIAL MEDICAL AND COSMETIC APPLICATIONS

Topic Editors:
Jinwei Zhang, University of Exeter, United Kingdom
Antje Labes, Fachhochschule Flensburg, Germany
Runying Zeng, Third Institute of Oceanography, China

Citation: Zhang, J., Labes, A., Zeng, R., eds. (2021). Marine Microbial-Derived Molecules and Their Potential Medical and Cosmetic Applications. Lausanne: Frontiers Media SA. doi: 10.3389/978-2-88971-331-8

Table of Contents

frontiers in Microbiology

EDITORIAL
published: 16 July 2021
doi: 10.3389/fmicb.2021.706152

Editorial: Marine Microbial-Derived Molecules and Their Potential Medical and Cosmetic Applications

Jinwei Zhang[1,2]*, *Runying Zeng*[3] and *Antje Labes*[4]

[1] Hatherly Laboratories, Institute of Biomedical and Clinical Sciences, University of Exeter Medical School, Exeter, United Kingdom, [2] European Centre for Environment and Human Health, Environment and Sustainability Institute, University of Exeter Medical School, Penryn, United Kingdom, [3] Engineering Innovation Center for the Development and Utilization of Marine Bioresources, Third Institute of Oceanography, Minstry of Natural Resources China, Xiamen, China, [4] Department of Energy and Biotechnology, Flensburg University of Applied Sciences, Flensburg, Germany

Keywords: marine microbial ecology, marine biotechnology, bioactive materials, secondary metabolites, enzymes, oligosaccharides, medical and cosmetic applications

Editorial on the Research Topic

Marine Microbial-Derived Molecules and Their Potential Medical and Cosmetic Applications

OPEN ACCESS

Edited by:
Jean Armengaud, Commissariat à l'Energie Atomique et aux Energies Alternatives (CEA), France

Reviewed by:
Christophe Hano, Université d'Orléans, France

***Correspondence:**
Jinwei Zhang
j.zhang5@exeter.ac.uk

Specialty section:
This article was submitted to Microbiotechnology, a section of the journal Frontiers in Microbiology

Received: *06 May 2021*
Accepted: *22 June 2021*
Published: *16 July 2021*

Citation:
Zhang J, Zeng R and Labes A (2021) Editorial: Marine Microbial-Derived Molecules and Their Potential Medical and Cosmetic Applications. Front. Microbiol. 12:706152. doi: 10.3389/fmicb.2021.706152

The marine environment is a vast, largely unexploited resource for acquiring a multitude of microbial communities with a number of uncharacterized taxonomic groups and novel biosynthetic capabilities. Marine habitats provide unique conditions for microbial growth and secondary metabolite expressions that are not found in terrestrial ecosystems. The co-evolution of many marine macroorganisms, especially invertebrates, with these microorganisms often leads to a very close association or symbiotic relationship between the host organism and specific microbial species driven by natural products. The ocean basin floor is covered in sediments of different types and origins. Marine sediments are considered to be an incredibly rich source of microbial taxonomic diversity, including "unculturable" microbes. "Unculturable" microbial diversity presents a vast gene pool for biotechnological exploitation. In this context the secondary metabolites produced by the microbial species and their biosynthetic pathways represent a resource in the discovery of novel molecules or enzymes for a wide number of applications especially in the medical and cosmetic field. Sustainable use of these resources is a methodological challenge for the exploitation of "unculturable" microbes and their novel gene clusters responsible for biosynthetic pathways for new bioactive compounds and enzymes. However, new culture techniques in addition to culture-independent methods, such as PCR amplification from microbial community DNA (metagenome) and functional or sequence-based screening of metagenomic DNA libraries are proving useful. In recent years, efforts to characterize marine microbial metagenomics and their associated compounds and enzymes have expanded significantly, but given the vastness of the marine environment and the different types of microbial habitats found there, there is still room for game-changing discoveries.

The scope of this Special Issue is to provide a broad and updated overview on marine microbial community dynamics, genome sequencing and gene editing technology, marine microbial-derived molecules, and their potential medical and cosmetic applications. The collection includes 13 original research papers from prominent researchers in the field and provides the readers of the journal with recent results in the area of microbial-derived molecules and their

potential application in medical and cosmetic fields. Therefore, this Special Issue promotes our understanding of marine-derived biomolecules and their applications.

Emerging infectious diseases and multi-drug resistant human pathogens are becoming a major threat to global health. There is an urgent need for new antibiotics to fight evolving bacterial infections, especially with respect to gram negative pathogens. The marine habitat was shown to be a good source for extremophiles, known to be potential resources for novel bioactive metabolites. Gao et al. isolated 237 acidophilic/aciduric fungi from Thai mangrove sediment in acidic medium, and identified seven genera including *Penicillium*, *Aspergillus*, *Talaromyces*, *Cladosporium*, *Phoma*, *Alternaria*, *Trichoderma*, in four taxonomic orders of phylum *Ascomycota*. Ninety-five percent of these isolates can grow under extremely acidic conditions (pH 2). Many of them showed cytotoxic, antimicrobial, anti-H1N1 activities. The metabolites obtained from a typical aciduric fungus *Pencillium oxalicum* OUCMDZ-5207 were identified as tetrahydroauroglaucin (1), flavoglaucin (2), and auroglaucin (3), among which compound (3) showed strong selective inhibition on A549 cells with IC50 5.67 μM. Cong et al. isolated 1,208 bacterial and fungus strains in 27 genera from Antarctica soil environments, and investigated their physiology, enzyme activity and antifungal activity, respectively. For example, four polyketones: versicone A (1), versicone B (2), 4-methyl-5,6-dihydro-2H-pyran-2-one (3), and (R)-(+)-sydowic acid (4), were found from *Aspergillus sydowii* strain MS19. Compound (1) displayed strong activity against *Candida albicans*, with a MIC value of 3.91 μg/mL. Sarveswariv et al. screened 42 *Actinobacteria* from a mangrove soil sample, and found the biofilm inhibitory potential of *Micromonospora* sp. RMA46 against *Vibrio cholerae*. They found that the ethyl acetate extract of RMA46, mainly 2-methoxy-4-vinyl phenol and hexahydro-3-(phenylmethyl)-pyrrolo [1,2-a] pyrazine-1,4-dione, inhibited the formation of *V. cholerae* biofilms and downregulated the quorum sensing global switches LuxO and HapR. This study highlights *Micromonospora* sp. RMA46 as a potential source of anti-infectives against *V. cholerae*.

The known peptide sublancin and a surfactin–like lipopeptide demonstrate broad antimicrobial activity against Gram positive bacteria and yeasts. *Bacillus* strains are well-known to produce surfactins however Sharma et al. highlight the lipopeptide synthesized by *Bacillus subtilis* strain A5 isolated from marine sediment, as a candidate to inhibit *Candida ssp.* showing synergistic action with fluconazole. The lipopeptide emulgel formulation showed antimicrobial activity *in vitro* and no skin irritation was observed in mice. Rehman et al. reported nine sorbicillinoid derivatives (1–9), including six new compounds, from a marine sponge-derived fungus *Trichoderma reesei* (HN-2016-018). They discovered two novel sorbicillinoids (1–2) with a characteristic naphthalene-trione ring and two rare sorbicillinoids (3–4) possessing a bicycle (3.2.1) lactone skeleton. Compound 3 represented the first reported sorbicillinoid with a propan-2-one side chain. Compound 5 displayed strong cytotoxic activity against A549, MCF-7, and HCT116 cell lines with the IC50 values of 5.1, 9.5, and 13.7 μM, respectively. Paderog et al. reported about the isolation of precursors of anti-cancer anthracycline shunt metabolites, bisanhydoaklavinone and 1-hydroxybisanhydroaklavinone from marine sediment-derived *Streptomyces sp.* strain DSD069 without genetic manipulation. These two substances have antibiotic activity against *S. aureus* at MIC90 of 6.25 and 50 μg/mL, respectively.

Chemical epigenetic or genetic manipulation has been widely applied to microbes to obtain novel secondary metabolites or enhance the production. Wu et al. investigated the marine gorgonian-derived fungus *Aspergillus versicolor* XS-20090066 by chemical epigenetic manipulation with histone deacetylase inhibitor and DNA methyltransferase inhibitor. The discovered two new nucleoside derivatives, kipukasins K (1) and L (2), and one new bisabolane sesquiterpene, aspergillusene E (7). Compounds 1 and 7 exhibited antibacterial activities against *Staphylococcus epidermidis* and *S. aureus* with the MIC values of 8–16 μg/mL. Compound 7 displayed potent anti-larval attachment activity against bryozoan *Bugula neritina* with the EC50 and LC50 values of 6.25 and 25 μg/mL, respectively. Yao et al. used gene knockout method and created a ΔCtiS mutant strain of from a marine-derived fungus *Penicillium steckii* P2648 for biosynthesis of antibacterial compounds 1, 2, and 3 (isoquinoline alkaloids). Compounds 1 and 2 were reported firstly from the natural resource in this study, showed antibacterial activities against *Staphylococcus aureus* and *Enterococcus faecalis* with the MIC values of 16–32 μg/mL. Atmosphere and room-temperature plasma (ARTP) mutagenesis is an easy and fast method to generate the random mutational library in different strains. Liu et al. used iterative ARTP mutagenesis to obtain mutants from *Streptomyces sp.* MG010 and achieved antibacterial activities significantly increased by 75%.

Most carrageenase degradation products are mixtures, which makes it difficult to purify each type of oligosaccharide. Gui et al. cloned and expressed the carrageenase gene Car3206 in *Escherichia coli* cells, based on the genome sequence of an Antarctic *Polaribacter* sp. strain NJDZ03. The purified recombinant Car3206 produces only disaccharides, which can significantly reduce the cost of product purification in industrial production. Chitosanase is a significant chitosan-degrading enzyme forms chitooligosaccharides. Zheng et al. discovered a new member of GH-46 chitosanase (CsnS) from deep-sea bacterium *Serratia* sp. QD07. CsnS was a cold-adapted enzyme with activity of 324 U/mL, and is favorable to the production of (GlcN)2 and (GlcN)3, may have potential applications in the food and pharmaceutical industries.

Alginate oligosaccharides (AOS) showed various biological activities, with great potentials in industrial and biomedical applications. Marine neoagaro-oligosaccharides (NAOS) produced by most marine β-agarases always possess low DPs ($\leq$6) and limited categories. Qu et al. developed a novel strategy, using truncated recombinant AgaM1 (trAgaM1), that can efficiently produce NAOS especially with various DPs $\geq$8. trAgaM1 produced NAOS with various DPs (4–12), for examples, neoagarodecaose (NA10), and neoagarododecaose (NA12) at final concentrations of 3.02, and 3.02 g/L, respectively. Jin et al. investigated AOS with varying degrees of polymerization (DP), namely, AOS (DP2), AOS (DP4–6), and AOS (DP8–12), from

a deep-sea agarolytic *Flammeovirga pacifica* strain WPAGA1. They found that AOS could enhance hair growth after 30-days treatment on the back skin of mice.

This Special Issue summarizes important findings related to the marine microbial community, diverse bioactive materials, and their potential applications. The issue provide new possibilities for exploration and research on the novelties of marine microbial natural products.

AUTHOR CONTRIBUTIONS

JZ conceptualized the Research Topic and was responsible for writing the whole passage. JZ, RZ, and AL were responsible for checking and revision. All authors have read and agreed to the published version of the manuscript.

FUNDING

JZ was supported by the University of Exeter Medical School (UK), NIH Grants R01 NS109358 (USA), and The Royal Society No. IEC\NSFC\201094 (UK).

Conflict of Interest: The authors declare that the research was conducted in the absence of any commercial or financial relationships that could be construed as a potential conflict of interest.

frontiers in Microbiology

ORIGINAL RESEARCH
published: 30 January 2020
doi: 10.3389/fmicb.2020.00085

Epigenetic Agents Trigger the Production of Bioactive Nucleoside Derivatives and Bisabolane Sesquiterpenes From the Marine-Derived Fungus *Aspergillus versicolor*

Jing-Shuai Wu[1,2], Guang-Shan Yao[1,2,3], Xiao-Hui Shi[1,2], Saif Ur Rehman[1,2], Ying Xu[4], Xiu-Mei Fu[1,2], Xiu-Li Zhang[1,2], Yang Liu[5] and Chang-Yun Wang[1,2]**

[1] Key Laboratory of Marine Drugs, The Ministry of Education of China, School of Medicine and Pharmacy, Institute of Evolution & Marine Biodiversity, Ocean University of China, Qingdao, China, [2] Laboratory for Marine Drugs and Bioproducts, Qingdao National Laboratory for Marine Science and Technology, Qingdao, China, [3] Institute of Oceanography, Minjiang University, Fuzhou, China, [4] Shenzhen Key Laboratory of Marine Bioresource and Eco-Environmental Science, Shenzhen Engineering Laboratory for Marine Algal Biotechnology, College of Life Sciences and Oceanography, Shenzhen University, Shenzhen, China, [5] Institute for Insect Biotechnology, Justus Liebig University Giessen, Giessen, Germany

OPEN ACCESS

Edited by:
Jinwei Zhang,
University of Exeter, United Kingdom

Reviewed by:
Mohamed Ashour,
Ain Shams University, Egypt
Weaam Ebrahim,
Heinrich Heine University Düsseldorf, Germany

***Correspondence:**
Yang Liu
Liu.Yang@agrar.uni-giessen.de
Chang-Yun Wang
changyun@ouc.edu.cn

Specialty section:
This article was submitted to Microbiotechnology, Ecotoxicology and Bioremediation, a section of the journal Frontiers in Microbiology

Received: 20 November 2019
Accepted: 15 January 2020
Published: 30 January 2020

Citation:
Wu J-S, Yao G-S, Shi X-H, Rehman SU, Xu Y, Fu X-M, Zhang X-L, Liu Y and Wang C-Y (2020) Epigenetic Agents Trigger the Production of Bioactive Nucleoside Derivatives and Bisabolane Sesquiterpenes From the Marine-Derived Fungus Aspergillus versicolor. Front. Microbiol. 11:85. doi: 10.3389/fmicb.2020.00085

Epigenetic agents, histone deacetylase inhibitor (SAHA) and DNA methyltransferase inhibitor (5-Aza), were added to Czapek-Dox medium to trigger the chemical diversity of marine-derived fungus *Aspergillus versicolor* XS-20090066. By HPLC and ^{1}H NMR analysis, the diversity of fungal secondary metabolites was significantly increased compared with the control. With the aid of MS/MS-based molecular networking, two new nucleoside derivatives, kipukasins K (**1**) and L (**2**) were obtained. Meanwhile, the yields of four known nucleoside derivatives were significantly enhanced. In addition, one new bisabolane sesquiterpene, aspergillusene E (**7**), along with ten known derivatives were also isolated. The structures were elucidated by comprehensive spectroscopic methods of NMR and HRESIMS analysis. Compounds **1** and **7** displayed antibacterial activities against *Staphylococcus epidermidis* and *Staphylococcus aureus* with the MIC values of 8–16 μg/mL. Our study revealed that the fungus *A. versicolor* XS-20090066 has been effectively induced by chemical epigenetic manipulation with a combination of SAHA and 5-Aza to produce new metabolites.

Keywords: histone deacetylase inhibitor, DNA methyltransferase inhibitor, *Aspergillus versicolor*, nucleoside derivatives, bisabolane sesquiterpenes, antibacterial activities, antifouling activities

INTRODUCTION

Marine-derived fungi are prolific sources of structurally novel and biologically potent natural products for drug discovery (Jin et al., 2016; Blunt et al., 2018). However, the continuous investigations on the secondary metabolites from marine-derived fungi lead to a high frequency of rediscovery of known compounds (Penesyan et al., 2010), which motivated the researchers

to develop suitable strategies to find new natural products (Rutledge and Challis, 2015). A large number of fungal genome sequences suggested that the capacity of fungi to produce secondary metabolites was far more than we anticipated (Keller, 2018). Most of the biosynthetic gene clusters are silent or expressed at low level under standard laboratory conditions. Several approaches have been applied to activate the silent biogenetic gene clusters, such as OSMAC, co-culture, gene manipulation and chemical epigenetic methods (Rutledge and Challis, 2015; Keller, 2018). Recently, chemical epigenetic manipulation has been widely applied to marine-derived fungi as a handy and effective method to activate their silent gene clusters to obtain cryptic secondary metabolites (He et al., 2015; Li et al., 2017). This approach has been successful to induce or change the metabolic pathways to yield new secondary metabolites or enhance the production of the given compounds.

The fungi of *Aspergillus* genus derived from marine environment has been extensively investigated for decades due to the respected biological and pharmacological activities of their secondary metabolites (Lee et al., 2013; Wang and Ding, 2018). Chemical epigenetic manipulation has also been successfully employed to marine-derived *Aspergillus* genus to mine new cryptic secondary metabolites. For example, four new meroterpenoids were obtained from a chemical-epigenetic culture of *Aspergillus terreus* OUCMDZ-2739 with a histone deacetylase inhibitor, 10 μM trichostatin A (TSA) (Sun et al., 2018). A series of new bisabolene-type sesquiterpenoids were produced by a sea sediment-derived fungus *Aspergillus sydowii* cultured with a DNA methyltransferase inhibitor, 5-azacytidine (5-Aza) (Chung et al., 2013). Three new eremophilane-type sesquiterpenes were isolated from a marine-derived fungus *Aspergillus* sp. SCSIOW2 treated simultaneously with histone deacetylase inhibitor, suberohydroxamic acid (SBHA) and DNA methyltransferase inhibitor, 5-Aza (Wang L.Y. et al., 2016). These examples strongly proved that epigenetic manipulation is a feasible approach to induce the production of cryptic secondary metabolites from marine-derived fungi, especially *Aspergillus* genus.

In our previous studies, the fungus *Aspergillus versicolor* XS-20090066 isolated from the gorgonian *Dichotella gemmacea* collected from the Xisha Islands coral reef in the South China Sea has been proved to produce a series of bioactive anthraquinones, diketopiperazine alkaloids, phenyl ethers and nucleoside derivatives (Chen et al., 2013, 2014a,b). Furthermore, six bisabolane-type sesquiterpenoids were obtained by adding DNA methyltransferase inhibitor 5-Aza to the rice solid medium during the cultivation procedure (Wang C.Y. et al., 2016). In the present study, in order to further mine the metabolic potential of *A. versicolor* XS-20090066, this strain was co-incubated with different epigenetic agents in Czapek-Dox liquid medium. By using a combination of histone deacetylase inhibitor, suberoylanilide hydroxamic acid (SAHA) and DNA methyltransferase inhibitor, 5-Aza, the HPLC profile and ^{1}H NMR spectra of the EtOAc extract of fungal culture were significantly changed comparing to the control without any epigenetic agent. A large scale fermentation with SAHA and 5-Aza led to the isolation of six nucleoside derivatives (**1**–**6**) and eleven bisabolane sesquiterpenes (**7**–**17**). Herein, we report the epigenetic manipulation of the fungal strain, and the isolation, structure elucidation and bioactivity evaluation of the isolated metabolites.

MATERIALS AND METHODS

General Experimental Procedure

Optical rotations were recorded on a JASCO P-1020 digital polarimeter. UV spectra were determined on a HITACHI UH 5300 UV spectrophotometer. ECD data were measured by a J-815-150S Circular Dichroism spectrometer. IR spectra were acquired on a Nicolet-Nexus-470 spectrometer with a method of KBr pellets. NMR spectra of compounds **1**-**6** were recorded by a JEOL JEM-ECP NMR spectrometer (600 MHz for ^{1}H NMR and 150 MHz for ^{13}C NMR). While compounds **7**-**17** and EtOAc extracts of cultures were measured by a JEOL JEM-ECP NMR spectrometer (500 MHz for ^{1}H NMR and 125 MHz for ^{13}C NMR), HRESIMS were measured on a Thermo MAT95XP high resolution mass spectrometer, (+)-ESIMS spectra on a Thermo DSQ EImass spectrometer, and (−)-ESIMS spectra on a Bruker amaZon SL ESImass spectrometer. The HPLC analysis and purification was performed on a Hitachi L-2000 HPLC system coupled with a Hitachi L-2455 photodiode array detector and using an analytical column (Kromasil 250 mm × 4.6 mm, 5 μm) and a semi-prepared C_{18} column (Kromasil 250 mm × 10 mm, 5 μm), respectively. For HPLC analysis, the mobile phase was consisted of 0.1% formic acid in acetonitrile (A) and 0.1% formic acid in water (B) with a flowrate of 0.8 mL/min with 10 μL injection volume (2 mg/mL), and recorded at 254 nm. The elution gradient was as follows: 0 min, 5% A; 10 min, 10% A; 60 min, 100% A; 70 min, 100% A. Silica gel (Qing Dao Hai Yang Chemical Group Co.; 300-400 mesh) and Sephadex LH-20 (Amersham Biosciences) were used for column chromatography (CC). Precoated silica gel plates (Yan Tai Zi Fu Chemical Group Co.; G60, F-254) were used for thin-layer chromatography. Artificial sea salt was purchased from Zhongyan Qingdao Salt Industry Co., Ltd.

Fungal Material

The fungus *A. versicolor* XS-20090066 was isolated from the fresh tissue of the inner part of the gorgonian *D. gemmacea*, which was collected from the Xisha Islands coral reef in the South China Sea in December 2009. This fungal strain was identified as *A. versicolor* according to its morphological traits and ITS sequence with the GenBank (NCBI) accession number MN880095, which had 99.82% sequence identity with 100% query cover to that of the *A. versicolor* strain ATCC 9577 (NCBI GenBank accession number AY373880). This strain was previously described as *Aspergillus* sp. XS-20090066 with NCBI GenBank accession number HM535361 (Chen et al., 2013; Wang C.Y. et al., 2016), *Aspergillus* sp. (Chen et al., 2014b), and *A. versicolor* (Chen et al., 2014a). The phylogenetic tree (**Supplementary Figure S1**) was constructed using the neighbor-joining method. The distance calculations, tree construction, and bootstrap analysis were performed with the software MEGA 7.

This fungal strain was deposited at the Key Laboratory of Marine Drugs, the Ministry of Education of China, School of Medicine and Pharmacy, Ocean University of China, Qingdao, China.

Molecular Networking

LC-MS/MS were analyzed on a UHPLC system (1290, Agilent Technologies) with a UPLC HSS T3 column (1.8 μm 2.1 × 100 mm, Waters) coupled to a quadrupole time-of-flight mass spectrometer 6545 (Q-TOF, Agilent Technologies) equipped with an ESI dual source in positive-ion mode. The ESI conditions were set as follows: the capillary temperature at 350°C, source voltage at 4 kV, and a sheath gas flow rate of 0.5 mL/min. The mass spectrometer was operated with an auto MS/MS mode. Mass spectra were recorded from *m/z* 50 to *m/z* 1500 in a speed of 6 spectra/sec, followed by MS/MS spectra of the twelve most intense ions from *m/z* 50 to *m/z* 1500 in a speed of 12 spectra/sec. The data were converted to mzXML format, a text-based format for mass data by using MSConvert, and uploaded to the Global Natural Products Social Molecular Networking Web site (GNPS). The parameters for generating molecular network were set with precursor mass tolerance *m/z* 0.02 Da, MS/MS fragment ion tolerance *m/z* 0.02 Da, minimum cosine score 0.7, minimum matched fragment ions 4, minimum cluster size 2, and network Top 10. The spectral library matching in GNPS was performed with the filtering parameter of identical minimum cosine score and matched fragment ion number. The generated molecular network was visualized and rearranged using Cytoscape 3.6.1.

Fermentation, Extraction and Isolation

The fungus *A. versicolor* XS-20090066 was cultivated in the Czapek-Dox medium (sucrose 30 g/L, sodium nitrate 3 g/L, K_2HPO_4 1 g/L, $MgSO_4 \cdot 7H_2O$ 0.5 g/L, KCl 0.5 g/L, $FeSO_4 \cdot 7H_2O$ 0.01 g/L, artificial sea salt, 30 g/L) with sixty 1 L Erlenmeyer flasks (300 mL each) by adding 100 μM SAHA or/and 100 μM 5-Aza, at room temperature for 30 days. The fermentation broth and mycelia were extracted repeatedly with equal amount of ethyl acetate (EtOAc) for three times, and concentrated *in vacuo* to give a crude extract of 53 g. The extract was subjected to silica gel CC using a step gradient elution with petroleum ether/EtOAc (10:1 to 1:4, v/v) to provide five fractions (Fr.1-Fr.5). Fr.2 was further subjected to silica gel CC with Hexane/EtOAc (10:1 to 1:2) to afford five sub-fractions (Fr.2.1-Fr.2.5). Fr.2.1 was isolated by Sephadex LH-20 CC eluted with CH_2Cl_2/MeOH (1:1) to provide compounds **13** (5.1 mg), **14** (4.4 mg) and **15** (4.2 mg). Fr.2.2 was purified by semi-preparative HPLC with MeOH/H_2O (50:50) to yield **8** (2.4 mg) and **9** (3.2 mg). Fr.2.3 was subjected to semi-preparative HPLC with MeOH/H_2O (50: 50) to yield **10** (1.7 mg). Fr.2.4 was separated by Sephadex LH-20 CC eluted with CH_2Cl_2/MeOH (1:1) and further purified by semi-preparative HPLC with MeOH/H_2O (45: 55) to obtain **7** (4.2 mg), **11** (2.4 mg) and **12** (3.2 mg). Fr.3 was subjected to Sephadex LH-20 CC eluted with CH_2Cl_2/MeOH (1:1) to provide three sub-fractions (Fr.3.1–Fr.3.3). Fr.3.1 was isolated by semi-preparative HPLC with MeOH/H_2O (50: 50) to obtain **16** (14.2 mg) and **17** (5.4 mg). Fr.3.2 was separated by semi-preparative HPLC with MeOH/H_2O (30:70) to yield **5** (17 mg) and **6** (22 mg). Fr.5 was isolated on ODS CC with MeOH/H_2O (30%→70%) to afford five fractions (Fr.5.1–Fr.5.5). Fr.5.2 was separated by Sephadex LH-20 with CH_2Cl_2/MeOH (1:1) and further purified by semi-preparative HPLC with MeOH/H_2O (30:70) to produce **1** (9.3 mg) and **2** (7.1 mg). Fr.5.3 was purified by semi-preparative HPLC with MeOH/H_2O (35:65) to give **3** (23.7 mg) and **4** (22.2 mg) (**Supplementary Figure S2**).

Kipukasin K (**1**): yellow oil; $[\alpha]\ ^{20}_D$ −29.4° (*c* 1.0, MeOH); UV (MeOH) λ_{max} (log ε) 214 (3.06), 260 (2.96) nm; IR (KBr) ν_{max} 3419, 3028, 2930, 1710, 1606 1226 cm^{-1}; ^1H and ^{13}C NMR data, see **Table 1**; HRESIMS *m/z* 543.1265 $[M-H]^-$ (calcd for $C_{25}H_{23}N_2O_{12}$, 543.1256).

Kipukasin L (**2**): yellow oil; $[\alpha]\ ^{20}_D$ −26.5° (*c* 1.0, MeOH); UV (MeOH) λ_{max} (log ε) 216 (3.24), 257 (3.16) nm; IR (KBr) ν_{max} 3420, 3028, 2927, 1712, 1610, 1234 cm^{-1}; ^1H and ^{13}C NMR data, see **Table 1**; HRESIMS *m/z* 543.1265 $[M-H]^-$ (calcd for $C_{25}H_{23}N_2O_{12}$, 543.1256).

Aspergillusene E (**7**): white powder; UV (MeOH) λ_{max} (log ε) 219 (1.96), 250 (1.36), 266 (1.52), 294 (1.04) nm; IR (KBr) ν_{max} 3315, 1623, 1453, 1258 cm^{-1}; ^1H and ^{13}C NMR data, see **Table 2**; HRESIMS *m/z* 215.1428 $[M-H_2O+H]^+$ (calcd for $C_{15}H_{19}O$, 215.1430).

TABLE 1 | ^1H NMR and ^{13}C NMR data for 1 and 2[a].

	1		2	
Position	**δ_C, type**	**δ_H, mult (*J* in Hz)**	**δ_C, type**	**δ_H, mult (*J* in Hz)**
2	151.2, C		150.9, C	
4	163.5, C		163.5, C	
5	102.8, CH	5.60, d (8.1)	102.8, CH	5.57, d (8.1)
6	141.1, CH	7.67, d (8.1)	141.7, CH	7.71, d (8.1)
1′	88.9, CH	5.82, d (6.2)	87.4, CH	5.98, d (5.5)
2′	71.3, CH	4.52, d (5.7)	74.8, CH	5.39, m
3′	72.9, CH	5.32, dd (5.7, 4.0)	68.8, CH	4.36, t (5.9)
4′	79.8, CH	4.37, dt (5.5, 4.0)	82.3, CH	4.07, m
5′	64.0, CH_2	4.44, dd (12.0, 5.5)	63.9, CH_2	4.49, dd (12.0, 3.6)
		4.53, td (12.0, 4.0)		4.33, td (12.0, 5.9)
1″	113.9, C		113.6, C	
2″	160.4, C		160.4, C	
3″	97.5, CH	6.31, d (2.1)	97.5, CH	6.25, d (1.8)
4″	159.0, C		159.1, C	
5″	109.6, CH	6.26, d (2.1)	109.6, CH	6.20, d (1.8)
6″	138.7, C		138.7, C	
7″	167.1, C		166.8, C	
8″	20.1, CH_3	2.21, s	20.1, CH_3	2.14, s
9″	56.2, CH_3	3.70, s	56.2, CH_3	3.62, s
1‴	120.4, C		120.4, C	
2‴	116.9, CH	7.40, d (2.1)	116.9, CH	7.33, d (2.1)
3‴	145.9, C		145.8, C	
4‴	151.6, C		151.5, C	
5‴	116.0, CH	6.83, d (8.3)	115.9, CH	6.78, d (8.3)
6‴	122.5, CH	7.35, dd (8.3, 2.1)	122.5, CH	7.31, dd (8.3, 2.1)
7‴	166.0, C		166.0, C	

[a] *600 MHz for ^1H NMR and 150 MHz for ^{13}C NMR in DMSO-d_6.*

TABLE 2 | ^{1}H NMR and ^{13}C NMR data for 7[a].

Position	δ_C, type	δ_H, mult (*J* in Hz)
2	154.5, C	
3	109.5, C	
3a	129.1, C	
4	118.7, CH	7.40, d (7.8)
5	121.4, CH	7.15, dd (7.8, 1.5)
6	138.8, C	
7	108.9, CH	7.34, d (1.5)
7a	153.8, C	
8	24.0, CH_2	2.73, t (7.1)
9	37.2, CH_2	1.53, m
10	27.5, CH	1.53, m
11	22.7, CH_3	0.91, d (5.4)
12	22.7, CH_3	0.91, d (5.4)
13	8.1, CH_3	2.13, s
14	63.5, CH_2	4.56, s

[a]*500 MHz for ^{1}H NMR and 125 MHz for ^{13}C NMR in DMSO-d_6.*

Biological Assay

Antibacterial activities were evaluated against six pathogenic bacterial strains, *Staphylococcus epidermidis* ATCC 12228, *Staphylococcus aureus* ATCC 25923, *Pseudomonas aeruginosa* ATCC 27853, *Bacillus cereus* ATCC 14579, *Escherichia coli* ATCC 25922, and *Sarcina lutea* ATCC 9341, using a broth micro dilution method according to the standards and guidelines recommended by Clinical and Laboratory Standards Institute (CLSI, 2012). Vancomycin was used as a positive control.

Antifungal activities were tested against *Candida albicans* ATCC 24433, *Candida tropicalis* ATCC 20962 and *Candida parapsilosis* ATCC 22019 using a broth micro dilution method according to the standards and guidelines recommended by CLSI (CLSI, 2012). Amphotericin B was used as a positive control.

The cytotoxic activities were evaluated by the SRB method (Skehan et al., 1990) using five human tumor cell lines A549, HCT116, MCF-7, Hela, and Hep G2. Adriamycin was used as a positive control.

The antifouling assay was performed using bryozoan larvae of *Bugula neritina* according to the method described by Xu et al. (2010). All of the isolated compounds were screened at a concentration of 25 μg/mL to test their preliminary inhibitory effects on larval settlement. Then the active compounds were further examined to measure their EC_{50} and LC_{50} values with a 2-fold dilution method. 5-Octylfuran–2(5H)-one (butenolide) and seanine 211 was used as a positive control.

RESULTS

Chemical Epigenetic Manipulation of *A. versicolor* XS-20090066

The chemical epigenetic manipulation on *A. versicolor* XS-20090066 was conducted in Czapek-Dox liquid medium by using histone deacetylase inhibitors (SAHA, SBHA, nicotinamide, and sodium butyrate) or/and DNA methyltransferase inhibitors (5-Aza and 2′-deoxy-5-Aza) in different concentrations (1–1000 μM), while cultivation without epigenetic modifiers was used as the control. By comparing of HPLC and ^{1}H NMR analysis, cultivation with 100 μM SAHA and 100 μM 5-Aza, respectively, displayed remarkable chemical diversity of the secondary metabolites (**Figures 1**, **2**). Furthermore, the concomitant of two inhibitors with the optimal combination of 100 μM SAHA and 100 μM 5-Aza led to an additive effect on the epigenetic regulation of the fungal metabolites as shown in the HPLC profile at R_t 18–30 min (**Figure 1**). In the ^{1}H NMR profiles of the cultures, multiple resonations of hydrogen signals from 6.0 to 8.0 ppm belonging to the characteristic signals of unsaturated aromatic hydrogens were observed from the EtOAc extracts of the epigenetic manipulated cultures compared with the control (**Figure 2**). Intriguingly, the culture with a combination of SAHA and 5-Aza achieved the strongest cumulative signals compared to the cultures treated with SAHA or 5-Aza separately. The molecular networking profiles revealed that diverse structures existed in the culture, including nucleoside derivatives, anthraquinones, diketopiperazine alkaloids, phenyl ethers, bisabolane sesquiterpenes, and other unidentified secondary metabolites (**Figure 3**). Compared to the control, new nodes induced by epigenetic manipulation were observed, especially treated with SAHA and 5-Aza simultaneously (**Figure 3**). Consequently, a large scale fermentation with Czapek-Dox liquid medium was carried out with adding both 100 μM SAHA and 100 μM 5-Aza. From the EtOAc extract, 17 compounds were isolated (**Figure 4**), including two new nucleoside derivatives, kipukasins K (**1**) and L (**2**), and one new bisabolane sesquiterpene, aspergillusene E (**7**), along with four known nucleoside derivatives, kipukasin I (**3**) (Chen et al., 2014a), kipukasin H (**4**) (Jiao et al., 2007), kipukasins D (**5**) (Jiao et al., 2007), and kipukasins E (**6**) (Chen et al., 2014a), and ten known bisabolane sesquiterpenes, (*E*)-5-(hydroxymethyl)-2-(6′-methylhept-2′-en-2′-yl)phenol (**8**) (Sumarah et al., 2011), (*Z*)-5-(hydroxymethyl)-2-(6′-methylhept-2′-en-2′-yl)phenol (**9**) (Sumarah et al., 2011), 7-deoxy-7,14-didehydrosydonol (**10**) (Chung et al., 2013), (7*R*)-(−)-sydonol (**11**) (Li et al., 2012), (7*R*)-(−)-methoxyethanol (**12**) (McMullin et al., 2015), (7*S*)-(+)-sydonol (**13**) (Nukina et al., 1981), (7*S*)-(+)-methoxyethanol (**14**) (Chung et al., 2013), aspergiterpenoid A (**15**) (Li et al., 2012), sydonic acid (**16**) (Hamasaki et al., 1978), and hydroxysydonic acid (**17**) (Hamasaki et al., 1978).

Structure Elucidation

Kipukasin K (**1**) was isolated as a yellow oil, and the molecular formula was determined as $C_{25}H_{24}N_2O_{12}$ based on its (−)-HRESIMS at *m/z* 543.1265 $[M - H]^-$ (calcd 543.1256), indicating 15 degrees of unsaturation. The planar structure was elucidated by the analysis of 1D/2D NMR (**Supplementary Figures S3–S11**). One 1,2-disubstituted olefin group (δ_H 5.60 (d, J = 8.1 Hz), δ_C 102.8 and δ_H 7.67 (d, J = 8.1 Hz), δ_C 141.1), and two amide carbonyls (δ_C 151.2 and δ_C 163.5) were observed in the ^{1}H and ^{13}C NMR spectra. One pentose moiety (δ_H 4.37 to 5.82, δ_C 64.0 to 88.9) was elucidated on the basis of the J-values (**Table 1**) and ^{1}H–^{1}H COSY of H-1′ to H-5′ (**Figure 5**). These NMR spectroscopic characteristics were similar to those

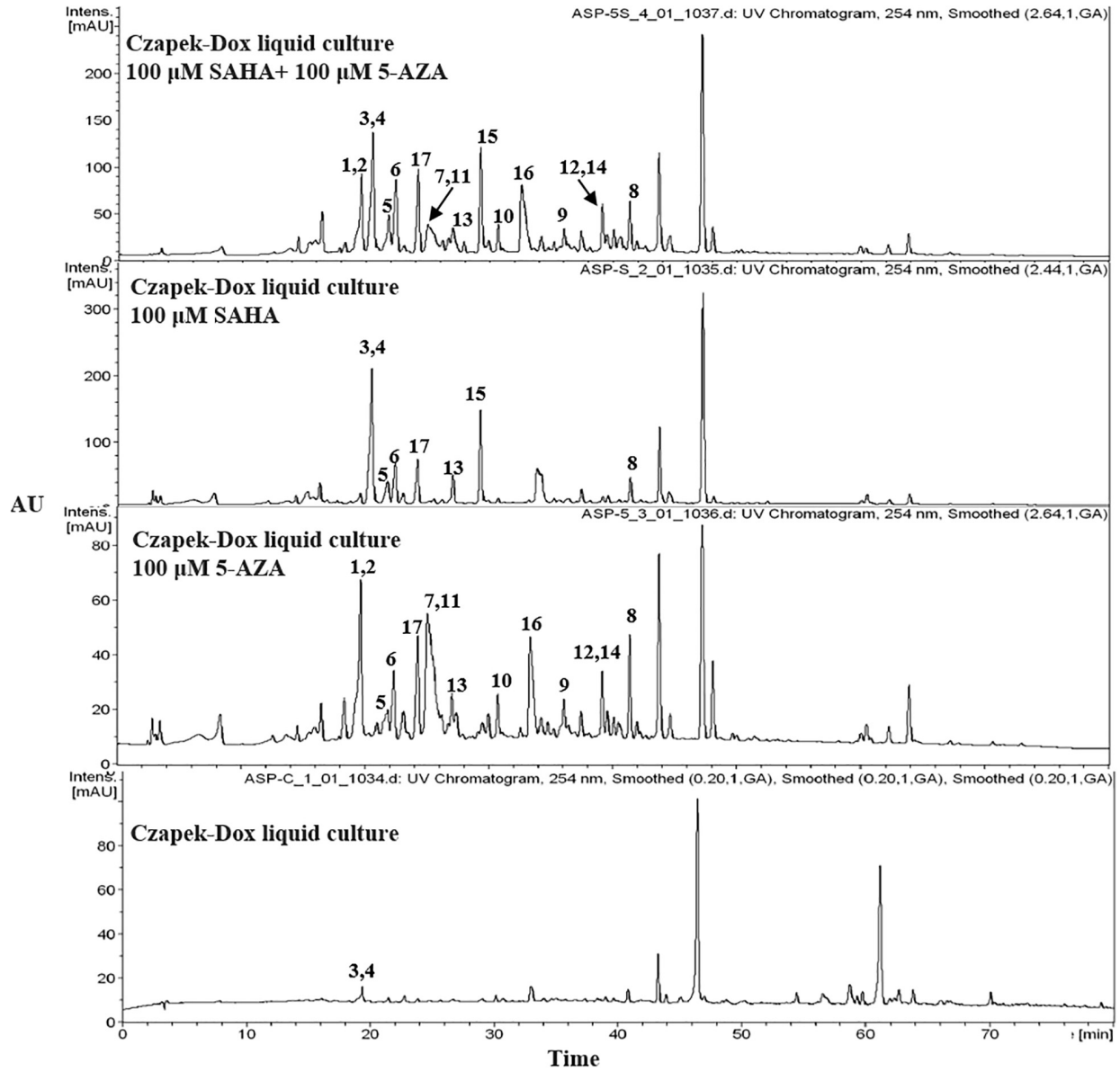

FIGURE 1 | HPLC profiles of EtOAc extracts of *A. versicolor* XS-20090066 with epigenetic agents.

of the typical uridine analog. The HMBC correlations from H-1′ to C-2/C-6 indicated that the pentose moiety was connected to N-1 (**Figure 5**). Careful analysis of the ^{1}H and ^{13}C NMR revealed the presence of 1,2,4,6-tetra-substituted [δ_H 6.26 (d, J = 2.1 Hz) and δ_H 6.31 (d, J = 2.1 Hz)] and 1,3,4-trisubstituted benzene [δ_H 6.83 (d, J = 8.3 Hz), δ_H 7.35 (dd, J = 8.3, 2.1 Hz), and δ_H 7.40 (d, J = 2.1 Hz)] moieties, as well as two ester carbonyls (δ_C 166.0 and δ_C 167.1). One methyl and one methoxyl were anchored at C-6″ and C-2″ of the 1,2,4,6-tetra-substituted benzene, respectively, based on the HMBC correlations from H-8″ to C-1″/C-5″/C-6″ and from H-9″ to C-2″. The above spectroscopic features of **1** were very similar to those of the co-isolated known nucleoside derivative kipukasin I (**3**). The 1,2,4,6-tetra-substituted aroyl unit was connected to C-3′ of the sugar moiety based on the HMBC correlation from H-3′ to C-7‴. The obvious difference was an additional 1,3,4-trisubstituted aroyl unit (protocatechuic ester moiety) in **1**. The HMBC correlation from H-5′ to C-7‴ suggested this moiety was located at C-5′.

Kipukasin L (**2**) was also isolated as a yellow oil. The molecular formula was established as $C_{25}H_{24}N_2O_{12}$ with 15 degrees of unsaturation based on the (−)-HRESIMS at m/z 543.1265 [M - H]$^-$ (calcd 543.1256). The ^{1}H and ^{13}C NMR spectra of **2** were very similar to those of **1** (**Supplementary Figures S12–S20**). The main difference was the chemical shifts of H-2′ (δ_H 5.39 in **2** vs. δ_H 4.52 in **1**) and H-3′ (δ_H 4.36 in **2** vs. δ_H 5.32 in **1**); C-2′ (δ_C

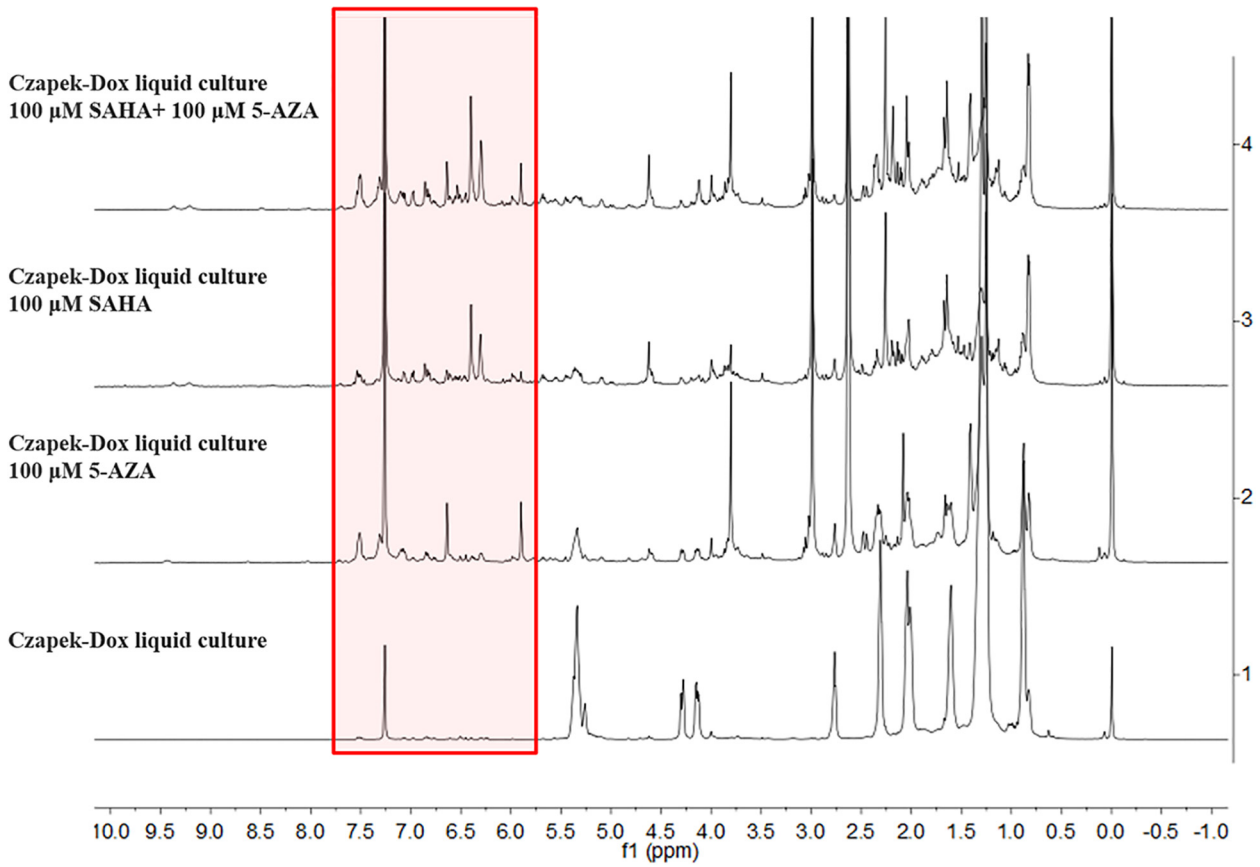

FIGURE 2 | ^{1}H NMR spectra of EtOAc extracts of *A. versicolor* XS-20090066 measured in $CDCl_3$ with 500 MHz, chemical shifts (δ) presented in ppm.

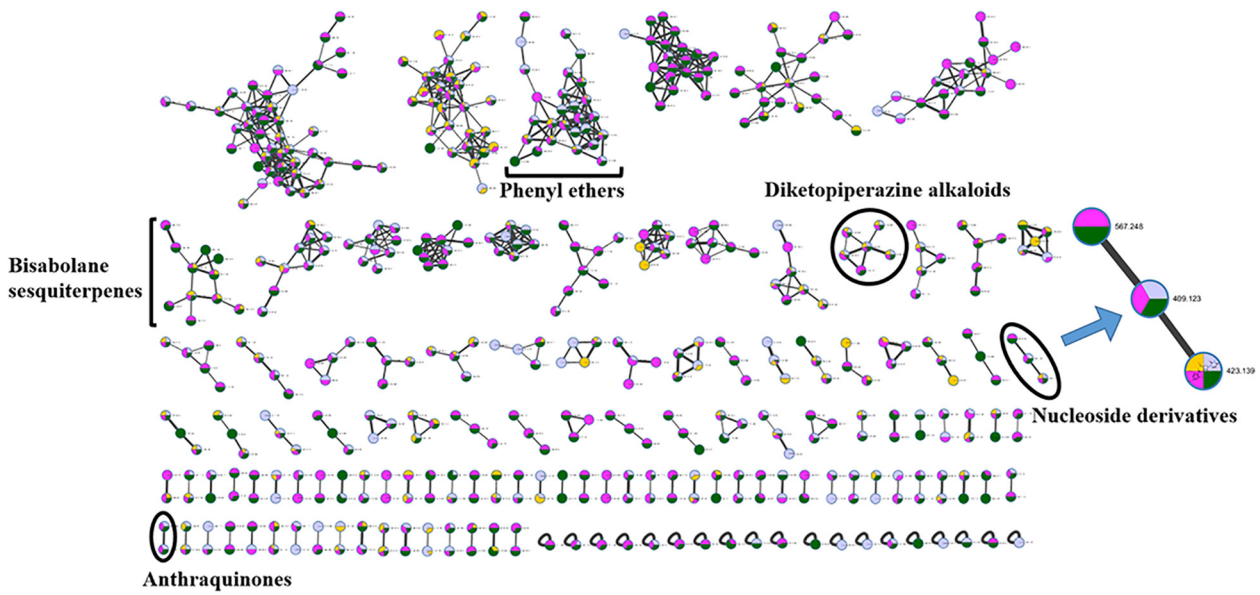

FIGURE 3 | Molecular networking of *A. versicolor* XS-20090066 treated with SAHA (yellow), 5-Aza (pink) and both of them (green), as well as the control (gray). The clusters marked are annotated as the GNPS (Global Natural Products Social Molecular Networking Web site) library matched compounds and their derivatives, and the cluster of interest is enlarged. The thickness of edges between the nodes indicates the degree of similarity between their respective MS^2 spectra.

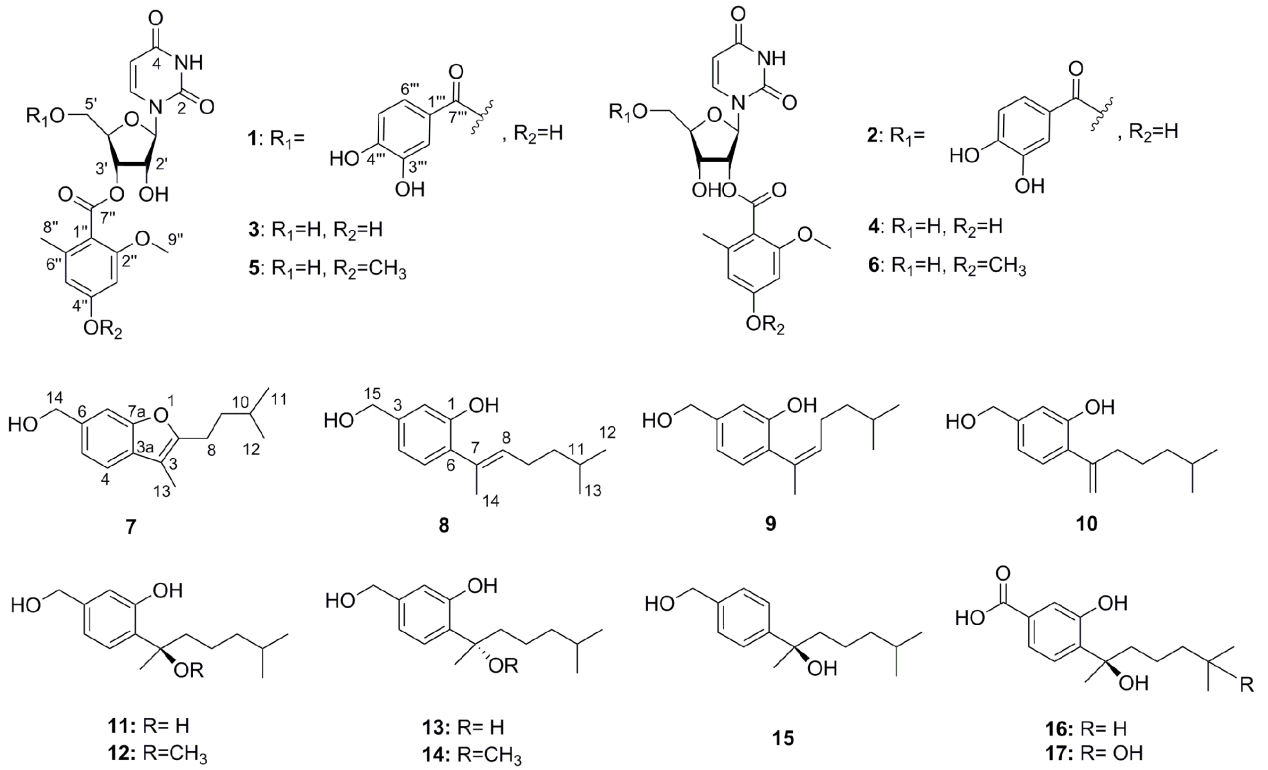

FIGURE 4 | The structures of compounds **1**–**17.**

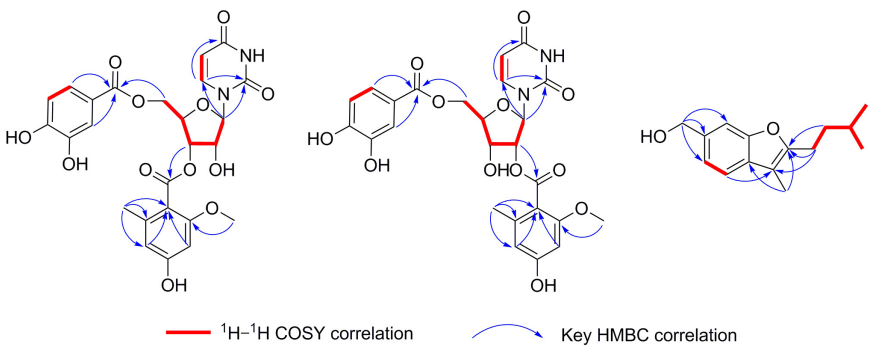

FIGURE 5 | The key ^{1}H–^{1}H COSY and HMBC correlations of compounds **1, 2,** and **7**.

74.8 in **2** vs. δ_C 71.3 in **1**) and C-3′ (δ_C 68.8 in **2** vs. δ_C 72.9 in **1**). It was suggested that the difference was the location of the tetra-substituted aroyl group. The HMBC correlation from H-2′ to C-7″ in **2** supported that it was located at C-2′ rather than C-3′ of ribose unit in **2** (**Figure 5**). Therefore, **2** is the regioisomer of **1**.

The ROESY correlations between H-6 and H-1′/H-2′, and H-1′ and H-4′ in compounds **1** and **2** were observed, suggesting that H-6, H-1′, H-2′ and H-4′ should be at the same side (**Supplementary Figure S21**). However, no correlation between 1,3,4-trisubstituted aroyl protons and 1,2,4,6-tetra-substituted aroyl protons or between aroyl protons and uracil olefin protons was observed from their ROESY spectra (**Supplementary Figures S8, S17**). Comparison of the chemical shifts of H-1′ (δ_H 5.82 in **1** and δ_H 5.98 in **2**) and their coupling constants (6.2 Hz in **1** and 5.5 Hz in **2**) with the reported ribose units confirmed that the sugar moieties in **1** and **2** were β-ribose (Ohigashi et al., 1989; Ostrowski et al., 2003). The absolute configurations of **1** and **2** were speculated based on the biogenetic considerations. The uridine unit could be established as uracil-1-β-D-ribofuranoside, identical to those of the co-isolated known nucleoside derivatives **3**–**6** (Jiao et al., 2007).

Aspergillusene E (**7**) was obtained as a white powder. The molecular formula was determined as $C_{15}H_{20}O_2$ with six degrees of unsaturation on the basis of its (+)-HRESIMS at *m/z* 215.1428

$[M - H_2O + H]^+$ (calcd 215.1430). The UV spectrum showed absorption bands of a benzofuran chromophore at 219, 250, 266, and 293 nm (Trofast, 1978). The ^{1}H NMR spectrum revealed the presence of one 1,2,4-trisubstituted benzene, one hydroxyl, three methylenes (one oxygenated), one methine, and three methyl groups (**Table 2** and **Supplementary Figure S22**). The ^{13}C NMR spectrum displayed the presence of 15 carbons, containing eight olefinic carbons (two oxygenated), one methine carbon, three methylene carbons (one oxygenated) and three methyl carbons (**Supplementary Figures S23, S24**). The isopentyl side chain, established by the ^{1}H–^{1}H COSY of H-8/H-9/H-10/H-11/H-12, was connected to C-2 based on the HMBC correlations from H-8 to C-2/C-3 and from H-9 to C-2 (**Figure 5** and **Supplementary Figures S25, S26**). As the presence of one benzene group and one olefinic group in the molecule occupied five degrees of unsaturation, another ring should exist in **7**, indicating a benzofuran moiety formed between C-2 and C-7a through one oxygen atom. The HMBC correlations from H-13 to C-2/C-3a revealed that the methyl was located at C-3. These spectroscopic characteristics were similar to the reported aspergillusene B, a bisabolane sesquiterpene from *A. sydowii* PSU-F154 (Trisuwan et al., 2011), except the oxygenated methylene group in **7** instead of a carboxyl group (**Supplementary Figures S27, S28**). The HMBC correlations from H-14 to C-5, C-6, and C-7 suggested that the oxygenated methylene was anchored at C-6 (**Figure 5**).

In our previous studies on this strain, four known nucleoside derivatives (**3**-**6**) were isolated from its rice culture (Chen et al., 2014a). By adding 5-Aza, six known bisabolane sesquiterpenes were harvested (Wang C.Y. et al., 2016). In present study, two new nucleoside derivatives (**1** and **2**), together with four known analogs were discovered by adding SAHA and 5-Aza simultaneously, which was confirmed by HPLC detection (**Figure 1**) and molecular networking analysis (**Figure 3**). Compounds **1** and **2** were newly emerged metabolites in the fungal culture relative to control (**Figure 1** and **Supplementary Figure S30**). Quantification analysis revealed that compounds **3** and **4** from the culture with a combination of SAHA and 5-Aza were upregulated approximately 365 fold and 81 fold, respectively, compared to those of control (**Supplementary Figures S29, S30** and **Supplementary Table S1**). In the enlarged cluster of molecular networking, the newly emerged node, belonging to nucleoside derivatives could only be observed in the extracts of culture with the presence of 5-Aza (**Figure 3**). In addition, eleven bisabolane sesquiterpenes including one new compound were mined, which further confirmed the effect of chemical epigenetic manipulation on this strain to produce bisabolane sesquiterpenes.

Bioassays of Compounds

The aroyl uridine derivatives have been reported to possess potential antibacterial activities. For example, kipukasins A and B, obtained from *A. versicolor* NRRL 35600 showed antibacterial activities against Gram-positive bacteria (Jiao et al., 2007). Chen et al. (2014a) reported the uridine derivatives kipukasins H/I exhibited antibacterial activity against *S. epidermidis*. For bisabolane sesquiterpenes, multiple activities have been reported, such as antimicrobial (Li et al., 2012; Guo et al., 2018), antiviral (Wang et al., 2014), and antifouling (Li et al., 2012) activities. In this study, all of the isolated compounds were evaluated for their antibacterial, antifungal, cytotoxic, and antifouling activities. Compounds **1** and **7** showed antibacterial activities against *S. epidermidis* and *S. aureus* with the MIC values of 8–16 μg/mL, respectively. When the hydroxyl at C-4″ in compounds **1**, **3,** and **4** was replaced by methoxyl in **2**, **5,** and **6**, the antibacterial activities were significantly decreased, respectively. While the hydroxyl at C-5′ in **3** and **4** was substituted by protocatechuic ester in **1** and **2**, no remarkable change was observed for the antibacterial activity. In addition, compound **7** exhibited antifungal activities against *Candida albicans* and *C. tropicalis* with the MIC values of 64 and 32 μg/mL, respectively. Unfortunately, none of the tested compounds showed cytotoxicity against human tumor cell lines A549, HCT116, MCF-7, Hela, and Hep G2. Interestingly, compound **7** exhibited anti-larval attachment activity against bryozoan *B. neritina* with the EC_{50} and LC_{50} values of 6.25 and 25 μg/mL, respectively. At the concentrations of 25 μg/mL, compounds **1**–**3**, **6**, and **14** could inhibit the larval settlement, while **8** could kill the larval.

CONCLUSION

In summary, the gorgonian-derived fungus *A. versicolor* XS-20090066 was effectively induced by chemical epigenetic manipulation with a combination of 100 μM SAHA and 100 μM 5-Aza to produce two new nucleoside derivatives and one new bisabolane sesquiterpene as well as more known derivatives. These induced metabolites exhibited antibacterial, antifungal and antifouling activities. Therefore, it could be concluded that chemical epigenetic manipulation should be a feasible and effective strategy to trigger the production of bioactive secondary metabolites from marine derived-fungi.

DATA AVAILABILITY STATEMENT

The datasets generated for this study can be found in the GenBank (NCBI) accession number MN880095.

AUTHOR CONTRIBUTIONS

C-YW and YL conceived and proposed the idea. J-SW contributed to the fermentation, extraction, isolation, and manuscript preparation. G-SY, X-HS, and YX contributed to the bioactivities test. J-SW, SR, X-MF, and X-LZ contributed to the data analysis, writing, revising, and proofreading of the manuscript. All authors read and approved the final version of the manuscript.

FUNDING

This work was supported by the National Natural Science Foundation of China (Nos. 81673350, 41830535, and U1706210),

the National Key Research and Development Program of China (No. 2018YFC0310900), the Open Research Fund Program of Qingdao National Laboratory for Marine Science and Technology (No. QNLM2016ORP0302), and the Taishan Scholars Program, China.

SUPPLEMENTARY MATERIAL

The Supplementary Material for this article can be found online at: https://www.frontiersin.org/articles/10.3389/fmicb.2020.00085/full#supplementary-material

REFERENCES

Blunt, J. W., Carrol, A. R., Copp, B. R., Davis, R. A., Keyzers, R. A., and Prinsep, M. R. (2018). Marine natural products. *Nat. Prod. Rep.* 35, 13–18.

Chen, M., Shao, C. L., Fu, X. M., Xu, R. F., Zheng, J. J., Zhao, D. L., et al. (2013). Bioactive indole alkaloids and phenyl ether derivatives from a marine-derived *Aspergillus* sp. *fungus*. *J. Nat. Prod.* 76, 547–553. doi: 10.1021/np300707x

Chen, M., Fu, X. M., Kong, C. J., and Wang, C. Y. (2014a). Nucleoside derivatives from the marine-derived fungus *Aspergillus versicolor*. *Nat. Prod. Res.* 28, 895–900. doi: 10.1080/14786419.2014.891114

Chen, M., Shao, C. L., Kong, C. J., She, Z. G., and Wang, C. Y. (2014b). A new anthraquinone derivative from a gorgonian-derived fungus *Aspergillus* sp. *Chem. Nat. Compd.* 50, 617–620. doi: 10.1007/s10600-014-1037-2

Chung, Y. M., Wei, C. K., Chuang, D. W., Mohaned, E. S., Hsieh, C. T., Asai, T., et al. (2013). An epigenetic modifier enhances the production of anti-diabetic and anti-inflammatory sesquiterpenoids from *Aspergillus sydowii*. *Bioorg. Med. Chem.* 21, 3866–3872. doi: 10.1016/j.bmc.2013.04.004

Clinical and Laboratory Standards Institute [CLSI] (2012). *Performance Standards for Antimicrobial Susceptibility Testing; Twenty- Second Informational Supplement. M100-S22*. Wayne, PA: Clinical and Laboratory Standards Institute.

Guo, Z. Y., Tan, M. H., Liu, C. X., Lv, M. M., Deng, Z. S., Cao, F., et al. (2018). Aspergoterpenins A–D: four new antimicrobial bisabolane sesquiterpenoid derivatives from an endophytic fungus *Aspergillus versicolor*. *Molecules* 23:1291. doi: 10.3390/molecules23061291

Hamasaki, T., Nagayama, K., and Hatsuda, Y. (1978). Two new metabolites, sydonic acid and hydroxysydonic acid, from *Aspergillus sydowi*. *Agric. Biol. Chem.* 42, 37–40. doi: 10.1271/bbb1961.42.37

He, X., Zhang, Z., Chen, Y., Che, Q., Zhu, T., Gu, Q., et al. (2015). Varitatin A, a highly modified fatty acid amide from Penicillium variabile cultured with a DNA methyltransferase inhibitor. *J. Nat. Prod.* 78, 2841–2845. doi: 10.1021/acs.jnatprod.5b00742

Jiao, P., Mudur, S. V., Gloer, J. B., and Wicklow, D. T. (2007). Kipukasins, nucleoside derivatives from *Aspergillus versicolor*. *J. Nat. Prod.* 70, 1308–1311. doi: 10.1021/np070241l

Jin, L. M., Quan, C. S., Hou, X. Y., and Fan, S. D. (2016). Potential pharmacological resources: natural bioactive compounds from marine-derived fungi. *Mar. Drugs* 14, 1–21.

Keller, N. P. (2018). Fungal secondary metabolism: regulation, function and drug discovery. *Nat. Rev. Microbiol.* 1, 167–177.

Lee, Y. M., Kim, M. J., Li, H., Zhang, P., Bao, B., Lee, K. J., et al. (2013). Marine-derived *Aspergillus* species as a source of bioactive secondary metabolites. *Mar. Biotechnol.* 15, 499–519. doi: 10.1007/s10126-013-9506-3

Li, D., Xu, Y., Shao, C. L., Zheng, C. J., Chen, Y. Y., Fu, X. M., et al. (2012). Antibacterial bisabolane-type sesquiterpenoids from the sponge-derived fungus *Aspergillus* sp. *Mar. Drugs* 10, 234–241. doi: 10.3390/md10010234

Li, G., Kusari, S., Golz, C., Laatsch, H., Strohmann, C., and Spiterller, M. (2017). Epigenetic modulation of endophytic *Eupenicillium* sp. LG41 by a histone deacetylase inhibitor for production of decalin-containing compounds. *J. Nat. Prod.* 80, 983–988. doi: 10.1021/acs.jnatprod.6b00997

McMullin, D. R., Green, B. D., and Miller, J. D. (2015). Antifungal sesquiterpenoids and macrolides from an endophytic *Lophodermium* species of *Pinus strobus*. *Phytochem. Lett.* 14, 148–152. doi: 10.1016/j.phytol.2015.10.006

Nukina, M., Sato, Y., Ikeda, M., and Sassa, T. (1981). Sydonol, a new fungal morphogenic substance produced by an unidentified *Aspergillus* sp. *Agric. Biol. Chem.* 45, 789–790. doi: 10.1271/bbb1961.45.789

Ohigashi, H., Kaji, M., Sakaki, M., and Koshimizu, K. (1989). 3-Hydroxyuridine, an allelopathic factor of an African tree, *Baillonella toxisperma*. *Phytochemistry* 28, 1365–1368. doi: 10.1016/s0031-9422(00)97747-1

Ostrowski, T., Maurizot, J. C., Adeline, M. T., Fourrey, J. L., and Clivio, P. (2003). Sugar conformational effects on the photochemistry of thymidylyl(3'-5')thymidine. *J. Org. Chem.* 68, 6502–6510. doi: 10.1021/jo030086p

Penesyan, A., Kjelleberg, S., and Egan, S. (2010). Development of novel drugs from marine surface associated microorganisms. *Mar. Drugs* 8, 438–459. doi: 10.3390/md8030438

Rutledge, P. J., and Challis, G. L. (2015). Discovery of microbial natural products by activation of silent biosynthetic gene clusters. *Nat. Rev. Microbiol.* 13, 509–520. doi: 10.1038/nrmicro3496

Skehan, P., Storeng, R., Scudiero, D., Monks, A., McMahon, J., Vistica, D., et al. (1990). New colorimetric cytotoxicity assay for anticancer-drug screening. *J. Natl. Cancer Inst.* 82, 1107–1112. doi: 10.1093/jnci/82.13.1107

Sumarah, M. W., Kesting, J. R., Sørensen, D., and Miller, J. D. (2011). Antifungal metabolites from fungal endophytes of *Pinus strobus*. *Phytochemistry* 72, 1833–1837. doi: 10.1016/j.phytochem.2011.05.003

Sun, K. L., Zhu, G. L., Hao, J. J., Wang, Y., and Zhu, W. M. (2018). Chemical-epigenetic method to enhance the chemodiversity of the marine algicolous fungus, *Aspergillus terreus* OUCMDZ-2739. *Tetrahedron* 74, 83–87. doi: 10.3390/md17010006

Trisuwan, K., Rukachaisirikul, V., Kaewpet, M., Phongpaichit, S., Hutadilok-Towatana, N., Preedanon, S., et al. (2011). Sesquiterpene and xanthone derivatives from the sea fan-derived fungus *Aspergillus sydowii* PSU-F154. *J. Nat. Prod.* 74, 1663–1667. doi: 10.1021/np200374j

Trofast, J. (1978). Chloromycorrhizinol A, a furochroman from an isolate of the roots of *Monotropa hypopitys*. *Phytochemistry* 17, 1359–1361. doi: 10.1016/s0031-9422(00)94589-8

Wang, C. Y., Liu, Y. F., Cao, F., and Wang, C. Y. (2016). Bisabolane-type sesquiterpenoids from a gorgonian-derived *Aspergillus* sp. fungus induced by DNA methyltransferase inhibitor. *Chem. Nat. Compd.* 52, 1129–1132. doi: 10.1007/s10600-016-1885-z

Wang, J. F., Lin, X. P., Qin, C., Liao, S. R., Wan, J. T., Zhang, T. Y., et al. (2014). Antimicrobial and antiviral sesquiterpenoids from sponge-associated fungus, *Aspergillus sydowii* ZSDS1-F6. *J. Antibiot.* 67, 581–583. doi: 10.1038/ja.2014.39

Wang, K. W., and Ding, P. (2018). New bioactive metabolites from the marine-derived fungi *Aspergillus*. *Mini-Rev. Med. Chem.* 18, 1072–1094. doi: 10.2174/1389557518666180305160856

Wang, L. Y., Li, M. J., Tang, J. Q., and Li, X. F. (2016). Eremophilane sesquiterpenes from a deep marine-derived fungus, *Aspergillus* sp. SCSIOW2, cultivated in the presence of epigenetic modifying agents. *Molecules* 21:473. doi: 10.3390/molecules21040473

Xu, Y., He, H., Schulz, S., Liu, X., Fusetani, N., Xiong, H., et al. (2010). Potent antifouling compounds produced by marine streptomyces. *Bioresour. Technol.* 101, 1331–1336. doi: 10.1016/j.biortech.2009.09.046

Conflict of Interest: The authors declare that the research was conducted in the absence of any commercial or financial relationships that could be construed as a potential conflict of interest.

frontiers in Microbiology

ORIGINAL RESEARCH
published: 24 April 2020
doi: 10.3389/fmicb.2020.00743

Anthracycline Shunt Metabolites From Philippine Marine Sediment-Derived *Streptomyces* Destroy Cell Membrane Integrity of Multidrug-Resistant *Staphylococcus aureus*

*Melissa June V. Paderog[1,2], Angelica Faith L. Suarez[3], Edna M. Sabido[3], Zhen Jie Low[4], Jonel P. Saludes[3,5,6] and Doralyn S. Dalisay[2,6,7]**

[1] Department of Pharmacy, College of Health and Allied Medical Professions, University of San Agustin, Iloilo City, Philippines, [2] Center for Chemical Biology and Biotechnology (C2B2), University of San Agustin, Iloilo City, Philippines, [3] Center for Natural Drug Discovery and Development (CND3), University of San Agustin, Iloilo City, Philippines, [4] Waters Pacific Pte Ltd, Singapore, Singapore, [5] Department of Chemistry, College of Liberal Arts, Sciences, and Education, University of San Agustin, Iloilo City, Philippines, [6] Balik Scientist Program, Philippine Council for Health Research and Development, Department of Science and Technology, Taguig, Philippines, [7] Department of Biology, College of Liberal Arts, Sciences, and Education, University of San Agustin, Iloilo City, Philippines

OPEN ACCESS

Edited by:
Jinwei Zhang,
University of Exeter, United Kingdom

Reviewed by:
Giorgia Letizia Marcone,
University of Insubria, Italy
Olga Vladimir Efremenkova,
Gause Institute of New Antibiotics Russian Academy of Medical Sciences, Russia

***Correspondence:**
Doralyn S. Dalisay
ddalisay@usa.edu.ph

Specialty section:
This article was submitted to Microbiotechnology, a section of the journal Frontiers in Microbiology

Received: *15 January 2020*
Accepted: *30 March 2020*
Published: *24 April 2020*

Citation:
Paderog MJV, Suarez AFL, Sabido EM, Low ZJ, Saludes JP and Dalisay DS (2020) Anthracycline Shunt Metabolites From Philippine Marine Sediment-Derived Streptomyces Destroy Cell Membrane Integrity of Multidrug-Resistant Staphylococcus aureus. Front. Microbiol. 11:743. doi: 10.3389/fmicb.2020.00743

The rise of antibiotic resistance (ABR) and the drying up of the pipeline for the development of new antibiotics demands an urgent search for new antibiotic leads. While the majority of clinically available antibiotics were discovered from terrestrial *Streptomyces*, related species from marine sediments as a source of antibiotics remain underexplored. Here, we utilized culture-dependent isolation of thirty-five marine sediment-derived actinobacterial isolates followed by a screening of their antibacterial activity against multidrug-resistant *S. aureus* ATCC BAA-44. Our results revealed that the crude extract of *Streptomyces griseorubens* strain DSD069 isolated from marine sediments collected in Romblon, Philippines displays the highest antibacterial activity, with 96.4% growth inhibition. The *S. aureus* ATCC BAA-44 cells treated with crude extract of *Streptomyces griseorubens* strain DSD069 showed cell membrane damage as demonstrated by (a) leakage and loss of vital cell constituents, including DNA and proteins, (b) irregular shrinkage of cells, and (c) increase membrane permeability. The antibiotic compounds were identified as Bisanhydroaklavinone and 1-Hydroxybisanhydroaklavinone with MIC value of 6.25 μg/mL and 50.00 μg/mL, respectively. Bisanhydroaklavinone and 1-Hydroxybisanhydroaklavinone are shunt metabolites in the biosynthesis of anticancer anthracycline derivatives namely doxorubicin, daunorubicin, and cinerubins. It is rare, however, that shunt metabolites are accumulated during fermentation of marine sediment-derived *Streptomyces* strain without genetic modification. Thus, our study provides evidence that natural bacterial strain can produce Bisanhydroaklavinone and 1-Hydroxybisanhydroaklavinone as antibiotic leads to combat ABR.

Keywords: antibacterial, Philippine marine sediments, anthracyclines shunt metabolites, multidrug-resistant *Staphylococcus aureus* (MDRSA), *Streptomyces*, cell membrane integrity, Bisanhydroaklavinone, 1-hydroxybisanhydroaklavinone

INTRODUCTION

With the increasing emergence of antibacterial resistance (ABR) among common pathogens, the quest to discover novel and new antibiotics is, therefore, urgent. ABR is the natural ability of bacteria to resist the effects of antibiotics, thereby rendering antibiotics less effective (Khan and Khan, 2016; Vestergaard et al., 2019). Various resistance mechanisms such as enzyme mutations, multidrug efflux-mediated resistance, production of antibiotic degrading enzymes, and modification of drug binding sites were developed by bacteria as their defense against antibiotics (Sriramulu, 2013; Vestergaard et al., 2019). These resistance mechanisms are developed rapidly, and the spread of multidrug-resistant strains is uncontrollable. Unfortunately, the ABR crisis is coupled with shortage of new antibiotics to replace those rendered ineffective by ABR strains. Therefore, urgent efforts to discover new antibiotics from underexplored sources are needed.

Members of the genus *Streptomyces* of the phylum Actinobacteria are soil saprophytes that are known producers of antibiotics (Shaik et al., 2017; Yang and Song, 2017; Kemung et al., 2018; Yang et al., 2020). These microorganisms contain high GC content in their DNA sequences and are reported to have antibiotic-producing biosynthetic gene clusters (BGC) (Hopwood, 2007; Dhakal et al., 2017; Romano et al., 2018) that produces about 75% of the clinically available antibacterial drugs in the market (Kemung et al., 2018). However, in the last 20 years, the re-discovery of previously characterized bioactive compounds and strain redundancy decreased the interest in these soil-dwelling bacteria as a source of novel bioactive compounds (Yang and Song, 2017; Almeida et al., 2019). Thus, *Streptomyces* living in other niches, such as the marine environment, gained value because of their chemodiversity (Chelvan et al., 2016; Dhakal et al., 2017; Yang and Song, 2017; Kemung et al., 2018; Romano et al., 2018; Al-Dhabi et al., 2019; Almeida et al., 2019).

In response to the ABR crisis and the challenges of finding new antibiotics, we collected marine sediments near Romblon, Philippines as a source of marine-derived Actinobacteria. We focused on isolating the Actinobacteria from marine sediments and screen their crude extracts against *Staphylococcus aureus* ATCC BAA-44, profiling antibacterial activity and determining their membrane disruption ability, and identifying the compound(s) responsible for antibiotic activity. We performed a culture-dependent isolation approach using the dry stamp and heat shock methods (Mincer et al., 2002; Jensen et al., 2005; Dalisay et al., 2013) utilizing minimal marine media to isolate marine sediment-derived Actinobacteria. We isolated 35 actinobacterial isolates with six isolates (17% hit rate) active against *S. aureus* ATCC BAA-44. *Streptomyces griseorubens* strain DSD069 showed the highest antibiotic activity. Its crude extract caused cell membrane damage and intracellular leakage, leading to compromised cell membrane integrity and death of *S. aureus* ATCC BAA-44. The antibiotic compounds were accumulated in the growth medium during fermentation, which were later identified as shunt metabolites in the biosynthesis of anticancer anthracycline derivatives such as doxorubicin, daunorubicin, and cinerubins. This work is the first report on the accumulation of anticancer anthracycline derivatives shunt metabolites by Philippine marine sediment-derived *Streptomyces* strain without genetic modification. Thus, our study provides evidence that natural bacterial strain can produce Bisanhydroaklavinone and 1-Hydroxybisanhydroaklavinone as antibiotic leads to combat ABR.

MATERIALS AND METHODS

Sample Collection and Culture-Dependent Isolation of Marine Actinobacteria

Sediment samples were collected from six sites near Alad and Lugbong islands of Romblon, Philippines. The sediments were collected 200–500 m away from the islands by SCUBA at a depth of 20–30 m. The sediment samples were placed in sterile cylindrical tubes and kept at 4°C until further processing. Dry stamp method (DSM) and heat shock method (HSM) (Mincer et al., 2002; Jensen et al., 2005; Dalisay et al., 2013) using selective minimal marine media (ISP4 and noble agar) (Dalisay et al., 2013) were used to grow the marine sediment-derived Actinobacteria. The inoculated plates were incubated at room temperature for 30 to 60 days.

Morphological Characterization of Marine Sediment-Derived Actinobacteria

Marine sediment-derived Actinobacteria were examined morphologically in terms of their mycelium production, specifically substratum mycelium (pigmentation) and aerial mycelium (spores). Spore size was measured using scanning electron microscopy (SEM). The spores were washed twice with PBS (0.1 M, pH 7.4), centrifuged, and fixed with glutaraldehyde solution (2.5% in PBS) for 1.5 h at 4°C. The fixed spores were dehydrated using gradient concentration of ethanol (30, 50, 85, 95, 100%) and twice with *t*-butyl alcohol before freezing at −20°C for 5 min. The spores were viewed under a scanning electron microscope, SEM (JEOL JSM 5510LV) (Fatima et al., 2019).

Extraction of Secondary Metabolites

Actinobacterial isolates were grown in marine medium 1 (MM1) agar (Dalisay et al., 2013) plates. Successive re-plating was done to obtain a pure isolate. Large-scale fermentation of the isolates was performed according to the method of Dalisay et al. (2013). Secondary metabolites were extracted using EtOAc and the extract partitioned with water. The EtOAc fractions were concentrated *in vacuo* and subsequently stored at −80°C until further use.

Multidrug-Resistant *Staphylococcus aureus* ATCC BAA-44

Staphylococcus aureus ATCC BAA-44 is a particular strain containing the SCC*mec* Type I gene. It is resistant to 18 clinically significant antibiotics namely ampicillin, amoxicillin/clavulanic acid, ciprofloxacin, cephalothin, doxycycline, gentamicin, erythromycin, imipenem, methicillin, penicillin, tetracycline, oxacillin, azithromycin, clindamycin, ceftriaxone, rifampin,

amikacin, and tobramycin [Staphylococcus aureus subsp. aureus Rosenbach (ATCC® BAA-44™), 2019].

Antibacterial Activity Assay

Agar Well Diffusion Assay

The preliminary screening of extracts against *S. aureus* ATCC BAA-44 was performed using agar well diffusion assay. The *S. aureus* ATCC BAA-44 (1×10^6 CFU/mL) in agar medium was prepared by pour plate technique. Thereafter, three wells were punched on the agar. The first well was filled with tetracycline (0.050 mg/well) as a positive control. The second well was filled with DMSO as a negative control, and the third well was filled with Actinobacteria crude extracts (2.0 mg/well). The samples were allowed to diffuse unto the agar for 1 h before incubation at 37°C for 18–24 h. Zone of inhibition was measured in mm after the incubation period. Extracts that exhibited zone of inhibition of more than 4.0 mm were considered to have antibacterial activity (Bredholt et al., 2008; Valli et al., 2012).

Microbroth Susceptibility Assay

The *S. aureus* ATCC BAA-44 (1×10^6 CFU/mL) in Mueller-Hinton broth (MHB) was prepared in a 96-well plate and exposed to different treatments [tetracycline 0.25 mg/mL in DMSO (positive control), DMSO (negative control), and crude extracts (2.5 mg/mL of DMSO)] for 18–24 h at 37°C. The bacterial density at OD 620 nm was measured after incubation using a microplate reader (Multiskan™ FC Thermo Fisher) and percent growth inhibitions were calculated.

Extracts with more than 50% growth inhibition were confirmed for antibacterial activity. The extract with the highest % growth inhibition against the multidrug-resistant *S. aureus* ATCC BAA-44 was further subjected to antibacterial activity profiling, mechanism of action assay, and chemical profiling for antibiotic compound identification (Langfield et al., 2004; Delgado-Andrade et al., 2006; Dalisay et al., 2013; Hayashi et al., 2014).

16S rRNA Gene Amplification and Sequencing

Actinobacterial DNA was extracted using the DNeasy Blood and Tissue Kit (Qiagen) according to the manufacturer's instruction. For 16S rRNA Gene amplification, universal primers 27F (5′-AGAGTTTGATCCTGGCTCAG-3′) and 1492R (5′-TACGGCTACCTTGTTACGACTT′) were used in PCR reaction. The reaction mixture (50 μL) contained 5 μL Taq Polymerase (5 units/μL), 5 μL $MgCl_2$ (50 mM), 5 μL Taq Buffer, 5 μL dNTPs (10 mM), 3 μL 27F primer (10 mM), 3 μL 1492R primer (10 mM), 19 μL nuclease-free H_2O (ultrapure water) and 100 ng/μL DNA template. The PCR conditions were as follows: initial denaturation at 98°C for 3 min; 35 cycles at 98°C for 10 s, 60°C for 10 s and 72°C for 60 s; and a 10-min final extension at 72°C (T100™ BioRad Thermal Cycler). The amplified products were cleaned using the QIAquick PCR cleanup kit (Qiagen) according to the manufacturer's protocol. The universal primers 27F, 518F, 800R, and 1492R were used to obtain the 1300–1500 bp gene sequences. The species-level affiliation of the sequenced 16S rRNA gene was determined using BLAST (Altschul et al., 1990). The phylogenetic tree was constructed using multiple alignments with maximum likelihood method in Mega 7.0 software (Kumar et al., 2016). Bootstrap analysis based on 1,000 replicates evaluated the resulting tree topologies.

Antibacterial Activity Profiling

Time-Kill Kinetics Assay

Following the same procedure in microbroth susceptibility, the assay was performed using 0.25 mg/mL tetracycline (positive control), DMSO (negative control), and 2.5 mg/mL of most active extract as treatments. In this assay, measurement of bacterial densities was obtained every 6 h (0, 6, 12, 18, and 24 h) within a 24 h period using microplate reader (Multiskan™ FC Thermo Fisher). Percent bacterial growth inhibition of the treatments at different time points was calculated and plotted (Tenover et al., 2004; Peck et al., 2012).

Minimum Inhibitory Concentration (MIC)

Two-fold serially diluted concentrations of extract (dilution range of 625 – 0.61 μg/mL) and tetracycline (dilution range of 62.5 – 0.061 μg/mL) was utilized, with DMSO as the negative control. The test bacterial strain (1×10^6 CFU/mL) was exposed to different treatments in a 96-well plate for 18–24 h at 37°C. The bacterial densities of different concentrations were measured at OD 620 nm using microplate reader (Multiskan™ FC Thermo Fisher). The corresponding % growth inhibition was calculated to identify the minimum concentration that could inhibit 90% of bacterial growth (du Toit and Rautenbach, 2000; Andrews, 2001; Delgado-Andrade et al., 2006).

Although tetracycline was listed as one of the antibiotics with resistance against *S. aureus* ATCC BAA-44, this antibiotic was used as the positive control in all the antibacterial assays covered in this work. We found that *S. aureus* ATCC BAA-44 has an MIC value of 31.25–50 μg/mL for tetracycline according to the protocol described in this work. Tetracycline susceptibility to *S. aureus* ATCC BAA-44 was also observed by other groups where MIC values were reported at 16 μg/mL (Rogers et al., 2010) and 64 μg/mL (Podoll et al., 2013).

Membrane Leakage Assay

Overnight grown broth culture of *S. aureus* ATCC BAA-44 (0.2 OD 620 nm) was prepared. Subsequently, the bacterial inoculum was exposed for 18–24 h to different treatments, namely 5% Tween 80 (positive control), DMSO (negative control), and the most active extract with concentrations of 2.50, 1.25, and 0.625 mg/mL in DMSO. The measurement of proteins and DNA that leaked out of the cell membrane was measured using a UV-Vis spectrophotometer (Shimadzu UV1280 Spectrophotometer) (Thombre et al., 2016; Tiwari et al., 2018). Leaked DNA was measured at 260 nm according to the method of Zhang et al. (2017), and proteins were measured by modifying the procedures of Bradford (1976). Here, proteins were directly measured at 280 nm instead of colorimetric measurement.

Transmission Electron Microscopy (TEM)

Bacterial cells of *S. aureus* ATCC BAA-44 (0.6 OD 620 nm) were exposed to the extract at 2.5 mg/mL concentration and

DMSO (negative control) for 24 h incubation period. Untreated bacterial cells were also prepared as a control. The extract-treated, DMSO-treated, and untreated cells were then processed to adhere to an aluminum film and then washed thrice with phosphate buffer saline (PBS) with a concentration of 0.1 M (pH 7.4). After washing, the cells were stained with 2% phosphotungstic acid and subjected to dehydration with a gradient concentration of ethanol (30, 50, 85, 95, 100%). The dehydrated cells were washed twice with *t*-butyl alcohol before freezing it at −20°C for 5 min. The cells were then placed in the TEM sample holder and coated with gold using a sputter. The cells were viewed using TEM (JEOL JEM 1010) (Schmid and Sakamoto, 2001; Karsha and Lakshmi, 2010; Bai et al., 2015).

Flow Cytometry

Overnight broth culture of *S. aureus* ATCC BAA-44 was utilized. The cells were harvested by centrifugation (4500 rpm for 5 min) and re-suspended in PBS (7.4 pH) to a final bacterial density of 0.05 OD 600 nm. The bacterial suspension in PBS was transferred to a 96-well plate. The bacterial suspensions were treated with vancomycin (7.5 mg/mL), DMSO, and active extract (2.5 mg/mL). Untreated cells (only bacterial suspension, negative control) and 70% ethanol-treated cells as positive control to represent dead cells were transferred onto their corresponding wells in 96-well plate. The plate was incubated for 4 h at 37°C. After incubation, the cells were centrifuged at 4500 rpm for 5 min and re-suspended in dye solution (optimized concentrations of the Live/Dead Cell Double Staining Kit of Sigma-Aldrich). Single stained cells were also prepared for fluorescence compensation in the flow cytometer. The plate was incubated at 37°C for 15 min (Nowakowska et al., 2015). After the incubation period, the cells were centrifuged (4500 rpm for 5 min) and resuspended in 100 μL PBS. Data were then acquired using Amnis™ FlowSight (Merck KGaA) imaging flow cytometer equipped with a 488 nm laser. Six thousand (6000) cell events were acquired per replicate, and 87% cell events were analyzed to eliminate cell debris. Propidium iodide fluorescence was measured at 642–745 nm band (Channel 5), and calcein fluorescence was measured at 505–560 nm band (Channel 2). The analysis was done using IDEA.6.2.188. Release.86x application software considering zero rfu as the lowest fluorescence unit. Propidium iodide fluorescing cells (R1) were gated as dead cells with permeant cell membranes, and calcein fluorescing cells (R2) were gated as live cells (Wu et al., 2016). The experiment was performed in triplicates.

Chemical Profiling

Thin-Layer Chromatography Profiling

Thin-layer chromatography (TLC) profile of the most active extract was carried out using pre-coated TLC plates (Merck TLC Silica Gel 60 W F254s–normal phase) and methanol–dichloromethane (1:13) as solvent system through one-way ascending technique. The developed chromatogram was visualized under UV light at 365 and 254 nm and retention factor (R_f) values of each band were calculated (Jayashree et al., 2014). Direct bioautography of the chromatogram was further performed by covering the surface of the TLC plate with a soft agar (MHA 0.8% agar) seeded with 1×10^6 CFU/mL of *S. aureus* ATCC BAA-44 and incubated overnight. The zone of inhibition of antibacterial components was visualized by detecting mitochondrial reductase enzyme activity of viable cells using a resazurin reduction-based reaction. The metabolically active viable cells convert resazurin (blue colored compound) to its reduced form resorufin (pink colored compound). Thus, the zone of inhibition appears as blue spot over a pink background (Choma and Grzelak, 2010; Choma and Jesionek, 2015; Jesionek et al., 2015).

Chromatographic Purification of Bioactive Compound

Guided by UV activity of bioactive bands in TLC-bioautography, the crude extract of the most active actinobacterial isolate was purified through a silica column (0.5 mm diameter × 54 mm height). Dichloromethane (DCM) followed by methanol-dichloromethane (1:13) was used as the mobile phase. Collected fractions were spotted onto a silica TLC plate and developed using methanol-dichloromethane (1:13). The fractions containing bioactive bands based on UV activity were pooled together and dried using a vacuum concentrator (Eppendorf™ Vacufuge™ Concentrator) at V-HV mode, 30°C for 2 h). Subsequently, the dried bioactive fraction was developed on a silica TLC plate using methanol-dichloromethane (1:13) as solvent. The identified bioactive bands based on R_f values in the TLC profile were isolated by preparative-TLC method using methanol-dichloromethane (1:13) solvent system.

LCMS Analyses of Bioactive Fraction

Mass spectrum for dereplication analysis were acquired using high-resolution mass spectrometer (Waters Xevo® G2-XS QTOF) equipped with high-performance system, StepWave™ ion source technology, XS collision cell technology, QuanTOF™ technology, UPLC/TOFMR for high transmission mode, and UPLC/MS^e for data acquisition. The solvent system was water with 0.1% (v/v) formic acid (solvent A) and acetonitrile with 0.1% (v/v) formic acid (solvent B). The analysis was performed with flow rate of 0.5 mL/min with an oven temperature at 40°C. The interface used for MS^e was electron spray ionization (ESI) with a collision energy of 6.0 eV for low energy and 10.0 eV for high energy. The scan time was set to 0.250 s using polarity positive mode with a mass range scan of m/z 50–900, and using a single UV wavelength of 254 nm. MS data were analyzed using Waters UNIFI Scientific Information System® and Chemspider™ Database.

RESULTS AND DISCUSSION

Members of the phylum Actinobacteria, which is exemplified by the genus *Streptomyces,* are well-known to produce bioactive compounds with various biological and pharmaceutical importance. Most of these compounds were isolated from terrestrial sources (Barka et al., 2016; Van Der Meij et al., 2017). However, there were reports recently, where their marine counterparts were also recognized as a source of bioactive compounds (Shaik et al., 2017; Yang and Song, 2017;

El-Gendy et al., 2018; Kemung et al., 2018; Subramani and Sipkema, 2019). The condition in the marine environment is remarkably different from that of the terrestrial environment. It is a hostile niche (Aneiros and Garateix, 2004; Imada, 2005; Valli et al., 2012), where marine microorganisms are exposed to low nutrition, high salinity, and high-pressure (Soliev et al., 2011; Almeida et al., 2019). As a result, marine microorganisms developed unique metabolic and physiological ability to survive by activating their environment adaptation genes (ENAs) (Almeida et al., 2019). Because of this, they produce different secondary metabolites that their terrestrial counterparts do not have (Imada, 2005; Zheng et al., 2011; Dholakiya et al., 2017).

In the last decade, marine sediments have become reference hotspots for bioprospecting of marine *Streptomyces* with antibiotic activities (Kamjam et al., 2017; Yang et al., 2020). Recent reports described that marine sediment-derived *Streptomyces* species are producers of diverse antibiotic compounds. This includes 2-alkyl-4-hydroxyquinoline antibiotics and antifungals produced by *Streptomyces* sp. strain MBTG13 isolated from sediments of Jeju Island, South Korea (Kim et al., 2019), polycyclic polyether compounds, terrosamycins A and B, produced by *Streptomyces* sp. RKND004 isolated from sediments of Prince Edward Island, Canada (Sproule et al., 2019), and oxazole-triene compound, inthomycin B, produced by *Streptomyces* sp. YB104 isolated from deep sediments in South Atlantic Ocean (Wu et al., 2018). These reports imply that *Streptomyces* thriving in underexplored niches such as marine sediments are resource for potential antibacterial compounds that are of diverse chemical characteristics.

As part of our natural drug discovery program for new antibiotics, we recovered 35 actinobacterial isolates from marine sediment samples collected near Romblon islands, Philippines using a culture-dependent isolation technique in selective minimal marine media (Mincer et al., 2002; Jensen et al., 2005; Dalisay et al., 2013). In this approach, we utilized two media (noble agar and ISP4) with components that mimic the sea water nutrients, pH, and salinity. Further, the media contain cyclohexamide to inhibit fungal contamination and the antibiotic rifamycin to select Actinobacteria (Mincer et al., 2002; Jensen et al., 2005; Hames-Kocabas and Uzel, 2012; Dalisay et al., 2013; Claverias et al., 2015; Jiang et al., 2016; Jose and Jha, 2017; Subramani and Sipkema, 2019).

The morphological characteristics of the actinobacterial isolates were profiled according to their aerial (spores) and substratum (pigmentation) mycelium (**Table 1**). Results showed diverse substratum mycelium production ranging from no pigmentation to yellowish, red-orange to red, and light yellowish-orange to brown. Although recovered from the same collection site, the isolates have varied growth period. Some (4 out of 35 isolates, 11%) grew for as fast as 33 days, while 14% (5 out of 35 isolates) were slow growers that required more than 100 days to develop. In terms of culture-dependent isolation, 29 isolates (82.9%) were recovered using dry stamp method while only six isolates (17.1%) were recovered using heat shock method. Besides, 60% (21 isolates) grew well in the noble agar medium while only 40% (14 isolates) grew well in the ISP4 medium. Our results revealed that the isolates in this study are diverse, as shown by the various diffusible pigments they produced, as well as growth variation in minimal marine media.

Antibacterial Activity Screening of Crude Extracts

The crude extracts of actinobacterial isolates (**Supplementary Figure 1**) were initially screened for antibacterial activity through agar well diffusion assay against *S. aureus* ATCC BAA-44. The results demonstrated that out of 35 crude extracts, seven (20%) showed antibacterial activity against *S. aureus* ATCC BAA-44 that exhibited zones of inhibition ranging from 4.1–15.0 mm (**Table 2**). Isolate DSD069 exhibited the highest zone of inhibition of 15.0 mm (±0.2 SD) at 2.0 mg/well, which is nearly equal to the activity of tetracycline at 14.0 mm (±0.1 SD) at 0.05 mg/well.

The results obtained from well-diffusion assay were further validated by microbroth susceptibility assay. Out of the seven crude extracts found active in well-diffusion assay, six extracts showed more than 50% growth inhibition (**Figure 1**) in microbroth susceptibility assay as confirmatory screening. Isolate DSD069 crude extract was found to show higher growth inhibition of 96.40% at 2.5 mg/mL against *S. aureus* ATCC BAA-44 in comparison to tetracycline that showed 95.48% at 0.25 mg/mL. Isolate DSD069 was selected for subsequent tests not only for its confirmatory high antibacterial activity against *S. aureus* ATCC BAA-44 but also for its broad antibacterial activities against eight target bacteria (**Supplementary Table 1**). Investigation of the antibacterial compounds against these target bacteria is ongoing and will be reported in due course.

16S rRNA Gene Sequence of Isolate DSD069

The identity of isolate DSD069 was determined using its 16S rRNA gene sequence. Using BLAST, the nearly complete 16S rRNA gene sequence (1411 bp) revealed 99.93% gene homology with *Streptomyces griseorubens* strain NBRC 12780, which was corroborated with the results obtained in phylogenetic analysis using Molecular Evolutionary Genetics Analysis (MEGA, V7) (**Supplementary Figure 2**). This result indicates that isolate DSD069 is a marine-derived *Streptomyces griseorubens* strain. The nearly complete 16S rRNA gene sequence was deposited in the GenBank with accession number MN818600. *S. griseorubens* strain DSD069 produced gray spores and no diffusible pigment when grown in marine ISP4 medium. SEM analysis of the spores revealed globular shape with size ranging from 1 to 2 μm (**Figure 2**).

Streptomyces griseorubens is a soil-derived actinobacterium (Pridham et al., 1957) that is involved in carbon and nitrogen recycling (Feng et al., 2014). Further, *S. griseorubens* possesses antibacterial activity against *Pseudomonas aeruginosa, S. aureus, Escherichia coli, S. pneumoniae,* and *Bacillus subtilis* (Al-Askar et al., 2014). A recent report described two lipocyclopeptide antibiotic compounds produced via non-ribosomal polypeptide synthetase (NRPS) biosynthetic gene cluster (BGC) in *Streptomyces griseorubens* strain INA 00887 (Tyurin et al., 2018). These antibiotics, namely, cryst-1 (Aspartocin B and C)

TABLE 1 | Isolation profile of marine sediment-derived actinobacterial strains.

Code	Collection site	Method of isolation	Incubation Period (days)	Medium for isolation and description of colonies		
				Medium	Mycelium	
					Aerial	Substratum
DSD044	Lugbung	DSM	33	Noble agar	Grayish-white	Red-orange
DSD045	Lugbung	DSM	33	Noble agar	Gray	Red-orange
DSD046	Lugbung	DSM	33	Noble agar	Gray	Red-orange
DSD047	Lugbung	DSM	33	Noble agar	Gray	None
DSD048	Lugbung	HSM	68	Noble agar	Gray	None
DSD049	Lugbung	HSM	68	Noble agar	Grayish-white	Red
DSD050	Lugbung	HSM	68	Noble agar	Gray	Light yellow-brown
DSD051	Lugbung	HSM	68	Noble agar	Gray	Light yellow-brown
DSD052	Lugbung	HSM	68	Noble agar	Gray	Light yellow-brown
DSD053	Lugbung	HSM	68	Noble agar	Gray	Red
DSD054	Alad	DSM	42	ISP4	Gray with some white portion	Brown
DSD055	Lugbung	DSM	42	ISP4	Gray	Yellowish-brown
DSD056	Lugbung	DSM	34	ISP4	Grayish with white portion	Yellowish-brown
DSD057	Lugbung	DSM	34	ISP4	Grayish with white portion	Yellowish-brown
DSD058	Lugbung	DSM	43	ISP4	Grayish with white portion	Yellowish
DSD059	Lugbung	DSM	43	ISP4	Grayish with white portion	Yellowish-brown
DSD060	Lugbung	DSM	43	ISP4	Gray	Yellowish
DSD061	Lugbung	DSM	43	ISP4	Gray	Yellowish
DSD062	Lugbung	DSM	43	ISP4	Gray	Yellowish
DSD063	Lugbung	DSM	43	ISP4	Gray	Yellowish
DSD064	Alad	DSM	34	Noble agar	Grayish-white	Yellowish-brown
DSD065	Alad	DSM	34	Noble agar	Gray	Yellowish-brown
DSD066	Alad	DSM	34	Noble agar	White	Yellowish
DSD067	Alad	DSM	34	Noble agar	White	Yellowish-brown
DSD068	Alad	DSM	34	Noble agar	Gray	None
DSD069	Lugbung	DSM	47	ISP4	Gray	None
DSD070	Alad	DSM	59	ISP4	Gray	Red
DSD071	Alad	DSM	103	Noble agar	White	Brownish-yellow
DSD072	Alad	DSM	103	Noble agar	White	Brownish
DSD073	Alad	DSM	103	Noble agar	White	Brownish
DSD074	Alad	DSM	67	ISP4	Gray	Red
DSD075	Alad	DSM	67	ISP4	Gray	Red
DSD076	Alad	DSM	103	Noble agar	White	Brownish
DSD077	Alad	DSM	103	Noble agar	White	Brownish
DSD078	Alad	DSM	67	Noble agar	Grayish white	Red

DSM, dry stamp method; HSM, heat shock method.

and cryst-2 (Aspartocin A), are two major components of crystallomycin complex, an antibiotic discovered 60 years ago when advanced analytical tools were not available to fully characterize the compounds (Tyurin et al., 2018). Although *S. griseorubens* is known to be terrestrial, a *S. griseorubens* strain was previously isolated from marine sediments collected from the seabed in Weihai, China (Ye et al., 2009). Interestingly, the strain required seawater for growth and biosynthesis of anticancer metabolites, indicating that the strain has evolved and developed genes for marine adaptation (i.e., marine adaptation genes, MAG) as a mechanism to adapt in marine environment (Ye et al., 2009). The same adaptive mechanism may possibly have contributed to the survival of *S. griseorubens* strain DSD069 in the marine environment, thus allowing to produce antibiotic metabolites.

Antibacterial Activity Profile of *Streptomyces griseorubens* Strain DSD069

Our results in the time-kill kinetics assay of the *S. griseorubens* strain DSD069 crude extract at 2.5 mg/mL against *S. aureus* ATCC BAA-44 showed a time-dependent antibacterial action, with a similar killing trend with that of tetracycline (0.25 mg/mL, positive control) (**Figure 3**). The crude extract (2.5 mg/mL) exhibited minimal antibacterial activity (58.11%) after 6 h

TABLE 2 | Agar well diffusion assay against multidrug-resistant *S. aureus*

Treatments	Zone of Inhibition (mm)
Tetracycline	14.0 ± 0.1
DSD047	4.1 ± 0.2
DSD061	8.0 ± 2.0
DSD062	5.9 ± 0.1
DSD065	5.8 ± 0.7
DSD067	4.3 ± 0.5
DSD069	15.0 ± 0.2
DSD070	4.8 ± 0.4

Data presented are mean zone of inhibition (mm) ± SD (standard deviation) of the bioactive marine sediment-derived actinobacterial isolates against S. aureus ATCC BAA-44 (1 × 10^6 CFU/mL) through agar well diffusion assay. Cultures of the test bacterial strains in Mueller-Hinton agar plates were exposed to treatments namely, Actinobacterial crude extract (2 mg/well), tetracycline - positive control (0.05 mg/well) and DMSO (negative control) for 18–24 h. The experiment was performed in three trials.

incubation time then gradually increased (89.59%) after 12 h and reached maximum inhibition (96.44%) after 24 h incubation period.

When tested by microbroth dilution assay to determine its minimum inhibitory concentration (MIC), the crude extract showed 2.44 μg/mL MIC value in comparison to tetracycline with MIC value of 31.25 μg/mL. These results suggest that at a lower concentration the crude extract exhibits strong antibacterial activity that is attributable to either a single antibacterial compound present in the crude extract or several compounds working synergistically to elicit a strong antibacterial action (Williamson, 2001; Yarnell, 2015).

Cell Membrane Disruption Assay

Bacterial cell membrane integrity was investigated through a leakage assay by measuring the leaked DNA and proteins. Results showed that the antibacterial activity is associated with membrane damage in a concentration-dependent manner (**Figure 4**). High absorbance values at 260 and 280 nm suggest leakage of DNA and proteins, respectively, which suggest that bacterial cell membrane integrity may have been compromised, allowing the intracellular materials (DNA and proteins) to leaked out of the cell. The percent of DNA and protein leakage of *S. griseorubens* strain DSD069 crude extract was calculated relative to 5% Tween 80, a known compound that affects cell membrane permeability (positive control) (Brown and Winsley, 1969). The result showed that *S. griseorubens* strain DSD069 crude extract exhibited 85.27% DNA leakage and 67.68% protein leakage at 2.5 mg/mL concentration.

This observation was further validated by TEM analysis. It was found that *S. aureus* ATCC BAA-44 cells exposed to *S. griseorubens* strain DSD069 extract at 2.5 mg/mL for 24 h showed cell membrane disruption (**Figure 4B**). The cells appeared with an irregular shape, collapsed, translucent, and formed aggregates of shrunken cells. These findings confer the cell membrane damaging effect of *S. griseorubens* strain DSD069 crude extract. While untreated cells and DMSO treated cells appeared to be spherical with smooth cell surface even on dividing cells; hence, indicating that the cell membranes are still intact.

To further assess the damaging effects of *S. griseorubens* strain DSD069 extract on cell membrane permeability and integrity, flow cytometry experiment using fluorescent dyes, calcein AM,

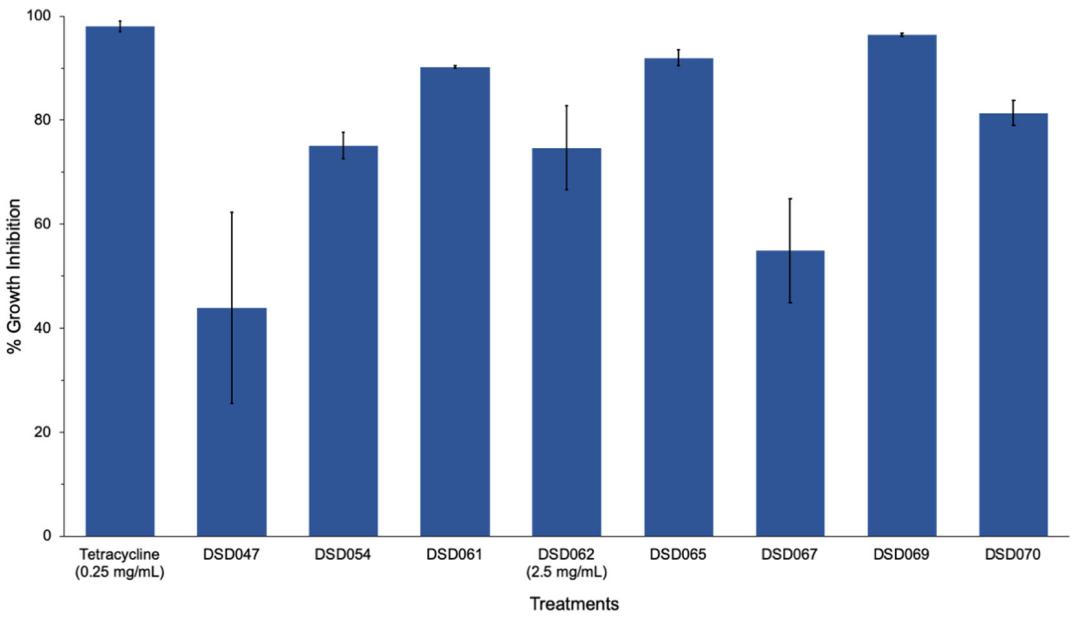

FIGURE 1 | Antibacterial activity of bioactive actinobacterial isolates against multidrug-resistant *Staphylococcus aureus*. Data illustrated are the percent growth inhibition (± SD) of the antibacterial isolates against *S. aureus* ATCC BAA-44 evaluated through microbroth susceptibility assay. Cultures of test bacterial strain (1 × 10^6 CFU/mL) were exposed to different actinobacterial extracts (2.5 mg/mL), positive control tetracycline (0.25 mg/mL), and DMSO (negative control) for 24 h. The percent growth inhibition were determined at 620 nm using the microtiter plate reader. The experiment was done in triplicates and performed in three trials.

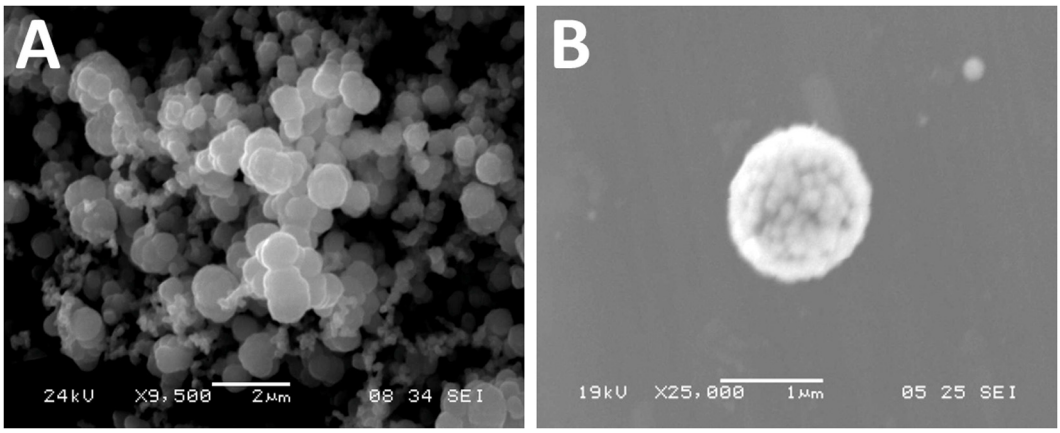

FIGURE 2 | Scanning electron photomicrograph of marine sediment-derived *Streptomyces griseorubens* strain DSD069. **(A)** Photomicrograph of spores at 9,500x magnification, and **(B)** photomicrograph of spore at 25,000x magnification.

and propidium iodide was performed. Calcein emits green fluorescence when intracellular esterases of live cells convert calcein AM to calcein. In contrast, red-fluorescent propidium iodide can only penetrate bacterial cells with compromised cell membrane permeability or integrity. Cell populations in the flow cytometer dot plots were clustered into two regions, namely dead or membrane-damaged cells (R1), which have strong propidium iodide fluorescence, and live cells (R2), which have strong calcein fluorescence (Wu et al., 2016). The untreated (99.07%) and DMSO-treated (99.10%) cells were mostly live cells, as indicated by high populations of calcein-fluorescing cells (**Figure 5**). Ethanol-treated cells, on the other hand, exhibited a high cell population (99.6%) fluorescing with propidium iodide, thus indicating that these cells were dead and have damaged cell membranes. After 4 h of incubation, *S. aureus* ATCC BAA-44 cells treated with *S. griseorubens* strain DSD069 crude extract at 2.5 mg/mL (the same concentration used in protein and DNA leakage assay and time kill assay) exhibited 76.54% of dead cells with damaged cell membrane as indicated by propidium iodide fluorescing cells and only 23.46% of calcein fluorescing cells (live cells). On the contrary, vancomycin at 7.5 mg/mL treatment exhibited only 3.82% of the dead and membrane-permeant cell population, and a large population of live cells fluorescing with calcein (96.18%) was observed. Previous reports on vancomycin time-kill kinetics against methicillin resistant *S. aureus* strains suggest onset antibacterial activity after 4 h incubation period (Singh et al., 2009) and more than 90% inhibition after 8 h incubation period (Foster et al., 1986). Moreover, this suggests the slow inhibiting action of vancomycin explaining why only a small percentage (3.82%) of the dead cell population was observed in our experiment.

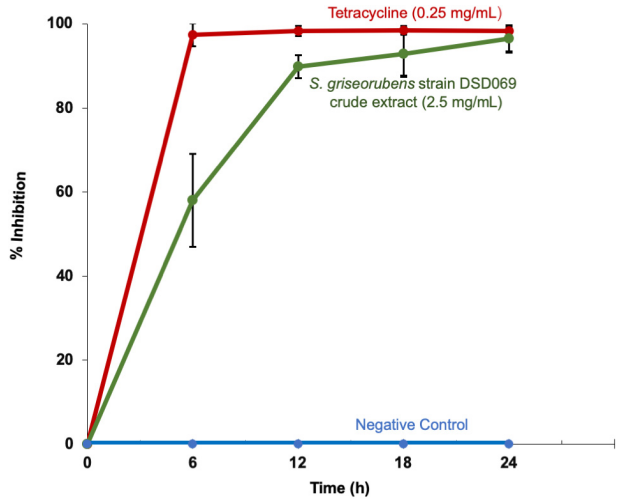

FIGURE 3 | Time-kill kinetics against multidrug-resistant *S. aureus* ATCC BAA-44. Data presented are the % growth inhibition (± SD) of the treatments at different time points. *S. aureus* ATCC BAA-44 (1×10^6 CFU/mL) was exposed to *S. griseorubens* strain DSD069 (2.5 mg/mL), 0.25 mg/mL tetracycline (positive control), and DMSO (negative control) for 24 h. Bacterial cell density was measured and corresponding % growth inhibition was calculated every 6 h interval from time 0 until 24 h incubation. The experiment was done in triplicates and performed in three trials.

Collectively, the results of the assays confirm that the loss of viability of multidrug resistant *S. aureus* ATCC BAA-44 when treated with *S. griseorubens* strain DSD069 crude extract is a consequence of cell membrane damage. The destruction of cell membrane is demonstrated by (a) leakage and loss of vital cell constituents, including DNA and proteins, (b) irregular shrinkage of cells, and (c) enhanced membrane permeability as shown by propidium iodide uptake.

Antibacterial Compounds From *Streptomyces griseorubens* Strain DSD069

To identify the compound/s responsible for the antibiotic activity against the multidrug resistant *S. aureus* ATCC BAA-44, thin layer chromatography (TLC) bioautography was performed. The bioautography assay result suggests that bands with R_f

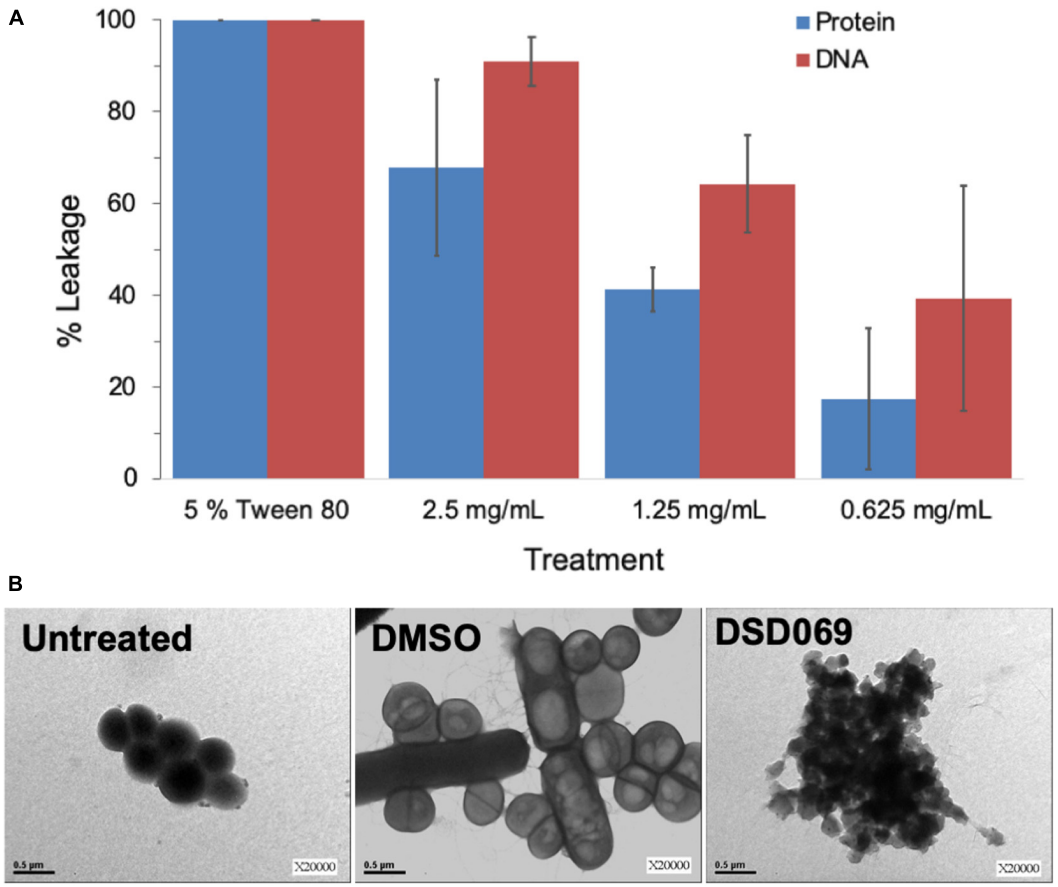

FIGURE 4 | Compromised cell membrane permeability and integrity. Data illustrated are **(A)** percent leakage of the UV_{260} (DNA) and UV_{280} (proteins) absorbing intracellular materials, and **(B)** TEM analysis of *S. aureus* ATCC BAA-44 exposed to different treatments namely, Untreated cells of *S. aureus* ATCC BAA-44 as a control, DMSO as a negative control, and *S. griseorubens* strain DSD069 crude extract (2.5 mg/mL).

values of 0.79 and 0.88 possessed antibacterial activity against *S. aureus* ATCC BAA-44 as indicated by the blue coloration in the bioautogram (**Supplementary Figure 3**). The bioactive band at R_f 0.79 has a characteristic intense orange fluorescence at 365 nm, while the band at R_f 0.88 has a dark orange fluorescence suggesting aromaticity.

Purification of the active components was done by passing 88.6 mg of *S. griseorubens* strain DSD069 crude extract through a silica column using dichloromethane followed by methanol-dichloromethane (1:13) as the mobile phase, which yielded 50 fractions (**Supplementary Figure 4**). The fractions were developed in a silica TLC plate using a methanol-DCM (1:13) solvent system and viewed under UV at 254 and 365 nm. Based on UV activity, fractions 37–42 were pooled together and dried that yielded 12.9 mg. Preparative silica TLC was used to further separate the bioactive bands at R_f 0.79 and R_f 0.88 and was designated as BAF1 and BAF2, respectively.

BAF1 was obtained as a yellow film. The molecular formula was determined as $C_{22}H_{16}O_6$ by high-resolution electrospray ionization mass spectrometry (HRESIMS) (*m/z* 377.10274 $[M + H]^+$, calcd. 377.10251), which indicated 15 degrees of unsaturation (**Figure 6**). MSe and dereplication analysis (Waters UNIFI Scientific Information System® and Chemspider™ database) revealed that BAF1 matched with Bisanhydroaklavinone, 1 (**Supplementary Figure 5**). On the other hand, BAF2 was also obtained as a yellow film. The molecular formula was determined as $C_{22}H_{16}O_7$ by high resolution electrospray ionization mass spectrometry (HRESIMS) (*m/z* 393.09733 $[M + H]^+$, calcd. 393.09743), which indicated 15 degrees of unsaturation (**Figure 6**). BAF2 matched with 1-Hydroxybisanhydroaklavinone, **2** (**Supplementary Figure 6**).

To investigate its antibacterial activity, microbroth susceptibility assay was performed at 100 mg/mL concentration against *S. aureus* ATCC BAA-44. Our results showed that **1** and **2** exhibited antibacterial activity of 92.09% and 99.14%, respectively. In comparison, tetracycline showed 93.40% inhibition at 50 µg/mL (**Supplementary Figure 7**).

The antibacterial activity against *S. aureus* ATCC BAA-44 was further confirmed by microbroth dilution assay to determined its minimum inhibitory concentration (MIC). Compound **1** strongly inhibits the growth of *S. aureus* ATCC BAA-44 as shown by its minimum inhibitory concentration (MIC) value of 6.25 µg/mL. Compound **2** and tetracycline displayed

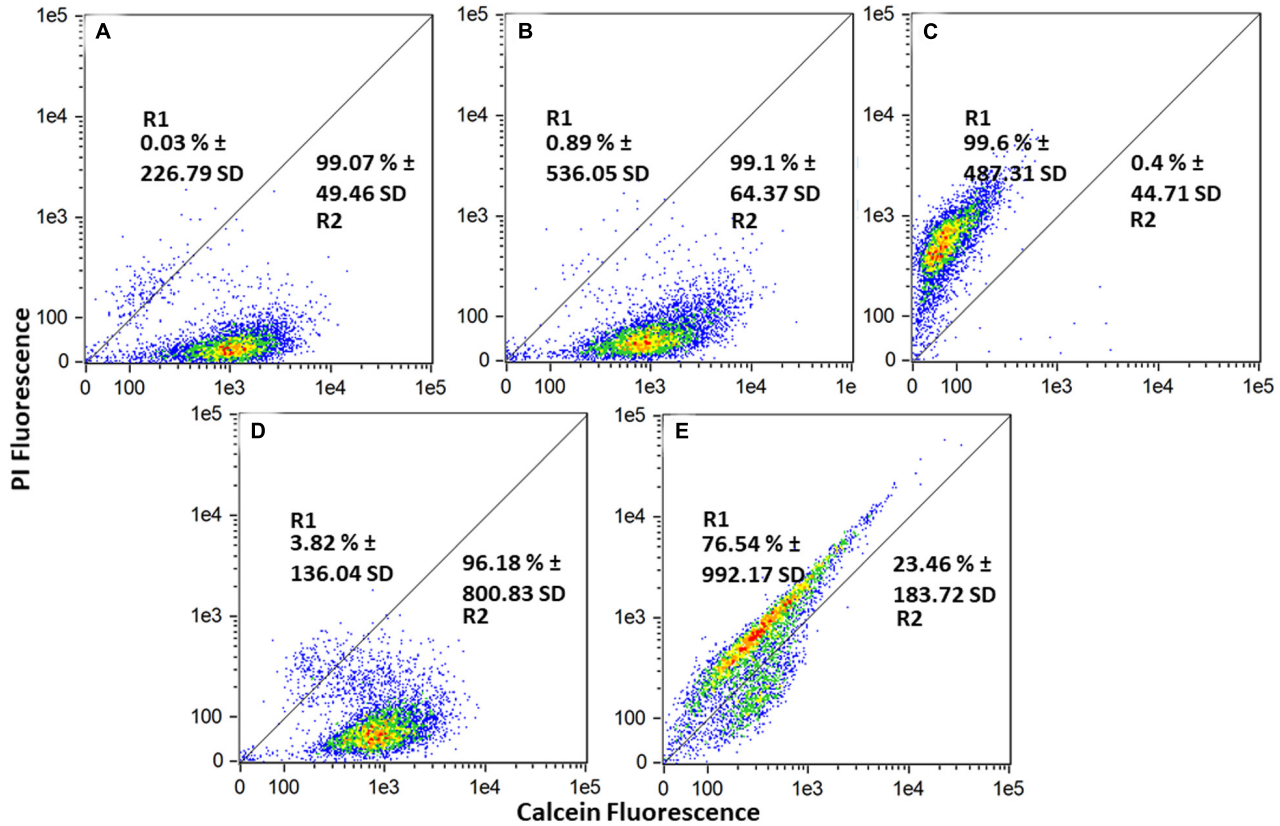

FIGURE 5 | Cell membrane permeability effect of *Streptomyces griseorubens* strain DSD069 crude extract. Data presented are flow cytometer scatter plots profile of various treatments namely: **(A)** Untreated, **(B)** DMSO, **(C)** 70% Ethanol, **(D)** Vancomycin, 7.5 mg/mL, and **(E)** *Streptomyces griseorubens* strain DSD069 crude extract, 2.5 mg/mL. The experiment was done in triplicates.

weak antibacterial activity against *S. aureus* ATCC BAA-44 with MIC value of 50 μg/mL and 50 μg/mL, respectively (**Supplementary Figure 8**).

Anthracycline Shunt Metabolites: Bisanhydroaklavinone (1) and 1-Hydroxybisanhydroaklavinone (2)

Compounds **1** and **2** are shunt metabolites of *Streptomyces* anthracycline glycosides such as the aclacinomycins (e.g., aclarubicin) (Eckardt and Bradler, 1965; Oki et al., 1975; Hori et al., 1977; Niemi et al., 1999), rhodomycins (e.g., daunorubicin and doxorubicin) (Brockmann and Franck, 1955; Arcamone et al., 1969; Grein, 1987), and cinerubins (cinerubin A and cinerubin B) (Corbaz et al., 1957; Eckardt et al., 1989). These anthracycline glycosides, however, are well known anticancer drugs (Egorin et al., 1981; Nitiss et al., 1997). Most of these bioactive anthracyclines are glycosides, containing one or more sugar moieties attached to the aglycone, which was reported to be an important structural requirement for their anticancer activities (Clark et al., 2004).

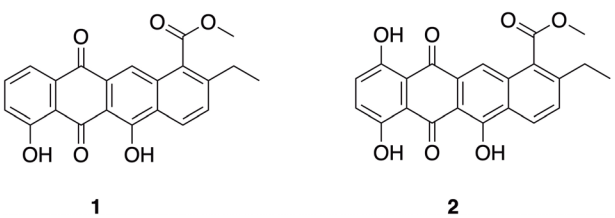

FIGURE 6 | Structures of anthracycline shunt metabolites: Bisanhydroaklavinone **(1)** and 1-Hydroxybisanhydroaklavinone **(2)**.

Compound **1** was previously reported to be a biosynthetic shunt product of block mutant strains of *Streptomyces galilaeus* as part of a study to understand the biosynthesis of aclacinomycins (Oki et al., 1980; Tobe et al., 1982). On the other note, **2** was reported as an isomer of Bisanhydro-δ-rhodomycinone and Bisanhydro-ε-rhodomycinone (Brockmann and Brockmann, 1963). Compound **2** is also known as η-pyrromycinone, a non-glycosidic compound isolated from a soil-derived *S. galilaeus* from Isle of Hidensee, Germany together with anticancer cinerubin A (Schlegel et al., 1987). No prior studies on the anticancer and antibiotic activity of **1** and **2** has been reported.

Chemical synthesis revealed that **1** could be derived from aklavinone and **2** from ε-pyrromycinone through hydrobromide/glacial acetic acid reaction and from 7-desoxyaklavinone and

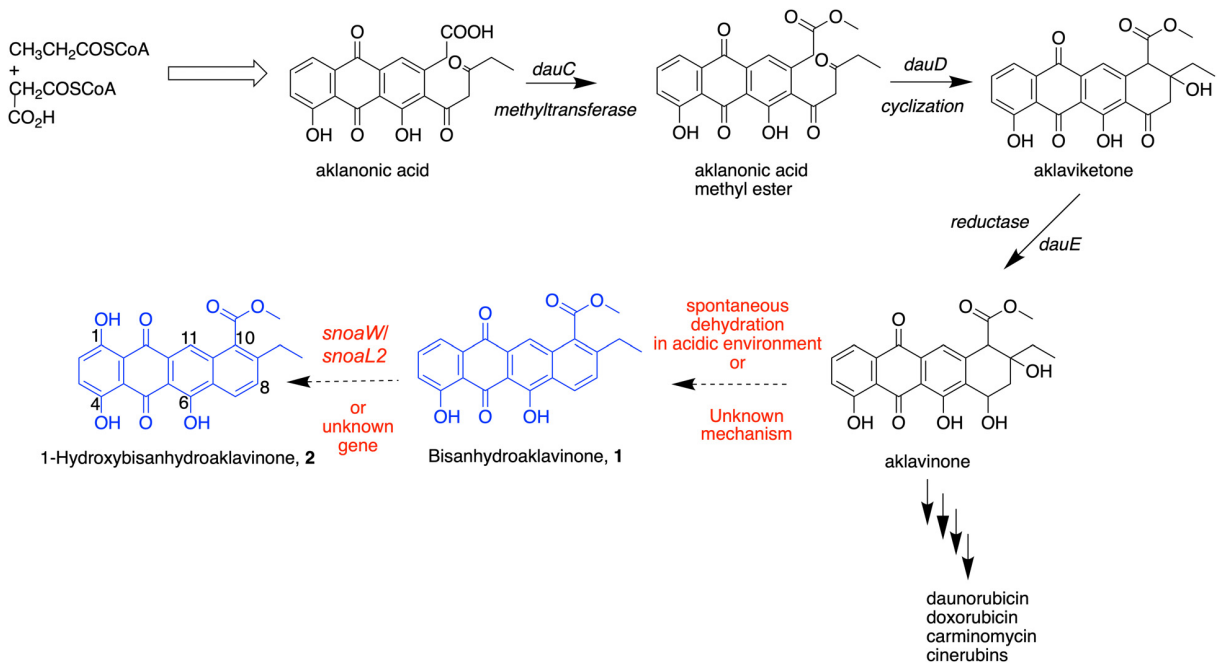

SCHEME 1 | Putative biosynthetic pathway of 1 and 2 in marine sediment-derived *Streptomyces griseorubens* strain DSD069.

ζ-pyrromycinone through Pd/Mohr or Pd/Kohle reaction, respectively (Eckardt, 1967). This chemical synthesis work supports the report that **1** and **2** can be double dehydration products of anthracyclinones produced by *Streptomyces* strains (Brockmann et al., 1965). This dehydration process, particularly on ring D of tetracenedione chromophore of these major aglycones, readily takes place in acidic conditions that resulted in the formation of 7,9-diols, which subsequently undergo bis-hydration further resulting to the aromatization of ring D (Lown, 1993). Compound **2** is hydroxylated at C-1 position of tetracenedione nucleus. This hydroxylation event was in the biosynthesis of anticancer cinerubins where AclR enzyme catalyzes the hydroxylation at C-1 position of aklavinone. The mechanism and reaction pathway of C-1 modification of the aglycone is not fully understood (Beinker et al., 2006). Interestingly, studies on the biosynthetic gene cluster of a similar anthracycline anticancer derivative, nogalomycin, involved a two-component monooxygenase SnoaW/SnoaL2 enzyme that is responsible for the hydroxylation at C-1 tetracenedione nucleus of aklavinone to 1-hydroxyaklavinone prior to glycosylation to form nogalomycin (Bechthold and Yan, 2012).

In this study, we found that **1** and **2** are metabolites accumulated in the biomass of marine sediment-derived *S. griseorubens* strain DSD069. Based on this finding, we propose in **Scheme 1** that the accumulation of dehydrated, non-glycosylated anthracyclinone compounds **1** and **2** was influenced by the acidity of the growth medium used in this study (pH 5.0–6.0) or perhaps other unknown mechanisms that favors the spontaneous dehydration and subsequent aromatization of ring D in the tetracenedione chromophore. This proposed mechanism is consistent with the previous report on spontaneous dehydration of aklavinone in an acidic environment to form Bisanhydroaklavinone (**1**) (Lown, 1993). Moreover, perhaps SnoaW/SnoaL2, AclR enzyme (C-1 hydroxylase) or similar functioning enzyme may have been well expressed in marine sediment-derived *S. griseorubens* strain DSD069 that may have favored the formation of 1-Hydroxybisanhydroaklavinone (**2**).

CONCLUSION

The findings in this study provide evidence on the potential of marine sediment-derived *Streptomyces* strains from Romblon, Philippines as a source of antibiotics against *S. aureus* ATCC BAA-44. Here, we found that *S. griseorubens* strain DSD069 exhibited its highest antibacterial activity by destroying the cell membrane of *S. aureus* ATCC BAA-44 as demonstrated by protein and DNA leakage and loss of vital cell constituents, irregular shrinkage of cells, and increase membrane permeability. We found that anthracycline shunt metabolites **1** and **2** are the major compounds produced by *S. griseorubens* strain DSD069 that are responsible for its antibacterial activity and plausibly causing the membrane damaging activity. The identification of the molecular target of anthracycline shunt metabolites **1** and **2** as well as their toxicity profiles warrants further investigation. Moreover, we have demonstrated that Philippine marine sediment-derived *S. griseorubens* strain DSD069 is a natural bacterial strain that can produce anthracycline shunt metabolites **1** and **2,** with potential as antibiotic leads to combat ABR. These anthracycline shunt metabolites were accumulated during the fermentation process. We proposed that the intermediate aglycone aklavinone in the biosynthesis

of anticancer anthracycline derivatives namely doxorubicin, daunorubicin, and cinerubins underwent spontaneous double dehydration to afford **1**, which subsequently converted to **2** via C-1 hydroxylation. These biosynthetic events are driven by mechanisms that are not yet fully understood in this study. Thus, the intriguing biosynthetic machinery found in Philippine marine-sediment derived *S. griseorubens* strain DSD069 that produce these shunt metabolites are interesting areas to look into for future studies.

DATA AVAILABILITY STATEMENT

The datasets generated for this study can be found in the GenBank with accession number MN818600.

AUTHOR CONTRIBUTIONS

DD conceptualized the study. DD and JS designed the experiments. MP, AS, ES, and ZL performed the experiments. MP, AS, ES, ZL, JS, and DD analyzed the data. MP, JS, and DD wrote and edited the manuscript.

FUNDING

This work was funded under the Grant-in-Aid (GIA) Program of the National Research Council of the Philippines (NRCP) and of the Department of Science and Technology (DOST) with grant numbers O-005 and D-138.

ACKNOWLEDGMENTS

Dr. Dalisay and Dr. Saludes thank the Balik Scientist Program of the Philippines Department of Science and Technology (DOST), through the Philippine Council for Health Research and Development (PCHRD) for the opportunity to serve the Filipino community through science, technology, and innovation. The *Balik* (Filipino word for Returning) Scientist Program (BSP) seeks highly trained Filipino scientists, technologists, experts, and professionals residing abroad to return to the Philippines and transfer their expertise to the local community for the acceleration of scientific, agro-industrial and economic development of the country. The authors thank Mr. Julius Tagomata and Mr. Cecilio Gonzales for collecting the marine sediment samples and the local government of Lugbong and Alad Islands, Romblon, Philippines for the permission.

SUPPLEMENTARY MATERIAL

The Supplementary Material for this article can be found online at: https://www.frontiersin.org/articles/10.3389/fmicb.2020.00743/full#supplementary-material

REFERENCES

Al-Askar, A. A., Rashad, Y. M., Hafez, E. E., Abdulkhair, W. M., Baka, Z. A., and Ghoneem, K. M. (2014). Characterization of alkaline protease produced by *Streptomyces griseorubens* E44G and its possibility for controlling *Rhizoctonia* root rot disease of corn. *J. Pure Appl. Microbiol.* 8, 221–230. doi: 10.1080/13102818.2015.1015446

Al-Dhabi, N. A., Ghilan, A. M., Esmail, G. A., Arasu, M. V., Duriapandiyan, Y., and Ponmurugan, K. (2019). Bioactivity assessment of the Saudi Arabian Marine *Streptomyces* sp. *Al-Dhabi*-90, metabolic profiling and its *in vitro* inhibitory property against multidrug resistant and extended-spectrum beta-lactamase clinical bacterial pathogens. *J. Infect Public Health* 12, 549–556. doi: 10.1016/j.jiph.2019.01.065

Almeida, E., Rincon, A., Jackson, S., and Dobson, A. (2019). Comparative genomics of marine sponge-derived *Streptomyces* spp. *isolates SM*17 and SM18 with their closest terrestrial relatives provides novel insights into environmental niche adaptations and secondary metabolites biosynthesis potential. *Front. Microbiol.* 10:1713. doi: 10.3389/fmicb.2019.01713

Altschul, S., Gish, W., Miller, W., Myers, E., and Lipman, D. (1990). Basic local alignment search tool. *J. Mol. Biol.* 215, 403–410.

Andrews, J. M. (2001). Determination of minimum inhibitory concentrations. *J. Antimicrob. Chemother.* 48, 5–16. doi: 10.1093/jac/48.suppl_1.5

Aneiros, A., and Garateix, A. (2004). Bioactive peptides from marine sources: pharmacological properties and isolation procedures. *J. Chromatogr. B Anal. Technol. Biomed. Life Sci.* 803, 41–53. doi: 10.1016/j.jchromb.2003.11.005

Arcamone, F., Cassinelli, G., Fantini, G., Grein, A., Orezzi, P., Pol, C., et al. (1969). Adriamycin, 14-Hydroxydaunomycin, a new antitumor antibiotic from *S. peucetius* var. caesius. *J. Biotechnol. Bioeng.* 11, 1101–1110. doi: 10.1002/bit.260110607

Bai, J., Wu, Y., Liu, X., Zhong, K., Huang, Y., and Gao, H. (2015). Antibacterial activity of shikimic acid from pine needles of cedrus deodara against *Staphylococcus aureus* through damage to cell membrane. *Int. J. Mol. Sci.* 16, 27145–27155. doi: 10.3390/ijms161126015

Barka, E. A., Vatsa, P., Sanchez, L., Gaveau-Vaillant, N., Jacquard, C., Klenk, H., et al. (2016). Taxonomy, physiology, and natural products of *Actinobacteria*. *Microbiol. Mol. Biol. R.* 80, 1–43. doi: 10.1128/MMBR.00019-15

Bechthold, A., and Yan, X. (2012). SnoaW/SnoaL2: a different two-component monooxygenase. *Chem. Biol.* 25, 549–551. doi: 10.1016/j.chembiol.2012.05.002

Beinker, P., Lohkamp, B., Peltonen, T., Niemi, J., Mäntsälä, P., and Schneider, G. (2006). Crystal structures of SnoaL2 and AclR: two putative hydroxylases in the biosynthesis of aromatic polyketide antibiotics. *J. Mol. Biol.* 359, 728–740. doi: 10.1016/j.jmb.2006.03.060

Bradford, M. (1976). A rapid and sensitive method for the quantitation of microgram quantities of protein utilizing the principle of protein-dye binding. *Anal. Biochem.* 72, 248–254. doi: 10.1016/0003-2697(76)90527-3

Bredholt, H., Fjaervik, E., Johnsen, G., and Zotchev, S. B. (2008). Actinomycetes from sediments in the Trondheim fjord, Norway: diversity and biological activity. *Mar. Drugs* 6, 12–24. doi: 10.3390/md6010012

Brockmann, H. Jr., Budzikiewicz, H., Djerassi, C., Brockmann, H., and Niemeyer, J. (1965). Das massenspektroskopische fragmentierungsverhalten der anthracyclinone. *Chemische Berichte* 98, 1260–1269. doi: 10.1002/cber.19650980436

Brockmann, H., and Brockmann, H. Jr. (1963). δ-Rhodomycine. *Chemische Berichte* 96, 1771–1778. doi: 10.1002/cber.19630960705

Brockmann, H., and Franck, B. (1955). Rhodomycinone und iso-rhodomycinne, rhodomycine. *Chemische Berichte* 80, 1792–1796. doi: 10.1002/cber.19550881132

Brown, M. R. W., and Winsley, B. E. (1969). Effect of polysorbate 80 on cell leakage and viability of *Pseudomonas aeruginosa* exposed to rapid changes of ph, temperature and tonicity free. *Microbiology* 56, 99–107. doi: 10.1099/00221287-56-1-99

Chelvan, Y., Chelvan, T., Pushpam, A., Karthik, R., Ramalingam, K. R., and Vanitha, M. C. (2016). Extraction and purification on antimicrobial compounds

from marine actinobacteria. *Res. J. Pharm. Technol.* 9, 381–385. doi: 10.5958/0974-360X.2016.00068.8

Choma, I., and Jesionek, W. (2015). TLC-direct bioautographu as a high throughput method for detection of antimicrobials in plants. *Chromatography* 2, 225–238. doi: 10.3390/chromatography2020225

Choma, I. M., and Grzelak, E. M. (2010). Bioautography detection in thin-layer chromatography. *J. Chromatogr. A* 1218, 2684–2691. doi: 10.1016/j.chroma.2010.12.069

Clark, B., Capon, R., Stewart, M., Lacey, E., Tennant, S., and Gill, J. (2004). Blanchaquinone: a new anthraquinone from an australian *Streptomyces* sp. *J. Nat. Prod.* 67, 1729–1731. doi: 10.1021/np049826v

Claverias, F., Undabarrena, A., Gonzales, M., Seeger, M., and Camara, B. (2015). Culturable diversity and antimicrobial activity of actinobacteria from marine sediments in Valparaiso Bay, Chile. *Front. Microbiol.* 6:737. doi: 10.3389/fmicb.2015.00737

Corbaz, R., Ettlinger, L., Keller-Schierlein, W., and Zahner, H. (1957). zur systematik der *Actinomyceten*. *Arch. Mikrobiol.* 26, 192–208. doi: 10.1007/bf00412100

Dalisay, D. S., Williams, D. E., Wang, X. L., Centko, R., Chen, J., and Andersen, R. J. (2013). Marine sediment-derived Streptomyces bacteria from British Columbia, Canada are a promising microbiota resource for the discovery of antimicrobial natural products. *PLoS One* 8:e77078. doi: 10.1371/journal.pone.0077078

Delgado-Andrade, C., Rufián-Henares, J. A., and Morales, F. J. (2006). Study on fluorescence of Maillard reaction compounds in breakfast cereals. *Mol. Nutr. Food Res.* 50, 799–804. doi: 10.1002/mnfr.200500249

Dhakal, D., Pokhrel, A. R., Shrestha, B., and Sohng, J. K. (2017). Marine rare actinobacteria: isolation, characterization, and strategies for harnessing bioactive compounds. *Front. Microbiol.* 8:1106. doi: 10.3389/fmicb.2017.01106

Dholakiya, R. N., Kumar, R., Mishra, A., Mody, K. H., and Jha, B. (2017). Antibacterial and antioxidant activities of novel. *Front. Microbiol.* 8:2420. doi: 10.3389/fmicb.2017.02420

du Toit, E. A., and Rautenbach, M. (2000). A sensitive standardised micro-gel well diffusion assay for the determination of antimicrobial activity. *J. Microbiol. Methods* 42, 159–165. doi: 10.1016/s0167-7012(00)00184-6

Eckardt, K. (1967). Rote Antibiotica aus Actinomyceten. Zur identifizierung einer reihe von anthracyclinonpigmenten aus *Streptomyces galilaeus* Stamm JA 3043 (Galirubine und Galirubinone). *Chem. Berichte.* 100, 2561–2568. doi: 10.1002/cber.19671000815

Eckardt, K., and Bradler, G. (1965). Zur kenntnis-einiger roter hydroxychinonfarbstoffe aus einem *Streptomyces*-stamm: galirubinine und galirubin. *Kurze Originalmitteilungen* 19, 539–540. doi: 10.1007/BF00645826

Eckardt, K., Schumann, G., Wagner, C., Stengel, C., Ihn, W., Novak, J., et al. (1989). Biosynthesis of anthracyclines: biotransformation of aklaviketone. *J. Basic Microbiol.* 5, 277–279. doi: 10.1002/jobm.3620290509

Egorin, M. J., Van Echo, D., Andrews, A., Fox, B. M., Nakazawa, H., Whitacre, M., et al. (1981). The clinical pharmacology of aclacinomycin A. *Anthracycline Antibiot. Canc. Ther.* 22, 527–540. doi: 10.1007/978-94-009-7630-6_48

El-Gendy, M. M. A. A., Mohamed, Z., Hekal, N., Ali, F., and Yousef, A. (2018). Production of bioactive metabolites from different marine endophytic *Streptomyces* species and testing them agianst methicillin-resistant *Staphylococcus aureus* (MRSA) and cancer cell lines. *BioTechnologia* 99, 13–35. doi: 10.5114/bta.2018.73559

Fatima, A., Aftab, U., Shaaban, K., Thorson, J., and Sajid, I. (2019). Spore forming actinobacterial diversity of cholistan desert pakistan: polyphasic taxonomy, antimicrobial potential and chemical profiling. *BMC Microbiol.* 19:49. doi: 10.1186/s12866-019-1414-x

Feng, H., Zhi, Y., Sun, Y., Wei, X., Luo, Y., and ZHuo, P. (2014). Draft genome sequence of a novel *Streptomyces grisorubens* strain, JSD-1, active in varbon and nitrogen recycling. *Genome Announc.* 2, 650–614. doi: 10.1128/genomeA.00650-14

Foster, J. K., Lentino, J. R., Strodtman, R., and DiVincenzo, C. (1986). Comparison of invitro activity of quinolone antibiotics and vancomycin against gentamicin- and methicillin-resistant *Staphylococcus aureus* by time-kill kinetic studies. *Antimicrob. Agents Chemother.* 30, 823–827. doi: 10.1128/AAC.30.6.823

Grein, A. (1987). Antitumor anthracyclines produced by *Streptomyces peucetius*. *Adv. Appl. Microbiol.* 32, 203–214. doi: 10.1016/S0065-2164(08)70081-9

Hames-Kocabas, E., and Uzel, A. (2012). Isolation strategies of marine-derived actinomycetes from sponge and sediment samples. *J. Microbiol. Methods* 88, 342–347. doi: 10.1016/j.mimet.2012.01.010

Hayashi, K., Fukushima, A., Hayashi-Nishino, M., and Nishino, K. (2014). Effect of methylglyoxal on multidrug-resistant *Pseudomonas aeruginosa*. *Front Microbiol.* 4:195. doi: 10.3389/fmicb.2013.00195

Hopwood, D. A. (2007). *Streptomyces in Nature and Medicine: The Antibiotic Makers*. New York: Oxford University Press.

Hori, S., Shirai, M., Hirano, S., Oki, T., Inui, T., Tsukagoshi, S., et al. (1977). Antitumor activity of new anthracycline antibiotics, aclacinomycin a and its analogs, and their toxicity. *Gann* 68, 685–690. doi: 10.20772/cancersci1959.68.5_685

Imada, C. (2005). Enzyme inhibitors and other bioactive compounds from marine actinomycetes. *Antonie Van Leeuwenhoek* 87, 59–63. doi: 10.1007/s10482-004-6544-x

Jayashree, B., Bibin, Y. S., Prabhu, D., Shanthirani, C. S., Gokulakrishnan, K., Lakshmi, B. S., et al. (2014). Increased circulatory levels of lipopolysaccharide (LPS) and zonulin signify novel biomarkers of proinflammation in patients with type 2 diabetes. *Mol. Cell. Biochem.* 388, 203–210. doi: 10.1007/s11010-013-1911-4

Jensen, P. R., Gontang, E., Mafnas, C., Mincer, T. J., and Fenical, W. (2005). Marine microorganism and drug discovery: current status and future potential. *Environ. Microbiol.* 7, 1039–1048. doi: 10.1111/j.1462-2920.2005.00785.x

Jesionek, W., Móricz, Á, Ott, P. G., Kocsis, B., Horváth, G., and Choma, I. M. (2015). TLC-Direct bioautography and LC/MS as complementary methods in identification of antibacterial agents in plant tinctures from the asteraceae family. *J. AOAC Int.* 98, 857–861. doi: 10.5740/jaoacint.SGE2-Choma

Jiang, Y., Li, Q., Chen, X., and Jiang, C. (2016). Isolation and cultivation methods of Actinobacteria – basics and biotechnological approach. *IntechOpen* 2, 39–57. doi: 10.5772/61457

Jose, P. A., and Jha, B. (2017). Intertidal marine sediment harbours actinobacteria with promising bioactive and biosynthetic potential. *Sci. Rep.* 7:10041. doi: 10.1038/s41598-017-09672-6

Kamjam, M., Sivalingam, P., Deng, Z., and Hong, K. (2017). Deep sea Actinomycetes and their secondary metabolites. *Front. Microbiol.* 8:760. doi: 10.3389/fmicb.2017.00760

Karsha, P. V., and Lakshmi, B. (2010). Antibacteria activity of black pepper (*Piper nigrum* Linn.) with special reference to its mode of action on bacteria. *Indian J. Nat. Prod. Resour.* 1, 213–215.

Kemung, H. M., Tan, L. T., Khan, T. M., Chan, K., Pusparajah, P., Goh, B., et al. (2018). *Streptomyces* as a prominent resource of future anti-MRSA Drugs. *Front. Microbiol.* 9:2221. doi: 10.3389fmicb.2018.02221

Khan, S., and Khan, A. (2016). Breaking the spell: combating multidrug resistant 'Superbugs'. *Front. Microbiol.* 7:174. doi: 10.3389/fmicb.2016.00174

Kim, H., Hwuang, J., Chung, B., Cho, E., Bae, S., Shin, J., et al. (2019). 2-Alkyl-4-hydroxyquinolines from a marine-derived *Streptomyces* sp. inhibit hyphal growth induction in *Candida albicans*. *Mar. Drugs* 17:133. doi: 10.3390/md17020133

Kumar, S., Stecher, G., and Tamura, K. (2016). MEGA7: molecular evolutionary genetics analysis version 7.0 for bigger datasets. *Mol. Biol. Evol.* 33, 1870–1874. doi: 10.1039/molbev/msw054

Langfield, R. D., Scarano, F. J., Heitzman, M. E., Kondo, M., Hammond, G. B., and Neto, C. C. (2004). Use of a modified microplate bioassay method to investigate antibacterial activity in the Peruvian medicinal plant *Peperomia galioides*. *J. Ethnopharmacol.* 94, 279–281. doi: 10.1016/j.jep.2004.06.013

Lown, W. J. (1993). Discovery and development of anthracycline antitumor antibiotics. *Chem. Soc. Rev.* 3, 165–176. doi: 10.1016/0163-7258(93)90006-Y

Mincer, T. J., Jensen, P. R., Kauffman, C. A., and Fenical, W. (2002). Widespread and persistent populations of a major new marine actinomycete taxon in ocean sediments. *Appl. Environ. Microbiol.* 68, 5005–5011. doi: 10.1128/AEM.68.10.5005-5011.2002

Niemi, J., Wang, Y., Airas, K., Ylihonko, K., Hakala, J., and Mantsala, P. (1999). Characterization of aklavinone-11-hydroxylase form *Streptomyces purpurascens*. *Biochim. Biophys. Acta* 1430, 57–64. doi: 10.1016/S0167-4838(98)00265-9

Nitiss, J., Pourquier, P., and Pommier, Y. (1997). Aclacinomycin a stabilizes topoisomerase 1 covalent complexes. *Canc. Res.* 57, 4564–4569.

Nowakowska, J., Stuehler, C., Egli, A., Battegay, M., Rauser, G., Bantug, G. R., et al. (2015). T cells specific for different latent and lytic viral proteins efficiently control Epstein-Barr virus-transformed B cells. *Cytotherapy* 17, 1280–1291. doi: 10.1016/j.jcyt.2015.06.003

Oki, T., Matsuzawa, Y., Yoshimoto, A., Numata, K., Kitamura, I., Hori, S., et al. (1975). New antitumor antibiotics, aclacinomycin A and B. *J. Antibiot.* 28, 830–834. doi: 10.7164/antibiotics.28.830

Oki, T., Yoshimoto, A., and Matsuzawa, Y. (1980). Biosynthesis of anthracycline antibiotics by *Streptomyces galilaeus*: i. glycosidation of various anthracyclines by an aclacinomycin-negative mutant and biosynthesis of aclacinomycins from aklavinone. *J. Antibiot.* 33, 1331–1340. doi: 10.7164/antibiotics.33.1331

Peck, K. R., Kim, M. J., Choi, J. Y., Kim, H. S., Kang, C. I., Cho, Y. K., et al. (2012). In vitro time-kill studies of antimicrobial agents against blood isolates of imipenem-resistant *Acinetobacter baumannii*, including colistin- or tigecycline-resistant isolates. *J. Med. Microbiol.* 61, 353–360. doi: 10.1099/jmm.0.036939-0

Podoll, J. D., Liu, Y., Chang, L., Walls, S., Wang, W., and Wang, X. (2013). Bio-inspired synthesis yields a tricyclic indoline that selectively resensitizes methicillin-resistant *Staphylococcus aureus* (MRSA) to β-lactam antibiotics. *Proc. Natl. Acad. Sci. U.S.A.* 110, 15573–15578. doi: 10.1073/pnas.1310459110

Pridham, T. G., Hesseltine, C. W., and Benedict, R. G. (1957). A guide for the classification of *Streptomyces* according to selected groups. Placement of strains in morphological sections. *Appl. Microbiol.* 6, 52–79. doi: 10.1128/aem.6.1.52-79.1958

Rogers, S. A., Huigens, R. W., Cavanagh, J., and Melander, C. (2010). Synergistic effects between conventional antibiotics and 2-aminoimidazole-derived antibiofilm agents. *Antimicrob. Agents Chemother.* 54, 2112–2118. doi: 10.1128/AAC.01418-09

Romano, S., Jackson, S., Patry, S., and Dobson, A. (2018). Extending the "One Strain Many Compounds" (OSMAC) principle to marine microorganisms. *Mar. Drugs* 16:244. doi: 10.3390/md16070244

Schlegel, B., Stengel, C., Schumann, G., Prauser, H., and Eckardt, K. (1987). Aklanonic acid-producing mutants of *Streptomyces galilaeus* and *Streptomyces peucetius* var. caesius. *J. Basic Microbiol.* 27, 107–111. doi: 10.1002/jobm.3620270212

Schmid, I., and Sakamoto, K. M. (2001). Analysis of DNA content and green fluorescent protein expression. *Curr. Protoc. Cytom.* 7, 295–304. doi: 10.1002/0471142956.cy0716s16

Shaik, M., Sankar, G. G., Iswarya, M., and Rajitha, P. (2017). Isolation and characterization of bioactive metabolites producing marine *Streptomyces parvulus* strain sankarensis-A10. *J. Genet. Eng. Biotechnol.* 15, 87–94. doi: 10.1016/j.jgeb.2017.02.004

Singh, S. R., Bacon, A. E. III, Young, D. C., and Couch, K. A. (2009). In vitro 24-hour time-kill studies of vancomycin and linezolid in combination versus methicillin-resistant *Staphylococcus aureus*. *Antimicrob. Agent Chemother.* 53, 4495–4497. doi: 10.1128/AAC.00237-09

Soliev, A. B., Hosokawa, K., and Enomoto, K. (2011). Bioactive pigments from marine bacteria: applications and physiological roles. *Evid. Based Complement. Alternat. Med.* 2011:670349. doi: 10.1155/2011/670349

Sproule, A., Correa, H., Decken, A., Haltli, B., Berrué, F., Overy, D. P., et al. (2019). Terrosamycins A and B, bioactive polyether ionophores from *Streptomyces* sp. *rknd*004 from Prince Edward Island sediment. *Mar. Drugs* 17:E347. doi: 10.3390/md17060347

Sriramulu, D. (2013). Evolution and impact of bacterial drug resistance in the context of cystitis disease and nosocomial setting. *Microbiol. Insights* 2013, 29–36. doi: 10.3147/MBI.S10792

Staphylococcus aureus subsp. aureus Rosenbach (ATCC® BAA-44™) (2019). Available online at: https://atcc.org/Products/All/BAA-44.aspx (accessed January, 2017).

Subramani, R., and Sipkema, D. (2019). Marine rare actinomycetes: a promising source of structurally diverse and unique novel natural products. *Mar. Drugs* 17:249. doi: 10.3390/md17050249

Tenover, F. C., Weigel, L. M., Appelbaum, P. C., McDougal, L. K., Chaitram, J., McAllister, S., et al. (2004). Vancomycin-resistant *Staphylococcus aureus* isolate from a patient in Pennsylvania. *Antimicrob. Agents Chemother.* 48, 275–280. doi: 10.1128/AAC.48.1.275-280.2004

Thombre, R., Shinde, V., Thaiparambli, E., Zende, S., and Mehta, S. (2016). Antomicrobial activity and mechanism of inhibition of silver nanoparticles against extreme halopholic aechaea. *Front. Microbiol.* 7:1424. doi: 10.3389/fmicb.2016.01424

Tiwari, V., Mishra, N., Gadani, K., Solanki, P. S., Shah, N. A., and Tiwari, M. (2018). Mechanism of antibacterial activity of zinc oxide nanoparticles against crabapenem-resistant *Acinetobacter baumannii*. *Front. Microbiol.* 9:1218. doi: 10.3389/fmicb.2018.01218

Tobe, H., Yoshimoto, A., and Ishikura, T. (1982). New anthracyclinone metabolites from two blocked mutants of *Streotimyces galilaeus* MA144-M1. *J. Antibiot.* 35, 1641–1645. doi: 10.7164/antibiotics.35.1641

Tyurin, A., Alferova, V., Paramonov, A., Shuvalov, M., Malanicheva, I., Grammatikova, N., et al. (2018). Crystallomycin revisited after 60 years: aspartocins B and C. *Med. Chem. Commun.* 9, 667–675. doi: 10.1039/c8md00002f

Valli, S., Suvathi, S. S., Aysha, O. S., Nirmala, P., Vinoth, K. P., and Reena, A. (2012). Antimicrobial potential of *Actinomycetes* species isolated from marine environment. *Asian Pac. J. Trop. Biomed.* 2, 469–473. doi: 10.1016/S2221-1691(12)60078-1

Van Der Meij, A., Worsley, S., Hutchings, M., and van Wezel, G. (2017). Chemical ecology of antibiotic production by *Actinomycetes*. *FEMS Microbiol. Rev.* 41, 392–416. doi: 10.1093/femsre/fux005

Vestergaard, M., Frees, D., and Ingmer, H. (2019). Antibiotic resistance and the MRSA problem. *Microbiol. Spectr.* 7:GPP3-0057-2018. doi: 10.1128/microbiolspec

Williamson, E. M. (2001). Synergy and other interactions in phytomedicines. *Phytomedicine* 8, 401–409. doi: 10.1078/0944-7113-00060

Wu, Q., Zhang, G., Wang, B., Li, X., Yue, S., Chen, J., et al. (2018). Production and identification of inthomycin b produced by a deep-sea sediment-derived *Streptomyces* sp. *YB*104 based on cultivation-dependent approach. *Curr. Microbiol.* 75, 942–951. doi: 10.1007/s00284-018-1469-1

Wu, Y., Bai, J., Zhong, K., Huang, Y., Qi, H., Jiang, Y., et al. (2016). Antibacterial activity and membrane-disruptive mechansism of 3-*p-trans*-coumaroyl-2-hydroxyquinic acid, a novel phenolic compound from pine needles of *Cedrus deodara*, against *Staphylococcus aureus*. *Molecules* 21:1084. doi: 10.3390/molecules21081084

Yang, N., and Song, F. (2017). Bioprospecting of novel and bioactive compounds from marine Actinomycetes isolated from South China Sea sediments. *Curr. Microbiol.* 75, 142–149. doi: 10.1007/s00284-017-1358-z

Yang, Z., He, J., Wei, X., Ju, J., and Ma, J. (2020). Exploration and genome mining of natural products from marine *Streptomyces*. *Appl. Microbiol. Biotechnol.* 104, 67–76. doi: 10.1007/s00253-019-10227-0

Yarnell, E. (2015). Synergi in herbal medicine. *J. Restor. Med.* 2014, 60–73. doi: 10.14200/jrm.2015.4.0104

Ye, L., Zhuo, Q., Liu, C., Luo, X., Na, G., and Xi, T. (2009). Identification and fermentation of a marine-derived *Streptomyces griseorubens* with anti-tumor activtiy. *Indian J. Mar. Sci.* 1, 14–21.

Zhang, J., Ye, K. P., Zhang, X., Pan, D. D., Sun, Y. Y., and Cao, J. X. (2017). Antibacterial activity and mechanism of action of black pepper ezzential oil on meat-borne *Escherichia coli*. *Front. Microbiol.* 7:2094. doi: 10.3389/fmicb.2016.02094

Zheng, L. H., Wang, Y. J., Sheng, J., Wang, F., Zheng, Y., Lin, X. K., et al. (2011). Antitumor peptides from marine organisms. *Mar. Drugs* 9, 1840–1859. doi: 10.3390/md9101840

Conflict of Interest: ZL was employed by Waters Pacific Pte Ltd.

The remaining authors declare that the research was conducted in the absence of any commercial or financial relationships that could be construed as a potential conflict of interest.

frontiers in Microbiology

ORIGINAL RESEARCH
published: 11 June 2020
doi: 10.3389/fmicb.2020.01167

Surfactin Like Broad Spectrum Antimicrobial Lipopeptide Co-produced With Sublancin From *Bacillus subtilis* Strain A52: Dual Reservoir of Bioactives

*Deepika Sharma[1], Shelley Sardul Singh[1], Piyush Baindara[1], Shikha Sharma[1], Neeraj Khatri[1], Vishakha Grover[2], Prabhu B. Patil[1] and Suresh Korpole[1]**

[1] Council of Scientific and Industrial Research (CSIR) – Institute of Microbial Technology, Chandigarh, India, [2] Dr. Harvansh Singh Judge Institute of Dental Sciences & Hospital, Panjab University, Chandigarh, India

An antimicrobial substance producing strain designated as A52 was isolated from a marine sediment sample and identified as *Bacillus* sp., based on 16S rRNA gene sequence analysis. The ANI and dDDH analysis of the genome sequence displayed high identity with two strains of *B. subtilis* sub sp. *subtilis*. Strain A52 yielded two antimicrobial peptides (AMPs) that differed in activity spectrum. MALDI mass spectrometry analysis of HPLC purified fractions revealed mass of peptides as 3881.6 and 1061.9 Da. The antiSMASH analysis of genome sequence unraveled presence of identical biosynthetic cluster involved in production of sublancin from *B. subtilis* sub sp. *subtilis* strain 168, which yielded peptide with identical mass. The low molecular weight peptide is found to be a cyclic lipopeptide containing C_{16} β-hydroxy fatty acid that resembled surfactin-like group of biosurfactants. However, it differed in fatty acid composition and antimicrobial spectrum in comparison to other surfactins produced by strains of *B. subtilis*. It exhibited broad spectrum antibacterial activity, inhibited growth of pathogenic strains of *Candida* and filamentous fungi. Further, it exhibited hemolytic activity, but did not show phytotoxic effect in seed germination experiment. The emulgel formulation of surfactin-like lipopeptide showed antimicrobial activity *in vitro* and did not show any irritation effects in animal studies using BALB/c mice. Moreover, surfactin-like lipopeptide displayed synergistic activity with fluconazole against *Candida*, indicating its potential for external therapeutic applications.

Keywords: sublancin, *B. subtilis*, *Candida*, synergistic, surfactin-like lipopeptide, emulgel

OPEN ACCESS

Edited by:
Jinwei Zhang,
University of Exeter, United Kingdom

Reviewed by:
Przemysław Bernat,
University of Lodz, Poland
Marcia Nitschke,
University of São Paulo, Brazil

****Correspondence:***
Suresh Korpole
suresh@imtech.res.in

Specialty section:
This article was submitted to Microbiotechnology, a section of the journal Frontiers in Microbiology

Received: *16 March 2020*
Accepted: *07 May 2020*
Published: *11 June 2020*

Citation:
Sharma D, Singh SS, Baindara P, Sharma S, Khatri N, Grover V, Patil PB and Korpole S (2020) Surfactin Like Broad Spectrum Antimicrobial Lipopeptide Co-produced With Sublancin From Bacillus subtilis Strain A52: Dual Reservoir of Bioactives. Front. Microbiol. 11:1167. doi: 10.3389/fmicb.2020.01167

INTRODUCTION

Development of drug resistance is a great threat to the effective treatment of infections caused by opportunistic or nosocomial pathogens (Davies and Davies, 2010; Prestinaci et al., 2015; Li and Webster, 2018; Laws et al., 2019). Clinically, most significant drug resistant nosocomial pathogens include *Staphylococcus aureus*, *Escherichia coli, Klebsiella* spp., *Shigella* spp., *Mycobacterium tuberculosis*, *Pseudomonas aeruginosa*, *Acinetobacter baumannii,* and *Enterobacter*

spp. (Alanis, 2005; Pande and Bhailume, 2014; Wong et al., 2017). *Candida* is a commensal fungus that is more often associated with infections in immunocompromised individuals. It has been reported to develop resistance to antibiotics like fluconazole, caspofungin, and amphotericin B commonly used to treat candidiasis (Eksi et al., 2013; Lum et al., 2015; Dagi et al., 2016; Ksiezopolska and Gabaldón, 2018). In 2019, Centers for Disease Control and Prevention (CDC) has included drug resistant *Candida* spp. in the list of organisms causing serious threat. In an attempt to combat such resistant pathogens, there is an urgent and compelling need to develop novel antimicrobials. To this effect, antimicrobial peptides (AMPs) including bacteriocins and lipopeptides with broad-spectrum antimicrobial activities have been found to be promising alternative candidates (Singh et al., 2014; Sharma et al., 2014; Lum et al., 2015; Raman et al., 2015; Lyu et al., 2016; Gwynne and Gallagher, 2018).

The genus *Bacillus* is a prolific producer of a wide range of antimicrobials and reported to produce peptide antimicrobial substances like bacteriocins, lipopeptides, and glycopeptides that are active against a variety of bacteria and fungi (Abriouel et al., 2011; Perez et al., 2018; Hashem et al., 2019; Miljkovic et al., 2019). According to their biosynthetic pathways, these bioactive molecules have been grouped mainly into two different classes: the first one comprises ribosomally synthesized peptides usually referred as bacteriocins and classified as ribosomally produced and post-translationally modified peptides (RiPPs) by Arnison et al. (2013). The other class comprises small antimicrobial cyclic lipopeptides synthesized enzymatically by non-ribosomal peptide synthetases (NRPS) and classified as post-ribosomal peptide synthetases (PRPS). Bacteriocins produced by *Bacillus* spp. display a high degree of target specificity against bacterial infections and also a broad spectrum of activity (Abriouel et al., 2011; Herzner et al., 2011; Ramachandran et al., 2014; Wu et al., 2019). Most of the compounds reported from *Bacillus* spp., largely belong to Class I bacteriocins that are known as lantibiotics (Klaenhammer, 1993) or lanthipeptides (Arnison et al., 2013). Sublancin is one of such lanthipeptide that has an S-linked glycocin produced by *B. subtilis* strain 168. It exhibits antimicrobial activity only against Gram-positive bacteria, including methicillin-resistant *Staphylococcus aureus* (MRSA) (Ren et al., 2018; Wang et al., 2018). Other strains of *B. subtilis* were reported to produces lipopeptides mostly pertaining to surfactins, iturins, and fengycins (Zhang and Sun, 2018). However, they differed in antimicrobial activity due to variations in length of fatty acid chains and/or amino acid composition (Mondol et al., 2013; Meena and Kanwar, 2015).

Marine ecosystem is a reservoir of multiple bacterial strains with ability to produce various bioactive compounds for survival (Debbab et al., 2010; Reen et al., 2015; Gupta et al., 2019; Paulsen et al., 2019). The genus *Bacillus* is a predominant microbial flora in marine ecosystem that differed with terrestrial strains in production of diverse classes of AMPs from species like *B. subtilis* (Ivanova et al., 1999; Berrue et al., 2009; Jin et al., 2012; Mondol et al., 2013; Tareq et al., 2014; Chen et al., 2017). Due to advancement in protein purification technology and characterization of AMPs, reports on bioactive from marine bacterial sources have also increased in the recent past. In light of the above facts, we have isolated a *Bacillus* strain from a marine sediment sample and explored the strain A52 for production of antimicrobial compounds, which have been characterized in detail.

MATERIALS AND METHODS

Strain Isolation and Identification

Strain A52 was isolated from a sediment sample obtained from marine environment (Bay of Bengal, West Bengal, India). During isolation of the bacteria on various media, a colony on nutrient agar (NA, Hi-media, India) with inhibitory zone in their surroundings was sub-cultured on NA and preserved as 20% (v/v) glycerol stocks at −80°C until further studies. All indicator strains used in this study were obtained from Microbial Type Culture Collection and Gene bank (MTCC), Chandigarh, India, and grown on recommended media. Phenotypic properties of strain A52 including morphology, physiology, and biochemical characteristics were performed using standard procedures (Smibert and Krieg, 1994). Identity of the strain was confirmed by BLAST search analysis of 16S rRNA gene sequence (Suresh et al., 2006). Further, taxonomic position of strain was determined by phylogenetic analysis of 16S rRNA gene sequence with the nearest type strains using MEGA version 7 (Kumar et al., 2016). Evolutionary distances were computed by Tamura-Nei method and expressed as units of the number of base substitutions per site to construct a neighbor-joining phylogenetic tree. The strain was further used for whole genome sequence.

Genome Sequence and Analyses

Genomic DNA of strain A52 was extracted and libraries were prepared. Sequencing of libraries was done as described earlier (Patil et al., 2016). Quality of obtained reads was checked using FastQC (Patel and Jain, 2012). Reads obtained were assembled using CLC Genomics Workbench 7.5 (CLC bio, Aarhus, Denmark). The average nucleotide identity (ANI) of strain A52 with genome sequences of other closely related members was calculated using ANI calculator (Yoon et al., 2017). Genome to genome distance calculator (GGDC) was used for the estimation of genetic relatedness using GGDC 2.0 web server[1] and calculations were performed by recommended formulae 2. Whole genome sequences of reference strains were downloaded from NCBI database in FASTA format. Pangenome analysis was performed using ultra-fast computational pipeline BPGA (Bacterial Pan Genome Analysis tool)[2] for core genome analysis.

Antimicrobial Activity of Strain A52

The antimicrobial activity was tested by well diffusion assay as mentioned earlier (Singh et al., 2014). Strain A52 was grown for 24 h in 500 ml of nutrient broth (NB, Hi-media, India) using 1000 ml flask and subsequently cells were removed by centrifugation (10,000 rpm for 15 min at 4°C). Supernatant was filtered through 0.22 μm filter (Millipore, United States) to obtain cell-free fermented broth (CFB) that was used for antimicrobial

[1]http://ggdc.dsmz.de/distcalc2.php

[2]https://iicb.res.in/bpga/index.html

assay (50 μl) against various indicator strains and the activity was measured as diameter of inhibition zone. Test strains used were *Staphylococcus aureus* (MTCC 1430), *Bacillus subtilis* (MTCC 121), *B. firmus* (MTCC 488), *B. licheniformis* (MTCC 429), *B. thuringiensis* (MTCC 1953), *Escherichia coli* (MTCC 1610), *Micrococcus luteus* (MTCC 106), *Steptococcus pyrogens* (MTCC 1928), *S. anginosus* (MTCC 1929), *S. oralis* (MTCC 2696), *S. mutans* (MTCC 497), *Candida albicans* (MTCC 1637), *C. albicans* (MTCC 183), *C. albicans* (MTCC 227), *C. tropicalis* (MTCC 184), *C. glabrata* (MTCC 3019), *C. haemulonii* (MTCC 2766), and *C. inconsplicue* (MTCC 1074). The phytopathogenic fungi employed in this study were *Alternaria brassicicola* (MTCC 2102), *Colletotrichum acutatum* (MTCC 1037), and *Fusarium moniliforme* (MTCC 158). Clinical isolates of *Candida* were provided by National Culture Collection of Pathogenic Fungi (NCCPF), PGIMER, Chandigarh, India.

Production and Purification of Antimicrobial Substances

Production of antimicrobial substances was pursued in NB. However, production was also tested in minimal medium [containing (g/l): disodium hydrogen phosphate, 7.9; potassium dihydrogen phosphate, 3.0; sodium chloride, 5.0; and ammonium chloride, 1.0] supplemented with 1% carbon (glucose, sucrose, glycerol, and starch) and nitrogen sources (yeast extract, ammonium chloride, and peptone). Overnight grown culture of strain A52 was inoculated to 1 L of medium and grown to late logarithmic growth phase on a rotary shaker at 30°C. Subsequently, CFB was mixed with activated Diaion HP-20 (Sigma-Aldrich, United States) resin (2%) and the antimicrobial substance was eluted in methanol. Methanol was evaporated using a rotavapour (BUCHI R-200, Switzerland) and was redissolved in Milli-Q water to offer as crude extract. CFB was also extracted by ethyl acetate solvent extraction using 1:1 ratio (Alajlani et al., 2016). Subsequently, solvent was removed on a rota vapor (BUCHI-200, Switzerland) and the extract was dissolved in minimal amount of methanol. For purification, these extracts were applied onto reverse phase high performance liquid chromatography (HPLC) (1260 Infinity, Agilent Technologies, United States) with a semi-preparative C18 column (Pursuit 10C18 250 mm × 21.2 mm). The solvent system comprised 0.12% aqueous trifluoroacetic acid (TFA, solvent A) and acetonitrile with 0.1% TFA (solvent B). The gradient of solvent B used to run the column was as follows: 0–60% for 0–45 min, 60–80% for 45–50 min, and 80–100% for 50–55 min. Elution from the column was monitored at 220 nm and the peaks of HPLC chromatogram were collected. These fractions were tested for antimicrobial activity and the active peaks were pooled through multiple runs, and solvent was evaporated. Peptides were suspended in water and used for characterization studies like thin layer chromatography (TLC), gel electrophoresis, and MALDI.

In-Gel Activity and TLC Overlay Bioautography

Purified antimicrobial peptides were analyzed on TLC plates (Silica gel 60 F_{254}, Merck, Germany) and used to determine the purity and antimicrobial activity of the compound by bioautographic assay (Zheng et al., 2005). About 50–60 μl of the peptide solution (100 μg/ml concentration) was loaded onto individual TLC silica gel plates in duplicates and were developed using a solvent system containing chloroform: methane: water (65:12:4 v/v). Subsequently, each TLC plate was dried, cut into two vertical parts, and one part of the TLC was used for direct detection of antimicrobial activity by overlaying on NA plate containing indicator strain (*S. aureus* MTCC 1430, ∼10^6 cells/ml). After allowing for 1 h of diffusion at 4°C, the TLC strip was removed and plates were incubated for 24 h at 37°C. The other part of TLC strip (5–10 μl of the peptide solution spot) was sprayed with ninhydrin and phosphomolybdic acid as a staining reagent to detect the presence of peptides and lipid moieties, respectively. Similarly, peptides were electrophoresed on 16% Tricine-SDS-PAGE and used for in-gel activity assay as described earlier (Baindara et al., 2016). *S. aureus* MTCC 1430 (∼10^6 cells/ml) was used as an indicator strain in assay.

Mass Spectrometry of Peptide

HPLC purified peptides and standard surfactin (Sigma, United States) were analyzed using Matrix-Assisted Laser Desorption Ionization (MALDI) to determine intact molecular weights of the peptides. The HPLC purified peptides were re-suspended in water (1 mg/ml) and 1 μl of peptide solution was mixed with 1 μl of matrix (CHCA, 10 mg/ml) and 2.0 μl of this mixture solution was spotted onto the MALDI 100 well stainless steel sample plate, allowed to air dry, and processed for MALDI analysis (AB Sciex 5800 MALDI-time of flight, TOF/TOF). Tandem mass spectrometry (MS/MS) data were acquired at 1,000 Hz in 1 kV MS/MS mode with 2,000 laser shots/spectrum in CID mode as mentioned earlier (Singh et al., 2014). The *de novo* sequence was generated using fragmentation pattern manually.

Collapse Drop Assay (CDA)

The surfactant property of peptide was determined using the qualitative drop-collapse assay (Youssef et al., 2004). Mineral oil (2 μl) was added to 96-well microtiter plate and equilibrated for 24 h at 37°C. After equilibration 5 μl of purified peptides (10 μg/ml) were added to the surface of the oil and drop shape was observed after 1 min using magnifying glass. Triton X-100 and water were used as positive and negative control, respectively.

Effect of pH, Temperature, and Proteolytic Enzymes

Sensitivity of purified peptides toward temperature, pH, and non-specific proteases was confirmed by performing bioassays. The pH stability was determined by adjusting the pH 2.0–12.0 of peptide aliquots (using 10 mM HCl or NaOH) and incubating for 4 h at room temperature. Samples were neutralized to pH 7.0 before processing for antimicrobial assay. To determine temperature susceptibility, peptides were incubated at different temperatures ranging from 37 to 100°C for 1 h and 121°C for 15 min and residual antimicrobial activity was determined at RT by well diffusion assay. Proteolytic enzymes trypsin and

proteinase K (Sigma, United States) were used at three different concentrations (0.1, 1.0, and 5.0 mg/ml) to observe their effect on the peptide. The enzyme solutions were prepared in 50 mM phosphate buffer (pH 7.0). All reactions were performed at 37°C for 6 h followed by deactivation of enzyme by heating the solution in boiling water for 5 min before performing the activity assay.

Determination of Minimum Inhibitory Concentration of Peptides

The minimum inhibitory concentration (MIC) of HPLC purified peptides was evaluated by using microtiter plate dilution assay. The peptide concentration was estimated using BCA protein assay (Thermo Fisher Scientific, United States) method as described by manufacturer. Actively growing test strains (5×10^5 CFU/ml) were inoculated in a 96-well plate with different concentrations of the peptides and plates were incubated for 24–48 h at 37°C (final volume in each well is 200 μl). OD was measured at 600 nm after 24 and 48 h for bacteria and yeast, respectively, using ELISA microplate reader (Thermo, United States). MIC against phytopathogenic fungi was determined using 96-well microtiter plate assay (Kaur et al., 2016). In 96-well microplates, 100 μl of fungal spore suspension (1×10^5 spores/ml) prepared in potato dextrose broth (PDB, Hi-media, India) was mixed with100 μl of fresh PDB containing different concentrations of lipopeptide. Control well contained 100 μl of fungal spore suspension and 100 μl of only medium. The microplates were incubated at 25°C and readings were recorded at 600 nm after 48 h. The lowest concentration showing no growth was considered as MIC. Each test was done in triplicate and optical density (OD_{600}) of peptide treated wells were compared with uninoculated wells (blank medium control).

Time Kill Assay

Purified AMPs were used to perform time kill assay against *S. aureus* MTCC 1430 as mentioned earlier (Baindara et al., 2016). Actively growing bacterial culture (0.2–0.3 OD at 600 nm) was centrifuged (10,000 rpm for 15 min at 4°C) and washed thrice with sterile PBS buffer. The pellet was suspended in PBS and subsequently treated with 2X and 5X MIC values of purified AMPs. Upon incubation for different time intervals, cells were removed from reaction mixture by centrifugation and washed with PBS buffer. Bacterial culture without AMP treatment was used as negative control. Samples were withdrawn at the end of different treatment time points starting from 0 to 8 h, bacterial cells were pelleted, serially diluted, and cell suspensions were plated on nutrient agar plates. For each treatment, negative controls were also processed under identical conditions and plated on NA. CFU at different time intervals were recorded after overnight incubation at 37°C.

Toxicity Testing

For hemolysis assay blood was collected from New Zealand white rabbit, centrifuged, washed three times, and resuspended in phosphate-buffered saline (PBS). Cells were counted using hemocytometer (adjusted to 2×10^8 cells/ml) and treated with different concentrations of peptides (between 10 and 200 μg/ml). They were incubated in a CO_2 incubator for 24 h at 37°C and processed to observe release of hemoglobin as described earlier (Singh et al., 2014). PBS and 0.1% Triton X-100 were used as agents for 0 and 100% hemolysis, respectively.

Phytotoxicity of lipopeptide was checked by treating sterilized *Vigna radiata* (Moong) seeds with different concentrations of A52 lipopeptide (20–60 μg/ml). Lipopeptide was replaced with water as control. Seeds were allowed to germinate and seedlings were maintained at room temperature under moist conditions. Seed germination (%) was recorded for treated and control seeds after 3 days of incubation (Kaur et al., 2016).

Electron Microscopic Studies

The effect of peptide on cell membrane was determined by scanning electron microscopy (SEM) and transmission electron microscopy (TEM) after treatment with AMPs. For this, test strains *S. aureus* MTCC 1430 and *C. albicans* MTCC 183 were cultured to mid-log phase in respective media. The cells were harvested by centrifugation at 10,000 × g for 10 min, washed thrice with 1X PBS, and re-suspended to adjust an OD_{600} of 0.2. The cell suspension was mixed with 2X and 5X MIC of AMPs and incubated at 37°C overnight. Following the incubation, cells were processed for SEM and TEM as described (Raje et al., 2006). The specimens were completely dried using freeze drier, coated with gold, and visualized under a scanning electron microscope (ZEISS, Germany). For TEM (JEOL, JEM 2100, United States), cells were treated with peptide, washed, and subjected to negative stain 0.1% sodium phosphotungstate (Sigma, United States) for visualization. Effect of A52 lipopeptide on fungal spore was observed through a phase contrast microscope (Nickon H600L, Japan).

Determination of Fractional Inhibitory Concentration

Fractional inhibitory concentration (FIC) testing was performed to determine the effect of A52 lipopeptide in combination with fluconazole against *C. albicans* MTCC 183. Varying concentrations of fluconazole (0.315–20 μg/ml) and A52 lipopeptide (0.375–12 μg/ml) were used individually or in combination to check the additive effect of antimicrobials. Next, to distinguish between the additive and synergistic effects, we determined the ΣFIC values (Chaturvedi et al., 2011). The interpretation of ΣFIC values was as follows: $\leq$ 0.5, synergistic; $>$ 0.5 to $<$ 4.0, indifferent (no antagonism), and $\geq$ 4.0, antagonistic.

Preparation of Emulgel Formulation

Gel base was prepared by dispersing carbopol 934 (Hi-media, India) in distilled water with constant stirring at moderate speed for overnight. Oil phase of the emulsion was made with cetomacrogol 1000, cetostearyl alcohol, white soft paraffin, propylene glycol in light liquid paraffin (Hi-media, India). Aqueous phase was prepared by dissolving peptides (0.5% w/v) in distilled water. The oily and aqueous phases were separately incubated in a water bath at 60°C. Upon obtaining uniformity, oily phase was added to the aqueous phase with

continuous stirring. Pre-heated gel base dispersion of carbopol 934 and vitamin ETPGS (Sigma, United States) were added to the emulsion steadily with continuous stirring to obtain homogenized gel. The temperature of the formulation was lowered to 40°C and isopropyl alcohol was added with continuous stirring. The pH was maintained at 6.8 ± 0.2 using saturated solution of citric acid. *In vitro* emulgel was characterized for its visual appearance under the microscope for the presence of any particle or grittiness. The pH of emulgel was determined by digital pH meter (Contech, India) by dissolving gel in distilled water. Gel extrudability or oozing out from the collapsible tube was determined by physical squeezing from a tube. Gel viscosity was measured using viscometer (Brookfield DV-l Prime, United States).

Skin Irritation Study

Skin irritation potential of lipopetide based emulgel formulation was evaluated by carrying out skin irritancy test using 8 weeks old BALB/c female mice (Draize et al., 1944). Mice dorsal surface hair was removed without damaging the skin surface about 24 h prior to the experiment. Mice were divided into three groups (n = 3): Group I: 20% sodium lauryl sulfate (SLS) solution (positive control); Group II: plain gel (negative control); and Group III: A52 emulgel. The formulation was topically applied to the hairless skin area (approximately 1 cm^2) and observations were recorded at 24, 48, and 72 h. Thus, the applied sites were observed for dermal reactions such as erythema and edema. The mean erythemal and edemal scores were recorded on the basis of their degree of severity caused by application of formulations as follows: no erythema/edema = 0, slight erythema/edema = 1, moderate erythema/edema = 2, and severe erythema/edema = 3.

Statistical Analysis

All results were obtained by performing triplicate experiments in three independent replicates and presented as the mean ± SD (standard deviation). Animal experiments were triplicates performed in two independent replicates. Statistical significance among groups (between treated and untreated groups during killing kinetics and treated and positive control groups during hemolysis) were calculated using student's t-test. A p-value of < 0.05 was considered significant ($^{*}p < 0.05$, $^{**}p < 0.005$, and $^{***}p < 0.0005$).

RESULTS

Characterization of Strain A52

A colony on nutrient agar plate showing inhibition activity was isolated and designated as A52. Microscopy examination revealed cells as Gram-positive, rod shaped, motile, and endospore forming. It was catalase positive but methyl red, citrate, and oxidase negative. Optimum growth was observed at 37°C and pH 7. It grew well in the presence of 5% NaCl concentration. Hydrolysis of esculin, starch, gelatin, and tween 20, 40, 60, and 80 was positive. BLAST analysis of strain A52 showed high identity with type species of *B. subtilis* subsp. *inaquosorum* KCTC 13429^T (99.93%), *B. tequilensis* KCTC 13622^T (99.93%), and *B. subtilis* subsp. *subtilis* NCIB 3610^T (99.86%). Neighbor-joining phylogenetic analysis of strain A52 16S rRNA gene resulted in formation of clade with *B. subtilis* subsp. *inaquosorum* KCTC 13429^T (**Figure 1A**), consistently. Nonetheless, the ANI and dDDH values obtained for *B. subtilis* subsp. *subtilis* NCIB 3610^T with strain A52 were found to be 98.43 and 86.0%. This higher identity with *B. subtilis* subsp. *subtilis* NCIB 3610^T indicates that the strain is pertaining to this subspecies. Similarly, ANI value for the other *B. subtilis* subsp. *spizizenii* TUB-10^T, *B. subtilis* subsp. *inaquosorum* KCTC 13429^T, and *B. tequilensis* KCTC 13622^T with A52 were found to be 93.07, 93.01, and 91.63%, respectively. Further, the dDDH values for *B. subtilis* subsp. *spizizenii* TUB-10^T, *B. subtilis* subsp. *inaquosorum* KCTC 13429^T, and *B. tequilensis* KCTC 13622^T with A52 were found to be 50.5, 50.10, and 44.9%, respectively. The 16S rRNA gene and draft genome sequences have been deposited at NCBI with accession numbers MT102928 and JAACYL000000000, respectively. The pangenome analysis revealed a total number of 3,710 core genes (**Figure 1B**) amongst all the closest relatives of *B. subtilis* strains that exhibited highest identity in dDDH. Maximum unique genes (332) were found in strain A52 in comparison to *B. subtilis* subsp. *subtilis* NCIB 3610^T and strain 168.

Purification and Characterization of A52 Peptides

The CFB obtained from 48 h fermented broth of strain A52 in NB showed promising activity against test strains including bacteria and fungi. Antimicrobial substance production (as measured by inhibition zone) was initiated at mid logarithmic phase (1.5 OD_{600}) and reached to the highest levels at an OD_{600} of 2.4. Likewise, strain A52 grown in minimal medium containing 1% glucose or sucrose as carbon source yielded the highest inhibition zone of 15 mm against indicator strain, *S. aureus*. Addition of starch or glycerol and peptone as carbon and nitrogen sources showed moderate antimicrobial production (12 mm). Nevertheless, antimicrobial substance production was comparable in NB (13 mm) and the same was used for large scale production (1 L) as optimized medium. In view of multiple antimicrobial production ability by strains of *B. subtilis*, the antimicrobial substance from strain A52 was extracted by two methods including Diaion HP-20 resin (reverse phase chromatography, which capture hydrophobic compounds) and ethyl acetate solvent extraction. Crude extracts obtained in both methods displayed presence of major and minor peaks in reverse phase-HPLC analysis. The major fraction collected at 24.6 min (**Figure 2A**) from Diaion HP-20 extract yielded a single band corresponding to molecular weight of 3 kDa and showed antimicrobial activity against *S. aureus* MTCC 1430 in in-gel assay (inset **Figure 2A**). The other peptide collected at RT 15.9 min (**Figure 2B**) from ethyl acetate extract also showed single band corresponding to 1 kDa. No antimicrobial activity was detected in in-gel assay, but *S. aureus* MTCC 1430 was inhibited in TLC based overlay bioautographic assay (inset **Figure 2B**). MALDI-MS analysis of purified antimicrobial peptide (peak at RT 24.6 min) displayed a mass of 3881.6 Da (**Figure 2C**). Similarly, peak at RT 15.9 min yielded strong

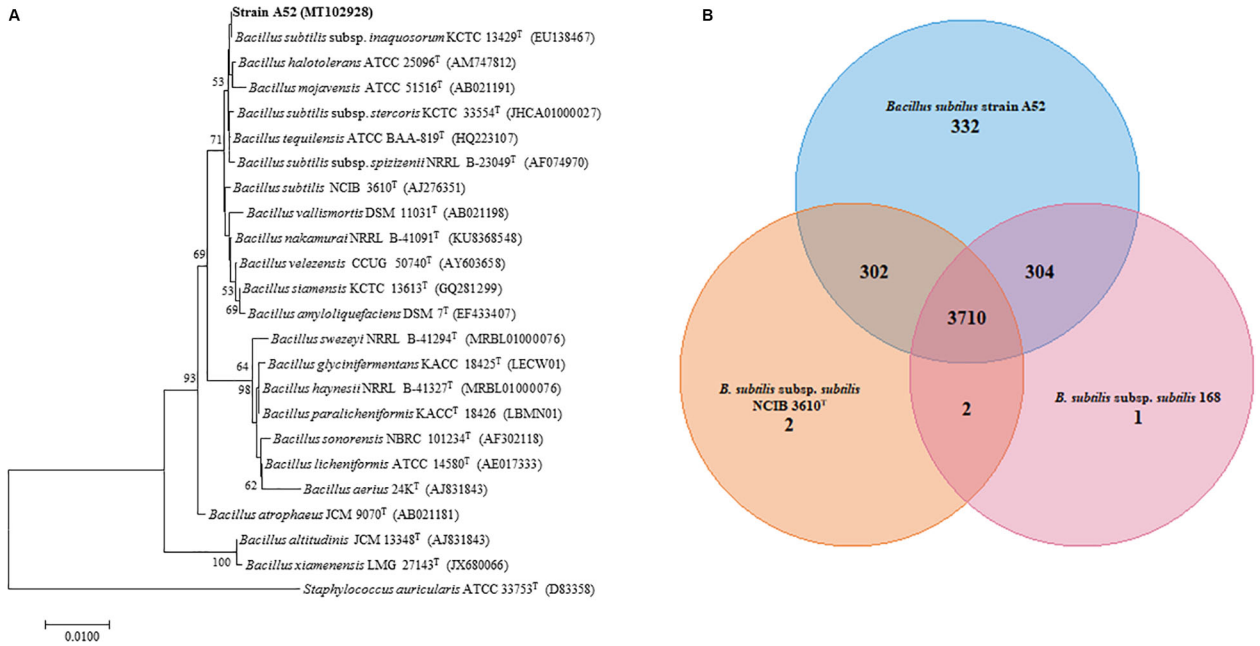

FIGURE 1 | Phylogenetic analysis to determine the taxonomic relation of strain A52. **(A)** Neighbor-joining phylogenetic tree based on 16S rRNA gene sequence of A52 and closely related members of genus *Bacillus*. It was reconstructed by computing evolutionary distances by Tamura-Nei method and expressed in the units of the number of base substitutions per site. The bootstraps values (percentage of 1,000 replicates) are indicated next to branch or nodes. Bar = 0.01nucleotide substitution per site nucleotide. **(B)** Venn diagram showing the number of unique, accessory and core genes of strain A52 along with *B. subtilis* ATCC 6051^T and *B. subtilis* subsp. *subtilis* strain 168 created. The number of unique genes of each species is shown in each corresponding circle, while the number of accessory genes is shown in the intersection area and number of core genes which is common for all strains.

signals at m/z 1061.9 and 1084.9 Da (**Figure 2D**) corresponding to protonated peptide ion $[M + H]^+$ and its sodium adduct $[M + Na]^+$. It also displayed an isomeric form of lipopeptide with m/z 1064.9 (**Supplementary Figure S1A**). Both peptides analyzed on TLC were stained with ninhydrin. Peptide with 1061.9 Da mass was also stained with phosphomolybdic acid and tested positive in CDA by exhibiting drop collapse.

Genome Sequence Analysis

The 4.22 Mb size draft genome was obtained in 59 contigs with an assembly coverage of ∼138X. The G + C content was 43.41 mol%. Analysis of genome sequence using RAST server revealed presence of 4,373 coding sequences (CDS) that contained various gene clusters including those associated with stress and electrolyte homeostasis required for adaptation of marine life, core metabolism, and synthesis of antimicrobial substances. Further, prediction of secondary metabolite biosynthesis gene clusters using antiSMASH identified the presence of eight complete biosynthetic gene clusters involved in synthesis of various antimicrobials secreted by different strains of *B. subtilis* (**Table 1**). Strikingly, peptide with mass of 3881.6 Da was matched with the mass of an antimicrobial glycocin known as sublancin 168, which showed 100% nucleotide identity with one of the biosynthetic clusters (**Figure 3A**). The other peptide with mass m/z 1061.9 Da was in agreement to the mass observed for standard surfactin (**Supplementary Figure S1B**). Consequently, the surfactin encoding non-ribosomal peptide synthatase gene cluster with 82% identity in strain A52 was analyzed in detail (**Figure 3B**). Furthermore, MS/MS fragmentation pattern resulted in formation of product ion at m/z 705.5, which is presumed to the loss of $[Glu + Ile/Leu + Leu + H]^+$, ion at m/z 609.2 $[Val + H]^+$, and ion at m/z 493.3 $[Asp + H]^+$ from precursor ion m/z 1061.7 Da (**Figure 3C**). The *de novo* sequence hypothesized for surfactin-like lipopeptide was in alignment with the presence of non-ribosomal synthetases encoding 7 amino acids including Glu^1-Leu/Ile^2-Leu^3-Val^4-Asp^5-Leu^6-Leu/Ile^7 and a β-OH hexadecane fatty acid chain.

Minimum Inhibitory Concentration, Killing Kinetics, and FIC

Sublancin purified from strain A52 showed activity against Gram-positive bacteria including various clinical strains of *Streptococcus* with MIC concentrations ranging between 2 and 10 μg/ml (**Table 2**). However, growth of few *Bacillus* species like *B. firmus* (MTCC 488), *B. licheniformis* (MTCC 429), *B. thuringiensis* (MTCC 1953) was not inhibited. No activity was detected against *E. coli* MTCC 1610 or fungal test strains. In contrast, surfactin-like lipopeptide showed broad spectrum antibacterial activity. Also, inhibited all test strains belonging to *Candida* and filamentous fungi (**Supplementary Figure S2**). The MIC values against bacterial indicator strains were lesser than sublancin (**Table 2**). Additionally, it was active against fluconazole resistant strains of *Candida* and filamentous fungi with MIC between 12 and 35 μg/ml (**Table 2**). Bactericidal kinetic

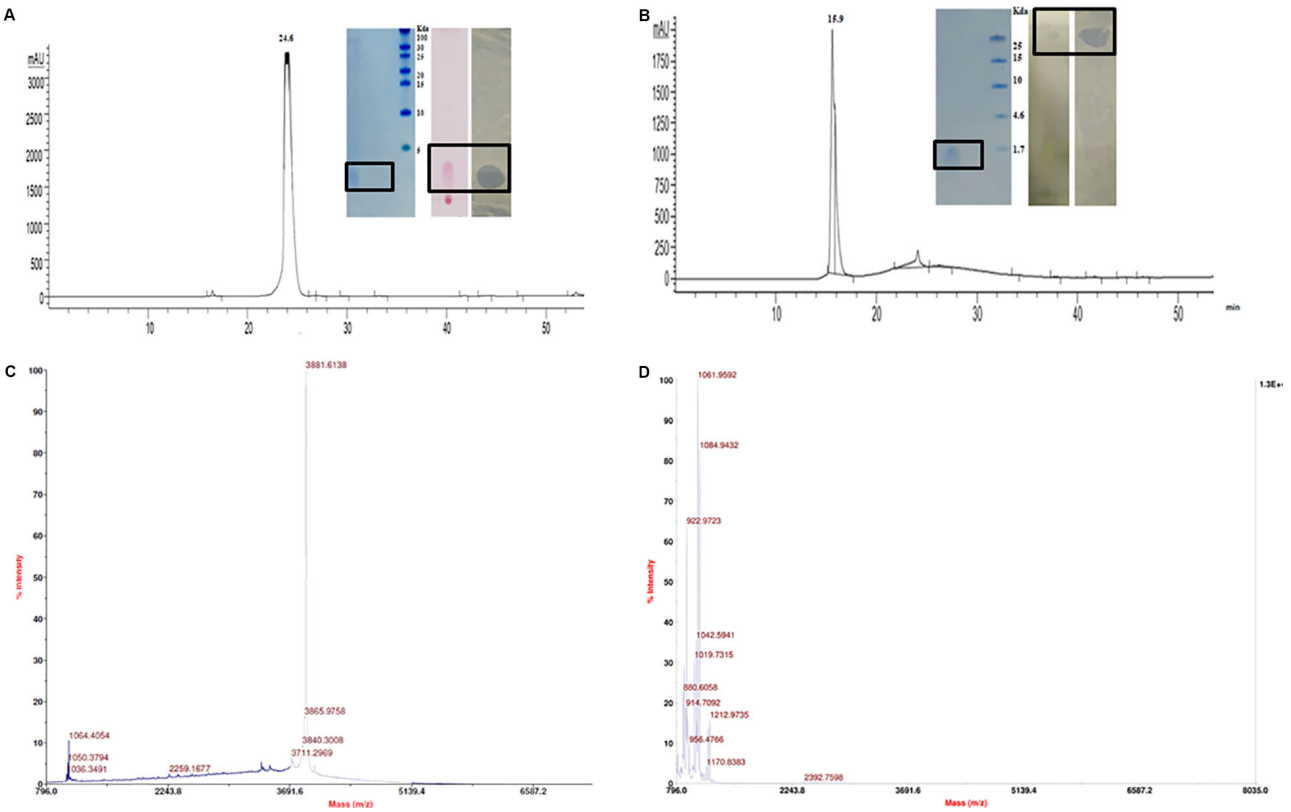

FIGURE 2 | Purification and characterization of antimicrobial peptides. **(A)** RP-HPLC profile of peptide inset showing Tricine–SDS-PAGE of peptide, TLC stained with ninhydrin and bioautography demonstrating a clear inhibition zone against *S. aureus*. **(B)** RP-HPLC profile of lipopeptide inset showing Tricine–SDS-PAGE of lipopeptide, TLC of with Phosphomolybdic acid and bioautography demonstrating a clear inhibition zone against *S. aureus*. **(C)** MALDI analysis of peptide **(D)** MALDI analysis of lipopeptide.

TABLE 1 | Different secondary metabolite clusters present in strain A52 and its closely related spp. (1) Strain A52, (2) *B. subtilis* subsp. *subtilis* strain 168, (3) *B. subtilis* subsp. *spizizenii* strain TUB-10^T, (4) *B. subtilis* subsp. *inaquosorum* KTCC 13429^T, (5) *B. tequilensis* KTCC 13622^T.

S. No.	Antimicrobial peptides	Class of antimicrobials	1	2	3	4	5	Peptide mass (Da)	References
1	Subtilosin A	Sactipeptide	+	+	+	+	+	3015.5	Babasaki et al., 1985
2	Bacilysin	NRPS dipeptide	+	+	+	+	+	271.1	Phister et al., 2004
3	Subtilin	Lanthipeptide	+	−	+	−	−	3321.7	Parisot et al., 2008
4	Bacillibactin	Siderophore	+	+	+	+	+	881.2	May et al., 2001
5	Sublancin 168	Lanthipeptide	+	+	−	−	−	3880.7*	Oman et al., 2011
6	Bacillaene	Polyene antibiotic	+	+	+	+	−	581.3	Butcher et al., 2007
7	Fengycin	Lipopeptide	+	+	−	+	+	1443.7	Villegas-Escobar et al., 2013
8	Surfactin	Lipopeptide	+	+	+	+	+	1058.6	Villegas-Escobar et al., 2013

**Molecular weight of reduced peptide.*

studies of sublancin A52 (5X MIC) using cells of *S. aureus* MTCC 1430 revealed reduction of bacterial load completely after 8 h of treatment (**Figure 4A**) whereas lipopeptide (5X MIC) showed complete killing of *S. aureus* MTCC 1430 within 7 h of treatment (**Figure 4B**). No reduction in CFU count was noticed for negative controls. A combination of the surfactin-like lipopeptide and fluconazole was found to reduce MIC of fluconazole against *C. albicans* MTCC 183. Remarkably, the treatment in combination led to four times decrease in the MIC of fluconazole in the presence of A52 surfactin-like lipopeptide (**Figure 4C**), suggesting their combinatorial effect to be synergistic (ΣFIC = 0.375).

Temperature and Enzyme Sensitivity

Sublancin from strain A52 was found to be stable up to 70°C and lost activity completely after autoclaving. It was also stable between pH 4.0 and 10.0. On the other hand, antimicrobial activity of the surfactin-like lipopeptide from strain A52 was not affected upon exposure to 100°C, but retained 89.0% activity after autoclaving (121°C for 15 min). It was found to be stable between

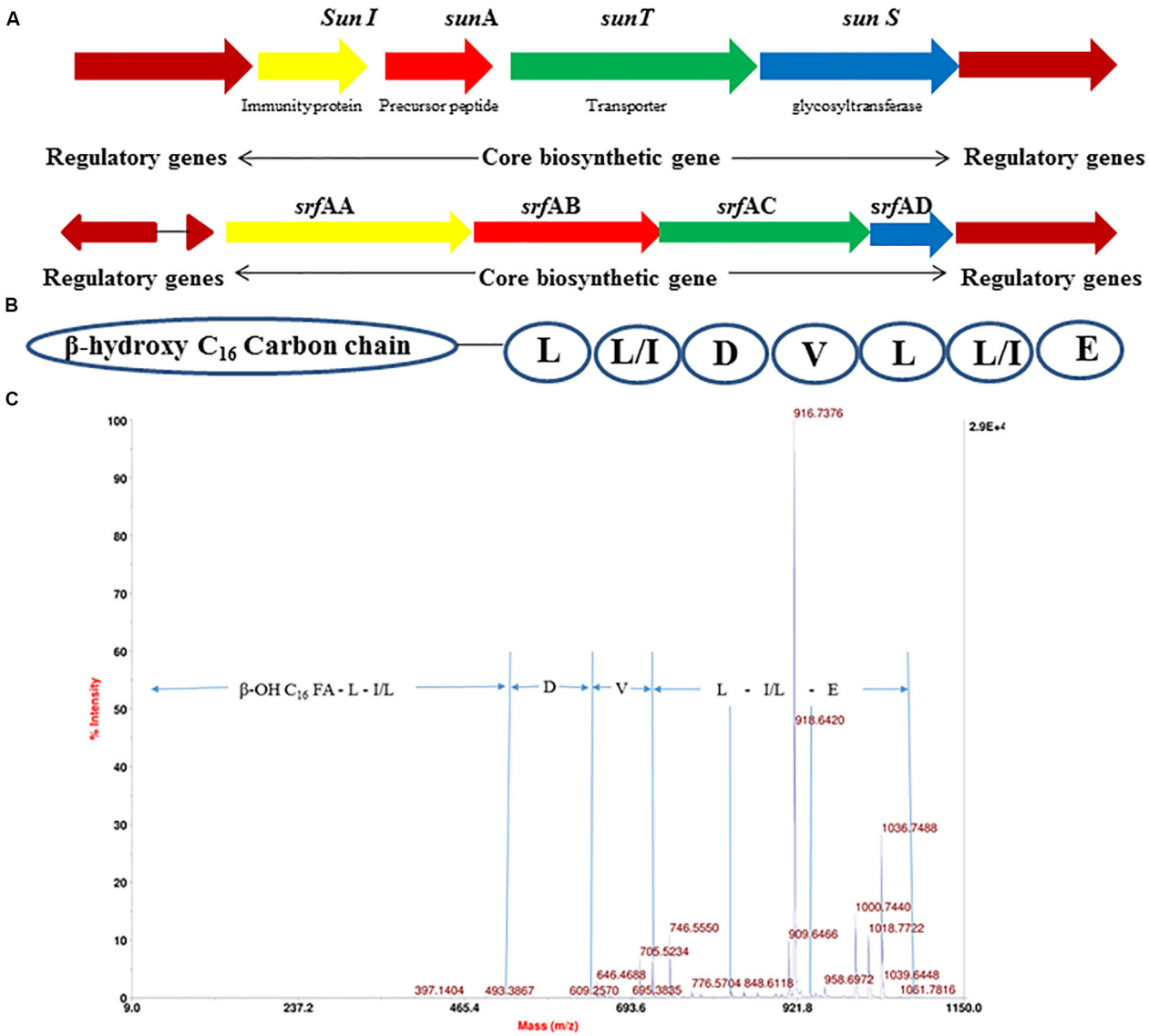

FIGURE 3 | Gene cluster of antimicrobial peptides from strain A52 genome sequence involved in biosynthesis of **(A)** sublancin, **(B)** surfactin, **(C)** fragmentation spectrum of surfactin isoform $[M + H]^+$ at m/z 1061.7 Da.

pH 4.0 and 10.0, however, complete loss in activity was noticed at pH 2.0 and 11.0. Studies on tolerance of the peptide to proteolytic enzymes revealed that both peptides were resistant to trypsin and proteinase K treatment (**Supplementary Table S1**). Additionally, lipopeptide was found to be stable to lipase treatment.

Microscopic Examination of Pathogens After Peptides Treatment

The images of untreated *S. aureus* cells showed smooth cell surface and appeared to be healthy and intact. The sublancin A52 treated cells showed altered morphology and shrinkage in TEM images, whereas the surfactin-like lipopeptide treated cells showed cell wall irregularities such as wall rupturing and cellular lysis (**Figures 5A,B**). Similarly, SEM images of surfactin-like lipopeptide treated *C. albicans* cells showed structural irregularity with disintegrated outer cell membrane resulting in dispersion of the intracellular contents while the control cells showed complete cell membrane and homogeneous cytoplasm (**Figure 5C**).

Hemolysis and Phytotoxicity

Sublancin from strain A52 did not show any hemolytic activity even at the 5X MIC concentration (**Figure 6A**) but surfactin-like lipopeptide demonstrated hemolytic activity at 1X MIC concentration (**Figure 6B**), which is almost equivalent to the activity shown by 1% Triton X-100. Surfactin-like lipopeptide was also able to lyse the spores formed by phytopathogenic fungus *A. brassicicola* MTCC 2102 (**Figure 6C**). It did not exhibit phytotoxicity in seed germination assay against *Vigna radiata*

TABLE 2 | MIC values of surfactin-like lipopeptide and sublancin from strain A52 against various test strains of bacteria, yeast, and filamentous fungi.

S. No.	Test organism	Strain number	MIC value (μg/ml)[$]				
			Fluconazole*	Amphotericin B*	Ampicillin[†]	Lipopeptide A52	Sublancin[#]
	Yeast						
1	*C. albicans*	MTCC 183	20	5	–	12	–
2	*C. albicans*	MTCC 1637	R	5	–	28	–
3	*C. albicans*	MTCC 227	R	5	–	24	–
4	*C. tropicalis*	MTCC 184	R	35	–	12	–
5	*C. glabrata*	MTCC 3019	R	25	–	16	–
6	*C. haemulonii*	MTCC 2766	R	100	–	20	–
7	*C. inconsplicue*	MTCC 1074	50	10	–	16	–
	Clinical Isolates						
8	*C. aurius*	470126	R	5	–	26	–
9	*C. rugos*	470141	5	5	–	16	–
10	*C. kefyr*	410004	R	50	–	26	–
11	*C. krusei*	440009	1	5	–	12	–
12	*C. albicans*	400054	R	5	–	16	–
13	*C. tropicalis*	420024	R	50	–	28	–
14	*C. parasilosis*	450030	10	50	–	28	–
15	*C. glabrata*	SKSS ID	R	100	–	16	–
16	*C. haemulonii*	470125	R	50	–	28	–
	Fungus						
17	*A. brassicicola*	MTCC 2102	R	50	–	25	–
18	*C. acutatum*	MTCC1037	R	R	–	35	–
19	*F. moniliforme*	MTCC 158	10	50	–	20	–
	Bacteria						
20	*S. aureus*	MTCC 1430	–	–	0.25	4	10
21	*B. subtilis*	MTCC 121	–	–	0.50	2	5
22	*B. cereus*	MTCC 430	–	–	0.50	2	5
23	*B. coagulans*	MTCC 492	–	–	0.50	2	8
24	*S. pyogenes*	MTCC 1928	–	–	0.03	2	2
25	*S. anginosus*	MTCC1929	–	–	0.25	4	6
26	*S. oralis*	MTCC 2696	–	–	0.40	4	8
27	*S. mutans*	MTCC 497	–	–	0.40	6	10
28	*M. luteus*	MTCC 106	–	–	0.20	1	2
29	*E. coli*	MTCC 1610	–	–	1.0	6	–

**Antifungal compounds that have no activity against bacteria. [†]Antibacterial broad spectrum. [#]Reported as narrow spectrum antibiotic by Paik et al. (1998). [$]Each test done in triplicate and optical density (OD_{600}) of antimicrobial peptide treated wells were compared with uninoculated wells (blank medium control).*

(Moong) seeds even at 60 μg/ml concentration. Indeed, there was no difference observed in germination and seedling formation between test and control (**Figure 6D**).

Emulgel Formulation and Properties

For preparation of emulgel, 50 mg of surfactin-like lipopeptide was dissolved in water and added to 10 g of emulgel formulation to make a final concentration of 0.5% w/w. The optimized chemical composition (%) used in the preparation of emulgel was propylene glycol (15.0%), cetomacrogol 1000 (2.5%), cetostearyl alcohol (7.5%), white soft paraffin (10.0%), liquid paraffin (2.5%), vitamin E TPGS (5.0%), carbopol 934 (0.5%), isopropyl alcohol (1.0%), and water (55.5%). *In vitro* assessment of emulgel formulation containing surfactin-like lipopeptide exhibited activity against *M. luteus* MTCC 106 and *C. albicans* MTCC 183 (**Supplementary Figure S3**). Individual testing of the above compounds at employed concentrations did not show antimicrobial activity against test strains. The emulgel was opaque and creamish in its appearance. The pH of emulgel was found to be 6.8 ± 0.2 and showed good extrudability. The viscosity of emulgel containing 0.5% w/w of carbopol was found to be 1451cP.

Skin Irritation Study

Results of skin irritancy of surfactin-like lipopeptide containing emulgel formulation determined using Draize test are summarized in **Supplementary Table S2**. The emulgel did not show any type of irritation as observed at time intervals of 24, 48, and 72 h after application. Dryness, hardening, and redness of skin was noticed at the site of SLS application which is known to cause irritation (**Figure 7A**). No effect was detected in negative control (**Figure 7B**). The results of emulgel formulation

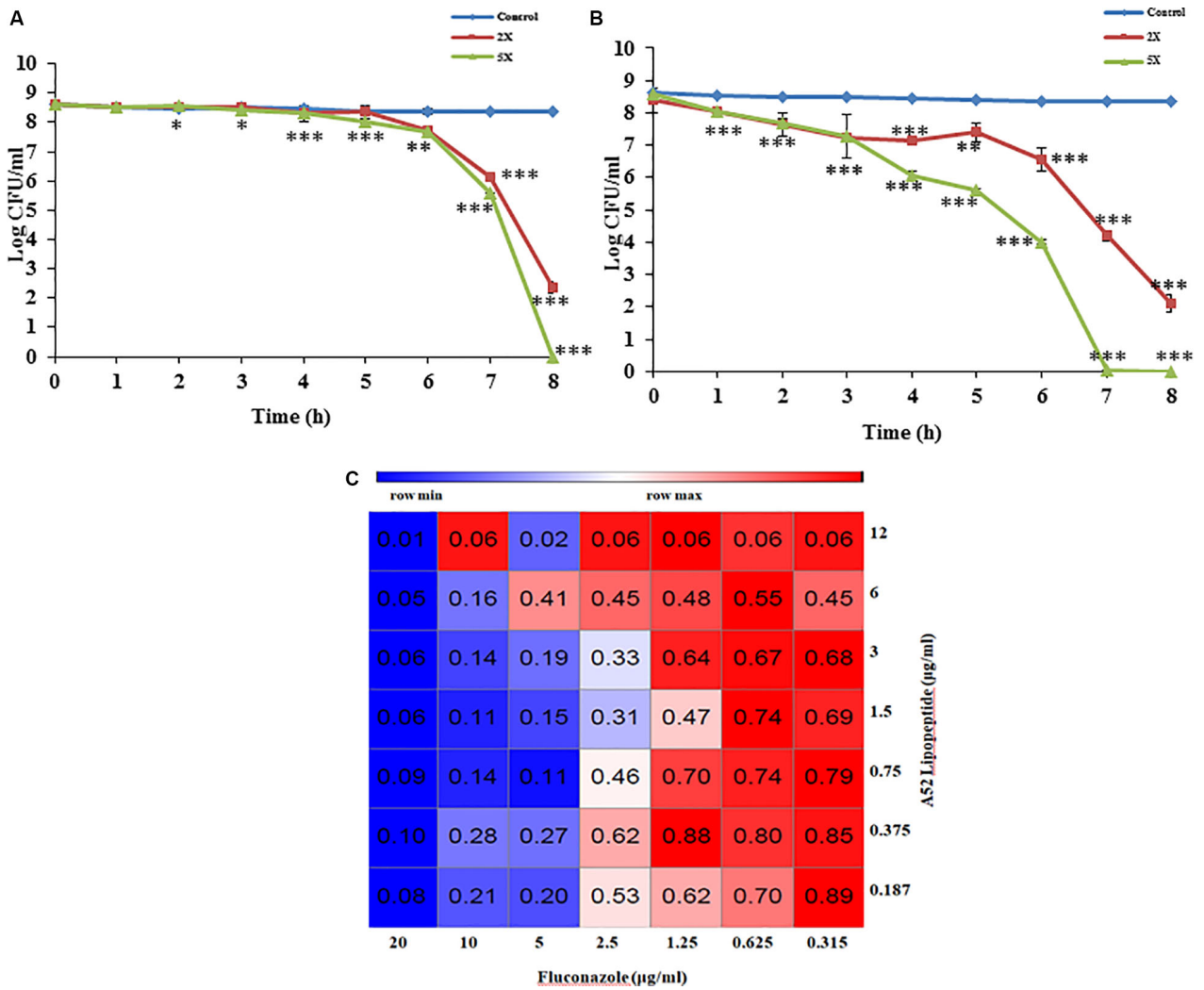

FIGURE 4 | Antimicrobial peptide mediated growth inhibition studies. **(A)** Killing kinetics of sublancin A52 (2X and 5X MIC) against *S. aureus* MTCC 1430. **(B)** Killing kinetics of surfactin-like lipopeptide (2X and 5X MIC) against *S. aureus* MTCC 1430. **(C)** The heat-map showing combination of surfactin-like lipopeptide from A52 and fluconazole inhibitory activity against indicator strain *C. albicans* MTCC 183. Addition lipopeptide (0.75 µg/ml) led to fourfold (2.5 µg/ml) decrease in MIC of fluconazole. The heat-map was generated using the morpheus software. *$p < 0.05$, **$p < 0.005$, and ***$p < 0.0005$.

application on skin was found to be similar with negative control (**Figure 7C**). There were no irritation symptoms observed even after 72 h upon application.

DISCUSSION

Increased resistance to antibiotics has resulted in difficulty to eliminate nosocomial and chronic infections. In the quest to develop novel antimicrobial agents, the marine ecosystem is favored environmental niche owing to the presence of diverse antimicrobial substances (Desjardine et al., 2007; Baindara et al., 2013; Ponnappan et al., 2015; Agrawal et al., 2017; Gupta et al., 2019). Therefore, in this study, we have explored a marine sediment bacterial isolate for antimicrobial production ability. Strain A52 was identified as a member of the genus *Bacillus,* taxonomically related to species *B. subtilis* (Tareq et al., 2014) and *B. tequilensis* (Rani et al., 2016). The ANI and dDDH of A52 genome sequence showed highest identity with *B. subtilis* subsp. *subtilis* NCIB 3610^T and followed by strain 168 (98.4 and 85.9%, respectively). Strain A52 mainly differed with both strains in number of unique genes, mostly involved in adaptation to marine environment. RAST, and bioinformatics analyses of genome sequence revealed the ability of strain A52 to produce multiple antimicrobials. Thus, strain A52 was grown in the presence of different carbon and nitrogen sources to test the possibility of multiple antimicrobials production as mentioned in **Table 1**. Since crude extract inhibited the growth of indicator strains pertaining to Gram-positive, Gram-negative bacteria, and *Candida*, we have analyzed the extract (including extracts from NB and MM with 1% glucose) on HPLC and detected the presence of two compounds with different spectrum of

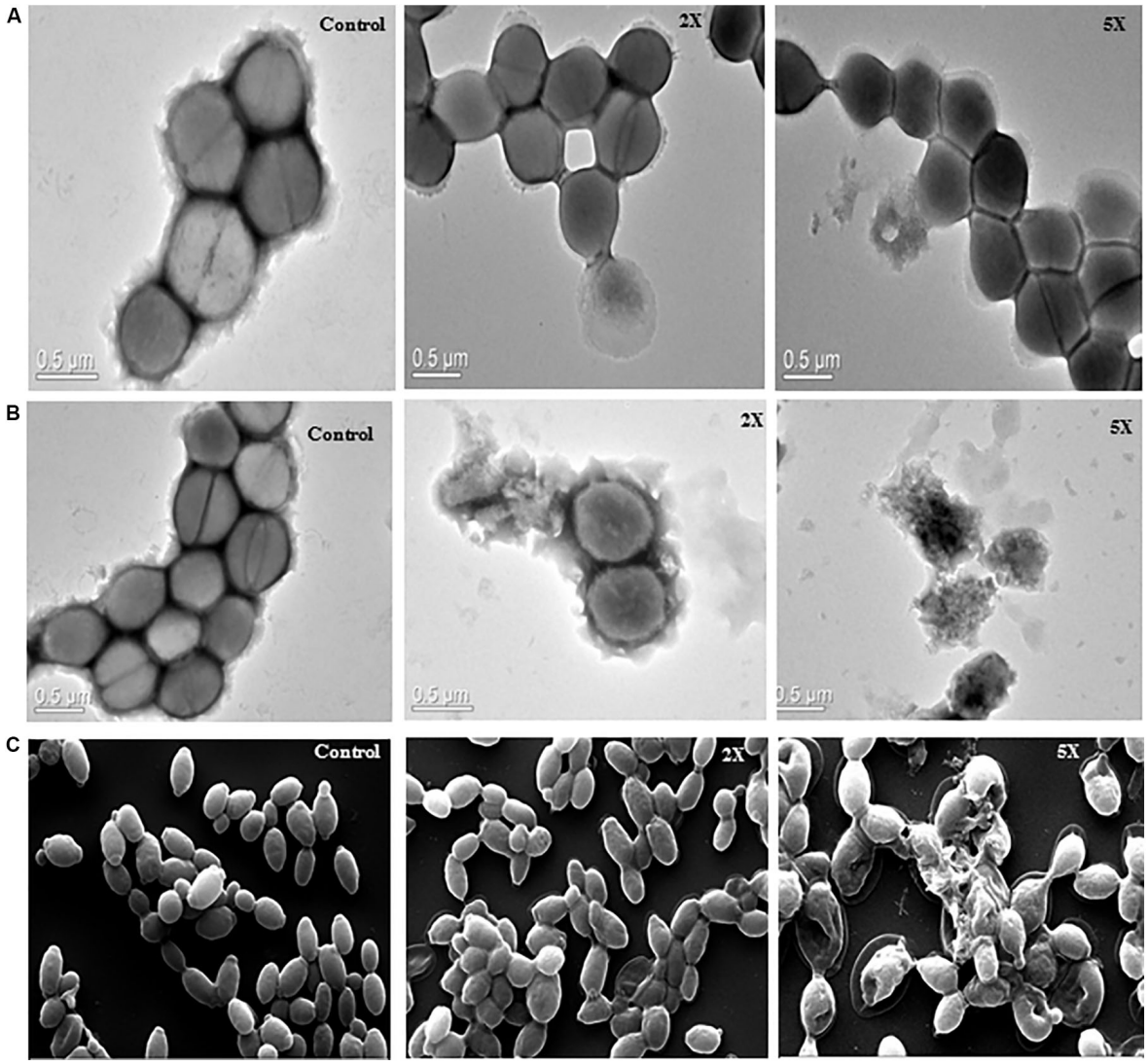

FIGURE 5 | Transmission electron microscopy images **(A)** sublancin A52 treated *S. aureus* MTCC 1430 cells, **(B)** surfactin-like lipopeptide treated *S. aureus* MTCC 1430 cells, **(C)** scanning electron microscopy images of *C. albicans* MTCC 183 (magnification 10000x) after treatment with A52 lipopeptide.

antimicrobial activity. Both purified compounds analyzed on TLC were stained with ninhydrin, indicating possible peptide nature of compounds. The low molecular weight compound stained with phosphomolybdic acid yielding a bluish black band, exposed association of a lipid group with the peptide. Lipopeptide presence was also confirmed with the increased surface diameter in collapse drop assay.

The validated mass of 3881 Da as detected for peptide from strain A52 is in alignment with the mass 3880.78 Da of reduced sublancin, a glycocin antimicrobial peptide produced by closest relative *B. subtilis* strain 168 (Oman et al., 2011; Wang et al., 2017). The reduced nature of peptide in this study is assumed to be due to the presence of acentonitrile in 0.1% TFA (Erlandsson and Hallbrink, 2005) as the peptide was not freeze dried to remove the solvent upon HPLC purification. The minor difference in mass may be due to instrument error (50 ppm deviation). Since sublancin belongs to the class of glycocins, which contains an unusual and essential glucosylated Cys residue (Gonzalo et al., 2014; Ji et al., 2015; Wang et al., 2017; Wu et al., 2019), we have verified the presence of sugar residue using α-naphthol reagent and confirmed the peptide as sublancin. Furthermore, the peptide inhibited the growth of only Gram-positive bacteria as described for sublancin (Oman et al., 2011). Number of Gram-positive test strains used for antimicrobial assay showed the ability of sublancin to kill various species of the genus *Bacillus* with few exceptions owing to the fact that sensitivity of various strains to the same bacteriocin is highly variable (Rasch and Knøchel, 1998). Sublancin is also reported to inhibit growth of methicillin resistant *Staphylococcus aureus* (MRSA) and showed protective ability in mice infection studies (Wang et al., 2017). TEM imaging of *S. aureus* cells treated with sublancin from A52 provided clear evidence that it possesses

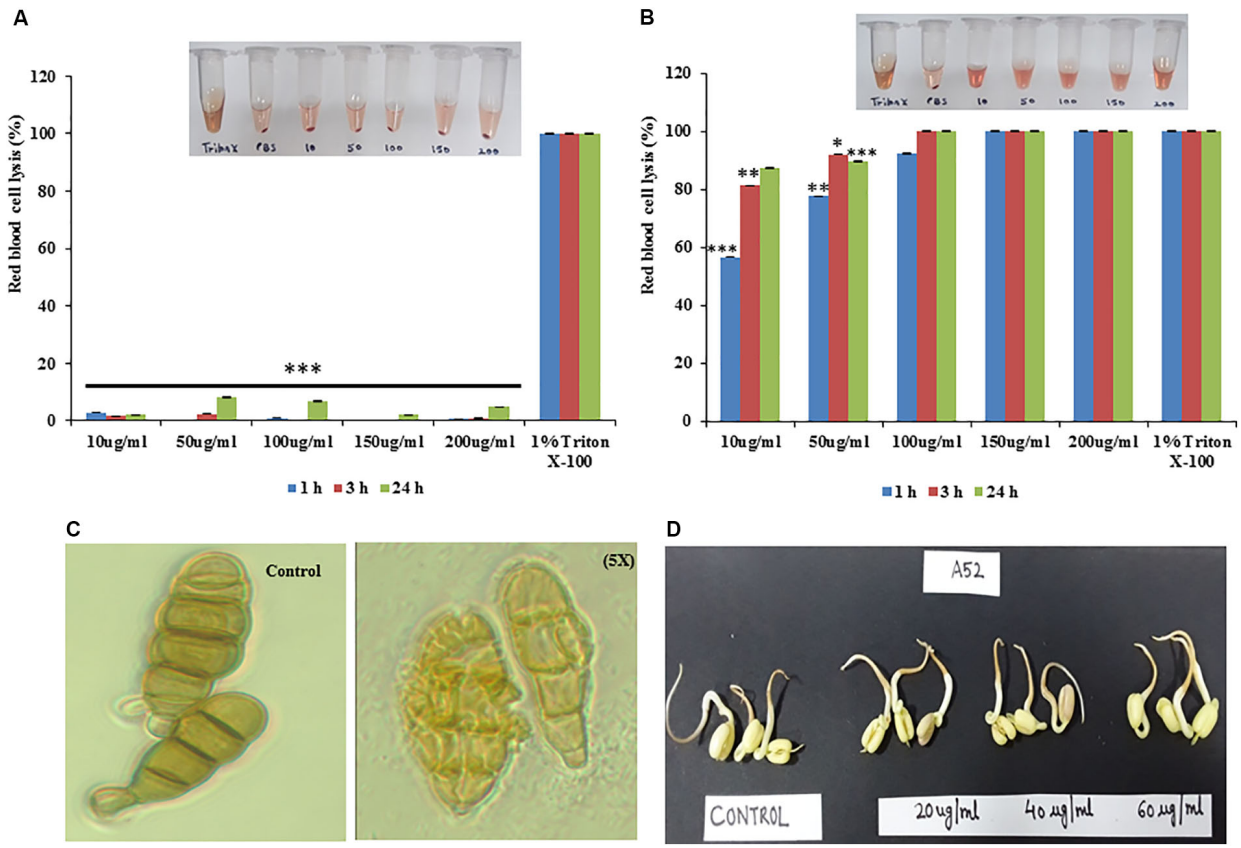

FIGURE 6 | Hemolytic properties of antimicrobial peptides from strain A52 **(A)** sublancin, **(B)** surfactin-like lipopeptide, **(C)** effect of surfactin-like lipopeptide on *A. brassicicola* spore, **(D)** Phytotoxicity of surfactin-like lipopeptide on seeds germination of *Vigna radiata*. $^{*}p < 0.05$, $^{**}p < 0.005$, and $^{***}p < 0.0005$.

bactericidal activity without cell lysis (**Figure 5A**), which is in accordance with recently studied mode of action of sublancin that reported negative effect on DNA replication, transcription, and translation (Wu et al., 2019). The thermal stability, broad pH range, and resistance to proteinase K and trypsin are in accordance with results observed earlier (Ji et al., 2015).

Likewise, the antiSMASH analysis for strain A52 genome sequence highlighted presence of a NRPS encoding genes with 82% nucleotide sequence identity to biosynthetic gene cluster involved in surfactin biosynthesis. As shown in mass spectrometry lipopeptide has a molecular weight of 1061 Da, which falls within the range of observed mass for surfactants. Combining the data from genes encoding NRPS clusters and mass obtained, we hypothesized that the lipopeptide consists of 7 amino acids as shown by the presence of specific synthetases which are commonly found in surfactin biosynthesis (Ma et al., 2016; Chen et al., 2017). The fatty acid moiety was identified as β-OH palmitic acid chain that has not been reported in surfactins produced by *B. subtilis* strains. Unlike other surfactins, the lipopeptide was found to be highly thermostable as it retained activity even after autoclaving. No reduction in activity was observed upon incubation with proteases or lipase. These results are in line with earlier reported lipopeptide properties in literature (Sharma et al., 2014; Jha et al., 2016; Chen et al., 2017).

Strikingly, surfactin-like lipopeptide produced by strain A52 showed broad spectrum antimicrobial activity against bacteria at low concentrations. Though inhibition of phytopathogenic fungi required higher concentrations, it was lesser than 25 μM that is generally employed to screen antifungal peptides and lipopeptides (Mircus et al., 2015). Earlier reports show that antimicrobial spectrum of lipopeptides were purely dependent on the length of their fatty acid moiety (Strieker and Marahiel, 2009; Mandal et al., 2013; Meir et al., 2017). Thus, it is pertinent to mention that the presence of different fatty acid resulted in broad spectrum antibacterial, anticandidial, and antifungal activities. SEM and TEM imaging of surfactin-like lipopeptide treated cells showed disruption of membrane due to possible pore formation resulting in scattering of cellular contents in their surroundings (**Figure 5**). This membrane lysis mechanism of action of lipopeptides makes the pathogens highly susceptible by decreasing the ability to develop resistance (Mangoni and Shai, 2011). In fact, surfactant-like lipopeptide was able to inhibit fluconazole resistant *Candida* by lowering the MIC of fluconazole in a synergistic combination. These results suggest that combined usage of the active compound with existing drugs shall contribute toward lowering the adverse effects associated with antifungal agents, while maintaining the effectiveness of the drug.

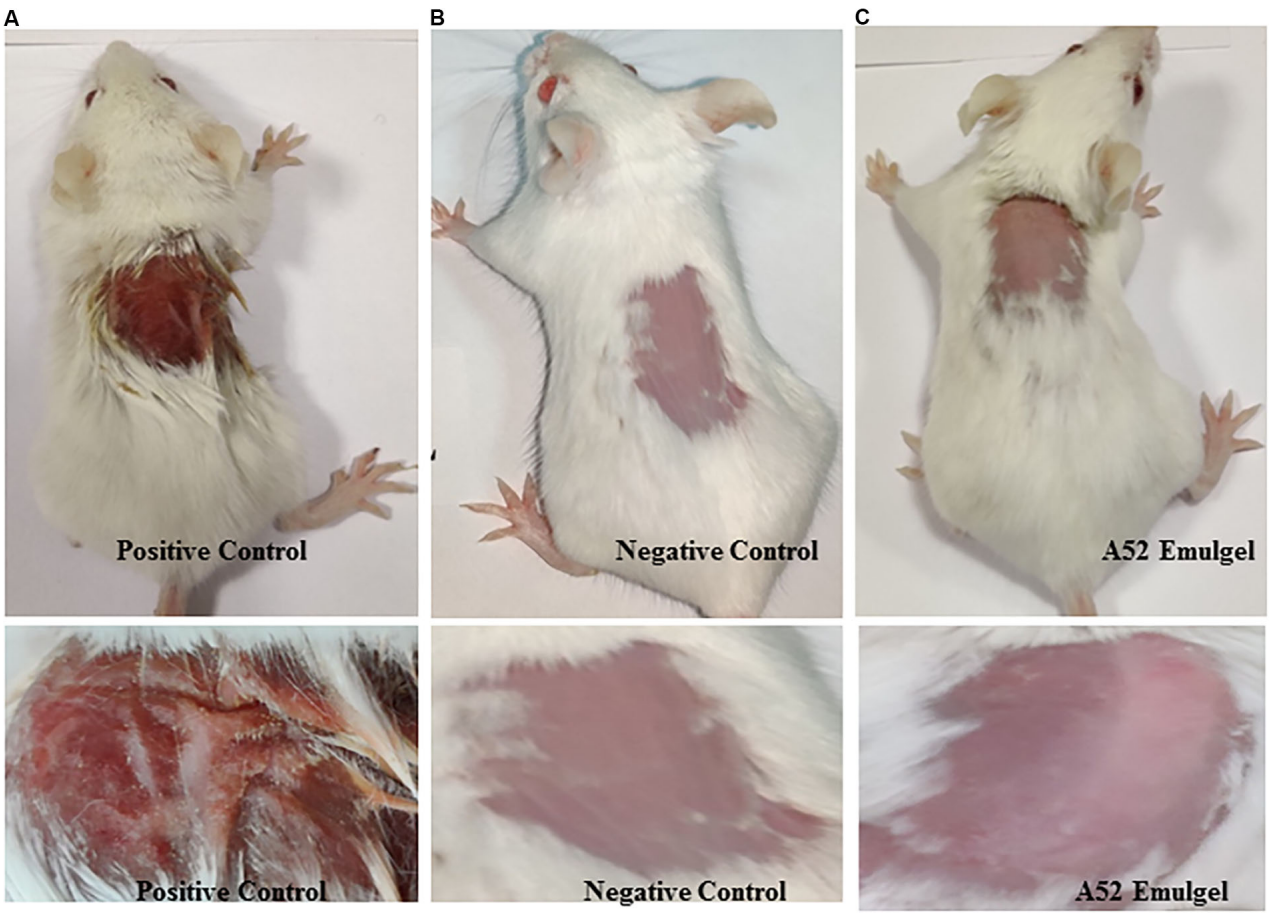

FIGURE 7 | Skin irritation study results at 72 h **(A)** positive control, 20% SLS treated, **(B)** negative control, plain gel, and **(C)** treated with emulgel containing surfactin-like lipopeptide.

For commercial application of biologically active compounds, it is imperative to explore their toxigenic potential for the relevant applications. Though lipopeptides cause hemolysis (Inès and Dhouha, 2015; Greber et al., 2018; Ramachandran et al., 2018), surfactin-like lipopeptide in this study showed promising potential for topical applications as evident from the emulgel experiment. The gel showed antimicrobial activity and did not show any skin irritation effect during experiment with BALB/c mice. Further, it was explored for phytotoxicity, where it showed no adverse effects in the seed germination process. Thus it may be developed as a crop-protective agent for use in agriculture field, but only upon detailed experiments, which are beyond the scope of this study. Considering broad activity with low MIC values and thermos-stability, surfactin-like lipopeptide secreted by strain A52 was found to be an appealing candidate for potential application as a topical therapeutic agent.

CONCLUSION

A novel broad spectrum antifungal lipopeptide has been reported from *B. subtilis* strain A52 isolated from marine sediment. It is simultaneously expressed with a well-known bacteriocin sublancin. The 1061.9 Da surfactin-like lipopeptide is highly effective against a diverse array of human and plant pathogenic fungi and has a broad spectrum antibacterial activity. Essentially, surfactin-like lipopeptide has shown synergistic activity with contemporary antifungal agent fluconazole, suggesting its promising role as a topical therapeutic agent.

DATA AVAILABILITY STATEMENT

The datasets generated for this study can be found in the genome sequence accession no. JAACYL000000000 and 16S rRNA gene sequence accession no. MT102928.

ETHICS STATEMENT

The animal study was reviewed and approved by the Institutional Animal Ethics Committee, Committee for the Purpose of Control and Supervision of Experiments on Animals approval no. 18/08.

AUTHOR CONTRIBUTIONS

DS, SSS, NK, and SK designed experiments. DS, SSS, PB, SS, PBP, NK, and SK performed experiments. DS, SSS, VG, PBP, and SK analyzed data. DS, SSS, VG, and SK prepared the manuscript.

FUNDING

This research was supported by grants from the Department of Science and Technology (DST), New Delhi, India (DS fellowship SR/WOS-A/LS-220/2017), SERB, DST, and CSIR, Government of India.

ACKNOWLEDGMENTS

We acknowledge the help of Dr. Lakhvir Kaur (Asst. Prof.), Department of Pharmaceutics Khalsa College of Pharmacy, Amritsar (India), for providing viscosity data of emulgel. We acknowledge technical help from Ms. Megha Sharma and we thank Dr. S. M. Mondal for standard surfactin analysis.

SUPPLEMENTARY MATERIAL

The Supplementary Material for this article can be found online at: https://www.frontiersin.org/articles/10.3389/fmicb.2020.01167/full#supplementary-material

REFERENCES

Abriouel, H., Franz, C. M., Omar, N. B., and Gálvez, A. (2011). Diversity and applications of *Bacillus* bacteriocins. *FEMS Microbiol. Rev.* 35, 201–232. doi: 10.1111/j.1574-6976.2010.00244.x

Agrawal, S., Acharya, D., Adholeya, A., Barrow, C. J., and Deshmukh, S. K. (2017). Nonribosomal peptides from marine microbes and their antimicrobial and anticancer potential. *Front. Pharmacol.* 8:828. doi: 10.3389/fphar.2017.00828

Alajlani, M., Shiekh, A., Hasnain, S., and Brantner, A. (2016). Purification of bioactive lipopeptides produced by *Bacillus subtilis* strain BIA. *Chromatographia* 79, 1527–1532. doi: 10.1007/s10337-016-3164-3

Alanis, A. J. (2005). Resistance to antibiotics: Are we in the post-antibiotic era? *Arch. Med. Res.* 36, 697–705. doi: 10.1016/j.arcmed.2005.06.009

Arnison, P. G., Bibb, M. J., Bierbaum, G., Bowers, A. A., Bugni, T. S., Bulaj, G., et al. (2013). Ribosomally synthesized and post-translationally modified peptide natural products: overview and recommendations for a universal nomenclature. *Nat. Prod. Rep.* 30, 108–160. doi: 10.1039/c2np20085f

Babasaki, K., Takao, T., Shimonishi, Y., and Kurahashi, K. (1985). Subtilosin A, a new antibiotic peptide produced by *Bacillus subtilis* 168: isolation, structural analysis, and biogenesis. *J. Biochem.* 98, 585–603. doi: 10.1093/oxfordjournals.jbchem.a135315

Baindara, P., Chaudhry, V., Mittal, G., Liao, L. M., Matos, C. O., Khatri, N., et al. (2016). Characterization of the antimicrobial peptide penisin, a class Ia novel lantibiotic from *Paenibacillus* sp. strain A3. *Antimicrob. Agents Chemother.* 60, 580–591. doi: 10.1128/AAC.01813-15

Baindara, P., Mandal, S. M., Chawla, N., Singh, P. K., Pinnaka, A. K., and Korpole, S. (2013). Characterization of two antimicrobial peptides produced by a halotolerant *Bacillus subtilis* strain SK. DU. 4 isolated from a rhizosphere soil sample. *AMB Express* 3:2. doi: 10.1186/2191-0855-3-2

Berrue, F., Ibrahim, A., Boland, P., and Kerr, R. G. (2009). Newly isolated marine *Bacillus pumilus* (SP21): a source of novel lipoamides and other antimicrobial agents. *Pure Appl. Chem.* 81, 1027–1031. doi: 10.1351/PAC-CON-08-09-25

Butcher, R. A., Schroeder, F. C., Fischbach, M. A., Straight, P. D., Kolter, R., Walsh, C. T., et al. (2007). The identification of bacillaene, the product of the PksX megacomplex in *Bacillus subtilis*. *Proc. Natl. Acad. Sci. U.S.A.* 104, 1506–1509. doi: 10.1073/pnas.0610503104

Chaturvedi, A. K., Engels, E. A., Pfeiffer, R. M., Hernandez, B. Y., Xiao, W., Kim, E., et al. (2011). Human papillomavirus and rising oropharyngeal cancer incidence in the United States. *J. Clin. Oncol.* 29, 4294–4301. doi: 10.1200/JCO.2011.36.4596

Chen, Y., Liu, S. A., Mou, H., Ma, Y., Li, M., and Hu, X. (2017). Characterization of lipopeptide biosurfactants produced by *Bacillus licheniformis* MB01 from marine sediments. *Front. Microbiol.* 8:871. doi: 10.3389/fmicb.2017.00871

Dagi, H. T., Findik, D., Senkeles, C., and Arslan, U. (2016). Identification and antifungal susceptibility of *Candida* species isolated from bloodstream infections in Konya. Turkey. *Ann. Clin. Microbiol. Antimicrob.* 15:36. doi: 10.1186/s12941-016-0153-1

Davies, J., and Davies, D. (2010). Origins and evolution of antibiotic resistance. *Microbiol. Mol. Biol. Rev.* 74, 417–433. doi: 10.1128/MMBR.00016-10

Debbab, A., Aly, A. H., Lin, W. H., and Proksch, P. (2010). Bioactive compounds from marine bacteria and fungi. *Microb. Biotechnol.* 3, 544–563. doi: 10.1111/j.1751-7915.2010.00179.x

Desjardine, K., Pereira, A., Wright, H., Matainaho, T., Kelly, M., and Andersen, R. J. (2007). Tauramamide, a lipopeptide antibiotic produced in culture by *Brevibacillus laterosporus* isolated from a marine habitat: structure elucidation and synthesis. *J. Nat. Prod.* 70, 1850–1853. doi: 10.1021/np070209r

Draize, J. H., Woodard, G., and Calvery, H. O. (1944). Methods for the study of irritation and toxicity of substances applied topically to the skin and mucous membranes. *J. Pharmacol. Exp. Ther.* 82, 377–390.

Eksi, F., Gayyurhan, E. D., and Balci, I. (2013). In vitro susceptibility of *Candida* species to four antifungal agents assessed by the reference broth microdilution method. *Sci. World J.* 2013:236903. doi: 10.1155/2013/236903

Erlandsson, M., and Hallbrink, M. (2005). Metallic zinc reduction of disulfide bonds between cysteine residues in peptides and proteins. *Int. J. Pept. Res. Ther.* 11, 261–265. doi: 10.1007/s10989-005-8113-1

Gonzalo, G. D. C. V., Zhu, L., Oman, T. J., and van der Donk, W. A. (2014). NMR structure of the S-linked glycopeptide sublancin 168. *Chem Biol.* 9, 796–801. doi: 10.1021/cb4008106

Greber, K. E., Ciura, K., Belka, M., Kawczak, P., Nowakowska, J., Bączek, T., et al. (2018). Characterization of antimicrobial and hemolytic properties of short synthetic cationic lipopeptides based on QSAR/QSTR approach. *Amino Acids* 50, 479–485. doi: 10.1007/s00726-017-2530-2

Gupta, V., Singh, S. S., Sidhu, C., Grover, V., Pinnaka, A. K., and Korpole, S. (2019). Virgicin, a novel lanthipeptide from *Virgibacillus* sp. strain AK90 exhibits inhibitory activity against Gram-positive bacteria. *World J. Microbiol. Biotechnol.* 35:133. doi: 10.1007/s11274-019-2707-9

Gwynne, P. J., and Gallagher, M. P. (2018). Light as a broad-spectrum antimicrobial. *Front. Microbiol.* 9:119. doi: 10.3389/fmicb.2018.00119

Hashem, A., Tabassum, B., and Allah, E. F. A. (2019). *Bacillus subtilis*: a plant-growth promoting rhizobacterium that also impacts biotic stress. *Saudi J. Biol. Sci.* 26, 1291–1297. doi: 10.1016/j.sjbs.2019.05.004

Herzner, A. M., Dischinger, J., Szekat, C., Josten, M., Schmitz, S., Yakéléba, A., et al. (2011). Expression of the lantibiotic mersacidin in *Bacillus amyloliquefaciens* FZB42. *PLoS One* 6:e22389. doi: 10.1371/journal.pone.0022389

Inès, M., and Dhouha, G. (2015). Lipopeptide surfactants: production, recovery and pore forming capacity. *Peptides* 71, 100–112. doi: 10.1016/j.peptides.2015.07.006

Ivanova, E. P., Vysotskii, M. V., Svetashev, V. I., Nedashkovskaya, O. I., Gorshkova, N. M., Mikhailov, V. V., et al. (1999). Characterization of *Bacillus* strains of marine origin. *Int. Microbiol.* 2, 267–271.

Jha, S. S., Joshi, S. J., and Geetha, S. J. (2016). Lipopeptide production by *Bacillus subtilis* R1 and its possible applications. *Braz. J. Microbiol.* 47, 955–964. doi: 10.1016/j.bjm.2016.07.006

Ji, S., Li, W., Baloch, A. R., Wang, M., and Cao, B. (2015). Improved production of sublancin via introduction of three characteristic promoters into operon

clusters responsible for this novel distinct glycopeptide biosynthesis. *Microb. Cell Fact.* 14:17. doi: 10.1186/s12934-015-0201-0

Jin, X. B., Sun, R. J., Zhu, J. Q., Xu, Z. J., Liu, Z., Wang, Q., et al. (2012). Isolation and identification of *Bacillus altitudinis* ZJ 186 from marine soil samples and its antifungal activity against *Magnaportheoryzae*. *Curr. Res. Bacteriol.* 5, 13–23. doi: 10.3923/crb.2012.13.23

Kaur, T., Kaur, A., Sharma, V., and Manhas, R. K. (2016). Purification and characterization of a new antifungal compound 10-(2, 2-dimethyl-cyclohexyl)-6, 9-dihydroxy-4, 9-dimethyl-dec-2-enoic acid methyl ester from *Streptomyces hydrogenans* strain DH16. *Front. Microbiol.* 7:1004. doi: 10.3389/fmicb.2016.01004

Klaenhammer, T. R. (1993). Genetics of bacteriocins produced by lactic acid bacteria. *FEMS Microbiol. Rev.* 12, 39–86.

Ksiezopolska, E., and Gabaldón, T. (2018). Evolutionary emergence of drug resistance in *Candida* opportunistic pathogens. *Genes* 9:461. doi: 10.3390/genes9090461

Kumar, S., Stecher, G., and Tamura, K. (2016). MEGA7: molecular evolutionary genetics analysis version 7.0 for bigger datasets. *Mol. Biol. Evol.* 33, 1870–1874. doi: 10.1093/molbev/msw054

Laws, M., Shaaban, A., and Rahman, K. M. (2019). Antibiotic resistance breakers: current approaches and future directions. *FEMS Microbiol. Rev.* 43, 490–516. doi: 10.1093/femsre/fuz014

Li, B., and Webster, T. J. (2018). Bacteria antibiotic resistance: new challenges and opportunities for implant-associated orthopedic infections. *J. Orthop. Res.* 36, 22–32. doi: 10.1002/jor.23656

Lum, K. Y., Tay, S. T., Le, C. F., Lee, V. S., Sabri, N. H., Velayuthan, R. D., et al. (2015). Activity of novel synthetic peptides against *Candida albicans*. *Sci. Rep.* 5:9657. doi: 10.1038/srep09657

Lyu, Y., Yang, Y., Lyu, X., Dong, N., and Shan, A. (2016). Antimicrobial activity, improved cell selectivity and mode of action of short PMAP-36-derived peptides against bacteria and *Candida*. *Sci. Rep.* 6:27258. doi: 10.1038/srep27258

Ma, Y., Kong, Q., Qin, C., Chen, Y., Chen, Y., Lv, R., et al. (2016). Identification of lipopeptides in *Bacillus megaterium* by two-step ultrafiltration and LC-ESIMS/MS. *AMB Express* 6:79. doi: 10.1186/s13568-016-0252-6

Mandal, S. M., Sharma, S., Pinnaka, A. K., Kumari, A., and Korpole, S. (2013). Isolation and characterization of diverse antimicrobial lipopeptides produced by *Citrobacter* and *Enterobacter*. *BMC Microbiol.* 13:152. doi: 10.1186/1471-2180-13-152

Mangoni, M. L., and Shai, Y. (2011). Short native antimicrobial peptides and engineered ultrashort lipopeptides: similarities and differences in cell specificities and modes of action. *Cell. Mol. Life Sci.* 4, 2267–2280. doi: 10.1007/s00018-011-0718-2

May, J. J., Wendrich, T. M., and Marahiel, M. A. (2001). The *dhb* operon of *Bacillus subtilis* encodes the biosynthetic template for the catecholic siderophore 2, 3-dihydroxybenzoate-glycine-threonine trimeric ester bacillibactin. *J. Biol. Chem.* 276, 7209–7217. doi: 10.1074/jbc.M009140200

Meena, K. R., and Kanwar, S. S. (2015). Lipopeptides as the antifungal and antibacterial agents: applications in food safety and therapeutics. *Biomed Res. Int.* 2015:473050. doi: 10.1155/2015/473050

Meir, O., Zaknoon, F., Cogan, U., and Mor, A. (2017). A broad-spectrum bactericidal lipopeptide with anti-biofilm properties. *Sci. Rep.* 7:2198. doi: 10.1038/s41598-017-02373-0

Miljkovic, M., Jovanovic, S., O'Connor, P. M., Mirkovic, N., Jovcic, B., Filipic, B., et al. (2019). *Brevibacillus laterosporus* strains BGSP7, BGSP9 and BGSP11 isolated from silage produce broad spectrum multi-antimicrobials. *PLoS One* 14:e0216773. doi: 10.1371/journal.pone.0216773

Mircus, G., Albert, N., Ben-Yaakov, D., Chikvashvili, D., Shadkchan, Y., Kontoyiannis, D. P., et al. (2015). Identification and characterization of a novel family of selective antifungal compounds (CANBEFs) that interfere with fungal protein synthesis. *Antimicrob. Agents Chemother.* 59, 5631–5640. doi: 10.1128/AAC.00850-15

Mondol, M. A. M., Shin, H. J., and Islam, M. T. (2013). Diversity of secondary metabolites from marine *Bacillus* species: chemistry and biological activity. *Mar. Drugs* 11, 2846–2872. doi: 10.3390/md11082846

Oman, T. J., Boettcher, J. M., Wang, H. A., Okalibe, X. N., and van der Donk, W. A. (2011). Sublancin is not a lantibiotic but an S-linked glycopeptide. *Nat. Chem. Biol.* 7, 78–80. doi: 10.1038/nchembio.509

Paik, S. H., Chakicherla, A., and Hansen, J. N. (1998). Identification and characterization of the structural and transporter genes for, and the chemical and biological properties of, sublancin 168, a novel lantibiotic produced by *Bacillus subtilis* 168. *J. Biol. Chem.* 273, 23134–23142. doi: 10.1074/jbc.273.36.23134

Pande, R. A., and Bhailume, P. V. (2014). Use of topical meropenem in management of hospital acquired *Pseudomonas* ocular infections. *J. Clin. Ophthalmol. Res.* 2, 23–25.

Parisot, J., Carey, S., Breukink, E., Chan, W. C., Narbad, A., and Bonev, B. (2008). Molecular mechanism of target recognition by subtilin, a class I lanthionine antibiotic. *Antimicrob. Agents Chemother.* 52, 612–618. doi: 10.1128/AAC.00836-07

Patel, R. K., and Jain, M. (2012). NGS QC Toolkit: a toolkit for quality control of next generation sequencing data. *PLoS One* 7:e30619. doi: 10.1371/journal.pone.0030619

Patil, P. P., Midha, S., Kumar, S., and Patil, P. B. (2016). Genome sequence of type strains of genus *Stenotrophomonas*. *Front. Microbiol.* 7:309. doi: 10.3389/fmicb.2016.00309

Paulsen, S. S., Strube, M. L., Bech, P. K., Gram, L., and Sonnenschein, E. C. (2019). Marine chitinolytic *Pseudoalteromonas* represents an untapped reservoir of bioactive potential. *mSystems* 4:e00060-19. doi: 10.1128/mSystems.00060-19

Perez, R. H., Zendo, T., and Sonomoto, K. (2018). Circular and leaderless bacteriocins: biosynthesis, mode of action, applications, and prospects. *Front. Microbiol.* 9:2085. doi: 10.3389/fmicb.2018.02085

Phister, T. G., O'Sullivan, D. J., and McKay, L. L. (2004). Identification of Bacilysin, Chlorotetaine, and Iturin A produced by *Bacillus* sp. Strain CS93 isolated from Pozol, a Mexican fermented maize dough. *Appl. Environ. Microbiol.* 70, 631–634. doi: 10.1128/AEM.70.1.631-634.2004

Ponnappan, N., Budagavi, D. P., Yadav, B. K., and Chugh, A. (2015). Membrane-active peptides from marine organisms-antimicrobials, cell-penetrating peptides and peptide toxins: applications and prospects. *Probiotics Antimicrob. Proteins* 7, 75–89. doi: 10.1007/s12602-014-9182-2

Prestinaci, F., Pezzotti, P., and Pantosti, A. (2015). Antimicrobial resistance: a global multifaceted phenomenon. *Pathog. Glob. Health* 109, 309–318. doi: 10.1179/2047773215Y.0000000030

Raje, M., Dhiman, R., Majumdar, S., Dass, T., Dikshit, K. L., and Kaur, R. (2006). Charged nylon membrane substrate for convenient and versatile high resolution microscopic analysis of *Escherichia coli* & mammalian cells in suspension culture. *Cytotechnology* 51, 111–117. doi: 10.1007/s10616-006-9027-2

Ramachandran, R., Chalasani, A. G., Lal, R., and Roy, U. (2014). A broad-spectrum antimicrobial activity of *Bacillus subtilis* RLID 12.1. *Sci. World J.* 2014:968487. doi: 10.1155/2014/968487

Ramachandran, R., Shrivastava, M., Narayanan, N. N., Thakur, R. L., Chakrabarti, A., and Roy, U. (2018). Evaluation of antifungal efficacy of three new cyclic lipopeptides of the class bacillomycin from *Bacillus subtilis* RLID 12.1. *Antimicrob. Agents Chemother.* 62:e01457-17. doi: 10.1128/AAC.01457-17

Raman, N., Lee, M. R., Lynn, D. M., and Palecek, S. P. (2015). Antifungal activity of 14-helical β-peptides against planktonic cells and biofilms of *Candida* species. *Pharmaceuticals* 8, 483–503. doi: 10.3390/ph8030483

Rani, P. R., Anandharaj, M., Hema, S., Deepika, R., and David Ravindran, A. (2016). Purification of antilisterial peptide (Subtilosin A) from novel *Bacillus tequilensis* FR9 and demonstrate their pathogen invasion protection ability using human carcinoma cell line. *Front. Microbiol.* 7:1910. doi: 10.3389/fmicb.2016.01910

Rasch, M., and Knøchel, S. (1998). Variations in tolerance of *Listeria monocytogenes* to nisin, pediocin PA-1 and bavaricin A. *Lett. Appl. Microbiol.* 27, 275–278.

Reen, F. J., Gutiérrez-Barranquero, J. A., Dobson, A. D., Adams, C., and O'Gara, F. (2015). Emerging concepts promising new horizons for marine biodiscovery and synthetic biology. *Mar. Drugs* 13, 2924–2954. doi: 10.3390/md13052924

Ren, H., Biswas, S., Ho, S., van der Donk, W. A., and Zhao, H. (2018). Rapid discovery of glycocins through pathway refactoring in *Escherichia coli*. *ACS Chem. Biol.* 13, 2966–2972. doi: 10.1021/acschembio.8b00599

Sharma, D., Mandal, S. M., and Manhas, R. K. (2014). Purification and characterization of a novel lipopeptide from *Streptomyces amritsarensis* sp. nov. active against methicillin-resistant *Staphylococcus aureus*. *AMB Express* 4:50. doi: 10.1186/s13568-014-0050-y

Singh, P. K., Sharma, S., Kumari, A., and Korpole, S. (2014). A non-pediocin low molecular weight antimicrobial peptide produced by *Pediococcus pentosaceus*

strain IE-3 shows increased activity under reducing environment. *BMC Microbiol.* 14:226. doi: 10.1186/s12866-014-0226-2

Smibert, R. M., and Krieg, N. R. (1994). "Phenotypic characterization," in *Methods for General and Molecular Bacteriology*, eds P. Gerhardt, R. G. Murray, W. A. Wood, and N. R. Krieg (Washington, DC: American Society for Microbiology), 607–654. doi: 10.1002/food.19960400226

Strieker, M., and Marahiel, M. A. (2009). The structural diversity of acidic lipopeptide antibiotics. *Chembiochem* 4, 607–616. doi: 10.1002/cbic.200800546

Suresh, K., Mayilraj, S., and Chakrabarti, T. (2006). *Effluviibacterroseus* gen. nov. sp. nov., isolated from muddy water, belonging to the family "*Flexibacteraceae*". Int. J. Syst. Evol. Microbiol. 56, 1703–1707.

Tareq, F. S., Lee, M. A., Lee, H. S., Lee, J. S., Lee, Y. J., and Shin, H. J. (2014). Gageostatins A-C, antimicrobial linear lipopeptides from a marine *Bacillus subtilis*. *Mar. Drugs*12, 871–885. doi: 10.3390/md12020871

Villegas-Escobar, V., Ceballos, I., Mira, J. J., Argel, L. E., Orduz Peralta, S., and Romero-Tabarez, M. (2013). Fengycin c produced by *Bacillus subtilis* EA-CB0015. *J. Nat. Prod.* 76, 503–509. doi: 10.1021/np300574v

Wang, S., Huang, S., Ye, Q., Zeng, X., Yu, H., and Qi, D. (2018). Prevention of cyclophosphamide-induced immunosuppression in mice with the antimicrobial peptide sublancin. *J. Immunol. Res.* 2018:4353580. doi: 10.1155/2018/4353580

Wang, S., Wang, Q., Zeng, X., Ye, Q., Huang, S., Yu, H., et al. (2017). Use of the antimicrobial peptide sublancin with combined antibacterial and immunomodulatory activities to protect against methicillin-resistant *Staphylococcus aureus* infection in mice. *J. Agric. Food Chem.* 65, 8595–8605. doi: 10.1021/acs.jafc.7b02592

Wong, D., Nielsen, T. B., Bonomo, R. A., Pantapalangkoor, P., Luna, B., and Spellberg, B. (2017). Clinical and pathophysiological overview of *Acinetobacter* infections: a century of challenges. *Clin. Microbiol. Rev.* 30, 409–447. doi: 10.1128/CMR.00058-16

Wu, C., Biswas, S., Garcia De Gonzalo, C. V., and van der Donk, W. A. (2019). Investigations into the mechanism of action of sublancin. *ACS Infect. Dis.* 5, 454–459. doi: 10.1021/acsinfecdis.8b00320

Yoon, S. H., Ha, S. M., Lim, J., Kwon, S., and Chun, J. (2017). A large-scale evaluation of algorithms to calculate average nucleotide identity. *Antonie Leeuwenhoek* 110, 1281–1286. doi: 10.1007/s10482-017-0844-4

Youssef, N. H., Dunacn, K. E., Nagle, D. P., Savage, K. N., Knapp, R. M., and McInerney, M. J. (2004). Comparison of methods to detect biosurfactant production by diverse microorganism. *J. Microbiol. Methods* 56, 339–347. doi: 10.1016/j.mimet.2003.11.001

Zhang, L., and Sun, C. (2018). Fengycins, cyclic lipopeptides from marine *Bacillus subtilis* strains, kill the plant-pathogenic fungus *Magnaporthe grisea* by inducing reactive oxygen species production and chromatin condensation. *Appl. Environ. Microbiol.* 84:e00445-18. doi: 10.1128/AEM.00445-18

Zheng, L., Chen, H., Han, X., Lin, W., and Yan, X. (2005). Antimicrobial screening and active compound isolation from marine bacterium NJ6-3-1 associated with the sponge *Hymeniacidon perleve*. *World J. Microbiol. Biotechnol.* 21, 201–206. doi: 10.1007/s11274-004-3318-6

Conflict of Interest: The authors declare that the research was conducted in the absence of any commercial or financial relationships that could be construed as a potential conflict of interest.

frontiers in Microbiology

ORIGINAL RESEARCH
published: 23 June 2020
doi: 10.3389/fmicb.2020.01334

Sorbicillinoid Derivatives From Sponge-Derived Fungus *Trichoderma reesei* (HN-2016-018)

*Saif Ur Rehman[1,2,3,4†], Lu-Jia Yang[1,2,3†], Ya-Hui Zhang[1,2,3], Jing-Shuai Wu[1,2,3], Ting Shi[1,2,3], Waqas Haider[1,2,3], Chang-Lun Shao[1,2,3] and Chang-Yun Wang[1,2,3]**

[1] Key Laboratory of Marine Drugs, The Ministry of Education of China, School of Medicine and Pharmacy, Ocean University of China, Qingdao, China, [2] Institute of Evolution & Marine Biodiversity, Ocean University of China, Qingdao, China, [3] Laboratory for Marine Drugs and Bioproducts, Qingdao National Laboratory for Marine Science and Technology, Qingdao, China, [4] Department of Pharmacy, Faculty of Medical and Health Sciences, University of Poonch Rawalakot, Rawalakot, Pakistan

Six new sorbicillinoids, trichoreeseione A (**1**) and B (**2**), trichodermolide B (**3**), 13-hydroxy-trichodermolide (**4**), 24-hydroxy-trichodimerol (**5**), 15-hydroxy-bisvertinol (**7**), together with three known analogs, trichodimerol (**6**), 24-hydroxy-bisvertinol (**8**), and bisvertinol (**9**), were isolated from the sponge-derived fungus *Trichoderma reesei* (HN-2016-018). Their structures including absolute configurations were elucidated by analysis of NMR, MS data, and calculated ECD spectra. Compounds **1** and **2** with a characteristic naphthalene-trione ring were firstly reported in sorbicillinoid family. Compounds **3** and **4** were two rare sorbicillinoids containing a unique bicycle [3.2.1] lactone skeleton, while **3** with a propan-2-one moiety was also recorded first time in this family. Compound **5** displayed cytotoxic activity against A549, MCF-7, and HCT116 cell lines with the IC_{50} values of 5.1, 9.5, and 13.7 μM, respectively.

Keywords: sponge-derived fungus, *Trichoderma reesei*, sorbicillinoid, naphthalene-trione, cytotoxic activity

OPEN ACCESS

Edited by:
Jinwei Zhang,
University of Exeter, United Kingdom

Reviewed by:
Tibor Kurtán,
University of Debrecen, Hungary
Weaam Ebrahim,
Heinrich Heine University Düsseldorf, Germany

***Correspondence:**
Chang-Yun Wang
changyun@ouc.edu.cn

† These authors have contributed equally to this work

Specialty section:
This article was submitted to Microbiotechnology, a section of the journal Frontiers in Microbiology

Received: *19 March 2020*
Accepted: *25 May 2020*
Published: *23 June 2020*

Citation:
Rehman SU, Yang L-J, Zhang Y-H, Wu J-S, Shi T, Haider W, Shao C-L and Wang C-Y (2020) Sorbicillinoid Derivatives From Sponge-Derived Fungus Trichoderma reesei (HN-2016-018). Front. Microbiol. 11:1334. doi: 10.3389/fmicb.2020.01334

INTRODUCTION

Sorbicillionids are a family of hexaketide metabolites with a characteristic sorbyl side chain residue (Harned and Volp, 2011), which was firstly isolated as an impurity in penicillin in 1948 (Andrade et al., 1992). Since then more than 100 analogs of sorbicillinoids have been isolated, which could be classified into monomeric, dimeric, trimeric, and polycyclic sorbicillinoids, and vertinolides according to their basic structural features (Harned and Volp, 2011). Sorbicillinoid family possesses extensive pharmacological effects including cytotoxic (Du et al., 2009; Ei-Elimat et al., 2015), antimicrobial (Ei-Elimat et al., 2015), antiviral (Peng et al., 2014), anti-inflammatory (Zhang et al., 2019), radical scavenging (Abe et al., 1998), and anti-diabetic activities (Cao et al., 2019). Majority of sorbicillionids were reported from 10 genera of fungi: *Penicillium*, *Phaeoacremonium*, *Trichoderma*, *Aspergillus*, *Phialocephala*, *Scytalidium*, *Clonostachys*, *Acremonium*, *Paecilomyces,* and *Verticillium* (Meng et al., 2016). In recent years, marine-derived fungi have emerged as an important resource for sorbicillinoids. Diverse sorbicillinoid analogs with unique skeletons have been reported from sponge associated fungi. For example, a group of sorbicillionids, saturnispols A–H possessing excellent antibacterial activity, especially against gram negative bacteria, were isolated from sponge-derived fungus *Trichoderma saturnisporum* DI-IA (Meng et al., 2018), while a series of dimeric and

monomeric sorbicillinoid derivatives with potent anti-inflammatory activity were reported from sponge-associated fungus *Trichoderma reesei* 4670 (Zhang et al., 2019).

During our recent research for exploration of new structurally diverse bioactive natural products from marine invertebrates and their symbiotic microorganisms (Liu et al., 2019), a variety of new secondary metabolites with multiple biological activities have been obtained from sponge-derived fungi (Li et al., 2012; Qi et al., 2013; Zhao et al., 2015; Wang et al., 2018). In this study, the strain *T. reesei* (HN-2016-018) isolated from an unidentified sponge collected from the South China Sea attracted our attention because the EtOAc extract from its fermentation broth exhibited cytotoxic activity. Chemical investigation led to the isolation of nine sorbicillionoid derivatives (**Figure 1**), including six new sorbicillionoids, trichoreeseione A (**1**), trichoreeseione B (**2**), trichodermolide B (**3**), 13-hydroxy-trichodermolide (**4**), 24-hydroxy-trichodimerol (**5**), and 24-hydroxy-bisvertinol (**7**), along with three known analogs, trichodimerol (**6**) (Andrade et al., 1992), 15 hydroxy-bisvertinol (**8**) (Zhang et al., 2019), and bisvertinol (**9**) (Trifonov et al., 1986). Herein, we report the isolation, structural elucidation, and cytotoxic activities of these compounds.

MATERIALS AND METHODS

General Experimental Procedure

The optical rotations were measured on a JASCO P-1020 digital polarimeter. IR spectra were recorded on a Nicolet-Nexus-470 spectrometer using KBr pellets (Thermo Electron, Waltham, MA, United States). UV spectra were recorded using a Milton Roy UV-Vis spectrophotometer. NMR spectra were acquired using a JEOL JEMECP NMR spectrometer (JEOL, Tokyo, Japan) (600 MHz for ^{1}H, 150 MHz for ^{13}C) and BRUKER AVANCE NEO NMR spectrometer (BRUKER, United States) (400 MHz for ^{1}H, and 100 MHz for ^{13}C), using TMS as an internal standard. ECD spectra were recorded on a JASCO J-815 circular dichroism spectrometer (JASCO Electric Co., Ltd., Tokyo, Japan). ESIMS spectra were measured on a Micromass Q-TOF spectrometer (Waters Corp., Manchester, United Kingdom). HPLC separation was performed using a Hitachi L-2000 HPLC system (Hitachi High Technologies, Tokyo, Japan) coupled with a Hitachi L-2455 photodiode array detector. A Kromasil C_{18} semi-preparative HPLC column (250 × 10 mm, 5 μm) (Eka Nobel, Bohus, Sweden) was used. Silica gel (Qingdao Marine Chemical Group Co., Qingdao, China) and Sephadex LH-20 (Amersham Biosciences Inc., Piscataway, NJ, United States) were used for column chromatography. Precoated silica gel GF254 plates (Yantai Zifu Chemical Group Co., Yantai, China) were used for analytical TLC.

Fungal Material

The fungal strain *T. reesei* (HN-2016-018) was separated from the internal fresh tissue of an unidentified sponge collected from the South China Sea in October 2016. The fungal strain was recognized on the basis of its morphological traits and by amplification and sequencing of the DNA sequences of the ITS region. The fungus was identified as *T. reesei* whose 500 base pair ITS sequence had 99% sequence identity to that of *T. reesei*. The phylogenetic tree (**Supplementary Figure S50**) was constructed using the neighbor joining method (Saitou and Nei, 1987). The distance calculations, tree construction, and bootstrap analysis were performed with the software MEGA 7 (Felsenstein, 1985). The strain was deposited in the Key Laboratory of Marine Drugs, the Ministry of Education of China, School of Medicine and Pharmacy, Ocean University of China, Qingdao, China, with the Gene Bank (NCBI) accession number MT367415.

Fermentation, Extraction, and Isolation

The fungal strain *T. reesei* (HN-2016-018) was cultivated in 80 L PDB medium at r.t. for 1 month. Broth and mycelia in fermented culture were separated by filtration. The filtrate was extracted three times with equal volume of EtOAc, and the mycelia were soaked in EtOAc (3 × 5000 mL). The TLC profiles of these two parts were similar, so these extracts were combined and obtained the EtOAc extract (103 g). The extract was subjected to VLC on silica gel (100–200 mesh) eluting with a combination solvent of PE/EtOAc in increasing polarity (90:10, 50:50, 30:70, 0:100) followed by CH_2Cl_2/MeOH (from 90:10 to 30:70) to obtain six fractions (Fr.1–Fr.6). Fr.3 was subjected to silica gel column chromatography (CC) to obtain two sub-fractions (Fr.3-1 and Fr.3-2). Fr.3-1 was chromatographed over a Sephadex LH-20 column using MeOH as mobile phase and afterward isolated by semi-preparative HPLC (75% MeOH/H_2O) to yield **1** (7.0 mg) and **2** (5.5 mg). Fr.3-2 was separated by HPLC (70% CH_3CN/H_2O) to give **4** (7 mg). Fr. 4 was fractionated with Sephadex LH-20 column using PE–CH_2Cl_2–MeOH (v/v, 2:1:1) as mobile phase to achieve four sub-fractions (Fr.4-1 to Fr.4-4). Pure compound **9** (10 mg) was obtained from Fr.4-1 by CC on Sephadex LH-20 with mobile phase CH_2Cl_2–MeOH (v/v, 1:1). Fr.4-2 was eluted with PE–EtOAc (v/v, 70:30) on silica gel CC and then purified with RP-HPLC (70% MeOH/H_2O) to afford **3** (6 mg). Fr.4-3 was processed with Sephadex LH-20 column and then further fractioned by RP-HPLC (65% MeOH/H_2O) to give **5** (8 mg) and **6** (25 mg). Fr.4-4 was subjected to RP-HPLC (45% MeOH/H_2O) to afford **7** (4.5 mg) and **8** (12 mg).

Trichoreeseione A (**1**) yellow oil; [α]25 D − 42.7 (*c* 0.1, MeOH); UV (MeOH) λ_{max} (log ε) 324 (4.784) nm; ECD (*c* 2.8 mM, MeOH) λmax (Δε) 227 (−8.9), 252 (+ 25.1), 288 (−20.8) nm; IR (KBr) ν_{max} 3614, 3566, 3525, 1700, 1683, 1509, 1398, 1026 cm^{-1}; ^{1}H and ^{13}C NMR see **Table 1**; HR-ESIMS *m*/*z* 357.1692 $[M + H]^+$ (calcd for $C_{21}H_{25}O_5$, 357.1697), 379.1511 $[M + Na]^+$ (calcd for $C_{21}H_{24}O_5Na$, 379.1516).

Trichoreeseione B (**2**) yellow oil; [α]25 D − 39.9 (*c* 0.1, MeOH); UV (MeOH) λ_{max} (log ε) 307 (4.236) nm; ECD (*c* 2.7 mM, MeOH) λmax (Δε) 226 (−6.8), 251 (+ 20.2), 286 (−18.2) nm; IR (KBr) ν_{max} 3629, 3567, 1700, 1683, 1650, 1521, 1457 cm^{-1}; ^{1}H and ^{13}C NMR see **Table 1**; HR-ESIMS *m*/*z* 373.1642 $[M + H]^+$ (calcd for $C_{21}H_{25}O_6$, 373.1646).

Trichodermolide B (**3**) yellow oil; [α]25 D + 64.2 (*c* 0.1, MeOH); UV (MeOH) λ_{max} (log ε) 308 (4.65) nm; ECD (*c* 1.40 mM, MeOH) λmax (Δε) 221 (−27.4), 267 (+27.1) nm; IR (KBr) ν_{max} 3023, 2934, 1785, 1721, 1683, 1634, 1597, 1436, 1381, 1186, 979 cm^{-1}; ^{1}H and ^{13}C NMR see **Table 2**; HR-ESIMS *m*/*z*

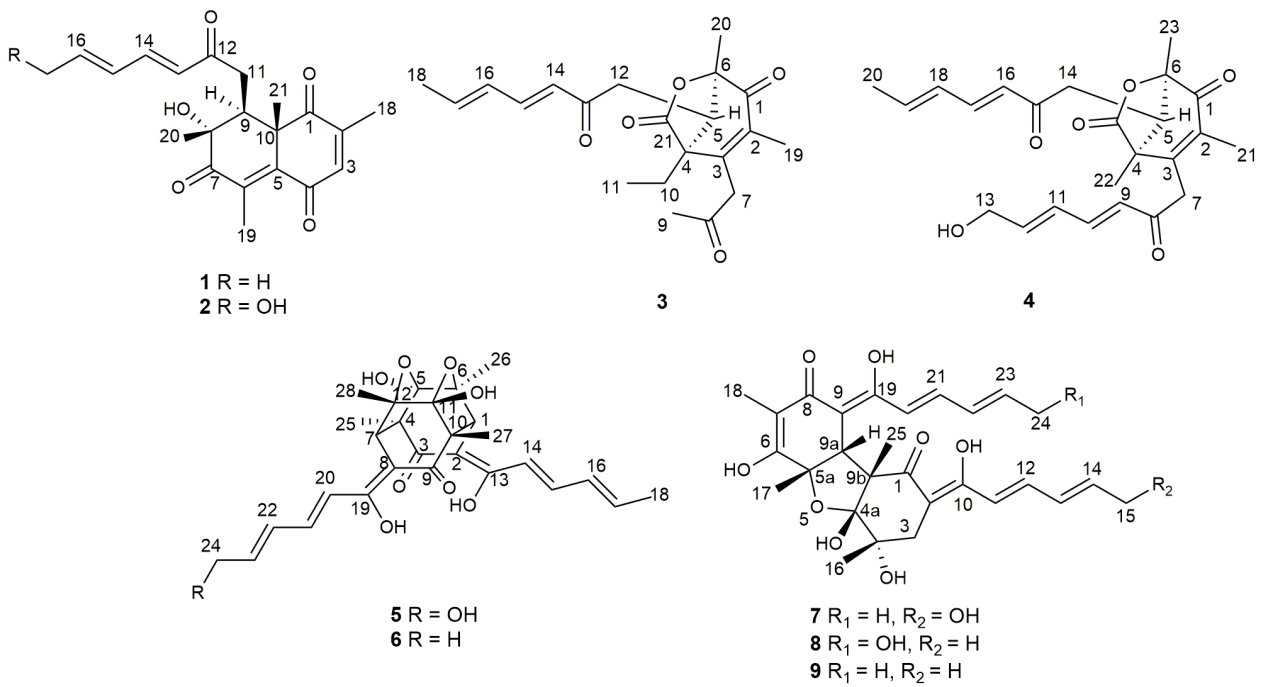

FIGURE 1 | Structures of isolated compounds **1**–**9**.

359.1861 $[M + H]^+$ (calcd for $C_{21}H_{27}O_5$, 359.1853), 381.1672 $[M + Na]^+$ (calcd for $C_{21}H_{26}O_5Na$, 381.1672).

13-Hydroxy-trichodermolide (**4**) yellow amorphous powder; [α]25 D + 27.6 (*c* 0.1, MeOH); UV (MeOH) λ_{max} (log ε) 272 (4.18) nm; IR (KBr) ν_{max} 3023, 2934, 1785, 1721, 1683, 1634, 1597, 1436, 1381, 1186, 979 cm^{-1}; ECD (*c* 1.12 mM, MeOH) λmax (Δε) 222 (−9.9), 266 (+7.8) nm; ^1H and ^{13}C NMR see **Table 2**; HR-ESIMS *m*/*z* 413.1956 $[M + H]^+$ (calcd for $C_{24}H_{29}O_6$, 413.1959), 435.1773 $[M + Na]^+$ (calcd for $C_{24}H_{28}O_6Na$, 435.1778).

24-Hydroxy-trichodimerol (**5**) yellow amorphous powder; [α]25 D − 405.6 (*c* 0.1, MeOH); UV (MeOH) λ_{max} (log ε) 358 (4.332) nm; ECD (*c* 1.07 mM, MeOH) λmax (Δε) 338 (+56.1), 383 (−83.5) nm; IR (KBr) ν_{max} 3435, 2979, 2933, 1615, 1297, 1178, 1121 cm^{-1}; ^1H and ^{13}C NMR see **Table 3**; HR-ESIMS *m*/*z* 513.2129 $[M + H]^+$ (calcd for $C_{28}H_{33}O_9$, 513.2130).

15-Hydroxy-bisvertinol (**7**) yellow powder; [α]25 D − 377 (*c* 0.1, MeOH); UV (MeOH) λ_{max} (log ε) 348 nm (3.874); ECD (*c* 1.95 mM, MeOH) λmax (Δε) 346 (+44.6), 403 (−71.4) nm; IR (KBr) ν_{max} 3739, 3390, 3265, 2933, 1711, 1612, 1556, 1361, 1027 cm^{-1}; ^1H and ^{13}C NMR see **Table 3**; HR-ESIMS *m*/*z* 513.2136 $[M - H]^-$ (calcd for $C_{28}H_{33}O_9$, 513.2130).

ECD Computational Methods

The MMFF94S force field was used for conformational searches of (8*R*,9*S*,10*S*)-**1**, (8*S*,9*R*,10*R*)-**1**, and (4*S*,5*R*,6*S*)-**3**, respectively. All conformers [20 for (8*R*,9*S*,10*S*)-**1**, 32 for (8*S*,9*R*,10*R*)-**1** and 19 for (4*S*,5*R*,6*R*)-**3**] were optimized at the B3LYP/6-31G(d) level using the Gaussian 09 and then further optimized at the B3LYP/6-311 + G(d) level. The ECD spectrum was calculated by the TDDFT method with the basis set at B3LYP/6-311++G(2d,p) level and simulated by Boltzmann distributions in SpecDis 1.62 (Bruhn et al., 2013).

Biological Assay

Human tumor cells, including colonic (HCT116 and SW480), lung carcinoma (A-549), hepatocellular carcinoma (HepG2), cervical carcinoma (HeLa), breast cancer (MCF-7), and human normal cells, including human umbilical vein endothelial cells (HUVEC) and hepatocytes CLiver cells were cultured in RPMI 1640 medium supplemented with 10% heat inactivated FBS (fetal bovine serum), 2 mM *L*-glutamine and combination of antibiotics penicillin 100 units/ml and streptomycin 100 g/ml were used to avoid contamination in culture medium. All samples were dissolved in DMSO. The adriamycin was used as a positive control and DMSO was used as a negative control (Wu et al., 2020).

The cytotoxicity of the isolated compounds was determined by sulphorhodamine B assay (Skehan et al., 1990). Cells in logarithmic growth stage were inoculated into 96-well tissue culture plates with 5000 cells/well (180 μL/well) for 24 h before treatment with the tested compounds to allow attachment of the cells to the plate. Cells were exposed to the six different concentrations (1.25, 2.5, 5, 10, 20, and 40 μM) in four parallel. After 72 h of drug action, cold trichloroacetic acid (TCA, 50% w/v) was added into each well to fix the cell. After several washings, cells were stained by 0.4% (w/v) SRB solution for 10 min in dark place. Excess stain was washed with 1% (v/v) glacial acetic acid. After drying overnight, the SRB-stained cells were dissolved with 150 μL/pore Tris solution and the color

TABLE 1 | ^{1}H (600 MHz) and ^{13}C NMR (150 MHz) spectroscopic data for compounds 1–2.

No.	1 in $CDCl_3$		2 in $CDCl_3$	
	δ_C type	δ_H, (*J* in Hz)	δ_C, type	δ_H, (*J* in Hz)
1	199.1, C		199.0, C	
2	148.8, C		148.7, C	
3	137.7, CH	6.75, s	137.7, CH	6.76, s
4	190.5, C		190.3, C	
5	147.6, C		147.6, C	
6	133.6, C		133.5, C	
7	202.5, C		202.3, C	
8	74.9, C		74.8, C	
9	41.9, CH	3.45, dd (7.5, 3.7)	42.0, CH	3.44, dd (7.7, 3.8)
10	54.4, C		54.3, C	
11	38.4, CH_2	2.94, dd (15.5, 7.5)	38.6, CH_2	2.96, dd (15.5, 7.7)
		2.84, dd (15.5, 3.7)		2.86, dd (15.5, 3.8)
12	198.8, C		198.5, C	
13	127.3, CH	6.27, d (15.5)	128.6, CH	6.38, d (15.5)
14	143.0, CH	7.30, dd (15.5, 9.7)	141.4, CH	7.34, dd (15.5, 10.9)
15	130.5, CH	6.21, m	129.4, CH	6.45, m
16	140.3, CH	6.20, m	141.6, CH	6.29, dt (15.5, 4.2)
17	18.9, CH_3	1.87, d (5.1)	62.9, CH_2	4.31, d (4.2)
18	17.0, CH_3	2.03, s	16.9, CH_3	2.04, s
19	12.9, CH_3	2.01, s	12.8, CH_3	2.02, s
20	22.4, CH_3	1.34, s	22.4, CH_3	1.34, s
21	21.5, CH_3	1.57, s	21.4, CH_3	1.57, s
8-OH		3.55, brs		3.76, brs

TABLE 2 | ^{1}H (600 MHz) and ^{13}C NMR (150 MHz) for compounds 3–4.

No.	3 in DMSO-d_6		4 in $CDCl_3$	
	δ_C, type	δ_H (*J* in Hz)	δ_C, type	δ_H (*J* in Hz)
1	191.2, C		191.2, C	
2	133.9, C		134.3, C	
3	150.9, C		149.3, C	
4	55.9, C		51.7, C	
5	50.0, CH	3.37, m	55.9, CH	3.33, dd (6.4, 4.3)
6	86.5, C		87.2, C	
7	44.7, CH_2	3.73, s	42.1, CH_2	3.67, d (5.4)
8	205.0, C		195.4, C	
9	30.5, CH_3	2.20, s	128.3, CH	6.20, d (15.5)
10	20.5, CH_2	1.25, dd (14.1, 7.2)	143.9, CH	7.24, dd (15.5, 10.9)
		2.03, dd (14.1,7.2)		
11	8.6, CH_3	0.82, t (7.2)	127.5, CH	6.46, m
12	35.0, CH_2	2.54, dd (18.1, 6.2)	143.6, CH	6.35, dt (15.5, 4.6)
		2.99, dd (18.1, 6.2)		
13	197.2		62.6, CH_2	4.34, d (4.6)
14	127.6, CH	6.14, d (15.5)	35.1, CH_2	3.23, dd (18.4, 6.4)
				2.46, dd (18.4, 4.3)
15	143.9, CH	7.17, dd (15.5, 10.1)	196.6, C	
16	130.6, CH	6.27, m	126.8, CH	6.11, d (15.5)
17	141.9, CH	6.32, m	144.2, CH	7.20, dd (15.5, 10.7)
18	19.1, CH_3	1.83, d (6.1)	130.2, CH	6.20, m
19	11.9, CH_3	1.70, s	141.7, CH	6.28, m
20	16.5, CH_3	1.37, s	18.9, CH_3	1.88, d (6.6)
21	174.7, C		11.6, CH_3	1.78, s
22			16.1, CH_3	1.23, s
23			16.2, CH_3	1.46, s
24			176.1, C	

intensity was measured in microplate reader at 540 nm. The IC_{50} values were analyzed using Graph Pad Prism 5 (GraphPad Software, Inc., La Jolla, CA, United States). The biological assay was carried out under proper aseptic environment to prevent contamination from bacteria, fungi, mycoplasma, and cross contaminations with other cell lines.

Statistical Analysis

The bioassay results were expressed as mean values ± SD. The IC_{50} values, i.e., the concentrations necessary for 50% inhibition, were calculated from the dose response curves using non-linear regression.

RESULTS

Structure Elucidation

Trichoreeseione A (**1**) was isolated as a yellow oil with a molecular formula $C_{21}H_{24}O_5$, based on its HR-ESIMS *m/z* 357.1692 $[M + H]^+$ (calcd for $C_{21}H_{25}O_5$, 357.1697 $[M + H]^+$), possessing 10 degrees of unsaturation. The ^{1}H NMR spectrum of **1** presented five olefinic protons, one methine, one methylene, five methyls, and one hydroxyl proton (δ_H 3.55, brs) (**Table 1**). The ^{13}C NMR spectrum exhibited the presence of 21 carbon signals, including eight olefinic carbons, four carbonyl groups and nine sp^3 hybridized carbons (**Table 1**), which indicated that two rings should be present in **1**. A substituted 2,6,8,10-tetra-methyl-8-hydroxy naphthalene 1,4,7-trione skeleton was deduced based on its spectroscopic features, combining with the key HMBC correlations from H-3 to C-1 and C-5, from H_3-18 to C-1, C-2, and C-3, from H_3-19 to C-4, C-5, C-6, and C-7, from H_3-20 to C-7, C-8, and C-9, and from H_3-21 to C-1, C-5, C-9, and C-10 (**Figure 2**). A typical sorbyl side chain was deduced from the ^{1}H-^{1}H COSY correlations H-13/H-14/H-15/H-16/H_3-17 and HMBC correlation from H-14 to C-12 (**Figure 2**). Further, the ^{1}H-^{1}H COSY signal H-9/H_2-11 and the HMBC correlations from H_2-11 to C-8, C-9, C-10, and C-12 (**Figure 2**) demonstrated that the sorbyl side chain was connected to C-9 bridged by CH_2-11.

The relative configuration of **1** was determined by coupling constants and NOESY spectrum (**Figure 3**). The *E*-configurations of double bonds in the sorbyl side chain were deduced on the basis of the large coupling constant ($J_{H-13/H-14}$ = 15.5 Hz) and the NOESY correlation between H-14 and H-16. The NOESY correlation between H_3-20 and H_3-21 indicated the same orientation of these two methyls, whereas the protons H_3-20 and H_3-21 were simultaneously correlated with H_2-11, reflecting that proton H-9 should locate at the other orientation. Therefore, the relative configuration of **1** was assumed as 8*R**,9*S**,10*S**. The

TABLE 3 | ^{1}H and ^{13}C NMR spectroscopic data for compounds 5 and 7.

No.	5[a] in CD_3OD		7[b] in CD_3OD	
	δ_C, type	δ_H, (*J* in Hz)	δ_C, type	δ_H, (*J* in Hz)
1	58.7, CH	3.08, s	195.3, C	
2	104.6[c], C		106.5, C	
3	201.3, C		36.5, CH_2	2.46, d (14.5)
				2.74, d (14.5)
4	61.0[d], C		74.3, C	
4a			107.3, C	
5	105.8, C			
5a			80.6, C	
6	80.4, C		169.1, C	
7	58.7, CH	3.09, s	110.7, C	
8	105.0[c], C		193.5, C	
9	201.9, C		102.6, C	
9a			55.1, CH	3.65, s
9b			60.6, C	
10	61.1[d], C		178.7, C	
11	105.8, C		123.6, CH	6.42, d (14.7)
12	80.4, C		142.3, CH	7.27, dd (14.7, 11.2)
13	175.9, C		129.7, CH	6.54, m
14	120.2, CH	6.31, d (14.7)	143.2, CH	6.26, dd (14.7, 4.3)
15	144.2, CH	7.28, dd (14.7, 11.1)	62.9, CH_2	4.22, d (4.3)
16	132.3, CH	6.37, m	22.8, CH_3	1.21, s
17	140.8, CH	6.21, dd (14.7, 6.6)	25.8, CH_3	1.43, s
18	18.9, CH_3	1.89, d (6.6)	7.1, CH_3	1.41, s
19	175.2, C		168.6, C	
20	122.1, CH	6.43, d (14.7)	121.8, CH	6.49, d (14.7)
21	143.1, CH	7.33, dd (14.7, 11.3)	139.4, CH	7.19, dd (14.7, 11.2)
22	129.7, CH	6.56, dd (14.7, 11.3)	132.5, CH	6.35, m
23	143.4, CH	6.27, dt (14.7, 4.4)	137.3, CH	6.11, dq (14.7, 6.6)
24	62.9, CH_2	4.22, d (4.4)	18.7, CH_3	1.87, d (6.6)
25	19.8, CH_3	1.37, s	20.1, CH_3	1.28, s
26	21.8, CH_3	1.35, s		
27	19.8, CH_3	1.37, s		
28	21.8, CH_3	1.35, s		

[a]Recorded at 600 MHz for ^{1}H NMR and at 150 MHz for ^{13}C NMR. [b]Recorded at 400 MHz for ^{1}H NMR and at 100 MHz for ^{13}C NMR. [c,d]Assignment of signals might be exchanged.

absolute stereochemistry of **1** was resolved by quantum chemical time-dependent density functional theory (TDDFT) calculation of its electronic circular dichroism (ECD) spectra of (8*R*,9*S*,10*S*)-**1** and (8*S*,9*R*10*R*)-**1**. The experimental ECD spectrum of **1** displayed the intense positive cotton effect at 252 nm and negative cotton effects at 227 and 288 nm, respectively, which were consistent with the theoretical ECD spectrum for (8*R*,9*S*,10*S*)-**1** (**Figure 4**). Therefore, the absolute configuration of **1** was determined as 8*R*,9*S*,10*S*.

Trichoreeseione B (**2**) was assigned a molecular formula of $C_{21}H_{24}O_6$ by HR-ESIMS, showing one additional oxygen atom compared to that of **1**. The NMR data of **2** (**Table 1**) suggested the same skeleton as **1**, apart from a hydroxy-methylene resonance (δ_H 4.31, δ_C 62.9) in **2** instead of the methyl signals (δ_H 1.87, δ_C 18.9) in **1**. The ^{1}H-^{1}H COSY and HMBC correlations confirmed the planar structure of **2**, in which a terminal hydroxy-methylene in the sorbyl side chain replaced the methyl group in **1** (**Figure 2**). The coupling constants, NOESY correlations (**Figure 3**), and ECD spectrum of **2** (**Figure 4**) demonstrated that its stereochemistry was the same as **1**. It is worth mentioning that compounds **1** and **2** represented the first example of sorbicillinoids with a characteristic naphthalene-trione ring.

Trichodermolide B (**3**) was given a molecular formula $C_{21}H_{26}O_5$ based on HR-ESIMS, indicating 9 degrees of unsaturation. The ^{1}H NMR and ^{13}C NMR data (**Table 2**) showed four carbonyls, three pairs of olefinic carbons, five methyls, three methylenes, one methine, and two quaternary carbons. These spectroscopic features suggested that **3** should be a sorbicillinoid analog and closely resembled to trichodermolide isolated from *Trichoderma longibrachiatum* (strain UAMH 4159) collected from cotton duck shelter (Andrade et al., 1996). The main differences were absence of four olefinic carbons, and addition of a propan-2-one moiety and one methylene. The HMBC correlations from H_2-7 to C-2, C-3 and C-4 suggested the propan-2-one moiety was attached to C-3. The ^{1}H-^{1}H COSY linkage between H_2-10 and H_3-11 indicated the presence of one ethylene group, which was located at C-4 based on the HMBC correlations from H_3-11 to C-4, and from H_2-10 to C-4, C-5, and C-21 (**Figure 2**).

The two double bonds in sorbyl side chain of **3** were also assigned as *E* configuration on the basis of their coupling constants ($J_{H-14/H-15}$ = 15.5 Hz), and the NOESY correlation between H-14/H-16 and H-15/H-17 (**Figure 3**). The relative configurations of the stereocenters at C-4, C-5, and C-6 were determined by NOESY spectrum. The NOESY correlations of H-5/H_3-20, and H-5/H_3-11 suggested the same side of these protons. Therefore, the relative configuration of **3** was assumed as 4*S**,5*R**,6*R**. The absolute configuration of **3** was determined by ECD calculation. The Boltzmann-weighted ECD curve of (4*S*,5*R*,6*R*)-**3** agreed with the experimental one (**Figure 4**), and hence, the absolute configuration of **3** was assigned as 4*S*,5*R*,6*R*.

13-Hydroxy-trichodermolide (**4**) has a molecular formula $C_{24}H_{28}O_6$ deduced by HR-ESIMS *m*/*z* 413.1956 $[M + H]^+$ (calcd. for $C_{24}H_{29}O_6$, 413.1959), indicating 11 degrees of unsaturation. The NMR data of **4** (**Table 2**) were very similar to those of trichodermolide isolated from *T. longibrachiatum* (strain UAMH 4159) (Andrade et al., 1996), except the terminal methyl group (δ_H 1.88, δ_C 18.9) at C-13 in trichodermolide was substituted by a hydroxy methylene group (δ_H 4.34, δ_C 62.6) in **4**.

The *E* configurations among the four double bonds in the side chains of **4** were confirmed by large coupling constant values ($J_{H-9/H-10}$ = $J_{H-11/H-12}$ = $J_{H-16/H-17}$ = 15.5 Hz) and the NOESY correlation between H-19/H-17 and H-16/H-18 (**Figure 3**). The relative configurations of three stereocenters, C-4, C-5, and C-6 of **4** were determined by comparison of its ^{1}H NMR data with already reported compound dihydro-trichodermolide (Li et al., 2011). The similarity of chemical shifts of H-5 (δ_H 3.33), H_2-14 (δ_H 3.23 and 2.46), and two methyl groups H_3-22 (1.23) and H_3-23 (δ_H 1.46) in **4** with those of in dihydro-trichodermolide, combing the NOESY correlations between H-5/H_3-22 and H-5/H_3-23, established that the relative configuration of **4** was in accordance with that of

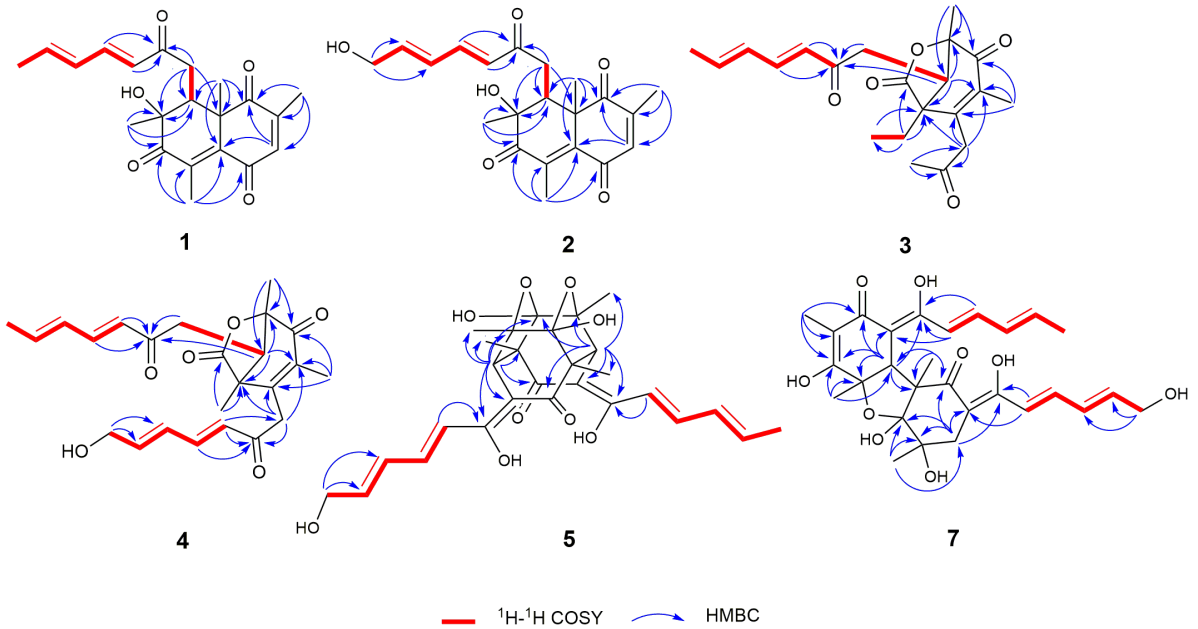

FIGURE 2 | Key ^{1}H–^{1}H COSY and HMBC correlations of **1**–**5** and **7**.

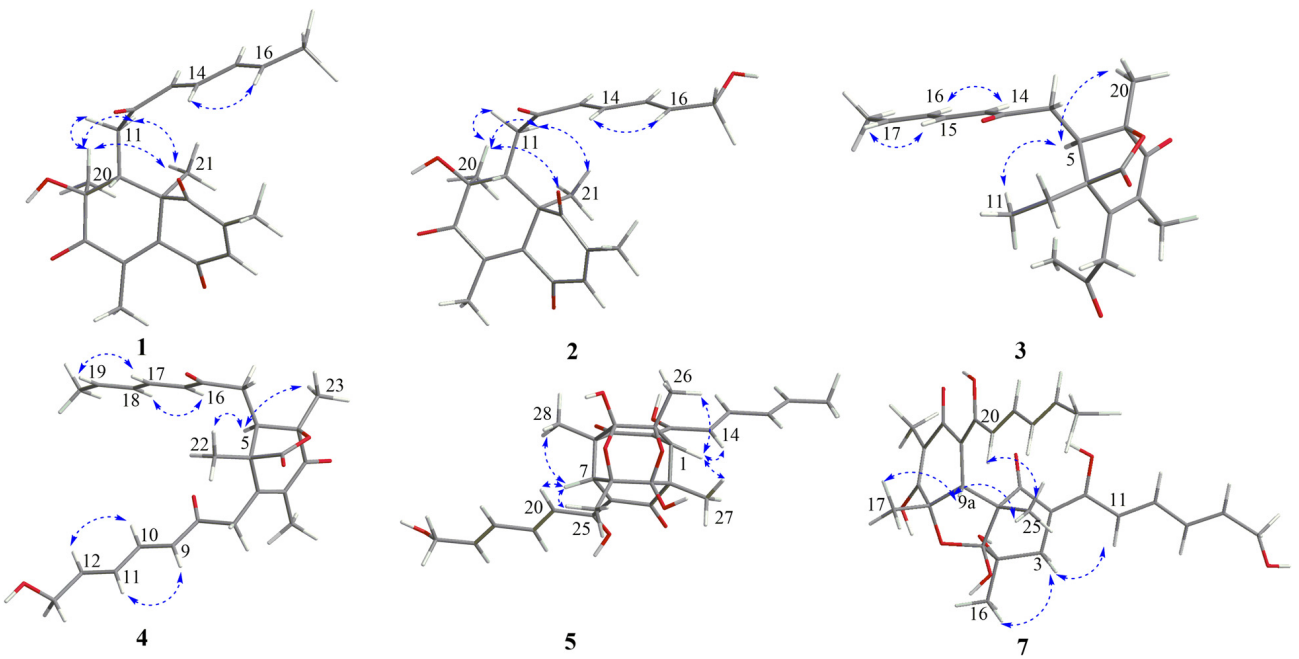

FIGURE 3 | Key NOESY correlations of **1**–**5** and **7**.

dihydro-trichodermolide. The absolute configuration of **4** was determined by comparing its ECD data (**Figure 4**) with those of known analogs (Andrade et al., 1996; Li et al., 2011; Cao et al., 2019). The ECD spectrum of **4** demonstrated nearly similar negative and positive cotton effects to those of reported analogs (**Figure 4** and **Supplementary Table S4**). Consequently, the absolute configuration of **4** was determined as 4*S*,5*R*,6*R*.

A literature survey revealed that bicycle (3.2.1) lactone skeleton was rare in the sorbicillinoid family. So far, only three compounds with this distinctive skeleton have been reported, including trichodermolide (Andrade et al., 1996), dihydro-trichodermolide (Li et al., 2011) and 13-hydroxy-dihydro-trichodermolide (Cao et al., 2019). In this study, two new sorbicillinoids (**3** and **4**) with a bicycle [3.2.1] lactone

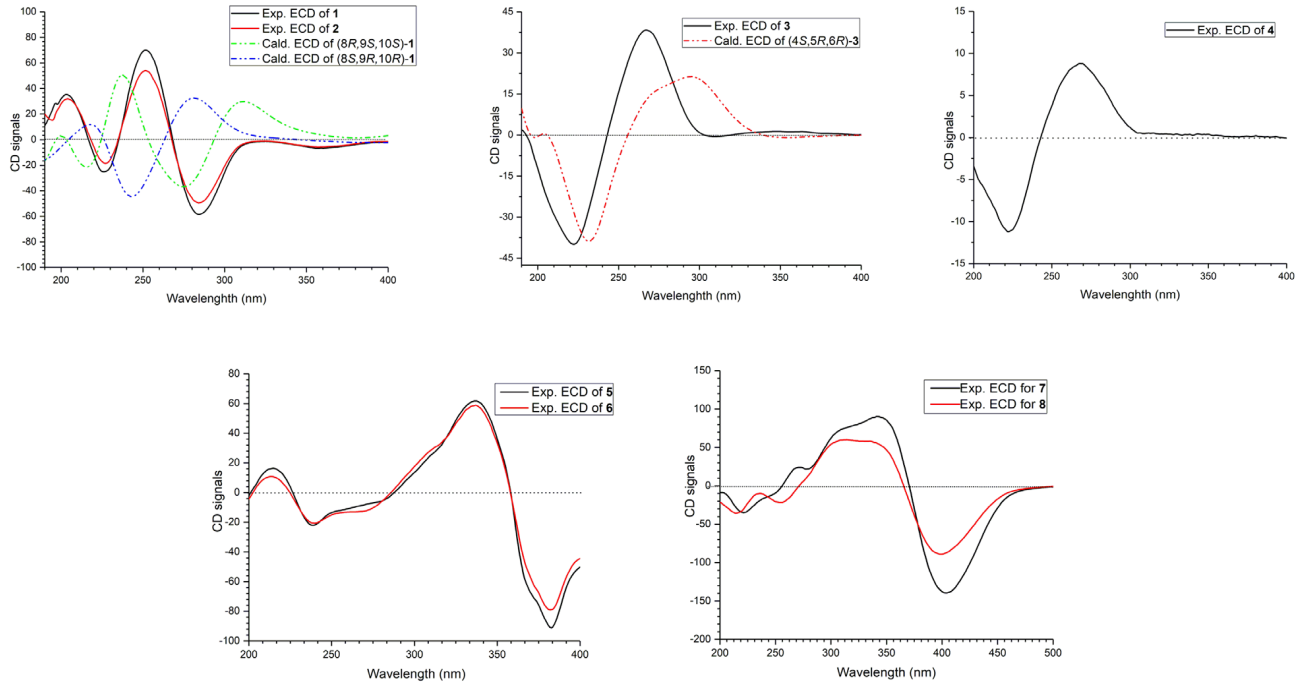

FIGURE 4 | ECD spectra of compounds **1**–**8**.

skeleton was discovered. Among them, **3** was unique in a sense that the propan-2-one side chain was reported first time for sorbicillinoid family.

24-Hydroxy-trichodimerol (**5**) was assigned the molecular formula $C_{28}H_{32}O_9$ by HR-ESIMS with 13 degrees of unsaturation. The NMR spectra (**Table 3**) of **5** exhibited resembling resonances with those of the co-isolated known compound trichodimerol (**6**), which was firstly isolated from *T. longibrachiatum* (strain UAMH 4159) (Andrade et al., 1992). The only obvious difference was the terminal methyl group (δ_H 1.89 δ_C18.8) at C-24 of sorbyl residue in **6** was replaced by a hydroxylated methylene group (δ_H 4.22, δ_C 62.9) in **5**.

The stereochemistry of the double bonds in the sorbyl chains in **5** was assigned as *E* configurations based on their coupling constants ($J_{H-14/H-15}$ = $J_{H-16/H-17}$ = $J_{H-20/H-21}$ = $J_{H-22/H-23}$ = 14.7 Hz). Moreover, in the NOESY spectrum, the correlations between H-1 and H-14, H_3-26, H_3-27, respectively, and between H-7 and H-20, H_3-25, H_3-28, respectively, were observed (**Figure 3**), suggesting the same relative configurations of **5** and **6**. The absolute configuration of **5** was determined by comparing its ECD spectrum with **6**. Compound **5** displayed strong positive Cotton effect at 338 nm (+62) and negative Cotton effect at 383 nm (−91), which was similar with that of **6** (**Figure 4**). Therefore, the absolute configuration of **5** was assumed as 1*R*,4*R*,5*R*,6*S*,7*R*,10*R*,11*R*,12*S* (**Figure 1**). It is worth noting that bisorbicillinoids possessing open-ended cage skeleton were uncommon active compounds (Zhai et al., 2016), of which trichodimerol was biomimetic total synthesized by Nicolaou et al. (2000).

15-Hydroxy-bisvertinol (**7**) displayed a $[M - H]^-$ ion at *m/z* 513.2136 in its HR-ESIMS, in accordance with the molecular formula $C_{28}H_{33}O_9$, which indicated 12 degrees of unsaturation. The 1D NMR and HSQC spectra displayed the presence of five methyls, two methylenes, nine methines, and twelve quaternary carbons. Careful examination of the NMR data of **7** (**Table 3**) disclosed that its skeleton has resemblance with the known compound bisvertinol (**9**), primarily isolated from fungus *Verticillium* intertextum (Trifonov et al., 1986). The obvious difference was that the methyl group at C-15 on one of the sorbyl side chains in **9** was replaced by a hydroxy methylene in **7**.

The relative configuration of **7** was addressed by the coupling constants, NOESY spectrum and biogenetic relationship. The large coupling constants of the four double bonds in the sorbyl chains ($J_{H-11/H-12}$ = $J_{H-13/H-14}$ = $J_{H-20/H-21}$ = $J_{H-22/H-23}$ = 14.7 Hz) reflected their *E*-configurations. In the NOESY spectrum, key cross peaks were observed between H-9a and H_3-25 and H_3-17 (**Figure 3**), indicating that the methyls H_3-17 and H_3-25 were at the same side with H-9a. The 4a-OH was deduced in the same face with H-9a, H_3-25 and H_3-17 by considering the higher stability of a *cis* 5-6 ring junction over a *trans* 5-6 ring junction (Andrade et al., 1992). The configuration of C-4 was presumed to be identical to that of the co-isolated **8** and **9** on the basis of biogenetic relationship. The experimental ECD spectra of **7** and **8** (**Figure 4**) were parallel to each other, possessing positive Cotton effect at 346 nm and negative at 403 nm, and both gave negative optical rotation values. Consequently, the absolute configuration of **7** was deduced as 4*S*,4a*R*,5a*S*,9a*R*,9b*R*.

The structures of known compounds, trichodermol (**6**) (Andrade et al., 1992), 24-hydroxy-bisvertinol (**8**) (Zhang et al., 2019), and bisvertinol (**9**) (Trifonov et al., 1986), were recognized by comparing their spectroscopic data (^{1}H and ^{13}C NMR, and MS) with those reported in the literature.

Bioassays of Compounds

All of the isolated new compounds (**1**–**5** and **7**) were assessed for their cytotoxic activities against five human tumor cell lines, including A549, HepG2, HCT 116, HeLa, MCF-7 and two healthy human cell lines HUVEC and CLiver. Compound **5** displayed cytotoxic activity against A549, MCF-7 and HCT 116 cell lines (**Figure 5**) with the IC_{50} values of 5.1, 9.5 and 13.7 μM, respectively, whereas displayed no significant cytotoxic activity against normal cell lines (HUVEC and CLiver) with the IC_{50} values higher than 40 μM. The selectivity index values (SI, IC_{50} normal cell line/IC_{50} cancer cell line) for compound **5** were found

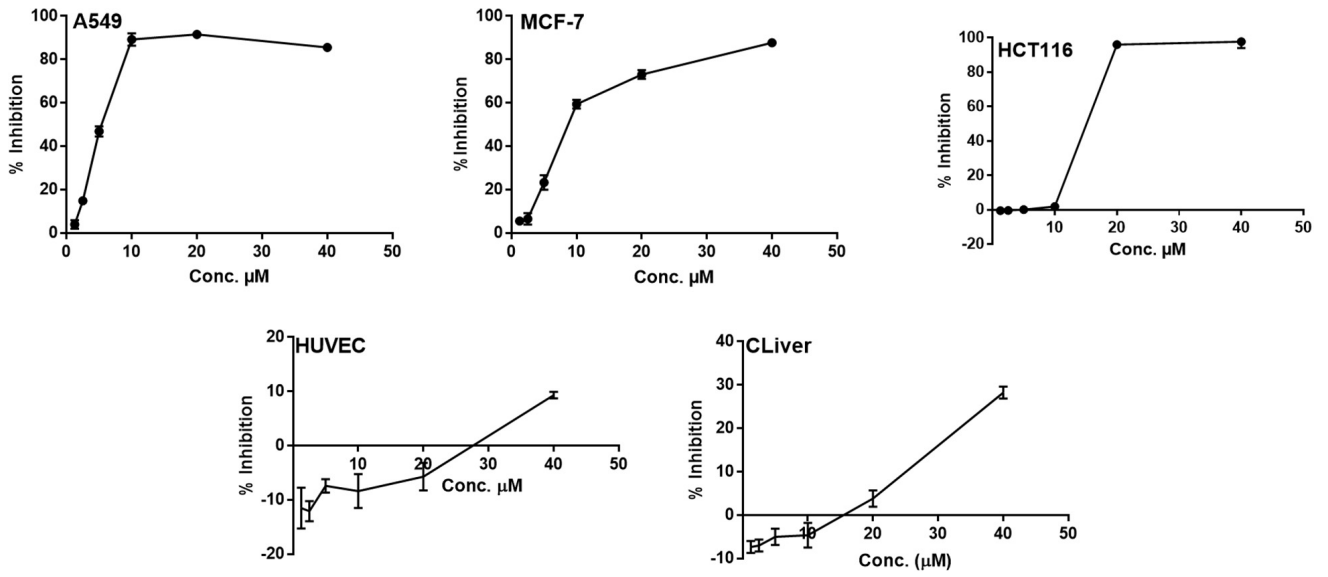

FIGURE 5 | The dose response curve of the cytotoxicity of compound **5** toward A549, MCF-7 HCT 116, HUVEC and CLiver cell lines. Cells were exposed to compound **5** with different concentrations for 72 h. Cell inhibition was determined by SRB stain.

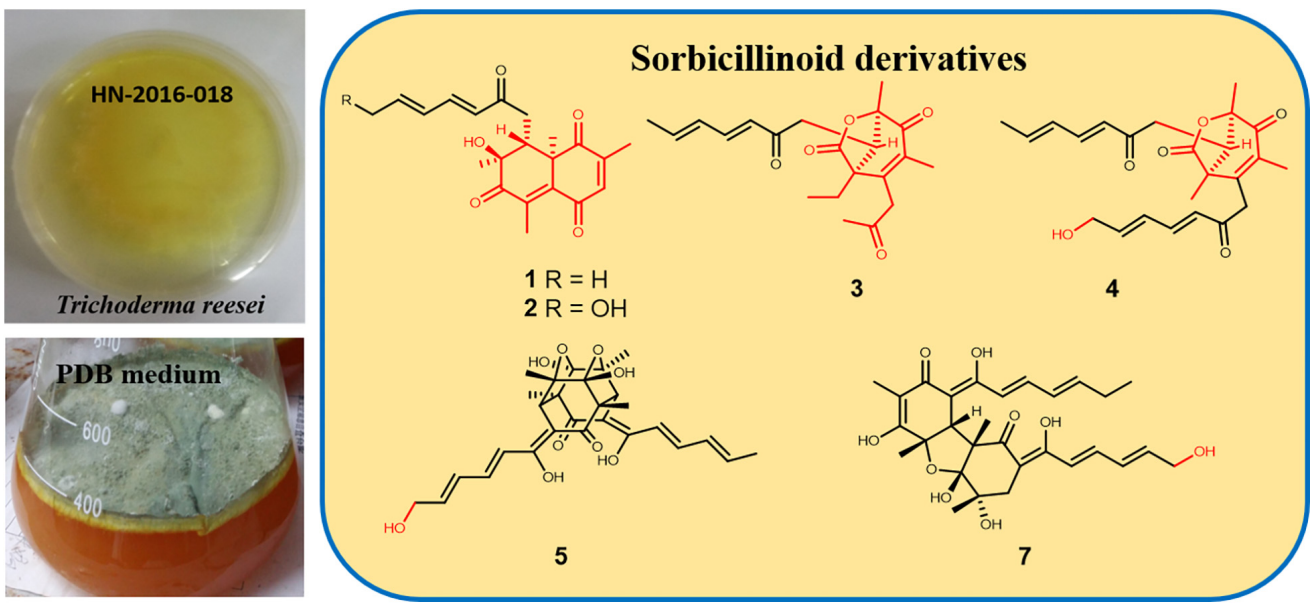

FIGURE 6 | Structural features of isolated sorbicillinoids.

to be higher than 7.8, 4.2, and 2.9, respectively, indicating its selective cytotoxicity.

CONCLUSION

In summary, we report here nine sorbicillinoid derivatives (**1**–**9**), including six new compounds, isolated from the sponge-derived fungus *T. reesei* (HN-2016-018). To date, more than 130 sorbicillinoid derivatives have been reported (Meng et al., 2016, 2018, 2019; Zhang et al., 2018, 2019; Cao et al., 2019; Wang et al., 2019; Yu et al., 2019). In this study, we discovered two novel sorbicillinoids (**1**–**2**) with a characteristic naphthalene-trione ring and two rare sorbicillinoids (**3**–**4)** possessing a bicycle (3.2.1) lactone skeleton (**Figure 6**), where only three compounds with such distinctive skeleton have been reported previously. Furthermore, compound **3** represented the first reported sorbicillinoid with a propan-2-one side chain, while a terminal hydroxylation at the side chain of compounds **2**, **4**, **5,** and **7** was also rare in the sorbicillinoid family. Compound **5** displayed strong cytotoxic activity against A549, MCF-7, and HCT116 cell lines. This study enriched the structural diversity of sorbicillinoids and provided the chemical entities for the development of marine bioactive natural products.

DATA AVAILABILITY STATEMENT

The original contributions presented in the study are included in the article/**Supplementary Material**, and further inquiries can be directed to the corresponding author/s.

AUTHOR CONTRIBUTIONS

C-YW and C-LS conceived of and proposed the idea. SR contributed to fermentation, extraction, and isolation. SR and L-JY contributed to the manuscript preparation. WH contributed to bioactivities test. SR, L-JY, J-SW, TS, and Y-HZ contributed to data analysis, write up, revision, and proofreading of the manuscript. All authors read and approved the final manuscript.

FUNDING

This work was supported by the Marine S&T Fund of Shandong Province for Pilot National Laboratory for Marine Science and Technology (Qingdao, China) (2018SDKJ0406-5), the National Natural Science Foundation of China (Nos. 41830535 and U1706210), and the National Science and Technology Major Project for Significant New Drugs Development, China (No. 2018ZX09735-004). We appreciated the Program of Open Studio for Druggability Research of Marine Natural Products, Pilot National Laboratory for Marine Science and Technology (Qingdao, China) directed by Kai-Xian Chen and Yue-Wei Guo, and the Taishan Scholars Program, China.

SUPPLEMENTARY MATERIAL

The Supplementary Material for this article can be found online at: https://www.frontiersin.org/articles/10.3389/fmicb.2020.01334/full#supplementary-material

REFERENCES

Abe, N., Murata, T., and Hirota, A. (1998). Novel DPPH radical scavengers, bisorbicillinol and demethyltrichodimerol, from a fungus. *Biosci. Biotech. Bioc.* 62, 661–666. doi: 10.1271/bbb.62.661

Andrade, R., Ayer, W. A., and Mebe, P. P. (1992). The metabolites of *Trichoderma longibrachiatum*. Part 1. isolation of the metabolites and the structure of trichodimerol. *Can. J. Chem.* 70, 2526–2535. doi: 10.1139/v92-320

Andrade, R., Ayer, W. A., and Trifonov, L. S. (1996). The metabolites of *Trichoderma longibrachiatum*. Part II The structures of trichodermolide and sorbiquinol. *Can. J. Chem.* 74, 371–379. doi: 10.1139/v96-042

Bruhn, T., Schaumlöffel, A., Hemberger, Y., and Bringmann, G. (2013). SpecDis: quantifying the comparison of calculated and experimental electronic circular dichroism spectra. *Chirality* 25, 243–249. doi: 10.1002/chir.22138

Cao, M. J., Zhu, T., Liu, J. T., Ouyang, L., Yang, F., and Lin, H. W. (2019). New sorbicillinoid derivatives with GLP-1R and eEF2K affinities from a sponge-derived fungus *Penicillium chrysogenum* 581F1. *Nat. Prod. Res.* 33, 1–7. doi: 10.1080/14786419.2019.1596099

Du, L., Zhu, T. J., Li, L. Y., Cai, S. X., Zhao, B. Y., and Gu, Q. Q. (2009). Cytotoxic sorbicillinoids and bisorbicillinoids from a marine-derived fungus *Trichoderma* sp. *Chem. Pharm. Bull.* 57, 220–223. doi: 10.1248/cpb.57.220

Ei-Elimat, T., Raja, H. A., Figueroa, M., Swanson, S. M., Falkinham, J. O., Lucas, D. M., et al. (2015). Sorbicillinoid analogs with cytotoxic and selective anti-*Aspergillus* activities from *Scytalidium album*. *J. Antibiot.* 68, 191–196. doi: 10.1038/ja.2014.125

Felsenstein, J. (1985). Confidence limits on phylogenies: an approach using the bootstrap. *Evolution* 39, 783–791. doi: 10.1111/j.1558-5646.1985.tb00420.x

Harned, A. M., and Volp, K. A. (2011). The sorbicillinoid family of natural products: isolation, biosynthesis, and synthetic studies. *Nat. Prod. Rep.* 28, 1790–1810.

Li, D., Xu, Y., Shao, C. L., Yang, R. Y., Zheng, C. J., Chen, Y. Y., et al. (2012). Antibacterial bisabolane-type sesquiterpenoids from the sponge-derived fungus *Aspergillus* sp. *Mar. Drugs* 10, 234–241. doi: 10.3390/md10010234

Li, D. H., Cai, S. X., Zhu, T. J., Wang, F. P., Xiao, X., and Gu, Q. Q. (2011). New cytotoxic metabolites from a deep-sea-derived fungus. *Phialocephala* sp., Strain FL30r. *Chem. Biodivers.* 8, 895–901. doi: 10.1002/cbdv.201000134

Liu, L., Zheng, Y. Y., Shao, C. L., and Wang, C. Y. (2019). Metabolites from marine invertebrates and their symbiotic microorganisms: molecular diversity discovery, mining, and application. *Mar. Life Sci. Tech.* 1, 60–94. doi: 10.1007/s42995-019-00021-2

Meng, J. J., Cheng, W., Heydari, H., Wang, B., Zhu, K., Konuklugil, B., et al. (2018). Sorbicillinoid-based metabolites from a sponge-derived fungus *Trichoderma saturnisporum*. *Mar. Drugs* 16:226. doi: 10.3390/md16070226

Meng, J. J., Gu, G., Dang, P. Q., Zhang, X. P., Wang, W. X., Dai, J. G., et al. (2019). Sorbicillinoids from the fungus *Ustilaginoidea virens* and their phytotoxic, cytotoxic, and antimicrobial activities. *Front. Chem.* 7:435. doi: 10.3389/fchem.2019.00435

Meng, J. J., Wang, X. H., Xu, D., Fu, X. X., Zhang, X. P., Lai, D. W., et al. (2016). Sorbicillinoids from fungi and their bioactivities. *Molecules* 21:715. doi: 10.3390/molecules21060715

Nicolaou, K. C., Vassilikogiannakis, G., Simonsen, K. B., Baran, P. S., Zhong, Y. L., Vidali, V. P., et al. (2000). Biomimetic total synthesis of bisorbicillinol, bisorbibutenolide, trichodimerol, and designed analogues of the bisorbicillinoids. *J. Am. Chem. Soc.* 122, 3071–3079. doi: 10.1021/ja9942843

Peng, J., Zhang, X., Du, L., Wang, W., Zhu, T., Gu, Q., et al. (2014). Sorbicatechols A and B, antiviral sorbicillinoids from the marine-derived fungus *Penicillium chrysogenum* PJX-17. *J. Nat. Prod.* 77, 424–428. doi: 10.1021/np400977e

Qi, J., Shao, C. L., Li, Z. Y., Gan, L. S., Fu, X. M., Bian, W. T., et al. (2013). Isocoumarin derivatives and benzofurans from a sponge-derived *Penicillium* sp. fungus. *J. Nat. Prod.* 76, 571–579. doi: 10.1021/np3007556

Saitou, N., and Nei, M. (1987). The neighbor-joining method: a new method for reconstructing phylogenetic trees. *Mol. Biol. Evol.* 4, 406–425.

Skehan, P., Storeng, R., Scudiero, D., Monks, A., McMahon, J., Vistica, D., et al. (1990). New colorimetric cytotoxicity assay for anticancer-drug screening. *J. Natl. Cancer I.* 82, 1107–1112. doi: 10.1093/jnci/82.13.1107

Trifonov, L. S., Hilpert, H., Floersheim, P., Dreiding, A. S., Rast, D. M., Skrivanova, R., et al. (1986). Bisvertinols: a new group of dimeric vertinoids from *Verticillium intertextum*. *Tetrahedron* 42, 3157–3179. doi: 10.1016/s0040-4020(01)87382-8

Wang, C. Y., Hao, J. D., Ning, X. Y., Wu, J. S., Zhao, D. L., Kong, C. J., et al. (2018). Penicilazaphilones D and E: two new azaphilones from a sponge-derived strain of the fungus *Penicillium sclerotiorum*. *RSC Adv.* 8, 3438–3453.

Wang, J. J., Li, K. L., Luo, X. W., Wu, Z. Y., Gu, T. W., Liao, S. R., et al. (2019). Sorbicillfurans A and B, two novel sorbicillinoid adducts from the fungus *Penicillium citrinum* SCSIO41402. *Org. Biomol. Chem.* 17, 8721–8725. doi: 10.1039/c9ob01595g

Wu, J. S., Yao, G. S., Shi, X. H., Rehman, S. U., Xu, Y., Fu, X. M., et al. (2020). Epigenetic agents trigger the production of bioactive nucleoside derivatives and bisabolane sesquiterpenes from the marine-derived fungus *Aspergillus versicolor*. *Front. Microbiol.* 11:85. doi: 10.3389/fmicb.2020.00085

Yu, J., Han, H., Zhang, X. Y., Ma, C. T., Sun, C. X., Che, Q., et al. (2019). Discovery of Two new sorbicillinoids by overexpression of the global regulator LaeA in a marine-derived fungus *Penicillium dipodomyis* YJ-11. *Mar. Drugs* 17:446. doi: 10.3390/md17080446

Zhai, M. M., Qi, F. M., Li, J., Jiang, C. X., Hou, Y., Shi, Y. P., et al. (2016). Isolation of secondary metabolites from the soil-derived fungus *Clonostachys rosea* YRS-06, a biological control agent, and evaluation of antibacterial activity. *J. Agric. Food Chem.* 64, 2298–2306. doi: 10.1021/acs.jafc.6b00556

Zhang, P. P., Deng, Y. L., Lin, X. J., Chen, B., Li, J., Liu, H. J., et al. (2019). Anti-inflammatory mono-and dimeric sorbicillinoids from the marine-derived fungus *Trichoderma reesei* 4670. *J. Nat. Prod.* 82, 947–957. doi: 10.1021/acs.jnatprod.8b01029

Zhang, Z. Z., He, X. Q., Che, Q., Zhang, G. J., Zhu, T. J., Gu, Q. Q., et al. (2018). Sorbicillasins A–B and scirpyrone K from a deep-sea-derived fungus, *Phialocephala* sp. FL30r. *Mar. Drugs* 16:245. doi: 10.3390/md16070245

Zhao, D. L., Shao, C. L., Gan, L. G., Wang, M., and Wang, C. Y. (2015). Chromone derivatives from a sponge-derived strain of the fungus *Corynespora cassiicola*. *J. Nat. Prod.* 78, 286–293. doi: 10.1021/np5009152

Conflict of Interest: The authors declare that the research was conducted in the absence of any commercial or financial relationships that could be construed as a potential conflict of interest.

frontiers in Microbiology

ORIGINAL RESEARCH
published: 10 July 2020
doi: 10.3389/fmicb.2020.01393

Exploration of Anti-infectives From Mangrove-Derived *Micromonospora* sp. RMA46 to Combat *Vibrio cholerae* Pathogenesis

Hema Bhagavathi Sarveswari[1], Shanthini Kalimuthu[1], Karthi Shanmugam[1], Prasanna Neelakantan[2] and Adline Princy Solomon[1]**

[1] *Quorum Sensing Laboratory, Centre for Research in Infectious Diseases, School of Chemical and Biotechnology, SASTRA Deemed to be University, Thanjavur, India,* [2] *Faculty of Dentistry, The University of Hong Kong, Pok Fu Lam, Hong Kong*

Vibrio cholerae, the etiological agent of cholera, employs quorum sensing (QS) pathways to control the expression of virulence factors, including the production of cholera toxin and biofilm formation. Acquired antibiotic resistance in *V. cholerae* draws attention to the development of novel therapeutics that counteract virulence, rather than the viability of the pathogen. In this context, we explored the anti-infective potential of rare marine Actinobacteria (RMA) from a mangrove ecosystem. Here, we report the effects of *Micromonospora* sp. RMA46 against *V. cholerae in vitro*. The RMA46 organic extract was non-bactericidal to *V. cholerae* cells and non-cytotoxic to macrophage RAW264.7 cell lines. RMA46 inhibited the formation of *V. cholerae* biofilms and downregulated the QS global switches LuxO and HapR, as well as other virulence genes including *ct*, *tcp*, and *hap*A. *In silico* molecular docking simulation of RMA46 ethyl acetate extract with LuxO and HapR revealed that 2-methoxy-4-vinylphenol and hexahydro-3-(phenylmethyl)-pyrrolo[1,2-*a*]pyrazine-1,4-dione could interact with the active sites of LuxO and HapR and potentially inhibit them. This study highlights *Micromonospora* sp. RMA46 as a potential source of anti-infectives against *V. cholerae*.

Keywords: anti-infectives, anti-virulence, anti-biofilm, rare marine Actinobacteria, *Micromonospora* species, marine compounds, *Vibrio cholerae*

OPEN ACCESS

Edited by:
Jinwei Zhang,
University of Exeter, United Kingdom

Reviewed by:
Srinivasan Ramanathan,
Fujian Agriculture and Forestry University, China
Shunmugiah Karutha Pandian,
Alagappa University, India

****Correspondence:***
Prasanna Neelakantan
prasanna@hku.hk
Adline Princy Solomon
adlineprinzy@biotech.sastra.edu;
adlineprincy@gmail.com

Specialty section:
This article was submitted to Microbiotechnology, a section of the journal Frontiers in Microbiology

Received: *02 April 2020*
Accepted: *29 May 2020*
Published: *10 July 2020*

Citation:
Sarveswari HB, Kalimuthu S, Shanmugam K, Neelakantan P and Solomon AP (2020) Exploration of Anti-infectives From Mangrove-Derived Micromonospora sp. RMA46 to Combat Vibrio cholerae Pathogenesis. Front. Microbiol. 11:1393. doi: 10.3389/fmicb.2020.01393

INTRODUCTION

Vibrio cholerae, a Gram-negative bacterium from the family Vibrionaceae, causes cholera, a self-limiting acute diarrheal disease (Zhu and Mekalanos, 2003). This contagious disease spreads primarily through the fecal–oral route and by consumption of contaminated food and water (Sack et al., 2004; Clemens et al., 2017). *V. cholerae* is classified into more than 200 serogroups on the basis of their lipopolysaccharide antigens, yet only two serogroups, O1 and O139, are associated with epidemic outbreaks of cholera (Wang et al., 2016). It is estimated that about 2.86 million people are affected by cholera in endemic countries, resulting in 95,000 deaths annually (Ali et al., 2015).

Antibiotic therapy is crucial for the treatment of cholera, as it abates the period of diarrhea, the amount of rehydration fluids, and the density of vibrios excreted in the stools (World Health Organization [WHO], 2019). Over the years, the rapid emergence of extensive drug-resistant (XDR) and multidrug-resistant (MDR) *V. cholerae* strains

possess a great public health threat, owing to their association with treatment failure and potential dissemination of resistance among other pathogens through mobile genetic elements (MGEs) (Chowdhury et al., 2016; Clemens et al., 2017; Verma et al., 2019; Gladkikh et al., 2020). The above caveats compel the need for developing novel strategies to thwart *V. cholerae* infection. Numerous studies have focused on developing compounds that target other fitness tactics of bacteria instead of developing newer antibiotics (Hema et al., 2016, 2017).

V. cholerae demonstrates extraordinary fitness by coordinated group behavior in expressing virulence factors through quorum sensing (QS) pathways (Miller and Mekalanos, 1984; Hammer and Bassler, 2003). There are two major parallel QS systems in *V. cholerae* comprising cholera autoinducer-1 (CAI-1), autoinducer 2 (AI-2), and their corresponding cognate inner membrane receptors (CqsS and LuxP/Q) (Miller et al., 2002; Rutherford et al., 2011). These individual receptors converge the information to a global response regulator, LuxO, in response to the low and high concentrations of their respective signals. Under low signal strength (LSS), the receptors function as kinases and phosphorylate LuxO, which activates the transcription of quorum regulatory RNAs (Qrrl-4) and controls the translation of two master regulators, AphA and HapR. The *qrr*1-4 small RNAs upregulate the expression of AphA and concurrently repress the expression of HapR (Rutherford et al., 2011). In turn, AphA regulates the expression of biofilm activator (VpsT), toxin-coregulated pilus (TCP), and cholera toxin (CTX), commencing the process of adhesion and production of CTX in humans (Lenz et al., 2004; Yang et al., 2010; Rutherford et al., 2011). These processes are key to the colonization of this bacterium in the intestine and form microcolonies. By contrast, under high signal strength (HSS), the receptors function as phosphatases, leading to dephosphorylation and inactivation of LuxO. This results in the downregulation of virulence and biofilm formation by the expression of hemagglutinin/protease A (HapA). HapA expression facilitates the dissemination of bacteria from the intestinal cells. Thus, LSS promotes infection, whereas HSS promotes bacterial detachment from the intestinal cells, resulting in dissemination (Zhu et al., 2002; Hammer and Bassler, 2003).

Anti-virulence therapy using synthetic and natural molecules that interfere with QS pathways in pathogens has been explored extensively. These molecules function either as an inhibitor or an agonist of the factors involved in QS signaling, affecting their biosynthesis, detection, signal transduction, and even as enzymes that inactivated the QS signal molecules (Defoirdt, 2018). Such QS molecules that occur naturally have been sourced from various plants, microorganisms, and higher organisms from a wide range of terrestrial and marine ecosystems. Among microorganisms, the phylum Actinobacteria has been a prodigious source of anti-virulence agents, providing a range of chemicals that interfere with the QS system of various human pathogens (Sarveswari and Solomon, 2019). In this work, we isolated and screened 42 rare marine Actinobacteria (RMA) from mangrove soil against rugose *V. cholerae* HYR14 biofilm and virulence. The organic solvent of RMA displaying a significant anti-biofilm activity was also analyzed for its potential to inhibit virulence mechanism through gene expression studies. Finally, the potential interaction of the active principles identified in the organic extract of RMA with the *V. cholerae* global response regulators LuxO and HapR was analyzed through *in silico* docking studies.

MATERIALS AND METHODS

Target Bacterial Strains and Culture Conditions

Vibrio cholerae biofilm-forming rugose strain, HYR14 obtained from NICED, India, was used throughout this study (Chowdhury et al., 2016). The strain was cultured in thiosulfate–citrate–bile salts–sucrose (TCBS) agar to confirm cell viability and propagated under standard growth conditions in Luria–Bertani (LB) broth at 37°C. An inoculum size of 0.2 (OD_{595}) $\approx 10^5$ cells were used for all the experiments (Hema et al., 2016).

Soil Sampling From Mangrove Ecosystem

Mangrove soil was sampled from Muthupet Mangrove Reserve, Tamil Nadu, India (**Supplementary Table S1**). Soil samples were collected using sterile containers from a site that was 20 m away from the shore and with 20 m depth. The samples were transported to the laboratory under cooling conditions and stored at 4°C in a dry condition prior to examination (Hong et al., 2009). The physio-chemical parameters such as salinity and temperature were measured using a handheld refractometer (Erma, Japan) during sample collection. The pH of the samples was determined using Eutech pH meter (Oakton, United States).

Pretreatment of Mangrove Soil and Selective Isolation of Rare Marine Actinobacteria

The soil was sieved through a large mesh to eliminate organic particles and was homogenized using a mortar and pestle. About 1 g of the homogenized samples was pretreated by 120°C for 60 min (dry heat) (Pisano et al., 1986) and by 1.5% of phenol for 30 min at 30°C (Pisano et al., 1986) and through moist heating with sterilized mangrove water at 50°C for 15 min (Takahashi, 2004). The pretreated soil samples were then serially diluted [1:10 (v/v) ratio] with sterile saline solution, and about 100 μl was spread plated on various isolation media. For selective isolation of RMA, International Streptomyces Project medium (ISP1 to ISP7) (Shirling and Gottlieb, 1966), actinomycetes isolation agar, starch casein agar, and humic acid–vitamin agar (Hayakawa and Nonomura, 1987) (HiMedia Laboratories, Mumbai, India) (**Supplementary Table S2**) supplemented with the filter-sterilized cycloheximide (40 μg/ml) and nalidixic acid (40 μg/ml) were used. The inoculated Petri plates were then incubated at 28°C for 4–6 weeks and regularly checked for the growth of actinomycetes-like colonies. Single discrete actinomycetes-like colonies grown on spread plated isolation media were re-subcultured on to ISP4 and actinomycetes isolation agar and further incubated at 28°C for the isolation of pure colonies

(Shirling and Gottlieb, 1966). Collection of pure colonies of the RMA isolates was stored at 4°C on ISP4 agar slants and also as lyophilized cultures for short-term and long-term storages, respectively.

Cultural, Morphological, and Biochemical Characterization of Rare Marine Actinobacteria Isolates

The RMA isolates collected from various isolation media were subjected to morphological characterization and biochemical analysis (Pridham and Gottlieb, 1948; Shirling and Gottlieb, 1966). Light microscopy was used to observe the morphologies of Actinobacteria isolates including the arrangement of mycelium and formation of spores by Gram's staining. The culture characteristics, including growth patterns on different media, pigmentation, colony color, presence, and color of aerial and substrate mycelium on various ISP media (ISP1 to ISP7), were determined.

Fermentation and Ethyl Acetate Extract Preparation

International Streptomyces Project medium no. 2 (ISP2) (0.5 g of peptone, 0.3 g of malt extract, 0.3 g of yeast extract, and 1.0 g of dextrose pH 6.2 ± 0.2) was used as fermentation medium for the exploration of the secondary metabolites produced by the 42 mangrove Actinobacteria isolates. The ISP2 medium was sterilized by autoclave at 121°C at 15 lb for 20 min. Initially, about four to five colonies from pure culture were inoculated into modified ISP2 media supplemented with 2.0 g/l of calcium carbonate in an Erlenmeyer conical flask and incubated at 150 rpm at 28°C for 7 days. After the incubation period, 5% (v/v) of well-grown culture from the calcium carbonate-supplemented ISP2 medium was inoculated into ISP2 media in an Erlenmeyer conical flask. The flask was incubated at 150 rpm at 28°C for 14 days. The uninoculated ISP2 medium served as a medium control, to ensure purity. After fermentation, the spent medium of the isolates was centrifuged at 5,000 rpm for 10 min, and the culture supernatant was filtered through a 0.2 μm nitrocellulose filter. The cell-free extracts were stored at -20°C. For the extraction of secondary metabolites by ethyl acetate, the cell-free filtrate was extracted twice with an equal volume of ethyl acetate, and the organic extract was condensed by evaporating ethyl acetate using a rotational evaporator (Heidolph Laborata, 4001) (Balasubramanian et al., 2017). The organic extract was resuspended in ethyl acetate and was used for further studies.

Efficacy of Rare Marine Actinobacteria Cell-Free Extract Against *Vibrio cholerae* HYR14 Biofilm

The antibiofilm activity of various dilutions of the 42 RMA cell-free extracts (50, 25, 12.50, 6.25, and 3.13%) was investigated. One hundred microliters (final volume) of LB broth containing various concentrations of RMA cell-free extract was aliquoted into a 96-well microtiter plate. Ten microliters of an overnight-grown culture of *V. cholerae* HYR14 strain that has been diluted up to 1:100 (OD_{595} = 0.2) was inoculated into each well, and the plates were incubated at 37°C for 24 h. Controls were included for all the experiments. After the incubation period, the plates were subjected to crystal violet staining. The medium and the planktonic cells present in the 96-well microtiter plates were aspirated at the end of the incubation period. The non-adherent HYR14 cells present in the wells were discarded by washing the wells thrice with sterile 1× phosphate-buffered saline. The microtiter plates were then air-dried for 20 min at ambient temperature to fix the adherent biofilms. To the dried wells, 100 μl of 0.2% (w/v) crystal violet was added and incubated for 20 min at room temperature. After the incubation period, the excess stain was washed off with sterile water twice, and the plates were air-dried completely. The bound crystal violet was solubilized by pipetting 100 μl of 33% glacial acetic acid into each well (Kaur et al., 2016). The absorbance of the wells was measured at 595 nm using an iMark™ microplate absorbance reader (Bio-Rad Laboratories, Inc., United States).

Nucleic Acid-Based Identification of Rare Marine Actinobacteria Strain Demonstrating *Vibrio cholerae* Biofilm Inhibitory Activity

The extraction of the genomic DNA of the RMA strain exhibiting a significant inhibitory activity against the *V. cholerae* HYR14 biofilm was performed using commercially available DNeasy Blood and Tissue kits (Qiagen, Germany) as per the manufacturer-recommended protocol (Ahmed et al., 2008). Until further use, the eluted DNA was stored at -20°C. Nested PCR targeting the 16SrRNA of the eubacterial genome was done using primers: forward primer (U1): 5′-TTGGAGAGTTTGATCCTGGCTC-3′ and reverse primer U4: 5′-GGACTACCAGGGTATCTA-3′ for the first round of nested PCR and forward primer (U2): 5′-TTGGAGAGTTTGATCCTGGCTC-3′) and reverse primer (U3): 5′-GCGGCTGGCACGTAGTTAG-3′ for the second round of nested PCR (Therese et al., 1998). The reaction conditions were set as described in Kharel (Sitaula) et al. (2018). The amplified product was then cyclo-sequenced, purified, and loaded to ABI3200 genetic analyzer (Applied Biosystems, United States) and sequenced as described previously (Aarthi et al., 2011). The obtained sequence was analyzed using BioEdit software (version 7.0.5.3) and was compared with 16S rRNA sequence database of National Center for Biotechnology Information (NCBI) using nucleotide BLAST (Altschul et al., 1990). The phylogenetic tree was constructed using the neighbor-joining method (Perrière and Gouy, 1996) and was validated using bootstrap analysis. The sequence was submitted to GenBank for accession number.

Quantification of Biofilm Formation and Eradication

To evaluate the effect of RMA46 organic extract on mature *V. cholerae* biofilm, 100 μl of fresh LB broth was aliquoted into a 96-well microtiter plate. This was inoculated with

10 μl of an overnight-grown culture of *V. cholerae* HYR14 strain that had been diluted up to 1:100 (OD_{595} = 0.2). The microtiter plate was incubated at 37°C for 24 h. After the incubation period, the non-adherent planktonic cells were aspirated gently without disturbing the biofilm. To the wells, 100 μl (final volume) of LB broth containing various concentrations of RMA46 organic extract (50–0.13 mg/ml) was aliquoted. The microtiter plate was incubated again at 37°C for 24 h. Following the incubation period, crystal violet assay was performed to evaluate the potential of RMA46 organic extract on eradication of *V. cholerae* biofilm. Untreated and vehicle controls were also included for all experiments (Balasubramanian et al., 2017).

To quantify the effect of RMA46 organic extract on the formation of *V. cholerae* biofilm, 100 μl (final volume) of LB broth containing various concentrations of RMA46 organic extract (50–0.13 mg/ml) was aliquoted into 96-well microtiter plate. Ten microliters of an overnight-grown culture of *V. cholerae* HYR14 strain that has been diluted up to 1:100 (OD_{595} = 0.2) was inoculated into each well, and the plates were incubated at 37°C for 24 h. After the incubation period, the plates were subjected to crystal violet staining. Untreated and vehicle controls were also included for all experiments.

For crystal violet staining, the medium and the planktonic cells present in the 96-well microtiter plates were aspirated at the end of the incubation period. The non-adherent HYR14 cells present in the wells were discarded by washing the wells thrice with sterile 1 × phosphate-buffered saline. The microtiter plates were then air-dried for 20 min at ambient temperature to fix the adherent biofilms. To the dried wells, 100 μl of 0.2% (w/v) crystal violet was added and incubated for 20 min at room temperature. After the incubation period, the excess stain was washed off with sterile water twice, and the plates were air-dried completely. The bound crystal violet was solubilized by pipetting 100 μl of 33% glacial acetic acid into each well (Kaur et al., 2016). The absorbance of the wells was measured at 595 nm using an iMark™ microplate absorbance reader (Bio-Rad Laboratories, Inc., United States).

Confocal Laser Scanning Microscopic Analysis

V. cholerae HYR14 (OD_{595} = 0.1) and RMA46 ethyl acetate extract at a concentration of (9.3 mg/ml) were inoculated into LB medium in cell culture plate containing sterile borosilicate coverslips and were incubated statically at 37°C for 24 h. After 24 h, the suspension was aspirated and removed carefully. The biofilms established on the coverslips were rinsed with 0.9% NaCl solution. Stock solutions of SYTO™ 9 green fluorescent stain (Thermo Fisher Scientific) and propidium iodide red fluorescent dyes (BacLight, Invitrogen Ltd.) were prepared at 1:1 ratio and stored at −20°C until further use. Briefly, 200 μl of the dyes was added to the coverslips and incubated at room temperature for 15 min under dark conditions. After incubation, the dyes were aspirated, and the coverslips were carefully washed with 0.9% NaCl. The washed coverslips were air-dried at ambient temperature and fixed on a sterile glass slide. These slides were observed under a 40× objective using a confocal laser scanning microscope (Olympus FLUOVIEW, FV1000). The biomass, average thickness, and roughness coefficient of biofilms were analyzed using COMSTAT package in MATLAB R2017b (Heydorn et al., 2000).

Cell Viability Assay

The effect of the RMA46 ethyl acetate extract on host cell viability was assayed using murine macrophages RAW264.7, cultured in Dulbecco's modified Eagle's medium (DMEM) supplemented with 10% fetal bovine serum (FBS), 1% penicillin/streptomycin (w/v), and 1% L-glutamine using the MTT (3-(4,5-dimethylthiazol-2-yl)-2,5-diphenyltetrazolium bromide) assay. About 1 × 10^4 RAW264.7 cells/well were seeded in a 96-well microtiter plate and incubated at 37°C in a CO_2 incubator for 24 h. After the incubation period, the cells were treated with various concentrations (0.13, 0.39, and 9.375 mg/ml) of *Micromonospora* sp. RMA46 ethyl acetate extract and incubated for another 24 h at 37°C in a CO_2 incubator. After 24 h, 1 mg/ml of MTT was added, and the microtiter plate was incubated at 37°C for 3 h. Dimethyl sulfoxide (DMSO) was added to dissolve the formazan crystals, and absorbance was read at 570 nm using a microplate reader spectrophotometer (Synergy H1) (Kartik et al., 2020).

Extraction of RNA and Quantitative Analysis of Virulence Gene Expression in *Vibrio cholerae* HYR14

Total RNA was extracted from the RMA46 extract-treated and untreated *V. cholerae* HYR14 from stationary phase culture (24 h) using RNeasy® Protect Bacteria Mini Kit (Qiagen), according to the manufacturer's guidelines. The purity and integrity of the isolated RNA were checked using NanoDrop (Thermo Fisher Scientific, United States). Preparation of cDNA was performed using the iScript™ cDNA Synthesis kit with a concentration of 100 ng following the manufacturer's guidelines. The following conditions were set for cDNA synthesis; 24°C for 5 min (annealing), 42°C for 30 min (extension), and 85°C for 5 min (inactivation). The effect of RMA46 ethyl acetate extract on the virulence gene expression in the HYR14 strain was analyzed by qRT-PCR using primers listed in **Supplementary Table S4**. The 16s rRNA was used as the reference gene. The relative gene expression was calculated using the $2^{-\Delta\ \Delta\ CT}$ method (Vezzulli et al., 2015; Hema et al., 2017).

Gas Chromatography–Mass Spectrometry Analysis

Separation and identification of the active compounds present in the ethyl acetate extract of RMA46 were performed with a PerkinElmer Clarus 500 GC-MS system. Helium was employed as a carrier gas at a flow rate of 1 ml/min, and the injector temperature was set at 280°C. The program of the column temperature was held at 50°C for 1 min

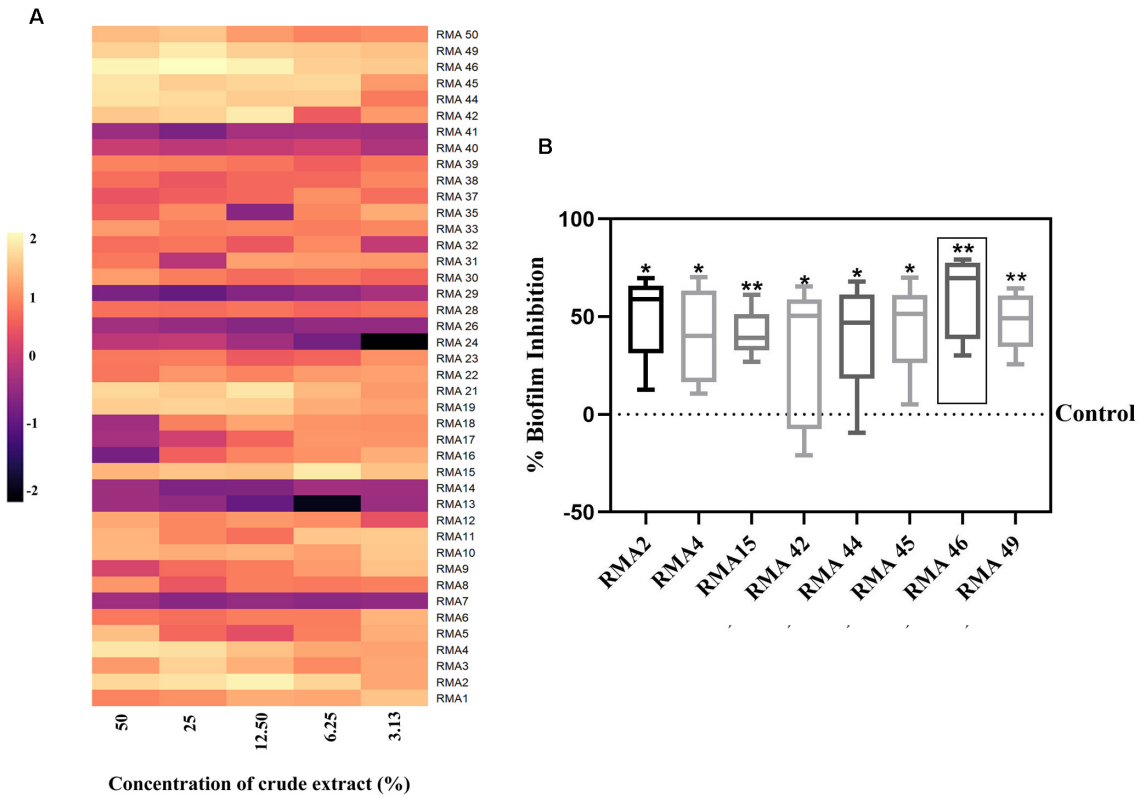

FIGURE 1 | (A) Effect of various concentrations of cell-free extract of 42 rare marine Actinobacteria (RMA) [50, 25, 12.50, 6.25, and 3.13% (v/v)] on 24 h biofilm of *Vibrio cholerae* HYR14. **(B)** Comparison of various concentrations [50, 25, 12.50, 6.25, and 3.13% (v/v)] of cell-free extracts of selected RMA strains that demonstrated significant HYR14 biofilm inhibitory activity. RMA46 displays the maximum ($p < 0.01$) inhibition than do all the other strains. A one-sample *t*-test was used for significance analysis. *$p < 0.05$, and **$p < 0.01$.

and increased at 10°C/min to 150°C (1 min hold), to 250°C for 1 min hold, and then at 15°C/min to 300°C (3 min hold). The mass spectrometer was operated at a mass range of 40–450 amu. One microliter of RMA46 extract dissolved in ethyl acetate was injected into the system. The separated compounds were identified by comparing their spectra with those in the National Institute of Standards and Technology (NIST) mass spectral library (Ravichandiran et al., 2012).

Computational Studies

Two-dimensional structures of the compounds identified in the *Micromonospora* sp. RMA46 ethyl acetate were drawn using MarvinSketch[1]. The ligands were prepared for molecular docking using LigPrep (Schrödinger, LLC, New York, NY, 2020). The primary structure of the ATP binding domain of LuxO (Q9KT84) was retrieved from Uniprot[2]. Protein BLAST (BLASTp) was performed for the query sequence against Protein Data Bank (PDB) to identify the structurally similar homolog. The QS signal integrator LuxO of *Photobacterium angustum* with the PDB accession number 5EP0 was chosen as the template. Homology modeling was performed using the protein structure prediction tool implemented in BioLuminate (Schrödinger, LLC, New York, NY, 2020). The modeled protein was subjected to a constrained energy minimization using GROMACS (Kutzner et al., 2019), and the quality of the modeled structure was further evaluated using the SAVES server[3]. The experimentally solved structure of HapR protein (2PBX) was downloaded and used for molecular docking simulations. Both the LuxO and HapR proteins were prepared using the protein preparation wizard (Sastry et al., 2013). A grid box was generated and was centered on the binding sites of the target proteins, and the docking simulation was performed using extra precision (XP) docking algorithm implemented in Glide (Schrödinger, LLC, New York, NY, 2020) (Friesner et al., 2006).

Statistical Analysis

GraphPad Prism software version 8.0.2 (GraphPad Software Inc., San Diego, CA, United States) was used for analyzing the data statistically. The significance was analyzed by Student *t*-test with p set at $p \leq 0.05$. All the assays were performed in triplicates, and the results have been expressed as mean ± SD.

[1]http://www.chemaxon.com

[2]www.uniprot.org

[3]https://servicesn.mbi.ucla.edu/SAVES

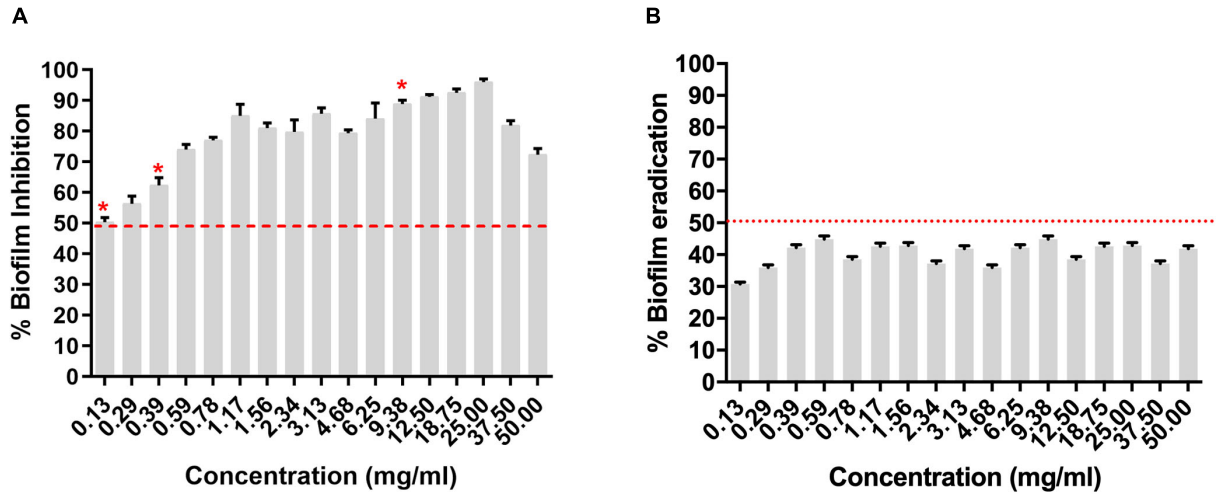

FIGURE 2 | (A) Dose-dependent inhibition of *Micromonospora* sp. RMA46 organic extract on the formation of *Vibrio cholerae* HYR14 biofilm. **(B)** Dose-dependent effect of RMA46 organic extract on preformed biofilm *V. cholerae* HYR14 biofilm. * Effective concentrations chosen for further studies.

RESULTS

Mangrove Soil Is Rich in Morphologically Distinct Rare Marine Actinobacteria

Non-*Streptomyces* like colonies that were selectively subcultured for the isolation of pure RMAs produced a wide range of colonies from round convex to dry, raised, irregularly edged colonies. These colonies also produced varied colony pigments from white, yellow, pink, orange, brownish-orange, gray, and black. Out of the 42 isolates, only one isolate (RMA44) produced diffusible pigment. Light microscopy revealed that a variety of structures including coccus, rod-coccus, coryneform, and short- and long-branched sometimes filamented hyphal formations. Many of these hyphal-producing strains also formed oval spores. The pattern of hyphae and spore formation also varied significantly among RMA isolates. A few isolates changed colony pigmentation from orange to black as the colonies got older (**Supplementary Table S3**). This showed that the mangrove soil supported a rich diversity of Actinobacteria.

Mangrove-Derived Rare Marine Actinobacteria Extract Could Attenuate *Vibrio cholerae* HYR14 Biofilm

The cell-free culture supernatants of all the 42 RMA isolates were screened for an anti-biofilm activity. The isolates RMA2, RMA4, RMA15, RMA42, RMA44, RMA45, RMA46, and RMA49 exhibited a $>$ 50% biofilm inhibitory activity (**Figure 1A**). However, the cell-free culture supernatant of RMA46 exhibited a consistent level of $\geq$ 30% inhibition of HYR14 biofilm without a bactericidal activity at all concentrations (v/v) chosen in the study (**Figure 1B** and **Supplementary Figure S1**). Therefore, the strain RMA46 was chosen for further investigations.

Isolate RMA46 Belongs to the Genus *Micromonospora*

The complete 16S rRNA sequence of the RMA46 strains (724 bp) determined in this study was deposited in GenBank database (accession number MK788184.1). To study the evolutionary relationship, similarity search of 16S rRNA sequence of RMA46 was performed against 16S rRNA database in National Center for Biotechnology Information (NCBI). The closely related sequences of RMA46 were used to construct the phylogenetic tree. The result showed that the strain RMA46 is closely related to *Micromonospora* sp. 171111 (accession number EF538723) and was clustered together in the phylogenetic tree (**Supplementary Figure S2**).

Micromonospora sp. RMA46 Ethyl Acetate Extract Effectively Inhibits Biofilm Formation by HYR14 Than by Eradicating Preformed Biofilms

The RMA46 organic extract (50–0.13 mg/ml) was evaluated for its *Vibrio cholerae* HYR14 biofilm inhibitory/disruptive potential. The RMA46 ethyl acetate extract inhibited HYR14 biofilms $\geq$ 50% at low concentrations (0.39–0.13 mg/ml). At higher concentrations (0.59–50 mg/ml), the RMA46 ethyl acetate extract effectively inhibited $>$ 70% of the HYR14 biofilm formation (**Figure 2A**). Overall, the data were consistent to show a dose-dependent increase in the inhibitory potential of RMA46 ethyl acetate extract against the *V. cholerae* HYR14 biofilm. On the contrary, the RMA46 ethyl acetate extract was unable to eradicate $>$ 50% of preformed biofilm (**Figure 2B**). Because the biofilm inhibitory concentration (BIC) of RMA46 ethyl acetate extract ranges from 50 to 90%, three effective BICs were chosen – BIC_{50} (0.13 mg/ml), BIC_{60} (0.39 mg/ml), and BIC_{90} (9.38 mg/ml) – to validate anti-infective potential.

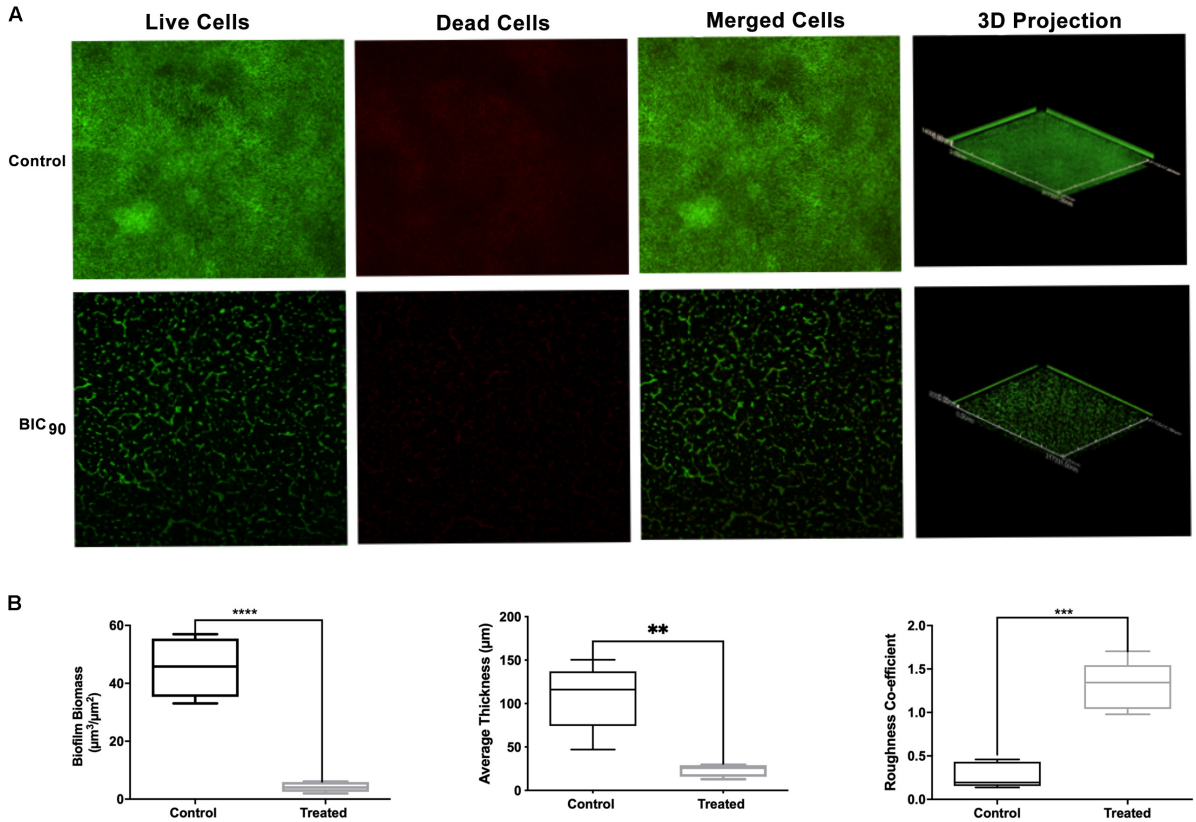

FIGURE 3 | (A) Confocal laser scanning microscopy of HYR14 biofilm in the presence of the RMA46 extract, visualized by red and green fluorescent vital dyes. **(B)** COMSTAT analysis on the biomass, average thickness, and roughness coefficient of HYR14 biofilm treated with RMA46 organic extract. Student's *t*-test was used for significance analyses. *$p < 0.05$ was considered significant. **$p < 0.01$, ***$p < 0.001$, and ****$p < 0.0001$.

RMA46 Ethyl Acetate Extract Affects the Thickness and Biomass of *Vibrio cholerae* Biofilm

Investigation on the effect of RMA46 ethyl acetate extract on HYR14 biofilm formation on coverslips was performed using confocal laser microscopy and COMSTAT analysis. Treatment with BIC_{90} (9.38 mg/ml) revealed a detached biofilm matrix, whereas the untreated control sample showed highly condensed and compact biofilms (**Figure 3A**). COMSTAT analysis revealed that the untreated *V. cholerae* formed thicker biofilms (107.7 μm) with higher biomass (45.4 $\mu m^3/\mu m^2$) and a roughness coefficient of 0.27. Yet the RMA46 ethyl acetate treated HYR14 biofilms was 23.2 μm and 4.2 $\mu m^3/\mu m^2$ in thickness and biomass, respectively. The roughness coefficient of the RMA46 treated HYR14 biofilm is 1.30. These results signify that RMA46 ethyl acetate leads to an irregular distribution and reduced biomass of HYR14 than does the untreated HYR14 biofilm (**Figure 3B**).

RMA46 Ethyl Acetate Extract Does Not Affect Mammalian Cell Viability

The effect of ethyl acetate extract of RMA46 on the viability of host cells was assessed against macrophage RAW264.7 cell lines. Three concentrations, representing BIC_{50}, BIC_{60}, and BIC_{90} (0.13, 0.39, and 9.37 mg/ml, respectively), were chosen to investigate the extract's lethality for 24 h. In all treatments compared with the control (untreated macrophage RAW264.7 cells), the viability of the cells was not affected, which indicated the non-toxic nature of the extract without affecting the cell viability (**Figure 4**).

RMA46 Extract Interferes With HYR14 Molecular Machinery

The real-time analysis of the expression pattern of *V. cholerae* HYR14 global switches (LuxO and HapR) and its downstream virulence genes – *ct*, *tcp*, small regulatory RNAs (*qrr2* and *qrr4*), *aphA*, and *hapA* – were quantified differentially under RMA46 organic (ethyl acetate) extract induced/uninduced state. At LSS, the global switch, LuxO is switched on to regulate the transcription of many other vital genes including the *tcp* and *ct* to encode toxin coregulated pilus and CTX, respectively. The small regulatory rRNA termed as *qrr*1-4 along with Hfq (RNA chaperone) binds with mRNA transcripts of *hap*R. HapR repression leads to the formation of biofilm. Similarly, at HSS, the de-repression of HapR leads to the suppression of biofilm formation and upregulation of protease

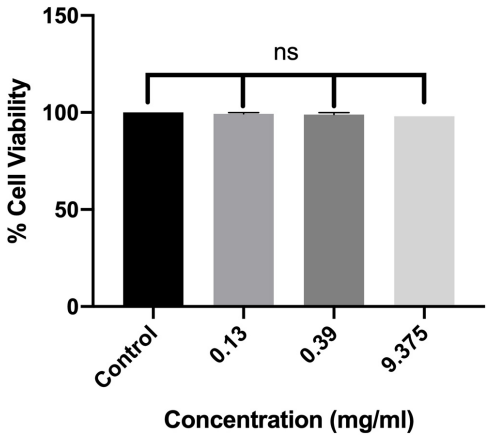

FIGURE 4 | Dose-dependent effect of RMA46 ethyl acetate extract on the cell viability. Experiments were performed in triplicates, and difference in mean values was compared with that of the untreated experiment control. One-way ANOVA was used for multiple comparison analyses. ns denotes not significant.

production, causing dissemination of *V. cholerae*. In this regard, the expression analysis at BIC_{50} showed a 2–3 $\log_2$ fold reduction in the expression of LuxO and HapR and its downstream virulence genes *hapA*, *tcp*, and *ct*. Similarly, the treated (BIC_{60}) cells showed a > 2 $\log_2$ fold downregulation in the expression of the global regulators (LuxO and HapR) and virulence genes (*tcp* and *ct*). Overall, the data were significant to show that RMA46 extract interferes with the HYR14 molecular machinery in a dose-dependent manner to downregulate to > 2–5 $\log_2$ fold, which confirmed that the entire virulence mechanism of *V. cholerae* has been switched off (**Figures 5A,B**).

Metabolic Profiling of RMA46 and Their Molecular Interaction With Active Sites of LuxO and HapR

With the use of gas chromatography–mass spectrometry (GC–MS), a total of 43 secondary metabolites were identified in the RMA46 extract belonging to different categories of secondary metabolites including alkanes (4.6%), alkenes (23.2%), carboxylic acids (25.5%), esters (6.9%), dairy ketone (4.6%), phenols (2.6%), and terpene (2.3%). The extract also contained aromatic monocyclic and heterocyclic compounds (20.9%) and other hydrocarbons (4.6%). Interestingly, the RMA46 extract also contained an oxaspiro compound (2.3%) (**Table 1** and **Supplementary Figure S3**).

QS global regulators: LuxO and HapR drive the virulence mechanism including biofilm and CTX production in *V. cholerae* in response to low and high environmental signals. Because

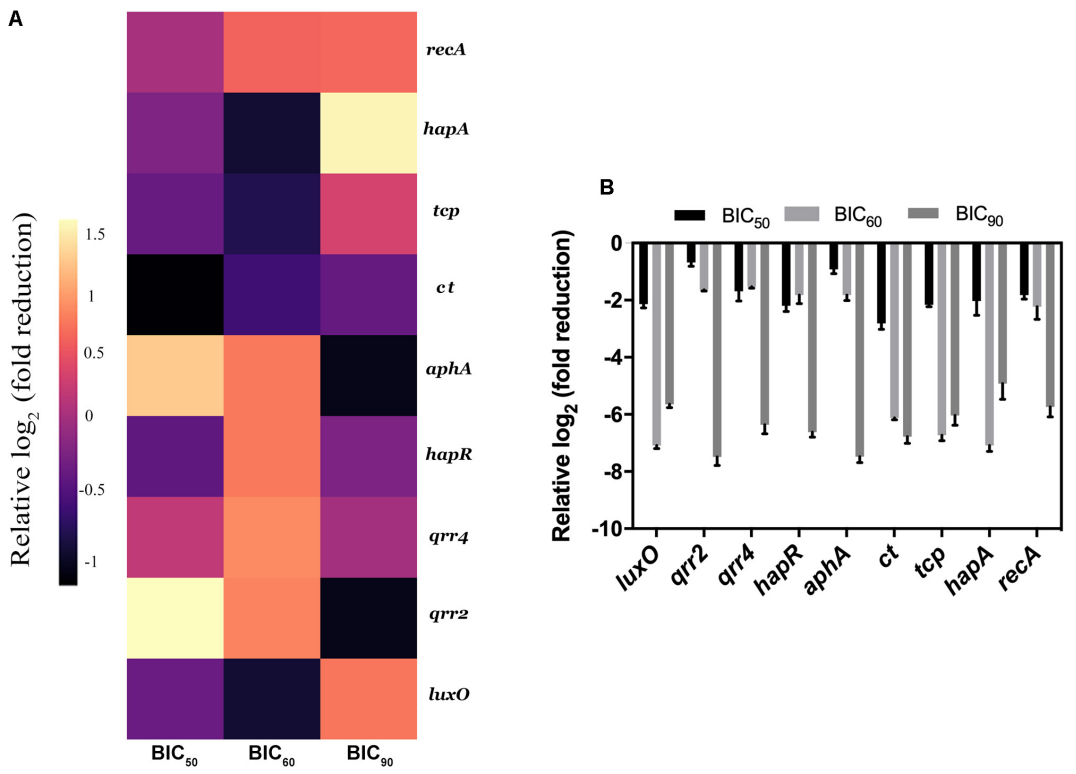

FIGURE 5 | Expression analysis of *Vibrio cholerae* virulence genes by quantitative PCR. **(A)** Heat map of real-time qRT-PCR to show the effect of RMA46 organic extract on virulence gene expression in *V. cholerae*. **(B)** Comparison between the various inhibitory concentration of RMA46 extract on HYR14 virulence-associated genes.

TABLE 1 | List of compounds identified in *Micromonospora* sp. RMA46 ethyl acetate extract using GC–MS.

S. no.	Class of compound	Name of the compound	Molecular weight (g/mol)	Retention time (min)	Peak area (%)
1	Carboxylic acids	2-Methoxy-propanoic acid	104	4.26	9.51
		3-Methyl-butanoic acid	102	5.60	2.96
		2-Methyl-butanoic acid	102	5.74	1.58
		4-Methyl-3-pentenoic acid	114.14	7.54	0.19
		α-Isopropylidene-aminooxy-propionic acid	145.15	9.11	0.99
		Benzoic acid	122.12	12.38	0.90
		Bis(2-methylpropyl)ester 1,2-benzenedicarboxylic acid	278.34	31.11	0.99
		N-[2-[4-(Acetyloxy)-3-methoxyphenyl]ethyl]-acetamide	251	33.78	1.31
		N-(3-Methylbutyl)acetamide	129.2	10.73	0.29
		N-(2-Phenylethyl)acetamide	163	21.88	2.47
		Bis(2-methylpropyl)ester 1,2-benzenedicarboxylic acid	278.34	31.11	0.99
2	Alkenes	1-Dodecene	168.31	11.05	0.83
		1-Tetradecene	196	15.19	4.26
		1*H*-Indene, 1-methylene-	128.17	11.67	0.68
		1-Non-adecene	266.5	23.56	7.66
		Hexadecane	266	23.80	0.56
		(*E*)-5-Octadecene	252.48	29.30	0.56
		Cetene	224.43	29.45	9.03
		3- Methyl-, (*E*)-5-undecene	168	15.51	0.09
		(*E*)-3-Eicosene	280	32.93	7.02
		1-Docosene	308	35.79	5.53
3	Alkanes	Dodecane	170.33	11.18	0.40
		Tetradecane	198	15.35	0.97
4	Phenols	2,4-Di-*tert*-butylphenol	206	20.99	0.95
		2-Methoxy-4-vinylphenol	150.177	14.31	1.06
5	Esters	2-Phenylethyl ester acetic acid	164	12.62	0.12
		Diphenyl ether	170.2	16.37	0.04
		2-Ethylhexyl salicylate	250	30.07	0.16
6	Aromatic heterocyclic compounds	2-Coumaranone	134	12.76	0.45
		2,3-Dihydro-benzofuran	120	13.32	1.50
		Biphenyl	154	15.92	0.11
		Hexahydro-pyrrolo[1,2-*a*]pyrazine-1,4-dione	154.17	31.36	2.25
		Hexahydro-3-(2-methylpropyl)-pyrrolo[1,2-*a*]pyrazine-1,4-dione	210	33.44	12.99
		Hexahydro-3-(phenylmethyl)-pyrrolo[1,2-*a*]pyrazine-1,4-dione	244	42.51	3.15
7	Heterocyclic hydrocarbon	4,5-Dimethyl-1,3-dioxane	116.16	6.34	0.11
8	Terpene	4-(1-Methylethyl)-2-cyclohexen-1-one	138.20	7.41	0.03
9	Aromatic hydrocarbon	1,4-Dichlorobenzene	147	8.11	0.14
10	Cyclic ketones	3-Methyl-1,2-cyclopentanedione	112.13	8.71	0.15
11	Aromatic monocyclic hydrocarbons	Phenylethyl alcohol	122.16	10.44	0.32
		Benzeneacetic acid	136	14.02	11.58
		Tetrahydro-4-hydroxy-6-pentyl-2*H*-pyran-2-one	186.25	20.68	0.09
12	Ketone	Benzophenone	182.22	26.30	0.58
13	Oxaspiro compound	7,9-Di-*tert*-butyl-1-oxaspiro(4,5)deca-6,9-diene-2, 8-dione	276.4	32.17	2.09

GC–MS, gas chromatography–mass spectrometry.

an experimentally solved structure of LuxO of *V. cholerae* is not available, we used a 1.6-Å resolution X-ray structure of the LuxO receiver-catalytic domain of *Photobacterium angustum*, which has 69% of sequence identity as a template for modeling *V. cholerae* LuxO (**Figure 6**). Any gaps observed during core modeling were subjected to loop modeling using Schrödinger PRIME (Jacobson et al., 2004). Then, the modeled protein was subjected to a constrain-based energy minimization using GROMACS. The Ramachandran plot of the modeled protein showed that PHI and PSI angles of the modeled proteins are within the allowed ranges, and the modeled protein was acceptable and hence used for further

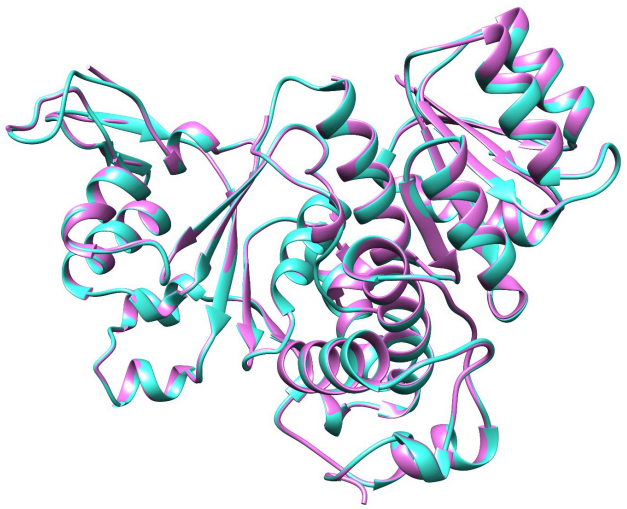

FIGURE 6 | Molecular superimposition of LuxO of *Photobacterium angustum* (template) and *V. cholerae*. The LuxO of *P. angustum* is represented in purple color and the LuxO of *V. cholerae* in turquoise color.

docking studies. For HapR, an existing X-ray structure of 2.2-Å resolution with putative ligand-binding domains was used. The small molecules identified in the RMA46 ethyl acetate extract identified using GC–MS was docked with the active sites of LuxO and HapR (**Figure 7**). Compound 2-methoxy-4-vinylphenol demonstrated an increased Glide score (-4.130) and Glide energy (-20.408 kcal/mol) with LuxO protein than did other molecules (**Figure 8**). The interaction pattern was observed as the ligand forms hydrogen bonding with the most crucial amino acid residues (GLN363 and TYR139) of the receiver-catalytic domain of ATP binding domain of LuxO. Similarly, the ligand, hexahydro-3-(phenylmethyl)-pyrrolo[1,2-*a*]pyrazine-1,4-dione, was found to have the highest affinity with the HapR protein with a Glide score of -4.543 and Glide energy of -30.465 kcal/mol and formed hydrogen bond interaction with SER165 amino acid.

DISCUSSION

The emergence of antimicrobial resistance among *Vibrio cholerae* is a burden on public health especially in developing countries (Das et al., 2019). An increase in the incidence of multidrug resistance *V. cholerae* could hurt cholera-controlling measures within a community (Mushayabasa and Bhunu, 2012). To subdue the emergence of antibiotic resistance, natural compounds that exert anti-virulence properties have been recognized as an alternative strategy (Narendrakumar et al., 2019a). Marine-derived Actinobacteria are a rich source of secondary metabolites that provide unique carbon scaffolds for the synthesis of advanced therapeutic agents for pathogens (Hassan and Shaikh, 2017). More than 3,000 compounds have been reported from marine bacteria most prevalently from the phylum Actinobacteria, which are known to inhibit drug-resistant bacterial pathogens (Rahman et al., 2010). The density of saprophytic Actinobacteria is high in mangrove soil owing to the detritus ecosystem found throughout the year (Saravanakumar et al., 2016). In this study, Actinobacteria strains were isolated from mangrove soil by various physical and chemical pretreatments by using a wide range of selective isolation media. It was observed that pretreatment of soil did not significantly affect the isolation of Actinobacteria strains. However, the application of starch casein agar and ISP no. 4 medium was most effective in the isolation of the Actinobacteria. The phylum Actinobacteria is one of the largest among the prokaryotes and encompasses many genera that are morphologically and phenotypically diverse.

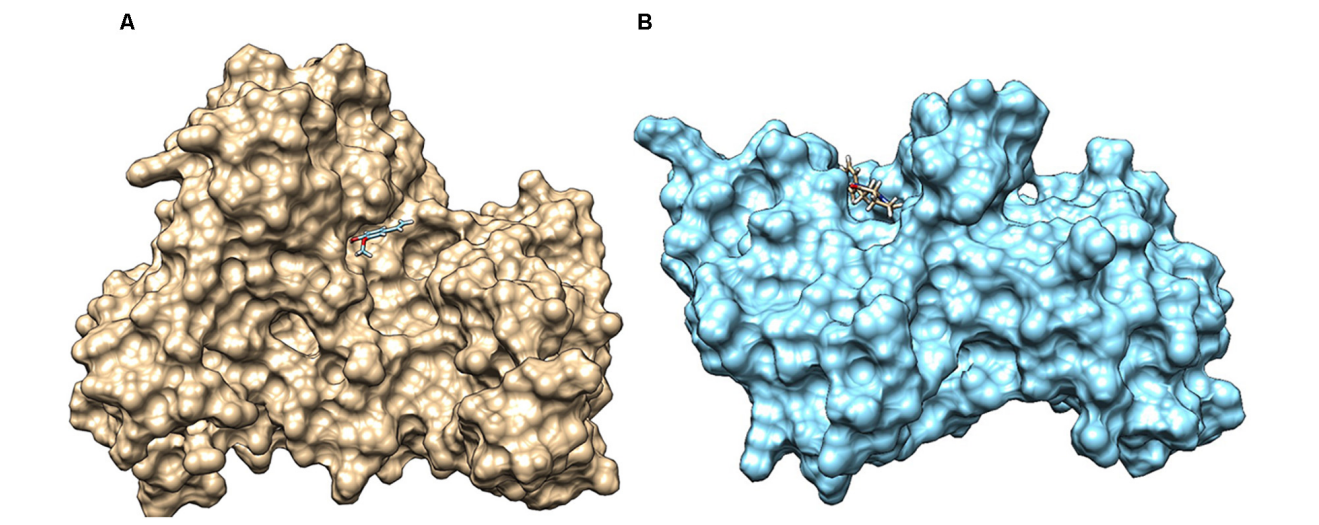

FIGURE 7 | (A) Docked complex of 2-methoxy-4-vinylphenol with LuxO of *Vibrio cholerae*, which forms hydrogen bond interaction with TYR129 and GLN363. **(B)** Interaction of hexahydro-3-(phenylmethyl)-pyrrolo[1,2-*a*]pyrazine-1,4-dione with HapR of *V. cholerae*, forming hydrogen bond with SER165. The *V. cholerae* response regulators are represented as surface (LuxO, gold color; and HapR, blue color), and the small molecules are represented as sticks.

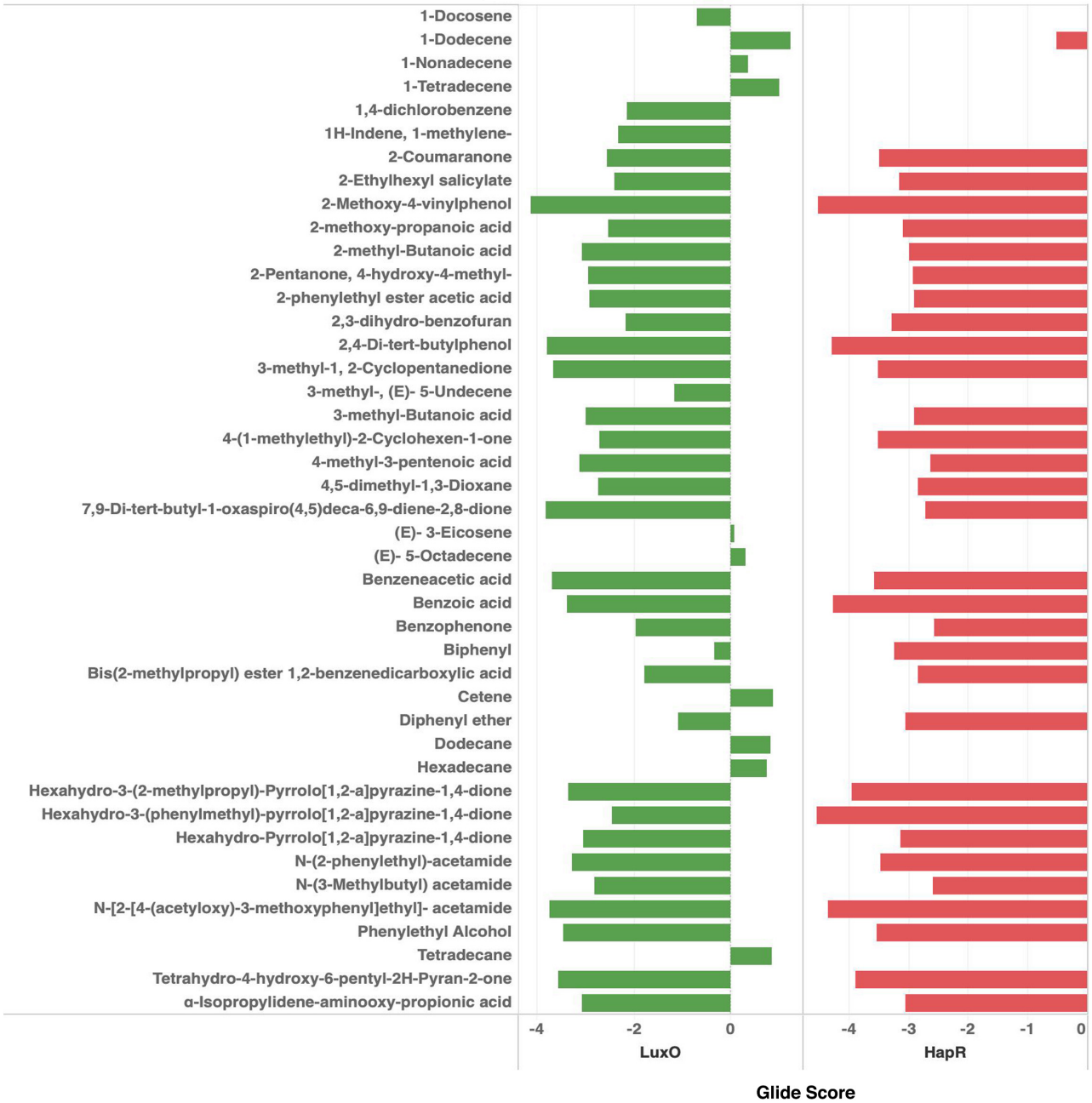

FIGURE 8 | Docking scores of the bioactive compounds identified in the ethyl acetate extract of RMA46 with LuxO and HapR of *Vibrio cholerae*.

The preliminary identification using light microscopy and colony morphology showed that the isolates were morphologically diverse, indicating the isolation of various genus. The isolated RMAs were screened using HYR14, a rugose *V. cholerae* O1 Ogawa biofilm-forming strain isolated during an outbreak in India. The strain is resistant to ampicillin, furazolidone, nalidixic acid, streptomycin, ciprofloxacin, erythromycin, and norfloxacin (Chowdhury et al., 2016). Because the rugose phenomenon is stable even after passage into humans and their potential to cause epidemics, the multidrug-resistant HYR14 strain was chosen for the screening the RMAs that can inhibit biofilm formation by *V. cholerae* for the current study (Morris et al., 1996; Chowdhury et al., 2016).

Although marine Actinobacteria account for 46% of the total Actinobacteria density exerting virulence inhibitory potential (Sarveswari and Solomon, 2019), the exploration for anti-virulence agents against *V. cholerae* had been very limited. Previously, culture supernatant of arctic derived rare Actinobacteria, *Nocardiopsis* sp. A731, had been reported

to exhibit a biofilm inhibitory activity against *V. cholerae* (Augustine et al., 2012). In our study, anti-biofilm phenotype-based screening of the RMA against HYR14 strain revealed that about 19% of the mangrove-derived isolates could inhibit the formation of *V. cholerae* biofilm. The study reinforces that the mangrove-derived Actinobacteria are a prospective source for anti-infectives against *V. cholerae*. Moreover, the HYR14 cell-free extract inhibits the formation of *V. cholerae* biofilms at a concentration (v/v) lesser than that of the *Nocardiopsis* sp. A731 reported by Augustine et al. (2012). In the same study, 200 μg/ml of *Streptomyces* sp. A745 diethyl ether fraction has been reported to suppress 60% of *V. cholerae* biofilm. Yet in our study, about 50% inhibition was observed at 130 μg/ml of RMA46 ethyl acetate extract. Although eight RMA isolates showed a significant activity against HYR14 biofilms, only the RMA46 strain that showed > 50% biofilm inhibition at least concentration was further subjected to nucleic acid-based identification. The sequence of the mangrove-derived *Micromonospora* sp. RMA46 was found to be closely related to the 16S rRNA sequence of another mangrove isolate *Micromonospora* sp. 171111. As both the strains were isolated from the mangrove region, the sequence similarity could reflect an environment selection among *Micromonospora* strains (Hong et al., 2009). The RMA46 ethyl acetate extract clearly eliminates the formation of HYR14 biofilm than its eradication. Previously, a non-significant impact on eliminating the preformed *V. cholerae* biofilms by natural products was attributed to their potential to affect the initial stages of biofilm formation including motility (Narendrakumar et al., 2019b). Hence, further studies with the *V. cholerae* HYR14 are needed to understand the mechanism of inhibition of biofilm formation.

The signal (autoinducer) strength influences the QS global switches (LuxO and HapR) to enhance the survivability and persistence of the intestinal pathogen, *V. cholerae* (Joelsson et al., 2007). At LSS, LuxO is positively regulated, and its synergistic interaction with the global response regulator, TsrA, enhances the production of *Vibrio* polysaccharide (VPS) TCP and CT to establish biofilm and virulence (Zheng et al., 2010).

When the signal strength is elevated (HSS), HapR is depressed, resulting in the upregulation of hemagglutinin/protease (HapA), facilitating the dispersal of *V. cholerae* cells within the biofilm matrix (Silva et al., 2003; Vance et al., 2003; Benitez and Silva, 2016). Also, HSS is directly proportional to the increased population size of *Vibrio* in an environment, which might lead to nutrient depletion. Interestingly, under nutrient-limited condition, the expression of HapA protease increases owing to the elevated intracellular cAMP pool. The cAMP binds to its allosteric receptor and exerts a positive feedback loop to activate CRP, RpoS, and HapR (Benitez and Silva, 2016). Our transcriptomic analysis revealed that the expression of major virulence genes and the response regulators of *V. cholerae* HYR14 is highly attenuated without affecting their growth in the presence of RMA46 ethyl acetate extract. This overall attenuation of the molecular machinery activated at LSS and HSS might be a combinatorial effect of two or more potential virulence attenuating bioactive molecules present in the RMA46 ethyl acetate extract against *V. cholerae*.

Genetically marine Actinobacteria are equipped to produce about 20 secondary metabolites (Lam, 2006). In this study, 43 secondary metabolites from various classes of chemical compounds have been identified. The RMA46 extract encompasses many chemicals from the class of carboxylic acid, and interestingly our group had previously reported the QS inhibitory effect of synthetically derived pyrazine-2-carboxylic acid on *V. cholerae* (Hema et al., 2017). The derivative of various other compounds reported in RMA46 has been reported to have other biological activities including antibacterial and anti-virulence activities against various other pathogens. This eventually exemplifies the potential of *Micromonospora* sp. RMA46 as a source for chemical structural templates for the development of anti-virulence agents. Docking of the 43 chemical compounds leads to the identification of 2-methoxy-4-vinylphenol and hexahydro-3-(phenylmethyl)-pyrrolo[1,2-*a*]pyrazine-1,4-dione to have the highest interacting capability with LuxO and HapR, respectively. The data corroborate our qRT-PCR data, which were also significant to show a complete blockage of virulence so as to prevent the colonization and dissemination of bacteria to persist infection. A derivative of 2-methoxy-4-vinylphenol has already been reported to have an inhibitory activity against LasIR/RhIIR circuit of *Pseudomonas aeruginosa* (Shah et al., 2019). Interestingly, hexahydro-3-(phenylmethyl)-pyrrolo[1,2-*a*]pyrazine-1,4-dione, also known as cyclo D-phenyalanyl-L-prolyl [Cyclo(Phe-Pro)], has been reported to attenuate the expression of genes associated with virulence in *V. cholerae*. Cyclo(Phe-Pro) inhibits the production of CTX and toxin coregulated pili in O1 El Tor strain by negatively affecting the transcription of genes *tcp*PH in *V. cholerae* (Bina and Bina, 2010). It was later shown that Cyclo(Phe-Pro) enhanced the ToxR-dependent transcription of *leu*O, which in turn repressed the downregulation of the ToxR regulon, altering the production of CT and TCP (Bina et al., 2013). However, the outcomes derived from this research support the bioprospecting of mangrove-derived *RMA* as sources of potential anti-infectives.

CONCLUSION

The pathogenesis of *Vibrio cholerae* is controlled via the QS-mediated communication process. The present study provides an insight in to the bioprospecting of mangrove-derived RMA to block QS-mediated response in *V. cholerae*. *Micromonospora* is one of the most productive genera among the phylum Actinobacteria in terms of the production of bioactive compounds. Yet the study of anti-virulence compounds with this genus is very limited. The Indian Ocean encompasses an astonishing source of marine microbial wealth, providing an opportunity to extensively exploit the RMA for the development of anti-virulence agents. The tapping of effective compounds from RMAs is achievable with the rapid development of modern technology in the field of

sampling, isolation, and identification strategies that open up novel mechanisms to arrest the development of rapid dissemination of antimicrobial resistance and pathogenesis of human and animal pathogens. To conclude, the identification of the anti-virulence property of *Micromonospora* sp. is another example of Actinobacteria as a treasure trove for pharmaceutically important compounds.

DATA AVAILABILITY STATEMENT

The datasets presented in this study can be found in online repositories. The names of the repository/repositories and accession number(s) can be found in the article/ **Supplementary Material**.

AUTHOR CONTRIBUTIONS

HS conducted all the experiments described in this study. SK supported the acquisition of images. KS designed the computational work. AS and PN designed the study and supervised all the experiments. HS and SK drafted the manuscript and it was reviewed by SK, PN, and AS.

FUNDING

The authors would like to thank the support of DST-SERB (EMR/2016/002296) and SASTRA Deemed to be University, Thanjavur, India.

ACKNOWLEDGMENTS

We thank Dr. Thandavarayan Ramamurthy, National Chair, Translational Health Science and Technology Institute, for the kind gift of *V. cholerae* strain HYR14.

SUPPLEMENTARY MATERIAL

The Supplementary Material for this article can be found online at: https://www.frontiersin.org/articles/10.3389/fmicb.2020.01393/full#supplementary-material

REFERENCES

Aarthi, P., Harini, R., Sowmiya, M., Malathi, J., Therese, K. L., and Madhavan, H. N. (2011). Identification of bacteria in culture negative and polymerase chain reaction (PCR) positive intraocular specimen from patients with infectious endopthalmitis. *J. Microbiol. Methods* 85, 47–52. doi: 10.1016/j.mimet.2011.01.010

Ahmed, W., Huygens, F., Goonetilleke, A., and Gardner, T. (2008). Real-time PCR detection of pathogenic microorganisms in roof-harvested rainwater in Southeast Queensland, Australia. *Appl. Environ. Microbiol.* 74, 5490–5496. doi: 10.1128/AEM.00331-08

Ali, M., Nelson, A. R., Lopez, A. L., and Sack, D. A. (2015). Updated global burden of cholera in endemic countries. *PLoS Negl. Trop. Dis.* 9:e0003832. doi: 10.1371/journal.pntd.0003832

Altschul, S. F., Gish, W., Miller, W., Myers, E. W., and Lipman, D. J. (1990). Basic local alignment search tool. *J. Mol. Biol.* 215, 403–410. doi: 10.1016/S0022-2836(05)80360-2

Augustine, N., Kerkar, S., and Thomas, S. (2012). Arctic actinomycetes as potential inhibitors of *Vibrio cholerae* biofilm. *Curr. Microbiol.* 64, 338–342. doi: 10.1007/s00284-011-0073-4

Balasubramanian, S., Othman, E. M., Kampik, D., Stopper, H., Hentschel, U., Ziebuhr, W., et al. (2017). Marine sponge-derived *Streptomyces* sp. SBT343 extract inhibits staphylococcal biofilm formation. *Front. Microbiol.* 8:236. doi: 10.3389/fmicb.2017.00236

Benitez, J. A., and Silva, A. J. (2016). *Vibrio cholerae* hemagglutinin(HA)/protease: an extracellular metalloprotease with multiple pathogenic activities. *Toxicon* 115, 55–62. doi: 10.1016/j.toxicon.2016.03.003

Bina, R. X., Taylor, D. L., Vikram, A., Ante, V. M., and Bina, J. E. (2013). *Vibrio cholerae* ToxR downregulates virulence factor production in response to cyclo(Phe-Pro). *mBio* 4:e00366-13. doi: 10.1128/mBio.00366-13

Bina, X. R., and Bina, J. E. (2010). The cyclic dipeptide cyclo(phe-pro) inhibits cholera toxin and toxin-coregulated pilus production in O1 El Tor *Vibrio cholerae*. *J. Bacteriol.* 192, 3829–3832. doi: 10.1128/JB.00191-10

Chowdhury, G., Bhadra, R. K., Bag, S., Pazhani, G. P., Das, B., Basu, P., et al. (2016). Rugose atypical *Vibrio cholerae* O1 El Tor responsible for 2009 cholera outbreak in India. *J. Med. Microbiol.* 65, 1130–1136. doi: 10.1099/jmm.0.000344

Clemens, J. D., Nair, G. B., Ahmed, T., Qadri, F., and Holmgren, J. (2017). Cholera. *Lancet* 390, 1539–1549. doi: 10.1016/S0140-6736(17)30559-7

Das, B., Verma, J., Kumar, P., Ghosh, A., and Ramamurthy, T. (2019). Antibiotic resistance in *Vibrio cholerae*: understanding the ecology of resistance genes and mechanisms. *Vaccine* 38, A83–A92. doi: 10.1016/j.vaccine.2019.06.031

Defoirdt, T. (2018). Quorum-sensing systems as targets for antivirulence therapy. *Trends Microbiol.* 26, 313–328. doi: 10.1016/j.tim.2017.10.005

Friesner, R. A., Murphy, R. B., Repasky, M. P., Frye, L. L., Greenwood, J. R., Halgren, T. A., et al. (2006). Extra precision glide: docking and scoring incorporating a model of hydrophobic enclosure for protein-ligand complexes. *J. Med. Chem.* 49, 6177–6196. doi: 10.1021/jm051256o

Gladkikh, A. S., Feranchuk, S. I., Ponomareva, A. S., Bochalgin, N. O., and Mironova, L. V. (2020). Antibiotic resistance in *Vibrio cholerae* El Tor strains isolated during cholera complications in Siberia and the Far East of Russia. *Infect. Genet. Evol.* 78:104096. doi: 10.1016/j.meegid.2019.104096

Hammer, B. K., and Bassler, B. L. (2003). Quorum sensing controls biofilm formation in *Vibrio cholerae*. *Mol. Microbiol.* 50, 101–114. doi: 10.1046/j.1365-2958.2003.03688.x

Hassan, S. S., and Shaikh, A. L. (2017). Marine actinobacteria as a drug treasure house. *Biomed. Pharmacother.* 87, 46–57. doi: 10.1016/j.biopha.2016.12.086

Hayakawa, M., and Nonomura, H. (1987). Humic acid-vitamin agar, a new medium for the selective isolation of soil actinomycetes. *J. Ferment. Technol.* 65, 501–509. doi: 10.1016/0385-6380(87)90108-7

Hema, M., Princy, S. A., Sridharan, V., Vinoth, P., Balamurugan, P., and Sumana, M. N. (2016). pyrizine-2-carboxylic acid and antibiotics against. *RSC Adv.* 6, 45938–45946. doi: 10.1039/C6RA04705J

Hema, M., Vasudevan, S., Balamurugan, P., and Adline Princy, S. (2017). Modulating the global response regulator, LuxO of V. cholerae quorum sensing system using a pyrazine dicarboxylic acid derivative (PDCApy): an antivirulence approach. *Front. Cell. Infect. Microbiol.* 7:441. doi: 10.3389/fcimb.2017.00441

Heydorn, A., Nielsen, A. T., Hentzer, M., Sternberg, C., Givskov, M., Ersboll, B. K., et al. (2000). Quantification of biofilm structures by the novel computer program COMSTAT. *Microbiology* 146, 2395–2407. doi: 10.1099/00221287-146-10-2395

Hong, K., Gao, A. H., Xie, Q. Y., Gao, H., Zhuang, L., Lin, H. P., et al. (2009). Actinomycetes for marine drug discovery isolated from mangrove soils and plants in China. *Mar. Drugs* 7, 24–44. doi: 10.3390/md7010024

Jacobson, M. P., Pincus, D. L., Rapp, C. S., Day, T. J. F., Honig, B., Shaw, D. E., et al. (2004). A hierarchical approach to all-atom protein loop prediction. *Proteins* 55, 351–367. doi: 10.1002/prot.10613

Joelsson, A., Kan, B., and Zhu, J. (2007). Quorum sensing enhances the stress response in *Vibrio cholerae*. *Appl. Environ. Microbiol.* 73, 3742–3746. doi: 10.1128/AEM.02804-06

Kartik, K. S., Muthusamy, S., Kadhirvel, S., and Mani, K. P. (2020). In-silico and in-vitro analysis of endocan interaction with statins. *Int. J. Biol. Macromol.* 146, 1087–1099. doi: 10.1016/j.ijbiomac.2019.09.235

Kaur, G., Balamurugan, P., Uma Maheswari, C., Anitha, A., and Princy, S. (2016). Combinatorial effects of aromatic 1, 3-disubstituted ureas and fluoride on *in vitro* inhibition of *Streptococcus mutans* biofilm formation. *Front. Microbiol.* 7:861. doi: 10.3389/fmicb.2016.00861

Kharel (Sitaula), R., Janani, M. K., Madhavan, H. N., and Biswas, J. (2018). Outcome of polymerase chain reaction (PCR) analysis in 100 suspected cases of infectious uveitis. *J. Ophthalm. Inflamm. Infect.* 8, 1–8. doi: 10.1186/s12348-017-0144-1

Kutzner, C., Páll, S., Fechner, M., Esztermann, A., de Groot, B. L., and Grubmüller, H. (2019). More bang for your buck: improved use of GPU nodes for GROMACS 2018. *J. Comput. Chem.* 40, 2418–2431. doi: 10.1002/jcc.26011

Lam, K. S. (2006). Discovery of novel metabolites from marine actinomycetes. *Curr. Opin. Microbiol.* 9, 245–251. doi: 10.1016/j.mib.2006.03.004

Lenz, D. H., Mok, K. C., Lilley, B. N., Kulkarni, R. V., Wingreen, N. S., and Bassler, B. L. (2004). The small RNA chaperone Hfq and multiple small RNAs control quorum sensing in *Vibrio harveyi* and *Vibrio cholerae*. *Cell* 118, 69–82. doi: 10.1016/j.cell.2004.06.009

Miller, M. B., Skorupski, K., Lenz, D. H., Taylor, R. K., and Bassler, B. L. (2002). Parallel quorum sensing systems converge to regulate virulence in *Vibrio cholerae*. *Cell* 110, 303–314. doi: 10.1016/S0092-8674(02)00829-2

Miller, V. L., and Mekalanos, J. J. (1984). Synthesis of cholera toxin is positively regulated at the transcriptional level by toxR. *Proc. Natl. Acad. Sci. U.S.A.* 81, 3471–3475. doi: 10.1073/pnas.81.11.3471

Morris, J. G., Sztein, M. B., Rice, E. W., Nataro, J. P., Losonsky, G. A., Panigrahi, P., et al. (1996). *Vibrio cholerae* O1 can assume a chlorine-resistant rugose survival form that is virulent for humans. *J. Infect. Dis.* 174, 1364–1368. doi: 10.1093/infdis/174.6.1364

Mushayabasa, S., and Bhunu, C. P. (2012). Assessing the impact of increasing antimicrobial resistance of *Vibrio cholerae* on the future trends of cholera epidemic. *ISRN Biomathematics* 2012, 1–10. doi: 10.5402/2012/127492

Narendrakumar, L., Gupta, S., Sen Johnson, J. B., Ramamurthy, T., and Thomas, S. (2019a). Molecular adaptations and antibiotic resistance in *Vibrio cholerae*: a communal challenge. *Microb. Drug Resist.* 25, 1012–1022. doi: 10.1089/mdr.2018.0354

Narendrakumar, L., Theresa, M., Krishnankutty Chandrika, S., and Thomas, S. (2019b). Tryptanthrin, a potential biofilm inhibitor against toxigenic *Vibrio cholerae*, modulating the global quorum sensing regulator, LuxO. *Biofouling* 35, 1093–1103. doi: 10.1080/08927014.2019.1696315

Perrière, G., and Gouy, M. (1996). WWW-query: an on-line retrieval system for biological sequence banks. *Biochimie* 78, 364–369. doi: 10.1016/0300-9084(96)84768-7

Pisano, M. A., Sommer, M. J., and Lopez, M. M. (1986). Application of pretreatments for the isolation of bioactive actinomycetes from marine sediments. *Appl. Microbiol. Biotechnol.* 25, 285–288. doi: 10.1007/BF00253664

Pridham, T. G., and Gottlieb, D. (1948). The utilization of carbon compounds by some actinomycetales as an aid for species determination. *J. Bacteriol.* 56, 107–114. doi: 10.1128/jb.56.1.107-114.1948

Rahman, H., Austin, B., Mitchell, W. J., Morris, P. C., Jamieson, D. J., Adams, D. R., et al. (2010). Novel anti-infective compounds from marine bacteria. *Mar. Drugs* 8, 498–518. doi: 10.3390/md8030498

Ravichandiran, V., Shanmugam, K., Anupama, K., Thomas, S., and Princy, A. (2012). Structure-based virtual screening for plant-derived SdiA-selective ligands as potential antivirulent agents against uropathogenic *Escherichia coli*. *Eur. J. Med. Chem.* 48, 200–205. doi: 10.1016/j.ejmech.2011.12.015

Rutherford, S. T., Van Kessel, J. C., Shao, Y., and Bassler, B. L. (2011). AphA and LuxR/HapR reciprocally control quorum sensing in vibrios. *Genes Dev.* 25, 397–408. doi: 10.1101/gad.2015011

Sack, D. A., Sack, R. B., Nair, G. B., and Siddique, A. (2004). Cholera. *Lancet* 363, 223–233. doi: 10.1016/S0140-6736(03)15328-7

Saravanakumar, K., Anburaj, R., Gomathi, V., and Kathiresan, K. (2016). Ecology of soil microbes in a tropical mangrove forest of south east coast of India. *Biocatal. Agric. Biotechnol.* 8, 73–85. doi: 10.1016/j.bcab.2016.08.010

Sarveswari, H. B., and Solomon, A. P. (2019). Profile of the intervention potential of the phylum actinobacteria toward quorum sensing and other microbial virulence strategies. *Front. Microbiol.* 10:73. doi: 10.3389/fmicb.2019.02073

Sastry, G. M., Adzhigirey, M., Day, T., Annabhimoju, R., and Sherman, W. (2013). Protein and ligand preparation: parameters, protocols, and influence on virtual screening enrichments. *J. Comput. Aided Mol. Des.* 27, 221–234. doi: 10.1007/s10822-013-9644-8

Shah, M. D., Kharkar, P. S., Sahu, N. U., Peerzada, Z., and Desai, K. B. (2019). Potassium 2-methoxy-4-vinylphenolate: a novel hit exhibiting quorum-sensing inhibition in: *Pseudomonas aeruginosa* via LasIR/RhlIR circuitry. *RSC Adv.* 9, 40228–40239. doi: 10.1039/c9ra06612h

Shirling, E. B., and Gottlieb, D. (1966). Methods for characterization of Streptomyces species. *Int. J. Syst. Bacteriol.* 16, 313–340. doi: 10.1099/00207713-16-3-313

Silva, A. J., Pham, K., and Benitez, J. A. (2003). Haemagglutinin/protease expression and mucin gel penetration in El Tor biotype *Vibrio cholerae*. *Microbiology* 149, 1883–1891. doi: 10.1099/mic.0.26086-0

Takahashi, Y. (2004). Exploitation of new microbial resources for bioactive compounds and discovery of new actinomycetes. *Actinomycetologica* 18, 54–61. doi: 10.3209/saj.18_54

Therese, K. L., Anand, A. R., and Madhavan, H. N. (1998). Polymerase chain reaction in the diagnosis of bacterial endophthalmitis. *Br. J. Opthalmol.* 82, 1078–1082. doi: 10.1136/bjo.82.9.1078

Vance, R. E., Zhu, J., and Mekalanos, J. J. (2003). A constitutively active variant of the quorum-sensing regulator LuxO affects protease production and biofilm formation in *Vibrio cholerae*. *Infect. Immun.* 71, 2571–2576. doi: 10.1128/IAI.71.5.2571-2576.2003

Verma, J., Bag, S., Saha, B., Kumar, P., Ghosh, T. S., Dayal, M., et al. (2019). Genomic plasticity associated with antimicrobial resistance in *Vibrio cholerae*. *Proc. Natl. Acad. Sci. U.S.A.* 116, 6226–6231. doi: 10.1073/pnas.1900141116

Vezzulli, L., Stauder, M., Grande, C., Pezzati, E., Verheye, H. M., Owens, N. J. P., et al. (2015). GbpA as a novel qPCR target for the species-specificdetection of *Vibrio cholerae* O1, O139, Non-O1/Non-O139 in environmental, stool, and historical continuous plankton recorder samples. *PLoS One* 10:e0123983. doi: 10.1371/journal.pone.0123983

Wang, R., Yu, D., Yue, J., and Kan, B. (2016). Variations in SXT elements in epidemic *Vibrio cholerae* O1 El Tor strains in China. *Sci. Rep.* 6, 1–8. doi: 10.1038/srep22733

World Health Organization [WHO] (2019). *Cholera*. Available online at: https://www.who.int/news-room/fact-sheets/detail/cholera (accessed January 29, 2020).

Yang, M., Frey, E. M., Liu, Z., Bishar, R., and Zhu, J. (2010). The virulence transcriptional activator aphA enhances biofilm formation by *Vibrio cholerae* by activating expression of the biofilm regulator VpsT. *Infect. Immun.* 78, 697–703. doi: 10.1128/IAI.00429-09

Zheng, J., Shin, O. S., Cameron, D. E., and Mekalanos, J. J. (2010). Quorum sensing and a global regulator TsrA control expression of type VI secretion and virulence in *Vibrio cholerae*. *Proc. Natl. Acad. Sci. U.S.A.* 107, 21128–21133. doi: 10.1073/pnas.1014998107

Zhu, J., and Mekalanos, J. J. (2003). Quorum sensing-dependent biofilms enhance colonization in *Vibrio cholerae*. *Dev. Cell* 5, 647–656. doi: 10.1016/S1534-5807(03)00295-8

Zhu, J., Miller, M. B., Vance, R. E., Dziejman, M., Bassler, B. L., and Mekalanos, J. J. (2002). Quorum-sensing regulators control virulence gene expression in *Vibrio cholerae*. *Proc. Natl. Acad. Sci. U.S.A.* 99, 3129–3134. doi: 10.1073/pnas.052694299

Conflict of Interest: The authors declare that the research was conducted in the absence of any commercial or financial relationships that could be construed as a potential conflict of interest.

frontiers in Microbiology

ORIGINAL RESEARCH
published: 03 September 2020
doi: 10.3389/fmicb.2020.570836

Diversity of Cultivable Microbes From Soil of the Fildes Peninsula, Antarctica, and Their Potential Application

Bailin Cong[1†], Xiaofei Yin[1†], Aifang Deng[1], Jihong Shen[1], Yongqi Tian[2*], Shaoyun Wang[2*] and Huanghao Yang[2]*

[1] The First Institute of Oceanography, Ministry of Natural Resources, Qingdao, China, [2] College of Biological Science and Engineering, Fuzhou University, Fuzhou, China

OPEN ACCESS

Edited by:
Runying Zeng,
State Oceanic Administration, China

Reviewed by:
Xinpeng Tian,
South China Sea Institute of Oceanology (CAS), China
Huansheng Cao,
Arizona State University, United States

***Correspondence:**
Jihong Shen
shenjihong@fio.org.cn
Yongqi Tian
tianyongqi@fzu.edu.cn
Shaoyun Wang
shywang@fzu.edu.cn

[†] These authors have contributed equally to this work

Specialty section:
This article was submitted to Microbiotechnology, a section of the journal Frontiers in Microbiology

Received: 09 June 2020
Accepted: 17 August 2020
Published: 03 September 2020

Citation:
Cong B, Yin X, Deng A, Shen J, Tian Y, Wang S and Yang H (2020) Diversity of Cultivable Microbes From Soil of the Fildes Peninsula, Antarctica, and Their Potential Application. Front. Microbiol. 11:570836. doi: 10.3389/fmicb.2020.570836

To explore the diversity and application potential of Antarctic microorganisms, 1208 strains bacteria and fungi were isolated from 5 samples collected from the Fildes Peninsula during China's 27th and 31st Antarctic expeditions. By using 16S and ITS sequence similarity alignment, 83 strains bacteria belonging to 20 genera and 30 strains fungi belonging to 7 genera were identified. Among them, 1 strains bacteria and 6 strains fungi showed low sequence similarity to the database, suggesting that they might be novel species. Physiological-biochemical characteristics showed that the identified bacteria could utilize many kinds of carbohydrates and that the identified fungi could produce several kinds of extracellular enzymes. The fungal strain MS-19, identified as *Aspergillus sydowii*, possesses the potential to produce antifungal activity agents based on an activity-guided approach. Further isolation yielded four polyketones: versicone A (**1**), versicone B (**2**), 4-methyl-5,6-dihydro-2H-pyran-2-one (**3**), and (*R*)-(+)-sydowic acid (**4**). It should be noted that **1** displayed strong activity against *Candida albicans*, with an MIC value of 3.91 μg/mL.

Keywords: Antarctica, cultivable microbes, novel species, enzymes, antifungal natural product

INTRODUCTION

Antarctica is located at the southernmost point of the earth, and the climate of Antarctica is very different from that of other places due to the Antarctic circulation. Antarctica has a simple and weak ecosystem because of the cold, dry climate and low level of nutrition (Chown et al., 2015). Few animals and plants can survive in this cold environment. Because of the special habitat, microbes in Antarctica evolved extraordinary resistance to low temperature, hypersalinity and radiation (Dong et al., 2015).

Scientists have collected and analyzed many samples from Antarctica to explore the biological diversity of this continent. Because of the rigorous environment, flowering plants and vertebrates have been rarely observed, and for those that have been observed, their main habitat was near the ocean. Lichens, mosses, nematodes, tardigrades, springtails and mites are much more abundant

in Antarctica compared with higher plants and animals (Velascocastrillon et al., 2014; Godinho et al., 2015). On the other hand, the microbes displayed extraordinary diversity. Cowan et al. reported the abundance of microbes discovered from hyperarid McMurdo Dry Valleys, and the dominant bacteria were *Acidobacteria*, *Actinobacteria*, and *Bacteroidetes* (Cowan et al., 2010). Teixeira et al. researched the bacterial diversity in rhizosphere soil from Antarctic vascular plants of Admiralty Bay and found that the most abundant phylum was *Firmicutes*, while *Bifidobacterium*, *Arcobacter* and *Faecalibacterium* were also prominent (Teixeira et al., 2010). In other warmer and wetter parts of Antarctica, such as the ice-free area of the Keller Peninsula, *Proteobacteria* are very abundant (Freckman and Virginia, 1997). Recently, research based on DNA sequencing was proven to be powerful for investigating the diversity of microbes. Huang et al. used the next-generation sequencing (NGS) method to prove that the ice-free area plateaus of Schirmacher Oasis contained bacteria belonging to 12 phyla and 110 genera (Huang et al., 2013), and Wang et al. reported the community structure of microorganisms sampled from different habitats (Wang et al., 2015). In summary, the incredible diversity of microorganisms in the soil of Antarctica has been reported in many studies.

Polar microorganisms are regarded as a source of cold-adapted and low-temperature enzymes and active natural products. Ray et al. isolated a strain of cold-adapted yeast, *Candida humicola*, from Schirmacher Oasis that produced high levels of protease at low temperature (Ray et al., 1992). Vazquez et al. (1995) isolated three strains of *Pseudomonas maltophilia* that displayed the highest levels of proteolytic activity at 20°C. Lario et al. (2015) analyzed a protease isolated from Antarctic algae and found that the purified protease presented optimal catalytic activity at pH 5.0 and 50°C and was stable in the presence of high concentrations of NaCl. On the other hand, an increasing number of active secondary metabolites have been found from different groups of polar microorganisms, including alkaloids, macrocyclic lipids, terpenes, peptides, quinones, polyketones and other structural types, showing antibacterial, antitumor, antiviral, immunomodulatory, antioxidant and other biological activities (Li et al., 2012; Chavez et al., 2015; Wang et al., 2016; Feng et al., 2019). These compounds with novel structures and wide activities are important lead compounds for drug research. Studies on these compounds provide a basis for the utilization of Antarctic bioresources, and the microorganisms of these studies might play important roles in future research and applications.

Since the first Antarctic expedition in 1984, Chinese scientists have devoted themselves to the research of this continent. The biodiversity of Antarctica was one of the questions that they focused on. Using samples collected from China's Antarctic expedition, we hoped to discover additional bacteria and fungi to increase our knowledge of the continent and identify putative enzymes and active natural products for industry and drug development. Moreover, cultivable strains can possibly be used for applications. The Fildes Peninsula is located in the southwest region of King George Island and is where the China Great Wall Station is located (**Figure 1**). We researched samples collected from the Fildes Peninsula, isolated and cultured microbes from soil, macroalgal rot, and sediment (**Supplementary Table S1**) and used 16S and ITS sequences to analyZe the evolutionary relationship of the isolated microbes. Herein, we report the isolation of 83 bacteria belonging to 20 genera and 30 fungi belonging to 7 genera from soil samples collected on the Fildes Peninsula. Furthermore, physical and chemical analyses showed that the bacteria could utilize many kinds of carbohydrates and that the fungi could produce several kinds of extracellular enzymes. At the same time, an *Aspergillus* strain named MS-19 was fermented, and four polyketones, versicone A (**1**), versicone B (**2**), 4-methyl-5,6-dihydro-2H-pyran-2-one (**3**), and (*R*)-(+)-sydowic acid (**4**), were isolated with an activity-guided approach. Among them, **1** and **2** displayed activities against *Fusarium oxysporum* and *Castanea anthracis,* especially **1**, which displayed strong activity against *Candida albicans*, with an MIC value of 3.91 μg/mL.

MATERIALS AND METHODS

Field Site and Sampling

Samples came from the Fildes Peninsula by China's 27th and 31st Antarctic expeditions. Soil, macroalgal rot and sediment samples were collected from Ardley Island – near the Fildes Peninsula, Antarctica. The collection location is shown in **Supplementary Table S1**. Sterile tools were used to collect rhizosphere soil at approximately 0–5 cm deep. Then, these soil samples were maintained at 4°C until culture and analysis. These samples were incubated at 8°C until the samples became dry. Approximately 1 g of soil was dissolved in 10 mL of sterile water and suspended. Ten-fold serial dilutions were performed, and the final concentration was 10^{-5}. Then, a 100 μL suspension was spread on a plate for culture. To identify bacteria, the culture medium 2216e (peptone 5 g, yeast extraction 1 g, agar 18 g, and seawater to 1000 mL; the medium was sterilized at 121°C for 20 min, and mycostatin was added to a final concentration of 100 μg/mL) was used. For fungi, the medium PDA (potato 200 g, glucose 10 g, agar 17 g, and seawater to 1000 mL; the medium was sterilized at 121°C for 20 min, and ampicillin was added to a final concentration of 100 μg/mL) was used. The culture temperature was 12°C with incubation for 1–2 weeks. These colonies were distinguished by colony morphology and pigmentation, and distinct colonies were chosen for pure culture and preservation. Bacteria were stored at −80°C with 30% glycerin, and fungi were stored at −80°C with 20% glycerin.

DNA Extraction, PCR Amplification and Molecular Phylogenetic Analysis

Bacteria were cultured in liquid medium for 1 week; then, the cells were collected for DNA extraction. Similarly, filtered fungi were cultured on PDA plates for 1 week. Approximately 50 mg of hyphae was ground in liquid nitrogen. DNA extraction was performed with the Genome DNA Extraction Kit (Tiangen, China). The universal primers 27F (5′-AGAGTTTGATCCTGGCTCAG-3′) and 1492R (5′-GGTTACCTTGTTACGACTT-3′) were used to amplify the bacterial 16S sequence. The reaction mixture contained 25 μL

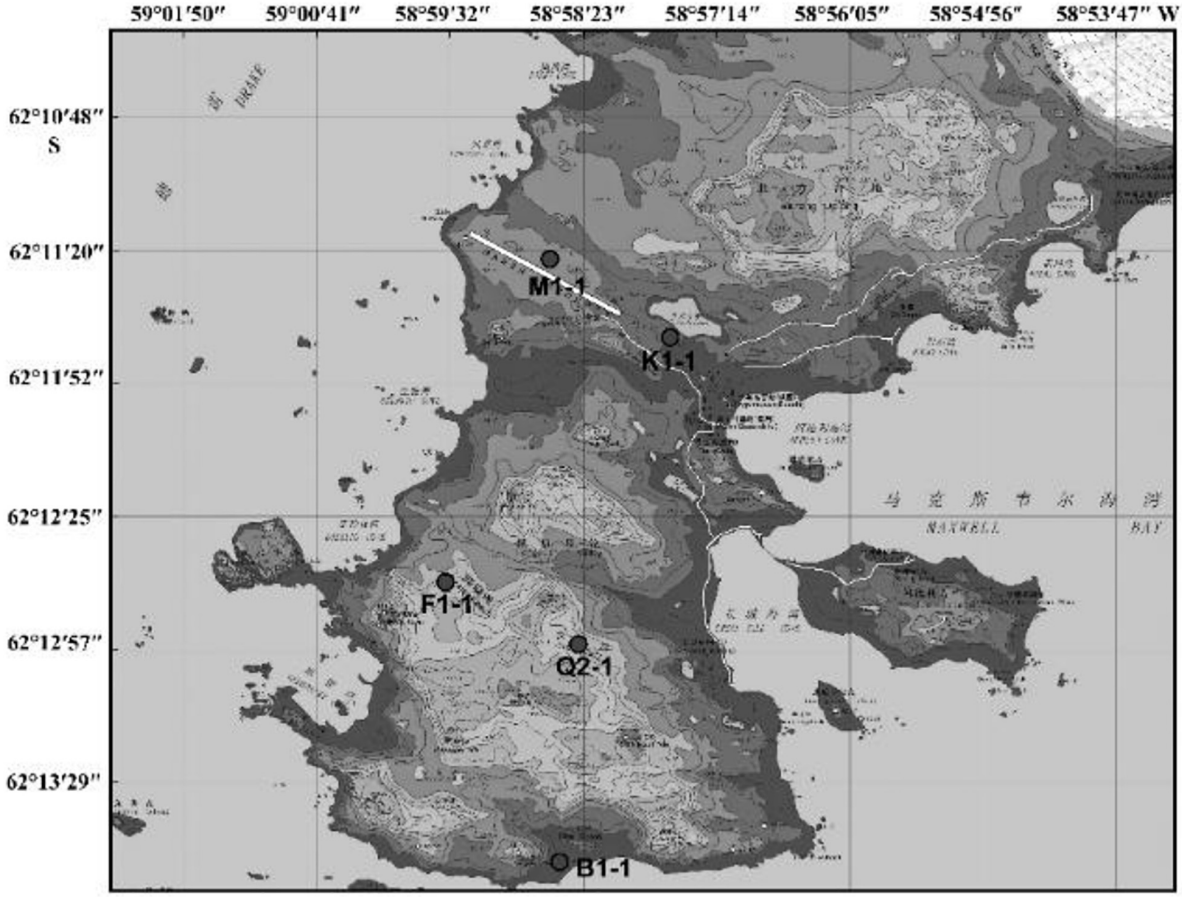

FIGURE 1 | The area where sampling was performed.

of 2 × Taq PCR MasterMix (Tiangen, China), 4 μL of both front and reverse primers, 1 μL of template DNA, and 20 μL of ddH_2O; the total volume was 50 μL. The PCR settings were denaturation at 94°C for 5 min; 30 cycles of denaturation at 94°C for 30 s, annealing at 55°C for 30 s, and elongation at 72°C for 90 s; and a final extension at 72°C for 10 min. Agarose gel electrophoresis was employed to confirm the PCR products, and the loading amount was 5 μL. To amplify fungal DNA, the universal primers ITS1 (5′-TCCGTAGGTGAACCTGCGG-3′) and ITS4 (5′-TCCTCCGCTTATTGATATGC-3′) were used (Hughes et al., 2009). The reaction mixture contained 25 μL of 2 × Taq PCR MasterMix (Tiangen, China), 6 μL of both forward and reverse primers, 1 μL of template DNA, and 18 μL of ddH_2O; the total volume was 50 μL. The PCR settings were denaturation at 94°C for 5 min; followed by 30 cycles of denaturation at 94°C for 30 s, annealing at 55°C for 30 s, and elongation at 72°C for 40 s; and a final extension at 72°C for 10 min. The PCR products were sent to Shanghai Sunny Biotechnology Co., Ltd. for sequencing. The 16S rDNA and ITS sequences were aligned to the GenBank database using BLAST analysis[1]. The phylogenetic tree was aligned by ClustalX, constructed by MEGA4.0 using the neighbor-joining method and visualized by the online tool iTOL[2]. Similarity comparison to type strains was completed by using the EzBioCloud Database[3].

Physiological-Biochemical Characteristics of Bacteria

To verify the physiology of the bacteria, the AP NE20 Kit was used according to the results of the 16S alignment. Typed strains of each genus or species were chosen for testing, and the culture temperature was set to 12°C. The protocol was provided by an API 20 NE Kit.

Physiological-Biochemical Characteristics of Fungi

To determine these fungi abilities to produce amylase, cellulase or caseinase activities, a chosen fungus was cultured on PDA culture with 7 colonies on each plate for approximately 2 weeks at 12°C. Then, the colonies were treated using the following protocols.

[1]https://blast.ncbi.nlm.nih.gov/Blast.cgi

[2]http://itol.embl.de/#

[3]http://eztaxon-e.ezbiocloud.net

TABLE 1 | Identification of culturable bacteria isolated from the soil of the Fildes Peninsula.

Genus	Stain no.	Most similar strain (ID)	Similarity	GenBank accession no.
Pseudomonas	1PF3	*Pseudomonas arsenicoxydans* VC-1(FN645213)	99.85%	KT991031
	1PQ2-6	*Pseudomonas migulae* CIP 105470(AF074383)	99.70%	KT991032
	1K1lan	*Pseudomonas migulae* CIP 105470(AF074383)	99.71%	KT991033
	1Q1lan-6	*Pseudomonas migulae* CIP 105470(AF074383)	99.71%	KT991034
	1EK3	*Pseudomonas migulae* CIP 105470(AF074383)	99.63%	KT991035
	1EQ1	*Pseudomonas migulae* CIP 105470(AF074383)	99.71%	KT991036
	1PK1	*Pseudomonas migulae* CIP 105470(AF074383)	99.71%	KT991037
	W3-1-3	*Pseudomonas migulae* CIP 105470(AF074383)	99.63%	KT991038
	2EK3	*Pseudomonas migulae* CIP 105470(AF074383)	99.63%	KT991039
	2PK7	*Pseudomonas graminis* DSM 11363(Y11150)	99.73%	KT991040
	2EK4	*Pseudomonas graminis* DSM 11363(Y11150)	99.78%	KT991041
	1F1lan	*Pseudomonas mandelii* CIP 105273(AF058286)	99.41%	KT991042
	1PM2	*Pseudomonas mandelii* CIP 105273(AF058286)	99.41%	KT991043
	1PF2-6	*Pseudomonas mandelii* CIP 105273(AF058286)	99.11%	KT991044
	1PK2	*Pseudomonas mandelii* CIP 105273(AF058286)	99.78%	KT991045
	2PM9	*Pseudomonas mandelii* CIP 105273(AF058286)	99.64%	KT991046
	1PM1	*Pseudomonas avellanae* BPIC631(AKBS01001374)	99.11%	KT991047
	1EK4-6	*Pseudomonas avellanae* BPIC631(AKBS01001374)	99.05%	KT991048
	1PM3	*Pseudomonas avellanae* BPIC631(AKBS01001374)	99.13%	KT991049
	2M2lan	*Pseudomonas avellanae* BPIC631(AKBS01001374)	99.12%	KT991050
	2PF3	*Pseudomonas avellanae* BPIC631(AKBS01001374)	98.46%	KT991051
	2PF2lan	*Pseudomonas avellanae* BPIC631(AKBS01001374)	99.13%	KT991052
	2PM4	*Pseudomonas avellanae* BPIC631(AKBS01001374)	99.05%	KT991053
	2PQ2	*Pseudomonas frederiksbergensis* JAJ28(AJ249382)	99.78%	KT991054
	2EK2	*Pseudomonas frederiksbergensis* JAJ28(AJ249382)	98.77%	KT991055
	Q1-3-2	*Pseudomonas frederiksbergensis* JAJ28(AJ249382)	99.78%	KT991056
	Q1-3-1	*Pseudomonas frederiksbergensis* JAJ28(AJ249382)	99.78%	KT991057
	1EQ2	*Pseudomonas meridiana* CMS 38(AJ537602)	99.41%	KT991058
	Q2-1-2	*Pseudomonas meridiana* CMS 38(AJ537602)	99.41%	KT991059
	2EM1	*Pseudomonas meridiana* CMS 38(AJ537602)	99.56%	KT991060
	2PQ3	*Pseudomonas meridiana* CMS 38(AJ537602)	99.49%	KT991061
	2PQ41	*Pseudomonas meridiana* CMS 38(AJ537602)	99.49%	KT991062
	2EQ1	*Pseudomonas meridiana* CMS 38(AJ537602)	99.56%	KT991063
	2EM5	*Pseudomonas meridiana* CMS 38(AJ537602)	99.56%	KT991064
Neptunomonas	1EF2	*Naphthovorans* NAG-2N-126(AF053734)	97.81%	KT991065
Psychrobacter	1EB1	*Psychrobacter glacincola* DSM 12194(AJ312213)	99.19%	KT991066
	1EB2	*Psychrobacter glacincola* DSM 12194(AJ312213)	99.49%	KT991067
	2EB3	*Psychrobacter glacincola* DSM 12194(AJ312213)	99.42%	KT991068
	2EB4	*Psychrobacter glacincola* DSM 12194(AJ312213)	99.49%	KT991069
	2EB5	*Psychrobacter glacincola* DSM 12194(AJ312213)	99.20%	KT991070
	2EB11	*Psychrobacter glacincola* DSM 12194(AJ312213)	99.20%	KT991071
	2EB12	*Psychrobacter glacincola* DSM 12194(AJ312213)	99.20%	KT991072
	2EB21	*Psychrobacter glacincola* DSM 12194(AJ312213)	99.20%	KT991073
	2PB1lan	*Psychrobacter urativorans* DSM 14009(AJ609555)	99.93%	KT991074
Luteibacter	2PK1	*Luteibacter rhizovicinus* LJ96(AJ580498)	97.77%	KT991075
	2PK6	*Luteibacter rhizovicinus* LJ96(AJ580498)	97.67%	KT991076
	2PK8	*Luteibacter rhizovicinus* LJ96(AJ580498)	97.75%	KT991077
Burkholderia	2PQ1	*Burkholderia udeis* LMG 27134(AY154367)	98.81%	KT991078
Massilia	2PK9	*Massilia aurea* AP13(AM231588)	98.01%	KT991079
	2PF3lan	*Massilia plicata* 76(AY966000)	98.17%	KT991080
	2PM4lan	*Massilia eurypsychrophila* B528-3(KJ361504)	99.33%	KT991081
	2PQ5	*Massilia eurypsychrophila* B528-3(KJ361504)	99.33%	KT991082
	2PM3lan	*Massilia eurypsychrophila* B528-3(KJ361504)	99.33%	KT991083

(Continued)

TABLE 1 | Continued

Genus	Stain no.	Most similar strain (ID)	Similarity	GenBank accession no.
Rugamonas	1K2lan	*Rμgamonas rubra* MOM 28/2/79(HM038005)	98.57%	KT991084
Janthinobacterium	K1-1	*Janthinobacterium svalbardensis* JA-1(DQ355146)	99.85%	KT991085
Duganella	2M1lan	*Duganella phyllosphaerae* T54(FR852575)	97.13%	KT991086
Planomicrobium	0.1a	*Planomicrobium okeanokoites* IFO 12536(D55729)	99.83%	KT991087
	1a	*Planomicrobium okeanokoites* IFO 12536(D55729)	99.83%	KT991088
Rhizobium	2PK3	*Rhizobium tubonense* CCBAU 85046(EU256434)	99. 08%	KT991089
	2PK7lan	*Rhizobium tubonense* CCBAU 85046(EU256434)	99. 80%	KT991090
Brevundimonas	N1-1-1	*Brevundimonas bullata* IAM 13153(D12785)	100%	KT991091
Sphingomonas	1PM7	*Sphingomonas aerolata* NW12(AJ429240)	99.32%	KT991092
	2PF4	*Sphingomonas glacialis* C16y(GQ253122)	99.77%	KT991093
	2PM11	*Sphingomonas glacialis* C16y(GQ253122)	99.85%	KT991094
Sulfitobacter	1EK2	*Sulfitobacter pontiacus* DSM 10014(Y13155)	99.77%	KT991095
Streptomyces	2PM10	*Streptomyces avidinii* NBRC 13429(AB184395)	99.77%	KT991096
Microterricola	1EM1	*Microterricola viridarii* KV-677(AB282862)	99.33%	KT991097
	2EM3	*Microterricola viridarii* KV-677(AB282862)	99.33%	KT991098
Arthrobacter	1EB3	*Arthrobacter antarcticus* SPC26(AM931709)	99.11%	KT991099
	1EF3-6	*Arthrobacter ginsengisoli'* DCY81(KF212463)	99.41%	KT991100
	D1-1-1	*Arthrobacter ginsengisoli'* DCY81(KF212463	99.48%	KT991101
	F1-1-1	*Arthrobacter ginsengisoli'* DCY81(KF212463)	99.33%	KT991102
	2PF1lan	*Arthrobacter ginsengisoli'* DCY81(KF212463)	99.63%	KT991103
	2EF1	*Arthrobacter ginsengisoli'* DCY81(KF212463)	99.48%	KT991104
	2EK1	*Arthrobacter ginsengisoli'* DCY81(KF212463)	99.41%	KT991105
	2EM2	*Arthrobacter ginsengisoli'* DCY81(KF212463)	99.48%	KT991106
	1M2lan	*Arthrobacter psychrochitiniphilus* GP3(AJ810896)	98.94%	KT991107
	1EM2	*Arthrobacter psychrochitiniphilus* GP3(AJ810896)	98.96%	KT991108
	M1-1-2	*Arthrobacter psychrochitiniphilus* GP3(AJ810896)	98.96%	KT991109
Gillisia	2EM4	*Gillisia hiemivivida* IC154(AY694006)	99.33%	KT991110
Pedobacter	2PM12	*Pedobacter panaciterrae* Gsoil 042(AB245368)	97.72%	KT991111
Mucilaginibacter	2PM7	*Mucilaginibacter dorajii* DR-f4(GU139697)	96.52%	KT991112
	2PK12	*Mucilaginibacter soli* R9-65(JF701183)	97.64%	KT991113

Amylase activity test on amylase medium: fresh iodine was added, and in the plates to stain several minutes. Then, the iodine was washed out. The colonies were checked to determine whether the surrounding area was a transparent circle. Cellulase activity test on cellulase medium: Congo red solution was added to the plate and incubated for 15 min. Then, the solution was washed out; NaCl solution was added, and the plate was incubated for 15 min. The colonies were checked to determine whether there was a transparent circle. Caseinase activity test on caseinase medium: the plate was covered with 40% trichloroacetic acid; transparency indicated a positive reaction.

Primary Screening for Antifungal Activity

The primary screening for antifungal activity was executed using 100 × 15 mm Petri plates containing 10 mL of PDA (Hong et al., 2013). Sterile blank paper disks (0.625 cm in diameter) were placed approximately 1 cm away from a central disk of the same size. An aliquot (8 μL, 500 μg/mL) in CH_3OH was introduced to each peripheral disk. The plates of *Fusarium oxysporum* and *Candida albicans were* incubated at 23°C for 72 h until mycelial growth from the central disk had enveloped. The peripheral disks containing the control (CH_3OH) produced crescents indicating inhibition around the disks containing samples with antifungal activity.

Extraction and Isolation

Aspergillus sydowii MS-19 was cultured on PDA plates at 20°C for 7 days. The seed medium consisting of malt extract (15 g), sea salt (10 g), and distilled water (1000 mL), pH 7.0, was inoculated with strain MS19, which was incubated at 25°C for 72 h on a rotating shaker (170 rpm). Mass scale fermentation of MS-19 was carried out using solid rice medium in 500 mL flasks (rice 80 g, sea salt 1.0 g, distilled water 80 mL) and inoculated with 10 mL of seed solution. Flasks were incubated at 20°C under a normal day night cycle. After 30 days, cultures from 20 flasks were harvested and subjected to organic extraction using ethyl acetate (EtOAc). The EtOAc extracts of solid MS19 rice medium were partitioned between petroleum ether and 90% aqueous MeOH. The resulting MeOH phase was fractionated using a silica column, Sephadex LH-20, and then semipreparative reversed-phase HPLC to obtain compounds **1**–**4** (**Figure 4**). The culture on solid rice medium was soaked in acetone, cut into small pieces and maintained for 1 day. The content was filtered and evaporated under vacuum using a Buchner funnel and extracted with EtOAc until exhaustion;

this process was repeated three times. The organic phase was collected and evaporated, and a dark brown oil crude extract (13.5 g) was obtained. The crude EtOAc extract was subjected to silica gel column chromatography (CC) eluted with petroleum ether/EtOAc in a gradient (v/v, 50:1, 30:1, 20:1, 10:1, 5:1, 1:1, 0:1), and 8 fractions (fractions 1–8) were obtained on the basis of TLC. Fr. 3 was purified by CC (petroleum ether/EtOAc, 5:2) to give 6 subfractions (fr. 3.1–3.6). Fr. 3.3 was further purified by (SP-RP) HPLC eluting with CH_3OH-H_2O (80:20) to afford compound **2** (4.5 mg). Fr. 4 was further purified by Sephadex LH-20 (petroleum ether/$CHCl_3$/MeOH, 5:2:1) to give 6 subfractions (fr. 4.1–4.6). Fr. 4.3 was further purified by (SP-RP) HPLC eluting with CH_3CN-H_2O (60:40, 1‰ TFA) to afford compounds **3** (4.0 mg) and **4** (38.3 mg). Compound **1** (3.7 mg) was isolated from fr. 4.2 by (SP-RP) HPLC using 80% MeCN.

Antifungal Activity Assay

The antifungal activity assay was performed using the broth microdilution method (Wang et al., 2016). Arrayed stock solutions of the tested compounds dissolved in DMSO were

TABLE 2 | Identification of culturable fungi isolated from the soil of the Fildes Peninsula.

Genus	Strain no.	Most similar strain (ID)	Similarity	GenBank accession no.
Geomyces	1PM6	*Geomyces pannorum* UFMGCB6110(KC485453)	100%	KT991114
	1EK1	*Geomyces pannorum* UFMGCB6110(KC485453)	98.10%	KT991115
	2PB5	*Geomyces pannorum* UFMGCB6110(KC485453)	100%	KT991116
	2PM1	*Geomyces pannorum* UFMGCB6110(KC485453)	100%	KT991117
	1PF2-8	*Geomyces pannorum* UFMGCB6049(KC485437)	100%	KT991118
	1PQ2-8	*Geomyces pannorum* UFMGCB6049(KC485437)	99.06%	KT991119
	1Q1lan-8	*Geomyces pannorum* UFMGCB6049(KC485437)	99.53%	KT991120
	1PQ1	*Geomyces pannorum* UFMGCB6049(KC485437)	100%	KT991121
	1EF3-8	*Geomyces pannorum* UFMGCB6049(KC485437)	100%	KT991122
	1PB1	*Geomyces pannorum* UFMGCB6049(KC485437)	100%	KT991123
	1	*Geomyces pannorum* UFMGCB6049(KC485437)	100%	KT991124
	4	*Geomyces pannorum* UFMGCB6049(KC485437)	100%	KT991125
	6	*Geomyces pannorum* UFMGCB6049(KC485437)	100%	KT991126
	2PB3	*Geomyces pannorum* UFMGCB6049(KC485437)	100%	KT991127
	2PB4	*Geomyces pannorum* UFMGCB6049(KC485437)	100%	KT991128
	2PB1	*Geomyces pannorum* UFMGCB6049(KC485437)	100%	KT991129
	2PB2	*Geomyces pannorum* UFMGCB6049(KC485437)	100%	KT991130
	2PQ6	*Geomyces pannorum* UFMGCB6049(KC485437)	99.76%	KT991131
	2PF1	*Geomyces pannorum* Geo-6(JF320819)	100%	KT991132
Pseudeurotium	W2-1	*Pseudeurotium desertorum* WL07-3(JX077048)	96.46%	KT991133
	2PM2	*Pseudeurotium desertorum* WL07-3(JX077048)	96.46%	KT991134
Rhizoscyphus	2PK2	*Rhizoscyphus monotropae* ATCC52305(AF169309)	91.82%	KT991135
Lecythophora	2PQ42	*Lecythophora fasciculata* IFM 50359(KT991136)	96.58%	KT991136
Rhodotorula	2PK13	*Rhodotorula rosulata* CBS10977(EU872492)	89.59%	KT991137
Mortierella	1PM5	*Mortierella elongatula* CBS 488.70(HQ630349)	95.91%	KT991138
	1EK4-8	*Mortierella elongatula* CBS 488.70(HQ630349)	95.12%	KT991139
	1PM4	*Mortierella elongatula* CBS 488.70(HQ630349)	95.91%	KT991140
	2EB6	*Mortierella elongatula* CBS 488.70(HQ630349)	95.91%	KT991141
	2EK5	*Mortierella elongatula* CBS 488.70(HQ630349)	95.91%	KT991142
Aspergillus	MS-19	*Aspergillus sydowii DBOF 102* (JQ724463)	99.13%	JX675047

TABLE 3 | Similarity comparison of all the sequences of potential novel species.

Microbial type	Strain no.	Most similar strain (ID)	Similarity
Bacteria	2PM7	*Mucilaginibacter dorajii* DR-f4(GU139697)	96.52%
Fungi	W2-1, 2PM2	*Pseudeurotium desertorum* WL07-3(JX077048)	96.46%
	1PM5, 1PM4, 2EB6, 2EK5	*Mortierella elongatula* CBS 488.70(HQ630349)	95.91%
	1EK4-8	*Mortierella elongatula* CBS 488.70(HQ630349)	95. 12%
	2PQ42	*Lecythophora fasciculata* IFM 50359 (KT991136)	96.58%
	2PK2	*Rhizoscyphus monotropae* ATCC52305(AF169309)	91.82%
	2PK13	*Rhodotorula rosulata* CBS10977(EU872492)	89.59%

diluted 100-fold with the proper culture medium for each pathogenic fungus, and preliminary screening was carried out under sterile conditions with 500 μg/mL (the highest concentration). Under a sterile environment, fungal suspensions (50 μL) of each pathogenic fungus were poured into wells containing 50 μL of 2-fold serially diluted single compounds in the corresponding culture medium for a final volume of 100 μL. The negative controls were treated with 1% DMSO. At the same concentrations, blank wells were prepared with the corresponding culture medium containing the tested compounds. The inoculated plates were incubated at 28°C. After incubation for 48 h, the optical density (OD) of each well was measured using a microplate reader at 600 nm. The minimum inhibitory concentration (MIC) values were derived from Probit analysis of the concentration, response data, with serially diluted concentrations of the tested compounds. The dilutions of the tested compounds were performed three times. Amphotericin B was used as a positive control against two fungi (*Fusarium oxysporum* and *Candida albicans*) with MIC values of 1.25 and 0.625 μg/mL, respectively.

RESULTS AND DISCUSSION

Diversity and Phylogeny of Soil Microorganisms

According to the cultivable results, we identified 83 strains of bacteria and 30 strains of fungi from soil, macroalgal rot and sediment samples collected on the Fildes Peninsula, Antarctica. By using 16S and ITS sequence similarity alignments, we

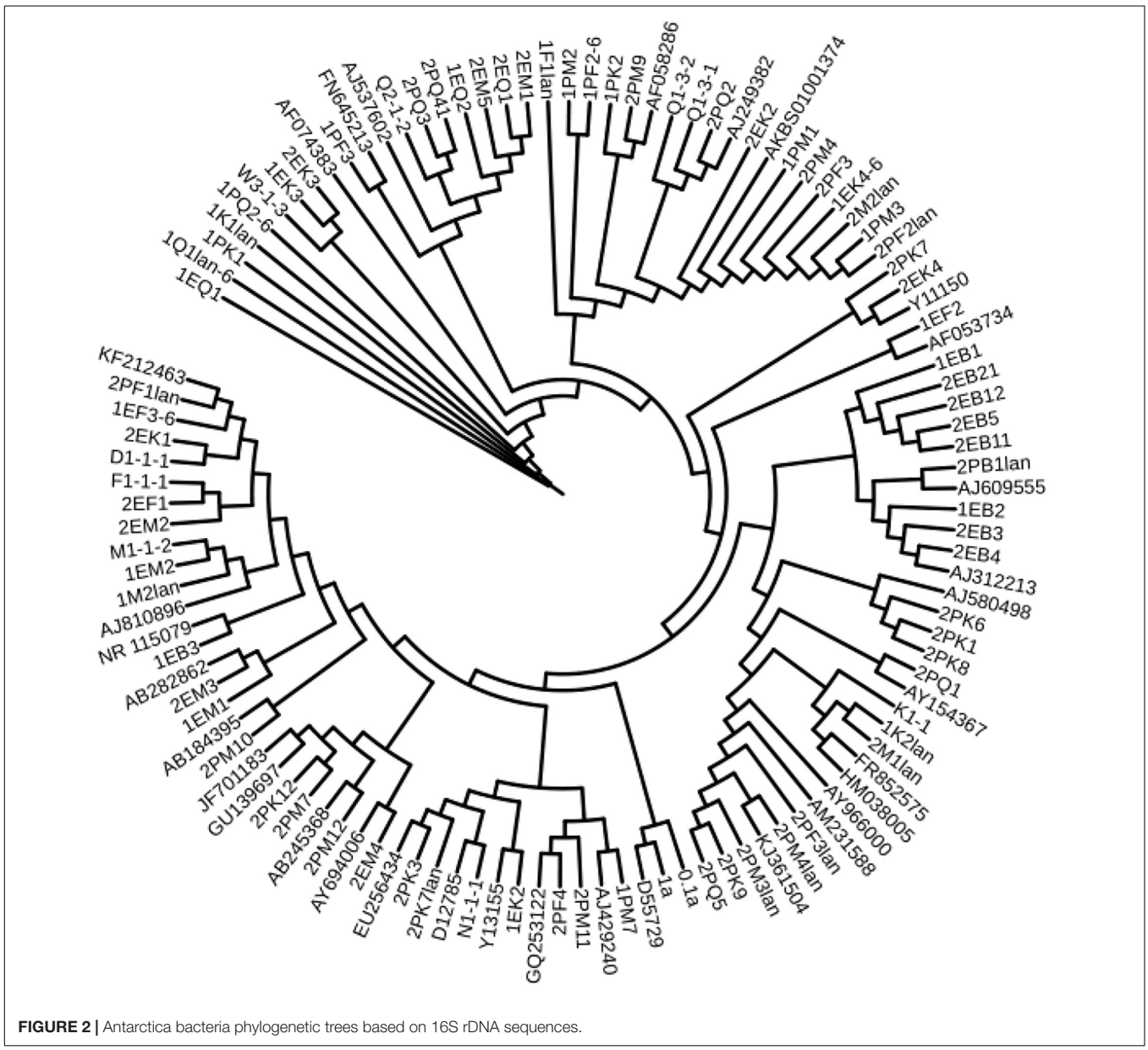

FIGURE 2 | Antarctica bacteria phylogenetic trees based on 16S rDNA sequences.

identified 33 apparently different species of bacteria belonging to 20 genera and 4 phyla and 8 species of fungi belonging to 6 genera and 4 classes. The 33 species of bacteria belonged to *Proteobacteria* (23), *Firmicutes* (1), *Actinobacteria* (5), and *Bacteroidetes* (4). The dominant bacterial genus was *Pseudomonas* (7). Distinct differences were observed among the 5 samples. The widespread genera *Pseudomonas* and *Massilia* belonged to *Proteobacteria*, while *Arthrobacter* belonged to *Actinobacteria*. *Pseudomonas* and *Massilia* were detected in samples F1-1, K1-1, M1-1, and Q2-1, while *Arthrobacte*r was detected in B1-1, F1-1, K1-1 and M1-1. Usually, we regarded a subject as a potential novel species if the 16S sequence similarity was < 97% (McCaig et al., 1999). From the 33 strains, we suggested that 1 may be novel species because of their low similarity, which is shown in **Table 3**. All the sequences we obtained have been submitted to GenBank, and their accession numbers are shown in **Tables 1**, **2**.

Fungi identification revealed 6 genera belonging to 4 classes: *Mortierella (Mortierellomycotina), Geomyces, Pseudeurotium, Hymenoscyphus (Leotiomycetes)*, Lecythophora (*Sordariomycetes*), *Rhodotorula* (*Microbotryomycetes*), and *Aspergillus*. The most abundant fungal genus was *Geomyces*. Several fungal strains with significant differences compared to typical strains were found. Usually, the subject was regarded as a potential novel species if the ITS sequence similarity was < 97% (Hughes et al., 2009). It was suggested that these 6 strains include 3 potential novel species might belong to 2 genera. From the results, we found that the microbes from the Fildes Peninsula, Antarctica, were plentiful although some of them never having been reported previously and should be investigated further (**Table 3**).

We used the neighbor-joining method to construct a phylogenetic tree according to the similarity of 16S and ITS sequences. The bootstrap value of each branch is the result of 1000 replications. The trees are shown in **Figures 2**, **3**.

Physiological-Biochemical Characteristics of Bacteria

Typical and putative novel strains were chosen from the cultured bacteria, and physical and chemical analyses were performed using the API NE20 Kit (bioMérieux). As shown in **Table 4**, 30, 23, 24, and 8 strains of them could produce α-glucosidase, protease, urease and β-galactosidase, respectively.

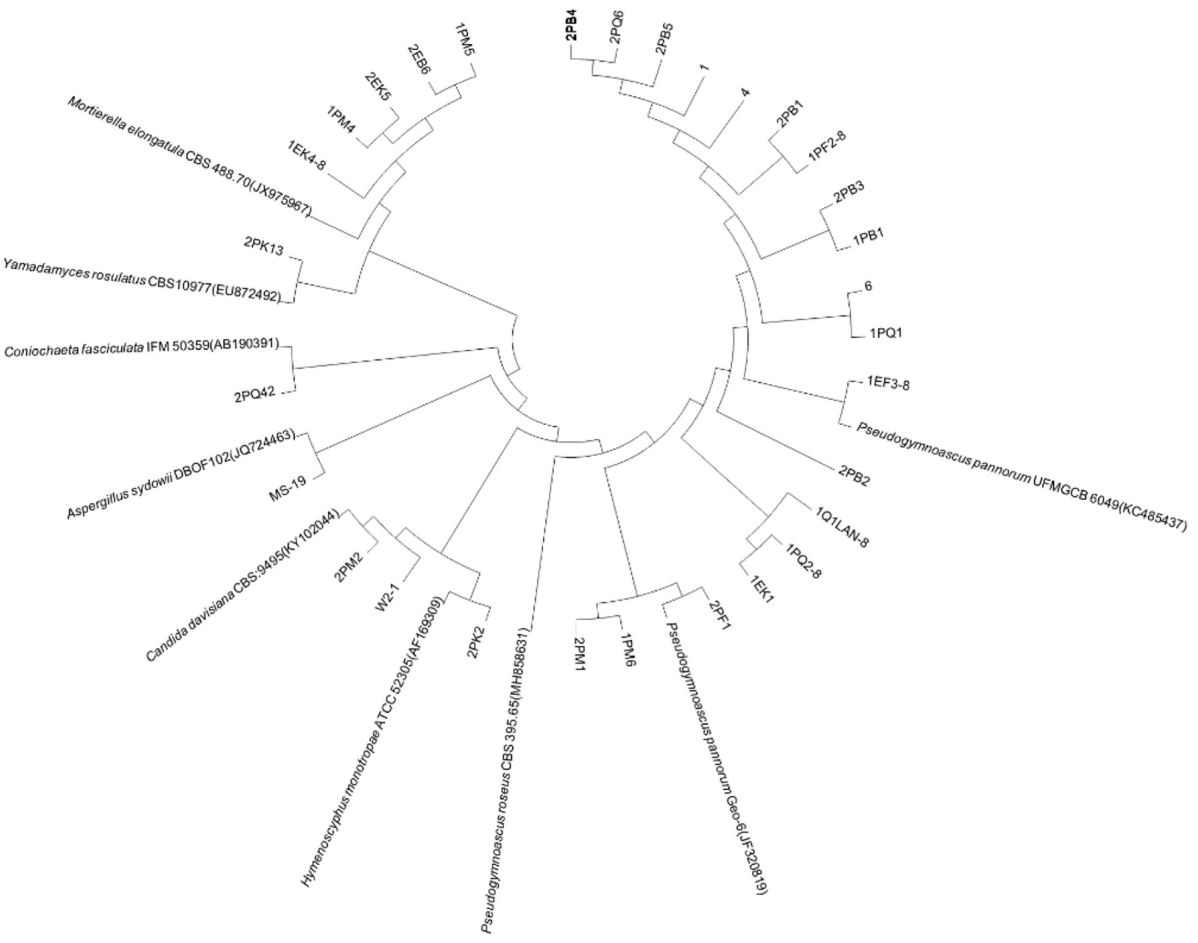

FIGURE 3 | Antarctica fungus phylogenetic trees based on ITS sequences.

TABLE 4 | API physiological and biochemical characterization of culturable bacteria.

Indicators	NO_3	TRP	GLU	ADH	URE	ESC	GEL	PNP	GLU	ARA	MNE	MAN	NAG	MAL	GNT	CAP	ADI	MLT	CIT	PAC
1PF3	−	−	±	+	+	+	+	−	+	+	+	+	+	−	+	+	−	+	+	−
1PQ2	−	−	−	+	+	+	+	−	+	+	+	+	+	±	+	+	±	+	+	±
2PK7	−	−	−	±	+	+	−	+	+	±	+	+	+	−	+	+	−	+	+	−
1PM2	+	−	−	−	+	+	+	−	−	−	−	−	−	−	−	−	−	−	+	−
1PM3	+	−	−	−	+	+	+	−	−	−	−	−	−	−	−	−	−	−	±	−
2EK2	+	−	−	±	±	+	+	−	+	−	−	+	−	−	+	+	±	+	+	−
2EM1	−	−	−	−	−	−	+	−	+	+	+	+	+	−	+	+	−	+	+	−
1EF2	+	−	−	−	+	+	+	−	−	−	−	−	−	−	−	−	±	−	+	−
2EB3	−	−	−	−	−	−	±	−	−	−	−	−	−	−	−	−	−	−	−	−
2PB1lan	+	−	−	−	+	+	+	−	−	−	−	−	−	−	−	−	−	−	−	−
2PK8	+	−	−	−	+	−	−	+	−	−	−	−	−	−	−	−	−	±	±	−
2PQ1	−	−	−	+	+	+	−	−	+	−	−	−	−	−	−	−	+	−	−	−
2PK9	−	−	−	−	+	+	−	−	−	−	−	−	−	−	−	−	−	−	+	−
2PF3lan	−	−	−	±	+	+	+	+	+	−	+	+	+	+	+	−	−	+	+	+
2PM3lan	+	−	−	−	−	+	+	−	+	+	+	+	+	+	+	+	+	+	+	±
1K2lan	+	−	−	+	+	+	−	−	−	−	−	−	−	−	−	−	±	±	−	−
K1-1	−	−	−	−	−	+	−	−	−	−	−	−	−	−	−	−	−	+	−	−
2M1lan	−	−	−	+	+	+	−	+	−	−	−	−	−	−	−	−	−	±	−	−
0.1a	+	−	−	−	−	+	+	−	+	−	−	−	−	−	−	−	−	−	−	±
2PK3	−	−	−	−	−	+	−	+	+	−	−	−	+	+	−	−	−	−	−	−
N1-1−1	+	−	+	+	+	+	−	+	+	−	+	+	+	+	+	+	−	+	+	+
1PM7	+	−	+	+	+	+	+	−	+	+	+	+	+	−	+	+	−	+	+	−
2PM11	−	−	−	−	+	+	+	−	−	−	−	+	+	−	+	−	−	+	+	−
1EK2	−	−	−	−	−	+	+	−	−	−	−	−	−	−	−	−	−	−	−	−
2PM10	+	−	−	−	+	+	+	−	−	−	−	−	−	−	−	−	−	−	+	−
1EM1	+	−	−	−	+	+	+	−	−	−	−	−	−	−	−	−	−	−	+	−
1EB3	+	−	−	−	+	+	+	−	−	−	−	+	−	−	−	+	−	+	+	−
2EF1	+	−	−	−	−	+	+	−	−	−	±	±	−	−	−	−	+	+	±	−
1EM2	+	−	−	−	+	+	+	−	−	−	−	−	−	−	−	−	±	±	−	−
2EM4	−	−	−	−	−	+	+	−	−	−	−	−	−	−	−	−	−	−	−	−
2PM12	+	−	−	−	+	+	±	−	±	±	−	−	−	−	−	−	−	−	+	−
2PM7	−	−	−	−	+	+	−	+	+	−	+	+	+	+	+	−	±	+	−	±
2PK12	−	−	+	+	+	+	+	+	+	+	+	+	+	±	+	+	±	+	+	+

*(**1**) N03, TRP, GLU, ADH, URE, ESC, GEL, and PNG represent nitrate reduction, indole synthesis, glucose fermentation, arginine dihydrolysis, urease, hydrolysis by α−glucosidase, protease and β−galactosidase, respectively. (**2**) GLU, ARA, MNE, MAN, NAG, MAL, GNT, CAP, ADI, MLT, CIT and PAC represent glucose, arabinose, mannose, mannitol, acetylglucosamine, maltose, potassium gluconate, capric acid, adipic acid, malate, sodium citrate and phenylacetic acid, respectively. (**3**) " + " represents positive reaction, "−" represents negative reaction, "±" represents weakly positive reaction.*

The tested bacteria displayed the ability to utilize a broad spectrum of organics. Strain 2EK2 could reduce nitrate to nitrite and nitrogen, produce arginine dihydrolase, urease, α-glucosidase and protease, and assimilate glucose, mannitol, potassium gluconate, capric acid, adipic, acid, malate and sodium citrate. 2PK7 could reduce nitrate to nitrite and nitrogen, produce arginine dihydrolase, urease, α-glucosidase, and β-galactosidase, and assimilate glucose, arabinose, mannose, mannitol, acetylglucosamine, potassium gluconate, capric acid, malate, and sodium citrate; 2PM3lan could reduce nitrate to nitrogen, produce α-glucosidase and protease and assimilate all 12 kinds of substrates tested. 2PF3lan could produce arginine dihydrolase, urease, α-glucosidase, and β-galactosidase and assimilate glucose, mannose, acetylglucosamine, maltose, potassium gluconate, malate, sodium citrate, and phenylacetic acid (**Table 4**).

Detection of Ectoenzyme Activities in Fungi

Extracellular enzymes were detected from typical and putative novel strains chosen from the culturable fungi. Results revealed that 7 strains were positive for amylase activity, 6 strains were positive for cellulase activity, and 10 strains were positive for caseinase activity. Six strains showed the abilities to produce all three enzymes (**Table 5**). The proportions of the strains encoding amylase, cellulase and caseinase were 53.85, 46.15, and 76.92%, respectively.

Primary Screening for Antifungal Activity

The EtOAc extract of rice fermentation of 30 fungi was prepared, and the antifungal activities of the 30 strains were screened by the filter paper method (Hong et al., 2013). A preliminary

TABLE 5 | Extracellular enzyme activity of culturable fungi.

Stain no.	Amylase	Cellulase	Caseinase
2PM1	−	−	−
1PQ1	+	+	+
1PQ2	+	+	+
2PF1	+	+	+
W2-1	−	−	±
2PK2	−	−	+
2PQ42	−	−	±
2PK13	+	−	+
1PM5	+	+	+
1EK4-8	−	−	−
1PM4	+	+	+
2EB6	+	±	+
2EK5	−	−	−

" + " represents positive, "− " represents negative, " ± " represents weakly positive.

screening revealed that only the fungus MS-19, identified as *Aspergillus sydowii*, was able to inhibit the growth of 2 pathogenic fungi (*F.oxysporum* and *C. albicans*). The neighbor-joining tree and morphological and microscopic characteristics of MS-19 are shown in **Supplementary Figure S1** and in previous literature (Cong et al., 2017).

Compound Identification

The EtOAc extract of rice fermentation of *Aspergillus sydowii* MS-19 was subjected to silica gel column chromatography and further purified by HPLC to obtain four known compounds (**1–4**) (**Figure 4**). The spectroscopic data of the identified compounds were compared with those reported in the literature, and versicone A (**1**), versicone B (**2**), 4-methyl-5,6-dihydro-2H-pyran-2-one (**3**), and (*R*)-(+)-sydowic acid (**4**) were identified. Compounds **1–3** were isolated from *Aspergillus sydowii* for the first time.

Compound **1** was obtained as a yellow amorphous solid. The ^{1}H NMR spectrum showed the presence of 3 methyl groups [δ_H 1.78 (s, H_3-18), δ_H 1.70 (s, H_3-19), δ_H 2.41 (s, H_3-14),], one methoxy group [δH 4.02 (s, H_3-21)], and 4 olefinic protons [δ_H 7.23 (s, H-1), δ_H 6.79, (d, J = 8.5 Hz, H-6), δ_H 7.58 (t, J = 8.5 Hz, H-7), δ_H 7.01 (dd, J = 8.5, 0.5 Hz, H-8)]. Analysis of the ^{13}C NMR data of **1** revealed 21 carbon signals, involving 3 methyl groups (δ_C 17.7, CH_3-14; δ_C 18.3, CH_3-19; δ_C 26.0, CH_3-18), one methoxy group (δ_C 56.8, CH_3-21), 2 oxygenated methylenes (δ_C 57.3, CH_2-20; δ_C 72.3, CH_2-15), 5 olefinic methines (δ_C 109.9, CH-8; δ_C 105.6, CH-6; δ_C 119.1, CH-1; δ_C 120.1, CH-16; δ_C 134.7, CH-7), 9 quaternary carbons including 4 oxygenated carbons (δ_C 152.9, C-3; δ_C 160.8, CH-5; δ_C 152.8, C-9; δ_C 157.6, C-12), and one carboxyl carbon (δ_C 179.9, C-13) (**Supplementary Table S2**). These signals were exactly the same as those of versicone A (Wang et al., 2016).

The resemblance of the ^{1}H and ^{13}C NMR data (**Supplementary Table S2**) of **2** and **1** indicated that they had the same skeleton. The main difference in the ^{1}H NMR spectra was the presence of a methoxy group at δ_H 3.89 in **2**, and in the ^{13}C NMR spectrum, a methoxy group at δ_C 57.4 in **2**. Therefore, **2** was presumed to be a product of the methylation of 1 at C-6 (δ_C 105.6 in **1**, δ_C 149.1 in **2**). This conclusion was supported because the NMR data of **2** was identical to that of versicone B. Versicones A-B were first discovered from the culture medium of *Aspergillus versicolour* SCSIO 05879 (Wang et al., 2016).

Compound **3** was isolated as a colorless oil. The ^{1}H NMR and ^{13}C NMR spectra showed the presence of one methyl group (δ_H 2.01, δ_C 22.6, CH_3-7), one methylene group [δ_H 2.38 (t, J = 6.0 Hz), δ_C 29.2, CH_2-4], one oxygenated methylene [δ_H 4.38 (t, J = 6.0 Hz), δ_C 65.9, CH_2-3], one methine [δ_H 5.83 (q = 1.5 Hz), δ_C 116.8, CH-6], and two quaternary carbons (δ_C 157.8, C-5; δ_C 164.8, C-1) (**Supplementary Table S3**). Through literature comparison, **3** was identified as 4-methyl-5,6-dihydro-2H-pyran-2-one (Hamasaki et al., 1975).

Compound **4** forms colorless needles, [α]25 D + 13.6 (*c* 0.20, $CHCl_3$). The NMR spectra indicated the presence of 20 protons and 15 carbons, including 3 methyls, 3 methylenes, 3 methine, and 6 quaternary carbons (**Supplementary Table S4**). Based on these data and the literature, **4** could easily be identified as sydowic acid (Ying et al., 2014).

Antifungal Activities

The antifungal activities of compounds **1–4** against two pathogenic fungi (*Fusarium oxysporum*, *Candida albicans*) were

TABLE 6 | Inhibitory effects of compounds **1–4** on pathogenic fungi.

Compound	Pathogenic fungi (MIC, μg/mL)	
	Fusarium oxysporum	*Candida albicans*
1	62.5	3.91
2	>500	125
3	>500	>500
4	>500	>500
Amphotericin B	1.25	0.625

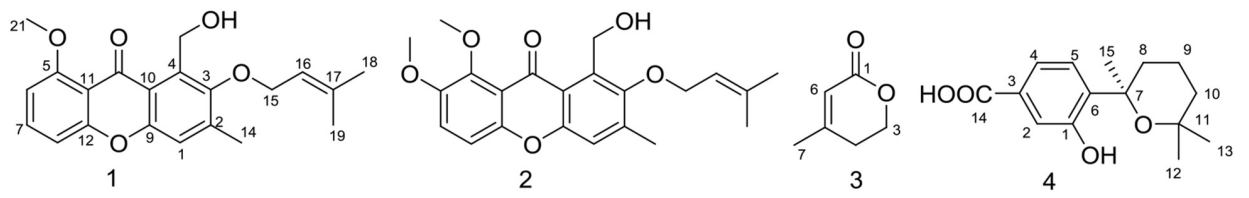

FIGURE 4 | Structure of compounds **1–4.**

preliminarily investigated. Amphotericin B was used as the corresponding positive control. Among them, **1** showed strong antifungal activity (MIC of 3.91 μg/mL) against *Candida albicans* compared with amphotericin B (MIC of 0.625 μg/mL). In addition, the antifungal activities of other compounds were not ideal (**Table 6**).

CONCLUSION

To better understand the biodiversity and the potential application of microbes living in Antarctica, we collected, isolated, cultured and analyzed the composition and function of microorganisms located on the Fildes Peninsula, Antarctica. Different kinds of culture media satisfy different microbial preferences, so we cultured the microbes in several media to obtain more species.

The bacteria we isolated from the soil collected on the Fildes Peninsula, Antarctica, included 33 species belonging to 4 phyla, *Proteobacteria* (23), *Firmicutes* (1), *Actinobacteria* (5), and *Bacteroidetes* (4), in 20 genera. A total of 7 species belonging to *Pseudomonas*, the dominant genus, were isolated, and 5 species belonging to *Arthrobacter* were obtained. This result was in accordance with Ding et al., who reported that the dominant genus belonged to *Gammaproteobacteria* (Ding et al., 2014). On the other hand, Dong et al. reported that the dominant genus belonged to the phylum Firmicutes (Dong et al., 2013). Compared with the *pyrosequencing* results from previous studies (Wang et al., 2015), many phyla were not detected, including *Acidobacteria* and *Verrucomicrobi*a. This might be because it is difficult to culture cells of these phyla (Hedlund, 2010; Thrash and Coates, 2010).

We isolated a fewer number of fungi than bacteria. Only 7 genera were recognized, *Mortierella*, *Geomyces*, *Hymenoscyphus*, *Pseudeurotium*, *Lecythophora Rhodotorula,* and *Aspergillus*, and the most common genus was *Geomyces*. Factors such as the variance of sampling places, sampling seasons, culture media, and methods might contribute to these differences. All 6 fungal genera we identified belonged to *Ascomycota* and *Basidiomycota*, and the results were consistent with those of Dong et al. (2015). In conclusion, we suggested that the microbes of the Fildes Peninsula are diverse; these results exceeded our estimation and provided a source for researching metabolism and biodegradation.

Among the isolated bacteria and fungi, 3 bacteria and five fungi had less similarity to references than others, suggesting that the 11 strains may be novel species. Usually, strains with 16S rDNA and ITS sequence similarity less than 97% could be regarded as novel species (McCaig et al., 1999; Hughes et al., 2009). Dong et al. reported several potential novel species (Dong et al., 2013), and one of them was verified as *Deinococcus antarcticus* sp. nov. (Dong et al., 2015). Although these putative novel species need to be further identified, this information could enrich our knowledge of Antarctica. To date, scientists have proven that many psychotropic and cold-resistant bacteria isolated from polar regions can synthesize enzymes that function at low temperatures. β-Galactosidase plays an important role in the degradation of cellulose (Pardee et al., 1959), and the strains detected in our study, including 2PK7, 2PK8, 2PF3lan, 2M1lan, 2PK3, N1-1-1, 2PM7, and 2PK12, could produce β-galactosidase. Previous reports have also shown that other fungal genera can synthesize β-galactosidase. Ding et al. obtained 2 strains of bacteria from Prydz Bay, Antarctica, that belonged to Microbacterium and Salegentibacter and could synthesize β-galactosidase (Ding et al., 2014). Turkiewicz et al. reported a novel species, *Thysanoessa macrura*, from the alimentary tract of Antarctic krill; this species could synthesize an intracellular cold-adapted β-galactosidase (Turkiewicz et al., 2003). All these strains that could synthesize β-galactosidase may provide candidates for industrial applications.

Macromolecules were utilized by microbes after hydrolysis (Thomas, 1980; Confer and Logan, 1997). By hydrolysing α-1,4-glycosidic bonds, α-glucosidase can produce glucose from polyoses such as amylose (der Maarel et al., 2002). Therefore, α-glucosidase plays an important role in the utilization of carbohydrates (Elbein, 1991). The strains 1PF3, 1PQ2, 2PK7, 1PM2, 2PB1lan, 2PF3lan, 2PM3lan, 2PM11, and EB3 could produce α-glucosidase, indicating that these strains were able to degrade polyose.

The tested strains showed broad-spectrum utilization of multiple kinds of carbohydrates. For example, 2EK2 could assimilate glucose, mannitol, potassium gluconate, capric acid, adipic acid, malate and sodium citrate; 1PF3, 2PK7, 2EM1, and 1PM7 could assimilate glucose, arabinose, mannose, mannitol, acetylglucosamine, potassium gluconate, capric acid, malate, and sodium citrate. N1-1-1 could assimilate glucose, mannose, mannitol, acetylglucosamine, maltose, potassium gluconate, capric acid, malate, sodium citrate and phenylacetic acid; 1PQ2, 2PM3lan, and 2PK12 could utilize all 12 kinds of carbohydrates tested. Therefore, these bacteria are substantial candidates for low-temperature applications.

The isolated fungi were tested to determine whether they could produce extracellular enzymes. The results showed that 7 of 13 had amylase activity, 6 of 13 had cellulase activity, and 10 of 13 had caseinase activity. Six strains displayed all three enzyme functions. Cellulase, amylase, and caseinase have important applications in industry (Souza, 2010; Kuhad et al., 2011; Shrestha et al., 2015). Because the testing temperature was set to 12°C, the testing results suggested that these Antarctic fungi had adapted to the extreme environment and may be a repository of low-temperature working enzymes. Former studies have provided suggestions for the utilization of biocatalysts (Robl et al., 2013).

In this paper, the antifungal activities of 30 fungi were also evaluated. As a result, the fungus MS-19, identified as *Aspergillus sydowii*, was able to inhibit the growth of *Castanea anthracis* and *Fusarium oxysporum*. Further isolation yielded four polyketones: versicone A (**1**), versicone B (**2**), 4-methyl-5,6-dihydro-2H-pyran-2-one (**3**), and (*R*)-(+)-Sydowic Acid (**4**). Among them, versicone A displayed strong activity against *Castanea anthracis* with an MIC value of 3.91 μg/mL. The results indicated that versicone A could be regarded as a lead compound against *Candida albicans*.

DATA AVAILABILITY STATEMENT

The datasets presented in this study can be found in online repositories. The names of the repository/repositories and accession number(s) can be found in the article/ **Supplementary Material**.

AUTHOR CONTRIBUTIONS

BC, XY, and AD contributed to isolation and identification of microbes of Antarctica. YT contributed to structure elucidation, NMR analysis, and bioactivities test. JS, SW, and HY were the project leader organizing and guiding the experiments and manuscript writing. All authors contributed to the article and approved the submitted version.

FUNDING

This work was supported by the National Key R&D Program of China (Grant No: 2018YFC1406701), Basic Scientific Fund for National Public Research Institutes of China (Grant No. 2018Q03), Chinese National Natural Science Foundation (Grant No. 41006102), and Natural Science Foundation of Fujian Province of China (Grant No. 2019J05032).

SUPPLEMENTARY MATERIAL

The Supplementary Material for this article can be found online at: https://www.frontiersin.org/articles/10.3389/fmicb.2020.570836/full#supplementary-material

REFERENCES

Chavez, R., Fierro, F., Garciarico, R. O., and Vaca, I. (2015). Filamentous fungi from extreme environments as a promising source of novel bioactive secondary metabolites. *Front. Microbiol.* 6:903. doi: 10.3389/fmicb.2015.00903

Chown, S. L., Clarke, A., Fraser, C. I., Cary, S. C., Moon, K. L., and McGeoch, M. A. (2015). The changing form of Antarctic biodiversity. *Nature* 522, 431–438. doi: 10.1038/nature14505

Confer, D. R., and Logan, B. E. (1997). Molecular weight distribution of hydrolysis products during the biodegradation of model macromolecules in suspended and biofilm cultures. II. Dextran and dextrin. *Water Res.* 31, 2137–2145. doi: 10.1016/s0043-1354(97)00050-x

Cong, B. L., Wang, N. F., Liu, S. H., Liu, F., Yin, X. F., and Shen, J. H. (2017). Isolation, characterization and transcriptome analysis of a novel Antarctic *Aspergillus sydowii* strain MS-19 as a potential lignocellulosic enzyme source. *BMC Microbiol.* 17:129. doi: 10.1186/s12866-017-1028-0

Cowan, D. A., Khan, N., Pointing, S. B., and Cary, S. C. (2010). Diverse hypolithic refuge communities in the McMurdo dry valleys. *Antarct. Sci.* 22, 714–720. doi: 10.1017/s0954102010000507

der Maarel, M. J., Der Veen, B. A., Uitdehaag, J. C., Leemhuis, H., and Dijkhuizen, L. (2002). Properties and applications of starch-converting enzymes of the α-amylase family. *J. Biotechnol.* 94, 137–155. doi: 10.1016/S0168-1656(01)00407-2

Ding, X., Cong, B., Zhang, Y., Jin, Y., Zhu, Q., Wang, N., et al. (2014). Biodiversity,physiological and biochemical characteristics of microorganisms in the sediments surface from the Prydz Bay,Antarctica. *Adv. Mar. Sci.* 32, 209–218. doi: 10.1016/s0377-8398(97)00021-2

Dong, N., Di, Z., Yu, Y., Yuan, M., Zhang, X., and Li, H. (2013). Exrtacellular enzyme activity and antimicrobial activity of culturable bacteria isolated from soil of Grove Mountains, East Antarctica. *Acta Microbiol. Sin.* 53, 1295–1306.

Dong, N., Li, H. R., Yuan, M., Zhang, X. H., and Yu, Y. (2015). *Deinococcus antarcticus* sp. nov., isolated from soil. *Int. J. Syst. Evol. Micr.* 65, 331–335. doi: 10.1099/ijs.0.066324-0

Elbein, A. D. (1991). Glycosidase inhibitors as antiviral and/or antitumor agents. *Semin. Cell Biol.* 2, 309–317.

Feng, W. Y., Chen, C. M., Mo, S. Y., Qi, C. X., Gong, J. J., Li, X. N., et al. (2019). Highly oxygenated meroterpenoids from the Antarctic fungus *Aspergillus terreus*. *Phytochemistry* 164, 184–191. doi: 10.1016/j.phytochem.2019.05.015

Freckman, D. W., and Virginia, R. A. (1997). Low-diversity Antarctic soil nematode communities: distribution and response to disturbanse. *Ecology* 78, 363–369. doi: 10.1890/0012-9658(1997)078[0363:ldasnc]2.0.co;2

Godinho, V. M., Gonçalves, V. N., Santiago, I. F., Figuered, H. M., Vitoreli, G. A., Schaefer, C. E., et al. (2015). Diversity and bioprospection of fungal community present in oligotrophic soil of continental Antarctica. *Extremophiles* 19, 585–596. doi: 10.1007/s00792-015-0741-6

Hamasaki, T., Sato, Y., and Hatsuda, Y. (1975). Isolation of new metabolites from *Aspergillus sydowi* and structure of sydowic acid. *Agric. Biol. Chem.* 39, 2337–2340. doi: 10.1271/bbb1961.39.2337

Hedlund, B. P. (2010). "Phylum XXIII. Verrucomicrobia phyl nov," in *Bergey's Manual® of Systematic Bacteriology*, ed. N. R. Krieg (New York, NY: Springer), 795–841. doi: 10.1007/978-0-387-68572-4_12

Hong, Y. X., Cai, X. X., Shao, B., Hong, J., Wang, S. Y., and Rao, P. F. (2013). Isolation of a thermostable trypsin inhibitor with exploitable potential. *Eur. Food Res. Technol.* 237, 457–465. doi: 10.1007/s00217-013-2013-y

Huang, J. P., Swain, A. K., Thacker, R. W., Ravindra, R., Andersen, D. T., and Bej, A. K. (2013). Bacterial diversity of the rock-water interface in an East Antarctic freshwater ecosystem, Lake Tawani(P)†. *Aquat. Biosyst.* 9, 1–4. doi: 10.1186/2046-9063-9-4

Hughes, K. W., Petersen, R. H., and Lickey, E. B. (2009). Using heterozygosity to estimate a percentage DNA sequence similarity for environmental species' delimitation across basidiomycete fungi. *New Phytol.* 182, 795–798. doi: 10.1111/j.1469-8137.2009.02802.x

Kuhad, R. C., Gupta, R., and Singh, A. (2011). Microbial cellulases and their industrial applications. *Enzym. Res.* 2011, 1–10. doi: 10.4061/2011/280696

Lario, L. D., Chaud, L. C., Almeida, M. D., Converti, A., Sette, L. D., and Pessoa, A. (2015). Production, purification, and characterization of an extracellular acid protease from the marine Antarctic yeast *Rhodotorula mucilaginosa* L7. *Fungal Biol.* 119, 1129–1136. doi: 10.1016/j.funbio.2015.08.012

Li, L. Y., Li, D. H., Luan, Y. P., Gu, Q. Q., and Zhu, T. J. (2012). Cytotoxic metabolites from the Antarctic psychrophilic fungus *Oidiodendron truncatum*. *J. Nat. Prod.* 75, 920–927. doi: 10.1021/np3000443

McCaig, A. E., Glover, L. A., and Prosser, J. I. (1999). Molecular analysis of bacterial community structure and diversity in unimproved and improved upland grass pastures. *Appl. Environ. Microbiol.* 65, 1721–1730. doi: 10.1016/S0003-4975(02)04832-4

Pardee, A. B., Jacob, F., and Monod, J. (1959). The genetic control and cytoplasmic expression of "Inducibility" in the synthesis of β-galactosidase by E. *coli*. *J. Mol. Biol.* 1, 165–178. doi: 10.1016/S0022-2836(59)80045-0

Ray, M., Devi, K. U., Kumar, G. S., and Shivaji, S. (1992). Extracellular protease from the antarctic yeast *Candida humicola*. *Appl. Environ. Microbiol.* 58, 1918–1923. doi: 10.1128/AEM.58.6.1918-1923.1992

Robl, D., Delabona, P. D., Mergel, C. M., Rojas, D. J., dos, S., Costa Pimentel, I. C., et al. (2013). The capability of endophytic fungi for production of hemicellulases and related enzymes. *BMC Biotechnol.* 13:94. doi: 10.1186/1472-6750-13-94

Shrestha, P., Ibáñez, A. B., Bauer, S., Glassman, S. I., Szaro, T. M., Bruns, T. D., et al. (2015). Fungi isolated from *Miscanthus* and sugarcane: biomass conversion, fungal enzymes, and hydrolysis of plant cell wall polymers. *Biotechnol. Biofuels* 8, 1–14. doi: 10.1186/s13068-015-0221-3

Souza, P. M. (2010). Application of microbial α-amylase in industry-A review. *Braz. J. Microbiol.* 41, 850–861. doi: 10.1590/S1517-83822010000400004

Teixeira, L. C., Peixoto, R. S., Cury, J. C., Sul, W. J., Pellizari, V. H., Tiedje, J., et al. (2010). Bacterial diversity in rhizosphere soil from Antarctic vascular plants of Admiralty Bay, maritime Antarctica. *ISME J.* 4, 989–1001. doi: 10.1038/ismej.2010.35

Thomas, F. (1980). The recognition of maltodextrins by *Escherichia coli*. *Eur. J. Biochem.* 108, 631–636. doi: 10.1111/j.1432-1033.1980.tb04758.x

Thrash, J. C., and Coates, J. D. (2010). "Phylum XVII. Acidobacteria phyl. nov," in *Bergey's Manual® of Systematic Bacteriology*, ed. N. R. Krieg (New York, NY.: Springer), 725–735. doi: 10.1007/978-0-387-68572-4_6

Turkiewicz, M., Kur, J., Białkowska, A., Cieśliński, H., Kalinowska, H., and Bielecki, S. (2003). Antarctic marine bacterium *Pseudoalteromonas* sp. 22b as a source of cold-adapted β-galactosidase. *Biomol. Eng.* 20, 317–324. doi: 10.1016/S1389-0344(03)00039-X

Vazquez, S., Merino, L. R., MacCormack, W., and Fraile, E. (1995). Protease-producing psychrotrophic bacteria isolated from Antarctica. *Polar Biol.* 15, 131–135. doi: 10.1007/BF00241051

Velascocastrillon, A., Gibson, J. A., and Stevens, M. I. (2014). A review of current Antarctic limno-terrestrial microfauna. *Polar Biol.* 37, 1517–1531. doi: 10.1007/s00300-014-1544-4

Wang, J. F., He, W. J., Huang, X. L., Tian, X. P., Liao, S. R., Yang, B., et al. (2016). Antifungal new oxepine-containing alkaloids and xanthones from the deep-sea-derived fungus *Aspergillus versicolor* SCSIO 05879. *J. Agric. Food Chem.* 64, 2910–2916. doi: 10.1021/acs.jafc.6b00527

Wang, N. F., Zhang, T., Zhang, F., Wang, E. T., He, J. F., Ding, H., et al. (2015). Diversity and structure of soil bacterial communities in the Fildes region (maritime Antarctica) as revealed by 454 pyrosequencing. *Front. Microbiol.* 6:1188. doi: 10.3389/fmicb.2015.01188

Ying, Y. M., Zhang, L. W., Shan, W. G., and Zhan, Z. J. (2014). Secondary metabolites of *Peyronellaea* sp. *XW*-12, an endophytic fungus of *Huperzia serrata*. *Chem. Nat. Compd.* 50, 723–725. doi: 10.1007/s10600-014-1063-0

Conflict of Interest: The authors declare that the research was conducted in the absence of any commercial or financial relationships that could be construed as a potential conflict of interest.

frontiers in Microbiology

ORIGINAL RESEARCH
published: 24 September 2020
doi: 10.3389/fmicb.2020.574771

Production of Neoagaro-Oligosaccharides With Various Degrees of Polymerization by Using a Truncated Marine Agarase

*Wu Qu[1], Dingquan Wang[1], Jie Wu[2], Zhuhua Chan[2], Wenjie Di[2], Jianxin Wang[1] and Runying Zeng[2,3]**

[1]Marine Science and Technology College, Zhejiang Ocean University, Zhoushan, China, [2]Third Institute of Oceanography, Ministry of Natural Resources, Xiamen, China, [3]Technical Innovation Center for Utilization of Marine Biological Resources, Ministry of Natural Resources, Xiamen, China

Bioactivities, such as freshness maintenance, whitening, and prebiotics, of marine neoagaro-oligosaccharides (NAOS) with 4–12 degrees of polymerization (DPs) have been proven. However, NAOS produced by most marine β-agarases always possess low DPs (≤6) and limited categories; thus, a strategy that can efficiently produce NAOS especially with various DPs ≥8 must be developed. In this study, 60 amino acid residues with no functional annotation result were removed from the C-terminal of agarase AgaM1, and truncated recombinant AgaM1 (trAgaM1) was found to have the ability to produce NAOS with various DPs (4–12) under certain conditions. The catalytic efficiency and stability of trAgaM1 were obviously lower than the wild type (rAgaM1), which probably endowed trAgaM1 with the ability to produce NAOS with various DPs. The optimum conditions for various NAOS production included mixing 1% agarose (w/v) with 10.26 U/ml trAgaM1 and incubating the mixture at 50°C in deionized water for 100 min. This strategy produced neoagarotetraose (NA4), neoagarohexaose (NA6), neoagarooctaose (NA8), neoagarodecaose (NA10), and neoagarododecaose (NA12) at final concentrations of 0.15, 1.53, 1.53, 3.02, and 3.02 g/L, respectively. The NAOS served as end-products of the reaction. The conditions for trAgaM1 expression in a shake flask and 5 L fermentation tank were optimized, and the yields of trAgaM1 increased by 56- and 842-fold compared with those before optimization, respectively. This study provides numerous substrate sources for production and activity tests of NAOS with high DPs and offers a foundation for large-scale production of NAOS with various DPs at a low cost.

Keywords: truncated agarase, neoagaro-oligosaccharide, various polymerization degrees, fermentation optimization, recombinant expression

OPEN ACCESS

Edited by:
Obulisamy Parthiba Karthikeyan, University of Houston, United States

Reviewed by:
Kris Niño Gomez Valdehuesa, The University of Manchester, United Kingdom
Xiaoqiang Ma, Singapore-MIT Alliance for Research and Technology (SMART), Singapore

***Correspondence:**
Runying Zeng
zeng@tio.org.cn

Specialty section:
This article was submitted to Microbiotechnology, a section of the journal Frontiers in Microbiology

Received: *21 June 2020*
Accepted: *02 September 2020*
Published: *24 September 2020*

Citation:
Qu W, Wang D, Wu J, Chan Z, Di W, Wang J and Zeng R (2020) Production of Neoagaro-Oligosaccharides With Various Degrees of Polymerization by Using a Truncated Marine Agarase. Front. Microbiol. 11:574771. doi: 10.3389/fmicb.2020.574771

INTRODUCTION

Agarose, the cell-wall component of marine algae, is a polysaccharide that consists of alternating disaccharide units of D-galactose and 3,6-anhydro-L-galactose (Ramos et al., 2016). Hydrolysis products of agarose, namely agaro-oligosaccharides (AOS) and neoagaro-oligosaccharides (NAOS), exhibit potential uses in food, pharmaceutical, and cosmetic industries (Chen et al., 2009;

Fu and Kim, 2010; Higashimura et al., 2013, 2016). Acid hydrolysis is a traditional method of degrading agarose into AOS (Xu et al., 2017), and alkalis are used to neutralize the pH value of AOS hydrolysate. However, a large amount of acids and alkalis used during the production process of oligosaccharides can be very harmful to the environment. Agarases from marine microorganisms, which can hydrolyze agarose under mild and environment-friendly conditions, are alternative solutions for acid hydrolysis to produce agarose-derived oligosaccharides (Lee et al., 2012). Agarases are mainly from marine environments and are classified as α- and β-agarases based on cleavage sites. Similar to the acids in hydrolysis, α-agarases cut the α-1,3-glycosidic bond in agarose to produce AOS, and β-agarases cut the β-1,4-glycosidic bond to produce NAOS (Yun et al., 2017). Therefore, enzymatic hydrolysis by β-agarases may be the most feasible method of NAOS production.

Agaro-oligosaccharides (AOS) and NAOS perform many biological activities. For instance, AOS possesses anti-inflammatory, carcinostatic, antioxidant, hepatoprotective, and α-glucosidase inhibitory properties (Chen et al., 2006; Enoki et al., 2010; Higashimura et al., 2013). NAOS exhibits hepatoprotective, freshness maintenance, skin whitening, and cholesterol-lowering activities (Hou et al., 2014; Ji et al., 2017; Jin et al., 2017; Kim et al., 2017). To compare the activities of AOS and NAOS, Xu et al. (2017) studied the antioxidant capacities of agar-derived oligosaccharides and reported that the scavenging ability of NAOS for hydroxyl radicals is greater than that of AOS. Therefore, NAOS might be more effective and valuable than AOS in certain fields.

According to the degree of polymerization (DP), NAOS are categorized as neoagarobiose (NA2), neoagarotetraose (NA4), neoagarohexaose (NA6), neoagarooctaose (NA8), neoagarodecaose (NA10), neoagarododecaose (NA12), and others. Scholars have investigated the bioactivities of NAOS (Hou et al., 2014; Jin et al., 2017). In general, the biological activities of NAOS are correlated with their DPs (Xu et al., 2018). For instance, NA4 and NA6 have high inhibition effects against α-glucosidase, tyrosinase, and melanin biosynthesis (Hong et al., 2017), and the probiotic activities of NA8, NA10, and NA12 are higher than those of NA4 and NA6 (Hu et al., 2006). However, simultaneously outputting these NAOS with various DPs of 4–12 by enzymes is difficult (Hou et al., 2015; Di et al., 2018) due to the problem with most β-agarases, that is, the DPs of NAOS produced by most agarases are usually low (≤6), and the types of NAOS produced by agarases are limited. In a recent study, a β-agarase called AgaXa was isolated from *Catenovulum* sp. X3 and degraded agarose into NA8 and NA10 as main end-products. However, the number of NAOS types is still limited, and almost all β-agarases can only produce 2–3 types of NAOSs (Xie et al., 2013). To solve the problems of simplistic and low DPs of agarase products, researchers mixed AgaXa with another β-agarase that can degrade agarose into NA4 and NA6 to simultaneously produce NAOS with various DPs of 4–12 (Li et al., 2007). However, the cost of fermenting two enzymes is higher than that of using only one enzyme. Thus, an effective method using a single agarase must be developed to produce NAOS with higher and various DPs.

agaM1 (GenBank accession number MG280837), a β-agarase gene, was isolated from mangrove sediment microbiome (Qu et al., 2018) and characterized through heterologous expression (Di et al., 2018). In the present study, we truncated AgaM1 and found that the truncated recombinant AgaM1 (trAgaM1) could hydrolyze agarose into NAOS with various DPs (NA4, NA6, NA8, NA10, and NA12) as end-products under specific reaction conditions. Moreover, the reaction conditions were optimized for large-scale production of NAOS. In addition, the production of trAgaM1 expressed in *Escherichia coli* cells was optimized in a shake flask and 5 L fermentation tank. Results provide the foundation for future large-scale production of marine NAOS with various DPs.

MATERIALS AND METHODS

Analysis, Cloning, and Expression of Truncated AgaM1 Gene

In our previous study (Di et al., 2018), the agarase gene *agaM1* was cloned and expressed in *E. coli* cells to obtain recombinant AgaM1 (rAgaM1). The conserved domains in the amino acid sequences of AgaM1 were predicted by using BLASTX on the NCBI website,[1] and a peptide without any annotation result was removed. PCR was performed to truncate the *agaM1* gene by using a forward primer (5'-CAATACGACTGGGATAA CATTGCAATTCC-3') and a reverse primer (5'-ATAGATT TCATCCACAAATGGATTCGGATATATAATTAAATCAG-3'). The PCR product was purified and ligated into the pEASY-Blunt E2 expression vector with the T7 promoter (TransGen Biotech Co. Ltd., China). Ultimately, 180 bp of nucleotide sequences were removed from the 3' end of the *agaM1* gene, resulting in the truncation of 60 amino acid residues from the C-terminal of the original rAgaM1. The truncated recombinant protein was called trAgaM1. *E. coli* BL21(DE3) cells harboring the recombinant plasmid were cultured in lysogeny broth (LB) to an OD600 of 0.6 at 37°C (250 rpm). Then, the cells were induced with 0.1 mmol/L isopropyl β-D-thiogalactoside (IPTG) at 17°C for 14 h (250 rpm) in a 250 ml shake flask with an initial liquid volume of 50 ml, which was set as the original condition for trAgaM1 production before optimization. After ultrasonication of the cells, trAgaM1 was purified using a nickel-affinity chromatography column (HisPur Ni-NTA Spin Column, Thermo Fisher Scientific, MA, United States). The unpurified and purified proteins were analyzed *via* 10% sodium dodecyl sulfate-polyacrylamide gel electrophoresis (SDS-PAGE). In detail, the unpurified samples with and without IPTG induction and three identical samples of purified proteins were loaded for SDS-PAGE. After the electrophoresis, two of the samples were stained by Coomassie brilliant blue, and the lane of the third sample was cut off for the activity stain as follows: sodium dodecyl sulfate (SDS) in the gel was removed by rinsing the gel thrice in phosphate buffer saline (PBS; pH 7.4) for approximately 20 min each time after electrophoresis. Subsequently, the gel was placed on the 1% (w/v) agar plate, and the plate was incubated at 30°C for 12 h. The agar plate was stained with iodine solution, and a clean zone could be observed at the position of trAgaM1. Protein concentration was determined using a Pierce BCA Protein Assay Kit (Thermo Fisher Scientific, MA, United States).

[1]https://blast.ncbi.nlm.nih.gov/

Enzyme Activity Assay

A total of 18.7 μg of the enzyme solution was mixed with 240 μl of Tris-HCl buffer (pH 9) containing 0.2% (w/v) melted agarose. Agarase activity (U) was defined as the amount of enzyme that produced 1 μmol of reducing sugar per minute under the optimum conditions. The content of reducing sugar was determined through 3,5-dinitrosalicylic acid (DNS) method (Miller, 1959). D-galactose was used for standard curve calculation of the reducing sugar content. The mixture was incubated at 50°C for 10 min and was incubated again at 100°C for 10 min with 750 μl of DNS. The amount of reducing sugar was measured by a spectrophotometer at a wavelength of 550 nm (OD550).

Characterization of trAgaM1

The optimum temperature and pH of trAgaM1 were assayed by incubating the reaction mixture under different temperatures (20–80°C) and pH buffers of citric acid-sodium citrate (0.1 mol/L citric acid, 0.1 mol/L sodium citrate, pH 3–6), PBS (0.2 mol/L Na_2HPO_4, 0.3 mol/L NaH_2PO_4, pH 7–8), and Tris-HCl (0.1 mol/L Tris base, pH 8–10). Agarase activity under the optimum condition was defined as 100%. The enzyme solution was incubated at 40 and 50°C for 3, 6, 12, 24, 36, and 60 h to determine the thermal stability of trAgaM1. Enzyme activity was measured using the aforementioned method. trAgaM1 activity without any treatment was defined as 100%. The effects of metal ions were assessed by determining trAgaM1 activity with $CaCl_2$, $NiSO_4$, $FeCl_2$, $BaCl_2$, $ZnSO_4$, KCl, $AgNO_3$, $MnSO_4$, $CdCl_2$, $CrCl_2$, $SrCl_2$, $CuCl_2$, NaCl, and $Mg(NO_3)_2$ at a final concentration of 1 mmol/L. trAgaM1 activity in the absence of any treatment was defined as 100%. All experiments were performed in triplicate.

Agarase activity was assayed at agarose concentrations of 2, 3, 4, 5, 6, 7, and 8 mg/ml under the optimum conditions to determine the kinetic parameters of trAgaM1. *Km* and *Vmax* were calculated using Lineweaver-Burke double reciprocal plot. Thin-layer chromatography (TLC) and high-performance liquid chromatography (HPLC) were used to identify the products of trAgaM1. The standards of NAOS and the products of trAgaM1 were placed into a silica gel 60 TLC plate (Merck, Darmstadt, Germany) and spread using a solvent system containing n-butanol/acetic acid/water (2:1:1; v/v/v). The spots of the products were visualized by spraying 10% (v/v) H_2SO_4 and heating them at 100°C for 10 min. For HPLC analysis (Waters Corporation, MA, United States), the mobile phase was 0.005 mol/L H_2SO_4. The column temperature was stabilized at 50°C. The flow rate of the mobile phase was 0.6 ml/min. The injection volume was 10 μl, and differential refractive index detector was used for NAOS detection. The HPLC column used for NAOS analysis was Aminex resin-based columns (Bio-Rad, MA, United States).

Determination of Substrate Utilization Rate of trAgaM1

Substrate utilization rate (SUR) was used as a key index for optimizing the production of NAOS with various DPs. In brief, a reduced dose of trAgaM1 was used to produce NAOS with high and various DPs at 50°C, and Tris-HCl (pH 9) was replaced by deionized water (pH 7.1) to prepare the agarose solution. Then, 200 ml of the reaction solution containing agarose (0.5, 1, 1.5, and 2%; w/v) and enzyme were incubated at 50°C for 3 h to measure the SUR of trAgaM1 under different conditions during optimization. The reaction solution was incubated on ice for 30 min and was centrifuged at 6,000 rpm for 15 min. After centrifugation, the supernatant was discarded, and the remaining agarose gel was resuspended with water and transferred to the original shake flask. The solution in the shake flask was dried in an oven at 80°C. The weight of flask was recorded every 24 h until the value did not change, and the constant weight value was used for the calculation of SUR. The weights of the shake flask before and after the experiment were measured using an electronic analytical balance. SUR was calculated as follows: SUR = (weight of shake flask after the experiment − weight of shake flask before the experiment)/original weight of agarose. The reaction solution containing inactivated trAgaM1 in boiling water bath was subjected to the same procedure and served as the control group. All experiments were performed in triplicate.

Optimization of trAgaM1 Expression in Shake Flask

The basic medium components for trAgaM1 expression were optimized from the following liquid mediums: LB (10 g of tryptone, 5 g of yeast extract, 10 g of NaCl, and 1 L of H_2O), super optimal broth (SOB, 20 g of tryptone, 5 g of yeast extract, 0.5 g of NaCl, and 1 L of H_2O), super optimal broth with catabolite repression (SOC, 20 g of tryptone, 5 g of yeast extract, 0.5 g of NaCl, 2.5 mmol/L KCl, 10 mmol/L $MgCl_2$, 20 mmol/L glucose, and 1 L of H_2O), and 2x YT growth medium (16 g of tryptone, 10 g of yeast extract, 5 g of NaCl, and 1 L of H_2O). The pH of these mediums was adjusted to 7.4 with NaOH and HCl (approximately 0.1 mol/L). The liquid medium was added with $MgCl_2$ (0, 10, 20, 30, and 40 mmol/L), glucose (1%, w/v), lactose (1%, w/v), maltose (1%, w/v), sucrose (1%, w/v), and glycerol (1%, w/v) to optimize trAgaM1 expression. The induction conditions including IPTG concentrations (0, 0.01, 0.1, 1, and 2 mmol/L) and induction temperatures (17, 22, 27, 32, and 37°C) were also optimized. Three natural osmolytes, namely proline, glutamate, and betaine, were added to the broth to a final concentration of 20 mmol/L (with and without 0.5 mol/L NaCl) to reduce the production of inclusion bodies. The feeding strategy was preliminarily studied. Briefly, 50 ml of 1.6% tryptone, 1% yeast extract, 10 mmol/L $MgCl_2$, 1% glycerol, and 30 mmol/L proline were fed into the broth after induction for 4 h. The production of trAgaM1 was conducted in a 250 ml shake flask with an initial liquid volume of 50 ml. The strain was first cultured to an OD600 value of 0.6 at 37°C (250 rpm), and the induction time was 16 h (250 rpm). After induction, the cells were broken by ultrasonic wave for assay of agarase activity. The agarase activity (U) per liter of the fermentation broth (total agarase activity, U/L) and the activity (U) produced per gram of the dry cells (specific productivity, U/g) were determined.

Preliminary Study on Production of trAgaM1 in 5 L Fermentation Tank

The components of the fermentation medium in the 5 L fermentation tank were as follows: 32 g of tryptone, 20 g of yeast extract, 10 g of NaCl, 200 g of glucose, 3.7 g of glycerol,

4.9 g of $MgCl_2$, 6.9 g of proline, 0.2 g of ampicillin, and 2 L of H_2O. The feeding medium contained 600 g of glucose, 10 g of yeast extract, 10 g of $MgCl_2$, 3.5 g of proline, 0.1 g of ampicillin, and 1 L of H_2O. First, 50 ml of bacterial culture with OD600 of 0.8 was inoculated into the fermentation medium and cultured at 37°C with a minute ventilation volume of 10 L and an agitator speed of 500 rpm. The broth pH was adjusted to 7.4 by adding 50% ammonia. The feeding medium was added into the fermentation medium after 6 h of inoculation at 2.5 ml/min. The broth was induced with IPTG at a final concentration of 0.1 mmol/L after 15 h of inoculation. Samples were taken every 3 h to determine total agarase activity and specific productivity.

RESULTS

Purification and Characterization of trAgaM1

Our study removed 60 amino acid residues without any annotation result on the NCBI database from the C-terminal of rAgaM1 (**Figure 1A**). The purified trAgaM1 was analyzed by 10% SDS-PAGE. The result showed that the molecular weight of trAgaM1 was approximately 70 kDa, which was consistent with the theoretical molecular weight of trAgaM1 (71.63 kDa; **Figure 1B**). The leaked expression was observed because the target protein band was also shown in the control group without IPTG induction, and the inclusion bodies were formed during the expression (**Figure 1B**). The concentration of the purified trAgaM1 was 80.53 mg/ml. The *Km* and *Vmax* values of trAgaM1 for agarose were 1.87 mg/ml and 192.31 U/mg, respectively (**Figure 1C**). The initial velocity of trAgaM1 reached a saturation point for agarose at a concentration of 6 mg/ml, and higher substrate concentration (8 mg/ml) showed an inhibition trend for the reaction velocity (**Figure 1D**). The optimum temperature and pH for trAgaM1 were 50°C and 9, respectively (**Figures 1E,F**). trAgaM1 maintained 87.1, 80.5, 79.1, 77.2, and 68.6% of the agarase activity after incubation for 1, 3, 6, 12, and 24 h, respectively, at 40°C. This finding indicated the good stability of trAgaM1 at 40°C. However, the agarase activity of trAgaM1 was lost after 3 h of incubation at 50°C (**Figure 1G**). Heavy metal ions, including Cu^{2+}, Sr^{2+}, Cr^{2+}, Cd^{2+}, Mn^{2+}, Ag^{+}, and Ba^{2+}, inhibited the trAgaM1 activity (**Figure 1H**). When excess enzyme was used, agarose was ultimately hydrolyzed into NA4 and NA6 within 60 min (**Figure 1I**).

Optimization of NAOS Production With Various DPs

Although excess trAgaM1 can completely degrade agarose into NA4 and NA6, the products of trAgaM1 were maintained at NAOS with DPs of 4–12 (**Figure 2D**) with a reduced dose of trAgaM1. Therefore, the production of NAOS with various DPs was optimized for large-scale NAOS generation, especially those with DPs higher than six.

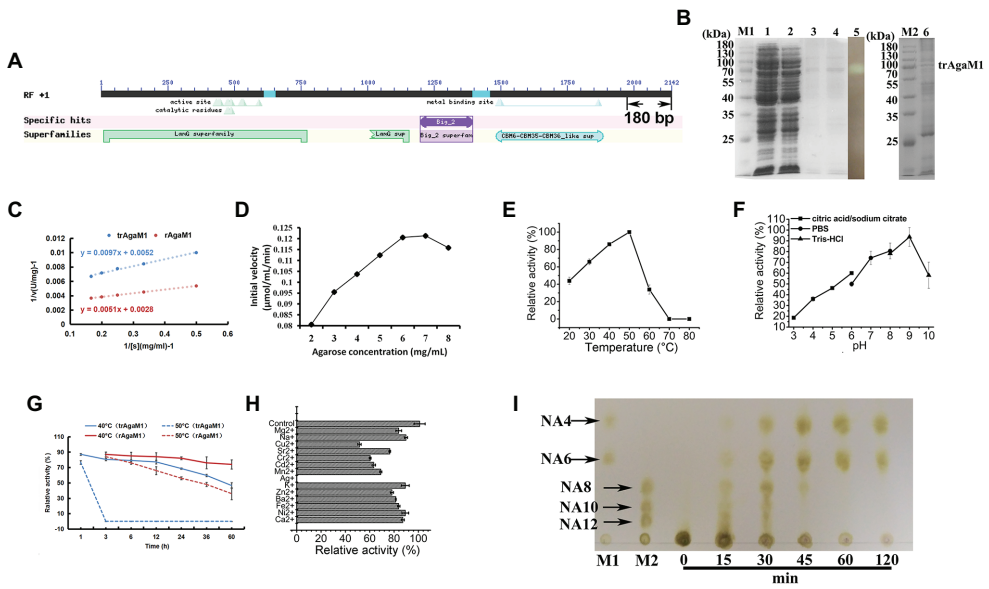

FIGURE 1 | (A) Conserved domains annotated in NCBI database and truncated peptides in AgaM1. **(B)** Analysis of truncated recombinant AgaM1 (trAgaM1) by 10% sodium dodecyl sulfate-polyacrylamide gel electrophoresis (SDS-PAGE). Lanes M1 and M2 represent the protein molecular standards; lanes 1 and 2 represent the supernatant of cell disruption liquid without and with isopropy-β-D-thiogalactoside (IPTG) induction, respectively. Lanes 3 and 4 show the purified trAgaM1, and lane 5 is the result of activity stain of trAgaM1 by iodine solution. Samples in lanes 3–5 are identical. Lane 6 shows the proteins in the form of inclusion bodies. **(C)** Determination of kinetic parameters of trAgaM1 by using Lineweaver-Burk plot. The result of trAgaM1 is compared with that of untruncated rAgaM1 from our previous study (Di et al., 2018). **(D)** Initial velocities of trAgaM1 at different agarose concentrations. **(E)** Effect of temperature on trAgaM1 activity. **(F)** Effect of pH on trAgaM1 activity. **(G)** Stability of trAgaM1 against 40 and 50°C. The result of trAgaM1 is compared with that of untruncated rAgaM1 from our previous study (Di et al., 2018). **(H)** Effect of metal ions on trAgaM1 activity. **(I)** Products of trAgaM1 as determined by thin-layer chromatography (TLC) with excess enzyme. Lanes M1 and M2 represent the molecular standard mixtures of neoagaro-oligosaccharides (NAOS) with polymerization degrees of 4–6 and 8–12, respectively.

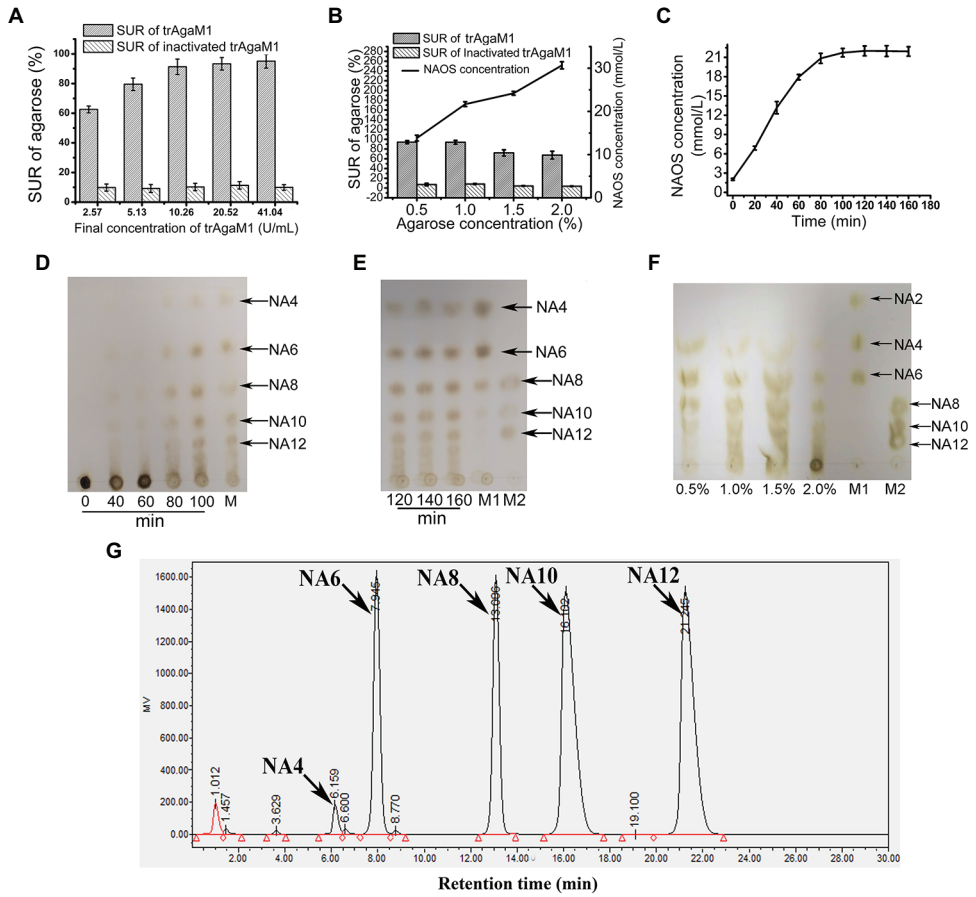

FIGURE 2 | (A) Optimization of trAgaM1 dose for the production of NAOS based on substrate utilization rate (SUR). **(B)** Optimization of agarose concentration for the production of NAOS based on SUR and yield of NAOS. **(C)** Optimization of reaction time for NAOS production based on NAOS yield. **(D)** trAgaM1 products from 0 to 100 min under optimized condition. M represents the molecular standard mixtures of NAOS with degrees of polymerization (DPs) of 4–12. **(E)** trAgaM1 products from 120 to 160 min under optimized condition. Lanes M1 and M2 represent the molecular standard mixtures of NAOS with DPs of 4–10 and 8–12, respectively. **(F)** Products of different agarose concentrations degraded by trAgaM1. **(G)** High-performance liquid chromatography (HPLC) result shows the composition and proportion of products degraded by trAgaM1 under optimum conditions. NA4, neoagarotetraose; NA6, neoagarohexaose; NA8, neoagarooctaose; NA10, neoagarodecaose; NA12, neoagarododecaose.

Discharge and filtration are needed after the hydrolysis reaction for the further preliminary purification of NAOS in the mass production. However, unhydrolyzed agarose and agar after degradation by trAgaM1 would re-solidify into colloidal solid when the temperature is less than approximately 40°C, thereby blocking the discharge pipes and apertures of the filter membranes. When clogging occurs, reheating is needed to remove the colloid, and the low SUR results in a waste of raw materials and an increase in labor costs. Thus, ensuring the degradation of most of the substrates is important for NAOS production, and SUR is the first factor to be considered. First, the dose of trAgaM1 used for NAOS production was optimized (**Figure 2A**). The SUR values increased with the trAgaM1 concentration; however, this value did not obviously increase when the final concentration of trAgaM1 was 10.26 U/ml. In consideration of the cost of trAgaM1 production, 10.26 U/ml was chosen as the optimized dose of trAgaM1 for NAOS production. Then, the agarose concentration was optimized. The NAOS production was improved by increasing the agarose concentration. However, the SUR values were 72 and 67.5% at agarose concentrations of 1.5 and 2%, respectively (**Figure 2B**), indicating that approximately 30% of agarose remained unreacted. The product DPs (4–12) were similar at agarose concentrations of 0.5, 1, and 1.5%; however, the DPs of products remained higher at a concentration of 2% than other agarose concentrations (**Figure 2F**). At concentrations of 0.5 and 1%, the SUR was high, and a higher amount of NAOS was produced with 1% agarose (**Figure 2B**). Therefore, 1% agarose was the most suitable for production because of its high NAOS yield and SUR.

Lastly, the reaction time was optimized. In theory, the NAOS yield increases with reaction time. However, the yield becomes stable at a certain level due to substrate reduction and enzyme activity loss. Further increasing the reaction time becomes meaningless. Thus, 200 ml of solution containing 10.26 U/ml (final concentration) trAgaM1 and 1% (w/v) agarose was incubated at 50°C for 3 h. The NAOS yield increased until

100 min (**Figure 2C**). The SUR of agarose at 100 min was 92.5 ± 2.87%, indicating that almost all of the substrates were degraded. Therefore, 100 min was the optimum reaction time for production.

Samples from the reaction solution under the aforementioned conditions were obtained and subjected to TLC for analyzing the DP of NAOS. NAOS with DPs of 4–12 were produced at 80 min, and the products remained stable from 80 to 160 min (**Figures 2D,E**). Thus, NAOS with various DPs were produced and served as the end-products of trAgaM1. In summary, the optimum conditions for producing NAOS with various DPs included mixing of 53.35 μg trAgaM1 at a final concentration of 10.26 U/ml with 1% agarose solution and incubating the mixture at 50°C for 100 min. Under the optimized condition, NAOS with DPs of 4–12 were produced with a yield of 9.25 g/L by per gram of trAgaM1. The yield ratio of these NAOS with DPs of 4–12 was 1.6:16.5:16.5:32.7:32.7 based on the peak area of each oligosaccharide (**Figure 2G**). Therefore, this strategy produced NA4, NA6, NA8, NA10, and NA12 at final concentrations of 0.15, 1.53, 1.53, 3.02, and 3.02 g/L, respectively.

Production Optimization of trAgaM1 in Shake Flask

The total agarase activity of 15.51 U/L was produced under the original production conditions. The culture medium was first optimized, and 2x YT was found to be the optimum medium for trAgaM1 expression (**Figure 3A**). The production of trAgaM1 increased by 4-fold with the addition of $MgCl_2$, and no obvious difference in the total activity was detected at different concentrations (10–40 mmol/L). However, $MgCl_2$ concentration affected the specific productivity of trAgaM1, and the maximum value was detected at 10 mmol/L (**Figure 3B**). Therefore, 10 mmol/L $MgCl_2$ was supplemented into the culture medium for succeeding experiments. Glycerol (1%) was the optimum

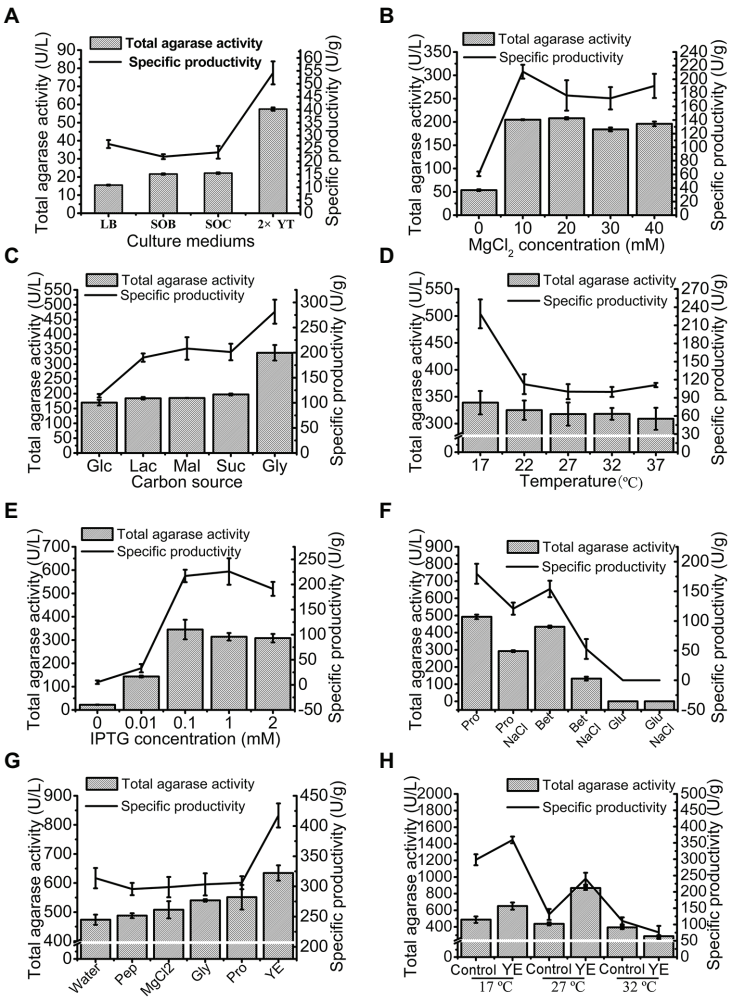

FIGURE 3 | Optimization of trAgaM1 expression in shake flask, including optimization of culture media **(A)**, $MgCl_2$ concentrations **(B)**, carbon sources **(C)**, induction temperatures **(D)**, IPTG concentrations **(E)**, additional natural osmolytes **(F)**, and feeding strategy **(G)**. The induction temperatures were re-optimized after the use of 20 mmol/L proline and feed strategy; the feeding groups without the use of proline served as controls **(H)**. Glc, glucose; Lac, lactose; Mal, maltose; Suc, sucrose; Gly, glycerol; Pro, proline; Bet, betaine; Glu, glutamate; Pep, peptone; and YE, yeast extract.

carbon source for trAgaM1 expression, leading to a total activity of approximately 1.5-fold greater than that with other carbon sources (**Figure 3C**). Therefore, 1% glycerol was used as the carbon source for subsequent optimization. The highest total activity and specific productivity were recorded at an induction temperature of 17°C (**Figure 3D**). IPTG at a concentration of 0.1 mmol/L was considered as the optimum condition for trAgaM1 production (**Figure 3E**). Accordingly, 0.1 mmol/L IPTG and 17°C were selected as the induction concentration and temperature for subsequent optimization. Furthermore, a leaked expression was observed because 22.08 U/L of total activity was still detected without any IPTG induction (**Figure 3E**), which is in accordance with the SDS-PAGE result (**Figure 1B**). Natural osmolytes (with and without 0.5 mol/L NaCl), including proline, glutamate, and betaine, were added into the reaction solution to reduce the production of inclusion bodies. NaCl and glutamate had negative effects on trAgaM1 production. However, betaine and proline without NaCl increased the production of trAgaM1. Furthermore, proline (20 mmol/L) increased the total activity and specific productivity to 492.23 U/L and 179.65 U/g, respectively. Therefore, the optimum medium components for trAgaM1 production included 2x YT medium, 10 mmol/L $MgCl_2$, 1% glycerol, and 20 mmol/L proline (**Figure 3F**).

The feeding strategy was preliminarily studied to improve the trAgaM1 production. Feeding yeast extract increased the total activity and specific productivity to 634.54 U/L and 417.46 U/g (**Figure 3G**), respectively. For large-scale production of trAgaM1, fed-batch fermentation was performed in a 5 L fermentation tank. However, the optimum induction temperature, which is lower than the normal temperature of water (approximately 25°C), was not reached due to the lack of refrigerating equipment in our fermentation tank. Therefore, the induction temperature was re-optimized. The presence of proline reduced the production of inclusion bodies at high temperatures. Therefore, the amount of trAgaM1 expressed in the supernatant with proline at 27°C was greater than that without proline at 27°C and with proline at 17°C (**Figure 3H**). Thus, 27°C was the optimum temperature for trAgaM1 production with the optimum medium components.

In summary, the optimum conditions for trAgaM1 production were as follows: induction of *E. coli* cells in the optimum medium (2x YT medium, 10 mmol/L $MgCl_2$, 1% glycerol, and 20 mmol/L proline) at 27°C with 0.1 mmol/L IPTG and feeding 50 ml of 1% yeast extract after induction for 4 h. Under these conditions, the total agarase activity and specific productivity of trAgaM1 increased by 56- and 9-fold after optimization, respectively.

trAgaM1 Production Through Fed-Batch Fermentation

To obtain large quantities of trAgaM1, we expressed the recombinant protein in a 5 L fermentation tank through a fed-batch strategy. The result showed that the trAgaM1 yield increased through high-density fermentation. The total agarase activity could reach 13,049.44 U/L, which was 842- and 15-fold higher than those obtained in a shake flask under the original and optimum conditions, respectively (**Figure 4**).

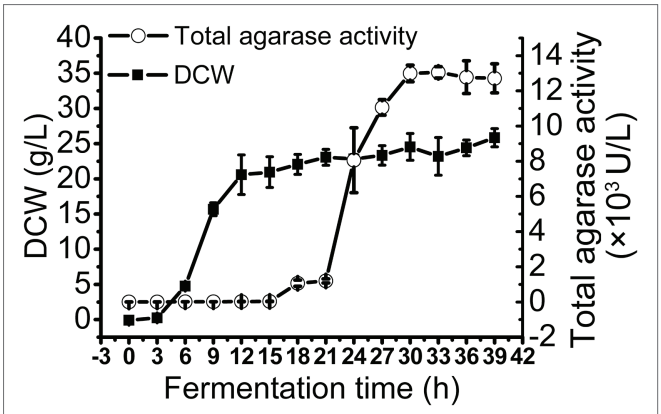

FIGURE 4 | Production of trAgaM1 in 5 L fermentation tank with glucose fed-batch strategy. DCW, dry cell weight.

DISCUSSION

NAOS with higher DPs might harbor greater biological activities (Xu et al., 2018). However, the bioactivities of NAOS with DPs greater than six have been hardly produced because NAOS with higher DPs are difficult to produce by using available agarases (Hou et al., 2015; Di et al., 2018). The production of NAOS with DPs of four and six was also important due to their biological activities (Jin et al., 2017). Therefore, a strategy for NAOS production with various DPs (e.g., 4–12) is crucial for their future biotechnological applications. In this study, a method to produce NAOS with DPs in the range of 4–12 was established and optimized, which enables the mass production of NAOS with various DPs by using a single enzyme.

Former studies showed that the truncation of amino acids from the C-terminal of agarases could change the enzymatic properties, for instance, the improvement of agarase activity (Ma et al., 2019). Therefore, our work aimed to obtain some special properties by the truncation of the original rAgaM1, and the results showed that NAOS with various DPs were produced by this truncated recombinant agarase, trAgaM1. Compared with the untruncated rAgaM1, two properties of trAgaM1 were varied (Di et al., 2018). First, the *Vmax* (192.31 U/mg) after truncation is 1.86-fold lower before truncation (357.14 U/mg; **Figure 1B**), suggesting the decreased catalytic efficiency of breaking the β-1,4-glycosidic bond. Second, the thermal stability at 50°C after truncation is weaker than the original agarase. The original agarase rAgaM1 maintained more than 65% of its activity after 10 h of pre-incubation at 50°C (Di et al., 2018). However, the agarase activity of trAgaM1 was completely lost after 3 h of pre-incubation at 50°C (**Figure 1C**). The effects of sequence deletion on the agarase characteristics are different. A total of 140 amino acid peptides with unknown function were truncated from the C-terminal of AgaG4, causing a 35-fold increase of agarase activity (Liu, 2015); however, the removal of 60 amino acids from AgaM1 in this study decreased the activity and stability of this agarase. Conversely, the truncated AgaO lost all the agarase activity (Han et al., 2016). Without the information of protein structures,

these differences cannot be scientifically and detailly explained. However, we speculated that these amino acids might strongly associate with the enzymatic activity and stability.

The optimum pH of trAgaM1 was 9; however, Tris-HCl buffer (pH 9) was replaced by deionized water (pH 7.1) for the production of various NAOS to avoid environmental pollution by alkaline solutions. We speculated that the non-optimum pH, along with the changes of activity and stability, probably provided the ability of trAgaM1 to produce NAOS with various DPs as end-products under certain conditions: although excess trAgaM1 can still degrade agarose into NA4 and NA6 (**Figure 1G**), some NAOS with higher DPs cannot be further degraded due to the non-optimum pH, weak activity of trAgaM1, and the activity lost throughout the reaction time with reduced amount of enzyme (10.26 U/ml), resulting in the production of NAOS with various DPs. In the previous study, the mutation of three amino acids endows agarase AgaD with the ability to produce NAOS with various DPs (David et al., 2018). The agarase activity of AgaD reduces 50-fold after the mutation (David et al., 2018), which is similar to the result in our study. Further comparison with other works is ineffective due to the scarce related studies. However, we infer that decreasing rather than increasing the activity is propitious to produce NAOS with high and various DPs. Therefore, NAOS with more diverse and higher DPs would be produced by the reformed β-agarase through truncation and/or other forms of amino-acid sequence modification in future works. The present study provides direction toward future NAOS production through enzyme modification.

The conditions for producing NAOS with various DPs were optimized in this study, which successfully resulted in NAOS with the highest SUR and yields. NAOS yield is always considered, whereas SUR is often neglected during production. SUR is greatly important for production because a low SUR results in the waste of substrate and labor cost and the loss of equipment. The SUR value of 92.5% can be reached after optimization. In addition, NAOS with various DPs are the intermediate products of most β-agarases and can be produced by many β-agarases theoretically if the reaction time is precisely controlled. Unfortunately, fully controlling the reaction time in the complex and extensive industrial production is unrealistic. In this study, NAOS with various DPs serve as the end-products under optimized conditions (**Figure 2D**), and these stable products make the reaction more flexible and easily controlled. In summary, the high SUR and yield of NAOS and the stable final products demonstrate that our method is a promising strategy for large-scale NAOS production.

Furthermore, the expression level of trAgaM1 was optimized to provide sufficient enzymes for NAOS production. During *E. coli* expression, the formation of inclusion bodies usually causes the low productivity of recombinant proteins (Le et al., 2011; Jhamb and Sahoo, 2012). Lowering the induction temperature is the most common method to reduce the production of inclusion bodies. However, refrigeration would consume additional energy during fermentation. Supplementing natural osmolytes, the so-called chemical chaperones, into the fermentation medium is an alternative method to decrease the formation of inclusion bodies (Diamant et al., 2010). Viscous osmolytes can significantly increase the stability of thermolabile proteins and reduce the rate of protein-folding, thereby improving the yields of the natively folded recombinant proteins (Diamant et al., 2001, 2010; de Marco et al., 2005). For the trAgaM1 fermentation, the total agarase activity with proline and betaine was increased by 1.4- and 1.2-fold compared with the treatment without osmolytes (**Figures 3E,F**). Additional NaCl can induce the osmolyte absorption into *E. coli* cells, which indirectly improves the yields of soluble recombinant proteins. However, trAgaM1 production with osmolytes decreased with additional NaCl regardless of the use of proline and betaine (**Figure 3F**). This finding was due to the salt concentration in 2x YT (0.5%), which was probably sufficient for osmolyte absorption, and the recombinant protein expression was inhibited by the additional NaCl (Duan et al., 2013). Importantly, proline increased the yield of trAgaM1 at high temperature, which then, increased the optimum induction temperature to 27°C (**Figure 3H**). This value is close to the room temperature, resulting in significant energy savings during the mass production because that the extra refrigeration and excessive heating were not incurred. In addition, natural osmolytes may also increase the yield of other recombinant proteins.

In conclusion, a strategy that can produce NAOS with various DPs was established and optimized in this study. Through this strategy, NAOS with DPs in the range of 4–12 as end-products can be produced using a single agarase trAgaM1 with high SUR and yield, which enables mass production. Moreover, the production of trAgaM1 was optimized, resulting in a total increase of 842-fold. The potential of natural osmolytes was also discussed based on our results. This study provides many substrate sources for the production and activity tests of NAOS with higher DPs and lays a foundation for the large-scale production of trAgaM1 and NAOS with various DPs at a low cost.

DATA AVAILABILITY STATEMENT

The datasets presented in this study can be found in online repositories. The names of the repository/repositories and accession number(s) can be found below: https://www.ncbi.nlm.nih.gov/genbank/, MG280837.

AUTHOR CONTRIBUTIONS

WQ and RZ designed this study. WQ, DW, and WD performed the experiments. WQ, JW, and DW analyzed the sequencing data. WQ, RZ, and DW wrote the paper. JW revised the paper. All authors contributed to the article and approved the submitted version.

FUNDING

This research was supported by grants from Scientific Research Foundation of Third Institute of Oceanography SOA under

contract no. 2017004; Xiamen Ocean Research and Development Institute Co-construction Project under contract no. K200302; National Key R&D Program of China under contract no. 2019YFD0901305; and Science and Technology Program of Zhoushan under contract no. 2019C21011.

ACKNOWLEDGMENTS

We thank Zhao Jing, Jin Min, and Wei Yachao for their assistance in writing the manuscript and enlightening the research ideas.

REFERENCES

Chen, S. K., Min, L. T., Jin, R. H., and Rongm, H. C. (2009). In vitro antioxidant activities of low-molecular-weight polysaccharides with various functional groups. *J. Agric. Food Chem.* 57, 2699–2704. doi: 10.1021/jf804010w

Chen, H., Yan, X., Zhu, P., and Lin, J. (2006). Antioxidant activity and hepatoprotective potential of agaro-oligosaccharides in vitro and in vivo. *Nutr. J.* 5:31. doi: 10.1186/1475-2891-5-31

David, B., Irague, R., Jouanneau, D., Daligault, F., Czjzek, M., Sanejouand, Y. H., et al. (2018). Internal water dynamics control the transglycosylation/hydrolysis balance in the agarase (AgaD) of *Zobellia galactanivorans*. *ACS Catal.* 7, 3357–3367. doi: 10.1021/acscatal.7b00348

de Marco, A., Vigh, L., Diamant, S., and Goloubinoff, P. (2005). Native folding of aggregation-prone recombinant proteins in *Escherichia coli* by osmolytes, plasmid- or benzyl alcohol-overexpressed molecular chaperones. *Cell Stress Chaperones* 10, 329–339. doi: 10.1379/csc-139r.1

Di, W., Qu, W., and Zeng, R. (2018). Cloning, expression, and characterization of thermal-stable and pH-stable agarase from mangrove sediments. *J. Basic Microbiol.* 58, 302–309. doi: 10.1002/jobm.201700696

Diamant, S., Eliahu, N., Rosenthal, D., and Goloubinoff, P. (2001). Chemical chaperones regulate molecular chaperones in vitro and in cells under combined salt and heat stresses. *J. Biol. Chem.* 276, 39586–39591. doi: 10.1074/jbc.M103081200

Diamant, S., Rosenthal, D., Azem, A., Eliahu, N., Ben-Zvi, A. P., and Goloubinoff, P. (2010). Dicarboxylic amino acids and glycine-betaine regulate chaperone-mediated protein-disaggregation under stress. *Mol. Microbiol.* 49, 401–410. doi: 10.1046/j.1365-2958.2003.03553.x

Duan, X., Chen, J., and Wu, J. (2013). Optimization of pullulanase production in *Escherichia coli* by regulation of process conditions and supplement with natural osmolytes. *Bioresour. Technol.* 146, 379–385. doi: 10.1016/j.biortech.2013.07.074

Enoki, T., Okuda, S., Kudo, Y., Takashima, F., Sagawa, H., and Kato, I. (2010). Oligosaccharides from agar inhibit pro-inflammatory mediator release by inducing heme oxygenase 1. *Biosci. Biotechnol. Biochem.* 74, 766–770. doi: 10.1271/bbb.90803

Fu, X. T., and Kim, S. M. (2010). Agarase: review of major sources, categories, purification method, enzyme characteristics and applications. *Mar. Drugs* 8, 200–218. doi: 10.3390/md8010200

Han, W., Cheng, Y., Wang, D., Wang, S., Liu, H., Gu, J., et al. (2016). Biochemical characteristics and substrate degradation pattern of a novel exo-type β-agarase from the polysaccharide-degrading marine bacterium *Flammeovirga* sp. strain MY04. *Appl. Environ. Microbiol.* 82, 4944–4954. doi: 10.1128/AEM.00393-16

Higashimura, Y., Naito, Y., Takagi, T., Mizushima, K., Hirai, Y., Harusato, A., et al. (2013). Oligosaccharides from agar inhibit murine intestinal inflammation through the induction of heme oxygenase-1 expression. *J. Gastroenterol.* 48, 897–909. doi: 10.1007/s00535-012-0719-4

Higashimura, Y., Naito, Y., Takagi, T., Uchiyama, K., Mizushima, K., Ushiroda, C., et al. (2016). Protective effect of agaro-oligosaccharides on gut dysbiosis and colon tumorigenesis in high-fat diet-fed mice. *Am. J. Physiol. Gastrointest. Liver Physiol.* 310, G367–G375. doi: 10.1152/ajpgi.00324.2015

Hong, S. J., Lee, J. H., Kim, E. J., Yang, H. J., Chang, Y. K., Park, J. S., et al. (2017). In vitro and in vivo investigation for biological activities of neoagarooligosaccharides prepared by hydrolyzing agar with β-agarase. *Biotechnol. Bioprocess Eng.* 22, 489–496. doi: 10.1007/s12257-017-0049-8

Hou, Y., Chen, X., Chan, Z., and Zeng, R. (2015). Expression and characterization of a thermostable and pH-stable β-agarase encoded by a new gene from *Flammeovirga pacifica* WPAGA1. *Process Biochem.* 50, 1068–1075. doi: 10.1016/j.procbio.2015.04.005

Hou, Y., Gao, J., Gu, L., Wang, S., and Zeng, R. (2014). Effects of agaro-oligosaccharide treatment on postharvest quality of cherry tomatoes during cold storage. *J. Food Process. Preserv.* 39, 949–955. doi: 10.1111/jfpp.12308

Hu, B., Gong, Q., Wang, Y., Ma, Y., Li, J., and Yu, W. (2006). Prebiotic effects of neoagaro-oligosaccharides prepared by enzymatic hydrolysis of agarose. *Anaerobe* 12, 260–266. doi: 10.1016/j.anaerobe.2006.07.005

Jhamb, K., and Sahoo, D. K. (2012). Production of soluble recombinant proteins in *Escherichia coli*: effects of process conditions and chaperone co-expression on cell growth and production of xylanase. *Bioresour. Technol.* 123, 135–143. doi: 10.1016/j.biortech.2012.07.011

Ji, H. Y., Cho, S. S., Kim, K. M., Ji, Y. K., Kim, E. J., Park, E. Y., et al. (2017). Neoagarooligosaccharides enhance the level and efficiency of LDL receptor and improve cholesterol homeostasis. *J. Funct. Foods* 38, 529–539. doi: 10.1016/j.jff.2017.09.053

Jin, M., Liu, H., Hou, Y., Chan, Z., Di, W., Li, L., et al. (2017). Preparation, characterization and alcoholic liver injury protective effects of algal oligosaccharides from *Gracilaria lemaneiformis*. *Food Res. Int.* 100, 186–195. doi: 10.1016/j.foodres.2017.08.032

Kim, J. H., Yun, E. J., Yu, S., Kim, K. H., and Kang, N. J. (2017). Different levels of skin whitening activity among 3,6-anhydro-l-galactose, agarooligosaccharides, and neoagarooligosaccharides. *Mar. Drugs* 15:321. doi: 10.3390/md15100321

Le, Y., Peng, J., Wu, H., Sun, J., and Shao, W. (2011). An approach to the production of soluble protein from a fungal gene encoding an aggregation-prone xylanase in *Escherichia coli*. *PLoS One* 6:e18489. doi: 10.1371/journal.pone.0018489

Lee, D. G., Jeon, M. J., and Lee, S. H. (2012). Cloning, expression, and characterization of a glycoside hydrolase family 118 beta-agarase from *Agarivorans* sp. JA-1. *J. Microbiol. Biotechnol.* 22, 1692–1697. doi: 10.4014/jmb.1209.09033

Li, J., Han, F., Lu, X., Fu, X., Ma, C., Chu, Y., et al. (2007). A simple method of preparing diverse neoagaro-oligosaccharides with beta-agarase. *Carbohydr. Res.* 342, 1030–1033. doi: 10.1016/j.carres.2007.02.008

Liu, H. (2015). Deletion of a non-catalytic region increases the enzymatic activity of a β-agarase from *Flammeovirga* sp. MY04. *J. Ocean Univ. China* 14, 841–848. doi: 10.1007/s11802-015-2800-0

Ma, J., Yan, Q., Yi, P., Yang, S., Liu, H., and Jiang, Z. (2019). Biochemical characterization of a truncated β-agarase from *Microbulbifer* sp. suitable for efficient production of neoagarotetraose. *Process Biochem.* 87, 119–127. doi: 10.1016/j.procbio.2019.08.021

Miller, G. L. (1959). Use of dinitrosalicylic acid reagent for determination of reducing sugar. *Anal. Biochem.* 31, 426–428.

Qu, W., Lin, D., Zhang, Z., Di, W., Gao, B., and Zeng, R. (2018). Metagenomics investigation of agarlytic genes and genomes in mangrove sediments in China: a potential repertory for carbohydrate-active enzymes. *Front. Microbiol.* 9:1864. doi: 10.3389/fmicb.2018.01864

Ramos, K. R., Valdehuesa, K. N., Cabulong, R. B., Moron, L. S., Nisola, G. M., Hong, S. K., et al. (2016). Overexpression and secretion of AgaA7 from *Pseudoalteromonas hodoensis* sp. nov in *Bacillus subtilis* for the depolymerization of agarose. *Enzym. Microb. Technol.* 90, 19–25. doi: 10.1016/j.enzmictec.2016.04.009

Xie, W., Lin, B., Zhou, Z., Lu, G., Lun, J., Xia, C., et al. (2013). Characterization of a novel β-agarase from an agar-degrading bacterium *Catenovulum* sp. X3. *Appl. Microbiol. Biotechnol.* 97, 4907–4915. doi: 10.1007/s00253-012-4385-5

Xu, S. Y., Kan, J., Hu, Z., Liu, Y., Du, H., Pang, G. C., et al. (2018). Quantification of neoagaro-oligosaccharide production through enzymatic hydrolysis and its anti-oxidant activities. *Molecules* 23:1354. doi: 10.3390/molecules23061354

Xu, X. Q., Su, B. M., Xie, J. S., Li, R. K., Yang, J., Lin, J., et al. (2017). Preparation of bioactive neoagaroligosaccharides through hydrolysis of *Gracilaria lemaneiformis* agar: a comparative study. *Food Chem.* 240, 330–337. doi: 10.1016/j.foodchem.2017.07.036

Yun, E. J., Yu, S., and Kim, K. H. (2017). Current knowledge on agarolytic enzymes and the industrial potential of agar-derived sugars. *Appl. Microbiol. Biotechnol.* 101, 5581–5589. doi: 10.1007/s00253-017-8383-5

Conflict of Interest: The authors declare that the research was conducted in the absence of any commercial or financial relationships that could be construed as a potential conflict of interest.

frontiers in Microbiology

ORIGINAL RESEARCH
published: 29 September 2020
doi: 10.3389/fmicb.2020.567060

Amelioration of Androgenetic Alopecia by Algal Oligosaccharides Prepared by Deep-Sea Bacterium Biodegradation

Min Jin[1,2†], Yu-Lei Chen[3†], Xiongfei He[4], Yanping Hou[1], Zhuhua Chan[1] and Runying Zeng[1,2]*

[1] Third Institute of Oceanography, Ministry of Natural Resources, Xiamen, China, [2] Southern Marine Science and Engineering Guangdong Laboratory, Zhuhai, China, [3] College of Food and Biological Engineering, Jimei University, Xiamen, China, [4] Aquabrain Biotech (Xiamen) Co., Ltd., Xiamen, China

OPEN ACCESS

Edited by:
Wen-Yong Lou,
South China University of Technology, China

Reviewed by:
Xunwei Wu,
Shandong University, China
Yao Nie,
Jiangnan University, China

***Correspondence:**
Runying Zeng
zeng@tio.org.cn

[†] These authors have contributed equally to this work

Specialty section:
This article was submitted to Microbiotechnology, a section of the journal Frontiers in Microbiology

Received: 29 May 2020
Accepted: 11 September 2020
Published: 29 September 2020

Citation:
Jin M, Chen Y-L, He X, Hou Y, Chan Z and Zeng R (2020) Amelioration of Androgenetic Alopecia by Algal Oligosaccharides Prepared by Deep-Sea Bacterium Biodegradation. Front. Microbiol. 11:567060. doi: 10.3389/fmicb.2020.567060

Androgenetic alopecia (AGA) is a dihydrotestosterone (DHT)-mediated hair loss disorder characterized by shortened anagen hair cycle. Oligosaccharides derived from seaweeds possess diverse biological functions. However, little is known about their effects on AGA. In this study, algal oligosaccharide (AOS) was characterized for its mitigation effects on key features involved in AGA pathogenesis, such as DHT- mediated cellular signaling and shortened anagen hair cycle. AOS with varying degrees of polymerization (DP), namely, AOS (DP2), AOS (DP4–6), and AOS (DP8–12), were prepared by agar biodegradation with *Flammeovirga pacifica* WPAGA1, an agarolytic bacterium isolated from deep-sea sediments. *In vitro* results showed that AOS with varying DPs significantly ameliorated the DHT-induced alterations of regulatory factors in human hair follicle dermal papilla cells in a dose- and DP-dependent manner, as revealed by the normalization of several hair-growth-stimulating or inhibitory factors. *In vivo* studies showed that AOS (DP2) extended the anagen phase and thereby delayed catagen progression in mice. Furthermore, AOS (DP2) stimulated dorsal hair growth in mice by increasing hair length, density, and thickness. Therefore, our findings indicated that AOS antagonized key factors involved in AGA pathogenesis, suggesting the potential application of AOS in the prevention and the treatment of AGA.

Keywords: androgenetic alopecia, algal oligosaccharides, dihydrotestosterone, deep-sea bacterium, anagen

INTRODUCTION

Androgenetic alopecia (AGA), commonly known as male pattern baldness, is an androgen-dependent hair loss disorder characterized by the progressive transformation of scalp terminal hairs into vellus hairs (Motofei et al., 2018). AGA is the most common type of progressive hair loss disorder in men and women (Lolli et al., 2017). AGA generally occurs after puberty, and its prevalence and incidence depend on age and race. Approximately 41.4% of Chinese men aged

more than 70 years are affected by AGA, and the overall prevalence of AGA in Chinese men is 21.3% (Wang et al., 2010). The prevalence of AGA is significantly higher in Caucasians than in Asians; more than 30% of white men will have AGA at age 30, and 80% will have the disorder at age 70 (Severi et al., 2003; Otberg et al., 2007). Although AGA is a benign condition, it can lead to negative psychological effects, which are associated with depression, anxiety, worries about aging, and low self-esteem, in men and women (Severi et al., 2003).

The known important causative factors involved in the pathogenesis of AGA are androgen, genetic factors, and age, although the complete molecular mechanisms have not been fully understood (Lolli et al., 2017). Androgen plays the most important role in the etiology of AGA. The main circulating androgen in men is testosterone. However, AGA appears more related to the most active androgenic compound, namely, dihydrotestosterone (DHT), which is converted from testosterone by 5α-reductase (Motofei et al., 2018). The affinity of androgen receptor (AR) for DHT is five times higher than that for testosterone. In hair follicles, AR is located in mesenchymal-derived dermal papilla cells, which are the action sites of DHT on scalp hair growth (Inui and Itami, 2011). Dermal papilla cells play fundamental roles in the induction and the maintenance of follicle epithelial cell growth and mediate the stimulating signals of DHT by secreting numerous growth factors and/or extracellular matrix factors on follicle cells (Botchkarev and Kishimoto, 2003; Blanpain et al., 2004; Roh et al., 2004). The released compounds have a paracrine effect on hair follicle epithelial cells as well as an autocrine effect on the dermal papilla itself (Lolli et al., 2017). Such factors include hair-growth-stimulating factors, such as vascular endothelial growth factor (VEGF) and insulin-like growth factor 1, and inhibitory factors, such as transforming growth factor beta 2 (TGF-β2) and Dickkopf 1 (DKK-1) (Blanpain et al., 2004; Lolli et al., 2017). DHT-induced alteration in regulatory paracrine factors will cause a progressive miniaturization of hair follicles, thereby shortening the anagen phase and eventually leading to a bald appearance (Pierard-Franchimont and Pierard, 2001; Inui et al., 2002; Lolli et al., 2017). Therefore, DHT-induced cellular signaling in dermal papilla cells and the subsequent shortening of anagen hair cycle serve as promising targets for AGA treatment.

Only two medications have been approved by the Food and Drug Administration to treat AGA, namely, minoxidil and finasteride. Although minoxidil has been used for more than 30 years to treat AGA, its precise mechanism of action on hair growth remains elusive (Messenger and Rundegren, 2004). Several primary mechanisms of minoxidil action are proposed: (a) minoxidil suppresses AR-mediated functions by decreasing AR transcriptional activity and reducing the expression of AR targets at the protein level (Hsu et al., 2014), (b) minoxidil exerts anagen prolongation effects by activating β-catenin pathway in dermal papilla cells (Kwack et al., 2011), (c) minoxidil stimulates hair follicle angiogenesis by inducing the expression of VEGF in dermal papilla cells (Lachgar et al., 1998), (d) minoxidil shows a cytoprotective activity by activating prostaglandin synthase-1 (Michelet et al., 1997), and (e) minoxidil increases blood flow by dilating hair follicle arteries (Messenger and Rundegren, 2004). Finasteride is a DHT synthesis inhibitor, which suppresses the conversion of testosterone to DHT by binding to 5α-reductase (Varothai and Bergfeld, 2014; Kelly et al., 2016; Adil and Godwin, 2017). Although minoxidil and finasteride have proven effective in ameliorating AGA with long-term daily use, their use is costly and leads to variable adverse effects that may even persist after treatment cessation. The most frequent adverse reactions related to minoxidil include scalp irritation, dryness, and allergic contact dermatitis (Tsuboi et al., 2012). The adverse effects of finasteride include mental/psychological impairment (lack of mental concentration, depression, suicidal ideations) and sexual disorders (decreased libido, erectile dysfunction, ejaculation disorder) (Motofei et al., 2016; Rowland et al., 2016). In this respect, alternative therapeutic or nutritional solutions for the treatment of AGA with less side effects should be identified. In the last two decades, algal oligosaccharides (AOS), especially oligosaccharides derived from agar (the major cell wall component of red algae), have been reported to possess diverse physiological and biological functions, such as anti-oxidation, liver injury protection, antitumor, immune modulation, and whitening and skin-moisturizing effects; hence, AOS have been an attractive compound in cosmetic, food, nutritional, and pharmaceutical industries (Enoki et al., 2010; Kim et al., 2010; Gao et al., 2017). In the present study, AOS with varying degrees of polymerization (DP) were prepared by agar biodegradation with *Flammeovirga pacifica* WPAGA1, a deep-sea agarolytic bacterium (Xu et al., 2012; Gao et al., 2017). Then, the mitigation effects of AOS on key features involved in AGA pathogenesis were characterized.

MATERIALS AND METHODS

Preparation of AOS With Varying DPs

AOS with varying DPs were prepared by agar biodegradation with a combination of three agarases, i.e., Aga2133, Aga4383 (Hou et al., 2015), and Aga2660. These enzymes were isolated from *F. pacifica* WPAGA1, a deep-sea bacterium that efficiently degrades agar (Xu et al., 2012; Gao et al., 2017). The three agarases show distinct endolytic activities on agar degradation, yielding various intermediate and end products, which are useful to produce AOS with varying DPs. Agar was degraded by recombinant Aga2133 to produce AOS (DP 8–12), an intermediate product at the early stage of degradation. Recombinant Aga4383 was used to degrade agar to yield AOS (DP4–6) as end products. The purified AOS (DP4–6) were then further hydrolyzed by recombinant Aga2260 to generate AOS (DP2) as end products. During each degradation process, samples were collected at different reaction time points and were heated at 100°C for 10 min to terminate the reaction. After centrifugation at 15,000 g and 4°C for 10 min, the supernatant was examined for AOS content through thin-layer chromatography (TLC) by using the method of Hou et al. (2015). After verification, the collected supernatant containing the desired AOS was lyophilized as AOS samples (DP2, DP4–6, and DP8–12) for further analysis.

Cell Culture and Treatment

Human hair follicle dermal papilla cells (hHFDPC) were obtained from Guangdong Biocell Biotechnology Co., Ltd. (Guangdong, China) and cultured in mesenchymal stem cell medium (ScienCell, United States) in a humidified atmosphere with 5% CO_2 at 37°C. All cell subcultures were performed at 70–80% cell confluence, digested with 0.25% trypsin, and inoculated into six-well plates or 96-well plates according to the experiment design.

hHFDPCs were harvested and inoculated into six-well plates at a density of 3×10^5 cells per well or into 96-well plates at a density of 10,000 cells per well and then cultured at 37°C for 24 h. The culture medium was added with 800 nM DHT to induce AGA-associated alterations in regulatory paracrine factors in hHFDPCs. Fresh culture medium alone was added as blank control. To assess the protective effects of AOS, an AOS sample of a given working concentration was added to the DHT-supplemented culture. The DHT-supplemented culture was added with 500 μM minoxidil as a positive treatment control. The cells were further cultured for 24 h and subjected to MTT assay, cytokine production measurement, or gene expression determination.

MTT Assay

hHFDPC cells were harvested, inoculated into 96-well plates at a density of 10,000 cells per well, and cultured at 37°C for 24 h. The growth medium was discarded and replaced with fresh medium containing various concentrations of the samples. In each plate, wells with culture medium but without cells were used as blank controls, and wells containing cells with medium and solvent only were used as solvent control. After 24 h of exposure to the samples, the cells were washed twice with phosphate-buffered saline gently, incubated in serum-free medium containing 0.5 mg/ml MTT at 37°C for 4 h, and extracted with 150 μl of dimethyl sulfoxide per well. The colored solution was detected for optical density (OD) at a wavelength of 490 nm by using Multiskan MS Analyzer (BioTek Epoch, United States). Cell viability was calculated by the following formula: viability rate (%) = (OD value of sample – OD value of blank control)/(OD value of solvent control – OD value of blank control) × 100.

Measurement of Secreted VEGF by ELISA

After 24 h of incubation, the culture supernatant was collected and centrifuged at 12,000 g and 4°C to remove cell debris. VEGF concentration in the culture supernatant from sample-treated hHFDPCs was detected using VEGF ELISA kits (Abcam, United States) following the manufacturer's protocol. OD at 450 nm was recorded using Multiskan MS Analyzer (BioTek Epoch).

Determination of the Expression of Hair-Growth-Related Genes by qPCR

Total RNA of hHFDPCs in each group was extracted by using RNAiso Plus Kit (TaKaRa, China). According to the manufacturer's instructions, total RNA was converted into first-strand cDNA by using a PrimeScript^{TM} RT reagent kit (TaKaRa). Quantitative real-time PCR was conducted to determine the transcript levels of β-catenin, TGF-β2, DKK1, and AR by using SYBR Green Real time PCR Master Mix (TaKaRa). GAPDH was used as the reference gene. The gene-specific primers used in this assay are listed in **Table 1**. The reaction was performed in the CFX96 Detection System (Bio-Rad, Hercules, CA, United States). The result was calculated by the $2^{-\Delta\Delta Ct}$ method.

In vitro Transdermal Permeability Experiments of AOS

The abdomen skin of Sprague–Dawley rats was fixed in a Franz diffusion pool. The donor solution was 500 μl of different AOS formulas (seven groups, **Table 2**). The receiving tank was added with 6 ml of physiological saline, and the water bath was equilibrated to 37°C at a fixed speed of 300 rpm. Subsequently, 1 ml of each sample was withdrawn and immediately replaced with an isothermal and equal volume of receiving solution at different time points (0.5, 1, 3, 4, and 5 h). The amount of AOS (DP2) in the sample was determined by the dinitrosalicylic acid method. The cumulative permeation per area of the skin (Q_n, μg/cm^2) was calculated according to the following equation, with the *in vitro* transdermal release curve plotted with time (hour) as the abscissa and Q_n (μg/cm^2) as the ordinate. The experiment was repeated three times.

$$Q_n = V_n C_n + \Sigma i = 1n - 1 C_i V_i A$$

where C_n is the drug concentration in the endothelial compartment at different times (mg/ml), C_i is the drug concentration in the samples at the final time point (mg/ml), V_n is the volume of the endothelial compartment, V_i is the sample volume, and A is the effective area of permeation.

TABLE 1 | Primers used in the qPCR assay.

Gene name	Forward primer (5′–3′)	Reverse primer (5′–3′)
β-catenin	TTAGCTGGTGGGCTGCAGAA	GGGTCCACCACTAGCCAGTATGA
TGFβ2	TTACACTGTCCCTGCTGCACTT	GGTATATGTGGAGGTGCCATCAA
DKK1	ATGCGTCACGCTATGTGCTG	TGGAATACCCATCCAAGGTGCTA
AR	CTCTCACATGTGGAAGCTGCAAG	TTTCCGAAGACGACAAGATGGAC
GAPDH	GCACCGTCAAGGCTGAGAAC	TGGTGAAGACGCCAGTGGA

TABLE 2 | Experimental design of algal oligosaccharide (AOS) transdermal permeation-enhancing formula.

Group No.	Penetration-enhancing formula
1	1% AOS (DP2)
2	1% AOS (DP2) + 1% glycerol
3	1% AOS (DP2) + 2% glycerol
4	1% AOS (DP2) + 1% PEG400
5	1% AOS (DP2) + 2% PEG400
6	1% AOS (DP2) + 1% glycerol + 1% PEG400
7	1% AOS (DP2) + 2% glycerol + 1% PEG400

Measurement of Hair Growth in Mice

Seven-week-old female C57BL/6 mice in the telogen stages of the hair cycle (Müller-Röver et al., 2001) were purchased from Zhejiang Vital River Laboratory Animal Technology Co., Ltd. (Zhejiang, China). After 7-day acclimation in the facility, mice were randomly divided into three groups ($n = 6$). The animal experiment design was adapted from the study of Kwack et al. (2011) but with specific modifications. The dorsal area (3 cm × 4 cm) of each mouse was synchronized to the anagen stage by depilation with a clipper and an electric shaver. At 10 days post-depilation, when all hair follicles in the depilated skin area entered anagen VI, the mice in different groups were wiped with 500 μl of vehicle sample (2% glycerol and 1% PEG 400), AOS alone sample (1% AOS DP2), or AOS formula (1% AOS DP2 with 2% glycerol and 1% PEG 400) daily for 10 days. Then, the mice were sacrificed to obtain skin specimens for morphological and histological observation. For hair length determination, hairs were plucked randomly from the treated dorsal area at 21 day, and the length of 30 hairs per mouse was measured manually. All experimental protocols were conducted in accordance with the guidelines for care and use of laboratory animals as approved by the Institutional Committee on the Care and Use of Animals of Third Institute of Oceanography, NMR (TIO-IACUC-03-2020-06-22).

Histological Analysis of Skin Specimens

Mouse skin specimens were fixed immediately in 10% neutral formalin, dehydrated using alcohol and xylene, and embedded in paraffin blocks. Five-micrometer sections were stained with hematoxylin and eosin and observed under a light microscope. Hair follicles at distinct hair cycle stages were classified and assigned according to the guideline described by Müller-Röver et al. (2001). To calculate the hair cycle score, hair follicles in anagen V–VI stage, early catagen stage (catagen I–III), mid-catagen stage (catagen IV–V), and late catagen stage (catagen VI–VIII) were arbitrarily attributed a score of 100, 200, 300, and 400, respectively. Fifty hair follicles identified on sections were scored for each mouse, and five mice were used for each group.

Statistical Analyses

All biological experiments were repeated three times independently. Data are expressed as mean ± standard deviation. GraphPad Prism 5 (GraphPad Software, San Diego, CA, United States) was utilized for analyzing the results. Numerical data were analyzed using one-way analysis of variance. Statistical significance between treatments was analyzed using Student's *t*-test.

RESULTS

Preparation of AOS With Varying DPs

AOS may exhibit different bioactivities depending on their composition (Gao et al., 2017). Therefore, we first sought to prepare AOS samples with varying compositions from agar. In our previous studies, the agarolytic bacterium *F. pacifica* WPAGA1 was isolated from the deep-sea sediments of the West Pacific Ocean (Xu et al., 2012). A genome sequence analysis of the strain identified three agarases (Aga2133, Aga4383, and Aga2660), which showed distinct endolytic activities toward agar and yielded various hydrolysis products (Hou et al., 2015; Gao et al., 2017). Thus, AOS samples were obtained by agar degradation with the enzymatic action of one or combined agarases (refer to "Materials and Methods" for details). The obtained hydrolysates were then characterized for oligosaccharide composition through TLC analysis (**Figure 1**). The hydrolysates with different oligosaccharide composition profiles were purified and lyophilized as AOS (DP2) sample (containing NA2, indicated with an arrow in **Figure 1A**), AOS (DP4–6) sample (containing NA4 and NA6, indicated with an arrow in **Figure 1B**), and AOS (DP8–12) sample (containing NA8, NA10, and NA12, indicated with an arrow in **Figure 1C**) for downstream *in vitro* and *in vivo* bioactivity assays.

Effects of Varying Doses of AOS on the Proliferation of hHFDPCs

The effects of varying concentrations of AOS on the proliferation of cultured hHFDPCs were investigated to determine the suitable dosage for *in vitro* experiments. Cultured hHFDPCs were treated with various concentrations of AOS with varying DPs (ranging from 0.1 to 10 mg/ml). As shown in **Figure 2**, treatment of AOS (DP2) up to 10 mg/ml did not influence the proliferation of hHFDPCs, whereas a high dose (10 mg/ml) of AOS (DP4–6) and AOS (DP8–12) inhibited the cell growth rate significantly ($p < 0.05$). Therefore, we selected three gradient doses of AOS (0.2, 1, and 5 mg/ml) for further *in vitro* experiments.

AOS Antagonized DHT-Induced Cellular Signaling in hHFDPCs

DHT could alter the secretion pattern of dermal papilla by enhancing the release of factors that inhibit keratinocyte growth as well as reducing the secretion of hair-growth-stimulating factors. In this study, DHT treatment with concentrations lower than 800 nM did not show obvious toxicity to hHFDPCs, while 1,000 nM DHT significantly decreased the cell viability (**Figure 3A**, $p < 0.01$). Thus, 800 nM DHT was used to induce alterations in regulatory paracrine factors in hHFDPCs. As predicted, the addition of 800 nM DHT significantly altered

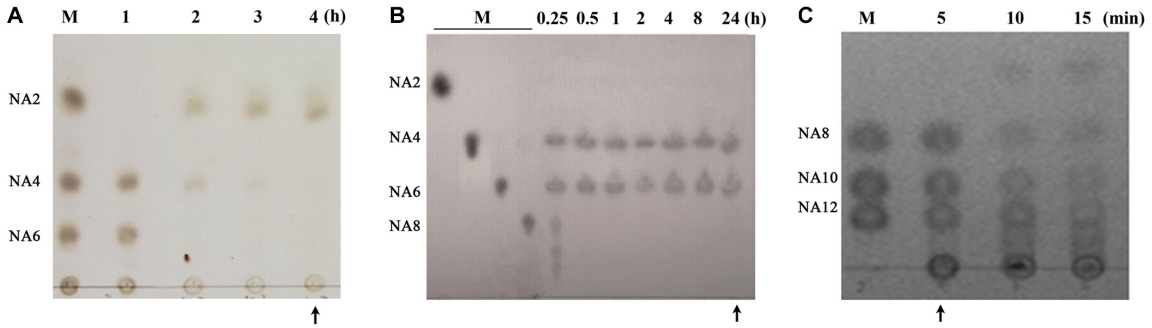

FIGURE 1 | Preparation of algal oligosaccharide (AOS) with varying DP from agar. **(A)** Preparation of AOS (DP2) by enzymatic degradation of AOS (DP4–6) with Aga2660. **(B)** Preparation of AOS (DP4–6) by enzymatic degradation of agar with Aga4383. This picture is adapted from the study of Hou et al. (2015). **(C)** Preparation of AOS (DP8–12) by enzymatic degradation of agar with Aga2133. M, agaroligosaccharide markers; NA2, neoagarobiose; NA4, neoagarotetraose; NA6, neoagarohexaose; NA8, neoagarooctaose; NA10, neoagarodecaose; NA12, neoagarododecaose. The hydrolysate indicated with an arrow in each thin-layer chromatography plate was purified and used in the following experiments.

the secretion pattern of regulatory factors in hHFDPCs as evidenced by the significant decrease in the concentration of VEGF ($p < 0.01$) and the significant increase in the expression levels of TGF-β2 ($p < 0.01$), DKK-1 ($p < 0.01$), and AR ($p < 0.01$) relative to the blank control group (**Figures 3B,C**). Minoxidil was used as a positive control for DHT-induced alteration treatment. As shown in **Figures 3B,C**, the addition of 500 μM minoxidil effectively ameliorated the DHT-induced alteration of secretion pattern in hHFDPCs. Similarly, the treatment of AOS exhibited apparent mitigation effects against DHT-induced alterations to some extent, as revealed by the partial or complete normalization of the levels of VEGF, TGF-β2, DKK-1, AR, and β-catenin (**Figures 3B,C**). The mitigation effects of AOS appeared mainly dependent on its dose and DP. In general, the mitigation effects of AOS increased with increasing concentration, but with some exceptions. For example, no obvious difference in the TGF-β2 expression level was found in hHFDPCs treated with different concentrations of AOS (DP 8–12). The minimum concentration required for taking effects differed between AOS with varying DPs. Specifically, either a low or a high concentration of AOS (DP2) could significantly elevate the VEGF concentration ($p < 0.05$), while only a higher concentration of AOS (DP4–6) or AOS (DP8–12) showed similar effects ($p < 0.05$). The results showed that AOS (DP2) exhibited the best mitigation effects because it attenuated all DHT-induced alterations tested, while no mitigation effects were observed for AOS (DP4–6) toward β-catenin and for AOS (DP8–12) toward β-catenin and TGF-β2. In some cases, the mitigation effects of AOS (DP2) were comparable with those of minoxidil. Hence, AOS (DP2) was selected for the following animal experiment.

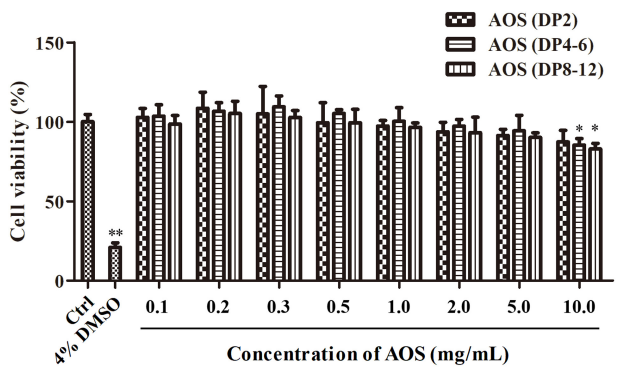

FIGURE 2 | Proliferation of cultured human hair follicle dermal papilla cells (hHFDPCs) treated with algal oligosaccharide (AOS) of varying doses. Different concentrations of AOS were added into cultured hHFDPCs, and cell viability was determined by 3-(4,5-dimethylthiazol-2-yl)-2,5-diphenyltetrazolium bromide assay. As a positive control, 4% dimethyl sulfoxide was included. Columns represent the mean of triplicate assays. Results that are significantly different from those in the blank control group are shown by asterisks (*$p < 0.05$, **$p < 0.01$).

AOS Prolonged the Duration of Anagen and Promoted Hair Growth in Mice

Seven groups of AOS permeation-enhancing formula (**Table 2**) were adopted as the donor solution onto rats' skin to evaluate the *in vitro* transdermal permeation of AOS (DP2). **Figure 4A** shows that AOS (DP2) alone barely penetrated into the rat skin within 5 h, although the permeation rate was accelerated at 1 h post-administration. Glycerol or PEG 400 alone enhanced the permeability of AOS by two to three times, while the combination of 2% glycerol and 1% PEG 400 improved the transdermal permeability of AOS upmost, with a value of 6.5-fold at 5 h post-administration. Hence, AOS with 2% glycerol and 1% PEG was applied in the mouse experiment.

Since one of the key features of AGA is shortened anagen period, we further sought to investigate whether AOS exert anagen prolongation effects in mice. The dorsal skin of 7-week-old female C57BL/6 mice was synchronized by depilation. After 10 days, when hair follicles in the depilated skin areas entered the anagen V–VI stage (as evidenced by the skin's black pigmentation) (Müller-Röver et al., 2001), the depilated areas were treated with vehicle (2% glycerol and 1% PEG 400), AOS alone (1% AOS DP2), or AOS formula (1% AOS

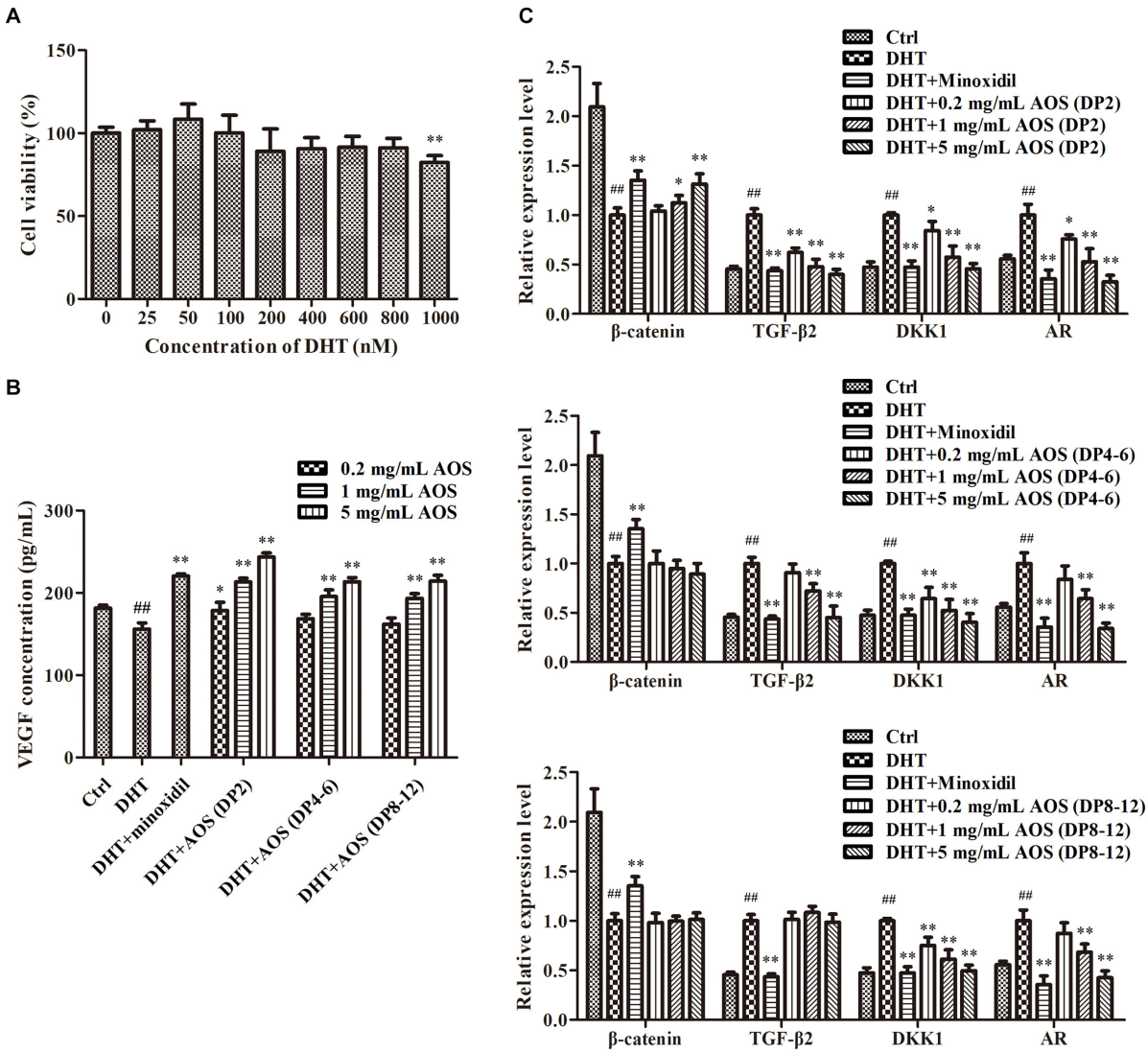

FIGURE 3 | Effects of algal oligosaccharide (AOS) with varying degrees of polymerization (DPs) on vascular endothelial growth factor (VEGF) secretion and hair-growth-related gene expression. **(A)** Influences of dihydrotestosterone (DHT) treatment on the growth of human hair follicle dermal papilla cells (hHFDPCs). Different concentrations of DHT were added into hHFDPCs. After 24 h, cell viability was determined by 3-(4,5-dimethylthiazol-2-yl)-2,5-diphenyltetrazolium bromide assay. **(B)** Effects of AOS with varying DPs on the VEGF secretion of hHFDPCs. Different concentrations of AOS were added into hHFDPCs, and the concentration of extracellular VEGF was determined by enzyme-linked immunosorbent assay. **(C)** Effects of AOS with varying DPs on hair-growth-related gene expression. GAPDH was used as the reference gene for internal control. For all figures, the control group was treated with culture medium. The final concentrations of DHT and minoxidil were 800 nM and 500 μM, respectively. Columns represent the mean of triplicate assays. Significant differences between DHT and control groups are indicated with double hash symbols ($^{\#\#}p < 0.01$). Results that are significantly different from those in the DHT group are shown by asterisks ($^{*}p < 0.05$, $^{**}p < 0.01$).

DP2 with 2% glycerol and 1% PEG 400) daily for 10 days (**Figure 4B**). A histological analysis showed more well-formed hair follicles in deep subcutis in both AOS alone and AOS formula group compared with those in the vehicle group, suggesting the extension of the anagen phase and the delayed catagen progression in mice treated with AOS alone or AOS formula (**Figure 4C**). Determination of the hair cycle score also showed a significantly lower value for both AOS alone and AOS formula group compared with the vehicle group (**Figure 4E**, $p < 0.05$), demonstrating that AOS significantly delayed the catagen progression of hair follicles. To confirm the hair-growth-promoting effects of AOS, the influences of AOS on hair morphology were further examined. As shown in **Figure 4C**, an apparent increase in hair density and thickness was observed in both AOS alone and AOS formula group compared with those in the vehicle group (**Figure 4C**). Besides these, the length of the dorsal hairs treated with AOS formula was significantly increased compared with that of the vehicle group (**Figure 4D**, $p < 0.05$), while no significant difference of hair length was found between the AOS alone group and the vehicle group ($p > 0.05$), suggesting that the AOS formula exerted better hair-growth-promoting effects than AOS alone.

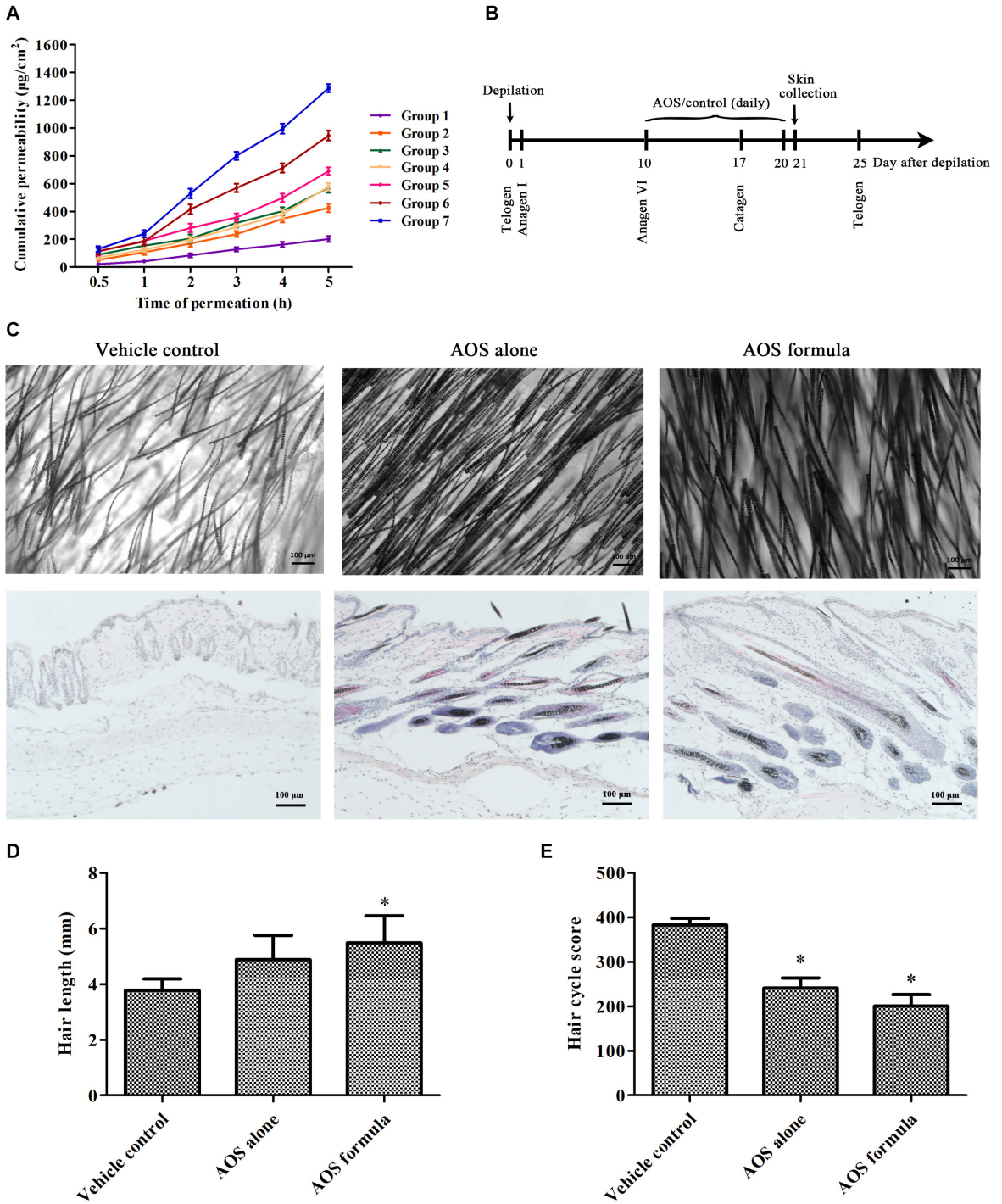

FIGURE 4 | Effects of algal oligosaccharide (AOS) on hair growth of mice. **(A)** *In vitro* transdermal permeation of different AOS penetration-enhancing formula. The abdomen skin of Sprague–Dawley rats was fixed in a Franz diffusion pool. Five hundred microliters of different AOS penetration-enhancing formulas was adopted as the donor solution. The amount of AOS (DP2) in the receiving tank was determined by the dinitrosalicylic acid method. The cumulative permeation per area of the skin (Q_n, μg/cm^2) was calculated. The experiment was repeated three times. **(B)** Scheme of the animal experiment. The back skin of C57BL/6 mice ($n = 6$) was treated with vehicle [2% glycerol and 1% polyethylene glycol (PEG) 400], AOS alone (1% AOS DP2), or AOS formula (1% AOS DP2 with 2% glycerol and 1% PEG 400) at anagen stage for 10 days. **(C)** Effects of AOS on hair follicle growth cycle and hair density. Representative morphological (top) and histological (bottom) images of skin tissue at day 21 are shown. **(D)** Effects of AOS on hair length. The length of randomly plucked hairs ($n = 30$) was measured. **(E)** Calculation of the hair cycle scores. Fifty hair follicles identified on sections were scored for each mouse, and five mice were used for each group. Each stage of the hair cycle has been scored as follows: anagen V–VI = 100, early catagen = 200, mid catagen = 300, late catagen = 400. The value indicates the mean hair cycle score per group (*$p < 0.05$).

DISCUSSION

AOS has received increasing attention because of its physiological and biological functions beneficial for the health of human beings (Han et al., 2016; Gao et al., 2017). However, to our best knowledge, no study has reported on the AGA amelioration activities of AOS. In the present study, we showed that AOS exhibited apparent antagonistic effects in a dose- and DP-dependent manner against DHT-mediated cellular signaling and anagen phase shortening. Since DHT-mediated cellular signaling and the subsequent shortening of the anagen phase play key roles in AGA pathogenesis, AOS may have potential applications in preventing or treating AGA.

Our study showed that AOS significantly ameliorated DHT-induced alteration in dermal papillae cells as revealed by the normalization of several key indices that are important in the pathogenesis of AGA (**Figure 3**). AOS induced several hair-growth-stimulating factors in dermal papillae cells, such as VEGF and β-catenin. VEGF promotes the generation of capillary vessels in hair follicles, thus nourishing the hair follicles and facilitating hair growth (Yano et al., 2001). VEGF can also induce the proliferation of dermal papilla cells through VEGFR-2-mediated activation of ERK (Li et al., 2012). Some studies have revealed the major role of the Wnt/β-catenin pathway in regulating hair growth (Van Mater et al., 2003), given that β-catenin can interact with AR in an androgen-dependent manner, thereby inhibiting Wnt signaling and hair growth (Chesire and Isaacs, 2002). This finding suggests a functional cross-talk between the AR and the Wnt signaling pathways. On the other hand, AOS suppressed several hair-growth-inhibitory factors, such as AR, TGF-β2, and DKK-1. AR is the binding site of DHT, at which DHT initiates AGA signaling in dermal papilla cells. A previous work reported the increased expression of AR in dermal papillae isolated from balding scalp tissue; thus, localized high levels of AR likely cause the patterned characteristic of balding scalp (Lolli et al., 2017). TGF-β2 suppresses the proliferation of hair follicle epithelial cells by stimulating the synthesis of certain caspases and subsequently activating cell apoptosis. TGF-β antagonists effectively prevent catagen-like morphological changes and promote the elongation of hair follicles *in vitro* and *in vivo* (Hibino and Nishiyama, 2004). DKK-1 was notably up-regulated in the dermal papillae cells of patients with AGA and inhibited hair growth by suppressing the Wnt signaling pathway (Kwack et al., 2012). Collectively, our findings showed that AOS could restore the DHT-induced alteration of regulatory factors in dermal papillae cells and thus may ameliorate AGA to some extent. However, it should be noted that AGA is a complicated disease, and DHT-induced alterations of hair-related genes do not necessarily lead to AGA. In this context, the potential application of AOS in ameliorating AGA may be limited.

The post-natal hair follicle is remodeled during cyclical periods of growth (anagen), regression (catagen), and rest (telogen) (Müller-Röver et al., 2001). The length of the rapid growth stage of anagen is believed to mainly contribute to hair length. One of the key features of AGA is shortened anagen period. Therefore, maintaining the anagen cycle is important for the treatment of AGA. Our results showed that AOS prolonged the anagen phase of hair follicles and promoted the growth of dorsal hair in mice. Similarly, a previous study suggested that minoxidil extended the anagen phase in mice by activating the β-catenin pathway in dermal papillae cells (Kwack et al., 2011).

Although the involvement of androgens in AGA is well established, most of the molecular mechanisms for the pathogenesis of the disorder are unknown (Lolli et al., 2017). In this regard, it is difficult to explore the fundamental mechanisms underlying the regulation effects of AOS on hair-growth-related factors and the anagen cycle. Nevertheless, we speculate that AOS likely exert their effects through their antioxidant activities. Oxidative stress is implicated in AGA pathogenesis. Balding dermal papillae cells from male patients with AGA underwent premature senescence *in vitro* compared with those from occipital scalp when challenged with environmental stress (Bahta et al., 2008; Upton et al., 2015). Bald dermal papillae cells are significantly more sensitive to oxidative stresses, and oxygen significantly alters their morphology, proliferation, migration, senescence, and TGF-β signaling (i.e., secreted higher levels of negative hair growth regulators, namely, TGF-β1 and β2) (Lolli et al., 2017).

Comparisons of the protective effects of AOS with varying DPs revealed a clear pattern, that is, the effects increased with decreasing DP (**Figure 3**). This finding may be due to the physical phenomenon that compounds with lower molecular weight have better abilities to migrate across the cell membrane. Similarly, AOS with lower DP is supposed to penetrate skin tissue more efficiently, thereby likely to exert better effects than AOS with higher DP when topically applied on skin. Indeed the hair-growth-promoting effect of AOS (DP2) was elevated when it was combined with penetration enhancers that improve its transdermal permeability (**Figure 4**). Several types of vehicles were reported to enhance the topical delivery efficiency of minoxidil on animals and humans, such as transcutol-containing vesicles (Mura et al., 2011), nanostructured lipid carrier gel (Uprit et al., 2013), and chitosan microparticles (Gelfuso et al., 2011). These types of vehicles may also be useful to improve the transdermal permeability of AOS and should be evaluated for their combined use with AOS in the future.

CONCLUSION

In conclusion, AOS significantly ameliorated the DHT-induced alterations of regulatory factors in hHFDPCs and prolonged the anagen phase of hair follicle in mice. Although the fundamental mechanism of the antagonistic effects of AOS against AGA key features is unknown, we speculated that AOS likely exhibited its effects through its antioxidant activities. AOS (DP2) exerted best effects because it likely penetrates the skin tissues and migrates across the cell membranes more efficiently than AOS with higher DP. Therefore, our study demonstrated that marine agarolytic microbes were useful for biodegrading agar to produce AOS with varying DP, which may have potential applications in the prevention and the treatment of DHT-induced AGA.

DATA AVAILABILITY STATEMENT

The raw data supporting the conclusions of this article will be made available by the authors, without undue reservation.

ETHICS STATEMENT

All experimental protocols were conducted in accordance with guidelines for care and use of laboratory animals approved by the Institutional Committee on the Care and Use of Animals of Third Institute of Oceanography, NMR (TIO-IACUC-03-2020-06-22).

AUTHOR CONTRIBUTIONS

RZ and ZC designed the experiments. MJ, Y-LC, XH, and YH performed the experiments, analyzed the data, and wrote the manuscript. All the authors edited and approved the final manuscript.

FUNDING

This work was financially supported by the Xiamen Marine and Fishery Development Special Fund Project (No. 19CZP008HJ06) and Xiamen Ocean Research and Development Institute Co-construction Project (No. K200302).

REFERENCES

Adil, A., and Godwin, M. (2017). The effectiveness of treatments for androgenetic alopecia: a systematic review and meta-analysis. *J. Am. Acad. Dermatol.* 77, 136–141. doi: 10.1016/j.jaad.2017.02.054

Bahta, A. W., Farjo, N., Farjo, B., and Philpott, M. P. (2008). Premature senescence of balding dermal papilla cells in vitro is associated with p16INK4a expression. *J. Invest. Dermatol.* 128, 1088–1094. doi: 10.1038/sj.jid.5701147

Blanpain, C., Lowry, W. E., Geoghegan, A., Polak, L., and Fuchs, E. (2004). Self-renewal, multipotency, and the existence of two cell populations within an epithelial stem cell niche. *Cell* 118, 635–648. doi: 10.1016/j.cell.2004.08.012

Botchkarev, V. A., and Kishimoto, J. (2003). Molecular control of epithelial–mesenchymal interactions during hair follicle cycling. *J. Invest. Derm. Symp. Proc.* 8, 46–55. doi: 10.1046/j.1523-1747.2003.12171.x

Chesire, D. R., and Isaacs, W. B. (2002). Ligand-dependent inhibition of β-catenin/TCF signaling by androgen receptor. *Oncogene* 21, 8453–8469. doi: 10.1038/sj.onc.1206049

Enoki, T., Okuda, S., Kudo, Y., Takashima, F., Sagawa, H., and Kato, I. (2010). Oligosaccharides from agar inhibit pro-inflammatory mediator release by inducing heme oxygenase 1. *Biosci. Biotech. Biochem.* 74, 766–770. doi: 10.1271/bbb.90803

Gao, B., Jin, M., Li, L., Qu, W., and Zeng, R. (2017). Genome sequencing reveals the complex polysaccharide-degrading ability of novel deep-sea bacterium *Flammeovirga pacifica* WPAGA1. *Front. Microbiol.* 8:600. doi: 10.3389/fmicb.2017.00600

Gelfuso, G. M., Gratieri, T., Simao, P. S., de Freitas, L. A. P., and Lopez, R. F. V. (2011). Chitosan microparticles for sustaining the topical delivery of minoxidil sulphate. *J. Microencapsul.* 28, 650–658. doi: 10.3109/02652048.2011.604435

Han, W., Cheng, Y., Wang, D., Wang, S., Liu, H., Gu, J., et al. (2016). Biochemical characteristics and substrate degradation pattern of a novel exo-type β-agarase from the polysaccharide-degrading marine bacterium *Flammeovirga* sp. strain MY04. *Appl. Environ. Microbiol.* 82, 4944–4954. doi: 10.1128/aem.00393-16

Hibino, T., and Nishiyama, T. (2004). Role of TGF-β2 in the human hair cycle. *J. Dermatol. Sci.* 35, 9–18. doi: 10.1016/j.jdermsci.2003.12.003

Hou, Y., Chen, X., Chan, Z., and Zeng, R. (2015). Expression and characterization of a thermostable and pH-stable β-agarase encoded by a new gene from *Flammeovirga pacifica* WPAGA1. *Proc. Bioch.* 50, 1068–1075. doi: 10.1016/j.procbio.2015.04.005

Hsu, C. L., Liu, J. S., Lin, A. C., Yang, C. H., Chung, W. H., and Wu, W. G. (2014). Minoxidil may suppress androgen receptor-related functions. *Oncotarget* 5:2187.

Inui, S., Fukuzato, Y., Nakajima, T., Yoshikawa, K., and Itami, S. (2002). Androgen-inducible TGF-β1 from balding dermal papilla cells inhibits epithelial cell growth: a clue to understand paradoxical effects of androgen on human hair growth. *FASEB J.* 16, 1967–1969. doi: 10.1096/fj.02-0043fje

Inui, S., and Itami, S. (2011). Molecular basis of androgenetic alopecia: from androgen to paracrine mediators through dermal papilla. *J. Dermatol. Sci.* 61, 1–6. doi: 10.1016/j.jdermsci.2010.10.015

Kelly, Y., Blanco, A., and Tosti, A. (2016). Androgenetic alopecia: an update of treatment options. *Drugs* 76, 1349–1364. doi: 10.1007/s40265-016-0629-5

Kim, H. T., Lee, S., Lee, D., Kim, H. S., Bang, W. G., Kim, K. H., et al. (2010). Overexpression and molecular characterization of Aga50D from Saccharophagus degradans 2-40: an exo-type β-agarase producing neoagarobiose. *Appl. Microbiol. Biotech.* 86, 227–234. doi: 10.1007/s00253-009-2256-5

Kwack, M. H., Kang, B. M., Kim, M. K., Kim, J. C., and Sung, Y. K. (2011). Minoxidil activates β-catenin pathway in human dermal papilla cells: a possible explanation for its anagen prolongation effect. *J. Dermatol. Sci.* 62, 154–159. doi: 10.1016/j.jdermsci.2011.01.013

Kwack, M. H., Kim, M. K., Kim, J. C., and Sung, Y. K. (2012). Dickkopf 1 promotes regression of hair follicles. *J. Invest. Dermatol.* 132, 1554–1560. doi: 10.1038/jid.2012.24

Lachgar, S., Charveron, M., Gall, Y., and Bonafe, J. (1998). Minoxidil upregulates the expression of vascular endothelial growth factor in human hair dermal papilla cells. *Br. J. Dermatol.* 138, 407–411. doi: 10.1046/j.1365-2133.1998.02115.x

Li, W., Man, X. Y., Li, C. M., Chen, J. Q., Zhou, J., Cai, S. Q., et al. (2012). VEGF induces proliferation of human hair follicle dermal papilla cells through VEGFR-2-mediated activation of ERK. *Exper. Cell Res.* 318, 1633–1640. doi: 10.1016/j.yexcr.2012.05.003

Lolli, F., Pallotti, F., Rossi, A., Fortuna, M. C., Caro, G., Lenzi, A., et al. (2017). Androgenetic alopecia: a review. *Endocrine* 57, 9–17.

Messenger, A., and Rundegren, J. (2004). Minoxidil: mechanisms of action on hair growth. *Br. J. Dermatol.* 150, 186–194. doi: 10.1111/j.1365-2133.2004.05785.x

Michelet, J. F., Commo, S., Billoni, N., Mahé, Y. F., and Bernard, B. A. (1997). Activation of cytoprotective prostaglandin synthase-1 by minoxidil as a possible explanation for its hair growth-stimulating effect. *J. Invest. Dermatol.* 108, 205–209. doi: 10.1111/1523-1747.ep12334249

Motofei, I. G., Rowland, D. L., Baconi, D. L., Tampa, M., Sârbu, M.-I., Păunicã, S., et al. (2018). Androgenetic alopecia; drug safety and therapeutic strategies. *Expert Opin. Drug Saf.* 17, 407–412.

Motofei, I. G., Rowland, D. L., Georgescu, S. R., Tampa, M., Baconi, D., Stefanescu, E., et al. (2016). Finasteride adverse effects in subjects with androgenic alopecia: a possible therapeutic approach according to the lateralization process of the brain. *J. Dermatol. Treat.* 27, 495–497. doi: 10.3109/09546634.2016.1161155

Müller-Röver, S., Foitzik, K., Paus, R., Handjiski, B., van der Veen, C., Eichmüller, S., et al. (2001). A comprehensive guide for the accurate classification of murine hair follicles in distinct hair cycle stages. *J. Invest. Dermatol.* 117, 3–15. doi: 10.1046/j.0022-202x.2001.01377.x

Mura, S., Manconi, M., Valenti, D., Sinico, C., Vila, A. O., and Fadda, A. M. (2011). Transcutol containing vesicles for topical delivery of minoxidil. *J. Drug Target.* 19, 189–196. doi: 10.3109/1061186x.2010.483516

Otberg, N., Finner, A. M., and Shapiro, J. (2007). Androgenetic alopecia. *Endocrin. Metab. Clin.* 36, 379–398.

Pierard-Franchimont, C., and Pierard, G. (2001). Teloptosis, a turning point in hair shedding biorhythms. *Dermatology* 203, 115–117. doi: 10.1159/000051723

Roh, C., Tao, Q., and Lyle, S. (2004). Dermal papilla-induced hair differentiation of adult epithelial stem cells from human skin. *Physiol. Genomics* 19, 207–217. doi: 10.1152/physiolgenomics.00134.2004

Rowland, D. L., Motofei, I. G., Popa, F., Constantin, V. D., Vasilache, A., Păunică, I., et al. (2016). The postfinasteride syndrome; an overview. *J. Mind Med. Sci.* 3, 99–107.

Severi, G., Sinclair, R., Hopper, J., English, D., McCredie, M., Boyle, P., et al. (2003). Androgenetic alopecia in men aged 40–69 years: prevalence and risk factors. *Br. J. Dermatol.* 149, 1207–1213. doi: 10.1111/j.1365-2133.2003.05565.x

Tsuboi, R., Itami, S., Inui, S., Ueki, R., Katsuoka, K., Kurata, S., et al. (2012). Guidelines for the management of androgenetic alopecia (2010). *J. Dermatol.* 39, 113–120. doi: 10.1111/j.1346-8138.2011.01361.x

Uprit, S., Sahu, R. K., Roy, A., and Pare, A. (2013). Preparation and characterization of minoxidil loaded nanostructured lipid carrier gel for effective treatment of alopecia. *Saudi Pharm. J.* 21, 379–385. doi: 10.1016/j.jsps.2012.11.005

Upton, J. H., Hannen, R. F., Bahta, A. W., Farjo, N., Farjo, B., and Philpott, M. P. (2015). Oxidative stress–associated senescence in dermal papilla cells of men with androgenetic alopecia. *J. Invest. Dermatol.* 135, 1244–1252. doi: 10.1038/jid.2015.28

Van Mater, D., Kolligs, F. T., Dlugosz, A. A., and Fearon, E. R. (2003). Transient activation of β-catenin signaling in cutaneous keratinocytes is sufficient to trigger the active growth phase of the hair cycle in mice. *Gene Dev.* 17, 1219–1224. doi: 10.1101/gad.1076103

Varothai, S., and Bergfeld, W. F. (2014). Androgenetic alopecia: an evidence-based treatment update. *Am. J. Clin. Dermatol.* 15, 217–230. doi: 10.1007/s40257-014-0077-5

Wang, T., Zhou, C., Shen, Y., Wang, X., Ding, X., Tian, S., et al. (2010). Prevalence of androgenetic alopecia in China: a community-based study in six cities. *Br. J. Dermatol.* 162, 843–847. doi: 10.1111/j.1365-2133.2010.09640.x

Xu, H., Fu, Y., Yang, N., Ding, Z., Lai, Q., and Zeng, R. (2012). *Flammeovirga pacifica* sp. nov., isolated from deep-sea sediment. *Int. J. Syst. Evol. Microbiol.* 62, 937–941. doi: 10.1099/ijs.0.030676-0

Yano, K., Brown, L. F., and Detmar, M. (2001). Control of hair growth and follicle size by VEGF-mediated angiogenesis. *J. Clin. Invest.* 107, 409–417. doi: 10.1172/jci11317

Conflict of Interest: XH was employed by the company Aquabrain Biotech (Xiamen) Co., Ltd.

The remaining authors declare that the research was conducted in the absence of any commercial or financial relationships that could be construed as a potential conflict of interest.

frontiers in Microbiology

ORIGINAL RESEARCH
published: 22 January 2021
doi: 10.3389/fmicb.2020.609952

Bioactive Metabolites From Acid-Tolerant Fungi in a Thai Mangrove Sediment

Hai Gao[1†], Yanan Wang[1†], Qiao Luo[1], Liyuan Yang[1], Xingxing He[1], Jun Wu[2], Konthorn Kachanuban[3], Pongthep Wilaipun[3], Weiming Zhu[1] and Yi Wang[1*]*

[1] School of Medicine and Pharmacy, Ocean University of China, Laboratory for Marine Drugs and Bioproducts of Qingdao National Laboratory for Marine Science and Technology, Qingdao, China, [2] School of Pharmaceutical Sciences, Southern Medical University, Guangzhou, China, [3] Faculty of Fisheries, Kasetsart University, Bangkok, Thailand

OPEN ACCESS

Edited by:
Runying Zeng, Third Institute of Oceanography, State Oceanic Administration, China

Reviewed by:
Lea Atanasova, University of Natural Resources and Life Sciences, Vienna, Austria
Samantha Chandranath Karunarathna, Kunming Institute of Botany, China
Yonghong Liu, Chinese Academy of Sciences, China

***Correspondence:**
Weiming Zhu
weimingzhu@ouc.edu.cn
Yi Wang
wangyi0213@ouc.edu.cn

† These authors have contributed equally to this work

Specialty section:
This article was submitted to Microbiotechnology, a section of the journal Frontiers in Microbiology

Received: *24 September 2020*
Accepted: *23 December 2020*
Published: *22 January 2021*

Citation:
Gao H, Wang Y, Luo Q, Yang L, He X, Wu J, Kachanuban K, Wilaipun P, Zhu W and Wang Y (2021) Bioactive Metabolites From Acid-Tolerant Fungi in a Thai Mangrove Sediment. Front. Microbiol. 11:609952. doi: 10.3389/fmicb.2020.609952

Despite being potentially useful extremophile resources, there have been few reports on acid-tolerant fungi and their bioactive metabolites. Acidophilic/aciduric fungi (n = 237) were isolated from Thai mangrove sediments in an acidic medium. Using fungal identification technology (including morphologic observation, chemical screening, and sequence comparisons) all the isolates were identified and 41 representative isolates were selected for analysis of the phylogenetic relationships (ITS rDNA, β-tubulin, calmodulin, and actin gene sequences). There were seven genera identified – *Penicillium*; *Aspergillus*; *Talaromyces*; *Cladosporium*; *Allophoma*; *Alternaria*; and *Trichoderma* – in four taxonomic orders of the phylum Ascomycota, and *Penicillium*, *Aspergillus,* and *Talaromyces* were the dominant genera. Acidity tolerance was evaluated and 95% of the isolates could grow under extremely acidic conditions (pH 2). Six strains were classed as acidophilic fungi that cannot survive under pH 7, all of which had an extraordinarily close genetic relationship and belonged to the genus *Talaromyces*. This is the first report on the acidophilic characteristics of this genus. The antimicrobial, anti-tumor, and antiviral activities of the fermentation extracts were evaluated. Nearly three-quarters of the extracts showed cytotoxic activity, while less than a quarter showed antimicrobial or anti-H1N1 activity. The typical aciduric fungus *Penicillium oxalicum* OUCMDZ-5207 showed similar growth but completely different chemical diversity at pH 3 and 7. The metabolites of OUCMDZ-5207 that were obtained only at pH 3 were identified as tetrahydroauroglaucin (**1**), flavoglaucin (**2**), and auroglaucin (**3**), among which auroglaucin showed strong selective inhibition of A549 cells with an IC_{50} value of 5.67 μM. These results suggest that acid stress can activate silent gene clusters to expand the diversity of secondary metabolites, and the bioprospecting of aciduric/acidophilic microorganism resources in Thai mangrove sediments may lead to the discovery of compounds with potential medicinal applications.

Keywords: acid-tolerant fungi, Thai mangrove sediment, genetic relationship, secondary metabolites, bioactive diversity

INTRODUCTION

Microbes are important drug producers, however, it is becoming more difficult to obtain new drugs and drug leads from common environmental microorganisms, with less discovery of new microorganisms occurring and duplication of research on their metabolites. Over the last 10 years, we have been investigating microbes and their metabolites from extreme environments. Extreme microorganisms are those that live in a special environment, including places with high temperatures (>50°C), low temperatures (<20°C), high pressure (>35 MPa), high salinity (>3% NaCl), high pH (>pH 9), and low pH (<pH 4) (Wilson and Brimble, 2009), where ordinary microbes cannot survive. The different physiological characteristics of extreme microorganisms can create unique metabolic pathways and their secondary metabolites can have remarkable chemical diversity and interesting bioactivity (Wang et al., 2009, 2011a,b,c, 2013; Zheng et al., 2009, 2010, 2013; Peng et al., 2011a,b, 2018; Fan et al., 2013, 2018; Lin et al., 2015; Qin et al., 2016; Wang M. M. et al., 2017; Jin et al., 2018).

Acid-tolerant microbes are a type of extreme microorganisms, which include acidophilic and aciduric microbes. The optimum pH for the growth of acidophiles is <pH 3, while aciduric microorganisms can tolerate both extremely acidic and neutral conditions (Johnson, 1998). There have been few studies on acidophilic fungi resources. In 2019, Martina et al. summarized the taxonomically identified indigenous acidophilic fungi, but only nine species (*Acidea extrema*, *Acidiella bohemica*, *Acidiella uranophila*, *Acidomyces acidophilus*, *Acidomyces acidothermus*, *Acidothrix acidophila*, *Coniochaeta fodinicola*, *Neohortaea acidophila*, and *Soosiella minima*) were listed. All these fungi were obtained from highly acidic habitats, including highly acidic soil, rivers, hot springs, mines, drainage, and acidophilic algae (Hujslová et al., 2019). Furthermore, Berkeley Pit Lake in the United States and mangrove sediments in China are acid-tolerant fungal habitats (Wang Y. et al., 2017). Although there has been a lack of investigation regarding the diversity of acidophilic fungi, this microbiota has the potential for a variety of applications, including bioremediation technologies (Deshmukh et al., 2016). For instance, acidophilic fungi have been reported to play an important role in the passive remediation of acid mine drainage and the degradation of environmental pollutants, such as phenolic compounds and polymerized rubber. The metabolites of acidophilic fungi also have potential medicinal value. In 2017, the Stierle group published a review of their work on the bioactive metabolites isolated from the abandoned acid metal mine, Berkeley Pit Lake (Stierle et al., 2017). By 2017, new compounds and bioactive compounds occupied 65 and 68% of all the compounds from aciduric microorganisms, respectively, suggesting that acid-tolerant fungi are potential medicinal resources (Wang Y. et al., 2017).

Mangroves are a special marine plant community distributed in the intertidal zone of tropical and subtropical regions. The particular nature of the environment means that mangrove sediments possess strong acidity and have the characteristics of high nutrition, high salinity, and strong reducibility. Although there have been some reports regarding microorganisms from mangroves, there have been few investigations of acidophilic or aciduric microorganisms. In our previous work, some novel bioactive compounds were obtained from acid-tolerant fungi in the soil of the mangrove rhizosphere of the China Mangrove Nature Reserve (Fan et al., 2013; Lin et al., 2015; Qin et al., 2016; Fan et al., 2018; Jin et al., 2018). Examples include new indole-diterpenoids with Anti-influenza virus activity from *Penicillium camemberti* OUCMDZ-1492 (Fan et al., 2013) and new anthraquinone derivatives with Anti hepatitis B virus activity from *Penicillium* sp. OUCMDZ-4736 (Jin et al., 2018). These results suggest that further investigation of the aciduric fungi obtained from mangrove sediments and their bioactive secondary metabolites are worthy of attention.

Previously, most studies of microbes from Thai mangroves have focused on bacteria and yeast (Limtong et al., 2007, 2008; Am-In et al., 2008, 2011; Atipan et al., 2012; Songsumanus et al., 2013; Wongwongsee et al., 2013; Hwanhlem et al., 2014; H-Kittikun et al., 2015; Wanapaisan et al., 2018). Fungi from Thai mangroves, especially acid-tolerant fungi and their bioactive metabolites under conditions of acidic stress, have not previously been investigated. In this paper, we report acid-tolerant fungi and their bioactive metabolites obtained from Thailand mangrove sediments. Using morphologic observations, chemical diversity comparisons, and analysis of the phylogenetic relationships of genes including internal transcribed spacer (ITS)-ribosomal DNA (rDNA), β-tubulin, calmodulin, partial actin gene sequences, the acid-tolerant fungi were identified and classified, and the biodiversity and biological characteristics were evaluated. Furthermore, acid tolerance and antibiotic biological activity (antibacterial, cytotoxicity, and antiviral activity) were also studied. A typical aciduric fungus – *Penicillium sp.* OUCMDZ-5207 – was analyzed under acidic and neutral conditions, and the metabolites at pH 3 and their cytotoxicity were studied.

MATERIALS AND METHODS

General Experimental Procedures

UV spectra were recorded on a Thermo Fisher Scientific NanoDrop One micro-spectrophotometer (Thermo Fisher Scientific, Waltham, MA, United States). ^{1}H NMR, ^{13}C NMR, and 2D NMR spectra were recorded on a Bruker Avance 500 MHz spectrometer with tetramethylsilane (TMS; Alfa Chemistry, United States) as an internal standard. Mass spectra were recorded on an Agilent 6200 Q-TOF MS system. TLC was performed on plates precoated with silica gel GF254 (10–40 μm, Qingdao Marine Chemical Ltd., Qingdao, China). Column chromatography was performed on silica gel (100–200, 200–300, and 300–400 mesh; Qingdao Marine Chemical Ltd., Qingdao, China), RP-18 gel (20–45 μm), and Sephadex LH-20 (Amersham Biosciences, United Kingdom). Medium-pressure liquid chromatography (MPLC; CXTH-3000, China) was performed using columns packed with RP-18 gel and an LC3000 system equipped with P3000A pump modules. Semipreparative high performance liquid chromatography (HPLC; Waters 1525,

United States) was performed using a column (YMC-pakODS-A, 10 × 250 mm, 5 μm, 4 mL/min).

Fungi Isolation

Fungi strains were isolated from the sediment around the roots of *Hibiscus tiliaceus*. Samples were collected from the mangrove habitat at PakMeng Beach, Thailand in October 2016. The samples were stored at −20°C and processed immediately for isolation and cultivation of the fungus after transport to the laboratory. The samples were then frozen at −20°C.

The gradient dilution method was used for fungi isolation. To remove superficial sediments and microbes, samples (1.0 g) were sterilized with 75% ethanol and rapidly washed three times with sterile water under sterile conditions. The samples were homogenized thoroughly and diluted to three different concentrations (0.1, 0.01, and 0.001) with sterile seawater. Then, 100-μL samples of each dilution were plated onto the corresponding isolation medium (**Table 1**) in triplicate. The acid medium was adjusted with citric acid and disodium hydrogen phosphate buffer solution to obtain the desired pH. The neutral medium was adjusted with NaOH. Chloramphenicol (100 μg/mL) was added to the medium to prevent the growth of bacteria during the incubation. The fungi were cultured at 28°C for at least 5 days. To ensure strain diversity, timely observations were conducted as much as possible. All the colonies were collected and purified on the plate repeatedly until a single colony was obtained, then inoculated onto slope media and stored at 4°C. Furthermore, these strains were also preserved in 20% glycerin liquid medium at −80°C.

TABLE 1 | Ingredient of media used for isolation and fermentation of microbial strains [a,b,c].

Microbes	Medium	Ingredient
Fungi sample	SWS	1.0 g peptone, 10.0 g soluble starch,20.0 g agar
	PDA	200.0 g potato extract, 20.0 g dextrose, 20.0 g agar
	GYP	10.0 g glucose,1.0 g yeast extract, 2.0 g peptone;20.0g agar
	MYPG	3.0 g yeast extract, 3.0 g malt extract, 5.0 g peptone,20.0 g glucose,1.0 g $K_2HPO_43H_2O$, 0.50g $MgSO_47H_2O$, 0.20 g $FeCl_36H_2O$, 20.0 g agar
	Martin medium	10.0 g peptone, 10.0 g glucose, 1.0 g $K_2HPO_43H_2O$, 0.50 g $MgSO_47H_2O$, 20.0 g agar
	Malt extract medium	30.0 g malt extract, 5.0 g tryptone, 20.0g agar
Pathogenic Microbes	Luria Bertani (LB)	5.0 g yeast extract, 10.0 g peptone, 5.0 g NaCl, 20.0 agar
	Zobell2116E	5.0 g peptone,3.0 g yeast extract, 20.0 g agar
	YPD	Peptone 2.0 g, yeast extract 1.0 g, glucose 2.0 g, 20.0 g agar

[a]All mediums were prepared with nature sterile seawater and adjusted to appropriate pH before autoclaving at 121°C for 20 min. [b] The liquid media without agar were used for fermentation of fungi in bioassay and compound isolation. [c] The 2216E, YPD, and LB media were used to culture aquatic and human pathogenic microbial strains in the antimicrobial test.

DNA Extraction, PCR Amplification, and Sequencing

Single fungal colonies were transferred with a sterilized toothpick to 50 μL of a lysis buffer for PCR with a Direct PCR kit (Takara) in a sterilized microtube. The microtubes were placed at 80°C for pre-degeneration for 15 min and then centrifuged at low speed. A 2-μL sample of the supernatant was used as the template to amplify the fungal gene fragment in a polymerase chain reaction (PCR). internal transcribed spacer (ITS)-ribosomal DNA (rDNA) sequences were amplified with the primers ITS1F (5′-CTTGGTCATTTAGAGGAAGTAA-3′) (Gardes and Bruns, 1993) and ITS4 (5′-TCCTCCGCTTATTGATATGC-3′) (White et al., 1990). For the sequencing of partial β-tubulin gene, βt2a (5′-GGTAACCAAATCGGTGCTGCTTTC-3′) and βt2b (5′-ACCCTCAGTG TAGTGACC CTTGGC-3′) were used as the primers (Glass and Donaldson, 1995). Partial calmodulin gene was amplified using the primers cmd5 (5′-CCGAGTACAAGGAGGCCTTC-3′) and cmd6 (5′-CCGATAGAGGTCATAACGTG-3′) (O' Donnell et al., 2000). For the sequencing of the partial actin gene, act-512F (5′-ATGTGCAAGGCCGGTTTCGC-3′) and ACT-783R (5′-TACGAGTCCTTCTGGCCCAT-3′) were used as the forward primer and reverse primer, respectively (Carbone and Kohn, 1999). The PCR reactions were performed in a final volume of 50 μL, which was composed of 2 μL of template DNA, 10 μL of 5 × PrimeSTAR Buffer (Mg2 + plus), 4 μL of dNTP Mix (2.5 mM of dATP, dCTP, dGTP and dTTP, respectively), 0.5 μL of forward primer (20 μM), 0.5 μL of reverse primer (20 μM), 0.5 μL of PrimeSTAR HS DNA Polymerase (2.5 U/μL), and 32.5 μL of ultrapure water. Amplification was carried out using the following thermal cycles: 30 cycles of 10 s at 98°C, 5 s at 55°C, and 60 s at 72°C. Then, the PCR products (5 μL) were loaded onto an agarose gel [1.2% agarose in 0.5 × TAE buffer and 5 μL of 1% ethidium bromide solution (m/v) per 100 mL of gel] and isolated using a gel extraction kit (E.Z.N.A., Omega, United States), according to the manufacturer's protocol after electrophoresis at 100 V for 35 min. PCR products were submitted for sequencing (Shanghai Personalbio Biotechnology Co., Ltd., China).

Phylogenetic Analysis

Fungal sequences were edited with Lasergene Software SeqMan (DNAStar Inc.). For preliminary identification, the sequences were compared with related sequences available in the National Center for Biotechnology Information (NCBI) to determine the identity of the sequence. All the fungal sequences were aligned using the CLC Sequence Viewer 6 software with the default parameters. All the identified ITS-rDNA sequences of the Thai mangrove fungi were submitted to NCBI GenBank and the accession numbers were obtained. All the sequences of β-tubulin,

calmodulin, partial actin gene were shown in **Supplementary Material**. A phylogenetic tree was generated with the neighbor-joining (NJ) method in the MEGA 4 software and 1,000 replicates were used for the bootstrap analysis. iTOL online software was used to process the phylogenetic tree. The reference sequences showing the highest homology to the sequences from the Thai mangrove fungi were amplified.

Preparation of Samples for Bioassay

The fungal strains were fermented with shaking at 28°C and 180 rpm for 7 day in a 500-mL conical flask containing 150 mL of Potato Dextrose Broth (PDB) liquid medium. The acid medium was prepared by adding citric acid and disodium hydrogen phosphate buffer solution. Three parallel lines were set for each experiment. The fermentation broth was extracted with an equal volume of ethyl acetate (EtOAc) three times. The dried extracts for bioassay were obtained by evaporation under reduced pressure.

Isolation and Identification of Compounds

Penicillium sp. OUCMDZ-5207 was isolated from the sediment around the roots of the mangrove plant, *H. tiliaceus*, at pH 2.0. The strain was fermented under static conditions at 26°C for 35 day in twenty 1000-mL Erlenmeyer flasks each containing 300 mL of PDB liquid medium at pH 3.0. The fermentation broths were harvested and extracted three times with an equal volume of ethyl acetate (EtOAc). Removal of the solvent in vacuum gave 3.2 g of EtOAc extract. The EtOAc extracts were separated on a silica-gel column eluting with petroleum ether (PE)–EtOAc (v/v100:1, 50:1, 25:1, 10:1, 5:1, 1:1, 1:2, 1:5, and 1:10) to obtain nine subfractions (Fr.1–Fr.9). Fr.3 (80.1 mg) was further subjected to purification with an HPLC ODS column (v/v acetonitrile $-H_2O$ 7:3) to give Fr.3-1–Fr.3-4. Fr.3-4 (10.3 mg) was further purified using a HPLC Polymer Stabilized Cholesteric Texture column (v/v acetonitrile–H_2O 13:20) to yield compounds 1 (3.21 mg, t_R 30 min) and 2 (4.32 mg, t_R 34 min). Fr.4 was further separated by Sephadex LH-20 column chromatography eluting with MeOH-CH_2Cl_2 (v/v 1:1) to give three subfractions (Fr.4-1–Fr.4-3). Fr.4-2 (5.6 mg) and subjected to silica gel column chromatography eluting with petroleum ether–EtOAc (v/v 35:1, 25:1, and 10:1) to give compound 3 (2.67 mg).

Tetrahydroauroglaucin (**1**): Light yellow amorphous solid. $C_{19}H_{26}O_3$. UV(MeOH) λ_{max} (logε) 240 (0.17), 275 (0.08), 392 (0.01) nm; ^{1}H-NMR (DMSO-d_6, 600 MHz) δ: 0.83 (3H, t, J = 6.7 Hz, H-7′), 1.26 (4H, m, H-5′, H-6′), 1.41 (2H, quintet, J = 7.3 Hz, H-4′), 2.62 (3H, s, H-4″), 2.19 (3H, s, H-5″), 2.46 (2H, q, J = 1.7 Hz, H-3), 3.16 (2H, d, J = 7.4 Hz, H-1″), 9.16 (1H, brs, 5-OH), 5.20 (1H, t, H-2″), 6.51 (1H, m, H-2′), 6.94 (1H, s, H-4), 5.78 (1H, dt, J = 15.9, H-1′), 9.99 (1H, s, 1-CHO), 11.60 (1H, s, 2-OH). ^{13}C-NMR (DMSO-d_6, 125 MHz) δ 197.3 (1-CHO), 152.9 (C-2), 146.9 (C-5), 140.5 (C-2′), 132.7 (C-3″), 127.7 (C-3), 124.7 (C-4), 125.7 (C-6), 121.6 (C-2″), 121.0 (C-1′), 117.4 (C-1), 33.2 (C-3′), 30.9 (C-5′), 28.4 (C-4′), 26.9 (C-1″), 25.6 (C-5″), 22.0 (C-6′), 17.7 (C-4″), 14.0 (C-7′). ESI-MS m/z 301[M-H]$^-$.

Flavoglaucin (**2**): Light yellow amorphous solid. $C_{19}H_{28}O_3$. UV(MeOH) λ_{max} (logε) 214 (1.33), 255 (0.99), 300 (0.76) nm; ^{1}H-NMR (DMSO-d_6, 600 MHz) δ: 11.68 (1H, s, 2-OH), 10.19 (1H, s, 7-CHO), 6.92 (1H, s, H-4), 5.18 (1H, d, J = 14.8 Hz, H-2″), 8.95 (1H, brs, 5-OH), 3.13 (2H, d, J = 7.4 Hz, H-1″), 2.80 (2H, t, J = 7.7 Hz, H-1′), 1.65 (3H, s, H-5″), 1.61 (3H, s, H-4″), 1.40 (2H, m, H-2′), 1.19–1.23 (8H, m, H-3′, 4′, 5′, 6′), 0.80 (3H, t, J = 6.7 Hz, H-7′) ^{13}C NMR (DMSO-d_6, 125 MHz) δ 197.2 (1-CHO), 153.2 (C-2), 146.9 (C-5), 132.5 (C-3″), 129.0 (C-3), 126.8 (C-6), 125.2 (C-4), 121.8 (C-2″), 117.6 (C-1), 31.3 (C-2′), 31.5 (C-4′), 29.0 (C-5′), 28.6 (C-3′), 26.7 (C-1″), 25.6 (C-5″), 23.2 (C-1′), 22.1 (C-6′), 17.7 (C-4″), 14.0 (C-7′). ESI-MS m/z 303[M-H]$^-$.

Auroglaucin (**3**): Yellow amorphous solid. $C_{19}H_{22}O_3$. UV(MeOH) λ_{max} (logε) 230 (1.47), 211 (1.22), 278 (1.13) nm. ^{1}H-NMR (DMSO-d_6, 600 MHz) δ: 11.71 (1H, s, 2-OH), 10.03 (1H, s, 7-CHO), 6.95 (1H, s, H-4), 5.18 (1H, t, J = 14.8 Hz, H-2″), 9.43 (1H, brs, 5-OH), 3.17 (2H, d, J = 7.3 Hz, H-1″), 6.82 (1H, d, J = 15.6 Hz, H-1′), 6.15 (1H, m, H-5′), 1.60 (3H, s, H-4″), 6.60 (1H, m, H-2′), 6.32 (2H, m, H-3′, 4′), 5.74 (1H, m, H-6′), 1.71 (3H, d, J = 6.8 Hz, H-7′); ^{13}C NMR (DMSO-d_6, 125 MHz) δ 196.9 (1-CHO), 153.3 (C-2), 147.7 (C-5), 131.2 (C-3″), 134.5 (C-3), 121.4 (C-6), 124.9 (C-4), 123.0 (C-2″), 116.9 (C-1), 124.5 (C-2′), 131.9 (C-4′), 128.4 (C-5′), 132.8 (C-3′), 26.9 (C-1″), 17.7 (C-5″), 130.9 (C-1′), 137.8 (C-6′), 25.6 (C-4″), 18.3 (C-7′). ESI-MS m/z 297[M-H]$^-$.

Anti-microbial Assay

The paper disk-agar diffusion method (Tamura et al., 1968) was used to evaluate the inhibition of pathogenic microorganisms, including nine aquatic pathogens (*Edwardsiella tarda*, *Vibrio parahaemolyticus*, *Vibrio Vulnificus*, *Vibrio alginolyticus*, *Aeromonas hydrophila*, *Pseudoalteromonas nigrifaciens*, *Shewanella marisflavi*, *Vibrio splendidus*, and *Bacillus cereus*) and eight human pathogens (*Staphylococcus aureus*, *Staphylococcus aureus* Rosenbach, *Escherichia coli*, *Bacillus subtilis*, *Clostridium perfringens*, *Candida albicans*, *Candida glabrata*, and *Pseudomonas aeruginosa*). The initial concentration of the EtOAc extract was 1 mg/mL. Ciprofloxacin and ketoconazole at concentrations of 0.1 mg/mL were used as positive controls. The pathogenic microorganisms were cultivated in a 50-mL centrifuge tube containing 30 mL of liquid medium and shaken at 28°C and 180 rpm for 12 h. LB medium was used for human pathogenic bacteria, 2116E medium for aquatic pathogenic bacteria, and YPD medium for human pathogenic fungi. The pathogenic strains were coated on a corresponding plate and incubated at 37°C for 30 min. Paper discs with 10 μL of the sample or positive controls (three parallels) were volatilized to dryness and placed onto an agar plate coated with the bacterial suspension. The plates were incubated for 12 h at 37°C. The negative control was methanol. Then, the diameters of the inhibition zones were recorded as the observed antibacterial activity.

Cytotoxic Assay

The cytotoxicity against human breast adenocarcinoma cell line MCF-7 and human lung adenocarcinoma cell line A549 was evaluated by the MTT method (Mosmann, 1983). The EtOAc

extracts, compounds, and positive control (adriamycin) were dissolved in dimethyl sulfoxide (DMSO), DMSO was a negative control. The cell lines were cultivated in RPMI-1640 medium with 10% FBS under a humidified atmosphere with 5% CO_2 at 37°C. Cell suspensions of MCF-7 and A549 (100 μL) were inoculated into 96-well plates (5×10^3 cells/well) and incubated under the above conditions for 24 h. Then, 100-μL samples with final concentrations of 100 μg/mL of extract, 10 μM of a compound, and 1 μM of adriamycin were added to each well in triplicate and the culture mediums were incubated for 72 h. The RPMI-1640 medium containing 5% FBS was used as a blank control. MTT (methylthiazolyldiphenyl-tetrazolium bromide) solution (20 μL; 5 mg/mL in FBS) was added into each well and the wells were incubated for 4 h at 37°C. The medium containing MTT was gently removed with a pipette and 150 μL of DMSO was added to each well to dissolve the formed formazan crystals. The absorbance was recorded on a Spectra Max Plus plate reader at 570 nm. The inhibition rate was calculated as [(OD blank - OD sample)/OD blank] × 100%.

Anti-H1N1 Assay

The cytotoxicity of the samples against MDCK cells was evaluated by the method described above. Non-toxic samples (inhibition rates <0) were evaluated for antiviral bioactivity against the influenza virus H1N1 [A/Puerto Rico/8/34 (H1N1), PR/8] by the MTT method. The Madin-Darby Canine Kidney (MDCK) cells were digested by trypsin as monolayer cells and incubated with the influenza virus H1N1 at 37°C for 1 h. Then, the culture medium was discarded and a new RPMI 1640 medium with 20 μL samples 50 μg/mL were added. The inhibition was evaluated by the MTT method the same as for cytotoxicity, as described above.

RESULTS AND DISCUSSION

Isolation and Phylogenetic Diversity of Aciduric Fungi Associated With Thai Mangrove Sediment

A total of 237 fungi strains were isolated from the acidic sediment collected from around the roots of *H. tiliaceus*, a mangrove plant from PakMeng Beach, Thailand. Six types of culture medium (**Table 1**) at two different pH values were used for isolation of the fungi. The acidity of the sediment sample was pH 5.0 and this pH value was used for the isolation. Additionally, pH 3.0 was used for the isolation to increase the possibility of obtaining acidophilic microbes. In total, 163 and 74 fungal strains were obtained under natural (pH 5.0) and acidic (pH 3.0) conditions, respectively. Duplicates were removed by detailed morphological observation, pigment formation, TLC characteristics, and HPLC fingerprint analysis of the crude extracts of the metabolites. After this assessment, there remained 95 individual fungi strains (72 at pH 5.0 and 23 at pH 3.0). These mangrove fungi grew better under natural conditions (pH 5.0) compared with the highly acidic environment (pH 3.0) (**Figure 1**). Compared with the other mediums used for isolation, the Martin medium was found to be more suitable for fungi growth, which may be related to the presence of more inorganic salts in this medium. The fungi may grow better in a medium rich in inorganic salts because of the characteristics of the natural fungal environment where the mangrove sediments are repeatedly washed by seawater and that deposits a large amount of inorganic salts.

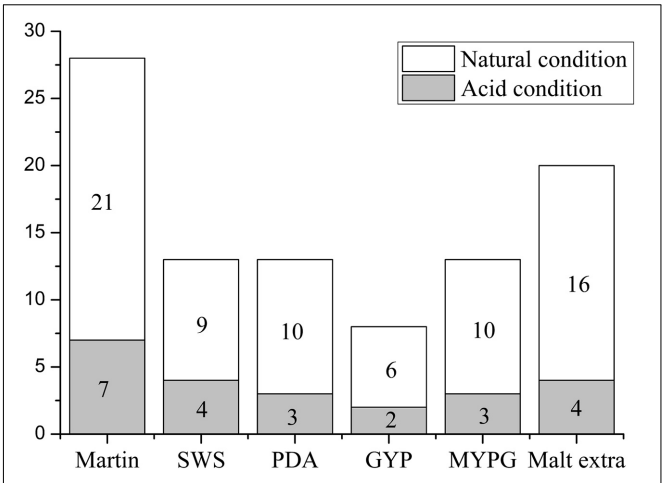

FIGURE 1 | Numbers of fungi isolated from Thai mangrove samples using different media under acidic (pH 3.0) and natural (pH 5.0) conditions (95 fungi strains, 72 at pH 5.0 and 23 at pH 3.0). The horizontal axis represents the type of culture medium (SWS: peptone starch agar; PDA: potato dextrose agar; GYP: glucose yeast extract peptone; and MYPG: malt extract yeast extract peptone glucose), and the vertical axis represents the number of fungi isolates.

We investigated research references on fungi derived from the semi-mangrove plant *H. tiliaceus* from 2008 to 2020 (Li et al., 2008, 2010; Yan et al., 2010, 2012; Wang et al., 2012). Most results discussed the plant endophyte and their metabolites. The fungal genera included *Aspergillus flavus*, *Penicillium commune*, and *Eurotium rubrum*, among which *A. flavus* strain was isolated from the roots, and the others were isolated from flowers or stems. There is no reference reported on pH adaptability of these fungi from the soil around *H. tiliaceus* roots. So it is the first time to report the characteristics of acid-tolerant rhizosphere fungi derived from *H. tiliaceus* of Thailand mangroves. Mangrove soil is a special acidic geological environment, but there have been few reports of acid-tolerant fungi from this environment. Generally, a highly acidic environment is not conducive to microbial growth; however, our results showed more than a quarter of the fungi (23/95) showed better growth in the highly acidic medium (pH 3.0), which indicated that the microbial community in mangrove sediments associated with *H. tiliaceus* in Thailand has distinctive acidophilic properties.

To investigate the phylogenetic relationship of these mangrove fungi, the ITS sequences were compared using Clustal X software, the isolates with duplicated ITS sequences were excluded, and the remaining 41 strains were analyzed for phylogenetic relationships. According to the blast results compared with the sequences already registered in the NCBI

TABLE 2 | Phylogenetic affiliations and the classification of 41 representative acid-tolerant fungal isolates from Thai mangrove samples.

Isolate No.	Class	Order	Family	Genus	Accession No.	Closest identified relative.	Identity (%)	Numbers
OUCMDZ-5020	Eurotiomycetes	Eurotiales	Aspergillaceae	*Penicillium*	MK358957	*Penicillium citrinum* NRRL 1841 (NR_121224.1)	99	12
OUCMDZ-5041					MK358954	*Penicillium oxalicum* NRRL 787 (NR_121232.1)	99	
OUCMDZ-5050					MK355522	*Penicillium polonicum* CBS 222.28 (NR_103687.1)	100	
OUCMDZ-5130					MK357071	*Penicillium chrysogenum* CBS 306.48 (NR_077145.1)	99	
OUCMDZ-5019					MK356475	*Penicillium rubens* CBS 129667 (NR_111815.1	99	
OUCMDZ-5207[a]					MK418548	*Penicillium tanzanicum* CBS 140968 (NR_158820.1)	99	
OUCMDZ-5226[a]					MK392091	*Penicillium lanosum* CBS 106.11 (NR_163539.1)	99	
OUCMDZ-5274[a]					MK393940	*Penicillium hetheringtonii* CBS 122392 (NR_111482.1)	99	
OUCMDZ-5004					MK351267	*Penicillium oxalicum* NRRL 787 (NR_121232.1)	100	
OUCMDZ-5237[a]					MK392099	*Penicillium commune* CBS 311.48 (NR_111143.1)	99	
OUCMDZ-4993					MK357511	*Penicillium flavigenum* CBS 419.89 (NR_103695.1)	100	
OUCMDZ-5022					MK355523	*Penicillium rubens* CBS 129667 (NR_111815.1)	100	
OUCMDZ-5122				*Aspergillus*	MK359012	*Aspergillus versicolor ATCC 957* (NR_131277.1)	99	10
OUCMDZ-5013					MK359008	*Aspergillus chevalieri NRRL 78* (NR_135340.1)	100	
OUCMDZ-5053					MK358986	*Aspergillus caesiellus CBS 470.65* (NR_077146.1)	99	
OUCMDZ-4990					MK358960	*Aspergillus flavus ATCC 16883* (NR_111041.1)	99	
OUCMDZ-5233[a]					MK418545	*Aspergillus terreus* ATCC 1012 (NR_131276.1)	99	
OUCMDZ-5064					MK355524	*Aspergillus welwitschiae* CBS 139.54 (NR_137513.1)	100	
OUCMDZ-5081					MK355967	*Aspergillus piperis* CBS 112811 (NR_077191.1)	99	
OUCMDZ-5232[a]					MK392093	*Aspergillus ochraceus* NRRL 398 (NR_077150.1)	100	
OUCMDZ-5076					MK351862	*Aspergillus ellipticus* ATCC 16903 (NR_138337.1)	100	
OUCMDZ-5210[a]					MK393941	*Aspergillus fumigatus* ATCC 1022 (NR_121481.1)	100	
OUCMDZ-5029			Trichocomaceae	*Talaromyces*	MK359023	*Talaromyces aurantiacus* CBS 314.59 (NR_103681.2)	97	11
OUCMDZ-5006					MK359011	*Talaromyces rogersiae* NRRL 62223 (NR_155914.1)	99	
OUCMDZ-5185[a]					MK358958	*Talaromyces variabilis* CBS 385.48 (NR_103670.2)	96	
OUCMDZ-5259[ab]						*Talaromyces liani* NRRL 1009 (NR_077206.1)	99	
OUCMDZ-5245[ab]						*Talaromyces minioluteus* CBS 642.68 (MN969409.1)	83	
OUCMDZ-4999					MK357489	*Talaromyces amestolkiae* CBS 132696 (NR_120179.1)	99	
OUCMDZ-5267[a]					MK392095	*Talaromyces siamensis* CBS 475.88 (NR_103683.2)	99	
OUCMDZ-5269[a]					MK418551	*Talaromyces australis* IBT 14256 (NR_147431.1)	99	
OUCMDZ-5221[a]					MK392092	*Talaromyces stollii* CBS 408.93 (NR_111781.1)	99	
OUCMDZ-5272[a]					MK392098	*Talaromyces erythromellis* CBS 644.80 (NR_121531.1)	96	
OUCMDZ-5252[a]					MK478881	*Talaromyces thailandensis* CBS 133147 (NR_147428.1)	99	
OUCMDZ-5058	Dothideomycetes	Capnodiales	Cladosporiaceae	*Cladosporium*	MK356562	*Cladosporium colombiae* CBS 274.80B (NR_119729.1)	99	4
OUCMDZ-5216[a]					MK421546	*Cladosporium phlei* CBS 358.69 (NR_120013.1)	100	
OUCMDZ-5036					MK357638	*Cladosporium oxysporum* CPC 14371 (NR_152267.1)	100	
OUCMDZ-5008					MK358961	*Cladosporium endophytica* MFLUCC 17 (NR_158360.1)	98	
OUCMDZ-5111		Pleosporales	Pleosporineae	*Allophoma*	MK356384	*Allophoma cylindrispora* UTHSC DI16 (NR_158276.1)	98	1
OUCMDZ-5040				*Alternaria*	MK357070	*Alternaria alstroemeriae* CBS 118809 (NR_163686.1)	99	2
OUCMDZ-5048					MK371740	*Alternaria eichhorniae* ATCC 22255 (NR_111832.1)	99	
OUCMDZ-5083	Sordariomycetes	Hypocreomycetidae	Hypocreaceae	*Trichoderma*	MK356149	*Trichoderma yunnanense* CBS 121219 (NR_134419.1)	99	1
Total Numbers	**3**	**4**	**5**	**7**				**41**

[a] *The strains were isolated at pH 3. Other strains were isolated at pH 5.* [b] *Phylogenetic affiliations were constructed based on ITS rDNA genes except for OUCMDZ-5259 and 5254 which were based on β-tubulin genes shown in* ***Supplementary Material****.*

gene databank, all the isolated fungi belonged to the Ascomycota phylum. These fungi showed 96–100% similarity to their closest relatives (**Table 2**). Based on the analysis of homology of the ITS rDNA gene, a phylogenetic relationship containing 41 representative fungi isolates was constructed by the neighbor-joining method (**Figure 2**). Considering the fact that the ITS phylogenetic analysis was not sufficient, different gene combinations were used for different genera. The β-tubulin gene was used for 33 isolates identified as *Penicillium*, *Talaromyces*, *Aspergillus* with the ITS genetic marker (**Supplementary Figure 2**). The phylogenetic relationship based on β-tubulin genes showed OUCMDZ-5245 and 5259 were clustered together with *Talaromyces* which were different from the ITS result *Penicillium*. Calmodulin and actin genes were used to analyze strain 5245 and 5259, respectively, and the results also showed that they all belonged to *Talaromyces*. At the level of genetic analysis, these two strains were considered more reliable as *Talaromyces*. Calmodulin and actin genes were used for analyzing OUCMDZ-5058, 5216, 5036, 5008, 5111 and 5083, 5040, 5048, respectively (**Supplementary Figures 3**, **4**). Except for strain 5111, all the identification results were corresponded to the ITS rDNA analyzing results. The actin gene was used for identification of 5111, and the result showed that 5111 belonged to *Allophoma* which was the same as the result of ITS. Combined with all the genetic analysis results, all the identified fungi belonged to one phylum (Ascomycota), three classes (Eurotiomycetes, Dothideomycetes, and Sordariomycetes), four orders (Eurotiales, Capnodiales, Pleosporales, and Hypocreomycetidae) and seven genera including *Penicillium* (12 isolates), *Aspergillus* (10 isolates), *Talaromyces* (11), *Cladosporium* (4), *Alternaria* (2), *Allophoma* (1), and *Trichoderma* (1). Among them, 80.5% of the strains belonged to the order Eurotiales. *Penicillium*, *Talaromyces*, and *Aspergillus* were the dominant genera in this mangrove ecosystem and were extensively distributed.

To understand the acid tolerance of these fungi, all the 41 strains obtained under (pH 3.0 and pH 5.0) were incubated under extremely acidic conditions (pH 2.0) and neutral conditions (pH 7), and the growth was observed. The results indicated that all of the 41 fungi strains could grow at pH 5.0, six (OUCMDZ-5221, 5252, 5259, 5267, 5269, and 5272) could not survive at pH 7.0 but grew well at pH 2.0, and two (OUCMDZ-4999 and 5111)

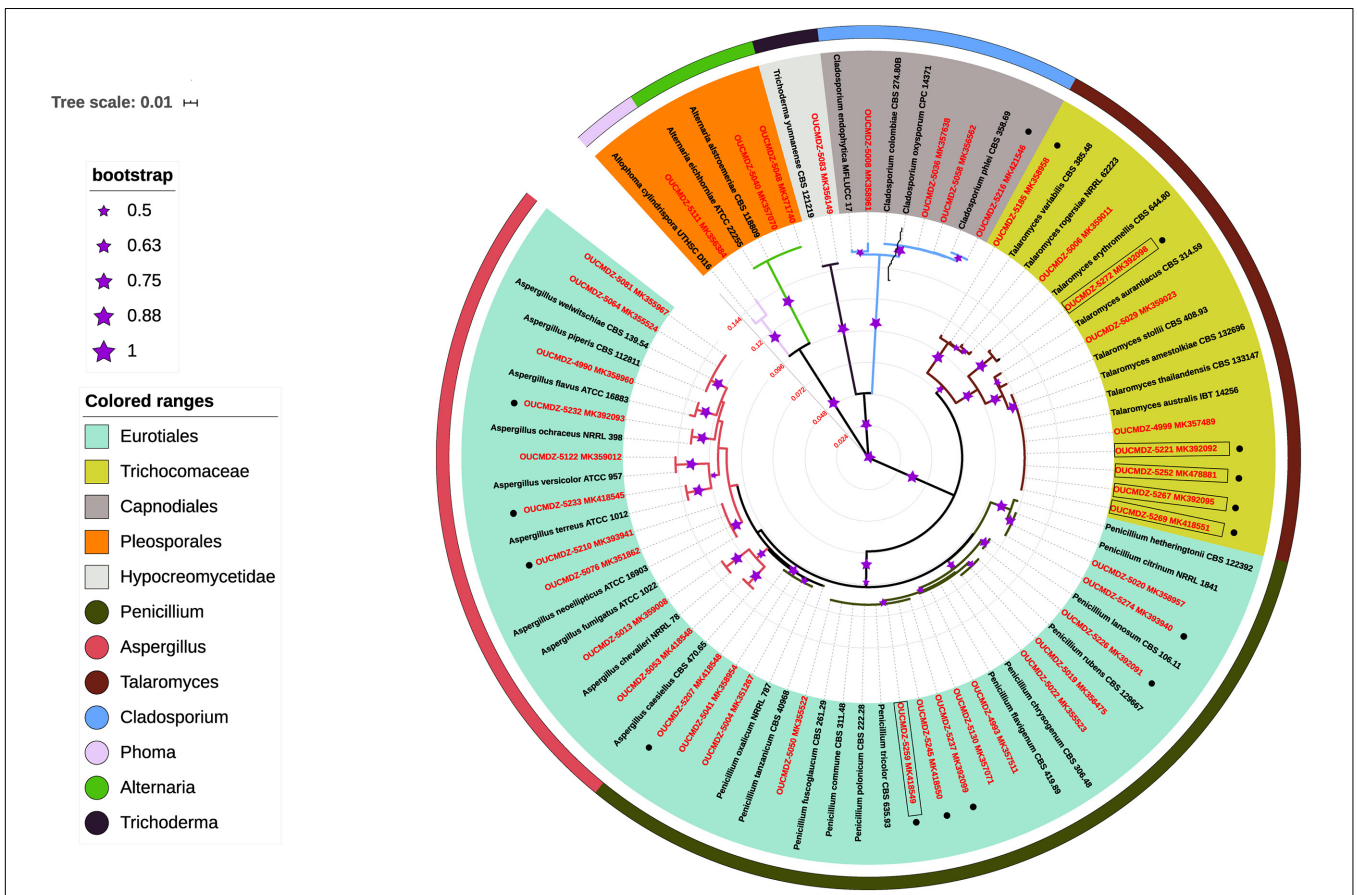

FIGURE 2 | Phylogenetic relationship of 41 representative fungal isolates based on ITS rDNA gene sequences using the neighbor-joining method. The scale bar represents 0.01 substitutions per nucleotide. Different orders and genera are represented by different colors. The size of the asterisk indicates different bootstrap values from 1000 replicates (a larger asterisk means a higher credibility). The red label indicates the strains isolated from the experiment, and the black label indicates the reference strains in the database. Acidophilic fungi are represented by boxes. The strains obtained under pH 3.0 are indicated by black spots.

could not survive at pH 2.0 or 3.0. The six isolates (OUCMDZ-5221, 5252, 5259, 5267, 5269, and 5272) can be characterized as acidophilic fungi that cannot survive in a neutral environment and have optimal growth at pH values between 2 and 5, and interestingly, all these six isolates belonged to the genus *Talaromyces*. These results came from the unrooted phylogenetic tree constructed with β-tubulin gene sequences (**Figure 3**).

All six acidophilic fungi were clustered in the branch of the genus *Talaromyces*. We summarized all the references on isolation and identification of *Talaromyces* since 2015 and found that no acidic culture conditions were involved in the isolation and culture process (including 34 new species of *Talaromyces*) (Adhikari et al., 2015; Visagie et al., 2015; Chen et al., 2016; Luo et al., 2016; Yilmaz et al., 2016a,b; Barbosa et al., 2018; Jiang et al., 2018; Rajeshkumar et al., 2019). However, in our experiments, all six acidophilic fungi isolates belonged to the genus *Talaromyces*. It was almost impossible to isolate these strains under neutral conditions. Although it was difficult to conclude whether the acidophilic fungi *Talaromyces* isolated by us were new species or not, these results revealed the acidophilic properties of the genus *Talaromyces* for the first time. This indicates that more samples of *Talaromyces* could be separated under acidic conditions.

The secondary metabolites of this genus have shown great potential in their chemical and bioactive diversity. Terpenoids, alkaloids, and polyketides with multiple bioactivities (including antibiotic, cytotoxic, and anti-HBV activity) have been reported as metabolites from *Talaromyces* (Hayashi et al., 2012; Kumar et al., 2013; Wu et al., 2015; Zhai et al., 2015; Fu et al., 2016; Guo et al., 2016; Xie et al., 2016; Zhao et al., 2016, 2019; Zhi et al., 2016; Cai et al., 2017; Küppers et al., 2017; Chen et al., 2018; Wang et al., 2018), with another review paper published in 2020 (Lan and Wu, 2020). Our investigation provides good

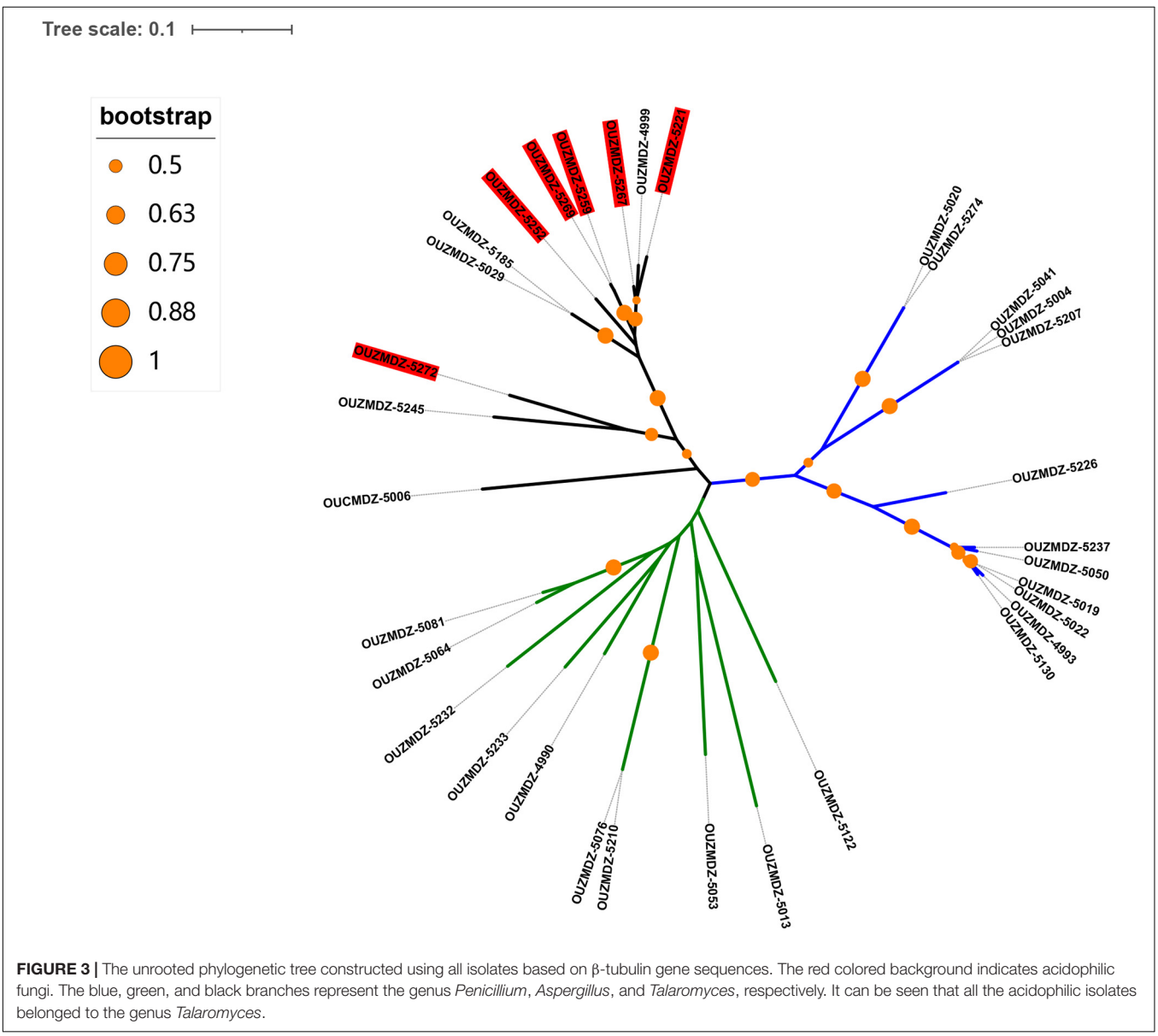

FIGURE 3 | The unrooted phylogenetic tree constructed using all isolates based on β-tubulin gene sequences. The red colored background indicates acidophilic fungi. The blue, green, and black branches represent the genus *Penicillium*, *Aspergillus*, and *Talaromyces*, respectively. It can be seen that all the acidophilic isolates belonged to the genus *Talaromyces*.

indications for future studies on the metabolites of this genus, which require further exploration. The mangrove sediments in Thailand are the best source of acid-tolerant microbes for investigating the acidophilic properties and diverse metabolites of the genus *Talaromyces*.

Bioactive Diversity of Aciduric Fungi Derived From Thai Mangrove Sediment

Forty-one representative fungi were fermented in a PDB medium at pH 3.0 and/or pH 7.0 based on the results of the growth of the isolates in the acid resistance assessment (detailed in **Supplementary Table 1**). All of the EtOAc extracts were tested for antimicrobial activity against nine aquatic and eight human pathogenic microbes. Nearly a quarter of the samples showed inhibitory effects (**Table 3**). The fungal strain OUCMDZ-5130 displayed broad-spectrum inhibitory effects against *C. albicans*, *C. glabrata*, *E. coli*, *V. alginolyticus*, *P. nigrifaciens*, *V. splendidus*, *S. aureus subsp. aureus* Rosenbach, *E. tarda*, and *B. cereus*. The strains OUCMDZ-5081, 5210, 5233, and 5245 showed weak antibacterial activity against the aquatic pathogens *P. nigrifaciens* and *V. alginolyticus*,

TABLE 3 | The antimicrobial activity of acid-tolerant fungal EtOAc extracts at 1000 μg/mL [a,b].

Strain No.	*C. albicans*	*C. glabrata*	*E. coli*	*V. alginolyticus*[d]	*P. nigrifaciens*[d]	*V. splendidus*[d]	*S. aureus*	*E. tarda*[d]	*B. cereus*[d]
OUCMDZ-5130	+	+	+++	++	+	−	++	++	+
OUCMDZ-5081	−	−	−	+	+	−	−	−	−
OUCMDZ-5210[c]	−	−	−	+	+	−	−	−	−
OUCMDZ-5233[c]	−	−	−	+	+	−	−	−	−
OUCMDZ-5245[c]	−	−	−	+	+	−	−	−	−
OUCMDZ-5048	−	−	−	−	+	−	−	−	−
OUCMDZ-5064	−	−	−	−	+	−	−	−	−
OUCMDZ-5040	−	−	−	−	−	+	−	−	+++
OUCMDZ-5020	−	−	−	−	+	−	−	−	++
OUCMDZ-4993	−	−	+	−	−	+	−	−	++

[a] *+++strong: inhibition zone diameter (IZD) ≥18 mm; ++moderate: IZD = 10–17 mm; + weak: IZD < 10 mm; − non-active: IZD = 0 mm.* [b] *IDZs of ciprofloxacin (positive control of bacteria) at 100 μg/mL were 18, 20, 21, 18, 21, 20, and 17 mm for E. coli, V. alginolyticus, P. nigrifaciens, V. splendidus, S. aureus Rosenbach, E. tarda, B. cereus, respectively. IDZs of ketoconazole (positive control of C. albicans and C. glabrata) at 100 μg/mL were 19, 22mm.* [c] *The fungal strains were fermented in PDA liquid medium at pH 3. Other fungal strains were fermented at pH 7.* [d] *Aquatic pathogens, the others were human pathogens.*

TABLE 4 | Cytotoxicity of acid-tolerant fungal EtOAc extracts at 100 μg/mL.

Strain No.	A549(%)	MCF-7(%)	Strain No.	A549(%)	MCF-7(%)
OUCMDZ-4993	34% ± 0.98	31% ± 1.09	OUCMDZ-5083	95% ± 1.43	75% ± 1.35
OUCMDZ-4990	83% ± 0.78	42% ± 1.02	OUCMDZ-5111	36% ± 0.65	17% ± 0.86
OUCMDZ-4999	45% ± 1.78	4% ± 0.36	OUCMDZ-5122	46% ± 1.23	4% ± 1.20
OUCMDZ-5004	84% ± 1.97	52% ± 1.05	OUCMDZ-5130	10% ± 0.23	30% ± 0.68
OUCMDZ-5006	61% ± 1.57	29% ± 0.79	OUCMDZ-5185[a]	47% ± 1.03	43% ± 1.09
OUCMDZ-5008	−105% ± 1.45	42% ± 0.79	OUCMDZ-5207[a]	53% ± 1.98	−68% ± 0.67
OUCMDZ-5013	71% ± 0.98	76% ± 0.86	OUCMDZ-5210[a]	27% ± 0.78	46% ± 0.32
OUCMDZ-5019	47% ± 1.62	22% ± 1.89	OUCMDZ-5216[a]	58% ± 0.67	44% ± 0.45
OUCMDZ-5020	45% ± 0.56	37% ± 1.79	OUCMDZ-5221[a]	87% ± 0.97	80% ± 0.78
OUCMDZ5022	65% ± 1.79	1% ± 1.90	OUCMDZ-5226[a]	84% ± 0.84	31% ± 0.45
OUCMDZ-5029	18% ± 1.45	19% ± 0.78	OUCMDZ-5232[a]	85% ± 0.78	54% ± 1.09
OUCMDZ-5036	21% ± 1.27	21% ± 1.67	OUCMDZ-5233[a]	91% ± 1.65	53% ± 0.12
OUCMDZ-5040	40% ± 1.68	53% ± 1.07	OUCMDZ-5237[a]	86% ± 1.79	82% ± 0.95
OUCMDZ-5041	83% ± 0.93	62% ± 0.54	OUCMDZ-5245[a]	86% ± 1.45	67% ± 1.35
OUCMDZ-5048	92% ± 0.79	−140% ± 0.56	OUCMDZ-5252[a]	43% ± 0.12	23% ± 0.45
OUCMDZ-5050	54% ± 0.98	51% ± 0.87	OUCMDZ-5259[a]	88% ± 0.67	57% ± 0.45
OUCMDZ-5053	−243% ± 1.67	25% ± 0.56	OUCMDZ-5267[a]	55% ± 0.69	44% ± 0.36
OUCMDZ-5058	40% ± 0.93	16% ± 0.98	OUCMDZ-5269[a]	71% ± 1.09	21% ± 0.98
OUCMDZ-5064	87% ± 1.23	47% ± 1.05	OUCMDZ-5272[a]	33% ± 1.08	54% ± 1.23
OUCMDZ-5076	76% ± 0.78	59% ± 0.97	OUCMDZ-5274[a]	80% ± 1.98	59% ± 1.45
OUCMDZ-5081	82% ± 0.67	24% ± 0.67			

Each datum represents the average inhibition and the standard deviation of three independent experiments. [a] *The fungal strains were fermented in PDA liquid medium at pH 3. Other fungal strains were fermented at pH 7.*

TABLE 5 | Anti-H1N1 activities of acid-tolerant fungal EtOAc extracts at 50 μg/ml [a].

Strain No.	Inhibition (%)	Strain No.	Inhibition (%)
OUCMDZ-5008	25% ± 0.32	OUCMDZ-5040	42% ± 1.07
OUCMDZ-5013	17% ± 1.45	OUCMDZ-5048	23% ± 0.69
OUCMDZ-5022	14% ± 0.67	OUCMDZ-5083	12% ± 1.09
OUCMDZ-5029	14% ± 0.98	OUCMDZ-5111	20% ± 1.56

The cytotoxicity of the sample against the MDCK cell was less than zero percent. Each datum represents the average inhibition and standard deviation of three independent experiments. The strains with an inhibition rate of less than 5% were considered to be inactive and are not presented in the table. [a] The fungal strains were fermented in PDA liquid medium at pH 7.

while the strains OUCMDZ-4993, 5020, and 5040 showed moderate antibacterial activity against the aquatic pathogen *B. cereus*. These fungi inhibited more aquatic pathogens than human pathogens.

The extracts were also evaluated for cytotoxicity against A549 and MCF-7 tumor cell lines at a concentration of 100 μg/mL (**Table 4**). The positive control adriamycin (1 μM) showed 80 and 72% inhibition of A549 and MCF-7 cells, respectively. The strains, which produced extracts that showed more than 50% inhibition, were defined as active strains. The results showed that 26 of the fungal strains (63.4%) were active, 13 of which had been fermented at pH 3. Eight strains, OUCMDZ-5013, 5041, 5076, 5083, 5221, 5237, 5245, and 5274, showed more than 60% inhibition of both A549 and MCF-7 cell lines. The strains OUCMDZ-5048 and 5207 only showed inhibitory activity against A549 cells with 92 and 53% inhibition, respectively. The strains OUCMDZ-5053 and 5008 stimulated the proliferation of A549 cells and inhibited the growth of MCF-7 cells.

Extracts of 41 fungi were evaluated for cytotoxicity against MDCK cell lines and the results showed that 28 strains (68.2%) were not cytotoxic at a concentration of 50 μg/mL. These non-cytotoxic strains were then selected to test for anti-H1N1 virus activity at the same concentration (**Table 5**). Eight strains, OUCMDZ-5008, 5013, 5022, 5029, 5040, 5048, 5083, and 5111, showed anti-H1N1 virus activity, among which OUCMDZ-5040 was the most active against the H1N1 virus with 42.1% inhibition, while the positive control, ribavirin, showed 47.0% inhibition at 50 μg/mL. Interestingly, all the strains with anti-H1N1 virus activity were fermented under neutral conditions (pH 7.0), which was different from the results relating to the anti-tumor activity (where 50.0% of the strains were fermented at pH 3.0).

The antimicrobial, cytotoxicity and antiviral activities of all the isolated aciduric and acidophilic fungal metabolites were evaluated. Nearly three-quarters of the fermentation extracts (26/41) showed cytotoxicity against A549 or/and MCF-7 cells, while less than a quarter of the isolates showed antimicrobial (10/41) or anti-H1N1 virus (8/41) activity (**Figure 4**). Most of the cytotoxic isolates were fermented under acidic conditions (pH 3), while all the isolates with anti-H1N1 virus activity were fermented under neutral conditions (pH 7.0). The metabolites of these acid-tolerant fungi did not show obvious antibacterial and antiviral activities but showed outstanding cytotoxic activities. These results suggest that an extremely acidic environment was not conducive to the growth of common microorganisms. However, these extreme conditions did not affect the survival of the acid-tolerant fungi, leading to the production of cytotoxic metabolites through population competition. These cytotoxic substances could potentially help mangrove plants to resist being eaten by other animals. More strains had inhibitory activity against aquatic pathogens than against human pathogens, which may be because the fungi exist in the rhizosphere environment of mangrove plants and protect the mangroves against pathogens.

The Metabolites From *Penicillium* sp. OUCMDZ-5207 at pH 3

The fungus strain OUCMDZ-5207 was identified as *Penicillium* according to the morphology and ITS sequences (Accession No. MK418548). No significant differences were observed in the growth or spore germination of OUCMDZ-5207 cultured at pH 3 and pH 7, but differences were found in

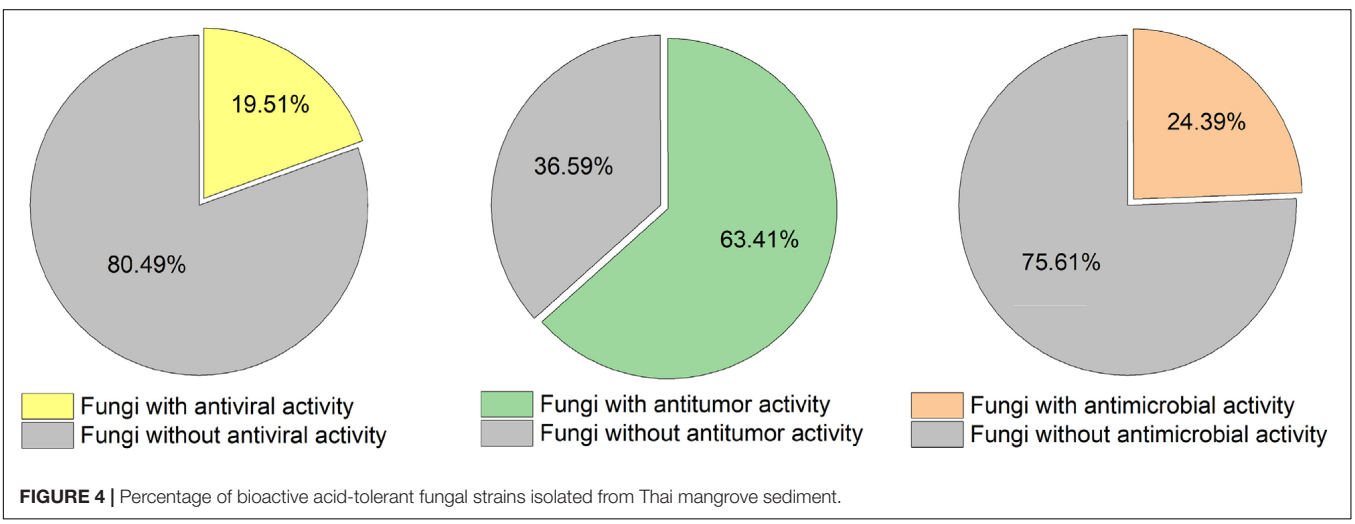

FIGURE 4 | Percentage of bioactive acid-tolerant fungal strains isolated from Thai mangrove sediment.

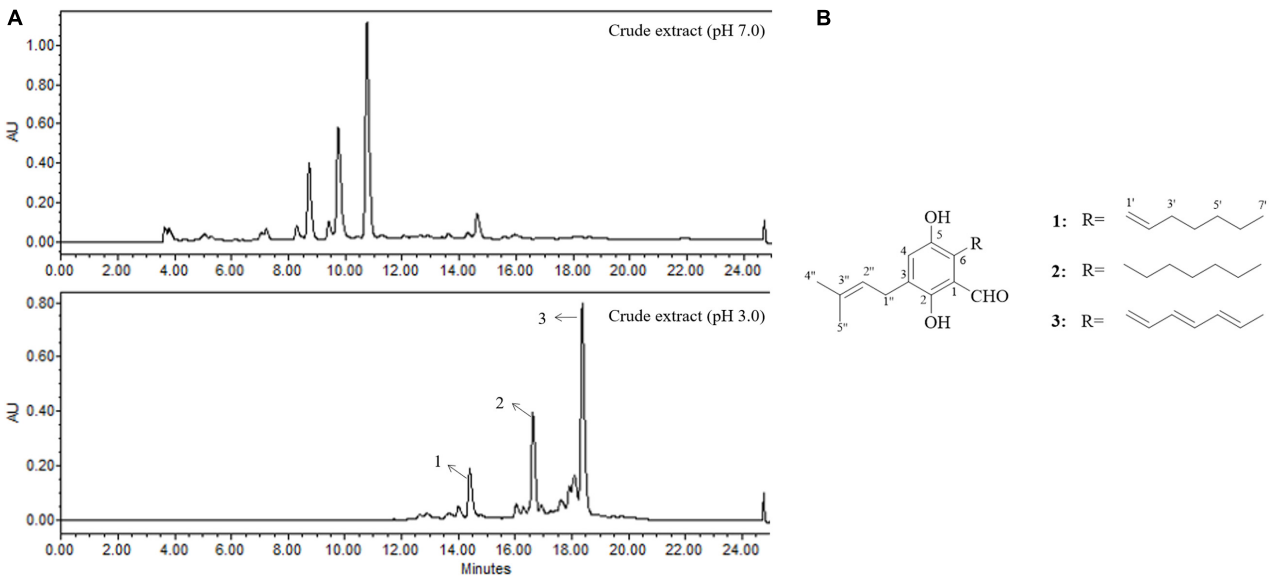

FIGURE 5 | (A) The HPLC profile of secondary metabolites from OUCMDZ-5207 at pH 7.0 and pH 3.0 (HPLC gradient elution: 0–25 min, 10–100% CH_3OH; UV wavelength: 300 nm; flow rate: 1 mL/min). **(B)** The chemical structures of compounds **1**–**3**.

the chemical diversity and the biomass under the acidic and neutral conditions (**Figure 5**). The EtOAc extracts fermented at pH 3 showed selective inhibitory activity against A549 cells with a 53% inhibition rate compared with a weak proliferative effect on MCF-7 cells. The metabolite yield at pH 3.0 (3.1240 g/L) far exceeded that at pH 7.0 (0.1236 g/L). Furthermore, compounds with retention times from 14 to 20 min were only produced at pH 3.0. Thus, strain OUCMDZ-5207 fermented at pH 3.0 was selected for chemical study, which resulted in the isolation and identification of three compounds that were only produced at pH 3.0, tetrahydroauroglaucin (**1**), flavoglaucin (**2**), and auroglaucin (**3**) (**Figure 5**; Miyake et al., 2009). Compounds 1–3 at a concentration of 10 μM showed cytotoxic activity against A549 and MCF-7 cells with 42 ± 0.96% and 53 ± 1.03%, 32 ± 0.45% and 27 ± 0.53%, and 79 ± 0.89% and 48 ± 1.09% inhibition, respectively. Compound 3 was the most active against A549 cells with an IC_{50} value of 5.67 μM (IC_{50} = 0.61 μM for the positive control, adriamycin). Compounds **1**–**3** have been previously reported to show good antimicrobial and antimalarial bioactivity, inhibition of LPS (Lipopolysaccharide)-induced NO release and opioid and cannabinoid receptor binding activity, and cytotoxicity against SF-268, MCF-7, NCI-H460, HeLa, and HepG-2 cells (Hamasaki et al., 1981; Miyake et al., 2009; Gao et al., 2011, 2012; Kim et al., 2014; Dzoyem et al., 2015; Liang et al., 2018; Elissawy et al., 2019).

To the best of our knowledge, there have been no previous reports of compounds **1**–**3** outlining that they exhibit cytotoxicity against A549. In the present study, compound **3** demonstrated strong selective inhibition against A549. When the environmental pH changed, the fungi respond to the ambient pH and transmit pH signals to the nucleus through transcriptional regulators, thereby regulating a series of gene expressions including secondary metabolite gene clusters. It has also been reported that pH sensing in filamentous fungi relies mainly on the regulatory pathway PacC, a global regulator of fungi, which regulates the transcription of secondary metabolite-related genes, such as aflatoxin, cephalosporin, and penicillin (Brakhage, 2013). This is a complex regulation system and it was difficult to conclude if this regulation system was related to our experimental results. However, these results do suggest that acid stress can activate silent gene clusters to expand the diversity of secondary metabolites and this strategy will lead to potential medicinal discovery.

CONCLUSION

Our investigation indicated that mangroves in Thailand are rich in aciduric and acidophilic microbial resources. These acid-tolerant microorganisms are potential medicinal resources. Acid stress can activate silent gene clusters to produce secondary metabolites that cannot be obtained under neutral conditions, which could be a useful strategy for expanding the diversity of available metabolites for potential medicinal use.

DATA AVAILABILITY STATEMENT

The datasets presented in this study can be found in online repositories. The names of the repository/repositories and accession number(s) can be found in **Table 2**.

AUTHOR CONTRIBUTIONS

All authors listed have made a substantial, direct and intellectual contribution to the work, and approved it for publication.

FUNDING

This work was supported by grants from the National Natural Science Foundation of China (No. 81973198), the Key Research and Development Program of Shandong (No. 2018GSF118070), and the National Science and Technology Major Project for Significant New Drug Development (No. 2018ZX09735004).

SUPPLEMENTARY MATERIAL

The Supplementary Material for this article can be found online at: https://www.frontiersin.org/articles/10.3389/fmicb.2020.609952/full#supplementary-material

REFERENCES

Adhikari, M., Yadav, D. R., Kim, S., Um, Y. H., Kim, H. S., Lee, H. B., et al. (2015). Discovery of two new talaromyces species from crop field soil in korea. *Mycobiology* 43, 402–407. doi: 10.5941/MYCO.2015.43.4.402

Am-In, S., Limtong, S., Yongmanitchai, W., and Jindamorakot, S. (2011). *Candida andamanensis* sp. nov., *Candida laemsonensis* sp. nov. and *Candida ranongensis* sp. nov., anamorphic yeast species isolated from estuarine waters in a Thai mangrove forest. *Int. J. Syst. Evol. Micr.* 61, 454–461. doi: 10.1099/ijs.0.022038-0

Am-In, S., Yongmanitchai, W., and Limtong, S. (2008). *Kluyveromyces siamensis* sp. nov., an ascomycetous yeast isolated from water in a mangrove forest in Ranong province, Thailand. *FEMS Yeast Res.* 8, 823–828. doi: 10.1111/j.1567-1364.2008.00396.x

Atipan, S., Akio, T., Vorasan, S., and Suppasil, M. (2012). Mangrove sediment, a new source of potential biosurfactant-producing bacteria. *Ann. Microbiol.* 62, 1669–1679. doi: 10.1007/s13213-012-0424-9

Barbosa, R. N., Bezerra, J. D. P., Souza-Motta, C. M., Frisvad, J. C., Samson, R. A., Oliveira, N. T., et al. (2018). New *Penicillium* and *Talaromyces* species from honey, pollen and nests of stingless bees. *Antonie Van Leeuwenhoek* 111, 1883–1912. doi: 10.1007/s10482-018-1081-1

Brakhage, A. A. (2013). Regulation of fungal secondary metabolism. *Nat. Rev. Microbiol.* 11, 21–32. doi: 10.1038/nrmicro2916

Cai, R. L., Chen, S. H., Long, Y. H., Li, C. H., Huang, X. S., and She, Z. G. (2017). Depsidones from *Talaromyces stipitatus* SK-4, an endophytic fungus of the mangrove plant *Acanthus ilicifolius*. *Phytochem. Lett.* 20, 196–199. doi: 10.1016/j.phytol.2017.04.023

Carbone, I., and Kohn, L. M. (1999). A method for designing primer sets for speciation studies in filamentous ascomycetes. *Mycologia* 91, 553–556. doi: 10.1080/00275514.1999.12061051

Chen, A. J., Sun, B. D., Houbraken, J., Frisvad, J. C., Yilmaz, N., Zhou, Y. G., et al. (2016). New *Talaromyces* species from indoor environments in China. *Stud. Mycol.* 84, 119–144. doi: 10.1016/j.simyco.2016.11.003

Chen, S. H., Ding, M., Liu, W. Y., Huang, X. S., Liu, Z. M., Lu, Y. J., et al. (2018). Anti-inflammatory meroterpenoids from the mangrove endophytic fungus, *Talaromyces amestolkiae*, YX1. *Phytochemistry* 146, 8–15. doi: 10.1016/j.phytochem.2017.11.011

Deshmukh, R., Khardenavis, A. A., and Purohit, H. J. (2016). Diverse metabolic capacities of fungi for bioremediation. *Indian J. Microbiol.* 56, 247–264. doi: 10.1007/s12088-016-0584-6

Dzoyem, J. P., Lannang, A. M., Fouotsa, H., Mbazoa, C. D., Nkengfack, A. E., Sewald, N., et al. (2015). Anti-inflammatory activity of benzophenone and xanthone derivatives isolated from *Garcinia* (*Clusiaceae*) species. *Phytochem. Lett.* 14, 153–158. doi: 10.1016/j.phytol.2015.10.003

Elissawy, A. M., Ebada, S. S., Ashour, M. L., Ei-Neketi, M., Ebrahim, W., and Singab, A. B. (2019). New secondary metabolites from the mangrove-derived fungus *Aspergillus* sp. AV-2. *Phytochem. Lett.* 29, 1–5. doi: 10.1016/j.phytol.2018.10.014

Fan, Y. Q., Wang, Y., Fu, P., Arthit, C., Pawinee, P., and Zhu, W. M. (2018). Secopaxilline A, an indole-diterpenoid derivative from an aciduric *Penicillium fungus*, its identification and semisynthesis. *Org. Chem. Front.* 5, 2835–2839. doi: 10.1039/c8qo00756j

Fan, Y. Q., Wang, Y., Liu, P. P., Fu, P., Zhu, T. H., Wang, W., et al. (2013). Indole-diterpenoids with Anti-H1N1 activity from the aciduric fungus *Penicillium camemberti* OUCMDZ-1492. *J. Nat. Prod.* 76, 1328–1336. doi: 10.1021/np400304q

Fu, G. C., Yang, Z. D., Zhou, S. Y., Li, X. M., Yu, H. T., Yao, X. J., et al. (2016). Wortmannines A-C, three novel wortmannin derivatives with an unusual five-membered B ring from the endophytic fungus *Talaromyces wortmannii* LGT-4. *Tetrahedron Lett.* 57, 4608–4611. doi: 10.1016/j.tetlet.2016.09.004

Gao, J. T., León, F., Radwan, M. M., Dale, O. R., Husni, A. S., Manly, S. P., et al. (2011). Benzyl derivatives with in vitro binding affinity for human opioid and cannabinoid receptors from the fungus *Eurotium repens*. *J. Nat. Prod.* 74, 1636–1639. doi: 10.1021/np200147c

Gao, J. T., Radwan, M. M., León, F., Wang, X. N., Jacob, M. R., Tekwani, B. L., et al. (2012). Antimicrobial and antiprotozoal activities of secondary metabolites from the fungus *Eurotium repens*. *Med. Chem. Res.* 21, 3080–3086. doi: 10.1007/s00044-011-9798-7

Gardes, M., and Bruns, T. D. (1993). ITS primer with enhanced specificity for basidiomycetes application to the identification of mycorrizae and rusts. *Mol. Ecol.* 2, 113–118. doi: 10.1111/j.1365-294X.1993.tb00005.x

Glass, N. L., and Donaldson, G. C. (1995). Development of primer sets designed for use with the PCR to amplify conserved genes from filamentous ascomycetes. *Appl. Environ. Microb.* 61, 1323–1330. doi: 10.1128/aem.61.4.1323-1330.1995

Guo, J., Ran, H. M., Zeng, J., Liu, D., and Xin, Z. H. (2016). Tafuketide, a phylogeny-guided discovery of a new polyketide from *Talaromyces funiculosus* Salicorn 58. *Appl. Microbiol. Biotechnol.* 100, 5323–5338. doi: 10.1007/s00253-016-7311-4

Hamasaki, T., Kimura, Y., Hatsuda, Y., and Nagao, M. (1981). Structure of a new metabolite, dihydroauroglaucin, produced by *Aspergillus chevalieri*. *Agric. Biol. Chem.* 45, 313–314. doi: 10.1080/00021369.1981.10864508

Hayashi, H., Oka, Y., Kai, K., and Akiyama, K. (2012). New chrodrimanin congeners, chrodrimanins D-H, from YO-2 of *Talaromyces* sp. *Biosci. Biotechnol. Biochem.* 76, 1765–1768. doi: 10.1271/bbb.120365

H-Kittikun, A., Biscola, V., El-Ghaish, S., Jaffrès, E., Dousset, X., Pillot, G., et al. (2015). Bacteriocin-producing *Enterococcus faecalis* KT2W2G isolated from mangrove forests in southern Thailand: purification, characterization and safety evaluation. *Food Control* 54, 126–134. doi: 10.1016/j.foodcont.2014.12.037

Hujslová, M., Bystrianský, L., Benada, O., and Gryndler, M. (2019). Fungi, a neglected component of acidophilic biofilms: do they have a potential for biotechnology? *Extremophiles* 23, 267–275. doi: 10.1007/s00792-019-01085-9

Hwanhlem, N., Chobert, J. M., and H-Kittikun, A. (2014). Bacteriocin-producing lactic acid bacteria isolated from mangrove forests in southern Thailand as potential bio-control agents in food: isolation, screening and optimization. *Food Control* 41, 202–211. doi: 10.1016/j.foodcont.2014.01.021

Jiang, X., Yu, Z., Ruan, Y., and Wang, L. (2018). Three new species of *Talaromyces* sect. Talaromyces discovered from soil in China. *Sci. Rep.* 8:4932. doi: 10.1038/s41598-018-23370-x

Jin, Y. Z., Qin, S. D., Gao, H., Zhu, G. L., Wang, W., Zhu, W. M., et al. (2018). An anti-HBV anthraquinone from aciduric fungus *Pennicillium* sp. OUCMDZ-4736 under low pH stress. *Extremophiles* 22, 39–45. doi: 10.1007/s00792-017-0975-6

Johnson, D. B. (1998). Biodiversity and ecology of acidophilic microorganisms. *FEMS Microbiol. Ecol.* 27, 307–317. doi: 10.1111/j.1574-6941.1998.tb00547.x

Kim, K. S., Cui, X., Lee, D. S., Ko, W., Sohn, J. H., Yim, J. H., et al. (2014). Inhibitory effects of benzaldehyde derivatives from the marine fungus *Eurotium* sp. SF-5989 on inflammatory mediators via the induction of heme oxygenase-1

in lipopolysaccharide-stimulated RAW264.7 macrophages. *Int. J. Mol. Sci.* 15, 23749–23765. doi: 10.3390/ijms151223749

Kumar, M., Qadri, M., Sharma, P. R., Kumar, A., Andotra, S. S., Kaur, T., et al. (2013). Tubulin inhibitors from an endophytic fungus isolated from *Cedrus deodara*. *J. Nat. Prod.* 76, 194–199. doi: 10.1021/np3006666

Küppers, L., Ebrahim, W., El-Neketi, M., Özkaya, F. C., Mándi, A., Kurtán, T., et al. (2017). Lactones from the sponge-derived fungus *Talaromyces rugulosus*. *Mar. Drugs* 15:359. doi: 10.3390/md15110359

Lan, D., and Wu, B. (2020). Chemistry and bioactivities of secondary metabolites from the genus *Talaromyces*. *Chem. Biodivers.* 17, e2000229. doi: 10.1002/cbdv.202000229

Li, D. L., Li, X. M., Li, T. G., Dang, H. Y., Proksch, P., and Wang, B. G. (2008). Benzaldehyde derivatives from *Eurotium rubrum*, an endophytic fungus derived from the mangrove plant *Hibiscus tiliaceus*. *Chem. Pharm. Bull.* 56, 1282–1285. doi: 10.1248/cpb.56.1282

Li, D. L., Li, X. M., Proksch, P., and Wang, B. G. (2010). 7-O-Methylvariecolortide A, a new spirocyclic diketopiperazine alkaloid from a marine mangrove derived endophytic fungus, *Eurotium rubrum*. *Nat. Prod. Commun.* 5, 1583–1586. doi: 10.1177/1934578X1000501014

Liang, T. M., Fang, Y. W., Zheng, J. Y., and Shao, C. L. (2018). Secondary metabolites isolated from the gorgonian-derived fungus *Aspergillus ruber* and their antiviral activity. *Chem. Nat. Compd.* 54, 559–561. doi: 10.1007/s10600-018-2406-z

Limtong, S., Yongmanitchai, W., Kawasaki, H., and Seki, T. (2007). *Candida thaimueangensis* sp. nov., an anamorphic yeast species from estuarine water in a mangrove forest in Thailand. *Int. J. Syst. Evol. Micr.* 57, 650–653. doi: 10.1099/ijs.0.64698-0

Limtong, S., Yongmanitchai, W., Kawasaki, H., and Seki, T. (2008). *Candida phangngensis* sp. nov., an anamorphic yeast species in the Yarrowia clade, isolated from water in mangrove forests in Phang-Nga Province, Thailand. *Int. J. Syst. Evol. Micr.* 58, 515–519. doi: 10.1099/ijs.0.65506-0

Lin, Y. W., Wang, L. P., Wang, Y., Wang, W., Hao, J. J., and Zhu, W. M. (2015). Bioactive natural products of *Aspergillus* sp. OUCMDZ-1914, an aciduric fungus from the mangrove soils. *Chin. J. Org. Chem.* 35, 1955–1960. doi: 10.6023/cjoc201504007

Luo, Y., Lu, X., Bi, W., Liu, F., and Gao, W. (2016). *Talaromyces rubrifaciens*, a new species discovered from heating, ventilation and air conditioning systems in China. *Mycologia* 108, 773–779. doi: 10.3852/15-233

Miyake, Y., Ito, C., Itoigawa, M., and Osawa, T. (2009). Antioxidants produced by *Eurotium herbariorum* of filamentous fungi used for the manufacture of karebushi, dried bonito (Katsuobushi). *Biosci. Biotechnol. Biochem.* 73, 1323–1327. doi: 10.1271/bbb.80887

Mosmann, T. (1983). Rapid colorimetric assay for cellular growth and survival: application to proliferation and cytotoxicity assays. *J. Immunol. Methods* 65, 55–63. doi: 10.1016/0022-1759(83)90303-4

O' Donnell, K., Nirenberg, H. I., Aoki, T., and Cigelnik, E. (2000). A Multigene phylogeny of the *Gibberella fujikuroi* species complex: detection of additional phylogenetically distinct species. *Mycoscience* 41, 61–78. doi: 10.1007/bf02464387

Peng, X. P., Wang, Y., Kunlai, S., Liu, P. P., Yin, X., and Zhu, W. M. (2011a). Cerebrosides and 2-Pyridone Alkaloids from the Halotolerant Fungus *Penicillium chrysogenum* grown in a hypersaline medium. *J. Nat. Prod.* 74, 1298–1302. doi: 10.1021/np1008976

Peng, X. P., Wang, Y., Liu, P. P., Hong, K., Chen, H., Yin, X., et al. (2011b). Aromatic compounds from the halotolerant fungal strain of *Wallemia sebi* PXP-89 in a hypersaline medium. *Arch. Pharm. Res.* 34, 907–912. doi: 10.1007/s12272-011-0607-0

Peng, X. P., Wang, Y., Zhu, G. L., and Zhu, W. M. (2018). Fatty acid derivatives from the halotolerant fungus *Cladosporium cladosporioides*. *Magn. Reson. Chem.* 56, 18–24. doi: 10.1002/mrc.4659

Qin, S. D., Wang, Y., Wang, W., and Zhu, W. M. (2016). Anti-H1N1-virus secondary metabolites from mangrove-derived aciduric fungus *Penicillium* sp. OUCMDZ-4736. *Chin. J. Mar. Drugs* 15, 21–28.

Rajeshkumar, K. C., Yilmaz, N., Marathe, S. D., and Seifert, K. A. (2019). Morphology and multigene phylogeny of *Talaromyces amyrossmaniae*, a new synnematous species belonging to the section Trachyspermi from India. *Mycokeys* 45, 41–56. doi: 10.3897/mycokeys.45.32549

Songsumanus, A., Tanasupawat, S., Igarashi, Y., and Kudo, T. (2013). *Micromonospora maritima* sp. nov., isolated from mangrove soil. *Int. J. Syst. Evol. Micr.* 63, 554–559. doi: 10.1099/ijs.0.039180-0

Stierle, A. A., Stierle, D. B., Decato, D., Priestley, N. D., Alverson, J. B., Hoody, J. et al. (2017). The berkeleylactones, antibiotic macrolides from fungal coculture. *J. Nat. Prod.* 80, 1150–1160. doi: 10.1021/acs.jnatprod.7b00133

Tamura, G., Suzuki, S., Takatsuki, A., Ando, K., and Arima, K. (1968). Ascochlorin, a new antibiotic, found by paper-disk agar-diffusion method. I. Isolation, biological and chemical properties of ascochlorin. (Studies on antiviral and antitumor antibiotics. I). *J. Antibiot.* 21, 539–544. doi: 10.7164/antibiotics.21.539

Visagie, C. M., Yilmaz, N., Frisvad, J. C., Houbraken, J., Seifert, K. A., Samson, R. A., et al. (2015). Five new *Talaromyces* species with ampulliform-like phialides and globose rough walled conidia resembling T. *Verruculosus*. *Mycoscience* 56, 486–502. doi: 10.1016/j.myc.2015.02.005

Wanapaisan, P., Laothamteep, N., Vejarano, F., Chakraborty, J., Shintani, M., Muangchinda, C., et al. (2018). Synergistic degradation of pyrene by five culturable bacteria in a mangrove sediment-derived bacterial consortium. *J. Hazard. Mater.* 342, 561–570. doi: 10.1016/j.jhazmat.2017.08.062

Wang, H., Lu, Z., Qu, H., Liu, P., Miao, C., Zhu, T., et al. (2012). Antimicrobial aflatoxins from the marine-derived fungus *Aspergillus flavus* 092008. *Arch. Pharm. Res.* 35, 1387–1392. doi: 10.1007/s12272-012-0808-1

Wang, H., Wang, Y., Liu, P. P., Wang, W., Fan, Y. Q., and Zhu, W. M. (2013). Purpurides B and C, two new sesquiterpene esters from the aciduric fungus *Penicillium purpurogenum* JS03-21. *Chem. Biodivers.* 10, 1185–1192. doi: 10.1002/cbdv.201200175

Wang, H., Wang, Y., Wang, W., Fu, P., Liu, P. P., and Zhu, W. M. (2011a). Anti-influenza virus polyketides from the acid-tolerant fungus *Penicillium purpurogenum* JS03-21. *J. Nat. Prod.* 74, 2014–2018. doi: 10.1021/np2004769

Wang, Y., Lu, Z. Y., Sun, K. L., and Zhu, W. M. (2011b). Effects of high salt stress on secondary metabolites production in the marine-derived fungus *Spicaria elegans*. *Mar. Drugs* 9, 535–542. doi: 10.3390/md9040535

Wang, Y., Zheng, J. K., Liu, P. P., Wang, W., and Zhu, W. M. (2011c). Three new compounds from *Aspergillus terreus* PT06-2 grown in a high salt medium. *Mar. Drugs* 9, 1368–1378. doi: 10.3390/md9081368

Wang, M. M., Wang, S. Y., Wang, W., Wang, Y., Wang, H., and Zhu, W. M. (2017). Inhibition effects of novel polyketide compound PPQ-B against influenza A virus replication by interfering with the cellular EGFR pathway. *Antivir. Res.* 143, 74–84. doi: 10.1016/j.antiviral.2017.04.007

Wang, W. J., Wan, X., Liu, J., Wang, J. P., Zhu, H. C., Chen, C. C., et al. (2018). Two new terpenoids from *Talaromyces purpurogenus*. *Mar. Drugs* 16:150. doi: 10.3390/md16050150

Wang, W. L., Wang, Y., Tao, H. W. T., Peng, X. P., Liu, P. P., and Zhu, W. M. (2009). Cerebrosides of the halotolerant fungus Alternaria raphanin isolated from a sea salt field. *J. Nat. Prod.* 72, 1695–1698. doi: 10.1021/np9002299

Wang, Y., Fan, Y. Q., Wang, Y. N., and Zhu, W. M. (2017). Research progress of natural products from aciduric microbes. *Chin. J. Antibiot.* 42, 255–260.

White, T. J., Bruns, T., Lee, S., and Taylor, J. (1990). "Amplification and direct sequencing of fungal ribosomal RNA genes for phylogenetics. PCR protocols: a guide to methods and applications," in *PCR Protocols. A Guide to Methods and Applications*, eds M. A. Innis, D. H. Gelfand, J. J. Sninsky, and T. J. White (San Diego: Academic Press), 315–322.

Wilson, Z. E., and Brimble, M. A. (2009). Molecules derived from the extremes of life. *Nat. Prod. Rep.* 26, 44–71. doi: 10.1039/b800164m

Wongwongsee, W., Chareanpat, P., and Pinyakong, O. (2013). Abilities and genes for PAH biodegradation of bacteria isolated from mangrove sediments from the central of Thailand. *Mar. Pollut. Bull.* 74, 95–104. doi: 10.1016/j.marpolbul.2013.07.025

Wu, B., Ohlendorf, B., Oesker, V., Wiese, J., Malien, S., Schmaljohann, R., et al. (2015). Acetylcholinesterase inhibitors from a marine fungus *Talaromyces* sp. Strain LF458. *Mar. Biotechnol.* 17, 110–119. doi: 10.1007/s10126-014-9599-3

Xie, X. S., Fang, X. W., Huang, R., Zhang, S. P., Wei, H. X., and Wu, S. H. (2016). A new dimeric anthraquinone from endophytic *Talaromyces* sp. YE3016. *Nat. Prod. Res.* 30, 1706–1711. doi: 10.1080/14786419.2015.1136888

Yan, H., Gao, S., Li, C., Li, X., and Wang, B. (2010). Chemical constituents of a marine-derived endophytic fungus *Penicillium commune* G2M. *Molecules* 15, 3270–3275. doi: 10.3390/molecules15053270

Yan, H. J., Li, X. M., Li, C. S., and Wang, B. G. (2012). Alkaloid and anthraquinone derivatives produced by the marine-derived endophytic fungus *Eurotium rubrum*. *Helv. Chim. Acta.* 95, 163–168. doi: 10.1002/hlca.201100255

Yilmaz, N., López-Quintero, C. A., Vasco-Palacios, A. M., Frisvad, J. C., Theelen, B., Boekhout, T., et al. (2016a). Four novel *Talaromyces* species isolated from leaf litter from Colombian Amazon rain forests. *Mycol. Prog.* 15, 1041–1056. doi: 10.1007/s11557-016-1227-3

Yilmaz, N., Visagie, C. M., Frisvad, J. C., Houbraken, J., Jacobs, K., and Samson, R. A. (2016b). Taxonomic re-evaluation of species in *Talaromyces* section Islandici, using a polyphasic approach. *Persoonia* 36, 37–56. doi: 10.3767/003158516X688270

Zhai, M. M., Niu, H. T., Li, J., Xiao, H., Shi, Y. P., Di, D. L., et al. (2015). Talaromycolides A-C, novel phenyl-substituted phthalides isolated from the green chinese onion-derived fungus *Talaromyces pinophilus* AF-02. *J. Agr. Food. Chem.* 63, 9558–9564. doi: 10.1021/acs.jafc.5b04296

Zhao, J. W., Yang, Z. D., Zhou, S. Y., Yang, L. J., Sun, J. H., Yao, X. J., et al. (2019). Wortmannine F and G, two new pyranones from *Talaromyces wortmannii* LGT-4, the endophytic fungus of *Tripterygium wilfordii*. *Phytochem. Lett.* 29, 115–118. doi: 10.1016/j.phytol.2018.11.023

Zhao, Q. H., Yang, Z. D., Shu, Z. M., Wang, Y. G., and Wang, M. G. (2016). Secondary metabolites and biological activities of *Talaromyces* sp. LGT-2, an endophytic fungus from *Tripterygium wilfordii*. *Iran J. Pharm. Res.* 15, 453–457. doi: 10.22037/IJPR.2016.1873

Zheng, J. K., Wang, Y., Wang, J. F., Liu, P. P., Li, J., and Zhu, W. M. (2013). Antimicrobial ergosteroids and pyrrole derivatives from halotolerant *Aspergillus flocculosus* PT05-1 cultured in a hypersaline medium. *Extremophiles* 17, 963–971. doi: 10.1007/s00792-013-0578-9

Zheng, J. K., Xu, Z. H., Wang, Y., Hong, K., Liu, P. P., and Zhu, W. M. (2010). Cyclic Tripeptides from the halotolerant fungus *Aspergillus sclerotiorum* PT06-1. *J. Nat. Prod.* 73, 1133–1137. doi: 10.1021/np100198h

Zheng, J. K., Zhu, H. J., Hong, K., Wang, Y., Liu, P. P., Wang, X., et al. (2009). Novel cyclic hexapeptides from marine-derived fungus, *Aspergillus sclerotiorum* PT06-1. *Org. Lett.* 11, 5262–5265. doi: 10.1021/ol902197z

Zhi, K. K., Yang, Z. D., Zhou, S. Y., Yao, X. J., Li, S., and Zhang, F. (2016). A new furanosteroid from *Talaromyces* sp. lgt-4, a fungal endophyte isolated from *Tripterygium wilfordii*. *Nat. Prod. Res.* 30, 2137–2141. doi: 10.1080/14786419.2016.1138301

Conflict of Interest: The authors declare that the research was conducted in the absence of any commercial or financial relationships that could be construed as a potential conflict of interest.

frontiers in Microbiology

ORIGINAL RESEARCH
published: 28 January 2021
doi: 10.3389/fmicb.2020.630309

Multi-omics Comparative Analysis of *Streptomyces* Mutants Obtained by Iterative Atmosphere and Room-Temperature Plasma Mutagenesis

*Tan Liu[1], Zhiyong Huang[2], Xi Gui[1], Wei Xiang[1], Yubo Jin[1], Jun Chen[1] and Jing Zhao[1,3]**

[1] College of Ocean and Earth Science, Xiamen University, Xiamen, China, [2] Tianjin Institute of Industrial Biotechnology, Chinese Academy of Sciences, Tianjin, China, [3] Fujian Collaborative Innovation Center for Exploitation and Utilization of Marine Biological Resources, Xiamen, China

Sponges, the most primitive multicellular animals, contain a large number of unique microbial communities. Sponge-associated microorganisms, particularly actinomyces, have the potential to produce diverse active natural products. However, a large number of silent secondary metabolic gene clusters have failed to be revived under laboratory culture conditions. In this study, iterative atmospheric room-temperature plasma. (ARTP) mutagenesis coupled with multi-omics conjoint analysis was adopted to activate the inactive wild *Streptomyces* strain. The desirable exposure time employed in this study was 75 s to obtain the appropriate lethality rate (94%) and mutation positive rate (40.94%). After three iterations of ARTP mutagenesis, the proportion of mutants exhibiting antibacterial activities significantly increased by 75%. Transcriptome analysis further demonstrated that the differential gene expression levels of encoding type I lasso peptide aborycin had a significant upward trend in active mutants compared with wild-type strains, which was confirmed by LC-MS results with a relative molecular mass of 1082.43 ($[M + 2H]^{2+}$ at m/z = 2164.86). Moreover, metabolome comparative analysis of the mutant and wild-type strains showed that four spectra or mass peaks presented obvious differences in terms of the total ion count or extracting ion current profiles with each peak corresponding to a specific compound exhibiting moderate antibacterial activity against Gram-positive indicators. Taken together, our data suggest that the ARTP treatment method coupled with multi-omics profiling analysis could be used to estimate the valid active molecules of metabolites from microbial crudes without requiring a time-consuming isolation process.

Keywords: ARTP mutagenesis, awaken cryptic gene clusters, antibacterial activity, transcriptome comparative analysis, metabolome comparative analysis

OPEN ACCESS

Edited by:
Jinwei Zhang,
University of Exeter, United Kingdom

Reviewed by:
Liya Liang,
University of Colorado Boulder, United States
Hui Wang,
Shantou University, China

****Correspondence:***
Jing Zhao
sunnyzhaoj@xmu.edu.cn
orcid.org/0000-0003-1895-7620

Specialty section:
This article was submitted to Microbiotechnology, a section of the journal Frontiers in Microbiology

Received: *17 November 2020*
Accepted: *28 December 2020*
Published: *28 January 2021*

Citation:
Liu T, Huang Z, Gui X, Xiang W, Jin Y, Chen J and Zhao J (2021) Multi-omics Comparative Analysis of Streptomyces Mutants Obtained by Iterative Atmosphere and Room-Temperature Plasma Mutagenesis. Front. Microbiol. 11:630309. doi: 10.3389/fmicb.2020.630309

INTRODUCTION

Marine sponges (phylum Porifera) are among the oldest Metazoans on Earth (Webster and Taylor, 2012). Due to their marine benthic environment and highly efficient filter-feeding abilities, sponges harbor abundant microorganisms, including bacteria, fungi, archaea, and microalgae (Cheng et al., 2020). In fact, our previous studies identified 363 strains from 49 sponge species, including 92

actinobacterial isolates with diverse antibacterial potential, in which most streptomycetes displayed moderate to strong antibacterial activity by using the minimal medium that inhibited several Gram-positive and -negative indicators (Liu et al., 2019). These marine symbionts can account for up to 40–60% of the sponges' total volume, most of which contribute to the nutrients and survival of the host (Hentschel et al., 2012). Moreover, many sponge-derived bioactive substances are synthesized, or partly synthesized, by sponge-associated microbial organisms rather than the sponges (Thomas et al., 2010). To date, more than 15,000 natural compounds have been obtained from marine sponges and symbionts, including alkaloids, peptides, terpenes, and polyketides (PKs) (Mehbub et al., 2014). Among these marine microorganisms, actinomycetes are the largest producers of secondary metabolites, with more than 10,000 compounds (approximately 45%) (Genilloud, 2017). Indeed, actinomycetes-associated secondary metabolites possess antimicrobial activity, 75% of which were isolated from *Streptomyces* (Avignone-Rossa et al., 2013).

Although many natural compounds have been discovered, they do not represent the full richness of what the marine actinobacterial groups can provide (Gerwick and Moore, 2012). However, isolating and characterizing new compounds with novel structures or activities has become increasing challenging. In recent decades, only two top-ranking microbial natural antibiotics, retapamulin (from fungal terpenoid pleuromutilin) and fidaxomicin (tiacumicin from *Actinoplanes deccanensis* tiacumicin), which only act against Gram-positive bacteria, have been launched (Mullane and Gorbach, 2011; Sun et al., 2018). Most other compounds are either derived from known antibiotics or are unable to meet the required standards of clinical trials. One associated drawback is that more than 99% of bacteria cannot be cultivated under laboratory conditions (Vartoukian et al., 2010). Additionally, secondary metabolite gene clusters generally remain silent or cryptic when strains are cultivated in the laboratory, likely due to a lack of environmental pressures (Seyedsayamdost, 2018). In fact, recent advances in whole genome sequencing and bioinformatics have revealed an abundance of cryptic biosynthetic gene clusters (BGCs), as much as 25–70 within actinobacterial genomes (Lee et al., 2020b). Therefore, it is crucial to awaken poorly expressed or silent gene clusters to effectively exploit the biosynthetic potential of these strains for the production of new compounds.

Unlike certain diverse molecular strategies capable of awakening these silent gene clusters, such as ribosome engineering, manipulation of regulatory genes, overexpression or replacement of promoters, and epigenetic perturbation, random gene mutations remain the only feasible method when the genomic sites of the desired phenotype are unknown, or the genetic regulation is complex (Rutledge and Challis, 2015). Unlike traditional mutation breeding methods, such as physical mutation, chemical mutation, DNA recombination, and protoplast fusion, atmospheric room-temperature plasma (ARTP) is a platform for microbial mutagenesis based on atmospheric-pressure discharge plasma with higher mutation rates and low treatment temperatures (Zhang et al., 2014). As of 2018, at least 14 fungi, and 24 bacteria, plants, and other microbial communities were successfully altered to improve the tolerance of their microorganisms to certain growth conditions, increasing biomass and optimizing relevant parameters or enhancing the production of enzyme activity or medicinal chemicals (Ottenheim et al., 2018). The ARTP system causes greater damage to DNA that results in various structural changes to the oligonucleotides, which accounts for the higher mutation rate compared to other methods, such as UV radiation or chemical mutagens (Wang et al., 2020).

Moreover, ongoing advances in gene mining, comparative transcriptomics, metabolomics, and other bioinformatic tools have made them promising methods for discovering natural products from actinomycetes (Boddy, 2014). By combining genome mining approaches with antiSMASH tools, bacterial PKs and non-ribosomal peptides (NRPs), as well as complex secondary metabolites with antimicrobial, antiviral, anti-infective, or anticancer properties, have been identified (Lee et al., 2020a). These new characterization methods have also predicted new biosynthetic pathways and their related natural compounds. For instance, Streptoseomycin and its BGC were identified from marine prawn symbiotic actinomycetes by genome mining (Zhang et al., 2018). Moreover, the metagenomic sequencing of sponge *Mycale hentscheli* symbionts identified more than 100 cryptic BGCs and linked them to diverse chemical substances with anticancer or antiviral abilities (Storey et al., 2020). Additionally, some novel putative BGCs have been identified in various unculturable microorganisms. RNA-seq (transcriptome sequencing) technology has also been widely applied to compare differential expression levels of secondary metabolic gene clusters that respond to the same or different compounds with specific ecological functions under different environmental conditions. For example, comparative transcriptomics was used to predict regulon and to identify its pleiotropic regulator, like DasR, representing the "switch" between primary and secondary metabolite processes that improves yields and awakens silent pathways (Nieselt et al., 2010). Comparative transcriptome and metabolomics not only provide new methods for gene mining and contributions to revealing the biosynthetic potential of silencing secondary metabolic gene clusters, but also offer a targeted scheme for the subsequent improvement of potentially active compounds that cannot be obtained for further analysis due to the poor expression of gene clusters.

In this study, iterative ARTP mutagenesis was applied to sponge-derived *Streptomyces* sp. MG 010 to obtain mutants with increased antimicrobial activity. Based on the gene mining, transcriptome, and metabolomic results, the transcriptional expression levels and corresponding metabolites of the BGCs encoding antimicrobial products were comparatively analyzed between mutants and the wild-type strain. This may provide valuable guidance for further studies on activating the silent or cryptic gene clusters of actinobacteria, while supporting further research on the related mechanisms of compound biosynthesis and the targeted development of bioactive products.

MATERIALS AND METHODS

Cultivation of *Streptomyces* sp. Strains

Streptomyces sp. MG010 was isolated from the marine sponge *Mycale* sp. located off the coast of Fujian, China. Gram-positive (*Staphylococcus aureus* ATCC 6538 and *Bacillus subtilis* ATCC 6633) and Gram-negative bacteria (*Escherichia coli* ATCC 25922 and *Vibrio alginolyticus* ATCC 33783) were used as indicators for the antibacterial activity assays.

ISP2 medium and LB medium were used for strain screening, fermentation, and antimicrobial bioassays. All media were sterilized at 115°C for 30 min before use (Bertani, 1951; Shirling and Gottlieb, 1966).

Preparation of Single Spore Suspension

Streptomyces sp. MG010 strain was inoculated into ISP2 solid medium and incubated at 28°C for 10 days. The mature spores were harvested using sterile cotton swabs scraped over the medium surface, and then washed twice with sterile saline. The spore pellets were then transferred to an Eppendorf tube with glass beads, and the spore chains were disrupted by shaking for 10 min. After centrifuging at 12,000 × *g* for 10 min and discarding the supernatant, the spore precipitate was carefully resuspended in 1 mL of sterile saline. The monospore suspension was counted using a blood counting chamber and the concentration was adjusted to 10^7–10^8 CFU/mL.

ARTP Mutagenesis

The operating parameters were as follows: an input voltage of 110 W, distance of 2 mm between the plasma torch nozzle exit and sample plate, pure helium used as the working gas, a gas flow rate of 10 slpm, and the temperature of the plasma jet was below 40°C. The monospore suspension (10 μL) was poured into a sterilized stainless-steel plate (6 mm diameter) and exposed to the ARTP plasma jet (SiQingYuan Inc., Wuxi, China) for different treatment times: 0, 30, 45, 60, 75, 90, 105, 120, 150, and 180 s.

To obtain the optimum mutation, the lethality and positivity rates of spores under different mutant treatment times were determined according to the following equations:

$$\text{Lethality rate}(\%) = (A - B)/A \times 100\% \quad (1)$$

where A is the total colony count of the sample without treatment and B represents the total colony count after the different mutant treatment times with ARTP.

$$\text{Positive rate}(\%) = C/D \times 100\% \quad (2)$$

where C is the total colony count of the mutants with increased antibacterial activity and D represents the total colony count of mutants with varying antibacterial activity.

Screening Process of the Iterative Mutant Strains

After treatment, the steel plates were placed into new 1.5 mL Eppendorf tubes and washed with 1 mL sterile saline. Then, 100 μL spore suspension was separately transferred onto ISP2 solid medium and cultured at 28°C for 5 days. Pure mutant colonies from the solid medium were selected and inoculated onto LB solid medium with typical indicative bacteria at 37°C for 1 day using the replica plating method. The diameters of the inhibitory zones were observed and measured. Next, 100 μL of the cell-free supernatants of the fermentation broths from potentially active mutants was drawn out for verification of the antibacterial activity using the Oxford Cup assay. The top mutants with increased antimicrobial activity were selected as the original isolates for the next round of ARTP mutagenesis. A total of three mutagenesis iterations were performed along with the screening methods (**Figure 1**). In addition, the genetic stability of the identified mutant isolates was evaluated by eight rounds of serial sub-cultivations.

RNA Extraction, and Transcriptome Sequencing and Analysis

The 16S rRNA gene sequences (∼1500 bp) of the MG010 strain were amplified and analyzed by the National Center of Biotechnology Information (NCBI) website[1] to select the most related reference strains. The nucleotide sequence data showed that *Streptomyces* sp. MG010 (GenBank accession number: MW186238) in this study shared 99% homology with *Streptomyces variabilis* strain HNS054 (GenBank accession number: ASM104418v1). Therefore, the *S. variabilis* strain HNS054 was chosen as the reference genome for subsequent experiments. Antibiotics and secondary metabolite analysis shell (antiSMASH) version 3.0.5 was used to analyze the potential to produce secondary metabolites.

Total RNA was extracted and purified from the wild-type strains (labeled NA1, NA2, and NA3) without testing their bioactivity against indicative bacteria, weakly bioactive mutants (labeled I1, I2, and I3), or the strongest bioactive mutants (labeled M1, M2, and M3) in the three parallel samples using the TIANGEN RNAprep Pure Micro Kit (TianGen, China) and RNA purification kit (TianGen, China), according to the manufacturer's instructions. The purity and concentration of the RNA (rRNA 28s/18s) were evaluated using a NanoDrop 2000 spectrophotometer (NanoDrop, Thermo Scientific, United States), and the integrity of the RNA was assessed using agarose gel electrophoresis. Then, all the RNA samples were subjected to RNA-seq library preparation and directed sequencing on the Illumina HiSeq platform (Meiji, China).

After filtering the low-quality sequences, a high content of unidentified nucleotides N, and adaptor-polluted sequences, clean reads were assembled using the software provided by sequencing platform Illumina. Clean reads were mapped to the reference *Streptomyces* sp. and the HNS054 genome (accession number: NZ_LDZX00000000.1, available at: https://www.ncbi.nlm.nih.gov/nuccore/NZ_LDZX00000000.1) using the software Bowtie2[2]. The abundance of gene transcripts from RNA-seq was quantified using the software RSEM package[3]. RPKM (reads per

[1]http://www.ncbi.nlm.nih.gov

[2]https://github.com/BenLangmead/bowtie2

[3]http://www.biomedsearch.com/nih/RSEM-accurate-transcriptquantification-from/21816040.html

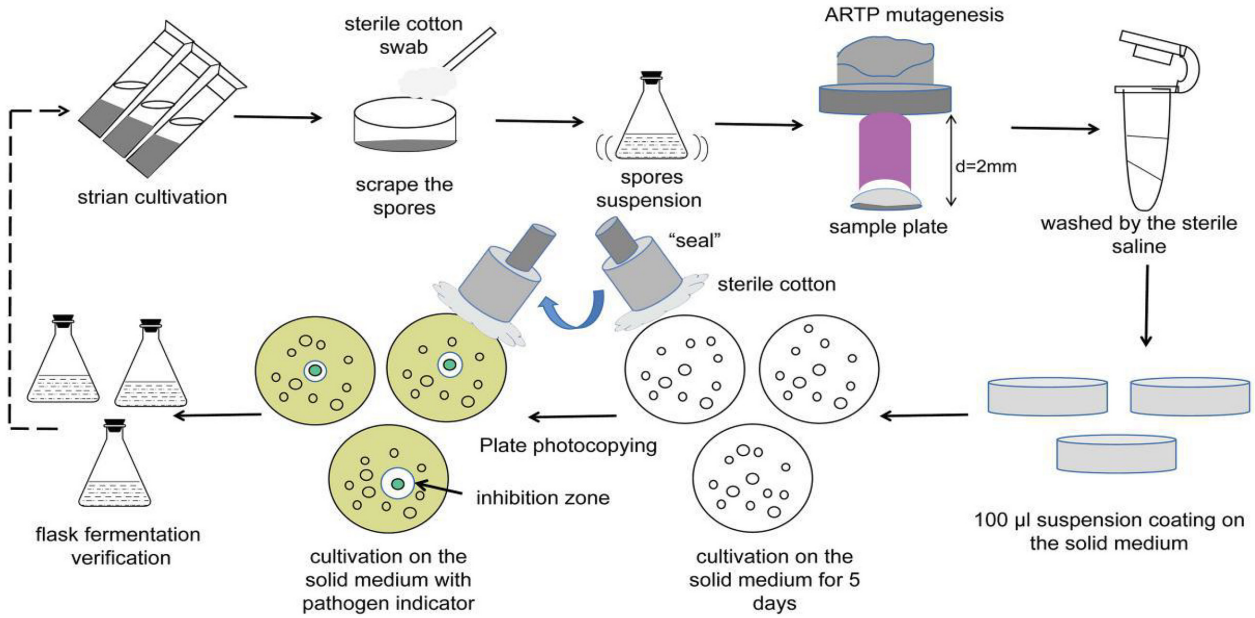

FIGURE 1 | Flow diagram of ARTP mutagenesis.

kilobase of exon model per million mapped reads) was used to indicate the abundance of a transcript. The edge R[4] was used to analyze differential expression analysis (fold change) and the related significance level between the wild and mutant strains. The false discovery rate (FDR) values below 0.05 or $\log_2 |\text{fold change}| \geq 1$ were considered to be significantly differentially expressed transcripts.

Gene functions were annotated by online programs and databases, including Gene Ontology (GO), Clusters of Orthologous Groups of protein (COG), and KEGG. Among these, GO terms enriched differentially expressed genes (DEGs) were analyzed using the Blast2GO software package[5]. The GO terms with significant expression (p-value < 0.05) were also enriched in KEGG pathways[6]; COG[7] terms were used as tools for functional annotation, classification, and protein evolution analysis. Other databases such as Nt (NCBI non-redundant nucleotide sequences), Nr (NCBI non-redundant protein sequences), and Pfam (Protein family) were also used to annotate gene functions.

Quantitative Real-Time (qRT)-PCR Analysis

A total of nine RNA samples were collected for quantitative real-time (qRT)-PCR analysis to verify the transcriptome data. The primers used for qRT-PCR were designed using the Premier 5 software. The detailed information for the primers is listed in **Supplementary Table S3**. The qRT-PCR reaction system was performed following the manufacturer's instructions using the SYBR Premix EX Tag kit (Takara, Japan), containing 10 μL of 2 × SYBR Premix EX Tag, 2 μL of each cDNA sample, 0.5 μL of Primer (10 μM), and added RNase Free H_2O up to a final volume of 20 μL. The reaction conditions were as follows: 95°C for 2 min; 40 cycles (95°C for 5 s; 60°C for 30 s) and 72°C for 30 s. The melting curve conditions were as follows: 95°C for 15 s; 60°C for 60 s; and 95°C for 15 s. The 16S rRNA of the wild strain was used as the reference gene in this study. QuantStudio 6 (Thermo Fisher Scientific, United States) was used to carry out all qRT-PCR reactions by detecting the SYBR fluorescence signal strength. Primer Quest Tool software was used to design primers with a product length of 100–300 bp (Invitrogen, ShangHai). The $2^{-\Delta\Delta Ct}$ method was used for data processing.

LC-MS Analyses of Wild Strain and Mutants

The wild-type strain (NA), weakly mutant strains (IA), and maximum antimicrobial activity of the mutant strains (MA) were first grown on ISP2 medium at 28°C for 5 days, after which the spores were inoculated into a 2.5 L Erlenmeyer flask containing 2.5 L ISP2 medium at 220 rpm and 28°C for 7 days. The crude extracts were obtained by extracting the fermentation broths with equal volumes of ethyl acetate and then butanone three times. The clarified supernatant was obtained by centrifuging the concentrates at 12,000 × g for 5 min. Both the ethyl acetate and butanone layers were collected and evaporated on a rotatory evaporator, and the concentrates were resolved in methanol (500 μL). The samples were adjusted to 5 mg/mL and analyzed by LC-MS with a linear gradient of 5–95% solvent B (solvent B: 0.1% formic acid + 100% CH_3CN; solvent A: 0.1% formic acid in H_2O) over 40 min at a rate of 1 mL/min with a UV length of 254 nm.

[4]http://www.bioconductor.org/packages/2.12/bioc/html/edgeR.html
[5]http://www.blats2go.com/b2ghome
[6]http://www.genome.jp/kegg
[7]http://www.ncbi.nlm.nih.gov/COG/

The free software MZmine2[8] was used to assess chromatograms by detecting, deconvoluting, aligning, and normalizing the data. Only those peaks with a high-quality mass intensity were retained, while the rest were discarded.

Antibacterial Activity Assay

The major predicted active fractions were collected by semi-preparative HPLC with a C_{18} column using a CH_3CN–H_2O elution system as previously described to identify the relatively pure peaks. The fractions were then dissolved in DMSO and adjusted to a uniform concentration of 100 μg/mL. Bacterial indicators were selected for antibacterial activity assays using the disk paper method. After cultivation for 24 h, the diameters of the bacteriostatic circles were measured.

RESULTS

Identified Mutations and Screening of the Mutants

The survival rate of *Streptomyces* sp. decreased with an increase in the mutagenesis time (**Figure 2A**). The lethal rates sharply increased when strains were exposed to ARTP before 75 s, and were observed to plateau at a treatment time of 75 s, with the death rate reaching 94% for the protection of the spore cell wall. Meanwhile, no spores survived treatments of 90 s or longer. Therefore, 75 s was chosen as the optimal exposure time for all subsequent experiments.

After three mutagenesis iterations, a total of 813 mutants were selected for antimicrobial activity screening. The mutation rates decreased as the positive mutation rates increased from 8.97 to 40.94%, indicating that interactive mutagenesis increased the possibility of emerging active strains (**Supplementary Table S1**). The antibacterial activities were then compared among the optimal mutants in each round (**Figure 2B**). Compared with the wild-type strain, the inhibitory diameter increased by 68% (first round), 71% (second round), and 75% (third round) after each round of ARTP treatment under the same culture conditions.

Mutant Stability

To detect the genetic stability of the mutant strains, eight rounds of subculture shake flask fermentation of the optimal mutants were conducted. The results indicated that the inhibitory activity of the identified mutant strains retained effective genetic stability (**Figure 2C**).

[8]http://mzmine.github.io/

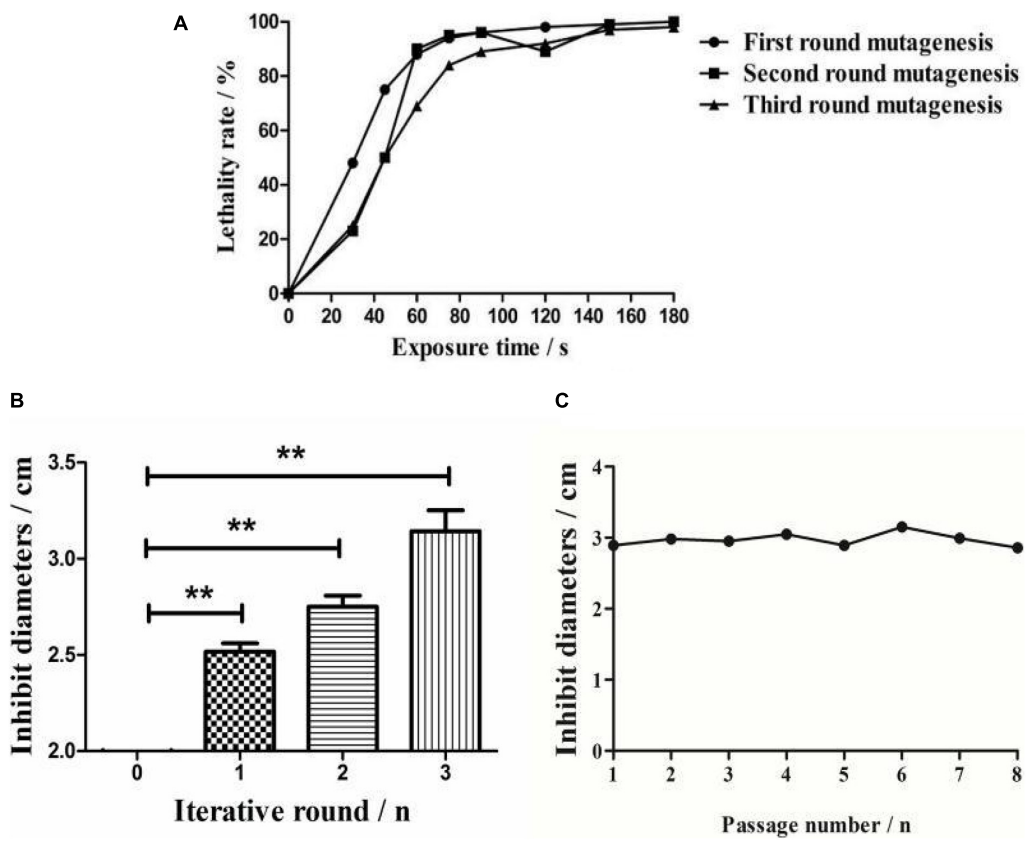

FIGURE 2 | Comparative analysis of ARTP mutagenesis process. **(A)** The lethality rate of the wild-type strain under different ARTP actuation durations. **(B)** Bacterial inhibition diameters of the wild-type strain and the active mutant strains after three iterations of ARTP mutagenesis. $^{**}P < 0.01$. **(C)** Generational fermentation of the mutant strains.

Partial characteristics, including the thermal stability and protease degradation activity, of one selected representative mutant were analyzed. The specific experimental methods are listed in **Supplementary Figure S5**. The bioactivity of the fermentation broth against indicative bacteria did not significantly differ when placed at 80°C for 4 h; however, no activity was observed above 80°C (**Supplementary Figures S5A,B**). The active substances from the fermentation broth were not sensitive to trypsin or chymotrypsin (**Supplementary Figure S5C**). Briefly, the results showed that the active substances of the mutant strains in the fermentation broth had excellent thermal stability and resistance to protease degradation.

RNA Sequencing and Comparative Analyses of Transcriptomic Profiles

The transcriptome of nine mutants (NA, IA, and MA in three parallels, respectively) were sequenced using the RNA-seq Illumina platform. In total, 177,898,864 clean reads were obtained from the NA, IA, and MA groups, among which 164,556,861 reads had a mapped ratio larger than 80%. The correlation coefficient between the wild strain and the mutants showed good quality of the collected cDNA reads (**Supplementary Figure S1A**). Compared with the wild strain, the clean reads mapping to the unique genes demonstrated that 1712 transcript genes of the IA mutants were significantly changed, including 956 upregulated and 756 downregulated genes, while 1812 transcript genes of the MA mutants were significantly changed, including 1145 upregulated and 676 downregulated genes (**Supplementary Figure S1B**). The significance of these gene transcriptions was determined by both FDR < 0.05 and $|\log_2 FC| \geq 1$.

Seven of the total 825 unigenes were annotated to three major functional groups using the GO categories, including biological process (4584 unigenes), molecular function (1900 unigenes), and cellular component (1341 unigenes; **Supplementary Figure S2A**). Comparing the NA and MA mutant strains, the most DEGs were found to be associated with biological processes, with equal numbers of upregulated and downregulated genes. Between the IA and MA mutants, remarkable changes were observed, with more upregulated than downregulated genes (**Supplementary Table S2**). Based on the DEGs, five of the total 123 unigenes were assigned to 23 function units based on the COG function annotation, with the largest number assigned to transcription (387 unigenes), accounting for 7.55% (**Supplementary Figure S2B**). A total of 5051 unigenes were also annotated to KEGG pathways involved in metabolic pathways (815 unigenes) and biosynthesis of secondary metabolites (370 unigenes), among which 20 pathways were significantly enriched, including ABC transporters, carbon metabolism, and biosynthesis of amino acids (**Supplementary Figure S2C**).

Comparison of DEGs in the Functional Gene Clusters

Comparative analysis using antiSMASH version 3.0.5 of functional gene clusters between the wild-type strain and mutants revealed a total of 21 gene clusters related to secondary metabolites that were significantly differentially expressed (**Table 1**). Using these DEGs, we conducted pairwise comparisons (**Figure 3**). The transcription results responding to ARTP mutagenesis illustrated that certain metabolic pathways, such as ribosomal metabolic processes, peptide and antibiotic biosynthesis and metabolism processes, transcription factors, and protein binding transport, became more active with an increase in antibacterial activity. Several gene clusters related to PKS or NRPS compounds were also differentially expressed between the NA and MA groups, such as cluster 11 and 12 (T1 PKS-NRPS), cluster 23 (T3 PKS), cluster 37 (NRPS), and cluster 51 (T2 PKS). Additionally, type I or IIIPK synthase and peptide synthase were significantly increased, although the numeric values of these transcriptome data (FPKM) ranged from 10 (at minimum) to 100 (at maximum) on average. Cluster 42, which was predicted to produce Lantipeptide, also showed higher gene expression levels and fold change differences in ABC transporter, membrane protein, and nitroreductase family deazaflavin-dependent oxidoreductase.

The expression levels of each gene in cluster 17 showed a trend toward significant upregulation, with FPKM ranging from 10 to 3000 on average. This gene cluster, 22,493 bp in length, located in 11,658–34,178 nt, was predicted to encode and synthesize lasso peptide compounds with a molecular weight of 2164 Da using antiSMASH software (**Figure 4A**). The gene cluster included the DNA-binding response regulator, sensor histidine kinase, export ABC transporter ATP-binding protein, lasso RiPP family leader peptide-containing protein, lasso peptide isopeptide bond-forming cyclase, lasso peptide biosynthesis PqqD family chaperone lasso peptide biosynthesis B2 protein, and ABC

TABLE 1 | Secondary metabolite gene clusters mined from *Streptomyces* sp. MG010.

Number	Type	Location	Size (bp)
Cluster 1	Butyrolactone	3080–12,864 nt	9784
Cluster 2	Terpene	1–13,395 nt	13,394
Cluster 3	Ectoine-butyrolactone	610–16,149 nt	15,539
Cluster 5	Nrps-otherks	1–36,205 nt	36,204
Cluster 7	Lantipeptide-nrps	1–49,526 nt	49,525
Cluster 11	T1 PKS-NRPS	33,563–76,741 nt	43,178
Cluster 12	T1 PKS-NRPS	1–84,193 nt	84,192
Cluster 17	Cyclic peptide	11,685–34,178 nt	22,493
Cluster 23	T3 PKS	1–40,029 nt	40,028
Cluster 26	Ectoine	76,656–87,054 nt	10,398
Cluster 30	Terpene	62,012–86,132 nt	24,120
Cluster35	Siderophore	43,911–55,683 nt	11,772
Cluster 37	NRPS	57,631–112,729 nt	55,098
Cluster 42	Lantipeptide	232,006–254,678 nt	22,672
Cluster 51	T2 PKS	210,177–252,686 nt	42,509
Cluster 55	Bacteriocin	1–10,280 nt	10,279
Cluster 59	Phenazine	20,971–41,870 nt	20,899
Cluster 63	Terpene	79,564–100,649 nt	21,085
Cluster 69	Siderophore	256,733–269,972 nt	13,239
Cluster 72	Terpene	402,937–425,093 nt	22,156
Cluster 77	Bacteriocin	203,204–213,419 nt	10,215

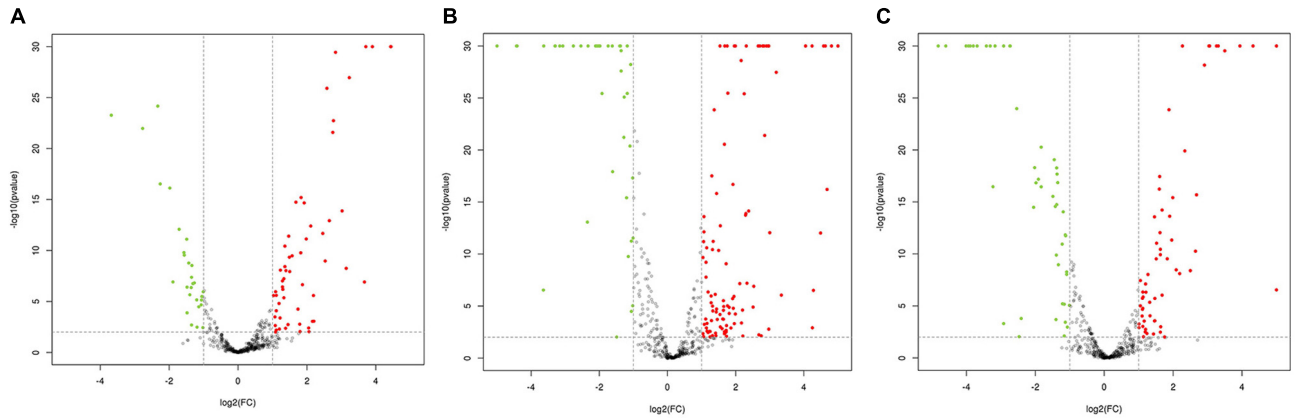

FIGURE 3 | Volcano plot of pairwise comparisons between samples. **(A)** Volcano plot of the comparisons between IA (Mutants with weak activity) and MA (Mutants with maximum activity); **(B)** Volcano plot of the comparisons between NA (Wild-type strain) and MA (Mutants with maximum activity); **(C)** Volcano plot of the comparisons between NA (Wild-type strain) and IA (Mutants with weak activity).

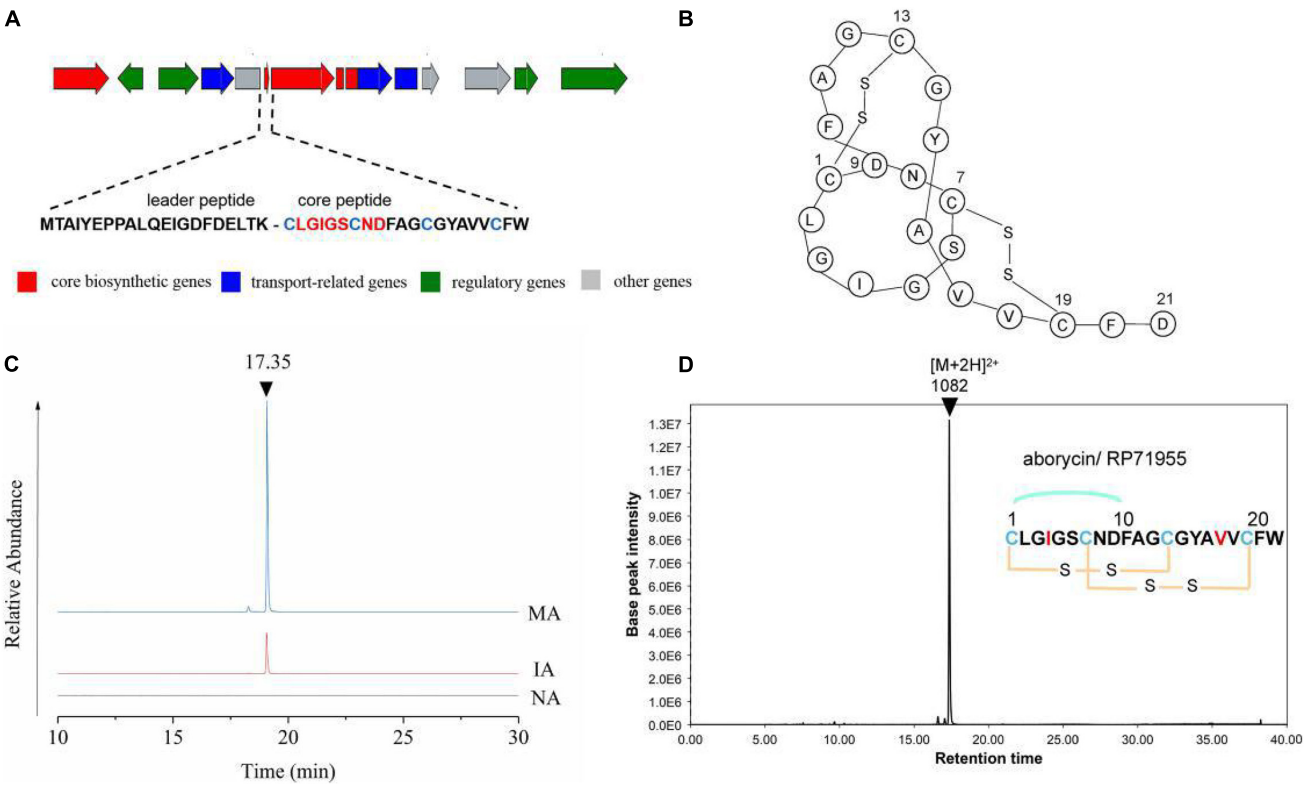

FIGURE 4 | Predicated lasso peptide data. **(A)** Gene cluster structure of lasso peptide. **(B)** Secondary structure of aborycin. **(C)** Comparative HPLC analysis of the lasso peptide in the extracted crudes of NA, IA, and MA groups. **(D)** Relative molecular mass of aborycin.

transporter ATP-binding protein (**Table 2**). Among these, AC003_RS25355 contained the complete leader peptide and core peptide encoding the lasso peptide compounds (**Figure 4B**).

qRT-PCR Results

To validate the confidence of the RNA-seq data, five genes were selected randomly from the NA, IA, and MA mutant strains for qRT-PCR analysis (**Supplementary Table S3**). The linear regression relationship of gene expression levels was effective, with R^2 of the NA, IA, and MA mutants reaching 0.9993, 0.998, and 1, respectively, while R^2 of the reference 16S rRNA genes reached 0.99 (**Supplementary Figure S3**). The fold changes in the gene expression differences between the qRT-PCR results and transcriptomic data showed that

TABLE 2 | Gene expression changes and function prediction of lasso peptide gene cluster.

Cluster	NA_mean_ fpkm	IA_mean_ fpkm	MA_mean_ fpkm	Predicted function
AC003_RS25335	20.08	22.39	32.52	Alpha/beta hydrolase
AC003_RS25345	173.77	144.33	339.3	DNA-binding response regulator
AC003_RS25350	79.02	87.69	68.57	Sensor histidine kinase
AC003_RS25355	15.13	233.47	3481.14	Export ABC transporter ATP-binnding protein
AC003_RS25360	11	125.51	1175.04	ABC transporter permease
AC003_RS35325	15.13	132.45	3080.16	Lasso RiPP family leader peptide-containing protein
AC003_RS25365	19.18	59.21	149.07	Lasso peptide isopeptide bond-forming cyclase
AC003_RS25370	2.59	7.7	68.71	Lasso peptide biosynthesis PqqD family chaperone
AC003_RS25375	9.07	12.59	73.23	Lasso peptide biosynthesis B2 protein
AC003_RS25380	16.16	14.33	102.59	ABC transporter ATP-binding protein
AC003_RS25385	5.51	13.73	92.72	ABC transporter
AC003_RS25390	2.99	10.56	86.5	DoxX family membrane protein
AC003_RS25400	7.75	14.07	55.72	CapA family protein
AC003_RS25405	275.92	120.82	183.81	DNA-binding response regulator
AC003_RS25415	41.58	34.11	23.66	AfsR/SARP family transcriptional regulator

although there was little deviation in these quantitative results, the up- and downregulated trends of these DEGs were the same (**Supplementary Figure S4** and **Supplementary Table S4**). The other eight genes (AC003_RS25345, AC003_RS25350, AC003_RS25355, AC003_RS35325, AC003_RS25365, AC003_RS25370, AC003_RS25375, and AC003_RS25380) in cluster 17 that predicted for lasso peptide also underwent several rounds of qRT-PCR analysis. Although the low gene expression level limited these results, significant differences were observed in the gene expression fold changes between the MA and NA mutants, thereby verifying that the changes in gene expression of the lasso peptide cluster were relatively accurate.

LC-MS and Antibacterial Activities Assay Results

The butanone-extracted samples of the wild-type strain (NA) and mutants (IA, MA) were analyzed by HPLC-MS. The results of metabolite profiling showed that the MA strain produced a higher yield of the putative lasso peptide (RT = 17.35 min) compared to the wild-type strain (NA) or IA (**Figure 4C**). LC-MS data further revealed a relative molecular mass of 1082.43 ($[M + 2H]^{2+}$ at m/z = 2164.86) (**Figure 4D**). The genomics and metabolomics analyses of this signal were both targeted to the molecule aborycin (Frechet et al., 1994). Therefore, ARTP mutagenesis might awaken the silent BGC and, to some extent, improve the production of this lasso peptide.

Additionally, the metabolic profiles of ethyl acetate extracted crudes between the wild strain (NA) and mutant strain (MA) were compared by LC-MS, determining their TIC (total ion count) and XIC (extracting ion current) (**Figure 5**). MA produced a series of low-molecular-weight compounds that did not contain in the NA, such as $[M + H]^+$ at m/z = 261.1231 (RT = 7.45 min), $[M + H]^+$ at m/z = 374.1642 (RT = 16.22 min), $[M + H]^+$ at m/z = 386.1256 (RT = 17.85 min), and $[M + H]^+$ at m/z = 304.2993 (RT = 20.25 min) (**Figures 5A,B**). To further predict these molecules, several online databases were used to identify the putative molecular formulas and structures (**Figure 5C**). Moreover, the spectroscopic data indicated that several unknown peaks with strong base peak intensities potentially represent new molecules with intriguing bioactivities. A panel of 12 putative fractions was used to detect potent antibacterial activities against the indicators (**Figure 5D**). Fractions B, D, E, and F were significantly different between the NA and MA in liquid chromatograms, among which fractions D, E, and F were against *S. aureus* with an MIC of 100 μg/mL. Meanwhile, component G and H did not exhibit antibacterial activities here, and the corresponding compounds could not be obtained from online databases, implying identification of novel compounds.

DISCUSSION

The first ARTP study was a report on *Streptomyces avermitilis* mutants that produced >40% more avermectins B1a than the wild-type strain (Wang et al., 2010). Over the past decade, more than 40 different microbial species involving 300 ARTP case studies have applied the ARTP mutagenesis method to improve the yield of diverse antibiotics, enzymes, and intermediate active metabolic compounds, particularly in actinomycetes (Ottenheim et al., 2018). Specifically, *Actinomyces* IN537 mutants increased acarbose yield by 62.5% compared to the original strain after treatment with ARTP (Ren et al., 2017). Moreover, iterative ARTP mutagenesis increased the transglutaminase (TGase) of bacterial fermentation by 27% with a maximum TGase activity of 5.85 U/mL (Jiang et al., 2017). Unlike most mutagenesis cases used to increase yields of known compounds for commercial high production demand, in the current study, mutants of the wild-type strain *Streptomyces* sp. MG010 were obtained by iterative ARTP with stronger antimicrobial activities, which not only indicated that silent gene clusters of *Streptomycete* strains have the potential to express active secondary metabolites,

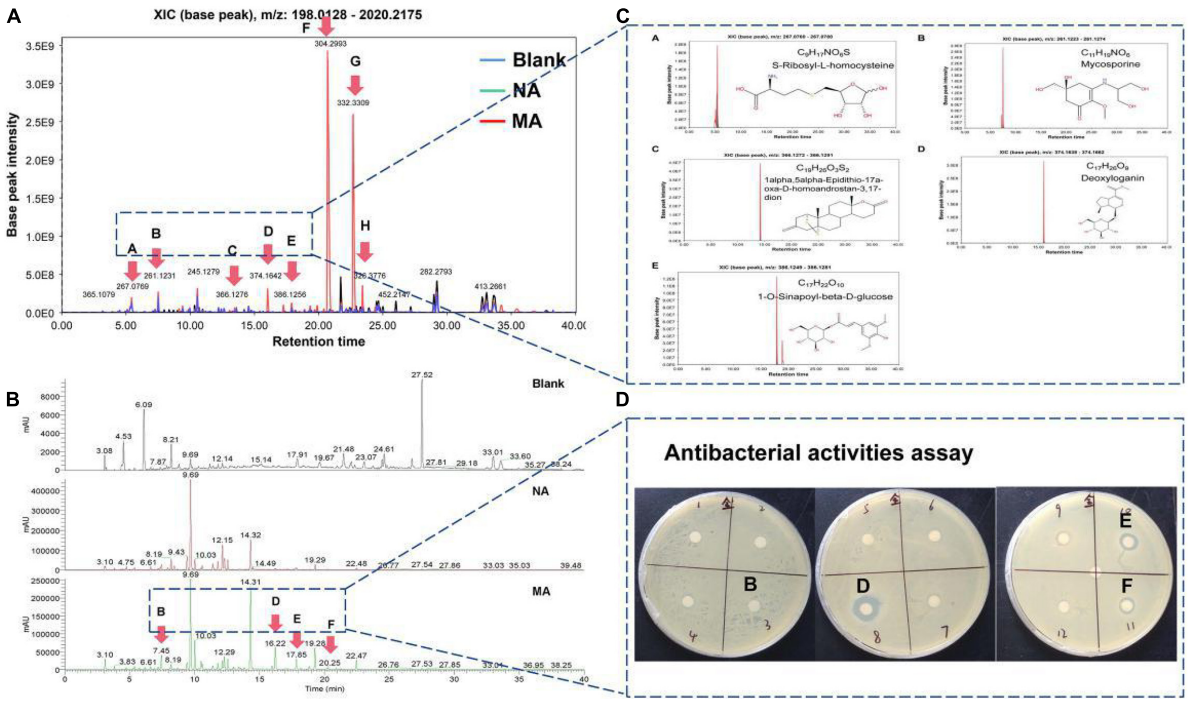

FIGURE 5 | Metabolic profiles of ethyl acetate extracted crudes between the wild-type strain (NA) and mutant strain (MA). **(A)** TIC (total ion chromatogram) of the NA, MA, and blank control. **(B)** XIC (extracted ion chromatogram) of the MA. **(C)** Putative molecular formulas and structures matched to the online database. **(D)** Antibacterial activity assay results.

but also suggested that mutagenesis likely represented a promising method for activating gene activity corresponding to unknown compounds. Previously, *Streptomyces coelicolor* A3 was induced by rare earth elements to express nine genes related to nine BGC, although several peaks were only detected via HPLC profiling (Tanaka et al., 2010). However, these unknown active compounds, as determined in this study, have the potential to be awakened by altering a single factor to evoke a stress response and to be the most promising factor for antagonizing pathogenic bacteria (Defraine et al., 2018).

For mutagenesis, the lethality rate curve should be accurately evaluated for different species, as for actinomycetes in this study, 75 s was the optimal interval; however, for other strains, such as bacteria or fungi, this may require much shorter or longer times. The appropriate balance of the death rate and the positive rate indicated a greater possibility to obtain active mutant strains. It is advisable to ensure the appropriate initial spore concentration (10^7–10^8 CFU/mL) and serial dilution density to obtain single colonies on the photocopied plates. In addition, the mutant efficiency tends to increase after several rounds of mutagenesis. Unlike conventional methods, iterative mutagenesis provides a driving force for mutation by increasing the degree of damage to intracellular DNA, which could improve and maintain the rapid mutation rates (Zhang et al., 2015). Therefore, it would be much wider and faster to awaken silent gene clusters and to enhance mutation range and efficiency.

Microorganisms, particularly actinomycetes, have played an important role in the field of natural product discovery, which often harbors various cryptic BGCs that are detected under laboratory conditions by analyzing genome sequencing (Niu, 2018). Stefano et al. (2018) stated the "One strain many compounds" (OSMAC) principle in marine microorganisms that suggests that more substances could be exploited from the existing strain resources. From the perspective of natural product production, major bottlenecks remain in the discovery of novel natural compounds. Our results show that although mutants with significantly increased antibacterial activity were obtained by ARTP treatment, due to the low expression level of these secondary gene clusters, the substances were not readily identified. Thus, the differences in the LC-MS data between the wild-type strains and mutants could be in favor of identifying these possible products. The comparative analysis showed that several small molecular compounds in the metabonomics profile did not exhibit obvious changes in the transcriptomic profile. Multi-omics analysis, combining the transcriptome with metabolic regulation levels, revealed more valuable information. Lu et al. (2018) used a multi-omics integrated analysis to study the enzyme production under the oxygen-limiting conditions of *Aspergillus niger*, which provides a holistic optimization target for industrial application. In this case, it was deduced that the integration of ARTP mutagenesis and multi-omics methods could improve the chances of mining active compounds in a more comprehensive way.

The lasso peptide is post-translationally modified by specific enzymes in which the peptide tails are trapped and locked in a ring (Li et al., 2014). This lasso topology makes the cyclic peptide very stable and difficult to obtain by chemical synthesis (Martin-Gomez and Tulla-Puche, 2018). With the development of in-depth sequencing technology of microbial genomics, there are two primary methods for the exploration of lasso peptide compounds, including screening methods of the McjB homology sequence and centering on the precursor to excavate lasso peptides (Semenova et al., 2005; Maksimov et al., 2012). Hence, multi-omics comparative analysis offers certain advantages over solely gene mining or other sequencing and screening methods. Moreover, it was speculated that iterative ARTP mutagenesis may activate silent gene clusters of secondary substances related to the generation of ribosome biosynthesis. In addition, the putative compounds mycosporines and mycosporine-like amino acids were considered as promising secondary metabolites for UV-photoprotection, and may be widely employed in chemical industries such as cosmetics and sunscreens (Kageyama and Waditee-Sirisattha, 2018). Deoxyloganin generally serves as a precursor of indole alkaloids (Battersby et al., 1970). Fraction F with an unknown compound structure also exhibited obvious bacteriostatic activity, which likely indicates a novel chemical.

Although mutants with strong antibacterial activities were obtained, the compounds extracted with the targeted molecular weights could not be identified due to the limited production. Moreover, the secondary metabolites of actinomycetes may be composed of a series of active components without the main active compounds, which may account for the failure of the separation process (Cai et al., 2002). The host strains were endowed with limited carrying capacity to express the active products, even under artificial or external pressures (Nepal and Wang, 2019). This could be reflected in the low expression of DEGs in the transcriptome profiles, which generally range from a few dozen to a few hundred FPKM. This suggests that even if the cryptic gene cluster could be awakened to express corresponding compounds above the test line, a sufficient threshold may not be achieved to allow for structural identification. Here the higher peak fractions, G and H, had no antibacterial activities, while other fractions with smaller peaks in the liquid chromatogram exhibited bioactivities, indicating that the ARTP mutagenesis activated the silenced gene clusters, however, failed to make induce high expression. Furthermore, several unknown promoters of secondary metabolic gene clusters were supposed to be inactive under laboratory conditions, which may cause short gene expression even if the gene cluster is functional (Myronovskyi and Luzhetskyy, 2016). The cluster activation may presumably disturb the original gene balance, which is non-negligible for the successful gene expression of the comprehensive metabolic pathway (Smanski et al., 2014). Moreover, inappropriate cultural conditions, or an inability to generate environmental signals necessary for streptomycetes in their natural environment, may impact the bioactivity yields (Craney et al., 2012). Future research should focus on improving the expression of these gene clusters or the yields of active compounds. In conclusion, our study provides an efficient method for the detection and identification of targeted bioactive complexes from extracted metabolite crudes of microbial culture mediums.

DATA AVAILABILITY STATEMENT

The datasets presented in this study can be found in online repositories. The names of the repository/repositories and accession number(s) can be found below: NCBI SRA, accession no: PRJNA679680.

AUTHOR CONTRIBUTIONS

TL was mainly responsible for the separation and purification of compounds, omics analysis, and article writing. ZH provided guidance on mutagenesis. XG, WX, and YJ were responsible for sampling and bacterial preliminary screening. JC provided guidance on omics analysis. JZ provided guidance on manuscript modification and overall framework construction. All authors contributed to the article and approved the submitted version.

FUNDING

This research was supported by grants from the National Natural Science Foundation of China (Grant No. 41876183) and the Fundamental Research Funds for the Central Universities (Grant No. 20720200045).

ACKNOWLEDGMENTS

We would like to thank Editage for its linguistic assistance during the preparation of this manuscript.

SUPPLEMENTARY MATERIAL

The Supplementary Material for this article can be found online at: https://www.frontiersin.org/articles/10.3389/fmicb.2020.630309/full#supplementary-material

REFERENCES

Avignone-Rossa, C., Kierzek, A. M., and Bushell, M. E. (2013). "Secondary metabolite production in *Streptomyces*," in *Encyclopedia of Systems Biology*, eds W. Dubitzky, O. Wolkenhauer, K.-H. Cho, and H. Yokota (New York, NY: Springer), 1903–1913. doi: 10.1007/978-1-4419-9863-7_1164

Battersby, A. R., Burnett, A. R., and Parsons, P. G. (1970). Preparation and isolation of deoxyloganin: its role as precursor of loganin and the indole alkaloids. *J. Chem. Soc. D Chem. Commun.* 13, 826–827. doi: 10.1039/c29700000826

Bertani, G. (1951). STUDIES ON LYSOGENESIS I. The mode of phage liberation by lysogenic *Escherichia coli*. *J. Bacteriol.* 62, 293–300. doi: 10.1128/JB.62.3.293-300.1951

Boddy, C. N. (2014). Bioinformatics tools for genome mining of polyketide and non-ribosomal peptides. *J. Ind. Microbiol. Biot.* 41, 443–450. doi: 10.1007/s10295-013-1368-1

Cai, Z., Lee, F. S. C., Wang, X. R., and Yu, W. J. (2002). A capsule review of recent studies on the application of mass spectrometry in the analysis of Chinese medicinal herbs. *J. Mass Spectrom.* 37, 1013–1024. doi: 10.1002/jms.370

Cheng, M. M., Tang, X. L., Sun, Y. T., Song, D. Y., and Li, G. Q. (2020). Biological and chemical diversity of marine sponge-derived microorganisms over the last two decades from 1998 to 2017. *Molecular* 25:853. doi: 10.3390/molecules25040853

Craney, A., Ozimok, C., Pimentel-Elardo, S. M., Capretta, A., and Nodwell, J. R. (2012). Chemical perturbation of secondary metabolism demonstrates important links to primary metabolism. *Chem. Biol.* 19, 1020–1027. doi: 10.1016/j.chembiol.2012.06.013

Defraine, V., Fauvart, M., and Michiels, J. (2018). Fighting bacterial persistence: current and emerging anti-persister strategies and therapeutics. *Drug Resist. Update* 38, 12–26. doi: 10.1016/j.drup.2018.03.002

Frechet, D., Guitton, J. D., Herman, F., Faucher, D., Helynck, G., James-Surcouf, E., et al. (1994). Solution structure of RP 71955, a new 21 amino acid tricyclic peptide active against HIV-1 virus. *Biochemistry* 33, 42–50. doi: 10.1021/bi00167a006

Genilloud, O. (2017). *Actinomycetes*: still a source of novel antibiotics. *Nat. Prod. Rep.* 34, 1203–1232. doi: 10.1039/C7NP00026J

Gerwick, W. H., and Moore, B. S. (2012). Lessons from the past and charting the future of marine natural products drug discovery and chemical biology. *Chem. Biol.* 19, 85–98. doi: 10.1016/j.chembiol.2011.12.014

Hentschel, U., Piel, J., Degnan, S. M., and Taylor, M. W. (2012). Genomic insights into the marine sponge microbiome. *Nat. Rev. Microbiol.* 10, 641–654. doi: 10.1038/nrmicro2839

Jiang, Y., Shang, Y.-P., Li, H., Zhang, C., Pan, J., Bai, Y.-P., et al. (2017). Enhancing transglutaminase production of *Streptomyces mobaraensis* by iterative mutagenesis breeding with atmospheric and room-temperature plasma (ARTP). *Bioresour. Bioprocess.* 4:37. doi: 10.1186/s40643-017-0168-2

Kageyama, H., and Waditee-Sirisattha, R. (2018). "Chapter 5 - Mycosporine-like amino acids as multifunctional secondary metabolites in *Cyanobacteria*: from biochemical to application aspects," in *Studies in Natural Products Chemistry*, ed. R. Atta Ur (Amsterdam: Elsevier), 153–194. doi: 10.1016/B978-0-444-64179-3.00005-0

Lee, N., Hwang, S., Kim, J., Cho, S., Palsson, B., and Cho, B. K. (2020a). Mini review: genome mining approaches for the identification of secondary metabolite biosynthetic gene clusters in *Streptomyces*. *Comput. Struct. Biotechnol. J.* 18, 1548–1556. doi: 10.1016/j.csbj.2020.06.024

Lee, N., Kim, W., Hwang, S., Lee, Y., Cho, S., Palsson, B., et al. (2020b). Thirty complete *Streptomyces* genome sequences for mining novel secondary metabolite biosynthetic gene clusters. *Sci. Data* 7:55. doi: 10.1038/s41597-020-0395-9

Li, Y. J., Zirah, S., and Rebuffat, S. (2014). *Lasso Peptides: Bacterial Strategies to Make and Maintain Bioactive Entangled Scaffolds*. Berlin: Springer press, doi: 10.1007/978-1-4939-1010-6

Liu, T., Wu, S. F., Zhang, R. Z., Wang, D. X., Chen, J., and Zhao, J. (2019). Diversity and antimicrobial potential of *Actinobacteria* isolated from diverse marine sponges along the Beibu Gulf of the South China Sea. *FEMS Microbiol. Ecol.* 95, 1–10. doi: 10.1093/femsec/fiz089

Lu, H., Cao, W., Liu, X., Sui, Y., Ouyang, L., Xia, J., et al. (2018). Multi-omics integrative analysis with genome-scale metabolic model simulation reveals global cellular adaptation of *Aspergillus niger* under industrial enzyme production condition. *Sci. Rep.* 8:14404. doi: 10.1038/s41598-018-32341-1

Maksimov, M. O., Pelczer, I., and Link, A. J. (2012). Precursor-centric genome-mining approach for lasso peptide discovery. *Proc. Natl. Acad. Sci. U.S.A.* 109, 15223–15228. doi: 10.1073/pnas.1208978109

Martin-Gomez, H., and Tulla-Puche, J. (2018). Lasso peptides: chemical approaches and structural elucidation. *Org. Biomol. Chem.* 16, 5065–5080. doi: 10.1039/C8OB01304G

Mehbub, M. F., Lei, J., Franco, C., and Zhang, W. (2014). Marine sponge derived natural products between 2001 and 2010: trends and opportunities for discovery of bioactives. *Mar. Drugs* 12, 4539–4577. doi: 10.3390/md12084539

Mullane, K. M., and Gorbach, S. (2011). Fidaxomicin: first-in-class macrocyclic antibiotic. *Expert. Rev. Anti. Infect. Ther.* 9, 767–777. doi: 10.1586/eri.11.53

Myronovskyi, M., and Luzhetskyy, A. (2016). Native and engineered promoters in natural product discovery. *Nat. Prod. Rep.* 33, 1006–1019. doi: 10.1039/C6NP00002A

Nepal, K. K., and Wang, G. (2019). *Streptomycetes*: surrogate hosts for the genetic manipulation of biosynthetic gene clusters and production of natural products. *Biotechnol. Adv.* 37, 1–20. doi: 10.1016/j.biotechadv.2018.10.003

Nieselt, K., Battke, F., Herbig, A., Bruheim, P., Wentzel, A., Jakobsen, ØM., et al. (2010). The dynamic architecture of the metabolic switch in *Streptomyces coelicolor*. *BMC Genom.* 11:10. doi: 10.1186/1471-2164-11-10

Niu, G. (2018). Genomics-driven natural product discovery in *Actinomycetes*. *Trends Biotechnol.* 36, 238–241. doi: 10.1016/j.tibtech.2017.10.009

Ottenheim, C., Nawrath, M., and Wu, J. C. (2018). Microbial mutagenesis by atmospheric and room-temperature plasma (ARTP): the latest development. *Bioresour. Bioprocess.* 5:12. doi: 10.1186/s40643-018-0200-1

Ren, F., Chen, L., and Tong, Q. (2017). Highly improved acarbose production of *Actinomyces* through the combination of ARTP and penicillin susceptible mutant screening. *World J. Microb. Biot.* 33:16. doi: 10.1007/s11274-016-2156-7

Rutledge, P. J., and Challis, G. L. (2015). Discovery of microbial natural products by activation of silent biosynthetic gene clusters. *Nat. Rev. Microbiol.* 13, 509–523. doi: 10.1038/nrmicro3496

Semenova, E., Yuzenkova, Y., Peduzzi, J., Rebuffat, S., and Severinov, K. (2005). Structure-activity analysis of microcin J25: distinct parts of the threaded lasso molecule are responsible for interaction with bacterial RNA polymerase. *J. Bacteriol.* 187, 3859–3863. doi: 10.1128/JB.187.11.3859-3863.2005

Seyedsayamdost, M. R. (2018). *Method for Awakening Silent Gene Clusters in Bacteria and Discovery of Cryptic Metabolites*. United States Patent Application 20170022532. Washington, DC: U.S. Patent and Trademark Office.

Shirling, E. B., and Gottlieb, D. (1966). Methods for characterization of *Streptomyces* species1. *Int. J. Syst. Bacteriol.* 16, 313–340. doi: 10.1099/00207713-16-3-313

Smanski, M. J., Bhatia, S., Zhao, D., Park, Y. J., Lauren, B. A. W., Giannoukos, G., et al. (2014). Functional optimization of gene clusters by combinatorial design and assembly. *Nat. Biotechnol.* 32, 1241–1249. doi: 10.1038/nbt.3063

Stefano, R., Stephen, J., Sloane, P., and Alan, D. (2018). Extending the "One strain many compounds" (OSMAC) principle to marine microorganisms. *Mar. Drugs* 16:244. doi: 10.3390/md16070244

Storey, M. A., Andreassend, S. K., Bracegirdle, J., Brown, A., Keyzers, R. A., Owen, J. G., et al. (2020). Metagenomic exploration of the marine sponge *Mycale hentscheli* uncovers multiple polyketide-producing bacterial symbionts. *mBio* 11:e02997-19. doi: 10.1128/mBio.02997-19

Sun, F., Zhang, H., Gonzales, G. B., Zhou, J., Li, Y., Zhang, J., et al. (2018). Unravelling the metabolic routes of retapamulin: insights into drug development of pleuromutilins. *Antimicrob. Agents Chemother.* 62:AAC.02388-17. doi: 10.1128/AAC.02388-17

Tanaka, Y., Hosaka, T., and Ochi, K. (2010). Rare earth elements activate the secondary metabolite-biosynthetic gene clusters in *Streptomyces coelicolor* A3(2). *J. Antibiot.* 63, 477–481. doi: 10.1038/ja.2010.53

Thomas, T. R. A., Kavlekar, D. P., and Lokabharathi, P. A. (2010). Marine drugs from sponge-microbe association—a review. *Mar. Drugs* 8, 1417–1468. doi: 10.3390/md8041417

Vartoukian, S. R., Palmer, R. M., and Wade, W. G. (2010). Strategies for culture of 'unculturable' bacteria. *FEMS Microbiol. Lett.* 309, 1–7. doi: 10.1111/j.1574-6968.2010.02000.x

Wang, L., Zhao, H., He, D., Wu, Y., Jin, L., Li, G., et al. (2020). Insights into the molecular-level effects of atmospheric and room-temperature plasma on mononucleotides and single-stranded homo- and hetero-oligonucleotides. *Sci. Rep.* 10:14298. doi: 10.1038/s41598-020-71152-1

Wang, L. Y., Huang, Z. L., Li, G., Zhao, H. X., Xing, X. H., Sun, W.-T., et al. (2010). Novel mutation breeding method for *Streptomyces avermitilis* using an atmospheric pressure glow discharge plasma. *J. Appl. Microbiol.* 108, 851–858. doi: 10.1111/j.1365-2672.2009.04483.x

Webster, N. S., and Taylor, M. W. (2012). Marine sponges and their microbial symbionts: love and other relationships. *Environ. Microbiol.* 14, 335–346. doi: 10.1111/j.1462-2920.2011.02460.x

Zhang, B., Wang, K. B., Wang, W., Bi, S. F., Mei, Y. N., Deng, X. Z., et al. (2018). Discovery, biosynthesis, and Heterologous production of Streptoseomycin, an

Anti-Microaerophilic bacteria Macrodilactone. *Org. Lett.* 20, 2967–2971. doi: 10.1021/acs.orglett.8b01006

Zhang, X., Zhang, C., Zhou, Q. Q., Zhang, X. F., and Wang, L. Y. (2015). Quantitative evaluation of DNA damage and mutation rate by atmospheric and room-temperature plasma (ARTP) and conventional mutagenesis. *Appl. Microbiol. Biot.* 99, 5639–5646. doi: 10.1007/s00253-015-6678-y

Zhang, X., Zhang, X. F., Li, H. P., Wang, L. Y., Zhang, C., Xing, X. H., et al. (2014). Atmospheric and room temperature plasma (ARTP) as a new powerful mutagenesis tool. *Appl. Microbiol. Biot.* 98, 5387–5396. doi: 10.1007/s00253-014-5755-y

Conflict of Interest: The authors declare that the research was conducted in the absence of any commercial or financial relationships that could be construed as a potential conflict of interest.

frontiers in Microbiology

ORIGINAL RESEARCH
published: 24 February 2021
doi: 10.3389/fmicb.2021.619731

Cloning and Characterization of a New Chitosanase From a Deep-Sea Bacterium *Serratia* sp. QD07

*Qiuling Zheng[1], Xiangjun Meng[2], Mingyang Cheng[1], Yanfeng Li[1], Yuanpeng Liu[1] and Xuehong Chen[1]**

[1] Department of Pharmacology, School of Basic Medicine, Qingdao University, Qingdao, China, [2] Qingdao Mental Health Center, Qingdao, China

Chitosanase is a significant chitosan-degrading enzyme involved in industrial applications, which forms chitooligosaccharides (COS) as reaction products that are known to have various biological activities. In this study, the gene *csnS* was cloned from a deep-sea bacterium *Serratia* sp. QD07, as well as over-expressed in *Escherichia coli*, which is a new chitosanase encoding gene. The recombinant strain was cultured in a 5 L fermenter, which yielded 324 U/mL chitosanases. After purification, CsnS is a cold-adapted enzyme with the highest activity at 60°C, showing 37.5% of the maximal activity at 0°C and 42.6% of the maximal activity at 10°C. It exhibited optimum activity at pH 5.8 and was stable at a pH range of 3.4–8.8. Additionally, CsnS exhibited an endo-type cleavage pattern and hydrolyzed chitosan polymers to yield disaccharides and trisaccharides as the primary reaction products. These results make CsnS a potential candidate for the industrial manufacture of COS.

Keywords: chitosanase, chitooligosaccharides, deep-sea bacterium, *Serratia* sp. QD07, fermenter

OPEN ACCESS

Edited by:
Jinwei Zhang,
University of Exeter, United Kingdom

Reviewed by:
Carlos Padilha,
Federal University of Rio Grande do Norte, Brazil
Guolin Cai,
Jiangnan University, China

****Correspondence:***
Xuehong Chen
chen-xuehong@163.com

Specialty section:
This article was submitted to Microbiotechnology, a section of the journal Frontiers in Microbiology

Received: *21 October 2020*
Accepted: *08 February 2021*
Published: *24 February 2021*

Citation:
Zheng Q, Meng X, Cheng M, Li Y, Liu Y and Chen X (2021) Cloning and Characterization of a New Chitosanase From a Deep-Sea Bacterium Serratia sp. QD07. Front. Microbiol. 12:619731. doi: 10.3389/fmicb.2021.619731

INTRODUCTION

Chitosan, the primary deacetylation product of chitin, is a linear cationic polysaccharide comprising of β-(1,4)-linked D-glucosamine (GlcN or D unit) and *N*-acetyl-D-glucosamine (GlcNAc or A unit) (Muanprasat and Chatsudthipong, 2017). The chitosan polymer is a natural alkaline polysaccharide, insoluble in most neutral liquids such as water (Naveed et al., 2019). Chitooligosaccharide (COS), the degradation product of chitosan, has aroused an increasing interest due to its excellent biological properties and potential applications. Of particular importance are its admirable biological activities including anti-microbial (Fernandes et al., 2008), anti-fungal (Mei et al., 2015), anti-oxidant (Ma et al., 2020), anti-inflammatory (Kunanusornchai et al., 2016), anti-obesity (Huang et al., 2015), anti-tumor (Suzuki et al., 1986; Zhao et al., 2019), anti-hypertensive (Huang et al., 2005), anti-HIV-1 (Artan et al., 2010), anti-Alzheimer's (Eom et al., 2013), and immune-enhancing effects (Zhang et al., 2014). It also shows promise as a drug/DNA delivery agent (Kumari et al., 2018; Li et al., 2019a; Wang et al., 2020). Therefore, COS is a promising candidate with potential application in several fields, including the medical and pharmaceutical industries.

Chitosanases (EC 3.2.1.132) are divided into five families: GH-5, GH-8, GH-46, GH-75, and GH-80 in the CAZy database (Thadathil and Velappan, 2014). Families GH-5 and GH-8 could hydrolyze chitosan and some other glycosides, while the families GH-46, GH-75 and GH-80

comprise chitosanases merely (Johnsen et al., 2010). Chitosanases catalyzed the breaking of the β-(1,4) glycosidic bonds in chitosan to yield low molecular weight chitosan (LMWC) or COS with different Degree of Polymerization (DP) (Brzezinski, 2011). Due to the substrate specificity of different chitosanases, the degradation of COS by different DP resulted in different biological activities. For example, the DP 1-3 inhibits matrix metalloproteinase-9 in human fibrosarcoma cells (Van Ta et al., 2006); the DP 2-6 (Qiao et al., 2011) exhibit anti-inflammatory activity; the DP6 shows anti-tumor activity (Xiong et al., 2009), whereas the DP 8-12 have higher anti-oxidant activity (Li et al., 2012).

Currently, COS can be produced by chemical, physical, electrochemical and enzymatic methods (Liang et al., 2018). Owing to the lack of contaminants and the easily controllable nature of the process, using chitosanases are relatively satisfactory tools to produce COS in enzymatic methods. Considering the lack of a suitable commercial chitosanase for the production of COS, we previously established an efficient affinity purification method to rapidly detect chitosanase in bacterial cultural supernatant (Li et al., 2019b), and several chitosanase-producing marine bacteria strains including a deep-sea bacterium *Serratia* sp. QD07 were successfully isolated. Chitosanase is mainly derived from bacteria (Luo et al., 2020), but to a lesser extent from fungi (Wang et al., 2008), plant tissues (Osswald et al., 1994) and viruses (Blanc et al., 2014). Although many chitosanases have been reported, there are only a few chitosanases with cold adaptability (Johnsen et al., 2010; Qin et al., 2018; Yang et al., 2019). The yield of chitosanase of microorganisms reported so far is different.

In this study, the gene *csnS* was cloned from *Serratia* sp. QD07, as well as expressed in *Escherichia coli*, which is a chitosanase encoding gene. Additionally, an efficient fermentation and purification method was established and the biochemical features of CsnS were characterized.

RESULTS AND DISCUSSION

Sequence Analysis of CsnS

The deep-sea bacterium *Serratia* sp. QD07 was isolated from a sample of sea mud in the South China Sea (depth: 1179 m). This strain proliferated rapidly in the selection medium containing chitosan [0.5% (w/v)] and showed high chitosanases activity. Results of the sequence analysis showed that its genome contained a putative chitosanase-encoding gene, *csnS*. In this study, the *csnS* gene was cloned from *Serratia* sp. QD07, which consisted of an intact open reading frame (ORF) of 756 base pairs, and an encoded protein, CsnS containing 251 amino acid residues. Signal peptide analysis revealed that the *N*-terminal of CsnS lacked signal peptide. The theoretical pI of CsnS was 5.56, as well as the molecular weight (MW) of CsnS was 27.1 kDa.

The phylogenetic tree was established by sequences analysis of CsnS and some other reported chitosanases from families GH-46, GH-75, and GH-80 (**Figure 1**). CsnS was inferred to belong to the glycoside hydrolyase-46 (GH-46) family. It was found that CsnS showed higher homology with a GH-46 chitosanase (GenBank: AAA19865.1), obtained from a species of the genus *Streptomyces*. In addition, the conservative domain database (CDD) search was conducted on NCBI, and CsnS was a recognized chitosanase with a conservative domain, belonging to the family GH-46. To further analyze its structure, multiple sequence alignment (MSA) between CsnS and seven other GH-46 chitosanases was established. Results from the MSA (**Figure 2**) showed that the enzyme contains some conserved regions with this chitosanase of family GH-46. The conserved sites Glu35 and Asp53 play vital roles in the hydrolysis of glycosides (Saito et al., 1999; Lyu et al., 2015). The regions 'AENS' (34–37), 'IGFC' (62–65), 'VMHG' (161–164), and sites Tyr47, Ile51, Asp53, Arg55, Thr58, Asp69, and Tyr125 are related to sugar binding (Lyu et al., 2014).

Fermentation and Purification of CsnS

The first phase of the process commenced with an original glycerol concentration of 10 g/L. At the beginning of the second stage, when OD 600 value was 1.0, IPTG (0.1 mM) was added, and the fermentation temperature was reduced to 20°C. The culture volume used for expression and purification is 50 mL. During the entire process, the feeding was controlled by maintaining the concentration of dissolved oxygen at 30% of air saturation. Once the enzyme activity decreased, the fermentation process was stopped (**Figure 3**). At the end of the process at 60 h, the extracellular CsnS activity was calculated to be 324 U/mL.

The recombinant CsnS was purified 1.7-fold using Ni-NTA-Sepharose column chromatography. Its MW was determined by sodium dodecyl sulfate-polyacrylamide gel electrophoresis (SDS-PAGE) to be about 27 kDa (**Figure 4**), corresponding to the predicted MW. The specific activity of purified CsnS was determined to be 412.6 U/mg. The activity recovery was 91.9%.

The Different Conditions on the Production of CsnS

Effects of Different Cell Density OD 600 on the Induction Cultivation Phase on CsnS

Cell density OD 600 was a critical parameter, which led to a significant effect on the extracellular activity at induction cultivation phase. As shown in **Supplementary Figure 1**, the induced cells reached 8 and the extracellular activity was 26 U/mL at OD 600. Whereas, when the induced cells reached 1, the extracellular activity was the highest, 81 U/mL, which was 3.1-fold higher than that of cell density (OD 600) at 8. Moreover, it was 2.1-fold higher than that at 4 of OD 600, which exhibited an extracellular activity of 38 U/mL. The extracellular activity was closer to cell density OD 600 at 1 and 2, after induction, and the extracellular activity of cell density OD 600 at 2 was 71 U/mL which was lower than OD 600 at 1. Consequently, at OD 600 of the induced cells reached 1 of OD 600, *E. coli* was more beneficial to the secretion expression.

Effects of Temperature on the Secretion of CsnS

Temperature is a key parameter in the production of recombinant proteins in *Escherichia coli*. Generally, the recombinant *E. coli* would grow slowly at low temperature, and low production rate always conduced low protein yields. However, the high

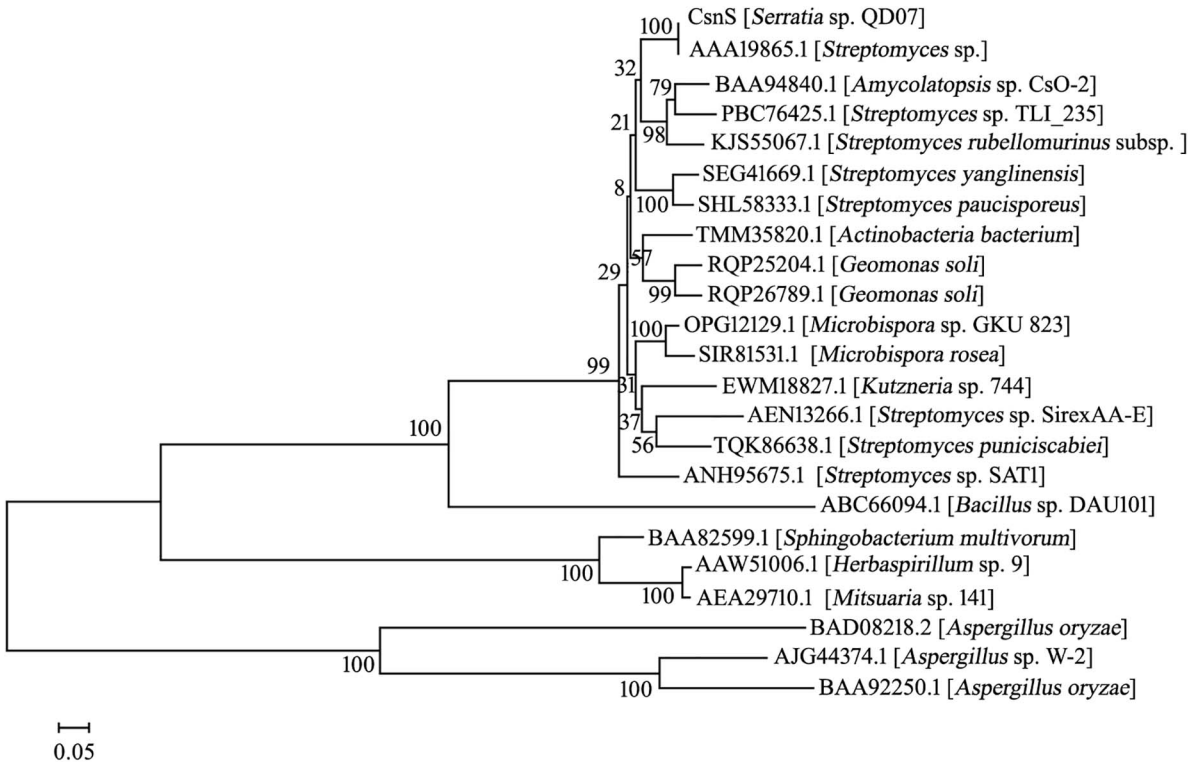

FIGURE 1 | The phylogenetic relationships between CsnS and other chitosanases from GH family 46, 75, and 80 is shown in the neighbor-joining tree. The bootstrap test of the tree repeated 1,000 times.

temperature would denature recombinant proteins and reduce enzyme activities. As shown in **Supplementary Figure 2**, under the induction temperature of 35°C, the number of OD 600-induced cells attained 8.9, while the extracellular activity was only 38 U/mL. By contrast, under the induction of 20°C, the coordination between protein synthesis and translocation was better, and extracellular activity was the highest, 82 U/mL, which was 2.1-fold higher than that under the induction of 35°C. The extracellular activity was 58 U/mL, 1.4-fold higher than that of 30°C. This high yield might be due to the low temperature which reduced the denaturation rate of the target proteins and allowed the freshly synthesized peptides to fold correctly. Although 15°C might be more suitable for CsnS production, the significantly lowered cell density limited its total protein yield. Consequently, *E. coli* was more favorable for secretion expression at a lower temperature of 20°C.

Effects of Concentration of IPTG on the Secretion of CsnS

The IPTG was added to induce the protein of CsnS expression. Actually, the IPTG was potentially toxic chemical that restrained cell growth with increasing concentration. Experiments were performed to investigate and identify the optimal induction concentration of IPTG. As shown in **Supplementary Figure 3**, at an induction concentration of 0.8 mM, OD 600 of the induced cells reached only 6.1, but the extracellular activity was also low and only 36 U/mL. When the induced concentration was 0.1 mM, the extracellular activity was the highest, 86 U/mL, 2.3-fold higher than that of 0.8 mM. Moreover, this activity was 1.4-fold higher than that of 0.4 mM, which exhibited the extracellular activity of 60 U/mL. The extracellular activity was closer at induction concentrations of IPTG at 0.1 mM and 0.2 mM, and the extracellular activity of induction concentrations at 0.2 mM was 77 U/mL. This low extracellular activity might be due to the low concentration of IPTG at 0.05 mM and high concentration of IPTG at 0.8 mM, which causes an inhibitory effect on the growth of *E. coli.* Consequently, at induction concentration of 0.1 mM, *E. coli* was more beneficial to the secretion expression.

Biochemical Properties of CsnS

The biochemical properties of recombinant CsnS were determined by the purified enzyme. As shown in **Figure 5A**, at 60°C, CsnS showed the highest activity. At the same time, CsnS exhibits 37.5% and 42.6% of its maximal activity at 0°C and 10°C, respectively, which is a cold-adapted enzyme. It can retain approximately 40% of enzyme activity at temperatures ranging from 0 to 100°C, which indicates the ruggedness of CsnS in extreme temperature conditions. Compared with temperature-sensitive enzymes, this kind of temperature-resistant enzyme has certain advantages in industrial production. On the one hand, the preparation cost of this kind of enzyme preparation is reduced, and the enzyme preparation has high stability, which can maintain the activity for a long time. On the other hand, the requirements for the reactor cooling system are reduced,

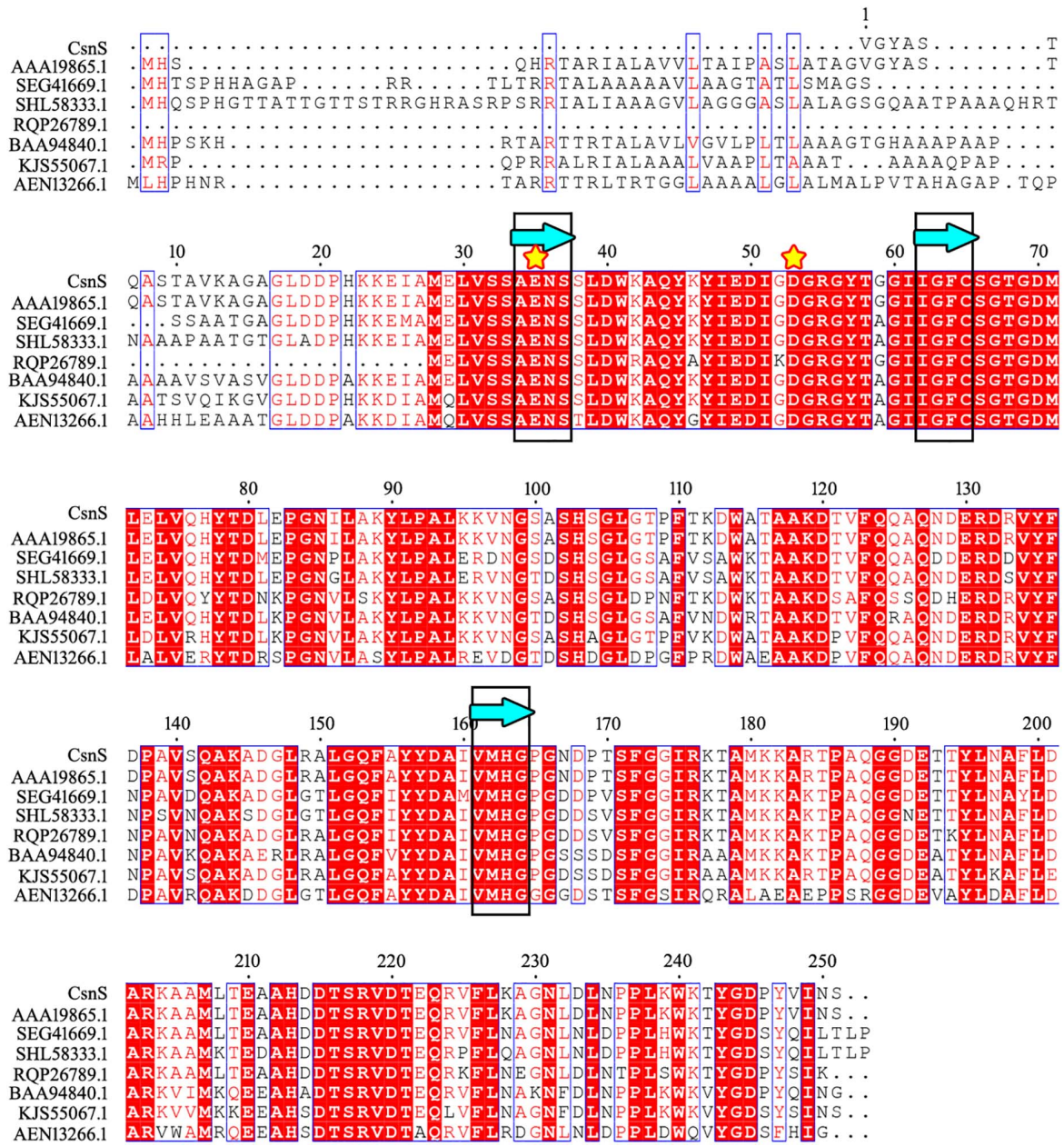

FIGURE 2 | Comparison of the sequence of CsnS with reported chitosanase activity from the GH-46 family: chitosanase from *Streptomyces* sp. N174 (GenBank number: AAA19865.1); chitosanase from *Streptomyces yanglinensis* (GenBank number: SEG41669.1); chitosanase from *Streptomyces paucisporeus* (GenBank number: SHL58333.1); chitosanase from *Geomonas soli* (GenBank number: RQP26789.1); chitosanase from *Amycolatopsis* sp. CsO-2 (GenBank number: BAA94840.1); chitosanase from *Streptomyces rubellomurinus subsp. indigoferus* (GenBank number: KJS55067.1); chitosanase from *Streptomyces* sp. SirexAA-E (GenBank number: AEN13266.1). The same sugar binding and catalytic sites are marked with blue bands (framed in black) and yellow stars, respectively.

which reduces energy consumption and pollution. In addition, CsnS has good enzyme activity at 60°C, and there are few hybrid bacteria living at 60°C, thus reducing the contamination of bacterial metabolites to products and improving the purity of products. After incubation at temperatures between 0 and 30°C for 2 h, the enzyme retained more than 80% of the initial activity (**Figure 5B**). These results show that the enzyme can be stored at room temperature and is capable of catalyzing hydrolysis at this temperature. This is a desirable property in industrial applications.

Assays to determine the optimal pH for CsnS activity were carried out with 0.3% (w/v) chitosan at pH 4.5–5.7. CsnS retained more than 60% of its activity in the experimental range and displayed optimal activity at pH 5.2 (**Figure 5C**). Additionally, the enzyme can retain more than 80% activity at pH 4.5–5.4. In order to study pH-stability of the enzyme, various buffers

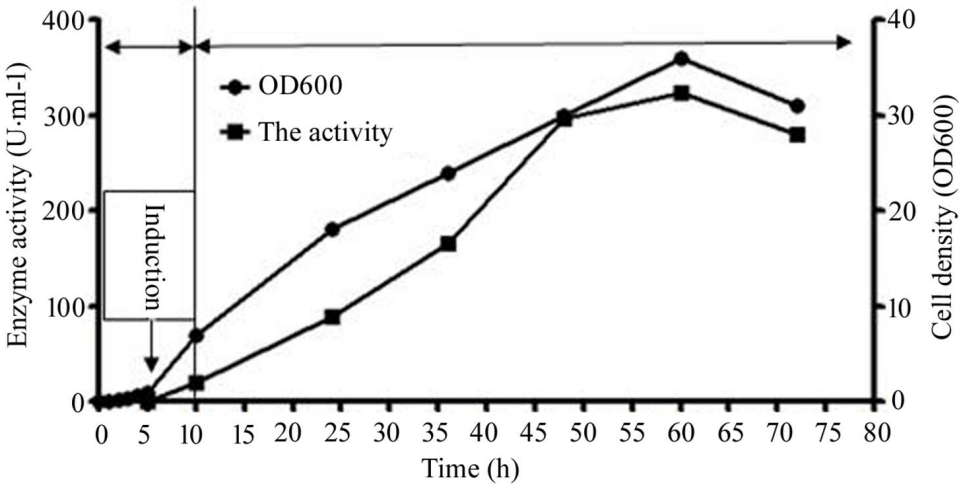

FIGURE 3 | The extracellular activity and cell growth of CsnS production by cultivation. And the entire culture procedure was distributed to three phases: the growth cultivation phase, the induction cultivation phase, and the fed-batch cultivation phase. Since OD 600 reached 1, the temperature was dropped to 20°C, as well as IPTG (0.1 mM) was added. Subsequently, the original glycerol was absolutely consumed, the feeding phase of fed-batch cultivation was initiated.

ranging from pH 3.4–9.4 were used in the assays (**Figure 5D**). The enzyme was found to be stable and retained more than 70% of its initial activity at a pH range of 3.4–8.2. At a higher pH value of 9.4, it retained about 35% of its original activity. Therefore, CsnS demonstrates high catalytic properties in either an acidic or alkaline environment and is stable over a broad range of pH. Because the fermentation process of pH sensing electrode sensor has been delayed, the pH of the fermentation medium is not fixed during the enzyme production process. Fortunately, pH has little effect on bacterial growth. Thus, pH fluctuations do not affect the enzyme activity of chitosanase during the fermentation process.

The effect of metal ions and reagents on the activities of CsnS was shown in **Table 1**. We found that except Cu^{2+} and Ni^{2+}, most metal ions can promote CsnS activity and maintain it above 70%. CsnS shows a strong ability to resist the interference of metal ions. Since most industrial equipments are constructed with metal, the non-reactivity of CsnS to metal ions could facilitate its use in the production process, thereby expanding its application efficiency.

Action Mode and Reaction Product Analysis

Thin-layer chromatography (TLC) was used to analyze the reaction products and the action modes of CsnS. As shown in **Figure 6**, no obvious chitooligosaccharides products appeared during the first 30 min of the reaction. When the substrate was hydrolyzed for 60 min, reaction products were observed, which were mainly a mixture of disaccharides (DP2), trisaccharides (DP3) and tetrasaccharides (DP4). With the extension of reaction time, the relative ratio of DP2 and DP3 oligomers enhanced, whereas those of the higher DP products reduced. Compared with CsnM (Zhou et al., 2019) we studied previously, the product increased DP-1 and DP-4. According to literature reports, DP2-4 chitosan oligosaccharide has a promising potential for a wide range of applications in the medical field, by virtue of its anti-inflammatory and anti-bacterial activities. These reaction products were similar to most known chitosanases, such as the CsnB from *Bacillus* sp. BY01 (Yang et al., 2019), CsnQ from *Bacillus* sp. Q1098 (Ma et al., 2020), Csn-BAC from *Bacillus* sp. MD-5 (Yang et al., 2020), and Csn-SP from *Bacillus* sp. DAU101 (Lee et al., 2006 and **Table 2**), all of which produced $(GlcN)_2$ and $(GlcN)_3$ as final products. Till date, the main products of chitosanases reported in the literature are mixtures of DP3-DP8, such as chitosanase from *Bacillus mycoides* TKU038 (Liang et al., 2016) and *Bacillus* sp. strain KCTC 0377BP (Choi et al., 2004), which are difficult to separate. We foresee CsnS as a potentially valuable agent in the manufacture of easily separable products in industrial production.

MATERIALS AND METHODS

Materials and Bacterial Cultures

We purchased *E. coli* strains BL21 (DE3) as well as expression vector, pET22b (+) from Takara (Dalian, China). From Aladdin Biochemical Technology Co., Ltd. (Shanghai, China), we purchased chitosan (degree of deacetylation $\geq$ 95%, viscosity: 100–200 mpa·s). And from Merck (Darmstadt, Germany), we purchased the thin-layer chromatography (TLC) silica gel plates.

Isolation of the Bacterial Strains *Serratia* sp. QD07

Deep-sea mud samples were collected from South China Sea (depth 1,179 m, E 118.16° N 22.01°) in August 2017. The samples were immersed, diluted, and spread on 2216E medium. Isolated colonies were cultured on chitosan selective medium containing 0.5% (w/v) chitosan, 0.1% (w/v) KH2PO4, 0.2% (w/v) K2HPO4, 0.07% (w/v) MgSO4,

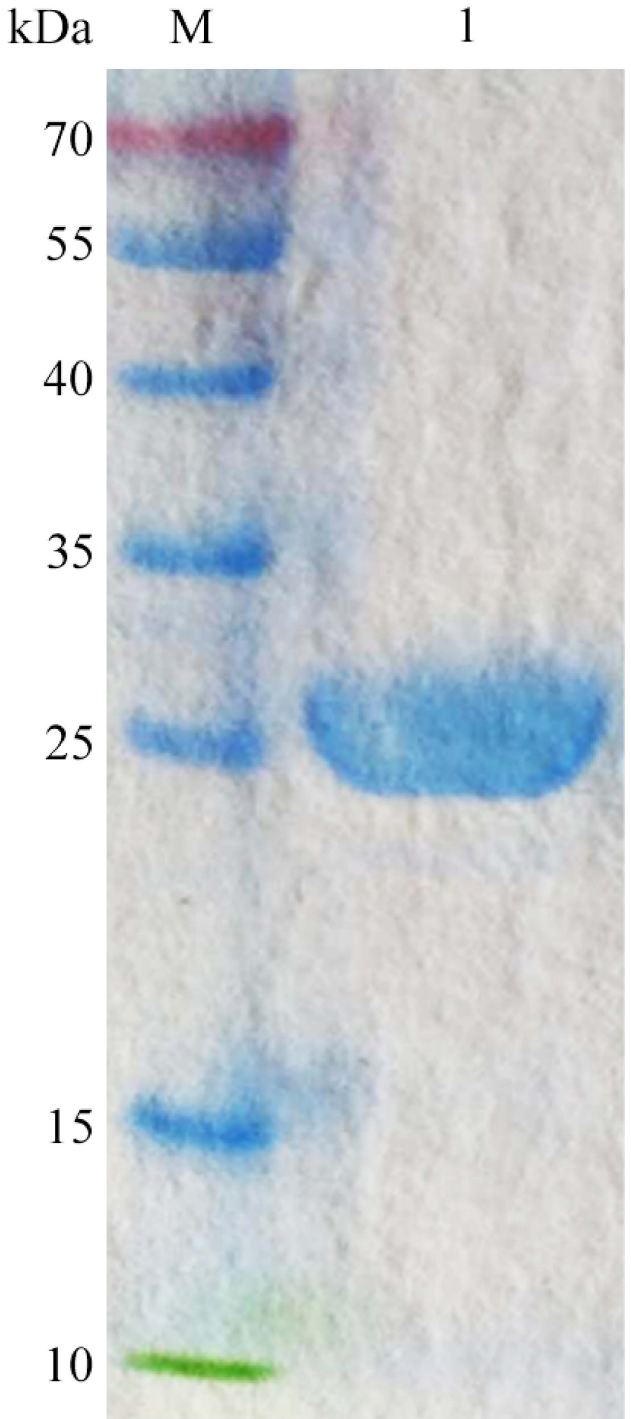

FIGURE 4 | SDS-PAGE analysis of the purified CsnS. M, molecular weight markers; 1, purified CsnS.

0.1% (w/v) NaCl, 0.01% (w/v) CaCl2, and 1% (w/v) agar. Strain QD07 was isolated and stored in our laboratory. Furthermore, this strain was identified as *Serratia* sp. QD07 using 16S rRNA gene sequence analysis (Genbank number: MT576555).

Sequence Analysis

The draft genome of *Serratia* sp. QD07 was determined by using our 2nd generation sequencer. A fictitious chitosanase encoding the gene *csnS* was identified and its protein sequence was registered in the GenBank database (Genbank number: MT241387). To further analyze the *csnS* gene sequence, we used the ORF search program[1] to determine the open reading frame (ORF). The signal peptide of CsnS via the SignalP 5.0 server[2] was analyzed. To improve phylogenetic analysis, using the Conserved Domain Database (CDD) to obtain domain and family information. For multi-sequence alignment, we used ClustalX2.1 and ESPript[3]. The phylogenetic tree was constructed by the MEGA 7.0 bootstrap adjacency binding method. In addition, it was using ExPASy[4] to determine the theoretical isoelectric point (pI) and MW of CsnS.

Expression of Recombinant Chitosanase

A polymerase chain reaction (PCR) was used to amplify the CsnS fragment without a terminator. The PCR primers used were Ep-CsnS-F and Ep-CsnS-R, which contained the recognition sites *Nco*I and *Xho*I, respectively. The amplified sequence was inserted into plasmid pET22b between the same recognition sites. *Escherichiacoli* BL21 (DE3) containing the recombinant plasmid pET22b-CsnS plasmid was inoculated into Luria-Bertani (LB) broth for growth at 37°C for 6 h.

High-Density Fermentation

60% glycerol stocks of the *E. coli* BL21-pET22b-CsnS cells were streaked on LB solid medium culture panel supplemented with 50 μg/mL ampicillin and incubated for 26 h at 37°C. *E. coli* colonies containing recombinant plasmid were inoculated in 5 mL LB medium containing 50 mg/mL ampicillin as well as incubated in a rotating shaking table (180 rpm) at 37°C overnight. The overnight cultivation (0.5 mL) was diluted to 50 mL Terrific Broth Medium (TB) including 50 mg/mL ampicillin and cultivated on a rotating shaking table (180 rpm) at 37°C before the optical density reading at 600 nm (OD 600) was 8.0. Accordingly, it was cultured in a bioreactor and fermented in a 5 L fermentation tank (BL Bio-5GJ, Shanghai, China). The 5% (v/v) seed culture was inoculated into TB medium. The complete culture process was divided into three stages. At the beginning of the first stage, the initial concentration of glycerol was 10 g/L at 37°C. When the OD 600 reading was 1.0, we moved to the second phase in which, isopropyl β-d-thiogalactoside (IPTG, 0.1 mM) was added to induce the protein formation. The cultivation temperature was decreased to 20°C and the sample was incubated. When glycerol in the medium was completely consumed, as indicated by a sudden increase in dissolved oxygen (DO) and it was reaching 60% of air saturation, we commenced the third phase. In this phase, we continued fermentation as a fed-batch with controlled feeding

[1]https://www.ncbi.nlm.nih.gov/orffinder/

[2]http://www.cbs.dtu.dk/services/SignalP/

[3]http://espript.ibcp.fr/ESPript/cgi-bin/ESPript.cgi

[4]https://web.expasy.org/cgi-bin/protparam/protparam

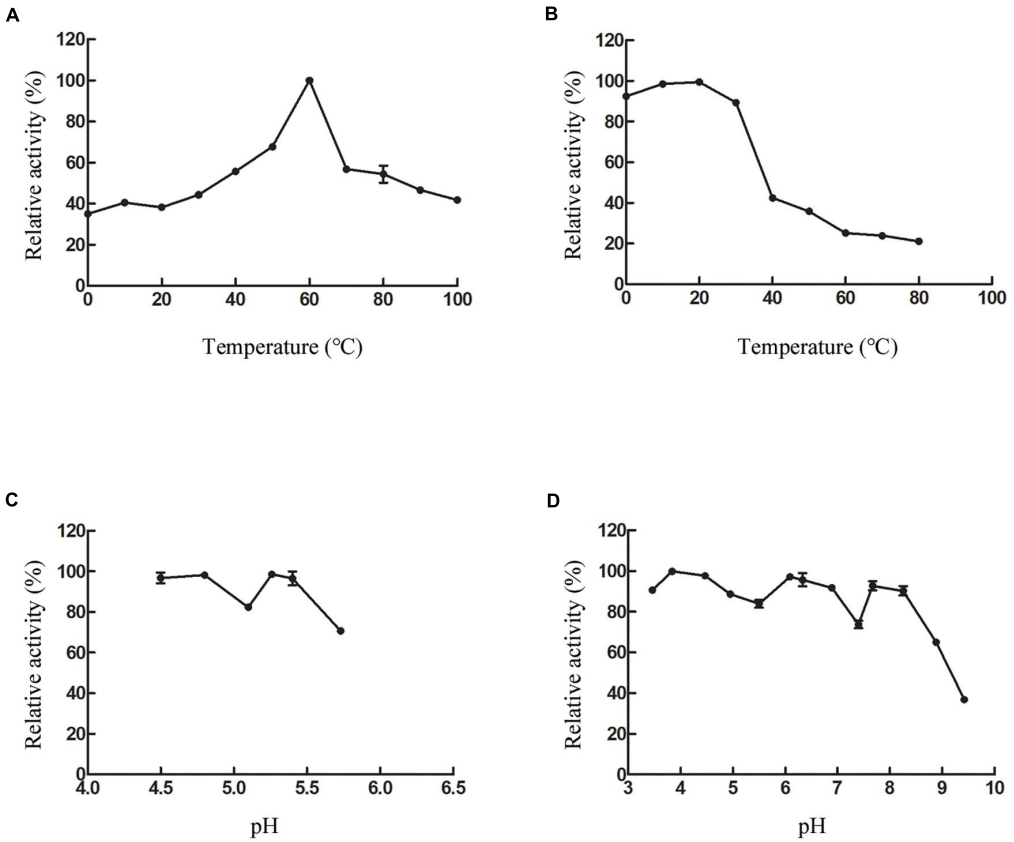

FIGURE 5 | Effect of temperature and pH on CsnS activity. **(A)** Effect of temperature on the activity of CsnS. **(B)** Thermal stability of CsnS. Enzyme was incubated for 2 h at 0–80°C. **(C)** Effect of pH on the activity of CsnS (Sodium acetate buffer pH 4.5–5.73). **(D)** pH stability of CsnS. The pH stability was analyzed by measuring the residual activity after pretreating the enzyme in different buffers at 4°C for 48 h (citric acid/Na2HPO4 buffer, pH 2.9–6.09; Na2HPO4/NaH2PO4 buffer, pH 6.33–7.40; Tris-HCl buffer, pH 7.67–8.25; glycine-NaOH buffer, pH 8.88–9.42). Data represent mean ± SD from three independent experiments.

to maintain a constant concentration of DO at 30% of air saturation. In the entire procedure, the pH was maintained at 7.0 throughout the addition of 20% (v/v) ammonia solution. The speed of cascade impeller was kept between 300 and 500 rpm, and the air source used compressed air with an airflow of 6 vvm.

Purification of Recombinant CsnS

The crude enzyme in the supernatant was harvested and centrifuged at 13,000 *g* at 4°C for 15 min. Phosphate buffers A (pH 8.0, 500 mM NaCl) and B (pH 8.0, 500 mM NaCl, 500 mM iminazole) were used in the purification process. Before the crude enzyme was loaded onto an Ni-NTA column in the AKTA150 automatic purification system, five column volumes of buffer A were used to wash the column in order to enable it to load proteins effectively. The sample loading speed was maintained at 1 mL/min. The target enzyme was eluted with buffer B by gradient elution. The enzyme purity and molecular mass were determined using SDS-PAGE.

The Fermentation Process of CsnS

In order to further optimize the fermentation, the recombinant strains containing CsnS were selected. To enhance the extracellular production of recombinant CsnS, we developed the process optimization strategies, as well as the effects of induction culture steps at various cell densities OD 600,

TABLE 1 | Effects of metal ions and reagents on the activity of CsnS.

Reagent added	Concentration (mM)	Relative activity (%)
None	–	100.0 ± 0.0
MgSO4	20	138.4 ± 3.3
$FeCl_3$	20	127.0 ± 3.1
$BaCl_2$	20	138.0 ± 4.4
$ZnCl_2$	20	114.3 ± 2.8
EDTA	20	131.4 ± 1.6
$FeSO_4$	20	140.3 ± 2.6
KCl	20	135.4 ± 0.1
$CuSO_4$	20	21.5 ± 0.4
Li_2SO_4	20	139.7 ± 3.1
$CoCl_2$	20	96.3 ± 3.8
SDS	20	119.3 ± 0.7
$(NH_4)_2SO_4$	20	141.4 ± 4.1
$Al_2(SO_4)_3$	20	140.7 ± 0.8
$CaCl_2$	20	139.2 ± 3.6
Nicl2	20	70.5 ± 0.8

Activity without addition of chemicals was defined as 100%. Data are shown as means ± SD (n = 3).

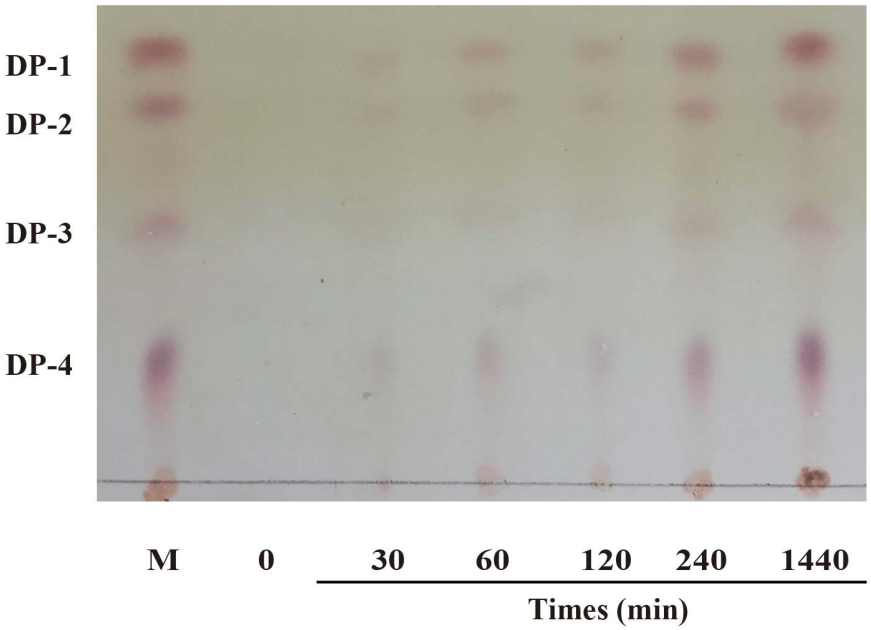

FIGURE 6 | TLC analysis of products after enzymatic hydrolysis.

TABLE 2 | Comparison of the CsnS properties with other reported chitosanases.

Name	GenBank no.	Orgnism source	Optimal pH	Stable pH range	Optimal temperature (°C)	Products (DP)	References
CsnS	MN963773	*Serratia* sp. QD101	5.8	3.4-8.8	60	2-3	This study
CsnQ	MN963773	*Bacillus* sp. Q1098	5.3	6.8-9.1	60	2	Mei et al., 2015
CsnB	MN531545	*Bacillus* sp. BY01	5.0	4.6-5.8	35	2-3	Liang et al., 2018
Csn-BAC	CP021911	*Bacillus* sp. MD-5	7.0	6.0-8.0	40	2-3	Li et al., 2019a
CS038	–	*Bacillus mycoides* TKU038	6.0	4.0-10.0	50	3-9	Lyu et al., 2015
CSN-SP	DQ316095	*Bacillus* sp. DAU101	7.5	–	50	2-3	Saito et al., 1999
chitosanase	AF334682	*Bacillus* sp. strain KCTC 0377BP	5.0	4.0-8.0	60	3-8	Luo et al., 2020
chitosanase	GQ487532	*Janthinobacterium* sp. 4239	5.0	–	45	1-2	Wang et al., 2020

induction temperatures, and various concentrations of IPTG were investigated.

Effects of Different Cell Density OD 600

To optimize the cell density OD 600 of induction for CsnS production, *Ecoli* strain harboring CsnS were induced at 0.5,1, 2, 4, and 8 in TB medium, respectively. The cell was incubated in 50 mL TB including 50 mg/mL ampicillin and cultured on a rotary shaker (180 rpm) at 37°C. When the optical density reached at various 600 nm (OD 600), and then reduced the temperature to 20°C. Accordingly, IPTG (0.1 mM) was added to induce the expression of target protein, and the cells were incubated for a further 24 h at 20°C sequentially.

Effects of Induction Temperature

To optimize the induction temperature of CsnS, *E.coli* strain containing CsnS were induced in TB medium at 15, 20, 25, 30, and 35°C, respectively. The cell was incubated in 50 mL TB including 50 mg/mL ampicillin, as well as cultured on a rotary shaker (180 rpm) at 37°C until the optical density at 600 nm (OD 600) attained 1. Accordingly, we put the shake flasks in a rotary shaker at various induction temperatures. Accordingly, IPTG (0.1 mM) was added to induce the expression of target protein, as well as the cultivation was continued for another 24 h at 20°C.

Effects of Different Concentrations of IPTG

The cells were incubated in 50 mL TB including 50 mg/mL ampicillin and placed in a rotary shaker (180 rpm) at 37°C and 600 nm (OD 600), until the optical density reached 1, and then dropped the temperature to 20°C. Various concentrations of IPTG (0.05, 0.1, 0.2, 0.4, and 0.8 mM) were added to induce the expression of the target protein, and the incubation at 20°C for an additional 24 h sequentially.

Assay of CsnS Activity

It was using the dinitrosalicylic acid method (DNS) to analyze CsnS activity. After diluting the enzyme in sodium acetate buffer (50 mM, pH 5.8), the enzymatic activity was measured using 100 μL enzyme and 900 μL 0.3% (w/v) chitosan at 60°C for

10 min. Next, 0.75 mL of 3,5-dinitrosalicylic acid was added into the mixture to reduce the reaction. Then, the mixture was boiled for 10 min and centrifuged to remove the debris, as well as the OD was determined at 520 nm. The mixture with inactivated enzyme constituted the control. One unit (U) of chitosanase was defined as the amount of chitosanase that delivered 1 μmol of reducing sugars per min under optimal conditions.

Effect of Temperature, pH and Metal Ions on CsnS

The enzyme was diluted 200 times with phosphate buffer (pH 7.0) for biochemical characteristic assays. The substrate chitosan 0.3% (w/v) at pH 5.8 was used in the assays to evaluate the influence of temperature and metal ions on the enzyme. The optimal reaction temperature of CsnS was determined, and its activity was measured at various reaction temperatures ranging from 0 to 100°C. Thermal stability was investigated by measuring the residual activity after pre-incubating the purified enzyme at 0–80°C for 2 h. In order to evaluate the effect of metal ions on CsnS, several solutions of metal ions at a final concentration of 20 mM solution were incubated with the purified enzyme at 4°C for 48 h and the enzyme activity was measured. To determine the optimal pH, the substrate chitosan (0.3% w/v) at varying pH (4.50–5.73) was prepared in sodium acetate buffer. Finally, to determine the effect of pH, the purified enzyme was incubated in various buffers with pH levels ranging from 3.4 to 9.4.

Analysis of CsnS Degradation Products

We used TLC to detect degradation products of CsnS, Purified CsnS (50 μL) was added to 450 μL of chitosan solution (3 mg/mL) and reacted at 60°C. The samples were subjected to several reaction times (10, 30, 60, 120, 240, and 1,440 min). The reaction was terminated by boiling the sample for 10 min. The inactivated samples (2 μL) were spotted on to a TLC plate and developed with *n*-propanol/30% ammonia (2:1) solution. The plates were sprayed with 0.5% ninhydrin in ethanol, and heated at 100°C for 20 min to visualize sugars.

CONCLUSION

In this study, CsnS, a new member of GH-46 chitosanase from deep-sea bacterium *Serratia* sp. QD07 was cloned as well as over-expressed in *E. coli*. The extracellular production of recombinant CsnS in a 5 L fermenter indicated a high enzyme activity of 324 U/mL. CsnS is a cold-adapted enzyme, which showed the highest activity at 60°C, and exhibited 37.5 and 42.6% of its maximal activity at 0°C and 10°C, respectively. Hydrolytic product analysis indicated that CsnS is an endo-type chitosanase, converting chitosan to $(GlcN)_2$ and $(GlcN)_3$. Therefore, we can conclude that CsnS has suitable properties and may have potential applications in the production of bioactive COS in the food and pharmaceutical industries.

DATA AVAILABILITY STATEMENT

The original contributions presented in the study are included in the article/**Supplementary Material**, further inquiries can be directed to the corresponding author/s.

AUTHOR CONTRIBUTIONS

QZ: formal analysis, writing – original draft preparation, conceptualization, and methodology. XM: editing, analysis, data curation, and software. MC: analysis. YL: software. YL: editing. XC: funding acquisition and supervision. All authors contributed to the article and approved the submitted version.

FUNDING

This work was supported by the National Natural Science Foundation of China (No. 81473384) and the Natural Science Foundation of Shandong Province (ZR2018BH036).

SUPPLEMENTARY MATERIAL

The Supplementary Material for this article can be found online at: https://www.frontiersin.org/articles/10.3389/fmicb.2021.619731/full#supplementary-material

Supplementary Figure 1 | Effects of different cell density OD600 in the induction cultivation phase on the extracellular activity in the shake flasks with TB medium at 0.5,1, 2, 4, and 8.

Supplementary Figure 2 | Effects of temperature on the extracellular activity and cell growth *Escherichia coli* strain which was grown in the shake flasks with TB medium at 15,20, 25, 30, and 35°C.

Supplementary Figure 3 | Effects of different concentrations of IPTG on the extracellular activity and cell growth in *Escherichia coli* strain which was grown in the shake flasks with TB medium at 0.05, 0.1, 0.2, 0.4, and 0.8 mM.

REFERENCES

Artan, M., Karadeniz, F., Karagozlu, M. Z., Kim, M. M., and Kim, S. K. (2010). Anti-HIV-1 activity of low molecular weight sulfated chitooligosaccharides. *Carbohydr. Res.* 345, 656–662. doi: 10.1016/j.carres.2009.12.017

Blanc, G., Mozar, M., Agarkova, I. V., Gurnon, J. R., Yanai-balser, G., Rowe, J. M., et al. (2014). Deep RNA sequencing reveals hidden features and dynamics of early gene transcription in *Paramecium bursaria Chlorella* virus 1. *PLoS One* 9:e90989. doi: 10.1371/journal.pone.0090989

Brzezinski, R. (2011). Uncoupling chitosanase production from chitosan. *Bioeng. Bugs* 2, 226–229. doi: 10.1186/1475-2859-10-7

Choi, Y. J., Kim, E. J., Piao, Z., Yun, Y. C., and Shin, Y. C. (2004). Purification and characterization of chitosanase from *Bacillus* sp. strain KCTC 0377BP and its application for the production of chitosan oligosaccharides. *Appl. Environ. Microbiol.* 70, 4522–4531. doi: 10.1128/aem.70.8.4522-4531.2004

Eom, T. K., Ryu, B., Lee, J. K., Byun, H. G., Park, S. J., and Kim, S. K. (2013). beta-secretase inhibitory activity of phenolic acid conjugated chitooligosaccharides. *J. Enzyme Inhib. Med. Chem.* 28, 214–217. doi: 10.3109/14756366.2011.629197

Fernandes, J. C., Tavaria, F. K., Soares, J. C., Ramos, O. S., Joao Monteiro, M., Pintado, M. E., et al. (2008). Antimicrobial effects of chitosans and chitooligosaccharides, upon *Staphylococcus aureus* and *Escherichia coli*, in food model systems. *Food Microbiol.* 25, 922–928. doi: 10.1016/j.fm.2008.05.003

Huang, L., Chen, J., Cao, P., Pan, H., Ding, C., Xiao, T., et al. (2015). Anti-obese effect of glucosamine and chitosan oligosaccharide in high-fat diet-induced obese rats. *Mar. Drugs* 13, 2732–2756. doi: 10.3390/md13052732

Huang, R., Mendis, E., and Kim, S. K. (2005). Improvement of ACE inhibitory activity of chitooligosaccharides (COS) by carboxyl modification. *Bioorg. Med. Chem.* 13, 3649–3655. doi: 10.1016/j.bmc.2005.03.034

Johnsen, M. G., Hansen, O. C., and Stougaard, P. (2010). Isolation, characterization and heterologous expression of a novel chitosanase from *Janthinobacterium* sp. strain 4239. *Microb. Cell Fact.* 9:5. doi: 10.1186/1475-2859-9-5

Kumari, M., Liu, C. H., and Wu, W. C. (2018). Protein moiety in oligochitosan modified vector regulates internalization mechanism and gene delivery: polyplex characterization, intracellular trafficking and transfection. *Carbohydr. Polym.* 202, 143–156. doi: 10.1016/j.carbpol.2018.08.131

Kunanusornchai, W., Witoonpanich, B., Tawonsawatruk, T., Pichyangkura, R., Chatsudthipong, V., and Muanprasat, C. (2016). Chitosan oligosaccharide suppresses synovial inflammation via AMPK activation: an in vitro and in vivo study. *Pharmacol. Res.* 113(Pt A), 458–467. doi: 10.1016/j.phrs.2016.09.016

Lee, Y. S., Yoo, J. S., Chung, S. Y., Lee, Y. C., Cho, Y. S., and Choi, Y. L. (2006). Cloning, purification, and characterization of chitosanase from *Bacillus* sp. DAU101. *Appl. Microbiol. Biotechnol.* 73, 113–121. doi: 10.1007/s00253-006-0444-0

Li, K., Xing, R., Liu, S., Qin, Y., Li, B., Wang, X., et al. (2012). Separation and scavenging superoxide radical activity of chitooligomers with degree of polymerization 6-16. *Int. J. Biol. Macromol.* 51, 826–830. doi: 10.1016/j.ijbiomac.2012.07.031

Li, S., Wang, L., Chen, X., Sun, M., and Han, Y. (2019a). Design and synthesis of a chitodisaccharide-based affinity resin for chitosanases purification. *Mar. Drugs* 17:68. doi: 10.3390/md17010068

Li, S., Wang, Y., Li, X., Lee, B. S., Jung, S., and Lee, M. S. (2019b). Enhancing the thermo-stability and anti-biofilm activity of alginate lyase by immobilization on low molecular weight chitosan nanoparticles. *Int. J. Mol. Sci.* 20:4565. doi: 10.3390/ijms20184565

Liang, S., Sun, Y., and Dai, X. (2018). A review of the preparation, analysis and biological functions of chitooligosaccharide. *Int. J. Mol. Sci.* 19:2197. doi: 10.3390/ijms19082197

Liang, T. W., Chen, W. T., Lin, Z. H., Kuo, Y. H., Nguyen, A. D., Pan, P. S., et al. (2016). An amphiprotic novel chitosanase from *Bacillus mycoides* and its application in the production of chitooligomers with their antioxidant and anti-inflammatory evaluation. *Int. J. Mol. Sci.* 17:1302. doi: 10.3390/ijms17081302

Luo, S., Qin, Z., Chen, Q., Fan, L., Jiang, L., and Zhao, L. (2020). High level production of a *Bacillus amlyoliquefaciens* chitosanase in *Pichia pastoris* suitable for chitooligosaccharides preparation. *Int. J. Biol. Macromol.* 149, 1034–1041. doi: 10.1016/j.ijbiomac.2020.02.001

Lyu, Q., Shi, Y., Wang, S., Yang, Y., Han, B., Liu, W., et al. (2015). Structural and biochemical insights into the degradation mechanism of chitosan by chitosanase OU01. *Biochim. Biophys. Acta* 1850, 1953–1961. doi: 10.1016/j.bbagen.2015.06.011

Lyu, Q., Wang, S., Xu, W., Han, B., Liu, W., Jones, D. N., et al. (2014). Structural insights into the substrate-binding mechanism for a novel chitosanase. *Biochem. J.* 461, 335–345. doi: 10.1042/bj20140159

Ma, C., Li, X., Yang, K., and Li, S. (2020). Characterization of a new chitosanase from a marine *Bacillus* sp. and the anti-oxidant activity of its hydrolysate. *Mar. Drugs* 18:126. doi: 10.3390/md18020126

Mei, Y. X., Dai, X. Y., Yang, W., Xu, X. W., and Liang, Y. X. (2015). Antifungal activity of chitooligosaccharides against the dermatophyte *Trichophyton rubrum*. *Int. J. Biol. Macromol.* 77, 330–335. doi: 10.1016/j.ijbiomac.2015.03.042

Muanprasat, C., and Chatsudthipong, V. (2017). Chitosan oligosaccharide: biological activities and potential therapeutic applications. *Pharmacol. Ther.* 170, 80–97. doi: 10.1016/j.pharmthera.2016.10.013

Naveed, M., Phil, L., Sohail, M., Hasnat, M., Baig, M., Ihsan, A. U., et al. (2019). Chitosan oligosaccharide (COS): an overview. *Int. J. Biol. Macromol.* 129, 827–843. doi: 10.1016/j.ijbiomac.2019.01.192

Osswald, W. F., Shapiro, J. P., Doostdar, H., Mcdonald, R. E., Niedz, R. P., Nairn, C. J., et al. (1994). Identification and characterization of acidic hydrolases with chitinase and chitosanase activities from sweet orange callus tissue. *Plant Cell Physiol.* 35, 811–820.

Qiao, Y., Bai, X. F., and Du, Y. G. (2011). Chitosan oligosaccharides protect mice from LPS challenge by attenuation of inflammation and oxidative stress. *Int. Immunopharmacol.* 11, 121–127. doi: 10.1016/j.intimp.2010.10.016

Qin, Z., Chen, Q., Lin, S., Luo, S., Qiu, Y., and Zhao, L. (2018). Expression and characterization of a novel cold-adapted chitosanase suitable for chitooligosaccharides controllable preparation. *Food Chem.* 253, 139–147. doi: 10.1016/j.foodchem.2018.01.137

Saito, J., Kita, A., Higuchi, Y., Nagata, Y., Ando, A., and Miki, K. (1999). Crystal structure of chitosanase from *Bacillus circulans* MH-K1 at 1.6-A resolution and its substrate recognition mechanism. *J. Biol. Chem.* 274, 30818–30825. doi: 10.1074/jbc.274.43.30818

Suzuki, K., Mikami, T., Okawa, Y., Tokoro, A., Suzuki, S., and Suzuki, M. (1986). Antitumor effect of hexa-N-acetylchitohexaose and chitohexaose. *Carbohydr. Res.* 151, 403–408. doi: 10.1016/s0008-6215(00)90359-8

Thadathil, N., and Velappan, S. P. (2014). Recent developments in chitosanase research and its biotechnological applications: a review. *Food Chem.* 150, 392–399. doi: 10.1016/j.foodchem.2013.10.083

Van Ta, Q., Kim, M. M., and Kim, S. K. (2006). Inhibitory effect of chitooligosaccharides on matrix metalloproteinase-9 in human fibrosarcoma cells (HT1080). *Mar. Biotechnol.* 8, 593–599. doi: 10.1007/s10126-006-6031-7

Wang, J., Zhou, W., Yuan, H., and Wang, Y. (2008). Characterization of a novel fungal chitosanase Csn2 from *Gongronella* sp. JG. *Carbohydr. Res.* 343, 2583–2588. doi: 10.1016/j.carres.2008.08.004

Wang, Y., Li, S., Jin, M., Han, Q., Liu, S., Chen, X., et al. (2020). Enhancing the thermo-stability and anti-bacterium activity of lysozyme by immobilization on chitosan nanoparticles. *Int. J. Mol. Sci.* 21:1635. doi: 10.3390/ijms21051635

Xiong, C., Wu, H., Wei, P., Pan, M., Tuo, Y., Kusakabe, I., et al. (2009). Potent angiogenic inhibition effects of deacetylated chitohexaose separated from chitooligosaccharides and its mechanism of action in vitro. *Carbohydr. Res.* 344, 1975–1983. doi: 10.1016/j.carres.2009.06.036

Yang, G., Sun, H., Cao, R., Liu, Q., and Mao, X. (2020). Characterization of a novel glycoside hydrolase family 46 chitosanase, Csn-BAC, from *Bacillus* sp. MD-5. *Int. J. Biol. Macromol.* 146, 518–523. doi: 10.1016/j.ijbiomac.2020.01.031

Yang, Y., Zheng, Z., Xiao, Y., Zhang, J., Zhou, Y., Li, X., et al. (2019). Cloning and characterization of a cold-adapted chitosanase from marine bacterium *Bacillus* sp. BY01. *Molecules* 24:3915. doi: 10.3390/molecules24213915

Zhang, P., Liu, W., Peng, Y., Han, B., and Yang, Y. (2014). Toll like receptor 4 (TLR4) mediates the stimulating activities of chitosan oligosaccharide on macrophages. *Int. Immunopharmacol.* 23, 254–261. doi: 10.1016/j.intimp.2014.09.007

Zhao, M., Gu, L., Li, Y., Chen, S., You, J., Fan, L., et al. (2019). Chitooligosaccharides display anti-tumor effects against human cervical cancer cells via the apoptotic and autophagic pathways. *Carbohydr. Polym.* 224:115171. doi: 10.1016/j.carbpol.2019.115171

Zhou, Y., Chen, X., Li, X., Han, Y., Wang, Y., Yao, R., et al. (2019). Purification and characterization of a new cold-adapted and thermo-tolerant chitosanase from marine bacterium *Pseudoalteromonas* sp. SY39. *Molecules* 24:183. doi: 10.3390/molecules24010183

Conflict of Interest: The authors declare that the research was conducted in the absence of any commercial or financial relationships that could be construed as a potential conflict of interest.

frontiers in Microbiology

ORIGINAL RESEARCH
published: 12 March 2021
doi: 10.3389/fmicb.2021.631039

Expression and Characterization of a Thermostable Carrageenase From an Antarctic *Polaribacter* sp. NJDZ03 Strain

*Yuanyuan Gui[1,2,3], Xiaoqian Gu[4], Liping Fu[2,3], Qian Zhang[2,3], Peiyu Zhang[1] and Jiang Li[2,3]**

[1] College of Environmental Science and Engineering Qingdao University, Qingdao, China, [2] Marine Bioresource and Environment Research Center, First Institute of Oceanography, Ministry of Natural Resources, Qingdao, China, [3] Key Laboratory of Ecological Environment Science and Technology, First Institute of Oceanography, Ministry of Natural Resources, Qingdao, China, [4] CAS and Shandong Province Key Laboratory of Experimental Marine Biology, Institute of Oceanology, Chinese Academy of Sciences, Qingdao, China

OPEN ACCESS

Edited by:
Runying Zeng, Third Institute of Oceanography, State Oceanic Administration, China

Reviewed by:
Lingling Wang, Dalian Ocean University, China
Dewi Seswita Zilda, Research Center for Marine and Fisheries Product Processing and Biotechnology, Indonesia

***Correspondence:**
Jiang Li
lijiang@fio.org.cn

Specialty section:
This article was submitted to Microbiotechnology, a section of the journal Frontiers in Microbiology

Received: *19 November 2020*
Accepted: *22 February 2021*
Published: *12 March 2021*

Citation:
Gui Y, Gu X, Fu L, Zhang Q, Zhang P and Li J (2021) Expression and Characterization of a Thermostable Carrageenase From an Antarctic Polaribacter sp. NJDZ03 Strain. Front. Microbiol. 12:631039. doi: 10.3389/fmicb.2021.631039

The complete genome of *Polaribacter* sp. NJDZ03, which was isolated from the surface of Antarctic macroalgae, was analyzed by next-generation sequencing, and a putative carrageenase gene *Car3206* was obtained. *Car3206* was cloned and expressed in *Escherichia coli* BL21(DE3). After purification by Ni-NTA chromatography, the recombinant Car3206 protein was characterized and the antioxidant activity of the degraded product was investigated. The results showed that the recombinant plasmid pet-30a-*car3206* was highly efficiently expressed in *E. coli* BL21(DE3). The purified recombinant Car3206 showed a single band on sodium dodecyl sulfate-polyacrylamide gel electrophoresis, with an apparent molecular weight of 45 kDa. The optimum temperature of the recombinant Car3206 was 55°C, and it maintain 60–94% of its initial activity for 4–12 h at 55°C. It also kept almost 70% of the initial activity at 30°C, and more than 40% of the initial activity at 10°C. These results show that recombinant Car3206 had good low temperature resistance and thermal stability properties. The optimum pH of recombinant Car3206 was 7.0. Car3206 was activated by Na^+, K^+, and Ca^{2+}, but was significantly inhibited by Cu^{2+} and Cr^{2+}. Thin-layer chromatographic analysis indicated that Car3206 degraded carrageenan generating disaccharides as the only products. The antioxidant capacity of the degraded disaccharides *in vitro* was investigated and the results showed that different concentrations of the disaccharides had similar scavenging effects as vitamin C on $O_{2\bullet}^-$, •OH, and DPPH•. To our knowledge, this is the first report about details of the biochemical characteristics of a carrageenase isolated from an Antarctic *Polaribacter* strain. The unique characteristics of Car3206, including its low temperature resistance, thermal stability, and product unity, suggest that this enzyme may be an interesting candidate for industrial processes.

Keywords: carrageenase, gene expression, enzymatic characterization, enzymatic hydrolysis, antioxidant capacity

INTRODUCTION

Carrageenans are high molecular weight sulfated polysaccharides that are important components of the cell walls of red seaweeds (*Rhodophyta*) (Hjerde et al., 2017). They are composed of alternating 3-linked β-D-galactopyranose and 4-linked α-D-galactopyranose or 4-linked 3,6-anhydro-α-D-galactopyranose disaccharide repeat units (Boulho et al., 2017). Carrageenans are linear sulfated polysaccharides that have been classified into κ-, ι-, and λ-carrageenan families according to the location and number of sulfate substitutions. Among them, κ-carrageenans are the most common in industrial production.

The molecular weight of seaweed polysaccharides is an important factor that affects their biological function (Jiao et al., 2011). Therefore, compared with carrageenans, carrageenan oligosaccharides have lower molecular weights, stronger tissue penetration abilities, and more extensive application fields (Sun et al., 2015). Numerous studies have shown that carrageenan oligosaccharides have many biological roles, including antitumor (Calvo et al., 2019), antiviral (Kalitnik et al., 2013), antioxidant (Sun et al., 2010), and immunomodulation activities (Huang et al., 2020). Carrageenan degradation methods include chemical methods, such as acid hydrolysis, that usually do not keep native constituents intact (Hjerde et al., 2017); physical methods that degrade carrageenans mainly by ultrasonic, microwave, or radiation, which do not change the composition and structure of oligosaccharides, but the reaction conditions are difficult to control (Abad et al., 2009); and biological enzymatic methods with carrageenases that degrade carrageenans, which can lead to more efficient production of single stereoisomers, fewer side reactions, and a lower environmental burden (Zhao et al., 2018), and is an ideal way to obtain carrageenan oligosaccharides. However, the carrageenase-producing bacteria isolated from nature have the disadvantages of low enzyme production and poor enzyme stability (Kang et al., 2014; Barbeyron et al., 2019). Microbial enzymes that hydrolyze carrageenan are of considerable interest because enzymatic degraded products of carrageenan are still in their infancy compared with other algal polymers such as agar and alginate (Michel et al., 2001a,b, 2006; Chauhan and Saxena, 2016). Therefore, obtaining highly efficient strains, especially of bacteria isolated for special environments, which degrade carrageenans and produce highly activity carrageenases is of great value. A large number of cold-adapted marine bacteria that degrade polysaccharides have been found in extreme environments, such as the Antarctic and deep seas (Jain and Krishnan, 2017), so the characterization of microorganisms from these environments may contribute to the discovery of novel polysaccharide-degrading enzymes for industrial applications.

Studies have shown that carrageenan oligosaccharides have strong antioxidant properties *in vitro* (Yuan et al., 2006). The term antioxidant generally refers to a compound that can scavenge reactive oxygen species (ROS). There are two types of ROS, oxygen-containing free radicals, which are associated with oxygen metabolism, and peroxides, which easily form free radicals (Cadenas and Davies, 2000). Oxygen-containing free radicals include superoxide ($O_2^{-\bullet}$), hydroxyl (•OH), and hydroperoxyl (HO_2) radicals, and peroxides include hydrogen peroxide (H_2O_2) and lipid peroxides (ROOH). Among the ROS, •OH, and $O_2^{-\bullet}$ have the highest toxicity and cause tissue lipid peroxidation, protein depolymerization, nucleic acid fracture, and polysaccharide depolymerization, all of which can harm organisms. Therefore, the scavenging rates of •OH and $O_2^{-\bullet}$ are important indicators that reflect the antioxidant effects of antioxidants. Synthetic antioxidants are commonly used in industry, but because of toxicological safety concerns their use is restricted (Qi et al., 2005). Carrageenan oligosaccharides are expected to be developed for use in the food processing and pharmaceutical industries as natural antioxidants.

In this study, we expressed and characterized a κ-carrageenase, Car3206, that was obtained from *Polaribacter* sp. NJDZ03, which was isolated from the surface of Antarctic macroalgae. After recombinant expression, the recombinant Car3206 was purified, and its enzymatic properties were characterized. The antioxidant activity of carrageenan oligosaccharides produced by Car3206 was investigated by measuring their ability to scavenge the superoxide, hydroxyl, and DPPH (1,1-diphenyl-2-picrylhydrazyl) radicals. The results will provide a good foundation for the future research and development of marine biological resources and industrial high-value production and utilization.

MATERIALS AND METHODS

Bacterial Strains, Plasmids, and Culture Conditions

A strain producing carrageenan lyase, *Polaribacter* sp. NJDZ03, was isolated from the surface of Antarctic macroalgae and was screened by detecting halo on carrageenan plates with Lugol's solution (Potassium iodide and Iodine) as chromogenic agent (**Supplementary Figure 1**). The strain *Polaribacter* sp. NJDZ03 preserved in the Key Laboratory of Marine Bioactive Substances, First Institute of Oceanography, Ministry of Natural Resources (Qingdao, China). This carrageenase-producing strain was grown at 15°C in a medium containing 0.5% tryptone, 0.1% yeast extract, and seawater. *Escherichia coli* BL21(DE3) (Tiangen Bio, Co., Ltd., Beijing, China) and *E. coli* DH5α (Tiangen) containing the pET-30a(His•Tag) plasmid (Takara Bio Inc., Beijing, China) were grown at 37°C in Luria–Bertani (LB) medium containing 10% tryptone, 5% yeast extract, and 10% NaCl or LB agar supplemented with kanamycin (50 mg/mL).

Cloning and Analysis of the Recombinant Car3206 Nucleotide and Amino Acid Sequences

Genomic DNA was extracted from *Polaribacter* sp. NJDZ03 using a Genomic DNA Extraction Kit (Takara, Shiga, Japan) and used as the template of PCR amplification. The forward and reverse primers were 5′-CGCCATATGATTAATAAATATAAAAGCGCA-3′ (underlined bases are the added *Nde*I site) and 5′-CCCAAGCTTCTGTATTGGTTATTGCTGCC-3′ (underlined bases are the added *Hind*III site). The PCR system (50 μL) was

as follows: Master Mix (Tiangen) 25 μL, forward and reverse primers 1 μL each, template 1 μL, and ddH_2O 22 μL. The PCR conditions were: 94°C for 2 min, and 35 cycles of 94°C for 30 s, 56°C for 30 s, and 72°C for 1.5 min, with a final extension step held at 72°C for 10 min. The PCR products were purified using a DNA purification kit (Takara, Shiga, Japan), then ligated into pET-30a(His•Tag), which was digested previously with *Nde*I (Takara) and *Hind*III (Takara). The constructed expression plasmid was transformed into *E. coli* DH5α cells. The transformed cells were screened using LB agar supplemented with kanamycin (50 mg/mL) at 37°C for 12 h, Then, the positive colonies were picked and put into the LB medium with kanamycin (50 mg/mL) at 37°C for 12 h. The PCR products were sequenced by the Shanghai Sangon Company.

The nucleotide and amino acid sequences were analyzed using GeneMark software[1]. BlastP and BlastN[2] searches were performed to identify the sequences and Motif Search[3] was used for motif analyses. The DNAMAN software package[4] was used for multiple sequence alignment.

Expression and Purification of the Recombinant Car3206 Protein

The *Car3206* gene was ligated into a pET-30a expression vector and transformed into *E. coli* BL21(DE3) cells. The cells harboring the pET30a–*Car3206* recombinant plasmid were grown in LB medium containing kanamycin (50 μg/mL) on a rotary shaker (150 rpm) at 37°C. When the OD_{600} reached 0.6, isopropyl-β-D-thiogalactopyranoside (IPTG) (0.5 mM) was added to the LB medium. Cultivation was continued for 16 h at 16°C and 120 rpm. Then, the cells were harvested by centrifugation (4°C, 7,500 × *g*, 20 min), resuspended in phosphate buffer (0.2 M Na_2HPO_4-NaH_2PO_4, pH 7.0), and disrupted using an ultrasonic cell disruptor (Biosafer, China). Cell debris was removed and the supernatant was obtained by centrifugation (4°C, 10,000 × *g*, 10 min). The target protein was purified using a His Bind Purification Kit (GE Healthcare, Co., Ltd., United States) and washed with binding buffer (20 mmol/L sodium phosphate, 0.5 mol/L NaCl, 20 mmol/L imidazole, pH 7.4). Then, the recombinant Car3206 was eluted using elution buffer (20 mM sodium phosphate, 500 mM NaCl, pH 7.4) with a linear gradient to 250 mM imidazole (Riera et al., 2003). The purity of the eluted recombinant Car3206 protein was analyzed by 12% sodium dodecyl sulfate-polyacrylamide gel electrophoresis (SDS-PAGE).

Assay of Car3206 Enzyme Activity

The enzymatic hydrolysis reaction system was as follows: 200 μL carrageenase was incubated with 1,800 μL phosphate buffer (0.2 M Na_2HPO_4-NaH_2PO_4, pH 7.0) containing 0.1% (w/v) carrageenan at 55°C for 45 min. The reducing oligosaccharide products in the reaction mixture were assayed using the 3,5-dinitrosalicylic acid method (Miller, 1959). One unit of enzyme (U) was defined as the amount of carrageenase needed to liberate 1 μM reducing sugar (measured as D-galactose) from carrageenan per min. All assays were performed in triplicate.

Characterization of the Recombinant Car3206 Protein

The optimum temperature for recombinant Car3206 activity was determined under standard assay conditions by varying the incubation temperature from 10 to 90°C. As the control, the highest enzyme activity was defined as 100%. The thermal stability of recombinant Car3206 was determined by incubating the enzyme solution at 45, 55, or 65°C for different times (1, 2, 3, 4, 5, 12, and 24 h) then measuring the residual enzyme activity under the standard assay conditions. As the control, the highest enzyme activity was defined as 100%.

The effect of pH on the recombinant Car3206 activity was assayed by incubating with 0.1% (w/v) carrageenan dissolved in different buffer systems, namely Na_2HPO_4-citric acid (pH 4.0–7.0), 0.05 M Tris–HCl (pH 7.1–8.9), and 0.05 M glycine-NaOH (pH 9.0–10.6) under standard assay conditions. As the control, the highest enzyme activity was defined as 100%.

The effects of various metal ions and a reagent on the activity of the recombinant Car3206 were determined by monitoring enzymatic activity in the presence of 5 mM of metal ions (Mn^{2+}, Sr^{2+}, Fe^{2+}, Fe^{3+}, Mg^{2+}, Ca^{2+}, Cr^{2+}, Cu^{2+}, Na^{+}, and K^{+}) and EDTA. Each test was conducted under standard assay conditions. As the control, the carrageenase activity without the metal ions or reagent was set as 100%.

Analysis and Preparation of Enzymatic Hydrolysis Products

Enzymatic hydrolysis products of carrageenan were determined by thin layer chromatography. We incubated 2 mL purified enzyme with 8 mL phosphate buffer (0.2 M Na_2HPO_4-NaH_2PO_4, pH 7.0) containing 0.1% (w/v) carrageenan at 55°C for 0.5, 1, and 6 h. The solutions were boiled for 10 min, then centrifuged (4°C, 10,000 × *g*, 10 min). The products at the different reaction times were added to Silica gel 60 F_{254} thin-layer chromatography plates (Merck, Germany) with the developing system (n-butanol:ethanol:water = 2:1:1, v/v/v). The resultant oligosaccharide spots were visualized by spraying with 10% (v/v) H_2SO_4 in ethanol and heating at 80°C for 15 min.

In addition, the 6-h hydrolysis product was collected, filtered, and concentrated using an Amicon Ultra-15 centrifugal filter unit (Millipore, Germany). The filtrate was evaporated, lyophilized, and collected as the oligosaccharide products for the antioxidant assay.

Antioxidant Activity of Enzymatic Hydrolysate

Scavenging Assay of Superoxide Radical ($O_2^{-\bullet}$)

The scavenging assay of $O_2^{-\bullet}$ was based on a modified phenazine-methosulfate (PMS)-NADH method (Siddhuraju and Becker, 2007). Briefly, 468 μM NADH, 60 μM PMS, and 150 μM NBS were prepared with phosphate buffer (0.1 M Na_2HPO_4-NaH_2PO_4, pH 7.4). Then, 1 mL NADH, 1 mL PMS, 0.5 mL carrageenan oligosaccharide samples at different concentrations,

[1]http://opal.biology.gatech.edu/GeneMark/

[2]http://blast.ncbi.nlm.nih.gov/Blast.cgi

[3]http://www.genome.jp/tools/motif/

[4]http://www.lynnon.com/

and 1 mL nitroblue tetrazolium (NBT) were added into the test tube in turn and mixed. The mixed solution was incubated at room temperature for 6 min, then the absorbance of each mixed solution was measured at 560 nm. The measurement was repeated three times and the results were averaged. The blank control group with distilled water instead of carrageenan oligosaccharide also was measured under the same conditions, and vitamin C (Vc) was used as the positive control. The concentration of Vc was 0.5 mg/mL and the concentrations of carrageenan oligosaccharides were 0.5, 1, 2, 4, and 8 mg/mL.

The scavenging capacity of a carrageenan oligosaccharide sample for the superoxide anion radical ($O_2^{-\bullet}$) was calculated as:

$$\text{Scavenging effect} = \frac{A_0 - A_1}{A_0} \times 100\%$$

where A_0 is the absorbance measured in the reaction solution of the blank control group and A_1 is the absorbance measured in the reaction solution of each experimental group.

Scavenging Assay of Hydroxyl Radical (•OH)

$FeSO_4$ can react with H_2O_2 to form hydroxyl radicals (•OH). The reaction equation is:

$$Fe^{2+} + H_2O_2 \rightarrow Fe^{3+} + OH^- + \bullet OH$$

The hydroxyl radical scavenging capacity was determined by the method of Jin et al. (2005) with modifications. Briefly, 1.5 mL of 5.0 Mm 1,10-phenanthroline solution (95% ethanol as solvent) was mixed with 2.0 mL of phosphate buffer (0.2 M Na_2HPO_4-NaH_2PO_4, pH 7.4), then 1.0 mL of 7.5 mM $FeSO_4$ solution was added. The solution was evenly mixed and 1.0 mL of 0.1% (w/v) H_2O_2 was added to start the reaction. Finally, redistilled water was added to a total volume if 10 mL, and this reaction system was used as the control group. For the experimental group, 1.0 mL Vc or carrageenan oligosaccharide at different concentrations was added, then 0.1% (w/v) H_2O_2 was added to start the reaction. Vc was used as a positive control. The mixture without scavengers (Vc or carrageenan oligosaccharides) and H_2O_2 was used as the blank control. The absorbance of each reaction solution was measured at 536 nm after incubation at 37°C for 1 h. The Vc concentration was 0.5 mg/mL, and the carrageenan oligosaccharide concentrations were 0.5, 1, 2, 4, and 8 mg/mL.

The scavenging capacity of a carrageenan oligosaccharide sample for hydroxyl radicals (•OH) was calculated as:

$$\text{Scavenging effect} = \frac{A_c - A_a}{A_b - A_a} \times 100\%$$

where A_a is the absorbance measured in the reaction solution of the control group, A_b is the absorbance measured in the blank control, and A_c is the absorbance measured in the reaction solution of each experimental group.

Scavenging Assay of DPPH Radical

The DPPH radical scavenging ability was assessed by the method of Sun and Ho (2005). Briefly, 2 mL of 0.15 mM DPPH radical (95% ethanol as solvent) was mixed with 2 mL carrageenan oligosaccharide at different concentrations. The Vc concentration was 0.5 mg/mL and the carrageenan oligosaccharide concentrations were 0.5, 1, 2, 4, and 8 mg/mL.

The scavenging capacity of carrageenan oligosaccharides to hydroxyl radicals (•OH) was calculated as:

$$\text{Scavenging effect} = \left(1 - \frac{A_i - A_j}{A_0}\right) \times 100\%$$

where A_i is the absorbance of the mixed solution measured at 517 nm after reacting in the dark for 30 min, A_j is the absorbance measured after the DPPH solution in the reaction system was replaced with 95% ethanol, and A_0. is the antioxidant (oligosaccharide sample or Vc) in the reaction system with distilled water instead.

RESULTS

Sequence Analysis and Expression of *Car3206*

A carrageenase-encoding gene, *Car3206*, was obtained from the whole genome of *Polaribacter* sp. NJDZ03 isolated from the surface of Antarctic macroalgae. The open reading frame of *Car3206* consisted of 1,203 bp, which encoded a protein of 400 amino acids with a calculated molecular weight of 44.5 kDa. Sequence similarity showed that the encoded carrageenase Car3206 belonged to the glycoside hydrolase family 16 (GH16). To our knowledge, this is the first report of a carrageenase isolated from an Antarctic *Polaribacter* strain.

The amino acid sequence of *Car3206* from the *Polaribacter* sp. strain shared high similarity with the sequences of other reported carrageenases. Multiple sequence alignment showed that the Car3206 sequence shared 90.75% homology with the orthologous sequence of *Pseudoalteromonas* sp. (GenBank: WP_007378515.1), 80.99% with *Vibrio* sp. (GenBank: QGN18698.1), 68.58% with *Shewanella* sp. 10N.286.48.A6 (GenBank: WP_102520062.1), 57.05% with *Aliagarivorans marinus* (GenBank: WP_084429454.1), and 56.66% with *Flavicella marina* (GenBank: WP_152285702.1). Based on the multiple alignment and NCBI's conserved domain database, 11 residues make up the active site (Ser_{139}, Ala_{141}, Trp_{143}, Glu_{162}, Asp_{164}, Glu_{167}, Asp_{178}, Asp_{180}, Gly_{206}, Ser_{255}, and Gly_{257}) and three residues make up the catalytic site (Glu_{162}, Asp_{164}, and Glu_{167}) (**Figure 1**; Michel et al., 2001a).

The carrageenase gene *Car3206* was expressed in *E. coli* BL21 (DE3) cells harboring pET-30a-Car3206 by IPTG induction. The crude carrageenase Car3206 was purified by Ni-NTA His Tag Kit affinity chromatography and analyzed by SDS-PAGE. A single band with an apparent molecular weight of 45 kDa was found (**Figure 2**), which is consistent with the calculated molecular weight.

Characterization of the Recombinant Car3206 Protein

The optimum temperature for Car3206 enzyme activity was 55°C (**Figure 3**). However, 44–90% activity was retained at low

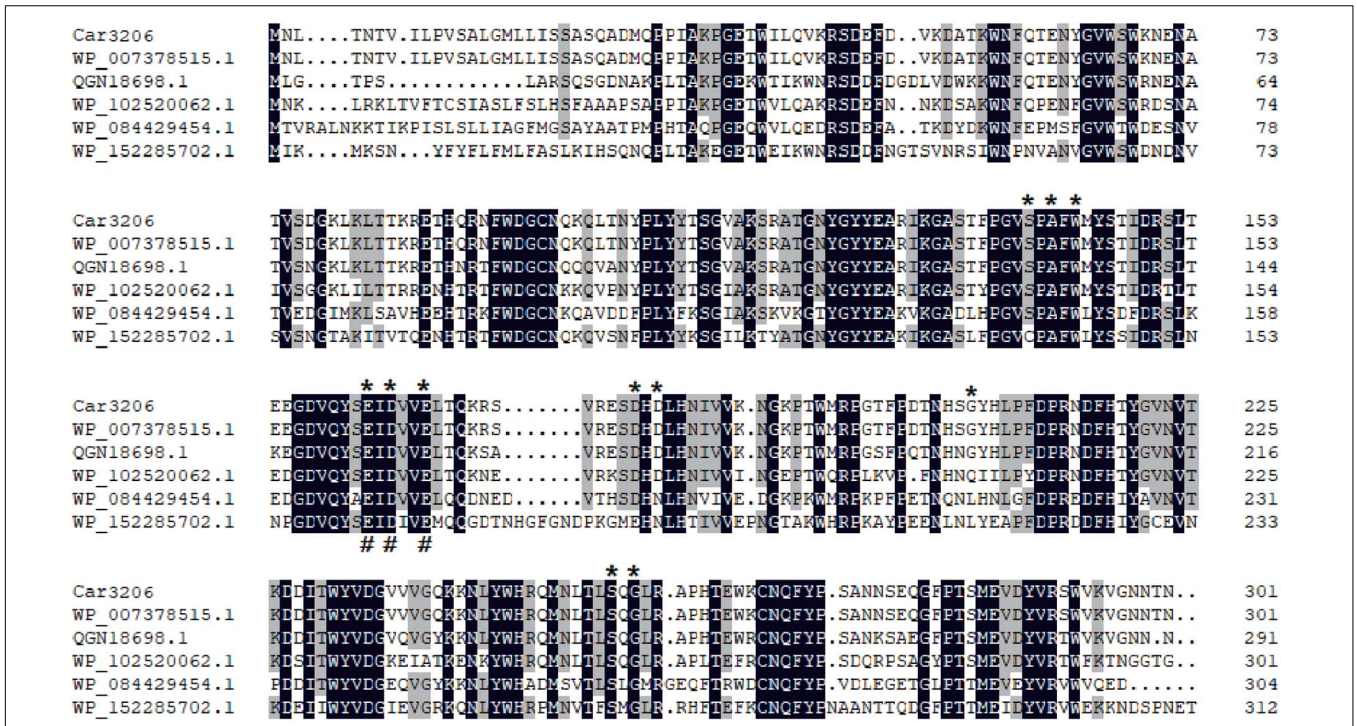

FIGURE 1 | Multiple sequence alignment of Car3206 protein sequences. The predicted κ-carrageenase amino acid sequence of *Car3206* was aligned with the deduced amino acid sequences of κ-carrageenase genes from *Pseudoalteromonas* sp. (GenBank: WP_007378515.1), *Vibrio* sp. (GenBank: QGN18698.1), *Shewanella* sp. 10N.286.48.A6 (GenBank: WP_102520062.1), *Aliagarivorans marinus* (GenBank: WP_084429454.1), and *Flavicella marina* (GenBank: WP_152285702.1). *indicates active sites; #indicates catalytic sites; black columns indicate identical amino acids; and gray columns indicate amino acids with ≥50% identity.

temperatures (10–45°C) and >85% activity was retained at 45–60°C, but at temperatures >60°C, the enzyme activity dropped sharply (**Figure 3**). The thermal stability analysis showed that recombinant Car3206 retained >90% of its enzyme activity after incubation at 45°C for 3 h and 50% of its enzyme activity after incubation for 12 h (**Figure 4**). At the optimal temperature of 55°C, 94% of the enzyme activity was retained after incubation for 3 h and 60% was retained after incubation for 12 h, which indicated that Car3206 had good thermal stability and low temperature tolerance.

The optimum pH for Car3206 enzyme activity was 7.0. Recombinant Car3206 was stable from pH 5.0–10.0, retaining >40% of the activity in this pH range (**Figure 4**).

The effects of metal ions on Car3206 enzyme activity are shown in **Figure 5**. Ca^{2+} significantly stimulated the enzyme activity, and Na^{+} and K^{+} slightly increased its activity. Conversely, Mn^{2+}, Sr^{2+}, Fe^{2+}, Fe^{3+}, and Mg^{2+} decreased Car3206 activity, and Cr^{2+} and Cu^{2+} sharply reduced its activity by 90%. EDTA is a chelating agent that almost inactivated Car3206, implying that metal ions play crucial role in Car3206 enzyme activity.

Hydrolysis Products of Carrageenan by Car3206 Activity

The thin layer chromatography result showed that Car3206 effectively degraded carrageenan (**Figure 6**). The only products were disaccharides and no intermediate products were detected. This result demonstrated that recombinant Car3206 hydrolyzed carrageenan to disaccharides as the end products through an exo-type mode of action.

Antioxidant Activity of the Hydrolysis Products

Assays of scavenging superoxide, hydroxyl, and DPPH radicals were used to assess the antioxidant activity. The superoxide, hydroxyl, and DPPH radicals scavenging activities of carrageenan oligosaccharides at concentrations of 0.5–8 mg/mL are shown in **Figure 7**. The results showed that all tested concentrations of the carrageenan oligosaccharide had scavenging effects on O_2^{-}•, •OH, and DPPH•, and the scavenging rate of enzymatic hydrolysis to the three kinds of radical increased with increasing carrageenan oligosaccharide concentrations. All these results indicated that the enzymatic hydrolysis products had similar antioxidant activity with vitamin C.

DISCUSSION

The development of marine bio-active substances has led to a focus on the biological activity of oligosaccharides. Oligosaccharides degraded from carrageenan are increasingly being used in medical, food, and industrial applications

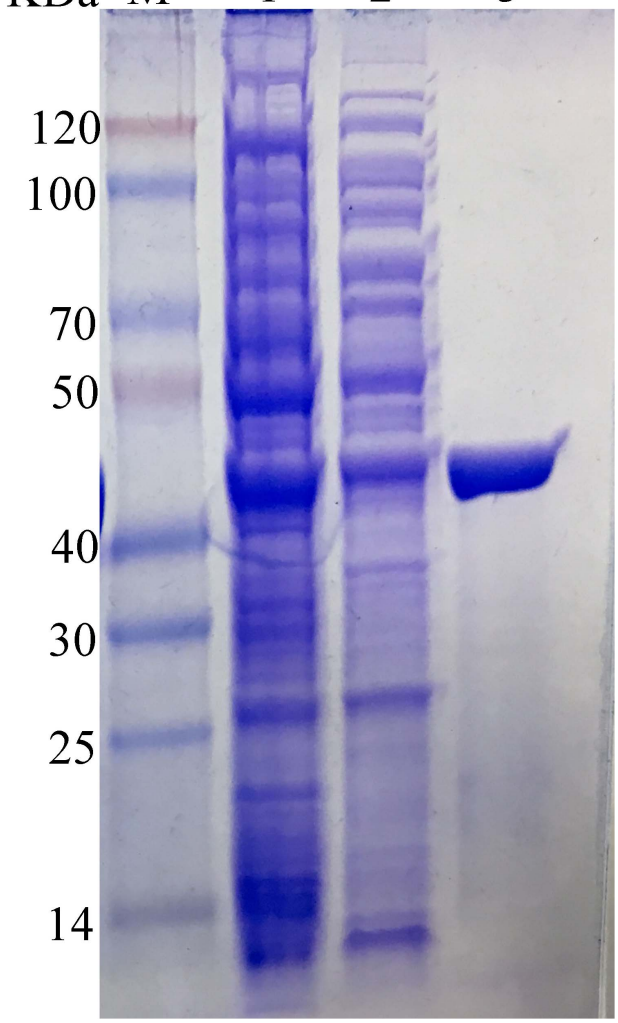

FIGURE 2 | SDS-PAGE of the purified recombinant carrageenase Car3206. M, protein marker; Lane 1, recombinant *Escherichia coli* BL21(DE3) cells harboring pET30a-Car3206 after induction; Lane 2, uninduced recombinant *E. coli* BL21(DE3) cells harboring pET30a-Car3206; Lane 3, purified recombinant Car3206.

(Zhu et al., 2020). Carrageenan oligosaccharides have been reported many times for their antioxidant activity and potential medicinal value (Sun et al., 2015; Calvo et al., 2019). These oligosaccharides are expected to be used as natural antioxidants to replace synthetic antioxidants that are potential safety hazards. Therefore, it is urgent to find novel microorganisms that produce carrageenases with high activity and high yield originated from special environment. Macroalgae are an important source of biomass in the marine environments of Antarctica, meanwhile, they are also a valuable source of novel and exploitable carbohydrate-active enzymes (Loque et al., 2010; Hettle et al., 2019). Antarctic macroalgae host complex and diverse microbiology communities. Among them, agarolytic and carrageenolytic strains have important ecological roles as agents to decompose the algal biomass in the marine environment of Antarctica. In this study, the carrageenase gene *Car3206* was obtained from the whole genome of *Polaribacter* sp. NJDZ03, which was isolated from the surface of Antarctic macroalgae. To our knowledge this is the first reported carrageenases isolated from an Antarctic *Polaribacter* strain. This result will deepen our knowledge of biodiversity of polysaccharide degrading bacteria, and provide a new idea for future research on the function and role of polysaccharide degrading bacteria in the marine carbon metabolism system of the Southern Ocean.

The extreme environment of cold and dry has created Antarctic microorganisms with special characteristics for them to thrive. For example, they produce cold-active or cold-adaptive enzymes that have been used in mechanism studies and are potential enzymes for commercial development (Bull et al., 2000). The genus *Polaribacter* is unique to the polar region. It means that *Polaribacter* sp. strain could use carrageenan of macroalgae as carbon source and decompose it into oligosaccharides by secreting carrageenan degrading enzyme, which is an important way for algae to return carbon fixed by photosynthesis to the atmosphere. Namely, *Polaribacter* sp. plays a role in the carbon cycle of the Southern Ocean. This result deepened our understand that these bacteria play an important role in the decomposition of algae, and on nutrient cycling dynamics in Antarctic marine ecosystems (Quartino et al., 2015). The special living environment in polar regions makes Car3206 have higher cold tolerance than other carrageenan degrading bacteria. Car3206 could maintain 44–67% of its maximal activity between 10 and 30°C (**Figure 3A**), indicating the cold-adapted feature of this enzyme. This feature allows enzymatic reactions to be carried out at lower temperatures and has the advantage for special applications, such as recovery of nucleic acid from low concentration agarose.

The cold-adapted GH16 κ-carrageenase Cgk16A has been reported to have a maximum activity of 52% at 15°C, but the activity quickly vanished at 30 and 40°C (Shen et al., 2018). Car3206 retains 44–90% activity at 10–45°C, unlike other carrageenases, indicating that Car3206 has both a high optimum temperature and good low temperature tolerance. Reaction temperature and thermostability are very important biochemical characteristic for industrial applications. Our results showed that the optimum temperature of the recombinant carrageenase Car3206 was 55°C. Most of the characterized carrageenases have maximum activity around 40–45°C; for example, the optimum temperature of κ-carrageenase S942 from *Pseudoalteromonas* sp. is 37°C (Lin et al., 2018), for the κ-carrageenase PpCgkCD from *Pseudoalteromonas porphvrae* LL1 it is 40°C (Zhao et al., 2018), and for κ-carrageenase PLJ30 from *Pseudoalteromonas carrageenovora* ASY5 is 45°C (Xiao et al., 2018; **Table 1**). However, the κ-carrageenase CgkX from *Pseudoalteromonas* sp. QY203 (Xu et al., 2015) and *P. carrageenovora* ASY5 (Li et al., 2016) have optimum temperatures similar to that of Car3206 (**Table 1**).

At high concentrations, carrageenan is highly viscous at room temperature and is an inhibitor of carrageenase degradation. The most commonly used method for obtaining low-viscosity carrageen is to increase the solution temperature. However, most

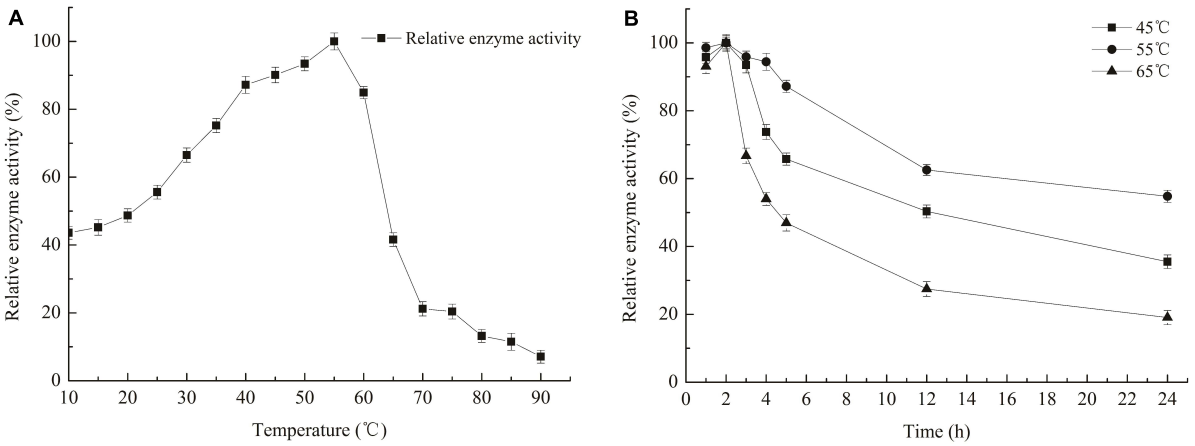

FIGURE 3 | Optimal temperature **(A)** and temperature stability **(B)** of recombinant carrageenase Car3206.

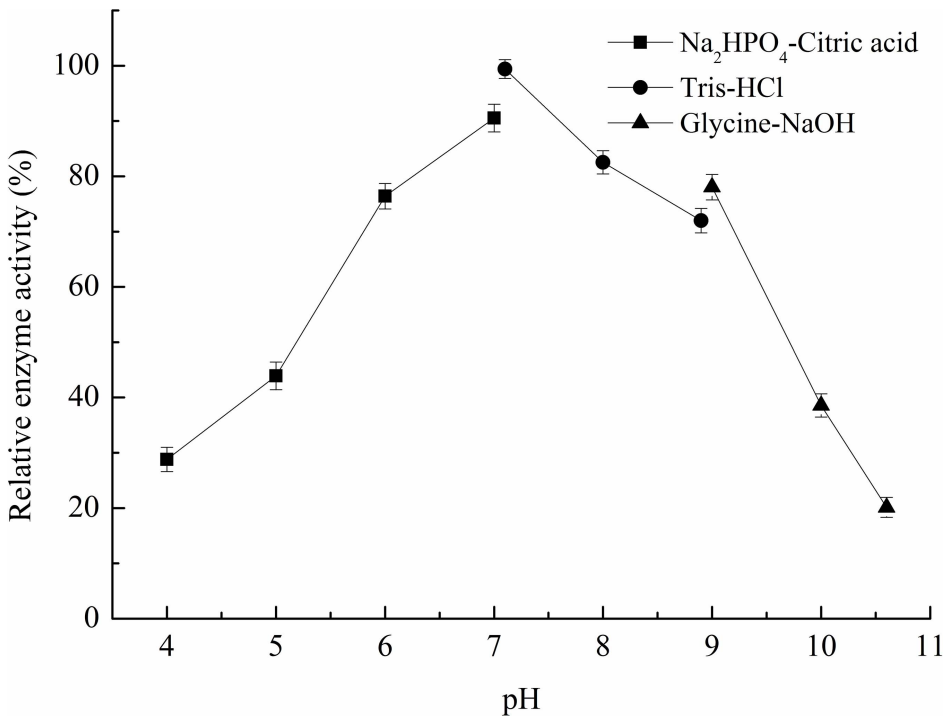

FIGURE 4 | Optimal pH of recombinant carrageenase Car3206.

reported carrageenan degrading enzymes are not stable above 40°C. Therefore, to prepare oligo-carrageenan on a commercial scale, it is necessary to select superior producer bacterial strains to improve the yield and thermostability of carrageenases (Li et al., 2019). The thermal stability results showed that Car3206 retained 96% activity after incubation at 55°C for 3 h, and 60% activity after incubation at 55°C for 12 h. The optimum temperature of κ-carrageenase PpCgkCD (Zhao et al., 2018) from *P. porphvrae* LL1 is 40°C, above 45°C the enzyme activity decreased sharply; when incubated at 40°C for 1 h it retained about 80% of its maximum activity, but enzyme activity was completely lost after incubation at 50°C for 1 h. The recombinant κ-carrageenase PLJ30 (Xiao et al., 2018) was stable after incubation at 45°C for 30 min and retained 80% of its maximum activity, when incubated at 50°C for 30 min it retained approximately 50% of its maximum activity, but lost approximately 80% of its activity after incubation at 45°C for 2 h. The κ-carrageenase CgkX (Xu et al., 2015) exhibited the outstanding stability at 0–40°C, where over 90% of the total activity was remained after the 1 h thermal treatment. However, the CgkX was almost inactivated after incubation at 50°C for 1 h. And the κ-carrageenase from *P. carrageenovora* ASY5 (Li et al., 2016) retained 95% of its

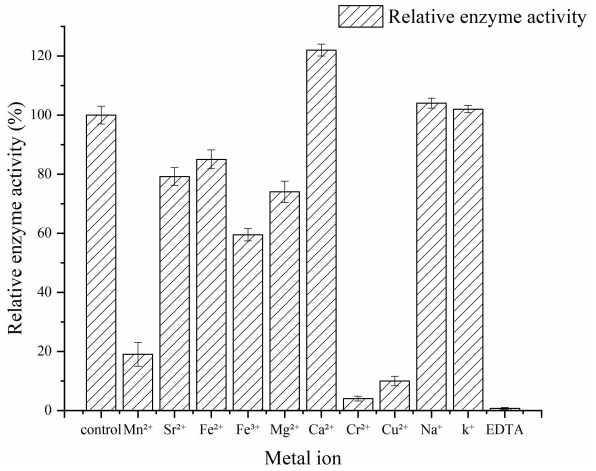

FIGURE 5 | Effects of metal ions on recombinant carrageenase Car3206.

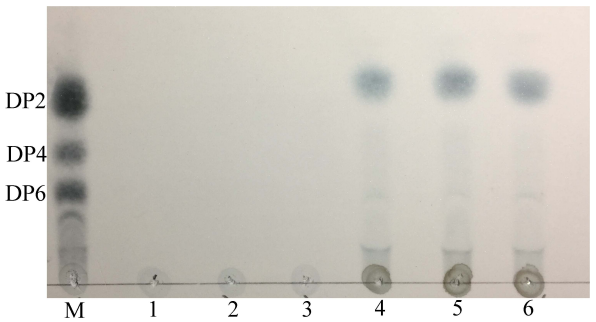

FIGURE 6 | Thin layer chromatography of the hydrolysis products of purified recombinant Car3206. M, standard mixture of carrageenan, disaccharide (DP2), tetrasaccharide (DP4), and hexasaccharide (DP6); Lane 1, recombinant Car3206; Lane 2, the substrate (0.1% carrageenan); Lane 3, products of carrageenan with inactivated Car3206 for 0.5 h; Lane 4, products of carrageenan with Car3206 for 0.5 h; Lane 5, products of carrageenan with Car3206 for 1 h; Lane 6, products of carrageenan with Car3206 for 6 h.

activity after incubation at 40°C for 1 h, and retained 60% of its maximum activity after incubation at 45°C for 1 h. Compared with other carrageenases, Car3206 has good thermal stability and high optimal temperature, which are the characteristics needed for industrial applications; making Car3206 a good candidate for industrial use (**Table 2**).

Metal ions had different effects on the carrageenase activity of recombinant Car3206 (**Table 1**). Car3206 activity improved significantly in the presence of Ca^{2+}, which is consistent with the results of a previous report (Liu et al., 2013). Ca^{2+} has significant effects on the activity of most known carrageenase, probably by forming metal–carbonyl coordination bonds with amino acids in the active centers of enzymes, thereby stabilizing the three-dimensional structure of the protein. Low concentrations of most metals, including Na^{+} and K^{+}, are known to increase carrageenase activity (Li et al., 2013, 2014), especially high concentrations of Na^{+} (up to 500 mmol/L) (Ma et al., 2013). Conversely, Cu^{2+} has a potential inhibitory effect on most carrageenases possibly because it competes with Ca^{2+} for the binding sites in the active centers of the enzymes; however, the exact catalytic mechanism needs further study.

In the study of the immune defense mechanism of carrageenan oligosaccharides, Guo et al. (2017) found that κ-carrageenan disaccharide can directly enter cells and affect cellular immune regulation because of its small molecular weight and less sulfate group. Therefore, the preparation of high quality carrageenan disaccharides has a great application prospect in the field of medicine. Oligo-carrageenan produced by the action of microbial enzymes can be more advantageous than produced by acid hydrolysis because enzymes are highly specific to their substrates and they generate oligo-derivatives are uniform in molecular weights (Yao et al., 2014). But Microbial enzymes which hydrolyze carrageenan is still in its infancy compared with that of other hydrocolloids such as agar and alginate (Chauhan and Saxena, 2016). The recombinant carrageenase Car3206 effectively degraded carrageenan into disaccharides. Both the recombinant carrageenase PLJ30 from *P. carrageenovora* ASY5 and CgkX from *Pseudoalteromonas* sp. QY203 degrade carrageenan into disaccharide and tetrasaccharide, the κ-carrageenase PpCgkCD from *P. porphyrae* LL1 degrades carrageenan into neo-κ-carrabiose and neo-κ-carratetraose (**Table 1**). Most carrageenase degradation products are mixtures, which makes it difficult to purify each type of oligosaccharide, whereas Car3206 produces only disaccharides, which can significantly reduce the cost of product purification in industrial production.

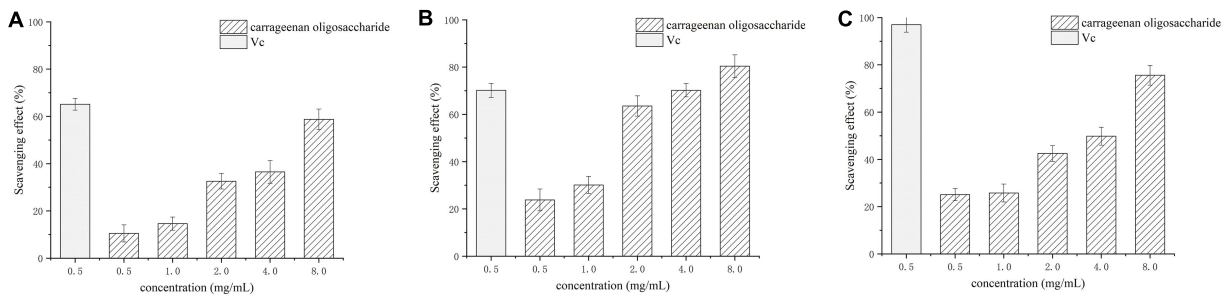

FIGURE 7 | Scavenging effect of κ-carrageenan oligosaccharide on superoxide radicals **(A)**, hydroxyl radicals **(B)**, and DPPH radicals **(C)**. Vc, vitamin C.

TABLE 1 | Comparison of Car3206 with carrageenases from other bacterial strains.

Enzyme	Source	Temperature	pH	Cation activators	Cation inhibitors	Products	References
Car3206	*Polaribacter* sp. NJDZ03 popolarba	55°C	7.0	Ca^{2+}, Na^{+}, and K^{+}	Mn^{2+}, Sr^{2+}, Fe^{2+}, Fe^{3+}, Mg^{2+}, Cr^{2+}, and Cu^{2+}	Disaccharide	This study
S942	*Pseudoalteromonas* sp.	37°C	7.0	Ca^{2+}, Na^{+}, and Mg^{2+}	Cu^{2+}, K^{+}, Zn^{2+}, and Mn^{2+}	–	Lin et al., 2018
PpCgkCD	*Pseudoalteromonas porphyrae* LL1	40°C	8.0	Ca^{2+}, K^{+}, and Mg^{2+}	Mn^{2+}, Fe^{2+}, Fe^{3+}, Zn^{2+}, Cu^{2+}, and Hg^{2+}	Neo-κ-carrabiose and neo-κ-carratetraose	Zhao et al., 2018
PLJ30	*Pseudoalteromonas carrageenovora* ASY5	45°C	6.5	Ag^{+} and Cd^{2+}	Sn^{2+}, Ba^{2+}, Ca^{2+}, Al^{3+}, Mg^{2+}, Sr^{2+}, Mn^{2+}, Zn^{2+}, Fe^{2+}, and Fe^{3+}	Disaccharide and tetrasaccharide	Xiao et al., 2018
CgkX	*Pseudoalteromonas* sp. QY203	55°C	7.0	Na^{+}	Zn^{2+}, Cu^{2+}, Ca^{2+}, Mg^{2+}, Al^{3+}, NH_4^{+}, Fe^{3+}, Ca^{2+}, and K^{+}	Disaccharide and tetrasaccharide	Xu et al., 2015
κ-carrageenase	*Pseudoalteromonas carrageenovora* ASY5	55°C	9.0	Na^{+}, K^{+}, Sn^{2+}, and Fe^{3+}	Cd^{2+}, Ba^{2+}, Mg^{2+}, Fe^{2+}, and Ca^{2+}	–	Li et al., 2016

TABLE 2 | Comparison of optimum temperature and thermal stability between Car3206 and other κ-carrageenases.

Enzyme	Source	Optimal temperature	Incubation conditions	relative activity	References
Car3206	*Polaribacter* sp. NJDZ03	55°C	55°C for 3 h 55°C for 12 h	96% 60%	This study
PpCgkCD	*Pseudoalteromonas porphyrae* LL1	40°C	40°C for 1 h 50°C for 1 h	80% 0%	Zhao et al., 2018
PLJ30	*Pseudoalteromonas carrageenovora* ASY5	45°C	45°C for 30 min 50°C for 30 min	80% 50%	Xiao et al., 2018
CgkX	*Pseudoalteromonas* sp. QY203	55°C	0–40°C for 1 h 50°C for 1 h	>90% 0%	Xu et al., 2015
κ-carrageenase	*Pseudoalteromonas carrageenovora* ASY5	55°C	40°C for 1 h 45°C for 1 h	95% 60%	Li et al., 2016

Wang et al. (2011) found that the antioxidant activity of carrageenan oligosaccharides with low sulfate content was better than that of those with high sulfate content, and low molecular weight oligosaccharides were shown to have higher antioxidant properties (Zhou et al., 2014), implying that the neocarrabiose from κ-carrageenan degradation may effectively promote antioxidant activity in cells and eliminate the damage caused by free radicals. We investigated the antioxidant capacity of the carrageenan disaccharides produced by Car3206 *in vitro* by measuring the scavenging effects on superoxide, hydroxyl, and DPPH radicals at concentrations of 0.5–8 mg/mL. The results showed that, at different concentrations, the disaccharides had obvious scavenging effects on $O_2^{-}\bullet$, •OH, and DPPH, and the scavenging effect tended to increase with increasing concentrations of the disaccharides. The scavenging capacity of the carrageenan disaccharides was similar to that of Vc at the same concentration, implying that this degraded product of carrageenan had high antioxidant potential.

In our study, the carrageenase gene *car3206* was successfully expressed in *E. coli* and high proportion soluble recombinant protein was obtained (**Figure 2**). Furthermore, recombinant Car3206 has an optimal activity at 55°C and more than 80% relative activity at 60°C which is important for applications where high concentration of carrageenan is required because at high temperature it is more soluble as well as more oligosaccharides production. Moreover, Car3206 showed good thermal stability which still maintained 60% activity after incubation at 55°C for 12 h, we know, the thermostability of the enzyme is another main factors for limiting its industrial production., In addition, the final degradation product of Car3206 is only disaccharide, which greatly simplify the separation process and reduced the production cost. In conclusion, our study also provides new ideas for the development and utilization of Antarctic microbial resources. The antioxidant capacity of carrageenan degradation products provides a path for research and industrial utilization of natural antioxidants in the future.

DATA AVAILABILITY STATEMENT

The raw data supporting the conclusions of this article will be made available by the authors, without undue reservation.

AUTHOR CONTRIBUTIONS

JL collected the samples, designed research, supervised the project, and analyzed data. YG performed the experiments and wrote the manuscript. XG, LF, and QZ performed the experiments and prepared figures. PZ analyzed the data.

All authors contributed to the article and approved the submitted version.

FUNDING

This research was supported by Impact and Response of Antarctic Seas to Climate Change (RFSOCC2020-2022), the National Key Research and Development Program of China (2018YFC1406704), and the Key Research and Development Program of Shandong Province, China (2018GHY115013).

SUPPLEMENTARY MATERIAL

The Supplementary Material for this article can be found online at: https://www.frontiersin.org/articles/10.3389/fmicb.2021.631039/full#supplementary-material

REFERENCES

Abad, L. V., Kudo, H., Saiki, S., Nagasawa, N., Tamada, M., Katsumura, Y., et al. (2009). Radiation degradation studies of carrageenans. *Carbohydr. Polym.* 78, 100–106. doi: 10.1016/j.carbpol.2009.04.009

Barbeyron, T., Zonta, E., Panse, S. L., Duchaud, E., and Michel, G. (2019). *Alteromonas fortis* sp. nov. a non-flagellated bacterium specialized in the degradation of iota-carrageenan, and emended description of the genus *Alteromonas*. Int. J. Syst. Evol. Microbiol. 69, 2514–2521. doi: 10.1099/ijsem.0.003533

Boulho, R., Marty, C., Freile-Pelegrín, Y., Robledo, D., Bourgougnon, N., and Bedoux, G. (2017). Antiherpetic (HSV-1) activity of carrageenans from the red seaweed *Solieriachordalis* (Rhodophyta, Gigartinales) extracted by microwave-assisted extraction (MAE). *J. Appl. Phycol.* 29, 2219–2228. doi: 10.1007/s10811-017-1192-5

Bull, A. T., Ward, A. C., and Goodfellow, M. (2000). Search and discovery strategies for biotechnology: the paradigm shift[J]. *Microbiol. Mol. Biol. Rev.* 64, 573–606. doi: 10.1128/MMBR.64.3.573-606.2000

Cadenas, E., and Davies, K. J. A. (2000). Mitochondrial free radical generation, oxidative stress, and aging. *Free Radic. Biol. Med.* 29, 222–230. doi: 10.1016/S0891-5849(00)00317-8

Calvo, G. H., Cosenza, V. A., Sáenz, D. A., Navarro, D. A., and Venosa, G. M. D. (2019). Disaccharides obtained from carrageenans as potential antitumor agents. *Sci. Rep.* 9:6654. doi: 10.1038/s41598-019-43238-y

Chauhan, P. S., and Saxena, A. (2016). Bacterial carrageenases: an overview of production and biotechnological applications. *3 Biotech* 6:146. doi: 10.1007/s13205-016-0461-3Guo

Guo, J., Zheng, Z., Chen, C., Lu, X., Zhang, Y., and Zheng, B. (2017). Enhanced production of κ-carrageenase and κ-carrageenan oligosaccharides through immobilization of *Thalassospira* sp. Fjfst-332 with magnetic Fe_3O_4-chitosan microspheres. *J. Agric. Food Chem.* 65, 7934–7943. doi: 10.1021/acs.jafc.7b02869

Hettle, A. G., Hobbs, J. K., Pluvinage, B., Vickers, C., and Boraston, A. B. (2019). Insights into the κ/ι-carrageenan metabolism pathway of some marine *pseudoalteromonas* species. *Commun. Biol.* 2:474. doi: 10.1038/s42003-019-0721-y

Hjerde, T., Christensen, B. E., and Smidsrod, O. (2017). The influence of the conformational state of κ- and τ-carrageenan on the rate of acid hydrolysis[J]. *Acta Mater.* 128, 249–257. doi: 10.1016/j.actamat.2017.02.019

Huang, Y., Zhang, L., Song, R., Mao, X., and Tang, S. (2020). A carrageenan/agarose composite sponge and its immunomodulatory activities toward raw264.7. *J. Biomed. Mater. Res. A* doi: 10.1002/jbm.a.37070

Jain, A., and Krishnan, K. P. (2017). A glimpse of the diversity of complex polysaccharide-degrading culturable bacteria from Kongsfjorden Arctic Ocean. *Ann. Microbiol.* 67, 203–214. doi: 10.1007/s13213-016-1252-0

Jiao, G. L., Yu, G. L., Zhang, J. Z., and Ewart, H. (2011). Chemical structure and bioactivities of sulfated polysaccharides from marine algae. *Mar. Drugs* 9, 196–233. doi: 10.3390/md9020196

Jin, Q., Liu, Y. F., Wang, X. G., and Dai, H. P. (2005). Sesamin as a natural antioxidant. *Chin. Cereals Oils Assoc.* 20, 89–92.

Kalitnik, A. A., Byankina Barabanova, A. O., Nagorskaya, V. P., Reunov, A. V., Glazunov, V. P., Solov'eva, T. F., et al. (2013). Low molecular weight derivatives of different carrageenan types and their antiviral activity. *J. Appl. Phycol.* 25, 65–72. doi: 10.1007/s10811-012-9839-8

Kang, D. H., Hyeon, J. E., You, S. K., Kim, S. W., and Han, S. O. (2014). Efficient enzymatic degradation process for hydrolysis activity of the carrageenan from red algae in marine biomass. *J. Biotechnol.* 192(Pt A), 108–113. doi: 10.1016/j.jbiotec.2014.09.019

Li, J., Pan, A. H., Xie, M. S., Zhang, P. P., and Gu, X. Q. (2019). Characterization of a thermostable κ-carrageenase from a hot spring bacterium and plant protection activity of the oligosaccharide enzymolysis product. *J. Sci. Food Agric.* 99, 1812–1819. doi: 10.1002/jsfa.9374

Li, J. J., Ni, H., Cai, H. N., Zhu, Y. B., and Xiao, A. F. (2016). Cloning, expression and enzymatic properties of κ-carrageenase from *Pseudoalteromonas carrageenovora*. *Mod. Food Sci. Technol.* 10, 72–77. doi: 10.13982/j.mfst.1673-9078.2016.10.012

Li, L., Ni, R., Shao, Y., and Mao, S. R. (2014). Carrageenan and its applications in drug delivery. *Carbohydr. Polym.* 103, 1–11. doi: 10.1016/j.carbpol.2013.12.008

Li, S. Y., Jia, P. P., Wang, L. N., Yu, W. G., and Feng, H. (2013). Purification and characterization of a new thermostable κ-carrageenase from the marine bacterium *pseudoalteromonas* sp. QY203. *J. Ocean Univ. China*. 12, 155–159. doi: 10.1007/s11802-013-1994-2

Lin, H., Li, R., Wang, R. Y., Jin, Q., and Miao, J. L. (2018). Screening, identification, enzyme-producing condition, and enzymatic property of carrageenase-producing Antarctic strain. *Chem. Bioeng.* 35, 47–52.

Liu, Z. M., Li, G. Y., Mo, Z. L., and Mou, H. J. (2013). Molecular cloning, characterization, and heterologous expression of a new κ-carrageenase gene from marine bacterium *Zobellia* sp. ZM-2. *Appl. Microbiol. Biotechnol.* 97, 10057–10067. doi: 10.1007/s00253-013-5215-0

Loque, C. P., Medeiros, A. O., Pellizzari, F. M., Oliveira, E. C., Rosa, C. A., and Rosa, L. H. (2010). Fungal community associated with marine macroalgae from Antarctica. *Polar Biol.* 33, 641–648. doi: 10.1007/s00300-009-0740-0

Ma, S., Duan, G. F., Chai, W. G., Geng, C. L., Tan, Y. L., Wang, L. S., et al. (2013). Purification, cloning, characterization and essential amino acid residues analysis of a new ι-carrageenase from *Cellulophaga* sp. QY3. *PLoS One* 8:e64666. doi: 10.1371/journal.pone.0064666

Michel, G., Chantalat, L., Duee, E., Barbeyron, T., and Dideberg, O. (2001a). The κ-carrageenase of *P. carrageenovora* features a tunnel-shaped active site: a novel insight in the evolution of Clan-B glycoside hydrolases. *Structure* 9, 513–525. doi: 10.1016/S0969-2126(01)00612-8

Michel, G., Chantalat, L., Fanchon, E., Henrissat, B., and Dideberg, O. (2001b). The iota-carrageenase of alteromonas fortis. a beta-helix fold-containing enzyme for the degradation of a highly polyanionic polysaccharide. *J. Bio. Chem.* 276, 40202–40209. doi: 10.1074/jbc.M100670200

Michel, G., Nyval-Collen, P., Barbeyron, T., Czjzek, M., and Helbert, W. (2006). Bioconversion of red seaweed galactans: a focus on bacterial agarases and carrageenases. *Appl. Microbiol. Biotechnol.* 71, 23–33. doi: 10.1007/s00253-006-0377-7

Miller, G. L. (1959). Use of dinitrosalicylic acid reagent for determination of reducing sugar. *Anal. Biochem.* 31, 426–428. doi: 10.1021/ac60147a030

Qi, H., Zhang, Q., Zhao, T., Chen, R., Zhang, H., Niu, X., et al. (2005). Antioxidant activity of different sulfate content derivatives of polysaccharide extracted from *ulva pertusa* (chlorophyta) in vitro. *Int. J. Biol. Macromol.* 37, 195–199. doi: 10.1016/j.ijbiomac.2005.10.008

Quartino, M. L., Vazquez, S. C., Latorre, G. E. J., and Mac Cormack, W. P. (2015). Possible role of bacteria in the degradation of macro algae desmarestia anceps montagne (phaeophyceae) in antarctic marine waters. *Rev. Argent. Microbiol.* 10, 274–276. doi: 10.1016/j.ram.2015.04.003

Riera, M., Pages, M., Issinger, O. G., and Guerra, B. (2003). Purification and characterization of recombinant protein kinase CK2 from Zea mays expressed in *Escherichia coli*. *Protein Expr. Purif.* 29, 24–32. doi: 10.1016/S1046-5928(03)00005-6

Shen, J., Chang, Y., Chen, F., and Dong, S. (2018). Expression and characterization of a κ-carrageenase from marine bacterium *Wenyingzhuangia aestuarii* OF 219: a biotechnological tool for the depolymerization of κ-carrageenan. *Int. J. Biol. Macromol.* 112, 93–100. doi: 10.1016/j.ijbiomac.2018.01.075

Siddhuraju, P., and Becker, K. (2007). The antioxidant and free radical scavenging activities of processed cowpea (*vigna unguiculata* (l.) walp.) seed extracts. *Food Chem.* 101, 10–19. doi: 10.1016/j.foodchem.2006.01.004

Sun, T., and Ho, C. T. (2005). Antioxidant activities of buckwheat extracts. *Food Chem.* 90, 743–749. doi: 10.1016/j.foodchem.2004.04.035

Sun, T., Tao, H. N., Xie, J., Zhang, S., and Xu, X. (2010). Degradation and antioxidant activity of κ-carrageenans. *J. Appl. Polym. Sci.* 117, 194–199. doi: 10.1002/app.31955

Sun, Y. J., Yang, B. Y., Wu, Y. M., Liu, Y., Gu, X., Zhang, H., et al. (2015). Structural characterization and antioxidant activities of κ-carrageenan oligosaccharides degraded by different methods. *Food Chem*. 178, 311–318. doi: 10.1016/j.foodchem.2015.01.105

Wang, P., Jiang, X. L., Jiang, Y. H., and Mou, H. J. (2011). Structure-function relationship of anti-ultraviolet radiation in series of marine derived characteristic oligosaccharides. *Nat. Prod. Res. Dev*. 23, 874–877. doi: 10.1631/jzus.B1000265

Xiao, A., Zeng, J., Li, J., Zhu, Y., Xiao, Q., and Ni, H. (2018). Molecular cloning, characterization, and heterologous expression of a new κ-carrageenase gene from *pseudoalteromonas carrageenovora* asy5. *J. Food Biochem.* 42:e12677. doi: 10.1111/jfbc.12677

Xu, X., Li, S., Yang, X., Yu, W., and Han, F. (2015). Cloning and characterization of a new κ-carrageenase gene from marine bacterium *pseudoalteromonas* sp. qy203. *J. Ocean Univ. China* 14, 1082–1084. doi: 10.1007/s11802-015-2652-7

Yao, Z., Wu, H., Zhang, S., and Du, Y. (2014). Enzymatic preparation of k carrageenan oligosaccharides and their anti-angiogenic activity. *Carbohydr. Polym.* 30, 359–367.

Yuan, H., Song, J., Zhang, W., Li, X., Li, N., and Gao, X. (2006). Antioxidant activity and cytoprotective effect of κ-carrageenan oligosaccharides and their different derivatives. *Bioorg. Med. Chem. Lett.* 16, 1329–1334. doi: 10.1016/j.bmcl.2005.11.057

Zhao, Y., Chi, Z., Xu, Y., Shi, N., Chi, Z., and Liu, G. (2018). High-level extracellular expression of κ-carrageenase in *Brevibacillus choshinensis* for the production of a series of κ-carrageenan oligosaccharides. *Process Biochem.* 64, 83–92.

Zhou, X. X., Xu, J., and Ding, Y. T. (2014). Alginate-derived oligosaccharides product by alginate lyase and detection of the antioxidant activity. *Food Ferment. Ind*. 2, 116–120.

Zhu, B., Ni, F., Xiong, Q., and Yao, Z. (2020). Marine oligosaccharides originated from seaweeds: source, preparation, structure, physiological activity and applications. *Crit. Rev. Food Sci. Nutr.* 61, 60–74. doi: 10.1080/10408398.2020.1716207

Conflict of Interest: The authors declare that the research was conducted in the absence of any commercial or financial relationships that could be construed as a potential conflict of interest.

frontiers in Microbiology

ORIGINAL RESEARCH
published: 04 June 2021
doi: 10.3389/fmicb.2021.600991

Genomic and Chemical Investigation of Bioactive Secondary Metabolites From a Marine-Derived Fungus *Penicillium steckii* P2648

Guangshan Yao[1], Xiaofeng Chen[1], Huawei Zheng[1], Danhua Liao[1,2], Zhi Yu[1,2], Zonghua Wang[1,2] and Jianming Chen[1]**

[1]*Institute of Oceanography, Minjiang University, Fuzhou, China,* [2]*Fujian Universities Key Laboratory for Plant-Microbe Interaction, College of Life Science, Fujian Agriculture and Forestry University, Fuzhou, China*

OPEN ACCESS

Edited by:
Jinwei Zhang,
University of Exeter, United Kingdom

Reviewed by:
Lijuan Liao,
Fujian Agriculture and Forestry University, China
Peng Zhang,
Chinese Academy of Agricultural Sciences (CAAS), China
Lu Liu,
Qingdao Institute of Bioenergy and Bioprocess Technology, Chinese Academy of Sciences (CAS), China

***Correspondence:**
Guangshan Yao
2616@mju.edu.cn
Jianming Chen
chenjm@tio.org.cn

Specialty section:
This article was submitted to Microbiotechnology, a section of the journal Frontiers in Microbiology

Received: *31 August 2020*
Accepted: *26 April 2021*
Published: *04 June 2021*

Citation:
Yao G, Chen X, Zheng H, Liao D, Yu Z, Wang Z and Chen J (2021) Genomic and Chemical Investigation of Bioactive Secondary Metabolites From a Marine-Derived Fungus Penicillium steckii P2648. Front. Microbiol. 12:600991. doi: 10.3389/fmicb.2021.600991

Marine fungi of the genus *Penicillium* are rich resources of secondary metabolites, showing a variety of biological activities. Our anti-bacterial screening revealed that the crude extract from a coral-derived fungus *Penicillium steckii* P2648 showed strong activity against some pathogenic bacteria. Genome sequencing and mining uncovered that there are 28 secondary metabolite gene clusters in P2648, potentially involved in the biosynthesis of antibacterial compounds. Chemical isolation and structural determination suggested citrinin is the dominant component of the crude extracts of P2648, and our further tests confirmed that citrinin showed excellent activities against various pathogenic bacteria. Moreover, the gene cluster containing a homolog of the polyketide synthase CitS was identified as the citrinin biosynthesis gene cluster through genetic analysis. Interestingly, three isoquinoline alkaloids were unexpectedly activated and isolated from the *Δcits* mutant and structural determination by using high-resolution electron spray ionization mass spectroscopy (HRESIMS), 1D, and 2D NMR. Further antibacterial assays displayed that compounds 1 and 2, but not compound 3, showed moderate activities against two antibiotic-resistant pathogenic bacteria with minimum inhibitory concentration (MIC) of 16–32 μg/ml. In conclusion, our results demonstrated that citrinin and isoquinoline alkaloids represent as the major antibacterial agents in the coral-associated fungus *P. steckii* P2648, and our genomic and chemical analyses present evidence in support of *P. steckii* P2648 as a potent natural products source for anti-bacterial drug discovery.

Keywords: isoquinoline alkaloids, anti-bacterial activities, coral-derived fungus, genome sequencing, *Penicillium steckii*

INTRODUCTION

Bacterial resistance to antibiotics, such as extended-spectrum β-lactamase (ESBL)-producing *Escherichia coli*, has become a global public health issue (Lee et al., 2006). The global spread of bacterial resistance significantly increased patient mortality and morbidity due to the shortage of suitable antibiotics (Peirano and Pitout, 2019). Given the richness and diversity in chemistry and biological activity, the fungal secondary metabolites are regarded as inexhaustible sources for new antibacterial

drugs (Abouelhassan et al., 2019). Species in the genus *Penicillium*, which are world widely distributed and mostly saprophytic, have since been considered as valuable resources of life-saving medicine and agrochemicals (Nielsen et al., 2017). The genus *Penicillium* consists of more than 350 of species, however, only a very limited number of them have been exploited for bioactive secondary metabolites. Among them, *Penicillium rubens* (also known as *Penicillium chrysogenum*) is one of the most prominent species and famous for its outstanding secondary metabolite penicillin, a paramount antibiotic for the therapy of infectious disease since World War II (Penalva et al., 1998). In addition, some other *Penicillium* fungi had been developed to produce series of pharmaceutical compounds, including the cholesterol-lowering drugs statins from *Penicillium citrinin* (Manu and Rogozea, 2016), mycophenolic acid from *Penicillium brevicompactum* (Anand and Srivastava, 2020), anti-cancer auranthine from *Penicillium aurantiogriseum* (Kalinina et al., 2018), and anti-Inflammation (3R, 7R)-7-acetoxyl-9-oxo-de-o-methyllasiodiplodin produced by *Penicillium* sp. (Liu et al., 2019).

Isoquinoline alkaloids constitute the largest classes of secondary metabolites with more than 2,500 defined structures, mainly produced by higher plants (Sato et al., 2007). Since the early 19th century, their complex structures and significant biological activities have attracted considerable attentions from researchers worldwide. However, so far, only a limited number of isoquinoline compounds were isolated from filamentous fungi, such as fumisoquins from *Aspergillus fumigatus* (Baccile et al., 2016), spathullins A and B from *Penicillium spathulatum* Em19 (Nord et al., 2019), imizoquins from *Aspergillus flavus* (Khalid et al., 2018), chaetolines A and B from *Chaetomium* sp (Ancheeva et al., 2018), and benzoisoquinoline-9-one from *Peyronellaea* sp. FT431(Li et al., 2019), and most were identified with anti-bacterial activities.

In our study, the genome of a coral-derived fungus *Penicillium steckii* P2648 was revealed by high-throughput sequencing, and founded to encode 28 of secondary metabolite gene clusters. The mycotoxin citrinin was identified as the major secondary metabolite of P2648 and showed antibacterial activities. The coding gene of citrinin cluster (*cits*) was genetically disrupted from P2648 genome. Besides, the disruption of *cits* compromised citrinin biosynthesis but caused the unanticipated accumulations of two anti-bacterial isoquinoline alkaloid compounds (Compound 1 and 2). Their chemical structures were classified by combining use of 1D, 2D-NMR, and MS. Taken together, our study demonstrated that citrinin endows the coral-derived *P. steckii* P2648 with prominent anti-bacterial features, while blocking the biosynthesis of citrinin will generate another two novel anti-bacterial isoquinoline alkaloids. Moreover, genetic dereplication approach will shed novel light on the study of secondary metabolites in marine-derived fungi.

MATERIALS AND METHODS

Fungal Identification

The fungal strain was isolated from a gorgonian which was collected from the South China Sea. For growth and conidiation, the fungal strain was cultured on the PDA agar (potato juice 20%, dextrose 2%, and agar 1%), YES (sucrose 15%, yeast extract 2%, and agar 1%), or GMM (sucrose 2%, $NaNO_3$ 3%, KH_2PO_4 1%, KCl 0.5%, $MgSO_4$ 0.1%, $FeSO_4$ 0.01%, and agar 1%) for 7 days at room temperature in the dark. For molecular identification of fungal strain, the genomic DNA of fungal strain was extracted from approximately 100 mg of mycelium, scraped from PDA plates, using a thermolysis method as previously reported (Zhang et al., 2010). The quality and quantity of DNA samples were measured with the NanoDrop Spectrophotometer (Thermo Scientific, Wilmington, Germany). The ITS fragment was amplified using the primer pair *ITS1/ITS4* (**Supplementary Table S2**), and 18S rRNA gene was obtained from our sequencing data. A phylogenetic tree based on ITS and 18 s rDNA sequences was constructed by using the MAGA X with the neighbor-joining method (Kumar et al., 2018).

Genome Sequencing

Genome sequencing of *P. steckii* P2648 was performed using the second-generation Illumina seq 4000 platform at Majorbio, China. The sequencing libraries were constructed using Illumina Paired-End DNA sample Prep Kit. Reads were assembled from raw data by using SOAPdenovo v2.04 program with a range of Kmers (17–92). Gene predictions were performed by using Maker2 program. Gene model annotations were carried out through sequence alignment in Cluster of Orthologous Groups of proteins (COG) database. Prediction of putative secondary metabolite biosynthesis gene cluster was carried out using the online AntiSMASH software. To use single-copy genes to plot species tree, the protein-coding genes from *P. steckii*, *Penicillium oxalicum*, *P. rubens*, *Penicillium griseofulvum*, *Penicillium brasilianum*, *Penicillium expansum*, and *Aspergillus nidulans* were downloaded from NCBI NR database. The single-copy genes were obtained by using OrthoFinder software. The phylogeny tree was constructed inferred from the amino acid sequences of 5,884 single-copy genes by IQ-TREE based on maximum likelihood algorithm. The phylogenetic tree was displayed by using iTOL.

Gene Deletion

Gene deletion strategy in P2648 was slightly modified from that we previously established in *P. oxalicum* (Yao et al., 2015). Double-joint PCR was used to construct a gene deletion cassette, using the *hph* gene amplified from plasmid pSilent-1 as the selectable marker. All primers that were used to amplify the 5'- and 3'-flanks were listed in **Supplementary Table S2** with the P2648 gDNA as the template. The entire gene deletion cassette was amplified with specific primers, using the 5'- and 3'-flanks for gene *citS* and *hph* mix as a template. The PCR products were transformed into the protoplasts of P2648 wild strain. For the preparation of protoplasts, approximately 10^9 cfu/ml of conidia was inoculated into 100 ml PDB Broth, shaken at 150 rpm for 12 h at 30°C. Mycelia were collected by using four-layers of cotton gauzes, transferred to a 50 ml

tube, and resuspended in 20 ml lysis filter-sterilized solution that contained 12 mg/ml lysing enzymes (Sigma, St Louis, MO, United States), 50 mM KC1, 1 M NaCl, and 1 mM $CaCl_2$. After shaken at 60 rpm, 30°C for 3–4 h, protoplasts were harvested by filtering through a two-layer of lens paper. The obtained protoplasts were washed twice with a solution of 0.5 M KC1, 50 mM $CaC1_2$, and 10 mmol Tris-HCl (pH 7.5). Fungal transformation and regeneration procedures were performed as described previously (Yao et al., 2015). Gene deletion mutants were preliminarily identified by PCR and then confirmed *via* RT-PCR. The primers used for verifying gene deletion mutants were listed in **Supplementary Table S2**.

Fermentation, Extraction, Isolation, and Structure Determination

The fungus *Δcits* mutant was cultivated in the rice medium (80 g of rice, 3 g of natural sea salt, and 100 ml of H_2O) in 1 L Erlenmeyer flask (20 flasks) at room temperature for 4 weeks. The fermented rice substrates were extracted three times with EtOAc (300 ml every time for each flask) and two times with MeOH (300 ml for each flask). The organic extracts were combined and concentrated under vacuum to afford a total extract (5.0 g), which was subjected to silica gel column chromatography (CC) using a step gradient elution with EtOAc-petroleum ether (0–100%) and then with MeOH-EtOAc (0–50%) to yield four fractions (Fr.1–Fr.4). Fr.3 was further subjected to silica gel CC, and eluted with $CHCl_2$-MeOH (40:1, v/v) to obtain subfractions Fr.3-1–Fr.3-4, Fr.3-2 was further purified by semi-preparative high performance liquid chromatography (HPLC) eluted with MeOH-H_2O (40:60, v/v) to give compounds 1 (14.0 mg) and 2 (19.0 mg). Fr.3-3 purified by Sephadex LH-20 CC with mixtures of $CHCl_2$-MeOH (1:1, v/v) to yield compound 3 (12.0 mg).

Optical rotations were recorded on a JASCO P-1020 digital polarimeter. IR was acquired on a Nicolet-Nexus-470 spectrometer with of KBr Pellet Method. The 1D and 2D NMR spectra were recorded in MeOD on a JEOL JEM-ECP NMR spectrometer with tetramethyl silane (TMS) as the internal standard. All NMR assignments were based on the ^1H-^1H COSY, HSQC, and heteronuclear multiple bond correlation (HMBC) spectroscopic data. High-resolution electron spray ionization mass spectroscopy (HRESIMS) data were acquired on a Thermo MAT95XP high-resolution mass spectrometer (Thermo Fisher Scientific, United States). HPLC analysis and purification were performed on a Hitachi L-2000 HPLC system coupled with a Hitachi L-2455 photodiode array detector and using an analytical Kromasil column (250 mm × 4.6 mm, 5 mm) and a semi-prepared C18 column (250 mm × 10 mm, 5 mm), respectively. The mobile phase consisted of 0.1% formic acid in acetonitrile (A) and 0.1% formic acid in water (B) with a flow rate of 1 ml/min with 10 ml injection volume, and recorded at 254 nm.

Antibacterial Activities Tests

The tested pathogenic bacterial strains include three common zoonotic pathogens (*E. coli* 25922, *Staphylococcus aureus* ATCC 2592, and *Pseudomonas aeruginosa* FRD1), two antibiotic-resistant bacteria [ESBL-producing *E. coli* (ATCC 35218) and vancomycin-resistant *Enterococcus faecalis* ATCC 51299]. The minimum inhibitory concentration (MIC) was determined by using a broth microdilution method according to the standards and guidelines recommended by Clinical and Laboratory Standards Institute (2012). Penicillin G sodium salt was used as anti-bacterial drug positive control.

RESULTS AND DISCUSSION

Genome Sequencing

During our screening of the marine-derived fungi for producing anti-bacterial natural products, the crude extract of gorgonian-derived fungus P2648 showed strong inhibition on the growth of both Gram-negative *E. coli* and Gram-positive *S. aureus* (MIC 50–100 μg/ml). Based on morphological characteristics and phylogenetic analysis of 18S rRNA and ITS sequence, P2648 was classified into the genus *Penicillium* with the highest sequence similarity (99.8%) to *P. steckii* (**Supplementary Figure S1**). Until now, no genome of marine-derived *P. steckii* had been sequenced. To investigate comprehensively the potential of marine-derived fungus P2648 in production of secondary metabolites, genomic DNA was isolated from the mycelia of strain P2648 and sequenced by using the Illumina Hiseq 4000 sequencing platform. The obtained genome of P2648 was assembled into 961 scaffolds of about 33.4 megabases (Mb), which is larger than that of model *P. steckii* strain IBT 24891 (**Table 1**). And, compared to other fungi in *Penicillium* genus, P2648 has a relatively larger genome in size (**Table 1**). A total of 12,098 protein-encoding genes were predicted, which comparable to both soil-derived *P. steckii* and *Penicillium* fungi. Among them, 10,343 (85.49%) genes have functional annotations in the COG database (**Supplementary Table S1**). Referring to the functional classification of COG, and among them, 279 genes (2.7%) are involved into secondary metabolite biosynthesis, transport, or metabolism (**Supplementary Table S1**).

To better understand the evolutional relationship, phylogenetic analysis was performed by using whole-genome alignment between P2648 and its relatives. The result showed that six *Penicillium* species and P2648 formed a clade with a high bootstrap support, in which P2648 showed closest relationship with *P. steckii* (**Figure 1A**). Therefore, together multi-loci DNA sequence and whole-genome alignment phylogenetic analysis confirmed that P2648 was one of

TABLE 1 | Genome features of marine fungus P2648 and six *Penicillium* fungi.

Strains	Genome size (Mbp)	GC%	Proteins
P2648	33.4	46.4	10,343
Penicillium steckii	32.1	45.1	10,362
P. citrinum	31.5	46.2	9,754
P. griseofulvum	29.1	47.3	9,630
P. rubens	32.5	48.9	11,460
P. expansum	32.4	47.5	11,060
P. oxalicum	30.2	50.6	9,979

P. steckii species. Sequence-synteny analyses between *P. steckii* and P2648 revealed that most of scaffolds showed synteny, however, extensive genetic divergences existed in the two *P. steckii* strains that were from different geographical regions (**Figure 1B**).

Secondary Metabolite Gene Cluster

The secondary metabolites of filamentous fungi constitute a rich resource of bioactive natural products with antibiotic activities, such as penicillin from *P. chrysogenum*. Interestingly, genes encoding biosynthetic pathway for secondary metabolite are often located in a gene cluster on chromosome to form the secondary metabolite biosynthetic gene clusters (SMBGC; Keller, 2015). Mining P2684 genome for gene clusters involved in the biosynthesis of secondary metabolites was performed by using the online antiSMASH tool. A total of 28 (SMBGCs) were identified from the genome of P2648, including nine of polyketide (PKS), 10 of non-ribosomal peptide (NRPS)-like (NRPS-like), four of NRPS, two of terpene (TE), three of PKS-NRPS hybrid, and one betalactone (**Table 2**).

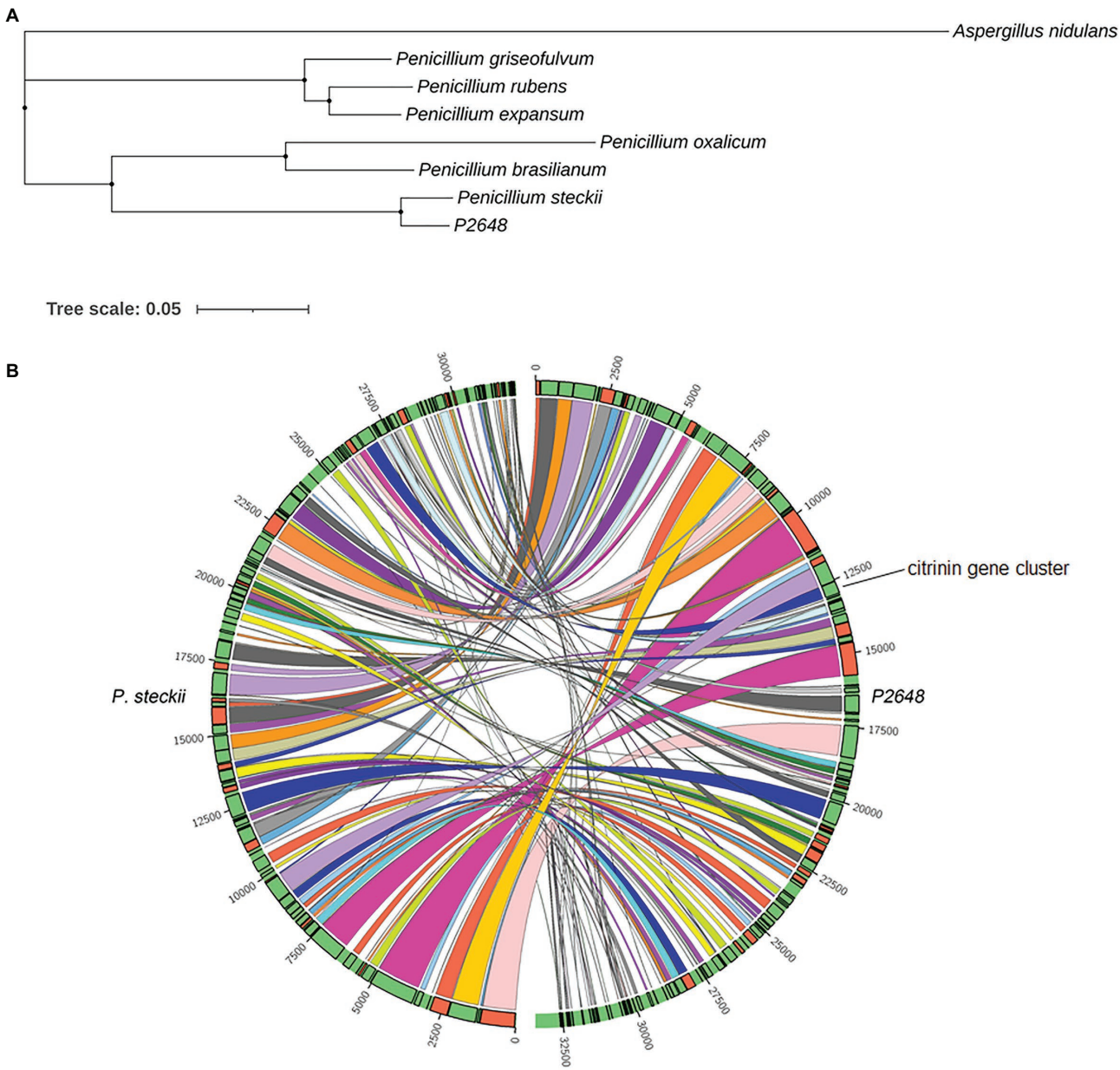

FIGURE 1 | Phylogenetic and synteny analysis of P2648 with other fungal species. **(A)** The maximum likelihood phylogeny was constructed inferred from the amino acid sequences of 5,884 single-copy genes by IQ-TREE. The phylogenetic tree was displayed by using iTOL. The single-copy genes were obtained by OrthoFinder tool. *Aspergillus nidulans* from *Aspergillus* genus was used as the outgroup; **(B)** Sequence-synteny analyses between marine-derived P2648 and soil-species, and the Circo plots represent syntenic blocks between P2648 and *Penicillium steckii*.

Based on antiSMASH prediction, we found that *P. steckii* P2648 has the potential to produce sorbocillin (**Table 2** and **Figure 2**). Sorbocillin and its derivatives, sorbicillinoids are a class of biologically active and structurally diverse fungal polyketides (Salo et al., 2016). Cluster 10 is consisted of three genes, two polyketide synthase (gene04233 and gene04234), and one FAD-dependent monooxygenase (gene04235). The two-polyketide synthases 04233 and 04234 showed high sequence similarities with the highly reducing iterative PKS SorA and the non-reducing iterative PKS SorbB, respectively (**Figure 2**). In sorbocillin biosynthesis, these two megaenzymes were reported to assemble the polyketide skeleton. And, the FAD-dependent monooxygenase 04235 from Cluster 10 showed high sequence similarity with the post-modification enzyme SobC (**Figure 2**). Together, our *in silico* analysis suggested that P2648 could produce sorbocillin and its analogs.

The polyketide cluster encoded by Cluster 3 showed 100% sequence similarity to the naphthopyrone cluster from *A. nidulans*, which responsible for biosynthesis of the yellow conidial wall pigment (Mayorga and Timberlake, 1992). In addition, Cluster 6 was predicted to biosynthesize secondary metabolites with structurally similar to nidulanin A and Cluster 22 showed high similarity to the terpene cluster squalestatin S1. Cluster 26 is composed of six genes, encoding FAD-dependent monooxygenase (gene10770), oxidoreductase (gene10771), o-methyltransferase (gene10772), monooxygenase (gene10773), non-reducing polyketide synthase (gene10774), and a transcription factor (gene10775). Among them, four of genes showed high sequence similarities with their counterparts involved in biosynthesis of TAN-1612 (Li et al., 2011). Therefore, we hypothesized that Cluster 26 potentially synthesize similar polyketide compounds.

Intriguingly, secondary metabolite products encoded by most of these SMBGCs in P2648 genome could not be assigned. In particular, three PKS/NRPS hybrid SMBGCs (Cluster 16, Cluster 20, and Cluster 24) were identified in P2648 genome, their secondary metabolite products remain to be determined. Also, we predicted 10 NRPS-like BGC gene clusters in P2648, no any compound could be assigned by bioinformatic analysis. Together, we have performed a comprehensive analysis and provide valued information on gene clusters for secondary metabolite biosynthesis by using both antiSMASH and gene cluster homology comparisons.

TABLE 2 | Secondary metabolite gene cluster in P2648.

Cluster	Type	Similarity to known BGC
Cluster 1	NRPS-like	
Cluster 2	NRPS-like	
Cluster 3	T1PKS	100% Naphthopyrone
Cluster 4	NRPS-like	
Cluster 5	Betalactone	
Cluster 6	NRPS	100% Nidulanin A
Cluster 7	NRPS	
Cluster 8	NRPS	
Cluster 9	T1PKS	
Cluster 10	T1PKS	100% Sorbicillin
Cluster 11	T1PKS	
Cluster 12	NRPS-like	
Cluster 13	T1PKS	
Cluster 14	T1PKS	
Cluster 15	NRPS-like	
Cluster 16	NRPS,T1PKS	
Cluster 17	NRPS-like	
Cluster 18	NRPS-like	
Cluster 19	NRPS-like	
Cluster 20	NRPS-like,T1PKS	
Cluster 21	NRPS-like	
Cluster 22	Terpene	50% Squalestatin S1
Cluster 23	NRPS-like	
Cluster 24	NRPS,T1PKS	
Cluster 25	T1PKS	
Cluster 26	T1PKS	50% TAN-1612
Cluster 27	Terpene	
Cluster 28	T1PKS	

Citrinin Is the Major Anti-bacterial Compound Produced by the Coral-Derived Fungus *P. steckii* P2648

To chemically identify the antibacterial agents, scaled fermentation of P2648 was performed by using a solid rice medium for 10 days. The ethyl acetate extracts of the fermentation were fractionated by using repeated positive and negative silica chromatography. A golden-yellow needle crystal (14 g) was obtained, which accounting for the largest population of total organic extracts (about 67%). Its structure was then identified to be as citrinin by comparing its ^{1}H NMR and ^{13}C NMR (**Table 3**) with previously reported NMR data (Blanc et al., 1995).

Identification of the Citrinin Biosynthetic Gene Cluster

No gene cluster for citrinin biosynthesis could be ascertained by antiSMASH analysis (**Table 2**). Therefore, to identify the gene cluster for citrinin biosynthesis, a manual BLAST search by using CitS coding gene from *Monascus ruber* as a query against the *P. steckii* P2648 genome was performed, and results showed that a putative citrinin polyketide cluster containing

TABLE 3 | ^{1}H (400 MHz) and ^{13}C (100 MHz) NMR spectroscopic data for citrinin ($CDCl_3$).

Position	Citrinin	
	δ_C, type	δ_H, mult. *J* in Hz
1	162.9, CH	8.25, s
3	81.7, CH	4.80, dq. 6.6, 0.8
4	34.6, CH	3.00, dq. 7.2, 0.9
4a	139.2, C	
5	123.1, C	
6	183.8, C	
7	100.3, C	
8	177.2, C	
8a	107.4, C	
9	18.2, CH_3	1.36, d. 6.7
10	18.5, CH_3	1.24, d. 7.2
11	9.4, CH_3	2.03, s
12	174.6, C	
8-OH		15.1, s
12-OH		15.9, s

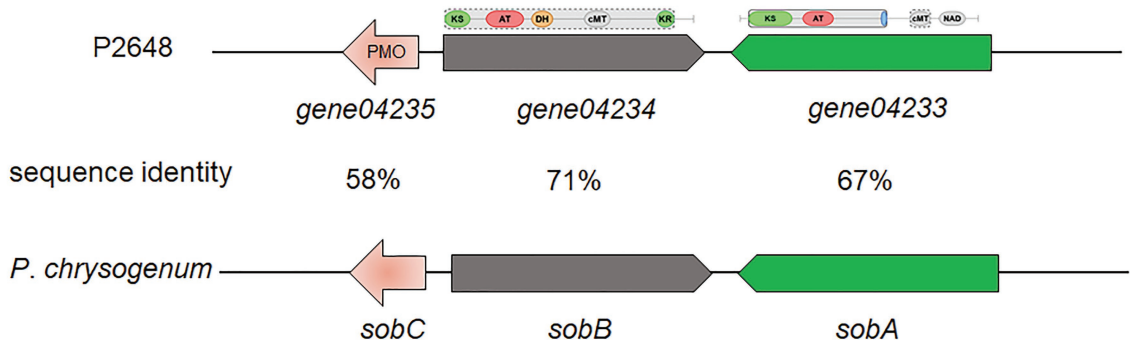

FIGURE 2 | The putative sorbocillin biosynthetic gene cluster of P2648 and the comparison of this cluster with the sorbocillin cluster reported for *P. chrysogenum*. PMO, monooxygenase; KS, ketosynthase domain; AT, acyltransferase; DH, dehydratase domain; cMT, carbon methyltransferase; KR, ketoreductase domain; and NAD, male sterility protein.

nine genes were identified (**Table 4**). And, the entire citrinin gene cluster showed synteny between P2648 and *P. steckii*. The gene04630 (the homolog of *cits*) encodes the polyketide synthase, synthesizing triply methylated pentaketide skeleton by using methylmalonyl-SCoA as the building block (He and Cox, 2016). The methyl at 12-site of methylated pentaketide is progressively oxidized to carboxylic acid by non-heme iron oxidase CitB, FAD-dependent oxidoreductase CitC, and followed by CitD. Then, the 3-carbonyl is reduced to ether by the dehydrogenase CitE. CtnR and CtnC are the pathway-specific transcription factor and transporter, respectively. To confirm the function of the putative polyketide cluster in the citrinin biosynthesis, the open reading frame (ORF) region of PKS gene *cits* was deleted from *P. steckii* wild-type strain P2648 (WT) genome by replacing with hygromycin phosphate transferase (*hph*) gene. A total of 21 hygromycin-resistance transformations were obtained by three cycles of genetic transformation, and two deletion mutants were further verified through RT-PCR with gene-specific primers (**Figure 3A**). Absence of *cits* gene had no detectable defects on both vegetative growth and conidiation of P2648 on various media (**Figure 3B**). As anticipated, the *Δcits* mutant produced a significant difference in secondary metabolite profiles when compared with WT (**Figure 4**). Citrinin dominates the fermentation extracts of WT, but no citrinin can be detected in *Δcits*, suggesting that CitS is essential for citrinin biosynthesis. Besides, intriguingly, as shown in **Figure 4**, several peaks with retention time from 26 to 28 min were emerged and enhanced in *Δcits* when compared with WT.

Three Isoquinoline Alkaloids Were Unexpectedly Accumulated in the *Δcits* Mutant

To further mine the induced metabolite potentials by obstructing citrinin synthesis, the secondary metabolites of *Δcits* were harvested by scaled fermentation. The organic extracts were fractionated by repeated silica gel chromatography, Sephadex LH-20, and semi-preparative HPLC, and finally obtained compounds 1–3 (**Figure 5**).

TABLE 4 | The citrinin biosynthesis gene cluster.

Gene ID	Description	Length	Functional annotation	Identity (%)
gene04631	CtnC	859	Transporter	79.33
gene04630	CitS	2,584	Polyketide synthase	74.81
gene04629	CitA	262	Oxydoreductase	78.76
gene04628	CitB	328	Iron/ascorbate oxidoreductase	81.76
gene04627	CtnR	552	$Zn(II)_2Cys_6$ transcriptional regulator	78.93
gene04626	CtiD	501	Aldehyde dehydrogenase	85.20
gene04625	unknown	128	Hypothetical protein	85.27
gene04624	CitE	915	Dehydrogenase	72.50
gene04623	CitC	463	FAD-dependent oxidoreductase	74.94

Compound 1 was obtained as a white powder. Its molecular formula was determined to be $C_{10}H_9NO_3$ on the basis of the HRESIMS (*m/z* 192.0653 $[M + H]^+$; calcd for $C_{10}H_{10}NO_3$, 192.0655) and the ^{13}C NMR data. The ^1H NMR data (**Table 5**) displayed four aromatic proton signals at δ_H 7.92 (1H, d, J = 8.0, 0.8 Hz, H-5),7.48 (1H, ddd, J = 7.2, 8.8, 1.2 Hz, H-7), 7.30 (1H, d, J = 8.0 Hz, H-8), and 7.24 (1H, ddd, J = 7.2, 8.0, 1.2 Hz, H-6); and an oxygenated singlet methyl proton resonance at δ_H 3.85. Additionally, the ^{13}C and HSQC spectra showed 10 carbon signals, attributable to one ester group carbonyl resonating at δ_C 161.6, eight aromatic or olefinic carbon signals at δ_C 153.0, 135.3, 130.4, 129.5, 122.6, 121.9, 115.9, and 114.9, and one oxygenated methyl signal at δ_C 59.2. The aforementioned NMR data indicated the presence of one 1,2 disubstituted aromatic ring and one olefinic bond and these groups accounted for six out of the seven degrees of unsaturation, requiring one additional ring in 1. Analysis of the COSY spectrum showed correlations of H-5/H-6, H-6/H-7, and H-7/H-8 (**Figure 6**). Based on the HMBC cross-peaks from H-5 to C-4/C-7/C-8a (**Figure 6**), from H-6 to C-4a/C-5/C-8a/C-8, from H-7 to C-5/C-8/C-8a, as well as from H-8 to C-4/C-4a/C-6 were used to connect the aromatic ring with the olefinic bond. The HMBC correlations from oxygenated methyl proton δ_H 3.85 to C-3 (δ_C 130.4)

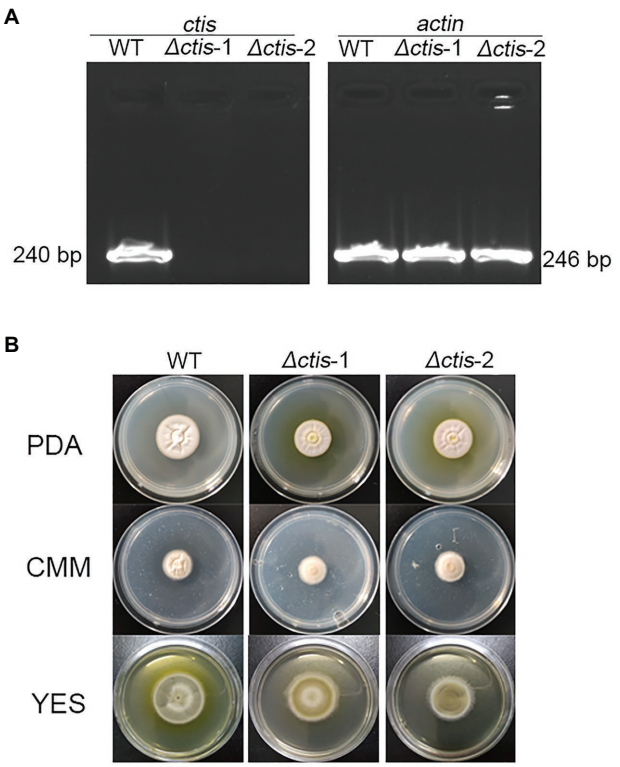

FIGURE 3 | Deletion of *citS* gene in P2648. **(A)** RT-PCR verification of gene deletion, the transcripts of *actin* gene were used as the control; **(B)** Conidia of *Δcits* and wild-type (WT) were inoculated on the PDA, CMM, and YES plates, culturing at 30°C for 7 days.

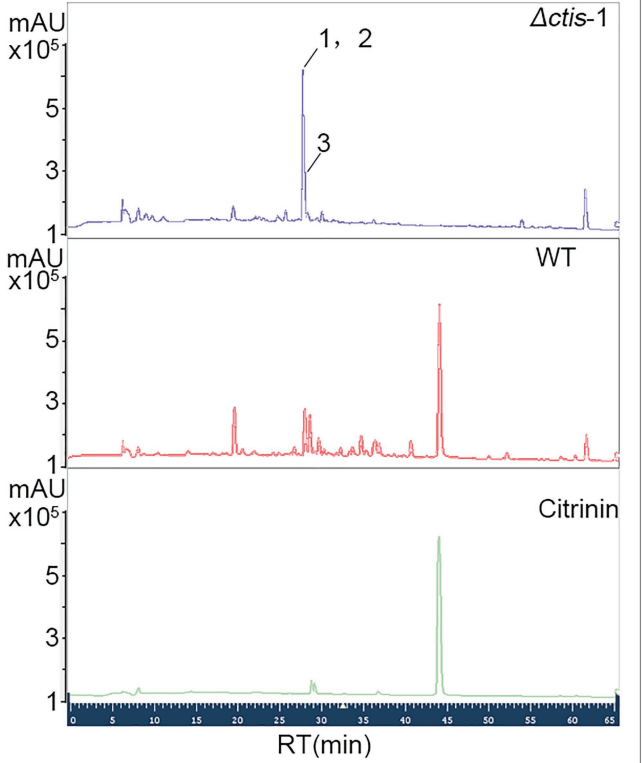

FIGURE 4 | High performance liquid chromatography (HPLC) analysis of secondary metabolite profiles of both *Δcits* mutant and WT strains. Conidia of *Δcits* and WT were inoculated in the rice medium and cultured at room temperate for 21 days, the secondary metabolites were extracted by using EtOAc, and then analyzed by HPLC.

demonstrated the groups of ■OCH_3 was anchored at C-3. Herein, compound 1 was elucidated as an isoquinoline alkaloid, 4-hydroxy-3-methoxy-2(1*H*)-quinolinone.

Compound 2 was also obtained as a white powder with the molecular formula $C_{11}H_{11}NO_3$ from HRESIMS (*m/z* 206.0808 $[M + H]^+$; calcd for $C_{11}H_{12}NO_3$, 206.0812), suggesting that 2 has one CH_2 mass unit more than 1. A careful comparison of the ^1H and ^{13}C NMR spectra of 2 (**Table 6**) with those of 1 showed a close structural relationship, with the only difference being the oxygenated methyl proton signal at δ_H 3.71 and the oxygenated methyl signal at δ_C 28.4. According to the HMBC cross-peaks from ■NCH_3 (δ_H 3.71) to C-2 and C-8a, the oxygenated methyl group was attached to the amide group. Therefore, compound 2 was characterized as 4-hydroxy-3-methoxy-1-methyl-2(1*H*)-quinolinone.

Compound 3 with the molecular formula $C_{11}H_{11}NO_2$ as determined by HRESIMS (*m/z* 190.0858 $[M + H]^+$; calcd for $C_{11}H_{12}NO_2$, 190.0863), was isolated as the white powder. The ^1H NMR spectrum (**Table 6**) was very similar to that of 2, with the notable difference being the addition of a singlet proton resonance at δ_H 7.99 in 3. Comparison of the ^{13}C NMR spectra of 3 with those of 2 displayed an unsubstituted olefinic carbon signal at δ_C 130.8. Combining the HMBC correlations from ■NCH_3 (δ_H 3.71) to C-2 and C-8a and

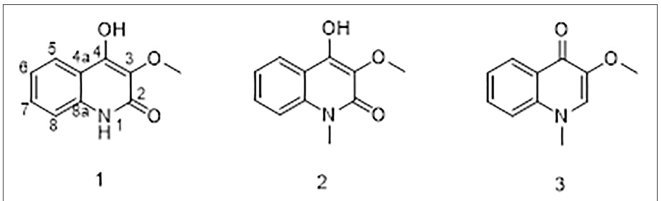

FIGURE 5 | Structures of compounds 1–3.

from ■OCH_3 (δ_H 3.89) to C-3, the structure of compound 3 was assigned as 3-methoxy-1-methyl-4(1*H*)-quinolone.

The unexpected accumulation of three isoquinoline alkaloids after the deletion of *citS* might cause by, at least, the redistribution of biosynthetic precursors. More specifically, in WT strain, citrinin is the dominant secondary metabolite, which obstructs the biosynthesis of other compounds by consuming most of the universal precursor substances, such as acetyl-CoA and malonyl-CoA. Elimination of the citrinin biosynthesis might increase the reserve pools of these precursors, which would be redirected into the biosynthesis pathway of isoquinoline alkaloids. Additionally, the deletion of *citS* also resulted in a low SM background, which consequently contributed to the discovery of those isoquinoline alkaloids with formerly low synthetic levels.

TABLE 5 | ^{1}H (400 MHz) and ^{13}C (100 MHz) NMR spectroscopic data for 1 and 2 (methanol-d_4).

Position	1		2	
	δ_C, type	δ_H, mult. *J* in Hz	δ_C, type	δ_H, mult. *J* in Hz
1-CH_3			28.4, CH_3	3.71, s
2	161.6, C		161.2, C	
3	130.4, C		130.2, C	
4	153.0, C		152.0, C	
3-OCH_3	59.2, CH_3	3.85, s	59.0, CH_3	3.82, s
4a	115.9, C		116.8, C	
5	122.6, CH	7.92, d. 8.0, 0.8	123.1, CH	8.02, d. 7.6
6	121.9, CH	7.24, ddd. 8.0, 7.2, 1.2	121.9, CH	7.30, ddd. 8.0, 6.8, 0.8
7	129.5, CH	7.48, ddd. 8.8, 7.2, 1.6	129.9, CH	7.60, ddd. 8.8, 7.2, 1.6
8	114.9, CH	7.30, d. 8.0	114.1, CH	7.51, d. 7.6
8a	135.3, C		136.8, C	

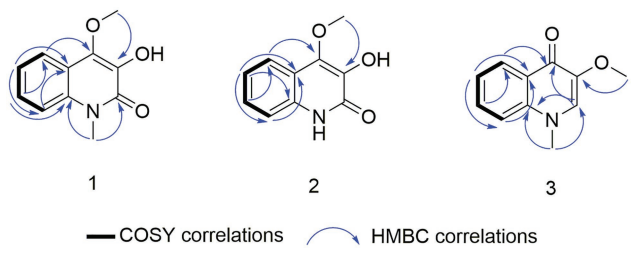

FIGURE 6 | COSY and key heteronuclear multiple bond correlation (HMBC) correlations for 1–3.

TABLE 6 | ^{1}H (400 MHz) and ^{13}C (100 MHz) NMR spectroscopic data for 3 (methanol-d_4).

Position	3	
	δ_C, type	δ_H, mult. *J* in Hz
1-CH_3	39.8, CH_3	3.99, s
2	130.8, CH	7.99, s
3	142.9, C	
3-OCH_3	56.8, CH_3	3.89, s
4	171.6, C	
4a	125.3, C	
5	125.5, CH	8.40, d. 8.4
6	122.9, CH	7.43, ddd. 8.0, 6.4, 1.2
7	131.7, C	7.78, ddd. 8.4, 6.8, 1.6
8	115.8, CH	7.72, d. 8.40
8a	139.0, C	

TABLE 7 | Antibacterial activity assays.

Compound	MIC (μg/ml)				
	E. coli ATCC 25922	*E. coli* ATCC 35218	*S. aureus* ATCC 2592	*E. faecalis* ATCC 51299	*P. aeruginosa* FRD1
1	32	32	16	32	>512
2	16	16	>512	16	>512
3	>512	>512	>512	>512	>512
Citrinin	16	16	16	4	>512
Penicillin sodium salt	4	256	8	8	4

Biological Activity Assay

The antibacterial activities of three isoquinoline alkaloids and citrinin against a variety of pathogenic bacteria were assessed using the broth microdilution method to determine the MICs (**Table 7**).

Citrinin displayed excellent biological activities against all tested pathogenic bacteria with MIC of from 4 to 16 μg/ml, except for *P. aeruginosa* FRD1. Compound 1 exhibited an MIC of 16–32 μg/ml against all tested pathogens expect for *P. aeruginosa* FRD1, and compound 2 also showed an MIC of 16 μg/ml against three pathogenic bacteria, including two *E. coli* and one *E. faecalis*. The most noteworthy result is that both compounds 1 and 2 showed obvious activities against two drug-resistant microbial bacterial pathogens *E. coli* ATCC 35218 and *E. faecalis* ATCC 51299, implying a different action mechanism from common antibiotics. Compound 3 did not show detectable biological activities against any of tested pathogenic bacteria. Compared with compounds 1 and 2, hydroxy at position 4 was oxidized to a carbonyl in compound 3, suggesting that the 4-hydroxy is essential for the anti-bacterial activities of isoquinoline alkaloids.

CONCLUSION

In the study, we reported the draft genome of a coral-derived fungus P2648. Whole-genome phylogenetic analysis demonstrated that P2648 is a novel strain of *P. steckii* species. The genome data and our bioinformatic analysis firstly revealed that *P. steckii* contains a large number of secondary metabolite cluster without assigned compounds. Further, our chemical investigation indicated that citrinin was identified as the dominant antibacterial agent of P2648, and a CitS-containing SMBGC was proved to be involved in citrinin biosynthesis in P2648. Surprisingly, three isoquinoline alkaloids were accumulated after blocking the biosynthesis of citrinin, and two of isoquinoline alkaloids showed moderate activities against two antibiotic-resistant pathogenic bacteria. In conclusion, our genomic and chemical analyses present evidence in support of *P. steckii* P2648 as a potent natural products source for anti-bacterial drug discovery.

DATA AVAILABILITY STATEMENT

The whole genome sequence of *P. steckii* P2648 has been deposited at NCBI database under the Bioproject number PRJNA671565.

AUTHOR CONTRIBUTIONS

GY, ZW, and JC conceived and designed the research work. GY, HZ, XC, DL, and ZY performed the experiments and analyzed the data. GY wrote the manuscript. HZ, XC, ZW, and JC revised the manuscript. All authors contributed to the article and approved the submitted version.

FUNDING

This work was supported by grants from Minjiang University (JAT190622, MYK19011, and MJY19019), China Ocean Mineral Resources R&D Association (DY135-B2-13), Project from Department of Fujian Science and Technology (2018N2001), and Program for Innovative Research Team in Science and Technology in Fujian Province University.

ACKNOWLEDGMENTS

We thank Chang-Yun Wang from Ocean University of China for providing gorgonian materials. We also thank a lot for Yao-Yao Zheng for his excellent technical assistance.

SUPPLEMENTARY MATERIAL

The Supplementary Material for this article can be found online at: https://www.frontiersin.org/articles/10.3389/fmicb.2021.600991/full#supplementary-material

Supplementary Figure S1 | Phylogenetic tree analysis of P2648 and related filamentous fungi. Phylogenetic tree of P2648 and all related strains were reconstructed based on a 18S RNA gene alignment using the MEGA X software package with the neighbor-joining method. Bootstrap analysis (1,000 replications) was used to provide confidence estimates for phylogenetic tree topologies, and the percentage values are indicated at nodes.

Supplementary Table S1 | Protein-encoding gene annotations.

Supplementary Table S2 | Primers used in this study.

REFERENCES

Abouelhassan, Y., Garrison, A. T., Yang, H., Chavez-Riveros, A., Burch, G. M., and Huigens, R. W. 3rd. (2019). Recent progress in natural-product-inspired programs aimed to address antibiotic resistance and tolerance. *J. Med. Chem.* 62, 7618–7642. doi: 10.1021/acs.jmedchem.9b00370

Anand, S., and Srivastava, P. (2020). Optimization strategies for purification of mycophenolic acid produced by *Penicillium brevicompactum*. *Appl. Biochem. Biotechnol.* 191, 867–880. doi: 10.1007/s12010-019-03204-w

Ancheeva, E., Mandi, A., Kiraly, S. B., Kurtan, T., Hartmann, R., Akone, S. H., et al. (2018). Chaetolines A and B, pyrano[3,2-f]isoquinoline alkaloids from cultivation of *Chaetomium* sp. in the presence of autoclaved *Pseudomonas aeruginosa*. *J. Nat. Prod.* 81, 2392–2398. doi: 10.1021/acs.jnatprod.8b00373

Baccile, J. A., Spraker, J. E., Le, H. H., Brandenburger, E., Gomez, C., Bok, J. W., et al. (2016). Plant-like biosynthesis of isoquinoline alkaloids in *Aspergillus fumigatus*. *Nat. Chem. Biol.* 12, 419–424. doi: 10.1038/nchembio.2061

Blanc, P. J., Laussac, J. P., Le Bars, J., Le Bars, P., Loret, M. O., Pareilleux, A., et al. (1995). Characterization of monascidin A from *Monascus* as citrinin. *Int. J. Food Microbiol.* 27, 201–213. doi: 10.1016/0168-1605(94)00167-5

Clinical and Laboratory Standards Institute (2012). Performance Standards for Antimicrobial Susceptibility Testing. Clinical and Laboratory Standards Institute (CLSI). Twenty-Second Informational Supplement. M100-S22.

He, Y., and Cox, R. J. (2016). The molecular steps of citrinin biosynthesis in fungi. *Chem. Sci.* 7, 2119–2127. doi: 10.1039/C5SC04027B

Kalinina, S. A., Kalinin, D. V., Hovelmann, Y., Daniliuc, C. G., Muck-Lichtenfeld, C., Cramer, B., et al. (2018). Auranthine, a benzodiazepinone from *Penicillium aurantiogriseum*: refined structure, absolute configuration, and cytotoxicity. *J. Nat. Prod.* 81, 2177–2186. doi: 10.1021/acs.jnatprod.8b00187

Keller, N. P. (2015). Translating biosynthetic gene clusters into fungal armor and weaponry. *Nat. Chem. Biol.* 11, 671–677. doi: 10.1038/nchembio.1897

Khalid, S., Baccile, J. A., Spraker, J. E., Tannous, J., Imran, M., Schroeder, F. C., et al. (2018). NRPS-derived isoquinolines and lipopetides mediate antagonism between plant pathogenic fungi and bacteria. *ACS Chem. Biol.* 13, 171–179. doi: 10.1021/acschembio.7b00731

Kumar, S., Stecher, G., Li, M., Knyaz, C., and Tamura, K. (2018). MEGA X: molecular evolutionary genetics analysis across computing platforms. *Mol. Biol. Evol.* 35, 1547–1549. doi: 10.1093/molbev/msy096

Lee, S. Y., Kotapati, S., Kuti, J. L., Nightingale, C. H., and Nicolau, D. P. (2006). Impact of extended-spectrum beta-lactamase-producing *Escherichia coli* and *Klebsiella* species on clinical outcomes and hospital costs: a matched cohort study. *Infect. Control Hosp. Epidemiol.* 27, 1226–1232. doi: 10.1086/507962

Li, Y., Chooi, Y. H., Sheng, Y., Valentine, J. S., and Tang, Y. (2011). Comparative characterization of fungal anthracenone and naphthacenedione biosynthetic pathways reveals an alpha-hydroxylation-dependent Claisen-like cyclization catalyzed by a dimanganese thioesterase. *J. Am. Chem. Soc.* 133, 15773–15785. doi: 10.1021/ja206906d

Li, C., Sarotti, A. M., Wu, X., Yang, B., Turkson, J., Chen, Y., et al. (2019). An unusual benzoisoquinoline-9-one derivative and other related compounds with antiproliferative activity from hawaiian endophytic fungus *Peyronellaea* sp. FT431. *Molecules* 24:196. doi: 10.3390/molecules24010196

Liu, Y., Li, D., Jiang, Q., Zhang, Q., Liu, P., Wang, L., et al. (2019). (3R, 7R)-7-acetoxyl-9-oxo-de-O-methyllasiodiplodin, a secondary metabolite of *Penicillium* sp., inhibits LPS-mediated inflammation in RAW 264.7 macrophages through blocking ERK/MAPKs and NF-kappaB signaling pathways. *Inflammation* 42, 1463–1473. doi: 10.1007/s10753-019-01009-x

Manu, P., and Rogozea, L. (2016). The discovery of statins. *Am. J. Ther.* 23, e980–e981. doi: 10.1097/MJT.0000000000000467

Mayorga, M. E., and Timberlake, W. E. (1992). The developmentally regulated *Aspergillus nidulans* wA gene encodes a polypeptide homologous to polyketide and fatty acid synthases. *Mol. Gen. Genet.* 235, 205–212. doi: 10.1007/BF00279362

Nielsen, J. C., Grijseels, S., Prigent, S., Ji, B., Dainat, J., Nielsen, K. F., et al. (2017). Global analysis of biosynthetic gene clusters reveals vast potential of secondary metabolite production in *Penicillium* species. *Nat. Microbiol.* 2:17044. doi: 10.1038/nmicrobiol.2017.44

Nord, C., Levenfors, J. J., Bjerketorp, J., Sahlberg, C., Guss, B., Oberg, B., et al. (2019). Antibacterial isoquinoline alkaloids from the fungus *Penicillium spathulatum* Em19. *Molecules* 24:4616. doi: 10.3390/molecules24244616

Peirano, G., and Pitout, J. D. D. (2019). Extended-spectrum beta-lactamase-producing *Enterobacteriaceae*: update on molecular epidemiology and treatment options. *Drugs* 79, 1529–1541. doi: 10.1007/s40265-019-01180-3

Penalva, M. A., Rowlands, R. T., and Turner, G. (1998). The optimization of penicillin biosynthesis in fungi. *Trends Biotechnol.* 16, 483–489. doi: 10.1016/S0167-7799(98)01229-3

Salo, O., Guzman-Chavez, F., Ries, M. I., Lankhorst, P. P., Bovenberg, R. A. L., Vreeken, R. J., et al. (2016). Identification of a polyketide synthase involved in sorbicillin biosynthesis by *Penicillium chrysogenum*. *Appl. Environ. Microbiol.* 82, 3971–3978. doi: 10.1128/AEM.00350-16

Sato, F., Inui, T., and Takemura, T. (2007). Metabolic engineering in isoquinoline alkaloid biosynthesis. *Curr. Pharm. Biotechnol.* 8, 211–218. doi: 10.2174/138920107781387438

Yao, G., Li, Z., Gao, L., Wu, R., Kan, Q., Liu, G., et al. (2015). Redesigning the regulatory pathway to enhance cellulase production in *Penicillium oxalicum*. *Biotechnol. Biofuels* 8:71. doi: 10.1186/s13068-015-0253-8

Zhang, Y. J., Zhang, S., Liu, X. Z., Wen, H. A., and Wang, M. (2010). A simple method of genomic DNA extraction suitable for analysis of bulk fungal strains. *Lett. Appl. Microbiol.* 51, 114–118. doi: 10.1111/j.1472-765X.2010.02867.x

Conflict of Interest: The reviewer LL declared a shared affiliation, with no collaboration, with three of the authors DL, ZY, and ZW to the handling editor at the time of the review.

The remaining authors declare that the research was conducted in the absence of any commercial or financial relationships that could be construed as a potential conflict of interest.

Advantages of publishing in Frontiers

OPEN ACCESS
Articles are free to read for greatest visibility and readership

FAST PUBLICATION
Around 90 days from submission to decision

HIGH QUALITY PEER-REVIEW
Rigorous, collaborative, and constructive peer-review

TRANSPARENT PEER-REVIEW
Editors and reviewers acknowledged by name on published articles

Frontiers
Avenue du Tribunal-Fédéral 34
1005 Lausanne | Switzerland

Visit us: www.frontiersin.org
Contact us: frontiersin.org/about/contact

REPRODUCIBILITY OF RESEARCH
Support open data and methods to enhance research reproducibility

DIGITAL PUBLISHING
Articles designed for optimal readership across devices

FOLLOW US
@frontiersin

IMPACT METRICS
Advanced article metrics track visibility across digital media

EXTENSIVE PROMOTION
Marketing and promotion of impactful research

LOOP RESEARCH NETWORK
Our network increases your article's readership